frontiers | Research Topics

Cell compartments and intracellular trafficking of lipids and proteins: Impact on biomedicine

Edited by
Silvana Zanlungo, Carlos Enrich, Volker Gerke, Emily Eden and Maria Isabel Colombo

Published in
Frontiers in Cell and Developmental Biology

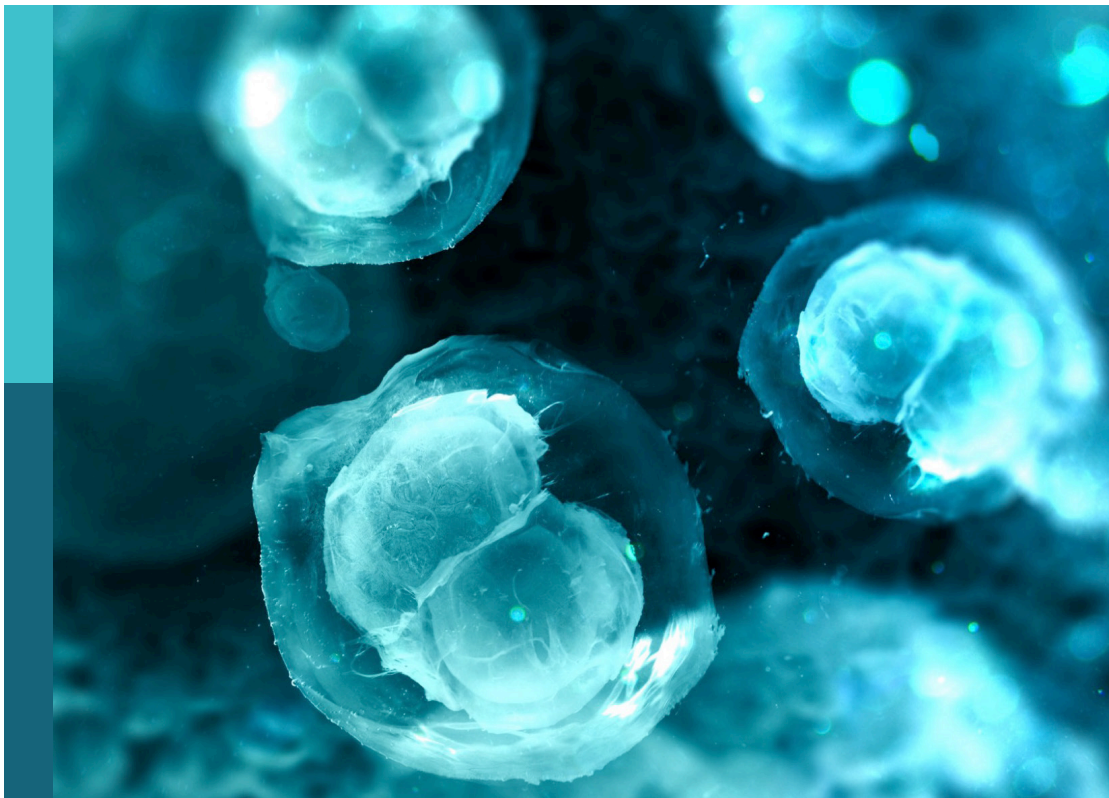

ISSN 1664-8714
ISBN 978-2-83250-994-4
DOI 10.3389/978-2-83250-994-4

About Frontiers

Frontiers is more than just an open access publisher of scholarly articles: it is a pioneering approach to the world of academia, radically improving the way scholarly research is managed. The grand vision of Frontiers is a world where all people have an equal opportunity to seek, share and generate knowledge. Frontiers provides immediate and permanent online open access to all its publications, but this alone is not enough to realize our grand goals.

Frontiers journal series

The Frontiers journal series is a multi-tier and interdisciplinary set of open-access, online journals, promising a paradigm shift from the current review, selection and dissemination processes in academic publishing. All Frontiers journals are driven by researchers for researchers; therefore, they constitute a service to the scholarly community. At the same time, the *Frontiers journal series* operates on a revolutionary invention, the tiered publishing system, initially addressing specific communities of scholars, and gradually climbing up to broader public understanding, thus serving the interests of the lay society, too.

Dedication to quality

Each Frontiers article is a landmark of the highest quality, thanks to genuinely collaborative interactions between authors and review editors, who include some of the world's best academicians. Research must be certified by peers before entering a stream of knowledge that may eventually reach the public - and shape society; therefore, Frontiers only applies the most rigorous and unbiased reviews. Frontiers revolutionizes research publishing by freely delivering the most outstanding research, evaluated with no bias from both the academic and social point of view. By applying the most advanced information technologies, Frontiers is catapulting scholarly publishing into a new generation.

What are Frontiers Research Topics?

Frontiers Research Topics are very popular trademarks of the *Frontiers journals series*: they are collections of at least ten articles, all centered on a particular subject. With their unique mix of varied contributions from Original Research to Review Articles, Frontiers Research Topics unify the most influential researchers, the latest key findings and historical advances in a hot research area.

Find out more on how to host your own Frontiers Research Topic or contribute to one as an author by contacting the Frontiers editorial office: frontiersin.org/about/contact

Cell compartments and intracellular trafficking of lipids and proteins: Impact on biomedicine

Topic editors

Silvana Zanlungo — Pontificia Universidad Católica de Chile, Chile
Carlos Enrich — University of Barcelona, Spain
Volker Gerke — University of Münster, Germany
Emily Eden — University College London, United Kingdom
Maria Isabel Colombo — Universidad Nacional de Cuyo, Argentina

Citation

Zanlungo, S., Enrich, C., Gerke, V., Eden, E., Colombo, M. I., eds. (2022). *Cell compartments and intracellular trafficking of lipids and proteins: Impact on biomedicine*. Lausanne: Frontiers Media SA. doi: 10.3389/978-2-83250-994-4

Table of contents

frontiers | Frontiers in Cell and Developmental Biology

TYPE Editorial
PUBLISHED 24 November 2022
DOI 10.3389/fcell.2022.1087214

OPEN ACCESS

EDITED AND REVIEWED BY
Vladimir Lupashin,
University of Arkansas for Medical Sciences, United States

*CORRESPONDENCE
Carlos Enrich,
enrich@ub.edu

SPECIALTY SECTION
This article was submitted to Membrane Traffic,
a section of the journal
Frontiers in Cell and Developmental Biology

RECEIVED 02 November 2022
ACCEPTED 18 November 2022
PUBLISHED 24 November 2022

CITATION
Zanlungo S, Enrich C, Gerke V, Eden ER and Colombo MI (2022), Editorial: Cell compartments and intracellular trafficking of lipids and proteins: Impact on biomedicine.
Front. Cell Dev. Biol. 10:1087214.
doi: 10.3389/fcell.2022.1087214

Editorial: Cell compartments and intracellular trafficking of lipids and proteins: Impact on biomedicine

Silvana Zanlungo[1], Carlos Enrich[2]*, Volker Gerke[3], Emily R. Eden[4] and María Isabel Colombo[5]

[1]Department of Gastroenterology, Faculty of Medicine, Pontificia Universidad Católica de Chile, Santiago, Chile, [2]Department of Biomedicine, Unit of Cell Biology, Faculty of Medicine and Health Sciences, Centre de Recerca Biomèdica CELLEX (IDIBAPS), University of Barcelona, Barcelona, Spain, [3]Institute of Medical Biochemistry, Centre for Molecular Biology of Inflammation, University of Münster, Münster, Germany, [4]UCL Institute of Ophthalmology, London, United Kingdom, [5]Laboratorio de Mecanismos Moleculares Implicados en El Tráfico Vesicular y la Autofagia, Instituto de Histología y Embriología de Mendoza (IHEM), Universidad Nacional de Cuyo- Consejo Nacional de Investigaciones Científicas y Tecnológicas (CONICET), Mendoza, Argentina

KEYWORDS

Endosomes, lysosomes, membrane contact sites, lysosome-related organelles, cholesterol, lysosomal storage diseases, disease models, lipid droplets

Editorial on the Research Topic
Cell compartments and intracellular trafficking of lipids and proteins: Impact on biomedicine

Endocytosis and cell compartments define eukaryotic cells and evolution has sculpted a complex subset of intracellular structures to arrange the modern cell. This process has been long, implicating each single organelle to eventually develop a functional consortium where spatio-temporal distribution becomes essential.

Because of this intrinsic extreme complexity minor alterations must be repaired, replaced, or undergo reorganization. This is also important when it comes to biochemical processes within and between cellular compartments developing a new concept that implicates cell compartments not to function as individual and isolated entities, but as a dynamic and regulated ensemble facilitating the intracellular trafficking of lipids and proteins. The diverse intracellular compartments contribute to a global cell homeostasis and alterations provide new insights relevant for a number of human diseases and offer opportunities for the design of innovative therapies and treatments.

In recent years we increasingly appreciate the complex organization of the crowded intracellular space. Sorting and trafficking along major routes travelled by vesicles implicate maturation, fission, and fusion of membranes and the most universal means of achieving compartmentalization is probably by the self-assembly of membranes into units, the organelles. These units maintain specific form and composition and emerge from elaborate and coordinated membrane trafficking pathways that manifest themselves

either as explicit membrane bound carriers or through regulated physical proximity of organelles (membrane contact sites). Indeed, the endoplasmic reticulum (ER) is the organelle "to rule them all"; it is the most extensive membrane compartment, lead regulator of membrane trafficking, the largest Ca^{2+} store and the compartment in charge for the biosynthesis of lipids, proteins and assembly of glycoconjugates (Wenzel et al., 2022).

The 14 articles in this collection cover only a small part of the wide panorama, but representative aspects are discussed to understand membrane trafficking across organelles from a wide biological, biophysical, or engineering perspectives and where protein sorting, membrane traffic, and organelle dynamics are the targets and alterations may be the cause of disease.

Endocytosis plays a key role in the regulation of signalling from cell surface receptors. In an original research article by Artyokov et al., endocytosis of death receptors is explored. Tumour necrosis factor (TNF)-associated ligand inducing apoptosis (TRAIL) binds cell surface death receptors DR4 and DR5, initiating a signalling cascade that results in apoptosis. Through unknown mechanisms, some cancer cells are resistant to TRAIL-induced apoptosis, limiting the anti-cancer potential. Here, Artyokov et al. determine the role of DR4 and DR5 endocytosis in conferring sensitivity to TRAIL-induced apoptosis. The authors demonstrate that TRAIL binding universally stimulated endocytosis of DR4 and DR5 in sensitive and resistant cells alike, concluding that sensitivity to TRAIL-induced apoptosis arises through post-endocytosis mechanisms.

Membrane lipid composition is a key determinant of endocytic traffic and receptor signalling and Hasegawa et al. review the importance of endosomal phosphatidylserine (PS) distribution on trafficking pathways. PS is the major anionic phospholipid in the plasma membrane but is also enriched on recycling endosomes where it recruits proteins involved in recycling and retrograde transport for cargo delivery to the plasma membrane and Golgi respectively. Here Hasegawa et al. discuss the role of PS flipping from luminal to cytosolic leaflets of recycling endosomes by the P_4-ATPase ATP8A in recycling and retrograde traffic. PS flipping is likely to be coordinated with the recently identified transport mechanism of newly synthesized PS from the ER to recycling endosomes at ER:endosome contact sites to promote recycling and retrograde transport (Kawasaki et al., 2022). Endosomal PS has also been implicated in YAP signalling, that regulates cell proliferation (Matsudaira et al., 2017), further demonstrating the importance of endosomal PS in membrane traffic and cell fate and Hasegawa et al. consider the potential significance of ATP8A1 mislocalisation in YAP signalling and Hermansky-Pudlak syndrome (HPS). On loss of the adaptor protein AP-3, that is defective in HPS, ATP8A1 accumulates on recycling endosomes, increasing the cytosolic exposure of PS, activating YAP and promoting cell division and migration.

The Research Topic continues to highlight the significance of the lipid environment in membrane traffic and disease. The importance of cholesterol transport and distribution inside of cells is a recurring theme (Ikonen, 2008; Lu, 2022). Here, a comprehensive review dissects the pathways for cholesterol efflux highlighting the state-of-the-art technology (Juhl and Wüstner). In addition, two original research articles study the role of cholesterol uptake in two pathogenic protozoa during infection. In *Toxoplasma gondii*, the relevance of cholesterol transport (Croce et al.) is underpinned using the cholesterol transport inhibitor U18666A demonstrating the potential of cholesterol for the recruitment of CHMP4, in MVBs formation, for optimum antigen presentation and parasite replication. Other related research (Okamoto et al.) addresses the problem of cholesterol uptake, in the pathogenic yeast *Candida glabrata*, as strategy to decrease antifungals susceptibility for proliferation and the possibilities of using ERG25 in the stabilization of sterol-rich lipid domains as therapy.

The family of low-density lipoprotein receptors (LDLR) plays a key role in cholesterol internalization and homeostasis (Go and Mani, 2012). This family comprises plasma membrane receptors that bind several unrelated ligands, which are subsequently endocytosed. Megalin is one of the members (Saito et al., 1994; Hussain et al., 1999), which has a critical function in recovering low molecular weight proteins, from the renal glomerular filtrate, (Leheste et al., 1999). Thus, alterations in the trafficking of this receptor may result in proteinuria (Marzolo and Farfan, 2011). In this collection, an original research article analyzes the post-transcriptional modulation of megalin in the Lowe Syndrome (LS) (Sandoval et al.). LS patients present mutations in a gene encoding a phosphatase known as OCRL1. Megalin is proteolytically cleaved in its ectodomain and in LS patients reduced levels of this megalin fragment are detected. In addition, the levels of the receptor in endocytic/recycling compartments increase in the proximal tubule renal cells. The authors show that silencing OCRL1 mimics the altered parameters found in LS patients with a significant decrease of megalin at the plasma membrane, indicative of a reduced recycling of the receptor. Furthermore, in these LS conditions the phosphorylation levels of megalin were reduced, explaining, in part, the altered recycling transport. Sandoval et al. also uncovered the role of insulin in the reduction of megalin phosphorylation and trafficking to the plasma membrane. The generation of this LS-mimicking cellular model may potentially help to develop novel therapeutic tools for this disease.

Lipid droplet (LD) landscape (Olzmann and Carvalho, 2019; Bosch et al., 2020) is also covered in this Research Topic emphasizing the great importance of LD as dynamic intracellular compartment found in most cells playing fundamental roles in lipid metabolism but having interactions and contacts with other organelles that remain elusive. Two reviews, one summarizing the major mechanisms of biogenesis and breakdown of LD (Fader Kaiser et al.) and a second review

about LD in the nucleus and their function at this novel subworld (McPhee et al.). Both articles discuss and dissect the molecular components to correlate with the involvement in human pathologies.

In the recent years the lysosome has emerged as an essential organelle for cellular homeostasis, being not only involved in the degradation of complex substrates but also able of sensing the nutrient environment and participate in signal transduction, thereby regulating fundamental processes such as cellular clearance and autophagy (Ballabio and Bonifacino, 2020). A review in this collection (Cabrera-Reyes et al.) focuses on lysosome homeostasis alterations in lipid-related disorders, particularly in prevalent diseases such as obesity and also in the less frequent Lysosomal Storage Diseases (LSDs), such as Niemann-Pick C (NPC) and Gaucher diseases and discusses the mechanisms involved in lysosomal alterations that are common among cells of metabolic tissues, including adipose tissue and the liver, which are primarily affected in these pathologies. An original research article of this collection (Marín et al.) explores the relevance of alterations in c-Abl tyrosine kinase signalling in the LSD Niemann-Pick type A (NPA), a fatal neurodegenerative disorder caused by the deficiency in acid sphingomyelinase (ASM) activity and characterized by an accumulation of sphingomyelin in lysosomes and dysfunction in the autophagy-lysosomal pathway. The results show the participation of c-Abl signalling in NPA neurodegeneration and autophagy-lysosomal alterations, supporting the potential use of c-Abl inhibitors for the clinical treatment of NPA patients.

Lysosome related organelles (LROs) are a unique class of intracellular compartments performing specialized functions in different types of cells. In vascular endothelial cells, the prominent LROs are Weibel-Palade bodies (WPBs). They serve as storage organelles for the blood clotting von-Willebrand factor and the leukocyte receptor P-selectin that are released *via* evoked exocytosis of WPBs following endothelial activation by inflammation or blood vessel damage (McCormack et al., 2017). The unique biogenesis and exocytotic response of WPBs are highlighted in one minireview of this series focussing on recent developments that identified factors involved in WPB maturation and WPB-actin as well as WPB-plasma membrane interactions in the course of exocytosis (Naß et al.). An original research article describes the interesting trafficking route of a vacuolar ATPase (vATPase) subunit on its way to maturing WPBs (Lu et al.). WPBs are acidic organelles, and the low intraluminal pH is required for the proper folding (tubulation) of VWF in the organelle. Recently, vATPase activity and the vATPase V0a1 subunit were reported to be required for proper WPB acidification and biogenesis of the organelle (Yamazaki et al., 2021; Terglane et al., 2022) and Lu et al. now extend this to another vATPase subunit, V0D1. Importantly, they show that this subunit is transported to WPBs in a manner requiring the HPS6 subunit of the endosomal BLOC-2 complex. Knockdown of HPS6 in primary human endothelial cells results in misshaped WPB and impaired VWF tubulation, a phenotype also seen in HPS6 deficient mouse endothelial cells. Lu et al. also report a direct interaction of the vATPase V0D1 subunit with HPS6 suggesting that the BLOC-2 complex is involved in transporting vATPase V0D1 from endosomes to WPBs for assembly of a functional vATPase in the limiting membrane of the organelle.

Macroautophagy is a degradative pathway that intersects with both the lysosomal and the proteosomal pathway to maintain cellular homeostasis by degrading and recycling critical components. Increasing evidence indicates that autophagy can be regulated, either in a positive or negative way, by the ubiquitin proteasome system, indicating that both systems function as an interconnected network (Korolchuk et al., 2010; Bustamante et al., 2018). An original research article of this series addressing this topic (Vargas et al.) identified an ER membrane protein called HERPUD1. Expression of a deletion mutant lacking the ubiquitin-like domain, critical for proteosomal degradation, negatively modulates autophagy. In addition, overexpression of this mutant leads to an increase in ER tubular stacks as well as an augment in the biogenesis of lysosomal vesicles. The authors propose that ER-lysosome intercommunication is promoted to favor cell survival under stress conditions, such as nutritional deficiency or certain drug treatments.

Finally, membrane contact sites (MCS) are now at the crest of the wave in cell biology (Prinz et al., 2020). The paradigm has changed, and compartments communicate by vesicular trafficking but also *via* dynamic close contacts with a plethora of tethers and molecular machineries in charge for transport and exchange of lipids, cholesterol, ions, and metabolites. MCS modulate endosome maturation, organelle positioning, metabolic platforms and for cellular homeostasis. A Mini Review in this collection (Enrich et al.) put together recent findings regarding a subset of annexins (Gerke et al., 2005) and discusses their multiple possibilities to regulate MCS dynamics, function and possible contribution to novel pathways providing new insights relevant for several human diseases and offering opportunities to design innovative treatments.

In summary, the present collection of research articles and reviews under this Research Topic highlights the advances in the field with novel insights to uncover the fine structure, distribution, and dynamics of molecular machineries and protein complexes in cell compartments. Throughout the collection, a relationship between the lipid environment and membrane trafficking/signalling pathways is emerging. The composition of membrane lipids is diverse and complex and key open questions remain about the maintenance of membrane lipid homeostasis and its influence over the endocytic pathway. A role for MCS in coordinating these dynamic and adaptable processes is becoming apparent but the picture in different physio/pathological situations is incomplete and key intracellular cholesterol transport mechanisms remain elusive. With improved understanding, new interventions to help in the cure of multiple human diseases become a possibility.

Author contributions

CE wrote the general introduction and final paragraph with inputs and edition by VG, ERE and SZ. Then, the fourteen short summaries of each article were divided according to the expertise in the field equally to SZ, CE, VG, ERE and MIC, and all authors approved it for publication. All authors listed have made a substantial, direct, and intellectual contribution to the work and approved it for publication.

Acknowledgments

We thank all contributing authors and reviewers for their support to the Research Topic.

Conflict of interest

The authors declare that the research was conducted in the absence of any commercial or financial relationships that could be construed as a potential conflict of interest.

Publisher's note

All claims expressed in this article are solely those of the authors and do not necessarily represent those of their affiliated organizations, or those of the publisher, the editors and the reviewers. Any product that may be evaluated in this article, or claim that may be made by its manufacturer, is not guaranteed or endorsed by the publisher.

References

Ballabio, A., and Bonifacino, J. S. (2020). Lysosomes as dynamic regulators of cell and organismal homeostasis. *Nat. Rev. Mol. Cell Biol.* 21 (2), 101–118. doi:10.1038/s41580-019-0185-4

Bosch, M., Sanchez-Alvarez, M., Fajardo, A., Kapetanovic, R., Steiner, B., Dutra, F., et al. (2020). Mammalian lipid droplets are innate immune hubs integrating cell metabolism and host defense. *Science* 370 (6514), eaay8085. doi:10.1126/science.aay8085

Bustamante, H. A., Gonzalez, A. E., Cerda-Troncoso, C., Shaughnessy, R., Otth, C., Soza, A., et al. (2018). Interplay between the autophagy-lysosomal pathway and the ubiquitin-proteasome system: A target for therapeutic development in alzheimer's disease. *Front. Cell. Neurosci.* 12, 126. doi:10.3389/fncel.2018.00126

Gerke, V., Creutz, C. E., and Moss, S. E. (2005). Annexins: Linking Ca2+ signalling to membrane dynamics. *Nat. Rev. Mol. Cell Biol.* 6 (6), 449–461. doi:10.1038/nrm1661

Go, G. W., and Mani, A. (2012). Low-density lipoprotein receptor (LDLR) family orchestrates cholesterol homeostasis. *Yale J. Biol. Med.* 85 (1), 19–28.

Hussain, M. M., Strickland, D. K., and Bakillah, A. (1999). The mammalian low-density lipoprotein receptor family. *Annu. Rev. Nutr.* 19, 141–172. doi:10.1146/annurev.nutr.19.1.141

Ikonen, E. (2008). Cellular cholesterol trafficking and compartmentalization. *Nat. Rev. Mol. Cell Biol.* 9 (2), 125–138. doi:10.1038/nrm2336

Kawasaki, A., Sakai, A., Nakanishi, H., Hasegawa, J., Taguchi, T., Sasaki, J., et al. (2022). PI4P/PS countertransport by ORP10 at ER-endosome membrane contact sites regulates endosome fission. *J. Cell Biol.* 221 (1), e202103141. doi:10.1083/jcb.202103141

Korolchuk, V. I., Menzies, F. M., and Rubinsztein, D. C. (2010). Mechanisms of cross-talk between the ubiquitin-proteasome and autophagy-lysosome systems. *FEBS Lett.* 584 (7), 1393–1398. doi:10.1016/j.febslet.2009.12.047

Leheste, J. R., Rolinski, B., Vorum, H., Hilpert, J., Nykjaer, A., Jacobsen, C., et al. (1999). Megalin knockout mice as an animal model of low molecular weight proteinuria. *Am. J. Pathol.* 155 (4), 1361–1370. doi:10.1016/S0002-9440(10)65238-8

Lu, A. (2022). Endolysosomal cholesterol export: More than just NPC1. *Bioessays.* 44 (10), e2200111. doi:10.1002/bies.202200111

Marzolo, M. P., and Farfan, P. (2011). New insights into the roles of megalin/LRP2 and the regulation of its functional expression. *Biol. Res.* 44 (1), 89–105. doi:10.4067/S0716-97602011000100012

Matsudaira, T., Mukai, K., Noguchi, T., Hasegawa, J., Hatta, T., Iemura, S. I., et al. (2017). Endosomal phosphatidylserine is critical for the YAP signalling pathway in proliferating cells. *Nat. Commun.* 8 (1), 1246. doi:10.1038/s41467-017-01255-3

McCormack, J. J., Lopes da Silva, M., Ferraro, F., Patella, F., and Cutler, D. F. (2017). Weibel-Palade bodies at a glance. *J. Cell Sci.* 130 (21), 3611–3617. doi:10.1242/jcs.208033

Olzmann, J. A., and Carvalho, P. (2019). Dynamics and functions of lipid droplets. *Nat. Rev. Mol. Cell Biol.* 20 (3), 137–155. doi:10.1038/s41580-018-0085-z

Prinz, W. A., Toulmay, A., and Balla, T. (2020). The functional universe of membrane contact sites. *Nat. Rev. Mol. Cell Biol.* 21 (1), 7–24. doi:10.1038/s41580-019-0180-9

Saito, A., Pietromonaco, S., Loo, A. K., and Farquhar, M. G. (1994). Complete cloning and sequencing of rat gp330/"megalin, " a distinctive member of the low density lipoprotein receptor gene family. *Proc. Natl. Acad. Sci. U. S. A.* 91 (21), 9725–9729. doi:10.1073/pnas.91.21.9725

Terglane, J., Menche, D., and Gerke, V. (2022). Acidification of endothelial Weibel-Palade bodies is mediated by the vacuolar-type H+-ATPase. *PLoS One* 17 (6), e0270299. doi:10.1371/journal.pone.0270299

Wenzel, E. M., Elfmark, L. A., Stenmark, H., and Raiborg, C. (2022). ER as master regulator of membrane trafficking and organelle function. *J. Cell Biol.* 221 (10), e202205135. doi:10.1083/jcb.202205135

Yamazaki, Y., Eura, Y., and Kokame, K. (2021). V-ATPase V0a1 promotes Weibel-Palade body biogenesis through the regulation of membrane fission. *Elife* 10, e71526. doi:10.7554/eLife.71526

frontiers in Cell and Developmental Biology

ORIGINAL RESEARCH
published: 30 September 2021
doi: 10.3389/fcell.2021.733688

Death Receptors DR4 and DR5 Undergo Spontaneous and Ligand-Mediated Endocytosis and Recycling Regardless of the Sensitivity of Cancer Cells to TRAIL

*Artem A. Artykov[1], Anne V. Yagolovich[1,2], Dmitry A. Dolgikh[1,2], Mikhail P. Kirpichnikov[1,2], Daria B. Trushina[3] and Marine E. Gasparian[1]**

[1] Department of Bioengineering, Institute of Bioorganic Chemistry (RAS), Moscow, Russia, [2] Faculty of Biology, Lomonosov Moscow State University, Moscow, Russia, [3] Department of X-Ray and Synchrotron Research, A.V. Shubnikov Institute of Crystallography of Federal Scientific Research Centre "Crystallography and Photonics" of Russian Academy of Sciences, Moscow, Russia

OPEN ACCESS

Edited by:
Silvana Zanlungo, Pontificia Universidad Católica de Chile, Chile

Reviewed by:
Curtis Okamoto, University of Southern California, United States
Natalia Bulgakova, The University of Sheffield, United Kingdom

***Correspondence:**
Marine E. Gasparian
marine_gasparian@yahoo.com

Specialty section:
This article was submitted to Membrane Traffic, a section of the journal Frontiers in Cell and Developmental Biology

Received: *30 June 2021*
Accepted: *06 September 2021*
Published: *30 September 2021*

Citation:
Artykov AA, Yagolovich AV, Dolgikh DA, Kirpichnikov MP, Trushina DB and Gasparian ME (2021) Death Receptors DR4 and DR5 Undergo Spontaneous and Ligand-Mediated Endocytosis and Recycling Regardless of the Sensitivity of Cancer Cells to TRAIL. Front. Cell Dev. Biol. 9:733688. doi: 10.3389/fcell.2021.733688

Tumor necrosis factor-associated ligand inducing apoptosis (TRAIL) induces apoptosis through the death receptors (DRs) 4 and 5 expressed on the cell surface. Upon ligand stimulation, death receptors are rapidly internalized through clathrin-dependent and -independent mechanisms. However, there have been conflicting data on the role of death receptor endocytosis in apoptotic TRAIL signaling and possible cell type-specific differences in TRAIL signaling have been proposed. Here we have compared the kinetics of TRAIL-mediated internalization and subsequent recycling of DR4 and DR5 in resistant (HT-29 and A549) and sensitive (HCT116 and Jurkat) tumor cell lines of various origin. TRAIL stimulated the internalization of both receptors in a concentration-dependent manner with similar kinetics in sensitive and resistant cell lines without affecting the steady-state expression of DR4 and DR5 in cell lysates. Using the receptor-selective TRAIL variant DR5-B, we have shown that DR5 is internalized independently of DR4 receptor. After internalization and elimination of TRAIL from culture medium, the receptors slowly return to the plasma membrane. Within 4 h in resistant or 6 h in sensitive cells, the surface expression of receptors was completely restored. Recovery of receptors occurred both from newly synthesized molecules or from trans-Golgi network, as cycloheximide and brefeldin A inhibited this process. These agents also suppressed the expression of cell surface receptors in a time- and concentration-dependent manner, indicating that DRs undergo constitutive endocytosis. Inhibition of receptor endocytosis by sucrose led to sensitization of resistant cells to TRAIL and to an increase in its cytotoxic activity against sensitive cells. Our results confirm the universal nature of TRAIL-induced death receptor endocytosis, thus cell sensitivity to TRAIL can be associated with post-endocytic events.

Keywords: DR5, DR4, receptor endocytosis, receptor recycling, membrane traffic, brefeldin A

INTRODUCTION

Cell surface receptor uptake and subsequent intracellular sorting for degradation or recycling regulates the specificity of downstream signaling. Some receptors are internalized continuously whereas others remain on the surface until a ligand is bound. In cancer cells the endocytic trafficking of signaling receptors such as receptor tyrosine kinases (RTKs), G protein–coupled receptors (GPCRs), and cytokine receptors is altered, affecting signaling pathways to enhance tumorigenesis and metastasis (Mellman and Yarden, 2013; Cendrowski et al., 2016; Schmid, 2017).

Ligand-mediated receptor internalization plays an important role in tumor necrosis factor (TNF) family member receptor signaling. Internalization of TNF-R1 and CD95 receptors is required for TNF- and FasL-mediated apoptosis signaling (Schütze and Schneider-Brachert, 2009; Schneider-Brachert et al., 2013). Studies have also been conducted to elucidate the role of death receptor internalization in binding to TNF-associated ligand inducing apoptosis (TRAIL). TRAIL induce apoptosis in cancer cells by activating death receptors DR4 and DR5 (LeBlanc and Ashkenazi, 2003). After stimulation with ligands, DR4 and DR5 rapidly internalize, and the role of this process in the regulation of TRAIL-mediated apoptosis is unclear. In some studies, inhibition of endocytosis by specific molecules or inactivation of dynamin increased TRAIL-mediated apoptosis (Kohlhaas et al., 2007; Zhang and Zhang, 2008; Zhang et al., 2009). Recently it was demonstrated that TRAIL selectively activated dynamin-1 to self-regulate death receptors endocytosis, attenuate apoptotic signaling and increase cell survival (Reis et al., 2017). In addition, clathrin-independent mechanisms were also suggested to participate in TRAIL death receptor internalization (Kohlhaas et al., 2007). Blocking caveola-mediated DR4 internalization by filipin III enhanced TRAIL-induced apoptosis (Zhao et al., 2009).

In contrast to the aforementioned studies, TRAIL-induced internalization of death receptors was proved important for apoptosis signaling. TRAIL-induced DR5 internalization is necessary for permeabilization of lysosomal membranes and apoptosis in malignant liver cells (Akazawa et al., 2009). Dominant-negative dynamin mutant and Rab7 silencing inhibit apoptotic signaling in human hepatocellular carcinoma cell lines Huh-7 and HNU 499, cholangiocarcinoma cell lines Mz-ChA-1 and HuCCT-1, but not in human cervical cancer cell line HeLa. Increased surface expression of endogenous lectin galectin-3 in metastatic colon adenocarcinoma LiM6-TR cells prevented the endocytosis of TRAIL receptors. Reduction of galectin-3 expression restored endocytosis of TRAIL receptors and TRAIL-dependent apoptosis (Mazurek et al., 2012). Thus, the role of internalization of TRAIL death receptors for signaling apoptosis is cell type-dependent. While DISC (death inducing signaling complex) formation and activation of caspase 8 at the plasma membrane are sufficient to induce apoptosis in type I cells, the induction of TRAIL-mediated apoptosis in type II cells may strongly depend on receptor internalization (Kohlhaas et al., 2007; Akazawa et al., 2009).

In addition to TRAIL-induced internalization, death receptors can also undergo constitutive endocytosis as a part of desensitizing mechanism. DR4 and DR5 constitutive endocytosis in breast cancer cell lines decreased their surface expression regardless of mRNA and total protein levels leading to TRAIL resistance (Zhang and Zhang, 2008).

A growing body of evidence indicates that the subcellular localization and the regulation of membrane transport of death receptors play an important role in determining apoptotic and non-apoptotic TRAIL signaling (Bertsch et al., 2014). In addition to its canonical location in the plasma membrane, TRAIL death receptors have been identified in the endosomes, lysosomes, autophagosomes, in the cytosolic compartment as well as in the nucleus (Zhang et al., 2000; Akazawa et al., 2009; Leithner et al., 2009; Di et al., 2013; Haselmann et al., 2014). It was also demonstrated that colon carcinoma cells can secrete extracellular vesicles coated with DR5 receptor, and competitive binding of TRAIL to DR5 on target cells and DR5 on vesicles leads to a decrease in apoptosis signaling (Setroikromo et al., 2020). The nuclear DR5 inhibits maturation of the microRNA let-7 in pancreatic cancer cell lines and increases their proliferation (Haselmann et al., 2014). Importin β1-mediated nuclear localization of DR5 limits TRAIL-induced death of tumor cells (Kojima et al., 2011). Later, the authors demonstrated that inhibition of importin β1 enhances the anticancer effect of an anti-DR5 agonist antibody in TRAIL-resistant tumor cells (Kojima et al., 2020). Recent studies demonstrated that death receptors DR4 and DR5 are constitutively localized to chromatin from the plasma membrane via clathrin-dependent endocytosis, and this process is greatly enhanced by TRAIL-mediated receptor endocytosis (Mert et al., 2019).

In this study, we showed that the death receptors DR4 and DR5 undergo constitutive and ligand-stimulated endocytosis with similar kinetics in TRAIL-sensitive and TRAIL-resistant tumor cell lines. Using the receptor-selective TRAIL variant DR5-B, we proved that death receptors can be internalize independently of each other. After internalization, the receptors slowly returned to the plasma membrane when TRAIL was washed out from culture medium. Within 6 h the surface expression of receptors was completely restored, regardless of the sensitivity of the tumor cells to TRAIL. The levels of receptors were restored through a combination of newly synthesized protein and recycling from endocytic compartments. Inhibition of receptor endocytosis by sucrose sensitized resistant cells to TRAIL and increased its cytotoxic activity against sensitive cells.

MATERIALS AND METHODS

Cell Lines and Culture Conditions

Human colorectal adenocarcinoma cell lines HT-29 and HCT116, Jurkat T-lymphoblastic leukemia cells, A549 human lung adenocarcinoma cell line were purchased from the Research Institute of Cytology, Russian Academy of Sciences (St. Petersburg, Russia). Nutrient medium DMEM supplemented

with 10% fetal calf serum was used to cultivate A549 and HCT116 cells and RPMI1640 medium supplemented with 10% fetal calf serum for HT-29 and Jurkat cells. All cells were cultured in a humidified incubator at 37°C in 5% CO_2. Cell culture media DMEM and RPMI1640 were purchased from PanEco (Moscow, Russia). Fetal bovine serum was from HyClone (Cramlington, United Kingdom).

Reagents

Recombinant proteins TRAIL (amino acid residues 114–280) and its DR5-selective mutant variant DR5-B were expressed in *Escherichia coli* and purified in our laboratory as previously described (Yagolovich et al., 2019). Brefeldin A and cycloheximide were purchased from Tocris (Bristol, United Kingdom). Pan-caspase inhibitor Z-VAD-FMK was from Santa Cruz Biotechnology (Dallas, TX, United States).

Cell Viability Assay

A549, HT-29, and HCT116 cells were seeded in 96-well plates at a density of 1×10^4 per well in 100 μl culture medium and incubated for 24 h in humidified atmosphere of 5% CO_2 (New Brunswick, Eppendorf, Germany) at 37°C. The culture medium was aspirated and 100 μl of fresh serum free medium supplemented with TRAIL or DR5-B was added to the wells. In the case of Jurkat, cells were harvested, washed with serum-free medium and plated in 96-well plates (5×10^4 cells per well) in 100 μl of culture medium without serum and 50 μl of TRAIL or DR5-B solutions at the appropriate concentrations were added to each well. The cells were incubated for 24 h, 10 μl of water soluble tetrazolium salts reagent (WST-1) (Sigma-Aldrich, St. Louis, MO, United States) was added to each well and incubation was continued for another 2 h at 37°C. The WST-1 assay is based on the cleavage of the tetrazolium salt WST-1 to formazan by cellular mitochondrial dehydrogenases. Viable cells have a high activity of mitochondrial dehydrogenases, which leads to the formation of the dye formazan. The optical density of the wells was measured using an iMark plate spectrophotometer (Bio-Rad, United States) at a wavelength of 450 nm with background subtraction at 655 nm.

Flow Cytometry

The assays were performed as described earlier, with some modifications (Artykov et al., 2020).

The cells were seeded in 6 well plate at a density of 2×10^5 cells per well in 2 ml of culture media and incubated for 24 h in humidified atmosphere of 5% CO_2 at 37°C. After washing with serum-free medium, the cells were incubated with TRAIL or DR5-B for the indicated time (5–60 min or 1–24 h). Cells were detached from the culture flasks with Versene solution, washed with ice-cold PBS, and resuspended in FACS buffer (PBS with 1% BSA). Cell suspensions were incubated for 1 h at 4°C with 5 μg/ml anti-DR4 (DR-4-02) or anti-DR5 (DR5-01-1) monoclonal antibodies (GeneTex, Irvine, CA, United States). Next the cells were washed twice and incubated with 20 μg/ml secondary antibodies Alexa Fluor 488 (Invitrogen, Waltham, MA, United States) for 1 h at 4°C, washed twice, and suspended in FACS buffer supplemented with propidium iodide. Mouse IgG1 (15H6, Genetex) was used as an isotype control. The cell surface expression of DR4 and DR5 was analyzed on a CytoFlex flow cytometer (Beckman Coulter, Brea, IN, United States).

Confocal Microscopy Analysis

Glass slides were placed in 6 well plates and 2×10^5 cells were seeded in each well. Cells were cultured in 2 ml of culture media and incubated for 24 h. After washing with serum-free medium cells were treated with 100 ng/ml or 1,000 ng/ml of TRAIL variants. At the indicated times, the medium was aspirated and the dishes were transferred to ice and washed with cold PBS. Subsequently, cells were fixed in 3% paraformaldehyde for 20 min. In order to analyze the expression of receptors only on the surface of the plasma membrane, the permeabilization step was skipped. After washing with ice-cold PBS and blocking in 3% BSA in PBS for 30 min, the primary antibodies to death receptors DR5 (DR5-01-1) and DR4 (DR-4-02) were added at a concentration of 2 μg/ml and the cells were incubated for 1 h at room temperature. The slides were washed three times with PBS and incubated with 4 μg/ml goat anti-mouse IgG Alexa Fluor 488 and Hoechst 33342 in the dark for 1 h at room temperature. The confocal LSM analysis was performed on Leica TCS SPE (Leica microsystems, Wetzlar, Germany) equipped with immersion ×100 objective with a 1.4 numerical aperture.

Statistical Analysis

Statistical analyses for each experiment were performed as described in the corresponding figure legends. Multiple comparison analyses for one-way ANOVA followed by Tukey test or followed by Dunnett's *post hoc* test were performed using GraphPad Prism 8. Experimental phenotypes were confirmed in at least three independent experiments.

RESULTS

TRAIL Decreases the Surface Expression of DR4 and DR5 Receptors in a Concentration-Dependent Manner

To study TRAIL-stimulated traffic of death receptors DR4 and DR5, two sensitive (HCT116 and Jurkat) and two resistant (HT-29 and A549) tumor cell lines were selected (**Figure 1A**). All cell lines expressed a comparable amount of death receptors on the cell surface, except that the level of the DR4 receptor was practically undetectable in Jurkat cells (**Figure 1B**). The absence of the surface expression of DR4 on Jurkat cells has been shown earlier in several studies (Jang et al., 2003; Merino et al., 2006). Thus, the traffic of this receptor in Jurkat cells was not investigated in the further experiments.

To analyze possible competition for receptor binding between TRAIL and antibodies, we used recombinant DR5 and DR4 extracellular domains captured at plates. The binding of anti-DR antibodies analyzed by ELISA (enzyme-linked immunosorbent assay) was not affected by TRAIL, indicating no competition (**Supplementary Figure 1** and **Supplementary Table 1**). In all cell lines, a decrease in surface expression of death receptors was measured during 1 and 24 h upon stimulation with TRAIL in a concentration-dependent manner (**Figure 1C**). Significant decrease of surface receptor expression was detected at TRAIL concentration of more than 10 ng/ml. The exception was Jurkat cells, where the effect was observed at lower concentrations of TRAIL probably because the ligand was not titrated by the DR4 receptor. The level of receptors on the cell surface did not differ significantly after incubation 1 or 24 h with high concentration of TRAIL (1,000 ng/ml), while at lower concentrations of ligand the number of receptors remaining on the plasma membrane was slightly lower after 24 h. These data indicated that TRAIL mediated downregulation of surface DRs in time- and concentration- dependent manner. It should be noted that the concentration of endogenous soluble TRAIL in blood is approximately 0.1–1 ng/ml, which is insufficient to stimulate the significant decrease of surface receptor exposure (Cheng et al., 2015). Thus, the possible physiological role of downregulation the surface expression of DR4 and DR5 upon stimulation of higher TRAIL concentrations currently remain unclear. To our knowledge, there are no publications describing a dramatic increase in the concentration of TRAIL under physiological conditions. The concentration of TRAIL in the blood rises sharply in clinical trials using high doses of the drug (5–20 mg/kg). According to pharmacokinetic profiles, after 1 h of drug administration, the concentration of TRAIL in the blood of patients was 20–150 ng/ml, depending on the dosage (Soria et al., 2010). Therefore, when treating the neoplastic diseases with TRAIL, it is extremely important to consider the effect of death receptor traffic on drug efficacy. In addition, numerous studies have shown that the surface expression of TRAIL DRs is upregulated under the influence of various chemotherapeutic and natural agents, what in turn can reduce the concentration of the ligand required to induce their internalization.

TRAIL Mediates Decrease of Surface Death Receptors With Similar Rate in Resistant and Sensitive Cell Lines

We then compared the kinetics of TRAIL-induced downregulation of the DR4 and DR5 receptors in sensitive (HCT116 and Jurkat) and resistant (A549 and HT-29) cell lines (**Figure 2A**). Cells were incubated with 100 ng/ml TRAIL for 5, 15, 30 min and then from 1 to 24 h, and the surface expression of receptors was determined by flow cytometry. According to the data, the bulk of both receptors were internalized within 1 h in all cell lines. One hour later, the process slowed down and after 2 h reached an equilibrium, in which the values practically did not change during 24 h. The flow cytometry data were confirmed by confocal microscopy analysis. To detect receptors only on the plasma membrane, the permeabilization step was excluded during samples preparation (**Figures 2B,C**). Obtained data clearly indicated that TRAIL induced decrease of DR4 and DR5 exposure in both TRAIL-sensitive HCT116 and TRAIL-resistant HT-29 cells with similar efficiency. Thus in both sensitive and resistant lines TRAIL does induce internalization despite the differences in the phenotype—apoptosis induction.

DR5-Selective TRAIL Variant DR5-B Internalizes Only DR5 Receptor

To elucidate the possible interaction of death receptors during internalization, a DR5-selective TRAIL variant was used. We have previously designed and purified TRAIL mutant variant DR5-B that selectively binds to DR5 receptor and lacks the affinity to DR4 and to decoy receptors DcR1 and DcR2 (Gasparian et al., 2009). TRAIL- and DR5-B-sensitive (HCT116) and resistant (HT-29) cells (**Figure 3A**) were incubated with ligands at a concentration of 1,000 ng/ml, and the time-dependent decrease of DR4 and DR5 surface expression was determined (**Figure 3B**). TRAIL and DR5-B stimulated the internalization of the DR5 receptor in both cell lines, but DR5-B worked faster and more efficiently. The rate of internalization as well as the absolute amount of internalized molecules was higher when cells were treated with DR5-B. After 5 min of incubation of HCT116 cells with DR5-B, 68% of DR5 was internalized, while TRAIL reduced the amount of this receptor by only 26%. The similar results were obtained in HT-29 cells. This is apparently due to the fact that TRAIL is titrated by the other receptors (DR4 or decoy receptors) as the dissociation constants of TRAIL and DR5-B to the DR5 receptor, determined earlier using surface plasmon resonance, practically did not differ (0.51×10^{-9} M and 0.71×10^{-9} M, respectively) (Gasparian et al., 2009). In contrast, the DR4 surface expression was not affected by DR5-B, whereas TRAIL reduced it by 90% in both lines. These data were confirmed by the confocal microscopy measurements of receptor exposure on the plasma membrane (**Figure 3C**). Our results are in good agreement with the data obtained in the work of Nahacka et al. (2018), where the authors compared the composition of DISC (death inducing signaling complex) formed by different DR-selective mutant variants of TRAIL. It was demonstrated that the DISC formed by DR5-B did not contain DR4 receptor in the HT-29 and PANC-1 cell lines, while in the DISC formed by TRAIL both DRs were detected. However, DR4 internalization by DR5-B was observed earlier after strong upregulation of the surface DRs by chemotherapeutic agents (Artykov et al., 2020). Obviously, increased expression of death receptors on the cell surface promotes the formation of heterodimers where the receptors can be internalized together as part of the same DISC (Szegezdi et al., 2012). Based on the obtained data, it can be assumed that DR5 can be internalized independently of DR4 receptor.

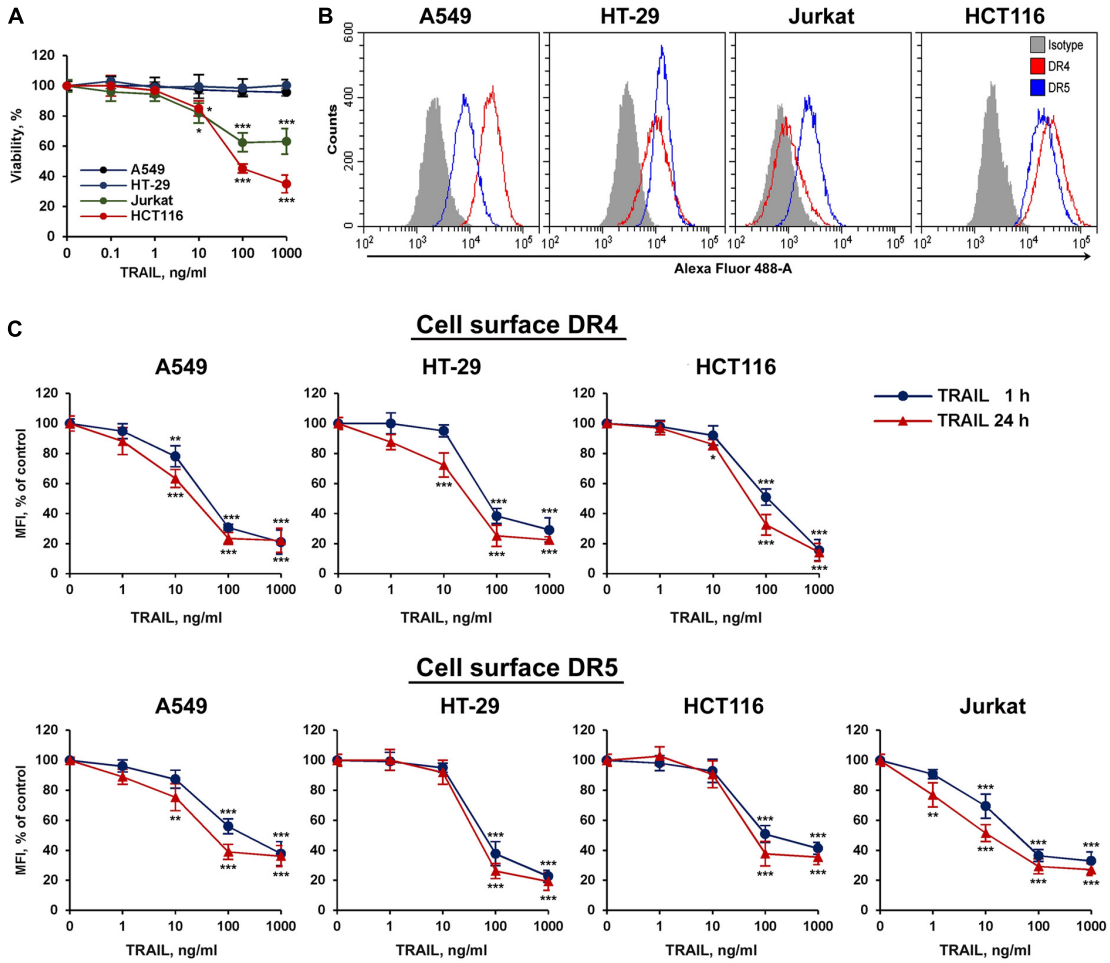

FIGURE 1 | TRAIL decreased surface expression of DR4 and DR5 receptors in concentration dependent manner. **(A)** Viability of HT-29, A549, HCT116, and Jurkat cells after TRAIL treatment for 24 h determined by WST-1 colorimetric assay. **(B)** Cell surface expression of TRAIL death receptors determined by flow cytometry. **(C)** Cells were treated with TRAIL in indicated concentrations for 1 or 24 h and surface expression of DR4 and DR5 was determined by flow cytometry. The data represent means ± SDs of triplicate assays. $^{*}p < 0.05$, $^{**}p < 0.01$, and $^{***}P < 0.001$ indicate significant difference from the control according to One-way ANOVA followed by Dunnett's *post hoc* test.

TRAIL Did Not Affect the Steady-State Expression of DR4 and DR5 in Cell Lysates

We then investigated the effect of TRAIL on the total expression of DR4 and DR5 receptors in cell lysates. TRAIL-sensitive (HCT116 and Jurkat) and TRAIL-resistant (HT-29 and A549) cells were incubated with 1,000 ng/ml TRAIL for 1, 2, 4, 6, and 24 h, and the receptors content was analyzed by Western blotting with monoclonal antibodies to DR4 and DR5 (**Figure 4A**). In all tested cells, we did not register significant changes in both DR4 and DR5 contents during the entire incubation period with TRAIL (**Figure 4B**). Usually the endocytosed receptors are shuttled to early endosomes, sorted to late endosomes and finally to the lysosomes for degradation. In the event when the cell is re-sensitized with a stimulatory agent, the receptor travels back to the plasma membrane directly or through recycling endosomes. Post-endocytic localization and trafficking of the TRAIL death receptors are poorly investigated. It has been shown that DR4 and DR5 receptors, after TRAIL stimulation, are transported from the plasma membrane to the nucleus or can co-localize with endosomes or lysosomes (Zhang et al., 2000; Akazawa et al., 2009; Mert et al., 2019). In any case, evidently during the incubation of cells with TRAIL, the rate of the supposed receptor degradation is comparable to the rate of synthesis of new molecules, and, therefore, the total level of protein in the cells remains stable.

Brefeldin A Inhibited the Recovery of Surface DR4 and DR5

We then investigated the kinetics of cell surface receptor recovery after TRAIL-induced endocytosis. For this, cells were incubated with TRAIL for 1 h, the ligand was washed off, and the surface expression of receptors was determined for 1, 2, 4, 6, and 24 h (**Figure 5A**). After removing the ligand from the culture medium,

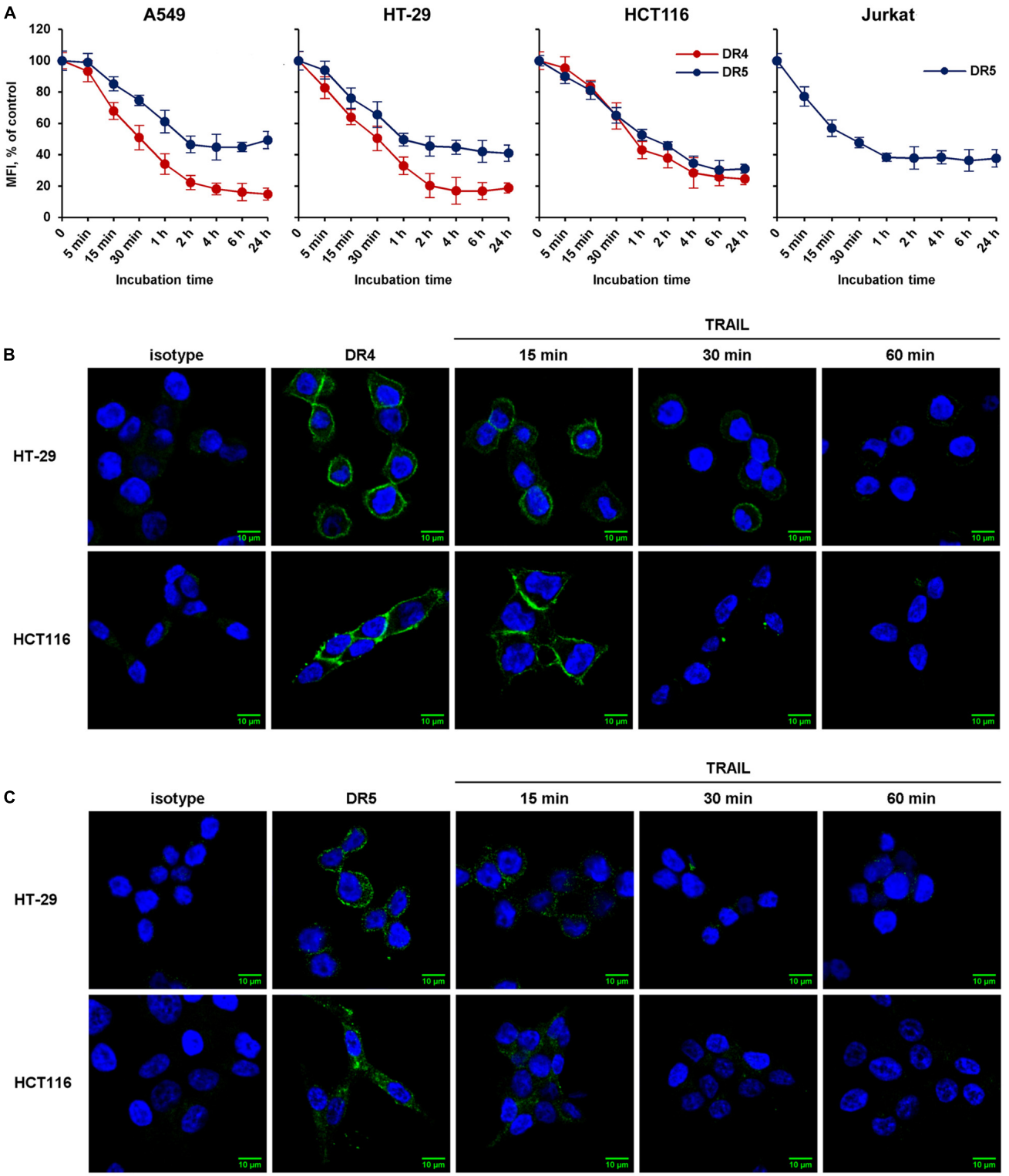

FIGURE 2 | The rate of TRAIL-mediated downregulation of surface DR4 and DR5 in resistant and sensitive tumor cell lines. **(A)** TRAIL-resistant (HT-29, A549) and TRAIL-sensitive (HCT116, Jurkat) cells were treated with 100 ng/ml TRAIL and surface expression of DR4 and DR5 was determined at indicated times by flow cytometry. The data represent means ± SDs of triplicate assays. Immunofluorescence staining of DR4 **(B)** and DR5 **(C)** receptors in HT-29 and HCT116 cells before and after TRAIL treatment analyzed by confocal LSM. To detect receptors only on the plasma membrane, the permeabilization step was excluded during samples preparation.

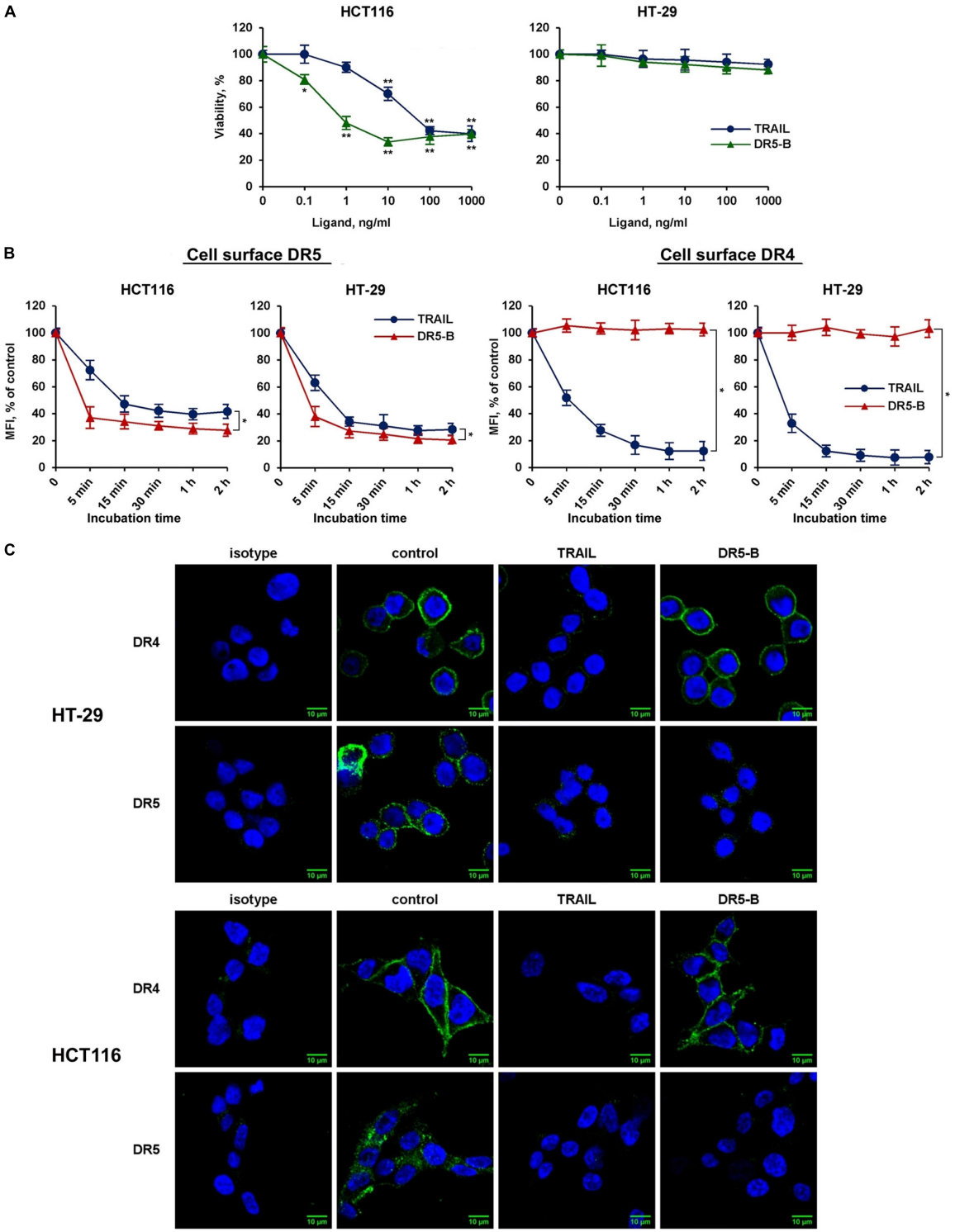

FIGURE 3 | DR5-selective variant of TRAIL DR5-B induced the decrease of surface expression of DR5 but not of DR4 receptor. **(A)** Viability of HT-29 and HCT116 cells after treatment with TRAIL or DR5-B at the indicated concentrations for 24 h as determined by the WST-1 colorimetric assay. The data represent means ± SDs of triplicate assays. *$p < 0.01$ and **$p < 0.001$ indicate significant difference from the control according to One-way ANOVA followed by Dunnett's *post hoc* test. **(B)** TRAIL-resistant HT-29 and TRAIL-sensitive HCT116 cells were treated with 1,000 ng/ml TRAIL or DR5-B and the surface expression of DR4 and DR5 was determined as shown in **Figure 2**. The data represent means ± SDs of triplicate assays. *$p < 0.001$ indicate significant difference between groups according to Two-way ANOVA. **(C)** Immunofluorescence staining of the DR4 and DR5 receptors in HT-29 and HCT116 cells before and after TRAIL treatment analyzed by confocal LSM. To detect receptors only on the plasma membrane, the permeabilization step was excluded during samples preparation.

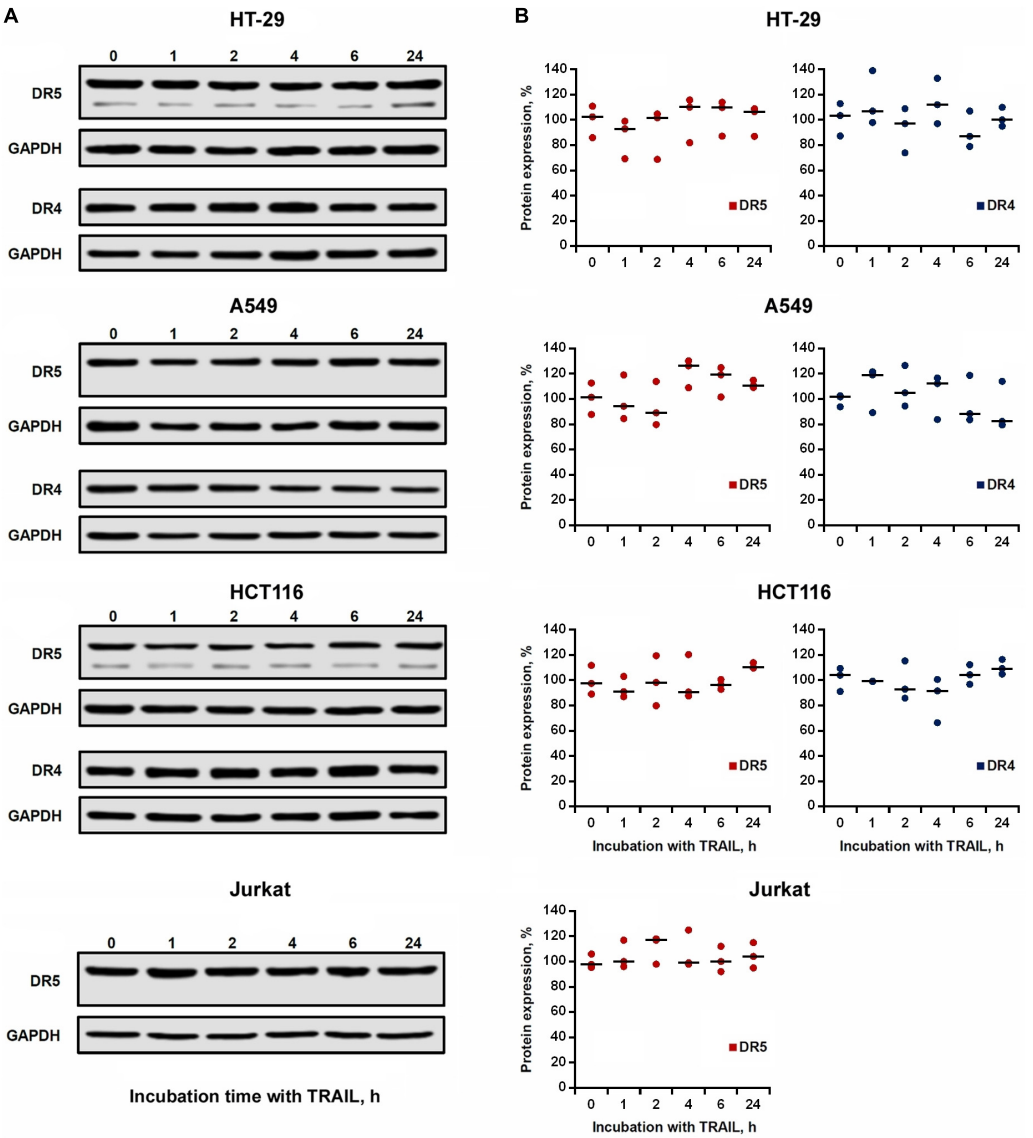

FIGURE 4 | Expression of DR4 and DR5 in cell lysates remained relatively stable after TRAIL treatment. **(A)** HT-29, A549, HCT116 and Jurkat cells were treated with 1,000 ng/ml TRAIL for 1, 2, 4, 6, and 24 h, and the expression of death receptors in cell lysates was analyzed by Western blotting. **(B)** Protein band intensities was calculated using the ImageJ software (http://rsbweb.nih.gov/ij/, NIH, Bethesda, MD, United States) and data were normalized to GAPDH. Data are expressed as the means ± SD of three independent experiments. The Dunnett's multiple comparisons tests following one-way ANOVA did not find a significant difference among means.

the amount of surface DR4 and DR5 increased slowly and after 4 h (in HT-29 and A549 cells) and 6 h (in HCT116 and Jurkat cells) reached values corresponding to that of untreated cells. It remains unclear whether faster DRs recovery plays an important role in cell resistance. Additional experiments are needed to verify this phenomenon. Interestingly, after prolonged (24 h) incubation, the number of receptors on the cell surface was even higher (20–30%) compared to TRAIL-untreated cells indicating that TRAIL promoted the upregulation of its death receptors surface expression. Brefeldin A (BFA), an potent ER stressor, which destroys Golgi compartments and depletes the delivery of substances to the cell surface from secretory pathway, significantly decreased DR5 and DR4 surface expression in time- (**Supplementary Figure 2** and **Supplementary Table 2**) and concentration-dependent manner in all cell lines (**Figures 5B,C** and **Supplementary Table 3**). Obtained data indicate that TRAIL receptors undergo spontaneous ligand-independent internalization regardless of the cell sensitivity. The recovery of surface DR4 and DR5 after TRAIL-stimulated endocytosis was also strongly inhibited by BFA in all cell lines. In addition, receptor surface levels were comparable after BFA treatment with and without TRAIL. These data indeed show the importance of the Golgi apparatus and indicate the existence of constitutive endocytosis of DRs. It was earlier shown that BFA leads to

TRAIL DRs accumulation in the Golgi apparatus, suggesting that this organelle forms a platform for DR signaling in stressed cells (van Raam et al., 2017). Recently it was demonstrated that endoplasmic reticulum (ER) stress initiated apoptosis through intracellular activation of DR5 independently of TRAIL and that misfolded proteins can directly engage with DR5 in the ER-Golgi intermediate compartment, where DR5 assembles pro-apoptotic caspase 8-activating complexes (Lam et al., 2020). Thus, the Golgi apparatus may be involved in the signaling of the post-endocytic DR4 and DR5 receptors.

Cell-Type Specific Action of Cycloheximide on the Expression and Recovery of Surface the DR4 and DR5

The effect of BFA on the receptor surface expression was unambiguous for all cell lines before and after TRAIL treatment (**Figures 5B,C** and **Supplementary Table 3**). However, the protein synthesis inhibitor cycloheximide (CHX) affected differently the expression of surface DRs in various cell types. CHX significantly inhibited both surface and total DR5 expression in A549 and HCT116 cells, whereas this effect was negligible in HT-29 and Jurkat cells (**Figures 6A–C** and **Supplementary Table 4**). Accordingly, after TRAIL-stimulated endocytosis, the surface restoration of this receptor was completely blocked in A549 and HCT116, but in HT-29 and Jurkat cells, it was only partially inhibited by CHX. The surface DR4 was virtually unaffected by CHX in HCT116 and A549 cells and decreased by about 20% in HT-29 cells (**Figure 6D** and **Supplementary Table 4**). However, the DR4 recovery after TRAIL stimulation was completely inhibited in HCT116 and HT-29 cells. Interestingly, CHX did not affect either DR4 surface expression in general or its recovery after TRAIL stimulation in A549 cells, indicating that DR4 recovery occurred from the intracellular compartments where it could be accumulated. Thus, the results of the experiment using CHX showed that there is no correlation between the sensitivity of cells to TRAIL and the balance between degradation, synthesis and recycling of receptors. Despite the fact that the effect of two inhibitors (BFA and CHX) was aimed at reducing the number of surface receptors, the inhibitory effect of BFA was more potent and universal either with or without TRAIL. Comparing the results in **Figures 5**, **6**, it can be seen that there are significant differences in the effects of BFA and CHX on the DRs surface expression. BFA significantly (by 60–70%) reduced the amount of DR5 on the surface of all tested cell lines, while CHX acted only on A549 and HCT116. In lines A549 and HCT116, the surface expression of DR4 was decreased by BFA, but not by CHX. These data indicated the important role of the Golgi apparatus in the restoration of post-endocytic receptors. Thus, it can be concluded that post-endocytic receptor recovery can occur not only from newly synthesized molecules, but also from the intracellular compartments, in particular from TGN. The inhibitory effects of BFA and CHX on the restoration of receptor surface expression indicated that TRAIL death receptors are continuously synthesized, externalized, internalized and degraded, and these processes are more pronounced for DR5 receptor.

Inhibition of Receptors Endocytosis by Hypertonic Sucrose Sensitized the Resistant Cells to TRAIL

We then investigated the role of ligand-mediated endocytosis of DR4 and DR5 on the cytotoxic activity of TRAIL. In our hands, the inhibitor of clathrin-mediated endocytosis dynasore or cholesterol-depleting agent filipin III did not significantly inhibit TRAIL-mediated endocytosis of DR4 or DR5 (**Supplementary Figure 3** and **Supplementary Table 5**). The hypertonic sucrose is known to non-selectively block the receptor endocytosis (Guo et al., 2015). TRAIL-mediated endocytosis of DR4 and DR5 was inhibited when cells were pretreated with sucrose at concentration 250 mM for 1 h (**Figures 7A,B** and **Supplementary Table 6**). In addition, A549 and HT-29 resistant cells were effectively sensitized to TRAIL when pre-incubated with 250 mM sucrose (**Figure 7C** and **Supplementary Table 7**). The cytotoxicity of TRAIL was also increased in HCT116 and Jurkat cells in the presence of sucrose. Hyperosmotic sucrose was highly cytotoxic to Jurkat cells during prolonged exposure (data not shown). Therefore, these cells were incubated with TRAIL for 3 h, which is insufficient to manifest the cytotoxic activity of TRAIL. Nevertheless, upon treatment of these cells with sucrose, a decrease in cell viability by TRAIL was observed in 3 h. The general caspase inhibitor z-VAD-FMK (10 μM) completely blocked the increased cytotoxic activity of TRAIL observed after incubation of cells in a hyperosmotic state, demonstrating that the decrease in cell viability is a result of the apoptotic mechanism activation induced by TRAIL but not by sucrose as hyperosmolarity itself did not induce apoptosis. Thus, the inhibition of TRAIL death receptor endocytosis by sucrose enhances the cytotoxic activity of TRAIL, suggesting that endocytosis is a defense mechanism for cell survival.

DISCUSSION

The cytokine TRAIL induces apoptosis through the death receptors DR4 or DR5, predominantly in cancer cells, but not in normal cells (Wajant, 2019). However, many cancer cells are resistant to DRs-mediated apoptosis due to a variety of mechanisms, and this is the reason for the low antitumor activity of its various therapeutic agonists (recombinant TRAIL variants or antibodies to receptors) in clinical trials (Micheau et al., 2013; Kretz et al., 2019). Although multiple proteins are involved in DR-mediated apoptosis, surface expression of death receptors is a prerequisite for the activation of TRAIL apoptosis signaling. Expression of DR4 and DR5 receptors is regulated at the transcriptional level by epigenetic modification, transcription factors, microRNA and RNA-binding proteins, as well as at post-translational level by ubiquitination and glycosylation (Song et al., 2010; van de Kooij et al., 2013; Micheau, 2018; Min et al., 2019). However, a high level of surface receptor expression does not always

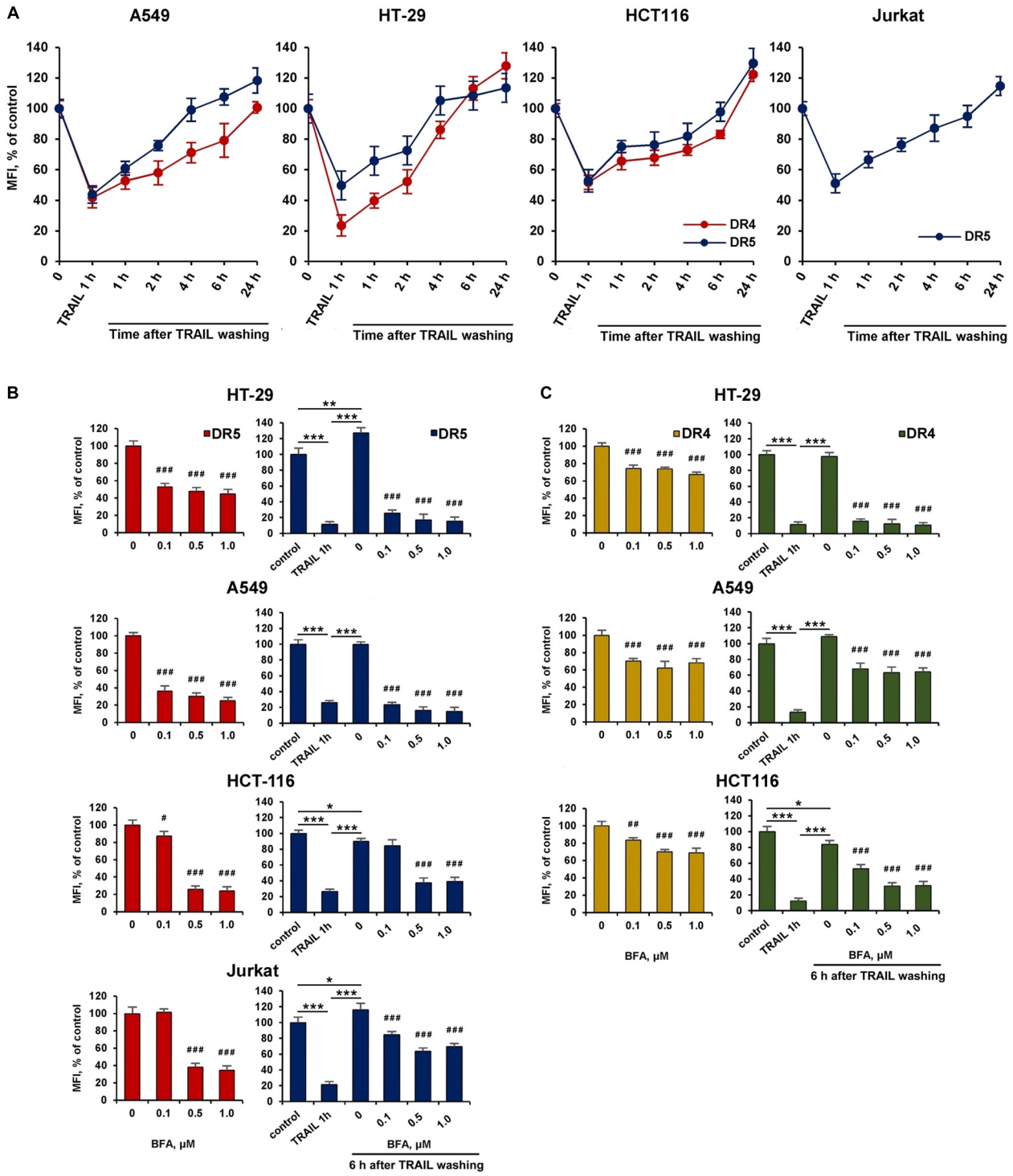

FIGURE 5 | Brefeldin A inhibited the recovery of surface DR4 and DR5 receptors. **(A)** HT-29, A549, HCT116, and Jurkat cells were treated with 1,000 ng/ml TRAIL for 1 h, the ligand was washed three times with ice-cold medium and the kinetics of surface receptor recovery was analyzed for 24 h by flow cytometry. Mean Fluorescence Intensity (MFI) values are presented as a percentage relative to control cells. Data represent means ± standard deviation of three analyzes. **(B)** Cells treated with Brefeldin A (BFA) before or after TRAIL (1 μg/ml) treatment at indicated concentrations for 6 h and the surface expression of DR5 **(B)** and DR4 **(C)** was determined by flow cytometry. Mean Fluorescence Intensity (MFI) values are presented as a percentage relative to BFA non-treated cells. Data represent means ± SD of three independent experiments. $^{*}p < 0.05$, $^{**}p < 0.01$, and $^{***}p < 0.001$ indicate significant difference between groups according to One-way ANOVA followed by Tukey test. $^{\#}p < 0.05$, $^{\#\#}p < 0.01$, and $^{\#\#\#}p < 0.001$ indicated significant difference from the untreated with BFA cells according to One-way ANOVA followed by Dunnett's *post hoc* test. Raw data for **(B,C)** are available in **Supplementary Table 3**.

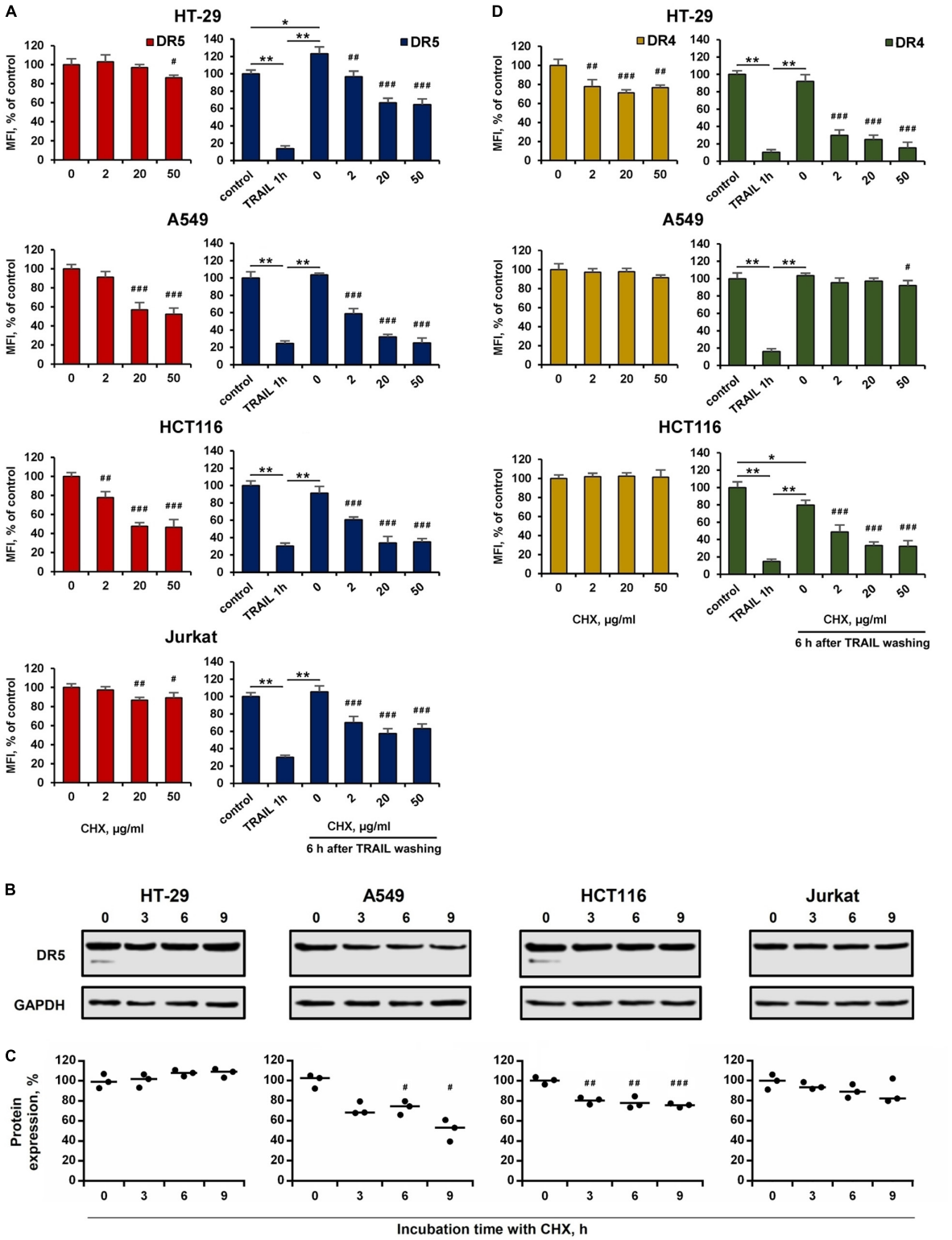

FIGURE 6 | Effect of cycloheximide on expression and recovery of surface DR4 and DR5. HT-29, A549, HCT116 and Jurkat cells were treated with cycloheximide (CHX) before or after TRAIL (1 μg/ml) treatment at indicated concentrations for 6 h and the surface expression of DR5 **(A)** and DR4 **(D)** was determined by flow cytometry. Mean Fluorescence Intensity (MFI) values are presented as a percentage relative to CHX non-treated cells. **(B)** Western blot analysis of DR5 receptor in cell lysates after treatment with 50 Âţg/ml CHX for 3, 6 and 9 h. **(C)** Protein band intensities calculated using the ImageJ software (http://rsbweb.nih.gov/ij/, NIH, Bethesda, MD, United States) and data were normalized to GAPDH. Data are expressed as the means ± SD of three independent experiments. Mean Fluorescence

(Continued)

FIGURE 6 | (Continued)
Intensity (MFI) values are presented as a percentage relative to BFA non-treated cells. Data represent means ± SD of three independent experiments. $^{*}p < 0.01$ and $^{**}p < 0.001$ indicate significant difference between groups to One-way ANOVA followed by Tukey test. $^{\#}p < 0.05$, $^{\#\#}p < 0.01$ and $^{\#\#\#}p < 0.001$ indicated significant difference from the untreated with CHX cells according to One-way ANOVA followed by Dunnett's posthoc test. Raw data for **(A,D)** are available in **Supplementary Table 4**.

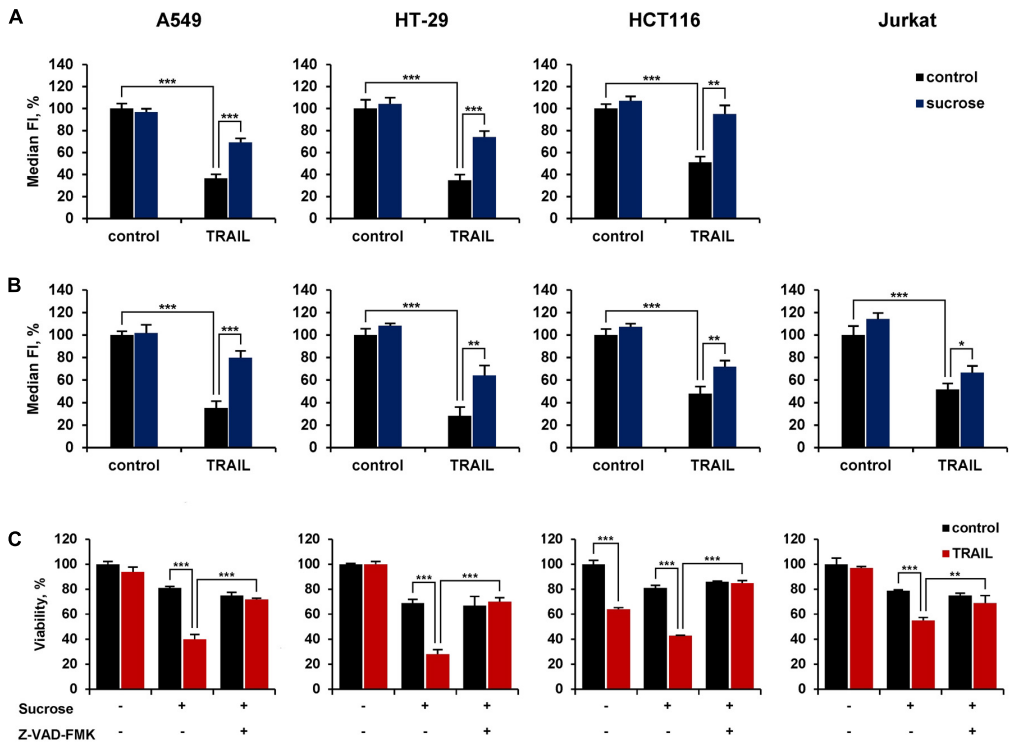

FIGURE 7 | Hypertonic sucrose inhibited TRAIL-mediated receptor endocytosis and sensitized resistant cells to TRAIL. HT-29, A549, HCT116 and Jurkat cells were treated with or without 250 mM sucrose for 1 h followed by treatment with 100 ng/ml TRAIL for another 1 h and the surface expression of DR4 **(A)** and DR5 **(B)** was determined by flow cytometry. **(C)** Cells were incubated with or without 250 mM sucrose for 1 h in the absence or presence of 10 μM Z-VAD-FMK followed by treatment with 100 ng/ml TRAIL for 16 h in the case of HT-29 and A549 cells, 7 h for HCT116 and 3 h for Jurkat cells. Viability was determined by WST-1 colorimetric assay. The results are presented as mean ± SD of triplicate independent experiments. $^{*}p < 0.05$, $^{**}p < 0.01$ and $^{***}p < 0.001$ indicate significant difference between groups according to One-way ANOVA followed by Tukey test. Raw data are available for **(A,B)** in **Supplementary Table 6** and for **(C)** in **Supplementary Table 7**.

correlate with the sensitivity to TRAIL (Chen et al., 2012). Numerous studies have demonstrated that DRs can be located in various cellular compartments such as autophagosomes, trans-Golgi network, and nucleus or even in the cytosol (Bertsch et al., 2014). The mechanisms of DRs expression and signaling have been extensively studied in the last two decades, but little research has focused on the regulation of their membrane transport.

In the present study, we compared the kinetics of TRAIL-mediated decrease of surface DR4 and DR5 receptors expression in TRAIL-resistant (HT-29, A549) and TRAIL-sensitive (HCT116, Jurkat) tumor cell lines. Both receptors surface expression was rapidly decreased after TRAIL binding in a concentration-dependent manner with similar kinetics in all tested cell lines. TRAIL-mediated rapid internalization of DR5 in Colo205 cells (Austin et al., 2006) or rapid internalization of TRAIL itself in BJAB, Hela (Kohlhaas et al., 2007), MDA-MB-231 and A549 (Zhang et al., 2009; Reis et al., 2017) and Huh-7 (Akazawa et al., 2009) cells have been described earlier. We measured for the first time the kinetics of TRAIL-mediated decrease in surface DR4 simultaneously with DR5 and showed that both receptors were internalized at the same rate. The receptor-selective TRAIL variant DR5-B decreased only surface DR5 but not DR4 indicating that death receptors can be internalized independently of each other. We did not observe changes to total death receptor levels during incubation of cells with TRAIL, since steady-state expression of DR4 and DR5 in cell lysates remained unchanged, possibly because the rate of putative degradation was equilibrated with the rate of synthesis of new molecules.

The recycling of DR4 and DR5 back to the plasma membrane after endocytosis was not investigated until now. Here we have demonstrated that both receptors slowly return to the plasma membrane after TRAIL washing from culture medium and within 6 h the surface expression of receptors was completely restored, regardless of the sensitivity of the tumor cells to TRAIL-induced apoptosis. The slow recycling pathway involves the transport of cargo proteins from the early endosome to the

endocytic recycling compartment (ERC) and from the ERC to the plasma membrane (Grant and Donaldson, 2009). The recovery of surface DR4 and DR5 was blocked by Golgi-disrupting agent BFA and partially suppressed by protein synthesis inhibitor CHX. Since TRAIL did not affect the stable expression of DRs in cell lysates. it can be assumed that the recovery of surface receptors can occur both from ERC (late endosomes and Golgi apparatus, or nucleus), where they accumulate, and from the newly synthesized molecules. It has recently been demonstrated that nuclear TRAIL-DRs are directly translocated from the plasma membrane through an initial clathrin-dependent endocytosis in a TRAIL-dependent manner, independently of its apoptotic activity (Mert et al., 2019). More research is needed to clarify how DRs endocytosis correlates with their recovery and how these processes are regulated.

We have also shown that TRAIL death receptors undergo constitutive endocytosis in the absence of a ligand. BFA decreased surface expression of both receptors in time- (1–6 h) and concentration-dependent manner, and this effect was more pronounced for DR5. The effect of brefeldin A was not associated with receptor degradation, since the content of DR5 in HT-29 and Jurkat cells or surface expression of DR4 in A549 and HCT116 cells were not affected by cycloheximide. The secretory stressors such as BFA and thapsigargin (Tg) have been shown to induce accumulation of death receptors in the Golgi apparatus and its compensatory expression (Lu et al., 2014; van Raam et al., 2017). Despite its importance, the details of TRAIL death receptors endosomal traffic have not been investigated. The signal recognition particle complex (SRP) is required for DR4, but not DR5 localization on the cell surface, indicating that receptors transport may be regulated in different ways (Ren et al., 2004). Recently it has been demonstrated that depletion of MLKL (Mixed lineage kinase domain-like) reduced the endosomal traffic and degradation of DR5, resulting in increased TRAIL cytotoxicity (Park et al., 2020). A deeper understanding of the molecular mechanisms that support DRs transport along the recycling pathway will provide a deeper understanding of the mechanisms of resistance of tumor cells to TRAIL and, probably, will determine new approaches to the treatment of tumor diseases.

Several studies have shown that the disruption of clathrin-dependent endocytosis of DRs by inactivation of dynamins (particularly by dynamin 1) leads to increased cell apoptosis (Austin et al., 2006; Reis et al., 2017). We did not observe any effect of the inhibitor of clathrin-mediated endocytosis dynasore on TRAIL-mediated DR4 or DR5 endocytosis. Dynasore is a cell-permeable inhibitor of dynamin GTPase activity that leads to the accumulation of late invaginated coated pits (Nankoe and Sever, 2006). One of the possible reasons for the lack of dynasore effect may be that antibodies to DRs cannot recognize receptors when they are in the O-shaped pits. Hyperosmotic sucrose blocks formation of type 1 coated pits by preventing clathrin and adaptors from interacting (Hansen et al., 1993). Under such conditions, the availability of receptors for antibodies is not impaired, and this is probably why we observed inhibition of TRAIL-mediated decrease in surface DRs upon pretreatment of cells with hyperosmotic sucrose. Resistant A549 and HT-29 cells were effectively sensitized to TRAIL-induced cell death under sucrose hyper-osmosis. Several studies have demonstrated that DR internalization is not required for the formation of the death inducing signaling complex (DISC) or for apoptosis (Kohlhaas et al., 2007; Zhang et al., 2009). However, the reasons for DISC inactivation after endocytosis remain unclear. In our experiments, the kinetics of receptor internalization practically did not differ in resistant and sensitive cells. However, the rate of DRs recovery in sensitive cells was relatively reduced. It can be assumed that the DISC components dissociate relatively faster after internalization in TRAIL-resistant cells, preventing the initiation of apoptosis.

Thus, we have demonstrated that the sensitivity of tumor cells is not related to the rate of TRAIL-mediated DR endocytosis. Based on our results it can be proposed that the post-endocytic events, such as the rate of DISC dissociation and accumulation of receptors in different compartments, or the rate of their degradation play a significant role in triggering apoptotic TRAIL signaling. Additional experimental data are needed to confirm this hypothesis.

DATA AVAILABILITY STATEMENT

The original contributions presented in the study are included in the article/**Supplementary Material**, further inquiries can be directed to the corresponding author/s.

AUTHOR CONTRIBUTIONS

AA, AY, MG, and DT performed the experiments and analyzed the data. DD and MK designed the research. MG wrote the manuscript. DD carefully revised the manuscript. All authors have read and approved the final manuscript.

FUNDING

This work was supported by Russian Science Foundation (Grant No. 21-14-00224, AA, MG, and DD production of recombinant TRAIL and DR5-B, TRAIL-mediated receptors traffic), by budgetary funding, AY, MK for western blot and ELISA analysis and of Lomonosov Moscow State University (Moscow, Russia). The confocal laser scanning microscopy study DT was performed using the equipment of the Shared Research Center FSRC "Crystallography and Photonics" RAS and supported by the Ministry of Science and Higher Education of the Russian Federation within the State assignment FSRC "Crystallography and Photonics" RAS.

SUPPLEMENTARY MATERIAL

The Supplementary Material for this article can be found online at: https://www.frontiersin.org/articles/10.3389/fcell.2021.733688/full#supplementary-material

REFERENCES

Akazawa, Y., Mott, J. L., Bronk, S. F., Werneburg, N. W., Kahraman, A., Guicciardi, M. E., et al. (2009). Death receptor 5 internalization is required for *Lysosomal Permeabilization* by TRAIL in malignant liver cell lines. *Gastroenterology* 136, 2365–2376.e7. doi: 10.1053/j.gastro.2009.02.071

Artykov, A. A., Belov, D. A., Shipunova, V. O., Trushina, D. B., Deyev, S. M., Dolgikh, D. A., et al. (2020). Chemotherapeutic agents sensitize resistant cancer cells to the DR5-specific variant DR5-B more efficiently than to TRAIL by modulating the surface expression of death and decoy receptors. *Cancers* 12:1129. doi: 10.3390/cancers12051129

Austin, C. D., Lawrence, D. A., Peden, A. A., Varfolomeev, E. E., Totpal, K., De Maziere, A. M., et al. (2006). Death-receptor activation halts clathrin-dependent endocytosis. *Proc. Natl. Acad. Sci. U.S.A.* 103, 10283–10288. doi: 10.1073/pnas.0604044103

Bertsch, U., Röder, C., Kalthoff, H., and Trauzold, A. (2014). Compartmentalization of TNF-related apoptosis-inducing ligand (TRAIL) death receptor functions: emerging role of nuclear TRAIL-R2. *Cell Death Dis.* 5:e1390. doi: 10.1038/cddis.2014.351

Cendrowski, J., Mamińska, A., and Miaczynska, M. (2016). Endocytic regulation of cytokine receptor signaling. *Cytokine Growth Factor Rev.* 32, 63–73. doi: 10.1016/j.cytogfr.2016.07.002

Chen, J.-J., Shen, H.-C. J., Rivera Rosado, L. A., Zhang, Y., Di, X., and Zhang, B. (2012). Mislocalization of death receptors correlates with cellular resistance to their cognate ligands in human breast cancer cells. *Oncotarget* 3, 833–842. doi: 10.18632/oncotarget.542

Cheng, W., Liu, F., Wang, Z., Zhang, Y., Zhao, Y.-X., Zhang, Q., et al. (2015). Soluble TRAIL concentration in serum is elevated in people with hypercholesterolemia. *PLoS One* 10:e0144015. doi: 10.1371/journal.pone.0144015

Di, X., Zhang, G., Zhang, Y., Takeda, K., Rosado, L. A. R., and Zhang, B. (2013). Accumulation of autophagosomes in breast cancer cells induces TRAIL resistance through downregulation of surface expression of death receptors 4 and 5. *Oncotarget* 4, 1349–1364. doi: 10.18632/oncotarget.1174

Gasparian, M. E., Chernyak, B. V., Dolgikh, D. A., Yagolovich, A. V., Popova, E. N., Sycheva, A. M., et al. (2009). Generation of new TRAIL mutants DR5-A and DR5-B with improved selectivity to death receptor 5. *Apoptosis* 14, 778–787. doi: 10.1007/s10495-009-0349-3

Grant, B. D., and Donaldson, J. G. (2009). Pathways and mechanisms of endocytic recycling. *Nat. Rev. Mol. Cell. Biol.* 10, 597–608. doi: 10.1038/nrm2755

Guo, S., Zhang, X., Zheng, M., Zhang, X., Min, C., Wang, Z., et al. (2015). Selectivity of commonly used inhibitors of clathrin-mediated and caveolae-dependent endocytosis of G protein–coupled receptors. *Biochimica et Biophysica Acta (BBA) Biomembranes* 1848, 2101–2110. doi: 10.1016/j.bbamem.2015.05.024

Hansen, S. H., Sandvig, K., and van Deurs, B. (1993). Clathrin and HA2 adaptors: effects of potassium depletion, hypertonic medium, and cytosol acidification. *J. Cell Biol.* 121, 61–72. doi: 10.1083/jcb.121.1.61

Haselmann, V., Kurz, A., Bertsch, U., Hübner, S., Olempska–Müller, M., Fritsch, J., et al. (2014). Nuclear death receptor TRAIL-R2 inhibits maturation of let-7 and promotes proliferation of pancreatic and other tumor cells. *Gastroenterology* 146, 278–290. doi: 10.1053/j.gastro.2013.10.009

Jang, Y. J., Park, K. S., Chung, H. Y., and Kim, H. I. (2003). Analysis of the phenotypes of Jurkat clones with different TRAIL-sensitivities. *Cancer Lett.* 194, 107–117. doi: 10.1016/s0304-3835(02)00680-8

Kohlhaas, S. L., Craxton, A., Sun, X.-M., Pinkoski, M. J., and Cohen, G. M. (2007). Receptor-mediated endocytosis is not required for tumor necrosis factor-related apoptosis-inducing ligand (TRAIL)-induced apoptosis. *J. Biol. Chem.* 282, 12831–12841. doi: 10.1074/jbc.M700438200

Kojima, Y., Nakayama, M., Nishina, T., Nakano, H., Koyanagi, M., Takeda, K., et al. (2011). Importin β1 protein-mediated nuclear localization of death receptor 5 (DR5) limits DR5/tumor necrosis factor (TNF)-related apoptosis-inducing ligand (TRAIL)-induced cell death of human tumor cells. *J. Biol. Chem.* 286, 43383–43393. doi: 10.1074/jbc.M111.309377

Kojima, Y., Nishina, T., Nakano, H., Okumura, K., and Takeda, K. (2020). Inhibition of importin b1 Augments the anticancer effect of agonistic anti-death receptor 5 antibody in TRAIL-resistant tumor cells. *Mol. Cancer Ther.* 19, 1123–1133.

Kretz, A.-L., Trauzold, A., Hillenbrand, A., Knippschild, U., Henne-Bruns, D., von Karstedt, S., et al. (2019). TRAILblazing strategies for cancer treatment. *Cancers* 11:456. doi: 10.3390/cancers11040456

Lam, M., Marsters, S. A., Ashkenazi, A., and Walter, P. (2020). Misfolded proteins bind and activate death receptor 5 to trigger apoptosis during unresolved endoplasmic reticulum stress. *Elife* 6:e52291. doi: 10.7554/eLife.52291

LeBlanc, H. N., and Ashkenazi, A. (2003). Apo2L/TRAIL and its death and decoy receptors. *Cell Death Differ* 10, 66–75. doi: 10.1038/sj.cdd.4401187

Leithner, K., Stacher, E., Wurm, R., Ploner, F., Quehenberger, F., Wohlkoenig, C., et al. (2009). Nuclear and cytoplasmic death receptor 5 as prognostic factors in patients with non-small cell lung cancer treated with chemotherapy. *Lung Cancer* 65, 98–104. doi: 10.1016/j.lungcan.2008.10.015

Lu, M., Lawrence, D. A., Marsters, S., Acosta-Alvear, D., Kimmig, P., Mendez, A. S., et al. (2014). Opposing unfolded-protein-response signals converge on death receptor 5 to control apoptosis. *Science* 345, 98–101. doi: 10.1126/science.1254312

Mazurek, N., Byrd, J. C., Sun, Y., Hafley, M., Ramirez, K., Burks, J., et al. (2012). Cell-surface galectin-3 confers resistance to TRAIL by impeding trafficking of death receptors in metastatic colon adenocarcinoma cells. *Cell Death Differ* 19, 523–533. doi: 10.1038/cdd.2011.123

Mellman, I., and Yarden, Y. (2013). Endocytosis and cancer. *Cold Spring Harbor Perspect. Biol.* 5:a016949. doi: 10.1101/cshperspect.a016949

Merino, D., Lalaoui, N., Morizot, A., Schneider, P., Solary, E., and Micheau, O. (2006). Differential inhibition of TRAIL-mediated DR5-DISC formation by decoy receptors 1 and 2. *Mol. Cell. Biol.* 26, 7046–7055. doi: 10.1128/MCB.00520-06

Mert, U., Adawy, A., Scharff, E., Teichmann, P., Willms, A., Haselmann, V., et al. (2019). TRAIL induces nuclear translocation and chromatin localization of TRAIL death receptors. *Cancers* 11:1167. doi: 10.3390/cancers11081167

Micheau, O. (2018). Regulation of TNF-related apoptosis-inducing ligand signaling by glycosylation. *IJMS* 19:715. doi: 10.3390/ijms19030715

Micheau, O., Shirley, S., and Dufour, F. (2013). Death receptors as targets in cancer: TRAIL clinical trials. *Br. J. Pharmacol.* 169, 1723–1744. doi: 10.1111/bph.12238

Min, K., Woo, S. M., Shahriyar, S. A., and Kwon, T. K. (2019). Elucidation for modulation of death receptor (DR) 5 to strengthen apoptotic signals in cancer cells. *Arch. Pharm. Res.* 42, 88–100. doi: 10.1007/s12272-018-01103-y

Nahacka, Z., Svadlenka, J., Peterka, M., Ksandrova, M., Benesova, S., Neuzil, J., et al. (2018). TRAIL induces apoptosis but not necroptosis in colorectal and pancreatic cancer cells preferentially via the TRAIL-R2/DR5 receptor. *Biochimica et Biophysica Acta Mol. Cell Res.* 1865, 522–531. doi: 10.1016/j.bbamcr.2017.12.006

Nankoe, S., and Sever, S. (2006). Dynasore puts a new spin on dynamin: a surprising dual role during vesicle formation. *Trends Cell Biol.* 16, 607–609. doi: 10.1016/j.tcb.2006.10.004

Park, S.-Y., Park, H.-H., Park, S.-Y., Hong, S. M., Yoon, S., Morgan, M. J., et al. (2020). Reduction in MLKL-mediated endosomal trafficking enhances the TRAIL-DR4/5 signal to increase cancer cell death. *Cell Death Dis.* 11:744. doi: 10.1038/s41419-020-02941-9

Reis, C. R., Chen, P.-H., Bendris, N., and Schmid, S. L. (2017). TRAIL-death receptor endocytosis and apoptosis are selectively regulated by dynamin-1 activation. *Proc. Natl. Acad. Sci. U.S.A.* 114, 504–509. doi: 10.1073/pnas.1615072114

Ren, Y.-G., Wagner, K. W., Knee, D. A., Aza-Blanc, P., Nasoff, M., and Deveraux, Q. L. (2004). Differential regulation of the TRAIL death receptors DR4 and DR5 by the signal recognition particle. *MBoC* 15, 5064–5074. doi: 10.1091/mbc.e04-03-0184

Schmid, S. L. (2017). Reciprocal regulation of signaling and endocytosis: Implications for the evolving cancer cell. *J. Cell Biol.* 216, 2623–2632. doi: 10.1083/jcb.201705017

Schneider-Brachert, W., Heigl, U., and Ehrenschwender, M. (2013). Membrane trafficking of death receptors: implications on signalling. *IJMS* 14, 14475–14503. doi: 10.3390/ijms140714475

Schütze, S., and Schneider-Brachert, W. (2009). "Impact of TNF-R1 and CD95 internalization on apoptotic and antiapoptotic signaling," in *Death Receptors and Cognate Ligands in Cancer Results and Problems in Cell Differentiation*, ed. H. Kalthoff (Berlin: Springer Berlin Heidelberg), 63–85. doi: 10.1007/400_2008_23

Setroikromo, R., Zhang, B., Reis, C. R., Mistry, R. H., and Quax, W. J. (2020). Death receptor 5 displayed on extracellular vesicles decreases TRAIL sensitivity of colon cancer cells. *Front. Cell Dev. Biol.* 8:318. doi: 10.3389/fcell.2020.00318

Song, J. J., Szczepanski, M. J., Kim, S. Y., Kim, J.-H., An, J. Y., Kwon, Y. T., et al. (2010). c-Cbl-mediated degradation of TRAIL receptors is responsible for the development of the early phase of TRAIL resistance. *Cell. Sign.* 22, 553–563. doi: 10.1016/j.cellsig.2009.11.012

Soria, J. C., Smit, E., Khayat, D., Bess, B., Yang, X., Hsu, C. P., et al. (2010). Phase 1b study of dulanermin (recombinant human Apo2L/TRAIL) in combination with paclitaxel, carboplatin, and bevacizumab in patients with advanced non-squamous non-small-cell lung cancer. *J. Clin. Oncol.* 28, 1527–1533. doi: 10.1200/JCO.2009.25.4847

Szegezdi, E., van der Sloot, A. M., Mahalingam, D., O'Leary, L., Cool, R. H., Muñoz, I. G., et al. (2012). Kinetics in signal transduction pathways involving promiscuous oligomerizing receptors can be determined by receptor specificity: apoptosis induction by TRAIL. *Mol. Cell. Proteo.* 11:M111.013730. doi: 10.1074/mcp.M111.013730

van de Kooij, B., Verbrugge, I., de Vries, E., Gijsen, M., Montserrat, V., Maas, C., et al. (2013). Ubiquitination by the membrane-associated RING-CH-8 (MARCH-8) ligase controls steady-state cell surface expression of tumor necrosis factor-related apoptosis inducing ligand (TRAIL) receptor 1. *J. Biol. Chem.* 288, 6617–6628. doi: 10.1074/jbc.M112.448209

van Raam, B. J., Lacina, T., Lindemann, R. K., and Reiling, J. H. (2017). Secretory stressors induce intracellular death receptor accumulation to control apoptosis. *Cell Death Dis.* 8:e3069. doi: 10.1038/cddis.2017.466

Wajant. (2019). Molecular mode of action of TRAIL receptor agonists-common principles and their translational exploitation. *Cancers* 11:954. doi: 10.3390/cancers11070954

Yagolovich, A. V., Artykov, A. A., Dolgikh, D. A., Kirpichnikov, M. P., and Gasparian, M. E. (2019). A new efficient method for production of recombinant antitumor cytokine TRAIL and its receptor selective variant DR5-B. *Biochemistry (Mosc)* 84, 627–636. doi: 10.1134/S0006297919060051

Zhang, X. D., Franco, A. V., Nguyen, T., Gray, C. P., and Hersey, P. (2000). Differential localization and regulation of death and decoy receptors for tnf-related apoptosis-inducing ligand (TRAIL) in human melanoma cells. *J. Immunol.* 164, 3961–3970. doi: 10.4049/jimmunol.164.8.3961

Zhang, Y., and Zhang, B. (2008). TRAIL resistance of breast cancer cells is associated with constitutive endocytosis of death receptors 4 and 5. *Mol. Cancer Res.* 6, 1861–1871. doi: 10.1158/1541-7786.MCR-08-0313

Zhang, Y., Yoshida, T., and Zhang, B. (2009). TRAIL induces endocytosis of its death receptors in MDA-MB-231 breast cancer cells. *Cancer Biol. Ther.* 8, 917–922. doi: 10.4161/cbt.8.10.8141

Zhao, X., Liu, Y., Ma, Q., Wang, X., Jin, H., Mehrpour, M., et al. (2009). Caveolin-1 negatively regulates TRAIL-induced apoptosis in human hepatocarcinoma cells. *Biochem. Biophys. Res. Commun.* 378, 21–26. doi: 10.1016/j.bbrc.2008.10.123

Conflict of Interest: The authors declare that the research was conducted in the absence of any commercial or financial relationships that could be construed as a potential conflict of interest.

Publisher's Note: All claims expressed in this article are solely those of the authors and do not necessarily represent those of their affiliated organizations, or those of the publisher, the editors and the reviewers. Any product that may be evaluated in this article, or claim that may be made by its manufacturer, is not guaranteed or endorsed by the publisher.

frontiers in Cell and Developmental Biology

REVIEW
published: 10 December 2021
doi: 10.3389/fcell.2021.790568

Alterations in Lysosome Homeostasis in Lipid-Related Disorders: Impact on Metabolic Tissues and Immune Cells

Fernanda Cabrera-Reyes[1,2], *Claudia Parra-Ruiz*[1,2], *María Isabel Yuseff*[1]* and *Silvana Zanlungo*[2]*

[1]Department of Cellular and Molecular Biology, Faculty of Sciences, Pontificia Universidad Católica de Chile, Santiago, Chile, [2]Department of Gastroenterology, Faculty of Medicine, Pontificia Universidad Católica de Chile, Santiago, Chile

Lipid-related disorders, which primarily affect metabolic tissues, including adipose tissue and the liver are associated with alterations in lysosome homeostasis. Obesity is one of the more prevalent diseases, which results in energy imbalance within metabolic tissues and lysosome dysfunction. Less frequent diseases include Niemann-Pick type C (NPC) and Gaucher diseases, both of which are known as Lysosomal Storage Diseases (LSDs), where lysosomal dysfunction within metabolic tissues remains to be fully characterized. Adipocytes and hepatocytes share common pathways involved in the lysosome-autophagic axis, which are regulated by the function of cathepsins and CD36, an immuno-metabolic receptor and display alterations in lipid diseases, and thereby impacting metabolic functions. In addition to intrinsic defects observed in metabolic tissues, cells of the immune system, such as B cells can infiltrate adipose and liver tissues, during metabolic imbalance favoring inflammation. Moreover, B cells rely on lysosomes to promote the processing and presentation of extracellular antigens and thus could also present lysosome dysfunction, consequently affecting such functions. On the other hand, growing evidence suggests that cells accumulating lipids display defective inter-organelle membrane contact sites (MCSs) established by lysosomes and other compartments, which contribute to metabolic dysfunctions at the cellular level. Overall, in this review we will discuss recent findings addressing common mechanisms that are involved in lysosome dysregulation in adipocytes and hepatocytes during obesity, NPC, and Gaucher diseases. We will discuss whether these mechanisms may modulate the function of B cells and how inter-organelle contacts, emerging as relevant cellular mechanisms in the control of lipid homeostasis, have an impact on these diseases.

Keywords: obesity, niemann-pick type C (NPC), gaucher disease (GD), lysosomal dysfunction, cathepsins, CD36, B cell activation and membrane contact sites (MCSs)

OPEN ACCESS

Edited by:
Angela Wandinger-Ness, University of New Mexico, United States

Reviewed by:
Frederick Maxfield, Cornell University, United States
Robert Zimmermann, University of Graz, Austria

***Correspondence:**
María Isabel Yuseff
myuseff@bio.puc.cl,
Silvana Zanlungo
szanlungo@uc.cl
silvana.zanlungo@gmail.com

Specialty section:
This article was submitted to Membrane Traffic, a section of the journal Frontiers in Cell and Developmental Biology

Received: *06 October 2021*
Accepted: *22 November 2021*
Published: *10 December 2021*

Citation:
Cabrera-Reyes F, Parra-Ruiz C, Yuseff MI and Zanlungo S (2021) Alterations in Lysosome Homeostasis in Lipid-Related Disorders: Impact on Metabolic Tissues and Immune Cells. Front. Cell Dev. Biol. 9:790568. doi: 10.3389/fcell.2021.790568

Abbreviations: ATX, autotoxin; BCR, B cell receptor; BMP, bis (monoacylglycero) phosphate; CTS, cathepsin; ER, endoplasmic reticulum; FAs, fatty acids; GD, Gaucher Disease; GILT, gamma-interferon-inducible lysosomal thiol reductase; HFD, high-fat diet; LDL, low-density lipoprotein; LDL-c, LDL-cholesterol; LDs, lipid droplets; LPA, lysophosphatidic acid; LSDs, Lysosomal Storage Diseases; MCSs, membrane contact sites; NAFLD, nonalcoholic fatty liver disease; NASH, nonalcoholic steatohepatitis; NPC, Niemann-Pick type C; PPAR-γ, peroxisome proliferator-activated receptor γ; STARD3, steroidogenic acute regulatory protein (StAR) D3; VLDL, low-density lipoprotein; WAT, white adipose tissue.

INTRODUCTION

Dyslipidemias are diseases that exhibit an imbalance or abnormal concentrations of lipids such as cholesterol, low-density lipoprotein (LDL) cholesterol (LDL-c), high-density lipoprotein (HDL), cholesterol (HDL-c) and triglycerides. Causes of dyslipidemias are classified as primary and secondary. The first ones are due to mutations in genes coding for proteins related to lipid metabolism and transport. Among the most common primary diseases is familial hypercholesterolemia, which is caused by autosomal dominant mutations in LDL receptors, increasing LDL-c levels (Helkin et al., 2016). Less frequent diseases related to the accumulation of lipids, include the Lysosomal Storage Diseases (LSDs), Niemann-Pick type C (NPC) and Gaucher diseases (Marques and Saftig 2019).

Secondary dyslipidemias are associated with an unhealthy lifestyle, including excessive drug and alcohol consumption, where the most frequent manifestation is obesity, which results from consumption of an unbalanced diet with high fat content (Klop, Elte, and Cabezas 2013). Obesity is a complex chronic disorder with a multifactorial etiology, considered to be an inflammatory disease that results from an excessive accumulation of fat and the disruption of metabolic homeostasis (Lee et al., 2013; Liu and Nikolajczyk 2019). The prevalence of obesity has increased exponentially in all countries in the past decades and has thus become a major heath burden (Popkin and Doak 2009; Blüher 2019).

Obesity-related pathogenesis results in energy imbalance within metabolic tissues, mainly affecting white adipose tissue (WAT) and the liver (Vázquez-Vela, Torres, and Tovar 2008). These tissues also acquire an inflammatory phenotype, where innate immune cells such as macrophages promote inflammation upon exposure to metabolic stress (Cousin et al., 2001; Weisberg 2003; Russo and Lumeng 2018). Inflammation is also promoted by cells of the adaptive immune system, such as B lymphocytes, which manage to infiltrate adipose and liver tissues (Wu et al., 2019), and produce pro-inflammatory cytokines and autoreactive antibodies (Aschermann et al., 2009; Winer et al., 2011; Kao et al., 2015; Srikakulapu and McNamara 2020). Interestingly, inflammation in response to obesity may be B cell-driven, where these cells have been proposed as potential therapeutic targets to overcome this disease (Shaikh et al., 2015).

Cells belonging to metabolic tissues, including adipocytes and hepatocytes, share common pathways that regulate metabolic functions. However, the organelles or cellular pathways within these cells that respond to and are affected by an excess of nutrients, remain incompletely understood. Metabolic functions, and cell signaling are regulated by interactions between the endoplasmic reticulum (ER) and a variety of organelles as well as lipidic structures, including mitochondria, Golgi, lysosomes, the plasma membrane, lipid droplets and the nucleus. There is a growing amount of evidence indicating that obesity leads to dysfunctional interactions between various organelles of different cell types. A prominent example is the dysregulation of mitochondrial dynamics, which affects their associations with the ER, promoting oxidative stress and a imbalance in lipid and glucose metabolism (Bournat and Brown 2010; Arruda et al., 2014; Ejarque et al., 2019).

Additionally, emerging evidence regarding lysosome function, an essential organelle involved in cellular homeostasis suggests that this organelle is susceptible to changes in lipid homeostasis in obesity and LSDs, especially those that accumulate lipids, such as NPC and Gaucher diseases (Dugail 2014; Cermak et al., 2016; Jaishy and Dale Abel 2016; Marques and Saftig 2019). Such dysfunctions can trigger an inflammatory response in adipocytes and hepatocytes, promoting the activation of immune cells and the persistence of a local inflammatory environment (Jaishy and Dale Abel 2016; Ballabio and Bonifacino 2020). Interestingly, B cells in obesity, NPC and Gaucher diseases could also present lysosome dysfunction due to an excess of nutrients, which can lead to alterations in their immune effector functions, such as the degradation and presentation of antigens, which depend on lysosomal activity. However, such functional aspects remain to be investigated.

This review will focus on lysosome homeostasis alterations in lipid-related disorders, particularly in prevalent diseases such as obesity and less frequent NPC and Gaucher diseases. We will discuss the mechanisms involved in lysosomal alterations that are common among cells of metabolic tissues, including adipose tissue and the liver, which are primarily affected in these pathologies. In this context, we will explore common pathways that are altered in the lysosome-autophagic axis, including cathepsins and CD36. We also speculate whether these mechanisms are also perturbed in cells of the adaptive immune system, specifically in B cells, since they rely on lysosomes to promote the processing and presentation of extracellular antigens. Finally, we will address the impact of lysosomal dysfunction on the functionality of MCS in obesity and NPC and Gaucher diseases.

ALTERATIONS IN LIPID METABOLISM IN LIVER AND ADIPOSE TISSUE IN LIPID-RELATED DISORDERS

Adipose tissue is classified into different types according to its function and appearance; among these are WAT and brown adipose tissue (BAT). WAT acts as an energy store by accumulating free fatty acids (FAs), while BAT is responsible for thermogenesis and energy expenditure (Vázquez-Vela et al., 2008). Adipose tissue is an endocrine organ that undergoes remodeling during metabolic diseases. For example, during obesity, adipocytes, which represent most of the WAT undergo hyperplasia and hypertrophy, as well as cellular death due to hypoxia, infiltration of immune cells with pro-inflammatory phenotypes and high levels of surrounding cytokines (Khan et al., 2020). It is widely described that obesity and its comorbidities are associated with an increased risk of nonalcoholic fatty liver disease (NAFLD) (Neuschwander-Tetri and Brent 2005). This occurs mainly because adipocytes diminish their capacity to store fat, causing chronic elevation of FAs, which are transported by blood circulation to the liver. Lipid accumulation in non-adipose tissues, such as muscle, heart and pancreas, including the liver, as well as an excess in the utilization of FAs cause deleterious effect on glucose metabolism, a term

known as lipotoxicity (Engin and Basak 2017; Yazıcı and Sezer 2017). In fact, in liver, FAs are stored as triglycerides in and repackaged as very low-density lipoprotein (VLDL), which then are transported to other tissues, producing global dyslipidemia. Furthermore, in the liver, FAs-induced lipotoxicity promotes ER and oxidative stress, as well as the release of cytokines from inflamed adipose tissue. This promotes inflammation and fibrosis, resulting in progression to nonalcoholic steatohepatitis (NASH) (Peverill et al., 2014; Rada et al., 2020). The increased delivery of FAs to the liver, circulating proinflammatory cytokines, such as TNF-α and interleukin 1β and other bioactive substances, including adipokines and hepatokines, as well as infiltrated immune cells contribute to the appearance of insulin resistance (Kahn and Flier 2000; Jung and Choi 2014; Shi et al., 2019). Overall, obesity causes significant metabolic defects within organs, which have been extensively discussed in previous reviews (Uranga and Keller 2019; Chait and den Hartigh 2020). Altogether, there is a close link between functional changes in WAT that directly affect the liver and vice versa.

Interestingly, changes in lipid metabolism may also contribute to lysosome dysfunction in the liver. Recent studies have underscored the importance of BMP [bis (monoacylglycero) phosphate or lysobisphosphatidic acid, LBPA], a key lysosomal phospholipid in the cellular pathophysiology of patients with lysosomal lipid accumulation, such as obesity and LSDs (Showalter et al., 2020). An increase in the circulating levels of BMP has been described in plasma of patients with NAFLD and NASH, as well as in plasma and livers of mice fed with a high-fat diet (HFD) (Grabner et al., 2019; Showalter et al., 2020). BMP is enriched in late endosomes/lysosomes, where its negative charge plays a key role in the formation of intraluminal vesicles, in lipid and cholesterol sorting, docking structures for the activation of lysosomal hydrolytic enzymes, and degradation of lipids and internal lysosomal membranes (Gallala and Konrad 2011; Pribasnig et al., 2015). In fact, BMP negative charges facilitate the adhesion of soluble positively charged hydrolases, allowing the degradation of lipids at the interface of inner lysosomal membranes (Gallala and Konrad 2011). In LSDs, Showalter et al. (2020) proposed that "accumulation of some glycolipid substrates triggers an adaptive mechanism to bolster BMP levels in an effort to promote the degradation of these species." Nevertheless, it remains to be determined whether altered levels of BMP are a mediator or a marker of pathological states.

On the other hand, the simplest bioactive phospholipid that is critical in the production and remodeling of intracellular lipids is lysophosphatidic acid (LPA). This phospholipid is implicated in the metabolism of adipose and liver tissues and in the pathogenesis and progression of obesity (Kaffe et al., 2019). In obesity or under conditions of increase lipids, there is an impact on organelle homeostasis and function in adipocytes and hepatocytes, with the lysosome one of the most altered, thus negatively influencing their cellular metabolic function, which will be discussed in the following sections.

Lysosomal Storage Diseases

LSDs, comprise approximately 70 hereditary diseases produced by mutations in genes encoding for lysosomal hydrolases, transporters or membrane proteins, leading most of the times to accumulation in this organelle of partially degraded substrates within this organelle (Platt et al., 2018). Particularly, LSDs with lipid accumulation show pronounced alterations in lipid metabolism and transport (Platt et al., 2018).

NPC disease is characterized by progressive neurodegeneration and visceral damage caused by mutations in either the *Npc1* (95% of the clinical cases) or *Npc2* genes. Both genes encode for lysosomal proteins involved in cholesterol efflux from lysosomes towards other compartments within the cell (Yañez et al., 2020). Therefore, unesterified cholesterol and other lipids with physicochemical affinity for cholesterol, such as glycosphingolipids, including sphingomyelin, sphingosine and BMP are accumulated in endosomes and lysosomes (Davidson et al., 2009;Neßlauer et al., 2019). Alterations in lysosomal cholesterol transport fail to maintain cellular, tissue, and whole-body lipid homeostasis (Beltroy et al., 2005; Kulinski and Vance 2007). In fact, in the liver, *de novo* synthesis of unesterified cholesterol increases to supply adequate amounts of cholesterol for the synthesis of bile acids or the turnover of membrane sterol (Xie, Turley, and Dietschy 2000; Beltroy et al., 2007). In this context, NPC cells, such as hepatocytes and fibroblast show decreased cholesterol esterification (Soccio and Breslow 2004; Maetzel et al., 2014), which is a key factor, because accumulation of unesterified cholesterol is associated with the infiltration of activated macrophages to metabolic tissues, which produce proinflammatory cytokines and other inflammatory factors and thereby play a critical role in parenchymal cell death (Liu et al., 2007; Liu et al., 2009). Importantly, the nervous system is particularly affected in this pathology, where Purkinje neurons are altered early during the onset of these diseases and are especially sensitive to loss of NPC1 function. Some of the neurological symptoms are associated with their death and early cerebellar degeneration. Moreover, dysfunction of non-neuronal cells in the brain, such as microglia and/or astrocytes, contribute to neurodegeneration (Vanier and Millat 2003). This leads to progressive damage such as generalized neurological deficits including ataxia, dystonia, seizures, and dementia that eventually lead to premature death that characterizes NPC disease (Wraith et al., 2009; Pallottini and Pfrieger 2020). Defects in cells of the nervous system are associated with the accumulation of lipids in lysosomes, which perturbs their interactions with other organelles, their functionality, motility, and cellular distribution, also contributing to a failure in autophagy (Oyarzún et al., 2019). How the accumulation of cholesterol caused by the loss of NPC1 leads to lysosomal dysfunction is not fully understood and will be addressed in this review.

Gaucher disease (GD) is one the most prevalent LSDs and is caused by mutations in the *GBA1* gene, which encodes for the (lysosomal) glucosylceramide degrading enzyme *β*-glucocerebrosidase [also named acid-*β*-glucosidase (GCase)]. GCase deficiency leads to lysosomal storage of glucosylceramide and its deacylated product, glucosylsphingosine. GD has been classified into three types: Type I; is characterized by organomegaly, cytopenia and adult onset non-neuropathic or visceral, Type II and III; both of them have an early onset and

progressive compromise brain functions (Nagral 2014; Platt et al., 2018). Cytopenia, splenomegaly and hepatomegaly, result from the infiltration of Gaucher cells, particularly phagocytic macrophages, to the bone marrow, spleen, and liver (Stirnemann et al., 2017; Marques and Saftig 2019). Among alterations reported for liver in GD type I patients, are oscillations in body weight (Kałużna et al., 2019), as well as metabolic abnormalities, including peripheral insulin resistance, dyslipidemia including low levels of high-density lipoprotein (Nascimbeni, Dalla Salda, and Carubbi 2018). Interestingly, a study carried out in patients with GD type 1 revealed high prevalence for liver steatosis (Nascimbeni et al., 2020) and alterations in liver including fibrosis, cirrhosis, and carcinoma (Starosta et al., 2020).

Although GD is considered a multisystemic disease due to the wide spectrum of symptoms, the molecular mechanisms underlying adipose and hepatic tissue alterations caused by the accumulation of glycosphingolipids in lysosomes, remain largely unknown. Most studies have addressed changes at the systemic level, where alterations have been reviewed mainly based on case reports, systematic reviews, and clinical trials (Kałużna et al., 2019). So far, several studies have focused on Gaucher cells (lipid-laden macrophages) that infiltrate liver tissue and the spleen and, in general, there is more information on GD type I, the most common and less aggressive type. In this scenario, current evidence obtained from studies in Gaucher disease suggest that lysosomal dysfunction is due to the accumulation of glucosylceramide and other lipids, such as cholesterol, in this organelle (Yañez et al., 2020). Observations made by immunofluorescence staining of dopaminergic neurons of patients with Parkinson's that carry mutations in the *GBA1* gene reveal that their lysosomes display a larger size (Kim et al., 2021). Additionally, evidence of lysosomal dysfunction has been reported in a Gaucher neuronopathic murine model after observing changes in the expression of lysosomal marker genes, as well as lower lysosomal biogenesis (Brown et al., 2019). In addition to this, an increase in the presence of multilamellar bodies has been observed in lysosomal structures and perinuclear lysosome clustering in fibroblasts of patients with Parkinson's disease that carry mutations in the *GBA1* gene (García-Sanz et al., 2017). These alterations in lysosomes also affect the autophagic pathway, where autophagic flux blockage has been observed in Gaucher mouse neurons (Farfel-Becker et al., 2014). Thus, considering that lysosomes are one of the most relevant organelles in sensing the homeostatic state of the cell, a better comprehension of the cellular mechanisms involved in the regulation of lysosome function is essential for the development of new therapeutic approaches to treat LSDs.

Cellular Pathways Involved in Defective Lysosome-Autophagic Axis

Lysosomes are intracellular organelles essential for the degradation and recycling of macromolecules released by endocytosis, phagocytosis, and autophagy (Appelqvist et al., 2013; Jaishy and Dale Abel 2016). These organelles not only participate in the degradation of molecules but are also highly dynamic complex organelles involved in detecting the state of cellular metabolism, controlling changes between anabolism/catabolism, participating in immune functions, plasma membrane repair, as well as cell adhesion and migration (Ballabio and Bonifacino 2020).

Autophagy provides the required molecular building blocks, such as amino acids, glucose, nucleotides, and FAs, which are used by starving cells. Additionally, autophagy regulates lipid metabolism including FAs oxidation, lipolysis, lipogenesis, ketogenesis, and cholesterol efflux (Martinez-Lopez and Singh 2015; Saito et al., 2019). Lipolysis involves the breakdown of triacylglycerols and esters by cytosolic lipases, while autophagy participates in part of this process, modulating lipoprotein trafficking, as well as, supplying and expanding lipid droplets (LDs) (Zhang et al., 2018a). However, lipid stores can also be accessed *via* lipophagy, a specific subset of selective autophagy that targets LDs and catabolizes their components into free FAs and glycerol (Kounakis et al., 2019). At present, abnormalities in lysosomal and autophagic function are associated with the pathogenesis of metabolic disorders, such as obesity and LSDs (Oyarzún et al., 2019; Wang, et al., 2017).

In this context, several studies have demonstrated the role of autophagy and lysosomes in regulating lipid storage within the two main organs that maintain lipid homeostasis: adipose and liver tissues (Christian, Sacco, and Adeli 2013; Lahiri, Hawkins, and Klionsky 2019). In fact, lipid-related disorders are characterized by a defect in the function of lysosomes that coexists both in the liver and adipose tissue, which negatively influences their metabolic function (Christian et al., 2013). In the next section, we will analyze the resulting lysosomal dysfunction and mechanisms involved including the role of cathepsins and the CD36 receptor as well as its relationship with autophagic functions.

LYSOSOMAL DYSFUNCTION COEXISTS IN ADIPOCYTES AND HEPATOCYTES IN LIPID-RELATED DISORDERS: RELEVANCE OF CATHEPSINS, AUTOPHAGY AND CD36 ALTERATIONS

Role of Cathepsins and Autophagy in Obesity

Several studies regarding lysosomal dysfunction in obese WAT and liver focus on cathepsins and autophagy function, because of their association with lipid storage (Ju et al., 2019; Mizunoe et al., 2019). Cathepsins are a group of proteases involved in intralysosomal protein degradation, which cleave different proteins and polypeptides (McGrath 1999; Turk 2001). These proteases have unique reactive-site properties and a tissue-specific expression pattern (Turk et al., 2012). The most abundant cathepsins (CTS) are L (CTSL) and B (CTSB), which are involved promoting autophagy (Kaminskyy and Zhivotovsky 2012). Moreover, they have been implicated in lysosomal dysfunction in obese murine models in adipose and liver, which display different alterations, such as, oxidative stress,

which lead to abnormal lysosomal pH (reduced acidification) (Pascua-Maestro et al., 2017). Such alterations attenuate the maturation of CSTL, causing the accumulation of autophagosomes, and the consequent, suppression of autophagic clearance (Inami et al., 2011; Mizunoe et al., 2017, Mizunoe et al., 2019). Moreover, increased CTSL and decreased CTSB expression at the transcriptional level have been recently observed in abdominal subcutaneous adipose tissue of overweight/obese men and women, but further research is required to establish whether such changes impact protein levels and activity (Xu et al., 2020).

In particular, human obese adipose tissues display high expression levels of autophagic genes, but exhibits attenuated adipocyte autophagic flux (Soussi et al., 2016; Mizunoe et al., 2017). A recent study revealed that omental adipose tissue of obese individuals and adipocytes treated with TNFα, a cytokine secreted within the adipose tissue microenvironment in obesity show an upregulation of lysosomal/autophagic genes (Ju et al., 2019). In contrast, this proinflammatory factor promotes autophagic flux and increases basal lipolysis, impairing triglyceride storage, where CTSB was required for the autophagic process (Ju et al., 2019). In fact, *CTSB* and *CTSD* gene expression are upregulated in obese WAT (Mizunoe et al., 2020). Lipolysis is exacerbated during obesity in WAT and induced overexpression of *CTSB* gene expression in adipocytes displays an increased basal lipolysis (Gaidhu et al., 2010; Mizunoe et al., 2020). Therefore, CTSB has been proposed as a therapeutic candidate for obese WAT. Autophagy is essential for the correct function of adipocytes. Accordingly, it has been reported that inhibition of autophagy by ATG5 or ATG7 knockdown or pharmacological inhibition in preadipocytes, impair their differentiation into mature WAT and lipid storage capacity (Zhang et al., 2016). Nevertheless, it remains to be determined whether upregulation of the expression of genes related to autophagy is sufficient to increase autophagic flux. There is currently a discrepancy regarding the effects on autophagy (enhanced or diminished) in adipose tissue of obese individuals, gene-modified obese animals or diet induced obesity models (García-Barrado et al., 2020). This has been discussed in detail by Zhang et al., 2018b; Zhang et al., 2018a).

Additionally, HFD or FAs exposure induces lysosomal membrane permeabilization in adipose tissue, leading to the release of lysosomal proteases, such as CTSB. The increase of cytosolic CTSB affects mitochondria, increasing ROS production and inducing mitochondrial dysfunction (Gornicka et al., 2012). In fact, *CTSB*$^{-/-}$ mice showed protection against adipocyte cell death (Gornicka et al., 2012). Interestingly, distinct cellular models have shown that cytosolic CTSB and CTSD participate in the degradation of the pro-apoptotic mediator Bid, which result in its activation and translocation to mitochondria. This translocation leads to cytochrome C release from mitochondria followed by caspase activation, triggering apoptotic cell death (Droga-Mazovec et al., 2008; Yadati et al., 2020). Therefore, we suggest that adipocytes could exhibit a similar mechanism, where cathepsins liberated to the cytosol due to lysosomal impairment induce mitochondrial damage and cell death, thus exacerbating lysosome dysfunction and cell damage. Overall, the role of autophagy and the participation of cathepsins in adipocyte function remains unclear.

In hepatocytes, ER stress alkalinizes lysosomal pH, which reduces the activity of CTSL, CTSB and CTSD, causing the accumulation of autophagosomes and suppressing autophagic clearance, which is associated with hepatic inflammation (Koga et al., 2010; Mizunoe et al., 2019). In line with these findings, autophagy-related proteins were also decreased in the liver of obese mice (Yang et al., 2010; Tong et al., 2019). On the other hand, extracellular CTSD function is relevant in the accumulation of hepatic lipids and intracellular CTSD is involved in essential processes, such as mitochondrial oxidative phosphorylation and electron transport function (Yadati et al., 2021). Recently, it was described that administration of the extracellular CTSD inhibitor reduced hepatic triglyceride levels in mice fed with a HFD, whereas intracellular or the extracellular CTSD inhibitor decreased hepatic cholesterol levels (Yadati et al., 2021). With these results the authors concluded that extracellular CTSD is involved in pathways related to lipids and inflammation.

Similar to adipocytes, a HFD also induces lysosomal membrane permeabilization and lipotoxicity in the liver of mice with NASH and NAFLD (Feldstein et al., 2006; Fucho et al., 2014). It has been reported that lysosome permeabilization is mediated by Bax, a pro-apoptotic mediator, which induces the release of cytosolic cathepsins (Feldstein et al., 2006). This results in caspase activation or mitochondrial membrane permeabilization mediated by caspase activation, triggering apoptosis and liver injury (Feldstein et al., 2006; Fucho et al., 2014; Jaishy and Dale Abel 2016).

Overall, these reports suggest that in obesity, autophagy is mostly downregulated in adipose tissue and in the liver. Also, that cathepsins are relevant in mediating the autophagy process and their release to the cytosol contributes to lysosome and cellular dysfunction through mitochondrial damage. However, more studies are needed to clarify the role of cathepsins in lysosomal dysfunction in these tissues in the context of obesity.

At present, several studies have focused on alterations in lysosomal distribution and dynamics, motility, and autophagic function involved in a variety of conditions, such as neurodegenerative diseases, cancer, and obesity (Seranova et al., 2017; Oyarzún et al., 2019). However, as expected, lysosomal dysfunction is also a common feature in LSDs, and their functional implications will be discussed in the following section.

Role of Cathepsins and Autophagy in Niemann-Pick Type C

This section will focus on the role of cathepsins and autophagy in hepatocytes in the context of NPC and Gaucher diseases, considering that most of the studies have been performed in the liver. An increase in the expression of CTSB, CTSD, CTSS, and CTSZ were recently observed in the liver and hepatocytes of *Npc1*$^{-/-}$ mice (Balboa et al., 2021; van der Lienden et al., 2021), suggesting that lysosomal proteases were increased. However, *Npc1*$^{-/-}$ mouse embryonic fibroblasts showed increased levels of mature CTSB and CTSD and normal lysosomal proteolytic

functions, suggesting that they remained unaffected (Sarkar et al., 2013). Interestingly, impaired clearance of autophagosomes has been observed in human dermal fibroblasts with mutations in *Npc1* and fibroblasts of *Npc1*$^{-/-}$ mice, which correlated with an inhibition of lysosomal protease activity produced by stored lipids (Elrick et al., 2012). In fact, NPC1-deficient lysosomes derived from HEK293T cells have proteolytic defects, where inhibition of mTORC1 by genetic and pharmacologic manipulation restores lysosomal proteolysis without correcting cholesterol storage (Davis et al., 2021). Regarding autophagic vesicle accumulation, an increase in levels of LC3-II (light chain 3 of microtubule-associated protein 1), a specific autophagosome maker, has been reported in the cerebellum, the hippocampus and livers of *Npc1*$^{-/-}$ mice as well as mouse embryonic fibroblasts (Pacheco et al., 2007; Sarkar et al., 2013; Meske et al., 2014). In addition, NPC1 iPSC (patient-specific induced pluripotent stem cells) show dysfunctional autophagic flux, where LC3-II and p62, an autophagy adaptor protein responsible for cargo delivery of ubiquitinated substrates, were significantly increased (Maetzel et al., 2014). However, it remains unclear whether an increase in the number of autophagosomes results from an increase in autophagic activity or a reduction in autophagy flux caused by impaired autophagosome-lysosome fusion (Dai et al., 2017). On the other hand, lysosome membrane permeabilization has been observed in NPC disease (Chung et al., 2016). As we have described before, lysosomal permeabilization promotes cytosolic release of CTSD, which triggers apoptosis in adipose and liver tissues of mice fed with a HFD. Interestingly, hippocampal neurons incubated with U18666A (a classic NPC1 inhibitor) have increased levels of *CTSD* mRNA and enzyme activity, which is associated with neuronal apoptosis (Amritraj et al., 2013). However, it has been reported that early lysosomal cholesterol accumulation induced by U18666A in human fibroblast attenuates apoptosis by preventing lysosome permeability and reducing CTSD release from lysosomes (Appelqvist et al., 2011). Cholesterol overload ultimately triggers lysosome membrane permeabilization, which disrupts lysosome homeostasis. Hence, we speculate that NPC livers could exhibit a similar mechanism thus contributing to lysosome dysfunction, but this remains to be investigated.

Role of Cathepsins and Autophagy in Gaucher Disease

Cathepsins have not been extensively studied in GD. However, in neuronopathic forms of GD changes in the subcellular distribution of CTSD have been detected in the brain and as well as an increase of CTSD in areas with neuronal loss, astrogliosis, and microgliosis, suggesting a role for CTSD in neuronal injury (Vitner et al., 2010). Also, GD mouse models show an increase of CTSD and CTSS in the liver and spleen, whereas patients with GD show increased serum levels of both proteases (Mistry et al., 2010; Afinogenova et al., 2019). Similar to NPC disease, there is evidence suggesting that autophagy is defective in GD. Primary fibroblasts deficient in saposin C have impaired autophagosome degradation associated with reduced CTSB and CTSD activity (Tatti et al., 2012; Seranova et al., 2017). Defects in the maturation and accumulation of autophagosomes including autophagic cargo were found in neurons and astrocytes cultured from mice deficient for glucocerebrosidase, prosaposin or glucosylceramidase (Farfel-Becker et al., 2014; Seranova et al., 2017). Additionally, LAMP2 and p62 accumulate in the brain of neuronopathic GD mouse models suggesting that autophagosome/lysosome function is compromised (Sun et al., 2010). In contrast, fewer autophagic vacuoles have been reported in peripherical blood mononuclear cells derived from GD patients with an increase of cytoplasmic localization of LC3A/B. This was accompanied by lysosome accumulation suggesting that constitutive autophagy is inactivated (Ivanova et al., 2019). In addition, neuronal mouse models of glucocerebrosidase deficiency showed a redistribution of CTSD from the lysosome to the cytosol suggesting that these cells also contain lysosomes with permeabilized membranes (Serrano-Puebla and Boya 2016). Similar to what was discussed in NPC disease, this cytosolic cathepsin may be promoting the mitochondrial damage that is observed in Gaucher disease (Cleeter et al., 2013; Osellame et al., 2013). Altogether, these data indicate common mechanisms coexisting among these diseases, where the functional deterioration of cathepsins is associated with impaired autophagy and their cytosolic distribution by lysosome membrane permeabilization is directly linked with lysosomal dysfunction and cellular damage (**Figure 1**).

Lysosomal Dysfunction in Obesity, Role of CD36 in Adipocytes and Hepatocytes

CD36 is a multifunctional immuno-metabolic receptor that belongs to the family of class B scavenger receptors. This receptor is primarily localized in caveolae and mediates FA uptake by endocytosis (Hao et al., 2020). This glycoprotein is widely expressed in tissues and different cell types, including adipocytes, hepatocytes, macrophages, monocytes, platelets, among others (Silverstein and Febbraio 2009). Scavenger receptors recognize modified self-antigens and are defined by their ability to bind oxidized-LDL, which is relevant in atherosclerosis pathogenesis, where the formation of lipid-laden foam cells promotes atherosclerotic plaques (Febbraio and Silverstein 2007; Silverstein and Febbraio 2009; Tian et al., 2020). In particular, CD36 binds these and other oxidized phospholipids, long-chain FA, and thrombospondin and its function varies according to each cell type (Gillotte-Taylor et al., 2001; Silverstein and Febbraio 2009). Evidence indicates that CD36 is not only a FA transporter but also an essential regulator of intracellular FA and immune homeostasis and has emerged as a relevant player connecting lysosomal dysfunction and lipid homeostasis alterations (Pepino et al., 2014; Rawnsley and Diwan 2020; Tian et al., 2020).

CD36 plays an important role in liver lipid homeostasis, lipophagy and autophagy, and its levels increase in hepatocytes exposed to high-fat diets as well as in hepatic steatosis and NAFLD (Bechmann et al., 2010; Love-Gregory and Abumrad 2011; Miquilena-Colina et al., 2011; Li et al., 2019). Indeed, in obesity, lipid accumulation and lysosomal dysfunction in

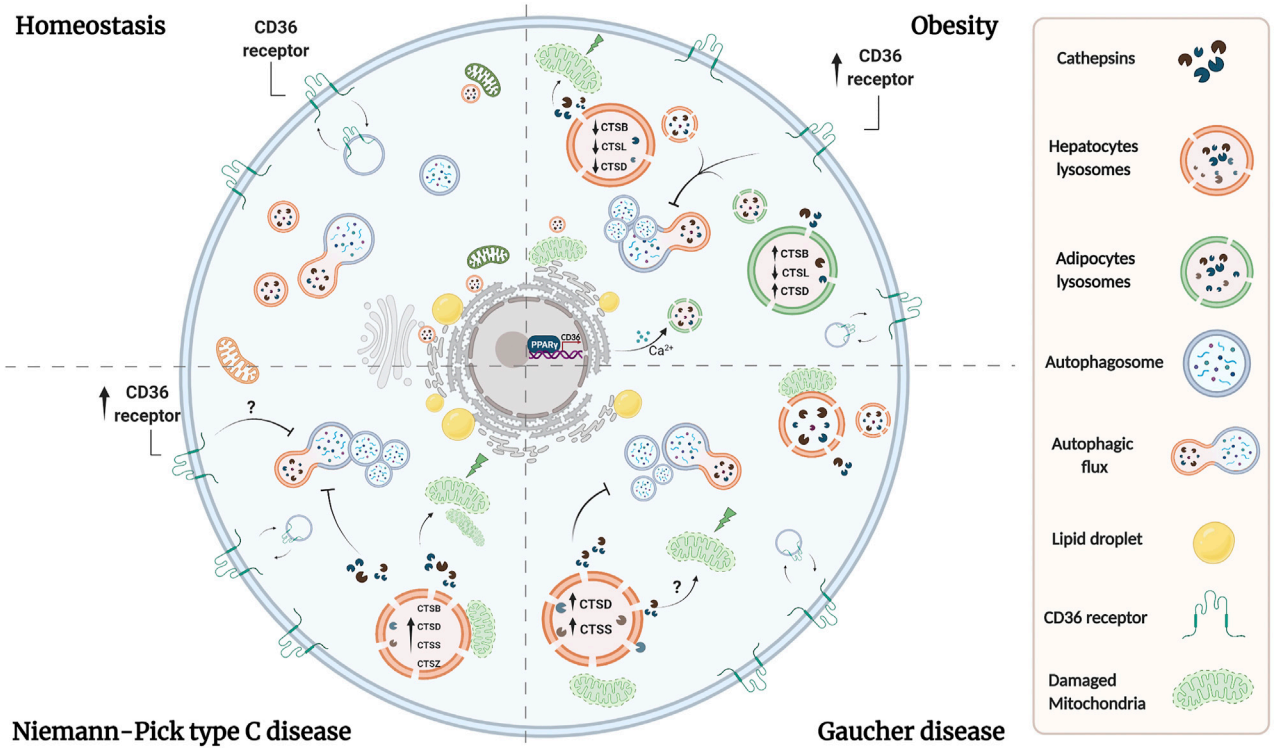

FIGURE 1 | Lysosomal dysfunction coexists in adipocytes and hepatocytes in lipid-related disorders. Overload of lipids induces permeabilization of lysosomal membrane in both adipose and liver tissues, leading to the release of lysosomal proteases. Reports have shown that cytosolic proteases increase ROS production and induce mitochondrial dysfunction, triggering apoptosis and liver injury. Whether similar alterations exist in adipocytes under these conditions, remains to be evaluated. Additionally, a imbalance in cathepsins levels exists in both tissues in obesity. Overall, obesity is associated with oxidative stress, which lead to alkalinization of lysosomal pH, causing the accumulation of autophagosomes, and suppression of autophagic clearance. In NPC and Gaucher diseases there are alterations in the levels or activity of cathepsins which are associated with proteolytic impairment and inhibition of autophagy, which altogether contribute to lysosome dysfunction probably by analogous mechanisms as those observed in obesity. On the other hand, dyslipidemia is associated with an increase in the expression of CD36 in adipocytes and hepatocytes, which leads also to an increase in lysosomal pH and an inhibition of autophagy. In adipocytes, CD36 mediates lysosomal calcium overload through the ER, and we speculate that a similar mechanism could occur in hepatocytes. Additionally, lipid uptake is mediated by an increase in CD36 expression in adipocytes and hepatocytes by PPAR-γ, which promotes lipid accumulation and contributes to lysosome dysfunction. Although the upregulation of CD36 in NPC liver has been observed, its role in NPC and Gaucher hepatic diseases remains unclear.

adipocytes and hepatocytes depends on the expression and role of CD36 (Koonen et al., 2007; Li et al., 2019; Rawnsley and Diwan 2020).

A recent study described an increase in the expression of CD36 in preadipocytes of mice fed with a HFD and also in obese patients (Luo et al., 2020). At a cellular level, CD36 was shown to interact with Fyn leading to the phosphorylation and activation of IP3R1 [inositol (1,4,5)-trisphosphate receptor 1], in FA-treated adipocytes. Consequently, an excess of calcium is transported from the ER to the lysosomes, generating an increase in lysosomal pH and in the production of inflammatory cytokines, while decreasing lipophagy and impairing lysosomal function (Luo et al., 2020; Rawnsley and Diwan 2020). Accordingly, lysosomal disruption is promoted by CD36/Fyn/IP3R1-mediated lysosomal calcium overload, which can be associated with a failure in autophagic flux observed in adipocytes of obese mice (Mizunoe et al., 2017). Additionally, activation of PPAR-γ (peroxisome proliferator-activated receptor γ), a nuclear receptor responsible for adipocyte differentiation and adipogenesis mediates FAs uptake through an increase of CD36 expression (Tontonoz and Spiegelman 2008; Cai et al., 2012). It has been reported that CD36 contributes to inflammation and cell death in adipose tissue of mice fed with a HFD (Cai et al., 2012). These findings indicate that CD36 participates in mediating the alteration of lysosomal calcium homeostasis and uptake of lipids in adipocytes, which leads to an alteration in autophagy and lysosomal function.

On the other hand, an increase in plasma LPA levels has been reported in mice fed with a HFD, which is associated with an increase in adipose tissue *ATX* (autotoxin) mRNA levels (Dusaulcy et al., 2011). Extracellular LPA is mainly produced from lysophosphatidylcholine by lysophospholipase D activity of ATX. Thus, LPA levels are closely related to the ATX protein content and/or activity (D'Souza et al., 2018; Ferry et al., 2003). The ATX-LPA pathway may contribute to obesity-induced insulin resistance by stimulating fibrosis, inflammation, and/or suppressing BAT, mitochondrial function and impairing PPAR-γ expression and activity. This last idea is supported by studies showing that mice with *ATX* deletion fed with an obesogenic diet present an increase in *PPAR-γ* mRNA levels (Dusaulcy et al.,

2011; D'Souza et al., 2018). Although, the data suggest that the ATX-LPA axis reduces PPAR-γ function, the specific mechanisms by which it contributes to obesity remains to be elucidated (Jose and Kienesberger 2021). In contrast, it has been reported that obese individuals have higher *PPAR-γ* mRNA levels, which contributes to an increase in the numbers of adipocytes (Vidal-Puig et al., 1997; McCann and Ratneswaran 2019). Interestingly, activation of PPAR-γ induces an increase in the number of small and insulin-sensitive adipocytes and up-regulates adiponectin, improving insulin sensitivity in the liver and muscle (Jakab et al., 2021). Therefore, more research is needed to address the precise role of ATX-LPA signaling and the PPAR-γ function in adipose tissue under obesity.

Additionally, studies have shown that the expression of CD36 under a HFD negatively regulates autophagy in hepatocytes. In mice with NASH, translocation of CD36 to the plasma membrane in hepatocytes is associated with lower AMPK (adenosine monophosphate-activated protein kinase) activity and lower FA oxidation (Zhao et al., 2018). Conversely, CD36 knockout mice fed with a HFD show increased autophagy/lipophagy, which promotes lipolysis and FAs catabolism by β-oxidation to produce energy, attenuating the accumulation of lipids (Li et al., 2019). In this report, the authors suggest that CD36 deficiency results in an increase in autophagy, which is correlated with a rise in the translocation of TFEB to the nucleus. Indeed, an increase in nuclear TFEB was observed upon knockdown of CD36 in human hepatoma cells in the presence of palmitic acid; however it was not quantified. In line with this work, inhibition of the internalization of CD36 by a deficiency of SNX10 (Sorting Nexin 10, a protein involved in protein sorting and membrane trafficking in endosomes) in lipid tissue-resident macrophages, suppresses the Lyn-AKT signaling pathway, which results in increased translocation of TFEB to the nucleus and enhances the function of the autophagy-lysosome system (Fan et al., 2020; You et al., 2020). Overall, one could speculate that, under obesity, translocation of TFEB could be inhibited in hepatocytes, thus decreasing the expression of genes related to lysosomal biogenesis and autophagy. This also suggests that an increase in CD36 expression in hepatocytes could cause an alteration of lysosomal calcium homeostasis as observed in adipocytes, enhancing lysosomal dysfunction.

Interestingly, the levels of CD36 in the liver are much higher in *ATG5*$^{-/-}$ mice, suggesting that the autophagy machinery also regulates CD36 expression (Li et al., 2018). Alternatively, in adipocytes, silencing of ATG5 led to a deterioration in the accumulation of triglycerides during adipogenesis and the inhibition of autophagy (Singh et al., 2009; Clemente-Postigo et al., 2020). The latter suggests that, in obesity, an increase in the expression of CD36 in adipocytes may be dependent on ATG5, which would contribute to the inhibition of autophagy through the aforementioned mechanisms.

On the other hand, elevated levels of plasma FA, induced by FA-rich diets, contribute to hepatic insulin resistance, increased glucose production and hepatic steatosis (Seppala-Lindroos 2002). Accordingly, it was shown that hepatocytes from obese rats require high insulin levels to translocate CD36 to the plasma membrane to improve the uptake of FA and the synthesis of triglycerides (Buqué et al., 2012). The authors of this work propose that hyperinsulinemia present in animal models and patients with insulin resistance and fatty liver may contribute to an increase in the expression of CD36 and in the accumulation of fat in the liver (Buqué et al., 2012). Conversely, CD36 deficiency decreased insulin resistance in primary adipocytes isolated from HFD-fed mice (Kennedy et al., 2011; Luo et al., 2020). Thus, based on the above, the expression of CD36 would also modulate the levels of insulin resistance. Consequently, high insulin levels observed in obesity may contribute to lysosomal dysfunction by generating an increase in the expression CD36, which together contribute to obesity-associated dyslipidemia.

Alternatively, similar to what was discussed in adipose tissue, several studies have shown that the hepatic expression of CD36 is positively regulated by activation of PPAR-γ under conditions of nutrient overload (Jung, Zhou, and Xie 2008; Pettinelli and Videla, 2011; Wang et al., 2020a; Yu et al., 2021). Interestingly (Yu et al., 2021), showed that hepatic extracellular galectin-3 promotes fatty acid uptake through CD36 in a PPAR-γ pathway-dependent manner (Yu et al., 2021). Indeed, galectin-3 is a lectin involved in liver inflammation, fibrosis, and related metabolic disorders (Iacobini et al., 2011; Pejnovic et al., 2013). Moreover, it has been reported, that hepatic extracellular galectin-3 is upregulated in NASH and its inhibition in mice fed with a HFD, reduced hepatic CD36 expression, the accumulation of lipids and hepatic steatosis (Iacobini et al., 2011; Yu et al., 2021). These findings indicate that CD36 expression in obese liver tissues is regulated by activation of PPAR-γ through galectin-3.

On the other hand, it has been reported that LPA is an agonist of PPAR-γ (McIntyre et al., 2003). LPA upregulates CD36 expression on the surface of monocytes through PPAR-γ stimulation and induces lipid accumulation through oxidized-LDL absorption (McIntyre et al., 2003). However, this mechanism has not yet been described in hepatocytes. Interestingly, LPA is involved in the progression of liver fibrosis, so it has been proposed as a therapeutic target (Kaffe et al., 2019). Therefore, we suggest that LPA (which increases with the overload of lipids) could participate as an agonist of PPAR-γ, promoting an increase in fatty acid uptake by CD36 in hepatocytes. Nevertheless, more research is required to demonstrate whether this mechanism contributes to lysosome dysfunction in obesity.

Concerning NPC disease, proteomic analysis from hepatocytes of *Npc1*$^{-/-}$ mice, performed by our group, showed an increase in the levels of CD36 protein levels (Balboa et al., 2021). Increased transcript levels of the CD36 in hepatocytes of *Npc1*$^{-/-}$ mice have been observed by our group and others (Vázquez et al., 2011; Dos Reis et al., 2020). Intriguingly, galectin-3 is increased in liver tissues from *Npc1*$^{-/-}$ mice (Cluzeau et al., 2012). In this sense, we propose that this galectin could be mediating lysosomal dysfunction by increasing CD36 expression through the PPAR-γ pathway.

Alternatively, LPA accumulation in liver tissues of *Npc1*$^{-/-}$ zebrafish, which reproduces the pathological features of NPC disease has been reported (Lin et al., 2018). Recently, lipidomic studies of liver tissue from *Npc1*$^{-/-}$ mice showed an increase of BMP (Pergande et al., 2019). However, they do not analyze the

levels of LPA. Based on this, it is possible to speculate that the hepatic levels of LPA increase in *Npc1*$^{-/-}$ mice. Under this scenario, we suggest that LPA may also promote the expression of CD36 in NPC hepatocytes through the PPAR-γ pathway (similar to what was discussed in obesity), promoting lysosome dysfunction. However, this requires further investigation.

On the other hand, BMP levels are increased in fibroblasts pretreated with U18666A, in fibroblasts derived from NPC1 patients, and fibroblasts and livers of *Npc1*$^{-/-}$ mice (Appelqvist et al., 2011; Moreau et al., 2019; Ilnytska et al., 2021). Interestingly, NPC1-deficient human fibroblasts incubated with BMP show a reduction in lysosomal cholesterol levels, which was associated with a direct interaction between BMP and NPC2, leading to an increase in lysosomal cholesterol efflux (McCauliff et al., 2019). This suggests that the increase in BMP compensates lipid accumulation at early stages until BMP production and the endosomal system collapse under lipid overload (Liu et al., 2014).

Interestingly, BMP levels were shown to be elevated in skin fibroblasts and plasma samples from patients with Gaucher disease (Meikle et al., 2008). However, its relevance remains unclear. Additionally, there are few studies that have evaluated the levels of LPA in Gaucher disease. LPA plasma levels seem to increase in Gaucher patients, but the results are not conclusive due to the low number of samples (Byeon et al., 2015). Overall, alterations in the expression or function of CD36 have not been reported in adipocytes in NPC or in Gaucher disease. Nevertheless, based on the evidence described in obesity, we speculate that CD36 expression and function could also be compromised in GD adipocytes and hepatocytes. Therefore, elucidating the role of CD36 may contribute to a better understanding of the dysregulated lysosomal function observed in both diseases.

Taken together, these findings show that in obesity, adipocytes and hepatocytes express higher levels of CD36, which leads to defective lysosome homeostasis and negatively regulates autophagic function. Thus, it is possible to speculate that CD36 could participate in the modulation of lysosomal dysfunction in NPC and Gaucher diseases (**Figure 1**). However, the mechanism by which these processes are controlled, requires further investigation.

ROLE OF LYSOSOMES IN THE IMMUNE RESPONSE OF B CELLS: IMPACT OF LIPID-RELATED DISORDERS

In recent years, several studies have suggested that B cells are also involved in adipose and liver tissues inflammation contributing to the pathogenesis of obesity. B cells are activated in adipose tissue during obesity (Shaikh et al., 2015; Srikakulapu and McNamara 2020) and in HFD-fed mice, these cells migrate to the liver, promoting inflammation, where macrophage differentiation to pro-inflammatory phenotypes secrete pro-inflammatory cytokines (Wu et al., 2019). Additionally, intrahepatic B cells might be involved in NAFLD by secretion of pro-inflammatory cytokines and IgG2a, a potent inducer of antibody-based inflammation (Zhang et al., 2016). Importantly, lysosomal function is critical for B cell activation during antigen recognition (Obino et al., 2017; Sáez et al., 2019). The question then arises as to whether such B cell functions are affected in obese patients. It is then necessary to understand how B cell activation occurs and the importance of lysosomes during this process.

B cell activation occurs when the B cell receptor (BCR) recognizes immobilized antigens on antigen-presenting cells, triggering an immune synapse. Activation of the BCR induces a signaling cascade that promotes the recruitment of lysosomes to the synapse, which depends on centrosome repositioning. These lysosomes fuse with the synaptic membrane, secreting their acidic content, facilitating the extraction, and processing of antigens. Activation of B cells induces an increase in the synthesis of MHC-II (type II major histocompatibility complexes) (Lankar et al., 2002; Yuseff et al., 2011). The synthesis of these molecules begins in the ER, where the αβ dimers of MHC-II are associated with an invariant chain that prevents binding to peptides and promotes their transport towards endo-lysosomes (Roche and Cresswell 1990). In this compartment, the invariant chain undergoes proteolysis by CTSS, an asparaginyl endopeptidase, generating a smaller fragment called CLIP. Subsequently, the H2DM chaperone catalyzes the exit of CLIP and the loading of the generated peptides into the MHC-II pocket (Lankar et al., 2002; Blum, Wearsch, and Cresswell 2013). Once the peptides are assembled, the MHC-II molecules are transported to the surface of B cells to be presented to the CD4$^+$ T lymphocytes to promote B-T cell cooperation (Lanzavecchia 1985; Mitchison 2004). This allows co-stimulation and proliferation of both cells and the differentiation of B cells into plasma cells that produce specific antibodies (Harwood and Batista 2010; Yuseff et al., 2011). The impact of lipid accumulation in lysosome function, as well as, in antigen extraction and presentation by B cells, remains to be addressed (**Figure 2**).

Role of CD36 in B Cells in Obesity

As previously mentioned, CD36 is expressed in adipocytes and hepatocytes, but has also been detected in immune cells, such as macrophages and dendritic cells as well as T and B cells (Urban et al., 2001; Corcoran et al., 2002; Won et al., 2008; Couturier et al., 2019). A study published recently by He et al. (2021) demonstrated that all peripheral human blood B cell populations express intracellular CD36 except naïve B cells (He et al., 2021). They found that CD36 colocalizes with LC3B upon the induction of autophagy and splenic B cells increase CD36 expression and autophagosome formation after LPS stimulation *in vitro*. Interestingly, B cells from CD36$^{-/-}$ mice have less autophagosome formation upon LPS stimulation (He et al., 2021) and exhibit defects in mitochondrial mobilization and also oxidative phosphorylation (He et al., 2021), as well as, reduced plasma cell formation, subsequent antibody production and proliferation. Remarkably, the expression of CD36 increases in T lymphocytes of adipose tissue and in the liver of mice fed with a HFD, but it is unclear whether it is preferentially expressed by a specific subset of cells (Couturier et al., 2019). However, the authors propose that there could also be an increase in the expression of CD36 in natural killer and B cells in these tissues (Couturier et al., 2019).

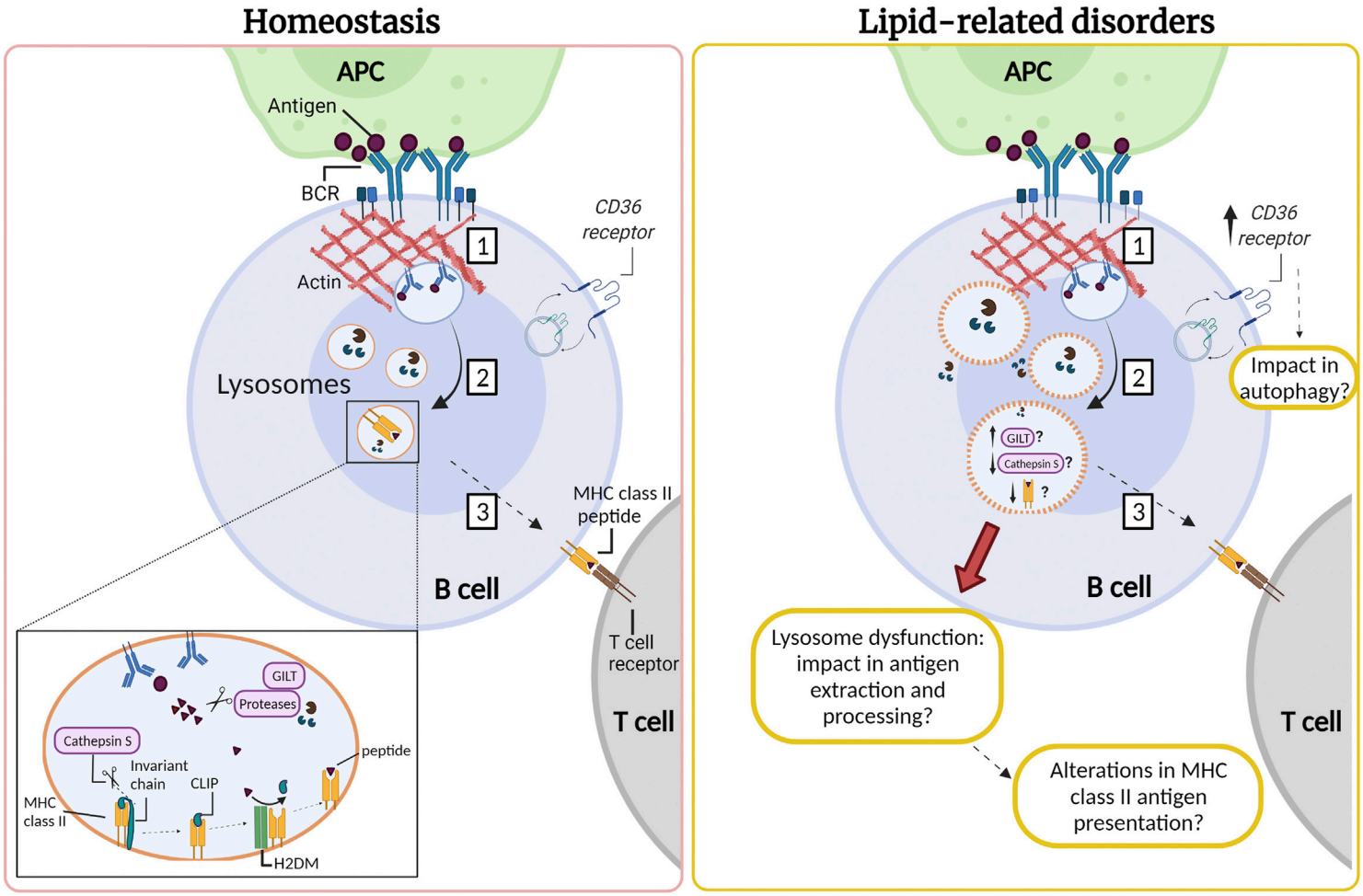

FIGURE 2 | Lysosomes are required for antigen processing in B cells: impact of lipid-related disorders. (1) The interaction of the B cell receptor (BCR) with antigens tethered at the surface of an antigen presenting cell (APC) gives rise to an immune synapse. Activation of the BCR triggers signaling cascades which induce extensive remodeling of the actin cytoskeleton at the synaptic interface, promoting membrane extensions and efficient BCR-antigen internalization into late endosomal compartments. (2) BCR-antigen converges into lysosomes which contain the accessory molecules, such as GILT, H2DM, proteases and MHC class II. MHC class II molecules are associated with the invariant chain, which undergoes proteolysis by cathepsin S generating a smaller fragment called CLIP. Subsequently, the H2DM chaperone catalyzes the exit of CLIP and the loading of antigenic peptides into the MHC-II pocket. (3) Next, MHC-II molecules are transported to the surface of the B cell to be presented to the $CD4^+$ T lymphocyte to promote B-T cell cooperation. We speculate that B cells that infiltrate the inflamed adipose and liver tissue in lipid-related disorders could also present lysosomal dysfunction resulting in lower cathepsin S levels or activity. Moreover, B cells might exhibit permeabilization of their lysosome membrane, similarly to observations in other cell types in lipid-related disorders. We suggest that in obesity there could also be an increase in the expression of CD36, which may be enhanced upon B cell activation. This might impact in autophagy, enhancing the canonical pathway and diminishing noncanonical autophagy. Such defects could impact the capacity of B cells to extract and process antigens, which relies on lysosome integrity. However, these functions remain to be evaluated and the question that arises is how are lysosomes in B cells affected by an excess of nutrients in obesity and LSDs?

As mentioned above, CD36 increases its expression under a HFD inhibiting autophagy in adipocytes and hepatocytes. In obesity, we speculate that B cells could also display elevated expression levels of CD36, which could regulate autophagy during their activation. B cell activation triggers a temporary change from basal to non-canonical autophagy, which is essential to control B cell differentiation (Martinez-Martin et al., 2017). Under these conditions, components from the autophagic machinery can be recruited to other pre-existing membranes, different from the phagophore, where they generally reside (Martinez-Martin et al., 2017). In this sense it has been described that ATG5 is necessary for the internalization and trafficking of BCR towards LAMP1 and MHC-II positive compartments, as well as for the optimal presentation of antigens to T cells (Arbogast et al., 2019). Additionally, it has been shown that activation of B cells with BCR ligands produces the colocalization of LC3 with the BCR and with MHC-II vesicles, showing an association of autophagic vesicles involving BCR and the MHC-II-mediated antigen presentation (Ireland and Unanue 2011). Therefore, it is tempting to speculate that in obesity there is an increase in the expression of CD36, which may be enhanced upon B cell activation. This may cause an imbalance in autophagy, enhancing the canonical pathway and diminishing noncanonical autophagy. In this sense, this could alter the lysosomal function, impairing the processing and presentation of antigens to T cells, as well as plasma cell formation and subsequent antibody production.

In contrast, B cells are also involved in adipose and liver tissue inflammation contributing to the pathogenesis caused by obesity. Several studies have shown that B cells in adipose and liver tissues in HFD-fed mice, enhance the activation of $CD4^+$ T lymphocytes and their differentiation into T helper (Th) 1 cells (Winer et al., 2011; Zhang et al., 2016). Interestingly, it has been reported that obese patients have low levels of PPAR-γ mRNA in peripheral blood mononuclear cells and protein levels in serum (Ramon et al., 2012). PPAR-γ-deficient T cells are hyperreactive to T cell receptor stimulation, which promotes greater B cell activation, thereby leading to autoantibody production (Park et al., 2014). We speculate that an imbalance in PPAR-γ activity in B cells in obesity could lead to the aforementioned defects. Thus, clarifying the role of PPAR-γ and its functional relationship with CD36, should help elucidate how a lipid overload impacts B cell activation, and affects antigen presentation to $CD4^+$ T lymphocytes.

Role of Cathepsins in B Cells in Obesity

Based on the role of cathepsins involved in antigen processing, it has been reported that gamma-interferon-inducible lysosomal thiol reductase (GILT) facilitates antigen processing since it reduces the disulfide bonds of proteins in the endo-lysosomal compartment. It has been hypothesized that the reduction of protein disulfide bonds that pass through the endocytic pathway may facilitate the processing of hidden epitopes so that they are not restricted by MHC-II (Singh and Cresswell 2010). As described previously, CTSS is essential for MHC-II processing and has disulfide bonds susceptible to this reduction since it is found in the lysosome together with GILT (Phipps-Yonas et al., 2013). Expression of GILT in primary B cells derived from mice decreases the expression and activity of CTSS but does not substantially alter the expression of other lysosomal proteins, such as H2DM, H2DO and CTSL (Phipps-Yonas et al., 2013). Interestingly, a transcriptomic study showed that the gene encoding for GILT was 1.72 times more expressed in the omental adipose tissue of severely obese men with metabolic syndrome compared to those without the syndrome (Turcot et al., 2012). Therefore, it is possible to speculate that dyslipidemia caused by obesity could induce an increase in the expression of GILT, and consequently a defect in lysosomal function by reducing the expression and activity of CTSS. Consistent with the previous idea, it has been reported that antigen presentation is defective in B cells derived from $CTSS^{-/-}$ or $CTSL^{-/-}$ Mice (Nakagawa et al., 1999). Additionally, CTSS regulates the level of mature CTSL in B cells, since it was shown that CTSL levels increase in the absence of CTSS, but in this study the activity of this enzyme was not detected (Honey et al., 2001). Thus, it is possible that a lower expression of CTSS could induce a dysregulation of CTSL, which could lead to a decrease in antigen processing, also altering the presentation of antigenic peptides on MHC-II to the T cells. As described in the previous section, reduction in levels of CTSL has been observed in adipose tissue and the liver in obesity. On the other hand, similar to what was discussed in obesity, B cells might exhibit permeabilization of their lysosome membrane. Such defects could impact the capacity of B cells to extract and process antigens, which relies on lysosome integrity. Based on these studies, it would be relevant to study the role of CD36 and/or cathepsins in B cell function associated with obesity.

Alteration of B Cell Functions in NPC and GD Diseases

In the majority of LSDs the pathology is primarily neuronal, but the immune system has also been implicated and predisposed towards suppression (Castaneda et al., 2008; Platt et al., 2016; Rigante et al., 2017). Lysosomal glycosphingolipid storage increased has been shown in splenic B cells derived from $Npc1^{-/-}$ mice and peripheral B cells from NPC1 patients (Lachmann et al., 2004; Vruchte et al., 2010). Additionally, results from our group showed that B lymphocytes treated with U18666A, exhibit lysosomal accumulation of unesterified cholesterol (Oyarzún et al., 2019) The lysosomes of NPC cells show a typical and concentrated perinuclear pattern, which results from an increase in the reverse transport of lysosomes, and their perinuclear clustering (Oyarzún et al., 2019). This is a key factor, because the correct distribution and motility of lysosomes promote a functional immune synapse between B cells with antigen-presenting cells. Also, the fusion of endolysosome compartments required to facilitate antigen uptake from presenting cells, is critical to achieve an efficient adaptive immune response (Yuseff et al., 2015). In fact, an excess of lipids in lysosomes of B cells might also promote the permeabilization of their lysosome membrane. However, these functions remain to be evaluated and the question that arises is how are lysosomes in B cells affected by an excess of lipid in LSDs? Thus, alterations in lysosome localization and function

could have an impact in B cell activation and its effector functions in NPC disease.

Levels of cytokines and chemokines are increased and participate in the initiation and propagation of the molecular pathogenesis of GD. The excess of glucosylceramide in GD cells can trigger and activate the release of interferon-γ, interleukin 4 and 6, and transforming growth factor-β by macrophages and dendritic cells. This promotes the development of T helper and follicular helper T cells required for the formation and activation of germinal centers that drive B-cell differentiation and thus have an impact on immunoglobulin (IgG, IgA, and IgM) production, triggering hypergammaglobulinemia, which contributes to inflammation (Fazilleau et al., 2009; Pandey and Grabowski 2013; Nguyen et al., 2020). Additionally, the accumulation of lipid rafts and glycosphingolipid storage in B cells in GD and NPC, leads to degradation of lipid raft-associated B cell receptor and thus altered immune responses (Vruchte et al., 2010). In fact, we speculate that it could disrupt BCR-dependent signaling and activation, which can be associated to the decrease in B cell levels observed in GD patients (Limgala et al., 2016). Alternatively, several patients with GD develop neoplasms and altered B-cell proliferation by mechanisms yet to be discovered (Pandey and Grabowski 2013; Cox et al., 2015). Thus, it is important to investigate the contribution of B cell functions and the implication of cathepsins and CD36 under the context of these diseases, where alterations in homeostatic pathways could converge in lysosomal dysfunction and their pathophysiological progress.

EMERGING CELLULAR MECHANISMS IN THE CONTROL OF LIPID HOMEOSTASIS: INTER-ORGANELLE CONTACTS

Recent studies have highlighted the importance of organelle contacts in mediating intracellular lipid flux. Compartments such as lysosomes, ER, mitochondria, Golgi complex, and lipid droplets physically interact and communicate with each other, but preserve their compartmentalization without membrane fusion. This form of communication has been denominated Membrane Contact Sites (MCSs), consisting of regions of apposition between two organelles (with a distance between 10 and 30 nm) through anchoring proteins, thus modulating the function of one or both compartments (Ballabio and Bonifacino 2020; Prinz et al., 2020). In recent years, MCSs have gained notorious interest because they are a communication system different from the diffusion of metabolites through membranes and vesicular transport; however, there is still much to be elucidated about the mechanisms that regulate their formation. Nonetheless, among the main functions described for MCSs are signaling between organelles, regulation of membrane dynamics, metabolic channeling, and lipid transport (Prinz et al., 2020). Therefore, alterations in lysosomal homeostasis and function due to lipid accumulation may have far-reaching consequences in communication and cross-regulation between organelles. Interestingly, inter-organelle contacts are involved in the pathogenesis of diseases that present alterations in cholesterol or triglyceride levels, as in obesity, NPC and Gaucher diseases.

Liver: Inter-organelle Contacts and Lipid Homeostasis in Obesity

Inside the cell, the nutritional context modulates mitochondria-ER membrane contacts, and alterations in this status induce a misbalance in lipid and glucose metabolism (Rieusset 2017). Accordingly, obesity leads to an increase in ER-mitochondrial interactions, resulting in mitochondrial calcium overload, compromised mitochondrial oxidative capacity, and increased oxidative stress, thus accelerating obesity-related pathologies, such as hepatic steatosis and glucose intolerance (Arruda et al., 2014).

Additionally, a recent study showed that the contact between mitochondria and the ER regulates the synthesis of VLDL in response to changes in lipid flux (Anastasia et al., 2021). This was evidenced after observing that hepatic depletion of the ER-resident Microsomal Triglyceride Transfer Protein (MTP), which plays a crucial role in VLDL biogenesis, promotes a phenotype reminiscent of hepatic dyslipidemia, as well as mitochondria wrapped by curved sheets of rough ER increasing the contact regions between them. This alteration reduces VLDL biogenesis and redirects hepatic free FAs flux towards LDs (Kozlitina et al., 2014; Anastasia et al., 2021). This is consistent with what has been described previously, where the accumulation of LDs increases the risk of metabolic disorders such as obesity and insulin resistance (Gross and Silver 2014; Wang et al., 2020b). In this sense, the authors conclude that there is a connection between intracellular and systemic control mechanisms to maintain lipid homeostasis (Anastasia et al., 2021).

On the other hand, a relevant type of membrane contact in lipid homeostasis is one formed by LD in tissues highly sensitive to lipid levels such as liver tissue. Interestingly, Krahmer et al. (2018) observed changes in the formation of MCSs in hepatocytes derived from HFD-fed mice and in the proteome associated with LDs. In this context, they found increased mitochondria-LDs contacts and increased binding of proteins belonging to different intracellular organelles (including those involved in MCSs between other organelles) to the surface of LDs. This highlights the tight modulation of metabolic processes by MCSs (Krahmer et al., 2018) (**Figure 3**).

Overall, these observations reinforce the notion that at least part of the intracellular mechanisms are altered during obesity in tissues that are key to metabolism, resulting from alterations in the communication of intracellular compartments. Considering that MCSs constitute a communication system based on the dynamic, efficient, and rapid transfer of lipids plus other metabolites, these contacts may be part of a central mechanisms underlying alterations in metabolic homeostasis.

Alterations of Inter-Organelle Contacts Sites in Dysfunctional Lysosomes in NPC and Gaucher Diseases

It is well known that MCSs between the ER and lysosomes are necessary to mediate intracellular homeostasis of cholesterol. Additionally, recent evidence in CHO and HeLa cells has shown that LDL-c can be transferred through contact regions established between the NPC1 transporter and the ER-localized

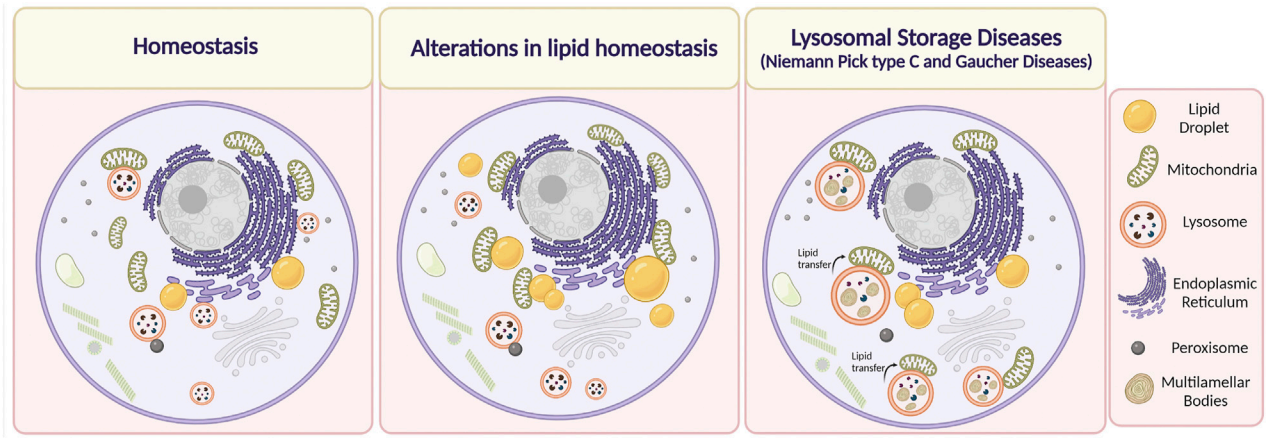

FIGURE 3 | Alterations in Membrane Contact Sites (MCSs) in lipid-related disorders. Under physiological conditions, the organelles are in close contact with each other depending on cell requirements. It has been described that alteration in lipid homeostasis, such as in the case of obesity, dyslipidemias, or after the administration of a high-fat diet induce an increase in MCSs between mitochondria and lipid droplets, and mitochondria and the endoplasmic reticulum. On the other hand, it has been reported that in Niemann Pick type C disease, lysosome-mitochondria MCSs increase, whereas, in the case of Gaucher disease, the duration of these contacts is higher. We speculate that there is an increase in the transfer of lipids between lysosome and mitochondria through MCSs that contributes to mitochondrial damage in NPC and Gaucher cells. Lipids are accumulated inside endolysosomes, in membrane reservoirs (Multilamellar bodies) (Created with BioRender.com).

Gramd1b sterol-transporter from late endosome/lysosomes toward the ER (Höglinger et al., 2019). Thus, when large amounts of LDL-c are internalized, a dynamic redistribution of the ER protein Gramd1b contacts NPC1 at lysosomes, promoting lysosomal cholesterol export. Moreover, the authors show that in the absence of functional NPC1, as in NPC disease, this inter-organelle contact is disrupted, contributing to cholesterol accumulation in lysosomes. Interestingly, the authors found that under these conditions, the lysosomes augment contacts with mitochondria. This is relevant because it might constitute a mechanism by which mitochondria raise their cholesterol levels to a pathological state, which can consequently trigger alterations in their function, thus compromising the metabolic state of the cell (Höglinger et al., 2019) (**Figure 3**).

On the other hand, MCSs between lysosomes and mitochondria are mediated by the lysosomal steroidogenic acute regulatory protein (StAR) D3 (STARD3) protein. This sterol transporter, also located in the lysosomal membrane, has been studied in the context of cholesterol transfer towards ER through MCSs formation (Alpy et al., 2013). Interestingly, we have shown that STARD3 protein levels in NPC were increased in hepatocytes, correlating with elevated cholesterol levels in mitochondria purified from livers of NPC mice, which might contribute to mitochondrial dysfunction (Balboa et al., 2017, 2021).

As mitochondrial dysfunction is observed in NPC disease, the expansion of MCSs between lysosomes and ER have been proposed as a potential strategy for new therapies for this disease (Yu et al., 2005; Kennedy et al., 2014). Interestingly, the number of MCSs between the ER and lysosomes is induced using agents that reduce cholesterol accumulation in NPC disease. For example, the well-known hydroxypropyl-γ-cyclodextrin (HPγCD) and hydroxypropyl-β-cyclodextrin (HPβCD) reduce the accumulation of cholesterol in fibroblasts derived from NPC1 patients (Singhal et al., 2018) and promote the association of lysosomes with the ER, without affecting MCSs between lysosomes and mitochondria. As mentioned initially, NPC1 deficiency disturbs autophagic flux, evidenced by the accumulation of autophagic vacuoles (Pacheco and Lieberman 2008). In fact, treatments with cyclodextrin, which enhances autophagy through the activation of TFEB and subsequent induction of lysosomal biogenesis induction, alleviates the intracellular accumulation of free cholesterol (Singhal et al., 2020). Added to this, it should be noted that functional recovery of contact sites has been successfully tested through their artificial expansion. In this context (Hoglinger et al., 2019) used a sterol-insensitive ORP1L mutant (ORP1L is a lysosome-anchored cholesterol sensor), that constitutively binds the protein VAP in the ER membrane, to act as an artificial tether while preventing the transportation of sterols, to expand ER-lysosome MCS. Remarkably, MCSs expansion by overexpression of this artificial tether rescued lysosomal cholesterol accumulation in NPC1-deficient HeLa cells (Höglinger et al., 2019). Similarly, Meneses-Salas et al. (2020) observed a recovery in the percentage of the endosome/lysosome surface in contact with the ER in CHO cells with mutations in the *Npc1* gene. This was observed after silencing Annexin A6, a member of the annexin family implicated in the regulation of endo- and exocytic pathways and cholesterol homeostasis by binding to membranes in a calcium-dependent manner (Meneses-Salas et al., 2020). Hence, this evidence reinforces MCSs as functional therapeutic targets.

Concerning GD, there is no available information regarding changes in MCSs formation in hepatocytes and other metabolic tissues. The unique information related to these types of alterations was provided by Kim et al. (2021), which observed that human iPSC-derived dopaminergic neurons were treated with an inhibitor of β-glucocerebrosidase activity (conduritol-b-

epoxide) exhibited prolonged tethering between mitochondria-lysosome MCSs (Kim et al., 2021) (**Figure 3**). Interestingly, in Gaucher and NPC cells there is a secondary accumulation of lipids besides glucosylceramide and cholesterol, respectively. In addition, NPC cells show mitochondrial damage and mitochondrial cholesterol accumulation (Balboa et al., 2017). Hence, it is possible to speculate that there is an increase in the transfer of lipids between lysosome and mitochondria, through MCSs that contributes to mitochondrial damage in NPC and Gaucher cells.

Therefore, the information obtained from the research in LSDs is summarized in the fact that the communication mediated by MCSs between compartments that are relevant for the sensing and modulation of lipid homeostasis, can undergo changes depending on key lysosomal proteins. Although the evidence provided in this area comes from non-metabolic cellular models, it is crucial to address whether similar alterations in contact sites are occurring in cells from metabolic tissues in the context of dyslipidemias. Hence, valuable information can be rescued from the understanding of major networks that regulate the intracellular metabolic state, and with it, of the organism.

Conclusions and Outstanding Questions

One of the critical organelles that respond to lipids excess are lysosomes. Several studies have conclusively shown that the lysosome-autophagic axis is affected by lipid overload in adipocytes and hepatocytes. Findings discussed in this review show that in an obese state, autophagy is mostly downregulated in adipose tissue and in the liver. Similarly, NPC and Gaucher diseases have an impairment in the clearance of autophagosomes along with proteolytic defects.

We also addressed commonly altered pathways in the lysosome-autophagic axis. On one side, various studies associate lysosomal dysfunction with altered levels of cathepsins. The eventual permeability of lysosomes and the release of cathepsins to the cytosol could lead to mitochondrial damage and promote lysosome dysfunction and cellular death in these tissues, where the overall evidence is not yet conclusive and more studies are needed to clarify how dysregulated cathepsins mediate lysosome defects in obesity, NPC, and Gaucher diseases. On the other hand, studies revealed that CD36 expression levels are increased in obese adipose and liver tissues, which negatively regulates autophagic function and leads to the failure of lysosomal homeostasis. In adipocytes, CD36/Fyn/IP3R1-mediated lysosomal calcium overload can also be associated with a failure in autophagic flux. Additionally, lipid uptake is mediated by an increase in CD36 expression in adipocytes and hepatocytes by PPAR-γ, which promotes lipid accumulation and contributes to lysosome dysfunction. Intriguingly, LPA is critical in lipid metabolism in obesity, and it is possible to speculate that the hepatic PPAR-γ-CD36 pathway is regulated by LPA. Even though upregulation of CD36 expression in NPC liver has been observed, its role in NPC and Gaucher hepatic diseases remains unclear. However, we believe that galectin 3 and LPA may also promote the expression of CD36 in NPC hepatocytes through the PPAR-γ pathway, contributing to lysosome dysfunction probably by analogous mechanisms observed in obesity.

Considering that B cells rely on lysosomes for the extraction and processing of antigens, it is relevant to elucidate how lysosomes and lysosomal hydrolases such as cathepsins, respond to an excess of nutrients in obesity and LSDs, and how these signals crosstalk with the activation of B cells during antigen recognition. Thus, we speculate that homeostatic alterations in CD36 and cathepsins described in obesity in adipocytes and hepatocytes could also be altered in B cells infiltrated in metabolic tissues, promoting functionals changes. Thus, it is essential to understand dysfunctions at this level, given that B cells are mediators of inflammation in adipose and liver tissues.

On the other hand, the studies of MCSs formed by lysosomes have dramatically increased in recent years given the relevance of its impact in lipid metabolism. The evidence suggests that they play a crucial role in the pathogenic mechanisms associated with obesity and its comorbidities, as well as in NPC and Gaucher diseases. In this context, it seems that an increase of MCSs between mitochondria- LDs and mitochondria-ER are also part of the altered cellular mechanisms, reflecting a misbalance in MCSs homeostasis. Thereby, unraveling these potentially disturbed pathways, including mechanisms that regulate MCSs involved in the control of lipid homeostasis will allow us to understand how responses of adipocytes, hepatocytes, and B cells are affected in obesity, NPC and Gaucher diseases. These findings will potentially unmask new key common targets in the modulation of lysosome function for the treatment of disorders related to lipids.

Outstanding Questions

From the perspective of lysosomal dysfunction observed in obesity, some outstanding questions that remain to be answered in future investigations are:

-How does CD36 coordinate autophagy in adipocytes and hepatocytes? Is there a relationship between the function of CD36 and lysosomal cathepsin activity? What is the implication of CD36 in the uptake of lipids and autophagy in the metabolic tissues of NPC and Gaucher diseases?

-How do LPA and the CD36-PPAR-γ pathway regulate lipid accumulation and lysosome dysfunction in adipocytes and hepatocytes, in obesity? How do LPA and galectin 3 coordinate the activation of this pathway in obesity? How does BMP promote lysosomal dysfunction in pathological states of obesity, NPC and Gaucher?

-Are MCSs altered in a similar fashion by the overload of lipids in adipose tissue and liver in obesity, NPC and Gaucher diseases? How is the formation of MCSs regulated under these conditions? Is there an increased lipid transfer in the transfer of lipids between lysosome and mitochondria through MCSs in LSDs? Does the increased lipid transfer in NPC and Gaucher diseases lead to mitochondrial dysfunction?

-With respect to B cells: Does CD36 coordinate lysosomal function in B cells and is it altered during obesity? How do lysosomes in B cells respond to an excess of nutrients in obesity and LSDs?

AUTHOR CONTRIBUTIONS

FC-R: Writing-Original draft preparation. FC-R, CP-R, MY, and SZ: Writing-Reviewing and Editing. FC-R and CP-R have created figures with BioRender.com. All authors have read and approved the final manuscript.

FUNDING

This work was supported by Agencia Nacional de Investigación y Desarrollo (ANID), FONDECYT Grants Number 1180900 (M-IY) and 1190334 (SZ), and by BECA VRI: VICERRECTORÍA DE INVESTIGACIÓN UC (FC-R and CP-R).

REFERENCES

Afinogenova, Y., Ruan, J., Yang, R., Kleytman, N., Pastores, G., Lischuk, A., et al. (2019). Aberrant Progranulin, YKL-40, Cathepsin D and Cathepsin S in Gaucher Disease. *Mol. Genet. Metab.* 128 (1–2), 62–67. doi:10.1016/j.ymgme.2019.07.014

Alpy, F., Rousseau, A., Schwab, Y., Legueux, F., Stoll, I., Wendling, C., et al. (2013). STARD3/STARD3NL and VAP Make a Novel Molecular Tether between Late Endosomes and the ER. *J. Cel Sci.* 126 (23), 5500–5512. doi:10.1242/jcs.139295

Amritraj, A., Wang, Y., Revett, T. J., Vergote, D., Westaway, D., and Kar, S. (2013). Role of Cathepsin D in U18666A-Induced Neuronal Cell Death. *J. Biol. Chem.* 288 (5), 3136–3152. doi:10.1074/jbc.M112.412460

Anastasia, I., Ilacqua, N., Raimondi, A., Lemieux, P., Ghandehari-Alavijeh, R., Faure, G., et al. (2021). Mitochondria-Rough-ER Contacts in the Liver Regulate Systemic Lipid Homeostasis. *Cel Rep.* 34 (11), 108873. doi:10.1016/j.celrep.2021.108873

Appelqvist, H., Nilsson, C., Garner, B., Brown, A. J., Kågedal, K., and Öllinger, K. (2011). Attenuation of the Lysosomal Death Pathway by Lysosomal Cholesterol Accumulation. *Am. J. Pathol.* 178 (2), 629–639. doi:10.1016/j.ajpath.2010.10.030

Appelqvist, H., Wäster, P., Kågedal, K., and Öllinger, K. (2013). The Lysosome: From Waste Bag to Potential Therapeutic Target. *J. Mol. Cel Biol.* 5 (4), 214–226. doi:10.1093/jmcb/mjt022

Arbogast, F., Arnold, J., Hammann, P., Kuhn, L., Chicher, J., Murera, D., et al. (2019). ATG5 Is Required for B Cell Polarization and Presentation of Particulate Antigens. *Autophagy* 15 (2), 280–294. doi:10.1080/15548627.2018.1516327

Arruda, A. P., Pers, B. M., Parlakgül, G., Güney, E., Inouye, K., and Hotamisligil, G. S. (2014). Chronic Enrichment of Hepatic Endoplasmic Reticulum-Mitochondria Contact Leads to Mitochondrial Dysfunction in Obesity. *Nat. Med.* 20 (12), 1427–1435. doi:10.1038/nm.3735

Aschermann, S., Lux, A., Baerenwaldt, A., Biburger, M., and Nimmerjahn, F. (2009). The Other Side of Immunoglobulin G: Suppressor of Inflammation. *Clin. Exp. Immunol.* 160 (2), 161–167. doi:10.1111/j.1365-2249.2009.04081.x

Balboa, E., Castro, J., Pinochet, M.-J., Cancino, G. I., Matías, N., Sáez, P. J., et al. (2017). MLN64 Induces Mitochondrial Dysfunction Associated with Increased Mitochondrial Cholesterol Content. *Redox Biol.* 12 (February), 274–284. doi:10.1016/j.redox.2017.02.024,

Balboa, E., Marín, T., Oyarzún, J. E., Contreras, P. S., Hardt, R., Van Den Bosch, T., et al. (2021). Proteomic Analysis of Niemann-Pick Type C Hepatocytes Reveals Potential Therapeutic Targets for Liver Damage. *Cells* 10, 2159. doi:10.3390/cells10082159

Ballabio, A., and Bonifacino, J. S. (2020). Lysosomes as Dynamic Regulators of Cell and Organismal Homeostasis. *Nat. Rev. Mol. Cel Biol.* 21 (2), 101–118. doi:10.1038/s41580-019-0185-4

Bechmann, L. P., Gieseler, R. K., Sowa, J.-P., Kahraman, A., Erhard, J., Wedemeyer, I., et al. (2010). Apoptosis Is Associated with CD36/Fatty Acid Translocase Upregulation in Non-alcoholic Steatohepatitis. *Liver Int.* 30 (6), 850–859. doi:10.1111/j.1478-3231.2010.02248.x

Beltroy, E. P., Liu, B., Dietschy, J. M., and Turley, S. D. (2007). Lysosomal Unesterified Cholesterol Content Correlates with Liver Cell Death in Murine Niemann-Pick Type C Disease. *J. Lipid Res.* 48 (4), 869–881. doi:10.1194/jlr.M600488-JLR200

Beltroy, E. P., Richardson, J. A., Horton, J. D., Turley, S. D., and Dietschy, J. M. (2005). Cholesterol Accumulation and Liver Cell Death in Mice with Niemann-Pick Type C Disease. *Hepatology* 42 (4), 886–893. doi:10.1002/hep.20868

Blüher, M. (2019). Obesity: Global Epidemiology and Pathogenesis. *Nat. Rev. Endocrinol.* 15 (5), 288–298. doi:10.1038/s41574-019-0176-8

Blum, J. S., Wearsch, P. A., and Cresswell, P. (2013). Pathways of Antigen Processing. *Annu. Rev. Immunol.* 31 (1), 443–473. doi:10.1146/annurev-immunol-032712-095910

Bournat, J. C., and Brown., C. W. (2010). Mitochondrial Dysfunction in Obesity. *Curr. Opin. Endocrinol. Diabetes Obes.* 17 (5), 446–452. doi:10.1016/j.lfs.2017.11.01910.1097/med.0b013e32833c3026

Brown, R. A., Voit, A., Srikanth, M. P., Thayer, J. A., Kingsbury, T. J., Jacobson, M. A., et al. (2019). mTOR Hyperactivity Mediates Lysosomal Dysfunction in Gaucher's Disease iPSC-Neuronal Cells. *Dis. Models Mech.* 12 (10). doi:10.1242/dmm.038596

Buqué, X., Cano, A., Miquilena-Colina, M. E., García-Monzón, C., Ochoa, B., and Aspichueta, P. (2012). High Insulin Levels Are Required for FAT/CD36 Plasma Membrane Translocation and Enhanced Fatty Acid Uptake in Obese Zucker Rat Hepatocytes. *Am. J. Physiology-endocrinology Metab.* 303 (4), E504–E514. doi:10.1152/ajpendo.00653.2011

Byeon, S. K., Lee, J. Y., Lee, J.-S., and Moon, M. H. (2015). Lipidomic Profiling of Plasma and Urine from Patients with Gaucher Disease during Enzyme Replacement Therapy by Nanoflow Liquid Chromatography-Tandem Mass Spectrometry. *J. Chromatogr. A.* 1381, 132–139. doi:10.1016/j.chroma.2015.01.004

Cai, L., Wang, Z., Ji, A., Meyer, J. M., and van der Westhuyzen, D. R. (2012). Scavenger Receptor CD36 Expression Contributes to Adipose Tissue Inflammation and Cell Death in Diet-Induced Obesity. *PLoS ONE* 7 (5), e36785. doi:10.1371/journal.pone.0036785

Castaneda, J. A., Lim, M. J., Cooper, J. D., and Pearce, D. A. (2008). Immune System Irregularities in Lysosomal Storage Disorders. *Acta Neuropathol.* 115 (2), 159–174. doi:10.1007/s00401-007-0296-4

Cermak, S., Kosicek, M., Mladenovic-Djordjevic, A., Smiljanic, K., Kanazir, S., and Hecimovic, S. (2016). "Loss of Cathepsin B and L Leads to Lysosomal Dysfunction, NPC-like Cholesterol Sequestration and Accumulation of the Key Alzheimer's Proteins,". Editor M. K. Lakshmana, 11, e0167428. doi:10.1371/journal.pone.0167428*PLOS ONE*11

Chait, A., and den Hartigh, L. J. (2020). Adipose Tissue Distribution, Inflammation and its Metabolic Consequences, Including Diabetes and Cardiovascular Disease. *Front. Cardiovasc. Med.* 7 (February), 1–41. doi:10.3389/fcvm.2020.00022

Christian, P., Sacco, J., and Adeli, K. (2013). Autophagy: Emerging Roles in Lipid Homeostasis and Metabolic Control. *Biochim. Biophys. Acta (Bba) - Mol. Cel Biol. Lipids* 1831 (4), 819–824. doi:10.1016/j.bbalip.2012.12.009

Chung, C., Puthanveetil, P., Ory, D. S., and Lieberman, A. P. (2016). Genetic and Pharmacological Evidence Implicates Cathepsins in Niemann-Pick C Cerebellar Degeneration. *Hum. Mol. Genet.* 25 (7), 1434–1446. doi:10.1093/hmg/ddw025

Cleeter, M. W. J., Chau, K.-Y., Gluck, C., Mehta, A., Hughes, D. A., Duchen, M., et al. (2013). Glucocerebrosidase Inhibition Causes Mitochondrial Dysfunction and Free Radical Damage. *Neurochem. Int.* 62 (1), 1–7. doi:10.1016/j.neuint.2012.10.010

Clemente-Postigo, M., Tinahones, A., El Bekay, R., Malagón, M. M., and Tinahones, F. J. (2020). The Role of Autophagy in White Adipose Tissue Function: Implications for Metabolic Health. *Metabolites* 10 (5), 179. doi:10.3390/metabo10050179

Cluzeau, C. V. M., Watkins-Chow, D. E., Fu, R., Borate, B., Yanjanin, N., Dail, M. K., et al. (2012). Microarray Expression Analysis and Identification of Serum Biomarkers for Niemann-Pick Disease, Type C1. *Hum. Mol. Genet.* 21 (16), 3632–3646. doi:10.1093/hmg/dds193

Corcoran, L., Vremec, D., Febbraio, M., Baldwin, T., and Handman, E. (2002). Differential Regulation of CD36 Expression in Antigen-Presenting Cells: Oct-2 Dependence in B Lymphocytes but Not Dendritic Cells or Macrophages. *Int. Immunol.* 14 (10), 1099–1104. doi:10.1093/intimm/dxf075

Cousin, B. a., Andr, M., Casteilla, L., and Pnicaud, L. (2001). Altered Macrophage-like Functions of Preadipocytes in Inflammation and Genetic Obesity. *J. Cel. Physiol.* 186 (3), 380–386. doi:10.1002/1097-4652(2001)9999:9999<000:aid-jcp1038>3.0.co;2-t

Couturier, J., Nuotio-Antar, A. M., Agarwal, N., Wilkerson, G. K., Saha, P., Kulkarni, V., et al. (2019). Lymphocytes Upregulate CD36 in Adipose Tissue and Liver. *Adipocyte* 8 (1), 154–163. doi:10.1080/21623945.2019.1609202

Cox, T. M., Rosenbloom, B. E., and Barker, R. A. (2015). Gaucher Disease and Comorbidities: B-Cell Malignancy and Parkinsonism. *Am. J. Hematol.* 90 (S1), S25–S28. doi:10.1002/ajh.24057

Dai, S., Dulcey, A. E., Hu, X., Wassif, C. A., Porter, F. D., Austin, C. P., et al. (2017). Methyl-β-cyclodextrin Restores Impaired Autophagy Flux in Niemann-Pick C1-Deficient Cells through Activation of AMPK. *Autophagy* 13 (8), 1435–1451. doi:10.1080/15548627.2017.1329081

Davidson, C. D., Ali, N. F., Micsenyi, M. C., Stephney, G., Renault, S., Dobrenis, K., et al. (2009). Chronic Cyclodextrin Treatment of Murine Niemann-Pick C Disease Ameliorates Neuronal Cholesterol and Glycosphingolipid Storage and Disease Progression. *PLoS ONE* 4 (9), e6951. doi:10.1371/journal.pone.0006951

Davis, O. B., Shin, H. R., Lim, C.-Y., Wu, E. Y., Kukurugya, M., Maher, C. F., et al. 2021. "NPC1-MTORC1 Signaling Couples Cholesterol Sensing to Organelle Homeostasis and Is a Targetable Pathway in Niemann-Pick Type C." *Developmental Cel* 56(3):260–276.e7. doi:10.1016/j.devcel.2020.11.016

Droga-Mazovec, G., Bojič, L., Petelin, A., Ivanova, S., Romih, R., Repnik, U., et al. (2008). Cysteine Cathepsins Trigger Caspase-dependent Cell Death through Cleavage of Bid and Antiapoptotic Bcl-2 Homologues. *J. Biol. Chem.* 283 (27), 19140–19150. doi:10.1074/jbc.M802513200

D'Souza, K., Paramel, G., and Kienesberger, P. (2018). Lysophosphatidic Acid Signaling in Obesity and Insulin Resistance. *Nutrients* 10 (4), 399. doi:10.3390/nu10040399

Dugail, I. (2014). Lysosome/Lipid Droplet Interplay in Metabolic Diseases. *Biochimie* 96 (1), 102–105. doi:10.1016/j.biochi.2013.07.008

Dusaulcy, R., Rancoule, C., Grès, S., Wanecq, E., Colom, A., Guigné, C., et al. (2011). Adipose-Specific Disruption of Autotaxin Enhances Nutritional Fattening and Reduces Plasma Lysophosphatidic Acid. *J. Lipid Res.* 52 (6), 1247–1255. doi:10.1194/jlr.M014985

Ejarque, M., Ceperuelo-Mallafré, V., Serena, C., Maymo-Masip, E., Duran, X., Díaz-Ramos, Monica., et al. (2019). Adipose Tissue Mitochondrial Dysfunction in Human Obesity Is Linked to a Specific DNA Methylation Signature in Adipose-Derived Stem Cells. *Int. J. Obes.* 43 (6), 1256–1268. doi:10.1038/s41366-018-0219-6

Elrick, M. J., Yu, T., Chung, C., and Lieberman, A. P. (2012). Impaired Proteolysis Underlies Autophagic Dysfunction in Niemann-Pick Type C Disease. *Hum. Mol. Genet.* 21 (22), 4876–4887. doi:10.1093/hmg/dds324

Engin, A. B., and Basak, Ayse. (2017). "What Is Lipotoxicity," in *Advances in Experimental Medicine and Biology*. Editors A. B. Engin and A. Engin (Cham: Springer International Publishing), 197–220. doi:10.1007/978-3-319-48382-5_8

Fan, Y., Yang, J., Li, H., Li, H., Zhang, S., Li, X., et al. (2020). SNX10 Deficiency Restricts Foam Cell Formation and Protects against Atherosclerosis by Suppressing CD36-Lyn Axis. *Can. J. Cardiol.* doi:10.1016/j.cjca.2020.05.010

Farfel-Becker, T., Vitner, E. B., Kelly, S. L., Bame, J. R., Duan, J., Shinder, V., et al. (2014). Neuronal Accumulation of Glucosylceramide in a Mouse Model of Neuronopathic Gaucher Disease Leads to Neurodegeneration. *Hum. Mol. Genet.* 23 (4), 843–854. doi:10.1093/hmg/ddt468

Fazilleau, N., Mark, L., McHeyzer-Williams, L. J., and McHeyzer-Williams, M. G. (2009). Follicular Helper T Cells: Lineage and Location. *Immunity* 30 (3), 324–335. doi:10.1016/j.immuni.2009.03.003

Febbraio, M., and Silverstein, R. L. (2007). CD36: Implications in Cardiovascular Disease. *Int. J. Biochem. Cel Biol.* 39 (11), 2012–2030. doi:10.1016/j.biocel.2007.03.012

Feldstein, A. E., Werneburg, N. W., Li, Z., Bronk, S. F., and Gores, G. J. (2006). Bax Inhibition Protects against Free Fatty Acid-Induced Lysosomal Permeabilization. *Am. J. Physiology-gastrointestinal Liver Physiol.* 290 (6), G1339–G1346. doi:10.1152/ajpgi.00509.2005

Ferry, G., Tellier, E., Try, A., Grés, S., Naime, I., Simon, M. F., et al. (2003). Autotaxin Is Released from Adipocytes, Catalyzes Lysophosphatidic Acid Synthesis, and Activates Preadipocyte Proliferation. *J. Biol. Chem.* 278 (20), 18162–18169. doi:10.1074/jbc.M301158200

Fucho, R., Martínez, L., Baulies, A., Torres, S., Tarrats, N., Fernandez, A., et al. (2014). ASMase Regulates Autophagy and Lysosomal Membrane Permeabilization and its Inhibition Prevents Early Stage Non-alcoholic Steatohepatitis. *J. Hepatol.* 61 (5), 1126–1134. doi:10.1016/j.jhep.2014.06.009

Gaidhu, M. P., Anthony, N. M., Patel, P., Hawke, T. J., and Ceddia, R. B. (2010). Dysregulation of Lipolysis and Lipid Metabolism in Visceral and Subcutaneous Adipocytes by High-Fat Diet: Role of ATGL, HSL, and AMPK. *Am. J. Physiology-cell Physiol.* 298 (4), C961–C971. doi:10.1152/ajpcell.00547.2009

Gallala, H. D., and Sandhoff, K. (2011). Biological Function of the Cellular Lipid BMP-BMP as a Key Activator for Cholesterol Sorting and Membrane Digestion. *Neurochem. Res.* 36 (9), 1594–1600. doi:10.1007/s11064-010-0337-6

García-Barrado, M., Iglesias-Osma, M., Pérez-García, E., Carrero, S., Blanco, E., Carretero-Hernández, M., et al. (2020). Role of Flavonoids in the Interactions Among Obesity, Inflammation, and Autophagy. *Pharmaceuticals* 13 (11), 342. doi:10.3390/ph13110342

García-Sanz, P., Orgaz, L., Bueno-Gil, G., Espadas, I., Rodríguez-Traver, E., Kulisevsky, J., et al. (2017). N370S -GBA1 Mutation Causes Lysosomal Cholesterol Accumulation in Parkinson's Disease. *Mov Disord.* 32 (10), 1409–1422. doi:10.1002/mds.27119

Gillotte-Taylor, K., Boullier, A., Witztum, J. L., Steinberg, D., and Quehenberger, O. (2001). Scavenger Receptor Class B Type I as a Receptor for Oxidized Low Density Lipoprotein. *J. Lipid Res.* 42 (9), 1474–1482. PMID: 11518768. doi:10.1016/s0022-2275(20)30281-9

Gornicka, A., Fettig, J., Eguchi, A., Berk, M. P., Thapaliya, S., Dixon, L. J., et al. (2012). Adipocyte Hypertrophy Is Associated with Lysosomal Permeability Both *In Vivo* and *In Vitro*: Role in Adipose Tissue Inflammation. *Am. J. Physiology-endocrinology Metab.* 303 (5), E597–E606. doi:10.1152/ajpendo.00022.2012

Grabner, G. F., Fawzy, N., Pribasnig, M. A., Trieb, M., Taschler, U., Holzer, M., et al. (2019). Metabolic Disease and ABHD6 Alter the Circulating Bis(Monoacylglycerol)Phosphate Profile in Mice and Humans. *J. Lipid Res.* 60 (5), 1020–1031. doi:10.1194/jlr.M093351

Gross, D. A., and Silver, D. L. (2014). Cytosolic Lipid Droplets: From Mechanisms of Fat Storage to Disease. *Crit. Rev. Biochem. Mol. Biol.* 49 (4), 304–326. doi:10.3109/10409238.2014.931337

Hao, J.-W., Wang, J., Guo, H., Zhao, Y.-Y., SunZhao, H.-H., Li, Y.-F., et al. (2020). CD36 Facilitates Fatty Acid Uptake by Dynamic Palmitoylation-Regulated Endocytosis. *Nat. Commun.* 11 (1), 1–16. doi:10.1038/s41467-020-18565-8

Harwood, N. E., and Batista, F. D. (2010). Early Events in B Cell Activation. *Annu. Rev. Immunol.* 28 (1), 185–210. doi:10.1146/annurev-immunol-030409-101216

He, C., Wang, S., Zhou, C., He, M., Wang, J., Ladds, M., et al. (2021). CD36 and LC3B Initiated Autophagy in B Cells Regulates the Humoral Immune Response. *Autophagy* 00 (00), 1–15. doi:10.1080/15548627.2021.1885183

Helkin, A., Stein, J. J., Lin, S., Siddiqui, S., Maier, K. G., and Gahtan, V. (2016). Dyslipidemia Part 1-Review of Lipid Metabolism and Vascular Cell Physiology. *Vasc. Endovascular Surg.* 50 (2), 107–118. doi:10.1177/1538574416628654

Höglinger, D., Burgoyne, T., Sanchez-Heras, E., Hartwig, P., Colaco, A., Newton, J., et al. (2019). NPC1 Regulates ER Contacts with Endocytic Organelles to Mediate Cholesterol Egress. *Nat. Commun.* 10 (1), 1–14. doi:10.1038/s41467-019-12152-2

Honey, K., Duff, M., Beers, C., Brissette, W. H., Elliott, E. A., Peters, C., et al. (2001). Cathepsin S Regulates the Expression of Cathepsin L and the Turnover of γ-Interferon-Inducible Lysosomal Thiol Reductase in B Lymphocytes. *J. Biol. Chem.* 276 (25), 22573–22578. doi:10.1074/jbc.m101851200

Iacobini, C., Menini, S., Ricci, C., Fantauzzi, C. B., Scipioni, A., Salvi, L., et al. (2011). Galectin-3 Ablation Protects Mice from Diet-Induced NASH: A Major Scavenging Role for Galectin-3 in Liver. *J. Hepatol.* 54 (5), 975–983. doi:10.1016/j.jhep.2010.09.020

Ilnytska, O., Jeziorek, M., Lai, K., Altan-Bonnet, N., Dobrowolski, R., and Storch, J. (2021). Lysobisphosphatidic Acid (LBPA) Enrichment Promotes Cholesterol Egress via Exosomes in Niemann Pick Type C1 Deficient Cells. *Biochim. Biophys. Acta (Bba) - Mol. Cel Biol. Lipids* 1866 (6), 158916. doi:10.1016/j.bbalip.2021.158916

Inami, Y., Yamashina, S., Izumi, K., Ueno, T., Tanida, I., Ikejima, K., et al. (2011). Hepatic Steatosis Inhibits Autophagic Proteolysis via Impairment of Autophagosomal Acidification and Cathepsin Expression. *Biochem. Biophysical Res. Commun.* 412 (4), 618–625. doi:10.1074/jbc.M10185120010.1016/j.bbrc.2011.08.012

Ireland, J. M., and Unanue, E. R. (2011). Autophagy in Antigen-Presenting Cells Results in Presentation of Citrullinated Peptides to CD4 T Cells. *J. Exp. Med.* 208 (13), 2625–2632. doi:10.1084/jem.20110640

Ivanova, M. M., Changsila, E., Iaonou, C., and Goker-Alpan, O. (2019). Impaired Autophagic and Mitochondrial Functions Are Partially Restored by ERT in Gaucher and Fabry Diseases. *PLoS ONE* 14 (1), e0210617–22. doi:10.1371/journal.pone.0210617

Jaishy, B., and Abel, E. D. (2016). Lipids, Lysosomes, and Autophagy. *J. Lipid Res.* 57 (9), 1619–1635. doi:10.1194/jlr.R067520

Jakab, J., Miškić, B., Mikšić, Š., Juranić, B., Ćosić, V., Schwarz, D., et al. (2021). Adipogenesis as a Potential Anti-obesity Target: A Review of Pharmacological Treatment and Natural Products. *Dmso* 14, 67–83. doi:10.2147/DMSO.S281186

Jose, A., and Kienesberger, P. C. (2021). Autotaxin-Lpa-Lpp3 Axis in Energy Metabolism and Metabolic Disease. *Ijms* 22 (17), 9575. doi:10.3390/ijms22179575

Ju, L., Han, J., Zhang, X., Deng, Y., Yan, H., Wang, C., et al. (2019). Obesity-associated Inflammation Triggers an Autophagy-Lysosomal Response in Adipocytes and Causes Degradation of Perilipin 1. *Cell Death Dis* 10 (2), 121. doi:10.1038/s41419-019-1393-8

Jung, U., and Choi, M.-S. (2014). Obesity and its Metabolic Complications: The Role of Adipokines and the Relationship between Obesity, Inflammation, Insulin Resistance, Dyslipidemia and Nonalcoholic Fatty Liver Disease. *Ijms* 15 (4), 6184–6223. doi:10.3390/ijms15046184

Kaffe, E., Magkrioti, C., and Aidinis, V. (2019). Deregulated Lysophosphatidic Acid Metabolism and Signaling in Liver Cancer. *Cancers* 11 (11), 1626. doi:10.3390/cancers11111626

Kahn, B. B., and Flier, J. S. (2000). Obesity and Insulin Resistance. *J. Clin. Invest.* 106 (4), 473–481. doi:10.1172/JCI10842

Kałużna, M., Trzeciak, I., Ziemnicka, K., Machaczka, M., and Ruchała, M. (2019). Endocrine and Metabolic Disorders in Patients with Gaucher Disease Type 1: A Review. *Orphanet J. Rare Dis.* 14 (1), 1–14. doi:10.1186/s13023-019-1211-5

Kaminskyy, V., and Zhivotovsky, B. (2012). Proteases in Autophagy. *Biochim. Biophys. Acta (Bba) - Proteins Proteomics* 1824 (1), 44–50. doi:10.1016/j.bbapap.2011.05.013

Kao, D., Danzer, H., Collin, M., Groß, A., Eichler, J., Stambuk, J., et al. (2015). A Monosaccharide Residue Is Sufficient to Maintain Mouse and Human IgG Subclass Activity and Directs IgG Effector Functions to Cellular Fc Receptors. *Cel Rep.* 13 (11), 2376–2385. doi:10.1016/j.celrep.2015.11.027

Kennedy, B. E., Madreiter, C. T., Vishnu, N., Malli, R., Graier, W. F., and Karten, B. (2014). Adaptations of Energy Metabolism Associated with Increased Levels of Mitochondrial Cholesterol in Niemann-Pick Type C1-Deficient Cells. *J. Biol. Chem.* 289 (23), 16278–16289. doi:10.1074/jbc.M114.559914

Kennedy, D. J., Kuchibhotla, S., Westfall, K. M., Westfall, Roy. L., Silverstein, R. L., Morton, R. E., et al. (2011). A CD36-dependent Pathway Enhances Macrophage and Adipose Tissue Inflammation and Impairs Insulin Signalling. *Cardiovasc. Res.* 89 (3), 604–613. doi:10.1093/cvr/cvq360

Khan, S., Chan, Y. T., Revelo, X. S., and Winer, D. A. (2020). The Immune Landscape of Visceral Adipose Tissue during Obesity and Aging. *Front. Endocrinol.* 11, 1–18. doi:10.3389/fendo.2020.00267

Kim, S., Wong, Y. C., Gao, F., and Krainc, D. (2021). Dysregulation of Mitochondria-Lysosome Contacts by GBA1 Dysfunction in Dopaminergic Neuronal Models of Parkinson's Disease. *Nat. Commun.* 12 (1). doi:10.1038/s41467-021-22113-3

Klop, B., Elte, J., and Cabezas, M. (2013). Dyslipidemia in Obesity: Mechanisms and Potential Targets. *Nutrients* 5 (4), 1218–1240. doi:10.3390/nu5041218

Koga, H., Kaushik, S., and Cuervo, A. M. (2010). Altered Lipid Content Inhibits Autophagic Vesicular Fusion. *FASEB j.* 24 (8), 3052–3065. doi:10.1096/fj.09-144519

Koonen, D. P. Y., Jacobs, R. L., Febbraio, M., Young, M. E., Soltys, C.-L. M., Ong, H., et al. (2007). Increased Hepatic CD36 Expression Contributes to Dyslipidemia Associated with Diet-Induced Obesity. *Diabetes* 56 (12), 2863–2871. doi:10.2337/db07-0907

Kounakis, K., Chaniotakis, M., Markaki, M., and Tavernarakis, N. (2019). Emerging Roles of Lipophagy in Health and Disease. *Front. Cel Dev. Biol.* 7 (SEP), 1–8. doi:10.3389/fcell.2019.00185

Kozlitina, J., Smagris, E., Stender, S., Nordestgaard, B. G., Zhou, H. H., Tybjærg-Hansen, A., et al. (2014). Exome-Wide Association Study Identifies a TM6SF2 Variant that Confers Susceptibility to Nonalcoholic Fatty Liver Disease. *Nat. Genet.* 46 (4), 352–356. doi:10.1038/ng.2901

Krahmer, N., Najafi, B., Schueder, F., Quagliarini, F., Steger, M., Seitz, S., et al. (2018). Organellar Proteomics and Phospho-Proteomics Reveal Subcellular Reorganization in Diet-Induced Hepatic Steatosis. *Developmental Cel* 47 (2), 205–221. e7. doi:10.1016/j.devcel.2018.09.017

Kulinski, A., and Vance, J. E. (2007). Lipid Homeostasis and Lipoprotein Secretion in Niemann-Pick C1-Deficient Hepatocytes. *J. Biol. Chem.* 282 (3), 1627–1637. doi:10.1074/jbc.M610001200

Lachmann, R. H., Te Vruchte, D., Lloyd-Evans, E., Reinkensmeier, G., Sillence, D. J., Fernandez-Guillen, L., et al. (2004). Treatment with Miglustat Reverses the Lipid-Trafficking Defect in Niemann-Pick Disease Type C. *Neurobiol. Dis.* 16 (3), 654–658. doi:10.1016/j.nbd.2004.05.002

Lahiri, V., Hawkins, W. D., and Klionsky, D. J. (2019). Watch what You (Self-) Eat: Autophagic Mechanisms that Modulate Metabolism. *Cel Metab.* 29 (4), 803–826. doi:10.1016/j.cmet.2019.03.003

Lankar, D., Vincent-Schneider, H., Briken, V., Yokozeki, T., Raposo, G., and Bonnerot, C. (2002). Dynamics of Major Histocompatibility Complex Class II Compartments during B Cell Receptor-Mediated Cell Activation. *J. Exp. Med.* 195 (4), 461–472. doi:10.1084/jem.20011543

Lanzavecchia, A. (1985). Antigen-Specific Interaction between T and B Cells. 1985. *J. Immunol.* 179 (11), 7206–7208.

Lee, H., Lee, I. S., and Choue, R. (2013). Obesity, Inflammation and Diet. *Pediatr. Gastroenterol. Hepatol. Nutr.* 16 (3), 143. doi:10.5223/pghn.2013.16.3.143

Lee, J. H., Zhou, J., and Xie, W. (2008). PXR and LXR in Hepatic Steatosis: A New Dog and an Old Dog with New Tricks. *Mol. Pharmaceutics* 5 (1), 60–66. doi:10.1021/mp700121u

Li, Y., Chao, X., Yang, L., Lu, Q., Li, T., Ding, W.-X., et al. (2018). Impaired Fasting-Induced Adaptive Lipid Droplet Biogenesis in Liver-specific Atg5-Deficient Mouse Liver Is Mediated by Persistent Nuclear Factor-like 2 Activation. *Am. J. Pathol.* 188 (8), 1833–1846. doi:10.1016/j.ajpath.2018.04.015

Li, Y., Yang, P., Zhao, L., Chen, Y., Zhang, X., Zeng, S., et al. (2019). CD36 Plays a Negative Role in the Regulation of Lipophagy in Hepatocytes through an AMPK-dependent Pathway. *J. Lipid Res.* 60 (4), 844–855. doi:10.1194/jlr.M090969

Limgala, R. P., Ioanou, C., Plassmeyer, M., Ryherd, M., Kozhaya, L., Austin, L., et al. (2016). Time of Initiating Enzyme Replacement Therapy Affects Immune Abnormalities and Disease Severity in Patients with Gaucher Disease. *PLoS ONE* 11 (12), e0168135–16. doi:10.1371/journal.pone.0168135

Lin, Y., Cai, X., Wang, G., Ouyang, G., and Cao, H. (2018). Model Construction of Niemann-Pick Type C Disease in Zebrafish. *Biol. Chem.* 399 (8), 903–910. doi:10.1515/hsz-2018-0118

Liu, B., Turley, S. D., Burns, D. K., Miller, A. M., Repa, J. J., and Dietschy, J. M. (2009). Reversal of Defective Lysosomal Transport in NPC Disease Ameliorates Liver Dysfunction and Neurodegeneration in the Npc1-/- Mouse. *Proc. Natl. Acad. Sci.* 106 (7), 2377–2382. doi:10.1073/pnas.0810895106

Liu, B., Xie, C., Richardson, J. A., Turley, S. D., and Dietschy, J. M. (2007). Receptor-Mediated and Bulk-phase Endocytosis Cause Macrophage and Cholesterol Accumulation in Niemann-Pick C Disease. *J. Lipid Res.* 48 (8), 1710–1723. doi:10.1194/jlr.M700125-JLR200

Liu, N., Tengstrand, E. A., Chourb, L., and Hsieh, F. Y. (2014). Di-22:6-Bis(Monoacylglycerol)Phosphate: A Clinical Biomarker of Drug-Induced Phospholipidosis for Drug Development and Safety Assessment. *Toxicol. Appl. Pharmacol.* 279 (3), 467–476. doi:10.1016/j.taap.2014.06.014

Liu, R., and Nikolajczyk, B. S. (2019). Tissue Immune Cells Fuel Obesity-Associated Inflammation in Adipose Tissue and beyond. *Front. Immunol.* 10. doi:10.3389/fimmu.2019.01587

Love-Gregory, L., and Abumrad, N. A. (2011). CD36 Genetics and the Metabolic Complications of Obesity. *Curr. Opin. Clin. Nutr. Metab. Care* 14 (6), 527–534. doi:10.1097/MCO.0b013e32834bbac9

Luo, X., Li, Y., Yang, P., Chen, Y., Wei, L., Yu, T., et al. (2020). Obesity Induces Preadipocyte CD36 Expression Promoting Inflammation via the Disruption of Lysosomal Calcium Homeostasis and Lysosome Function. *EBioMedicine* 56, 102797. doi:10.1016/j.ebiom.2020.102797

Maetzel, D., Sarkar, S., Wang, H., Abi-Mosleh, L., Xu, P., Cheng, A. W., et al. (2014). Genetic and Chemical Correction of Cholesterol Accumulation and Impaired Autophagy in Hepatic and Neural Cells Derived from Niemann-Pick Type C Patient-specific IPS Cells. *Stem Cel Rep.* 2 (6), 866–880. doi:10.1016/j.stemcr.2014.03.014

Magro dos Reis, I., Houben, T., Oligschläger, Y., Bücken, L., Steinbusch, H., Cassiman, D., et al. (2020). Dietary Plant Stanol Ester Supplementation Reduces Peripheral Symptoms in a Mouse Model of Niemann-Pick Type C1 Disease. *J. Lipid Res.* 61 (6), 830–839. doi:10.1194/jlr.RA120000632

Marques, A. R. A., and Saftig, P. (2019). Lysosomal Storage Disorders - Challenges, Concepts and Avenues for Therapy: beyond Rare Diseases. *J. Cel Sci.* 132 (2), jcs221739. doi:10.1242/jcs.221739

Martinez-Lopez, N., and Singh, R. (2015). Autophagy and Lipid Droplets in the Liver. *Annu. Rev. Nutr.* 35 (1), 215–237. doi:10.1146/annurev-nutr-071813-105336

Martinez-Martin, N., Maldonado, P., Gasparrini, F., Frederico, B., Aggarwal, S., Gaya, M., et al. (2017). A Switch from Canonical to Noncanonical Autophagy Shapes B Cell Responses. *Science* 355 (6325), 641–647. doi:10.1126/science.aal3908

McCann, M. R., and Ratneswaran, A. (2019). The Role of PPARγ in Childhood Obesity-Induced Fractures. *Genes Nutr.* 14 (1), 31. doi:10.1186/s12263-019-0653-7

McCauliff, L. A., Langan, A., Li, R., Ilnytska, O., Bose, D., Waghalter, M., et al. (2019). Intracellular Cholesterol Trafficking Is Dependent upon NPC2 Interaction with Lysobisphosphatidic Acid. *ELife* 8, 1–31. doi:10.7554/eLife.50832

McGrath, M. E. (1999). The Lysosomal Cysteine Proteases. *Annu. Rev. Biophys. Biomol. Struct.* 28 (1), 181–204. doi:10.1146/annurev.biophys.28.1.181

McIntyre, T. M., Pontsler, A. V., Hilaire, St., Silva, A. R., St. Hilaire, A., Xu, Y., et al. (2003). Identification of an Intracellular Receptor for Lysophosphatidic Acid (LPA): LPA Is a Transcellular PPAR Agonist. *Proc. Natl. Acad. Sci.* 100 (1), 131–136. doi:10.1073/pnas.0135855100

Meikle, P. J., Duplock, S., Blacklock, D., Whitfield, P. D., Macintosh, G., Hopwood, J. J., et al. (2008). Effect of Lysosomal Storage on Bis(Monoacylglycero) Phosphate. *Biochem. J.* 411 (1), 71–78. doi:10.1042/BJ20071043

Meneses-Salas, E., García-Melero, A., Kanerva, K., Blanco-Muñoz, P., Morales-Paytuvi, F., Bonjoch, J., et al. (2020). Annexin A6 Modulates TBC1D15/Rab7/StARD3 Axis to Control Endosomal Cholesterol Export in NPC1 Cells. *Cell. Mol. Life Sci.* 77 (14), 2839–2857. doi:10.1007/s00018-019-03330-y

Meske, V., Erz, J., Priesnitz, T., and Ohm, T.-G. (2014). The Autophagic Defect in Niemann-Pick Disease Type C Neurons Differs from Somatic Cells and Reduces Neuronal Viability. *Neurobiol. Dis.* 64, 88–97. doi:10.1016/j.nbd.2013.12.018

Miquilena-Colina, M. E., Lima-Cabello, E., Sanchez-Campos, S., Garcia-Mediavilla, M. V., Fernandez-Bermejo, M., Lozano-Rodriguez, T., et al. (2011). Hepatic Fatty Acid Translocase CD36 Upregulation Is Associated with Insulin Resistance, Hyperinsulinaemia and Increased Steatosis in Non-alcoholic Steatohepatitis and Chronic Hepatitis C. *Gut* 60 (10), 1394–1402. doi:10.1136/gut.2010.222844

Mistry, P. K., Liu, J., Yang, M., Nottoli, T., McGrath, J., Jain, D., et al. (2010). Glucocerebrosidase Gene-Deficient Mouse Recapitulates Gaucher Disease Displaying Cellular and Molecular Dysregulation beyond the Macrophage. *Proc. Natl. Acad. Sci.* 107 (45), 19473–19478. doi:10.1073/pnas.1003308107

Mitchison, N. A. (2004). T-cell-B-cell Cooperation. *Nat. Rev. Immunol.* 4 (4), 308–312. doi:10.1038/nri1334

Mizunoe, Y., Kobayashi, M., Hoshino, S., Tagawa, R., Itagawa, R., Hoshino, A., et al. (2020). Cathepsin B Overexpression Induces Degradation of Perilipin 1 to Cause Lipid Metabolism Dysfunction in Adipocytes. *Sci. Rep.* 10 (1), 1–12. doi:10.1038/s41598-020-57428-6

Mizunoe, Y., Kobayashi, M., Tagawa, R., Nakagawa, Y., Shimano, H., and Higami, Y. (2019). Association between Lysosomal Dysfunction and Obesity-Related Pathology: A Key Knowledge to Prevent Metabolic Syndrome. *Ijms* 20 (15), 3688. doi:10.3390/ijms20153688

Mizunoe, Y., Sudo, Y., Okita, N., Hiraoka, H., Mikami, K., Narahara, T., et al. (2017). Involvement of Lysosomal Dysfunction in Autophagosome Accumulation and Early Pathologies in Adipose Tissue of Obese Mice. *Autophagy* 13 (4), 642–653. doi:10.1080/15548627.2016.1274850

Moreau, D., Vacca, F., Vossio, S., Scott, C., Colaco, A., Paz Montoya, J., et al. (2019). Drug-induced Increase in Lysobisphosphatidic Acid Reduces the Cholesterol Overload in Niemann-Pick Type C Cells and Mice. *EMBO Rep.* 20 (7), 1–15. doi:10.15252/embr.201847055

Nagral, A. (2014). Gaucher Disease. *J. Clin. Exp. Hepatol.* 4 (1), 37–50. doi:10.1016/j.jceh.2014.02.005

Nakagawa, T. Y., Brissette, W. H., Lira, P. D., Griffiths, R. J., Petrushova, N., Stock, J., et al. (1999). Impaired Invariant Chain Degradation and Antigen Presentation and Diminished Collagen-Induced Arthritis in Cathepsin S Null Mice. *Immunity* 10 (2), 207–217. doi:10.1016/s1074-7613(00)80021-7

Nascimbeni, F., Dalla Salda, A., and Carubbi, F. (2018). Energy Balance, Glucose and Lipid Metabolism, Cardiovascular Risk and Liver Disease Burden in Adult Patients with Type 1 Gaucher Disease. *Blood Cel Mol. Dis.* 68, 74–80. doi:10.1016/j.bcmd.2016.10.012

Nascimbeni, F., Lugari, S., Cassinerio, E., Motta, I., Cavicchioli, A., Dalla Salda, A., et al. (2020). Liver Steatosis Is Highly Prevalent and Is Associated with Metabolic Risk Factors and Liver Fibrosis in Adult Patients with Type 1 Gaucher Disease. *Liver Int.* 40 (12), 3061–3070. doi:10.1111/liv.14640

Neuschwander-Tetri, B. A., and Brent, A. (2005). Nonalcoholic Steatohepatitis and the Metabolic Syndrome. *Am. J. Med. Sci.* 330 (6), 326–335. doi:10.1097/00000441-200512000-00011

Neßlauer, A.-M., Gläser, A., Gräler, M., Engelmann, R., Müller-Hilke, B., Frank, M., et al. (2019). A Therapy With Miglustat, 2-Hydroxypropyl-SS-Cyclodextrin and Allopregnanolone Restores Splenic Cholesterol Homeostasis in Niemann-Pick Disease Type C1. *Lipids Health Dis.* 18 (1), 146. doi:10.1186/s12944-019-1088-2

Nguyen, Y., Stirnemann, J., Lautredoux, F., Cador, B., Bengherbia, M., Yousfi, K., et al. (2020). Immunoglobulin Abnormalities in Gaucher Disease: An Analysis of 278 Patients Included in the French Gaucher Disease Registry. *Ijms* 21 (4), 1247. doi:10.3390/ijms21041247

Obino, D., Diaz, J., Sáez, J. J., Ibañez-Vega, J., Sáez, P. J., Alamo, M., et al. (2017). Vamp-7-dependent Secretion at the Immune Synapse Regulates Antigen Extraction and Presentation in B-Lymphocytes. *MBoC* 28 (7), 890–897. doi:10.1091/mbc.E16-10-0722

Osellame, L. D., Rahim, A. A., Hargreaves, I. P., Richard-Londt, A., Brandner, S., Waddington, S. N., et al. (2013). Mitochondria and Quality Control Defects in a Mouse Model of Gaucher Disease-Links to Parkinson's Disease. *Cel Metab.* 17 (6), 941–953. doi:10.1016/j.cmet.2013.04.014

Oyarzún, J. E., Lagos, J., Vázquez, M. C., Valls, C., De la Fuente, C., Yuseff, M. I., et al. (2019). Lysosome Motility and Distribution: Relevance in Health and Disease. *Biochim. Biophys. Acta (Bba) - Mol. Basis Dis.* 1865 (6), 1076–1087. doi:10.1016/j.bbadis.2019.03.009

Pacheco, C. D., Kunkel, R., and Lieberman, A. P. (2007). Autophagy in Niemann-Pick C Disease Is Dependent upon Beclin-1 and Responsive to Lipid Trafficking Defects. *Hum. Mol. Genet.* 16 (12), 1495–1503. doi:10.1093/hmg/ddm100

Pacheco, C. D., and Lieberman, A. P. (2008). The Pathogenesis of Niemann-Pick Type C Disease: a Role for Autophagy? *Expert Rev. Mol. Med.* 10 (1), e26. doi:10.1017/S146239940800080X

Pallottini, V., and Pfrieger, F. W. (2020). Understanding and Treating Niemann-Pick Type C Disease: Models Matter. *Ijms* 21 (23), 8979. doi:10.3390/ijms21238979

Pandey, M. K., and Grabowski, G. A. (2013). Immunological Cells and Functions in Gaucher Disease. *Crit. Rev. Oncog* 18 (3), 197–220. doi:10.1615/critrevoncog.2013004503

Park, H.-J., KimKim, D.-H., Kim, W.-J., Kim, J. Y., Senejani, A. G., Hwang, S. S., et al. (2014). PPARγ Negatively Regulates T Cell Activation to Prevent Follicular Helper T Cells and Germinal Center Formation. *PLoS ONE* 9 (6), e99127. doi:10.1371/journal.pone.0099127

Pascua-Maestro, R., Diez-Hermano, S., Lillo, C., Ganfornina, M. D., and Sanchez, D. (2017). Protecting Cells by Protecting Their Vulnerable Lysosomes: Identification of a New Mechanism for Preserving Lysosomal Functional Integrity upon Oxidative Stress. *Plos Genet.* 13 (2), e1006603. doi:10.1371/journal.pgen.1006603

Pejnovic, N. N., Pantic, J. M., Pantic, I. P. I. G., Zdravkovic, N. S., Djukic, A. L., Arsenijevic, N. N., et al. (2013). Galectin-3 Deficiency Accelerates High-Fat Diet-Induced Obesity and Amplifies Inflammation in Adipose Tissue and Pancreatic Islets. *Diabetes* 62 (6), 1932–1944. doi:10.2337/db12-0222

Pepino, M. Y., Kuda, O., Samovski, D., and Abumrad, N. A. (2014). Structure-Function of CD36 and Importance of Fatty Acid Signal Transduction in Fat Metabolism. *Annu. Rev. Nutr.* 34, 281–303. doi:10.1146/annurev-nutr-071812-161220

Pergande, M. R., Serna-Perez, F., Mohsin, S. B., Hanek, J., and Cologna, S. M. (2019). Lipidomic Analysis Reveals Altered Fatty Acid Metabolism in the Liver of the Symptomatic Niemann-Pick, Type C1 Mouse ModelLipidomic Analysis Reveals Altered Fatty Acid Metabolism in the Liver of the Symptomatic Niemann–Pick, Type C1 Mouse Model. *PROTEOMICS* 19 (18), 1800285. doi:10.1002/pmic.201800285

Pettinelli, P., and Videla, L. A. (2011). Up-Regulation of PPAR-γ mRNA Expression in the Liver of Obese Patients: an Additional Reinforcing

Lipogenic Mechanism to SREBP-1c Induction. *J. Clin. Endocrinol. Metab.* 96 (5), 1424–1430. doi:10.1016/j.cmet.2008.03.003

Peverill, W., Powell, L., and Skoien, R. (2014). Evolving Concepts in the Pathogenesis of NASH: Beyond Steatosis and Inflammation. *Ijms* 15 (5), 8591–8638. doi:10.3390/ijms15058591

Phipps-Yonas, H., Semik, V., and Hastings, K. T. (2013). GILT Expression in B Cells Diminishes Cathepsin S Steady-State Protein Expression and Activity. *Eur. J. Immunol.* 43 (1), 65–74. doi:10.1002/eji.201242379

Platt, F. M., d'Azzo, A., Davidson, B. L., Neufeld, E. F., and Tifft, C. J. (2018). Alessandra D'Azzo, Beverly L. Davidson, Elizabeth F. Neufeld, and Cynthia J. TifftLysosomal Storage Diseases. *Nat. Rev. Dis. Primers* 4 (1), 27. doi:10.1038/s41572-018-0025-4

Platt, N., Speak, A. O., Colaco, A., Gray, J., Smith, D. A., Williams, I. M., et al. (2016). Immune Dysfunction in Niemann-Pick Disease Type C. *J. Neurochem.* 136, 74–80. doi:10.1111/jnc.13138

Popkin, B. M., and Doak, C. M. (2009). The Obesity Epidemic Is a Worldwide Phenomenon. *Nutr. Rev.* 56 (4), 106–114. doi:10.1111/j.1753-4887.1998.tb01722.x

Pribasnig, M. A., Mrak, I., Grabner, G. F., Taschler, U., Knittelfelder, O., Scherz, B., et al. (2015). α/β Hydrolase Domain-Containing 6 (ABHD6) Degrades the Late Endosomal/Lysosomal Lipid Bis(monoacylglycero)phosphate. *J. Biol. Chem.* 290 (50), 29869–29881. doi:10.1074/jbc.M115.669168

Prinz, W. A., Toulmay, A., and Balla, T. (2020). The Functional Universe of Membrane Contact Sites. *Nat. Rev. Mol. Cel Biol.* 21 (1), 7–24. doi:10.1038/s41580-019-0180-9

Rada, P., González-Rodríguez, Á., García-Monzón, C., Valverde, Á. M., and Valverde, Á. M (2020). Understanding Lipotoxicity in NAFLD Pathogenesis: Is CD36 a Key Driver? *Cel Death Dis.* 11 (9), 802. doi:10.1038/s41419-020-03003-w

Ramon, S., Bancos, S., Thatcher, T. H., Murant, T. I., Moshkani, S., Sahler, J. M., et al. (2012). Peroxisome Proliferator-Activated Receptor γ B Cell-Specific-Deficient Mice Have an Impaired Antibody Response. *J.I.* 189 (10), 4740–4747. doi:10.4049/jimmunol.1200956

Rawnsley, D. R., and Diwan, A. (2020). Lysosome Impairment as a Trigger for Inflammation in Obesity: The Proof Is in the Fat. *EBioMedicine* 56, 102824. doi:10.1016/j.ebiom.2020.102824

Rieusset, J. (2017). Endoplasmic Reticulum-Mitochondria Calcium Signaling in Hepatic Metabolic Diseases. *Biochim. Biophys. Acta (Bba) - Mol. Cel Res.* 1864 (6), 865–876. doi:10.1016/j.bbamcr.2017.01.001

Rigante, D., Cipolla, C., Basile, U., Gulli, F., and Savastano, M. C. (2017). Overview of Immune Abnormalities in Lysosomal Storage Disorders. *Immunol. Lett.* 188 (July), 79–85. doi:10.1016/j.imlet.2017.07.004

Roche, P. A., and Cresswell, P. (1990). Invariant Chain Association with HLA-DR Molecules Inhibits Immunogenic Peptide Binding. *Nature* 345 (6276), 615–618. doi:10.1038/345615a0

Russo, L., and Lumeng, C. N. (2018). Properties and Functions of Adipose Tissue Macrophages in Obesity. *Immunology* 155 (4), 407–417. doi:10.1111/imm.13002

Sáez, J. J., Diaz, J., Ibañez, J., Bozo, J. P., Cabrera Reyes, F., Alamo, M., et al. (2019). The Exocyst Controls Lysosome Secretion and Antigen Extraction at the Immune Synapse of B Cells. *J. Cel Biol.* 218 (7), 2247–2264. doi:10.1083/jcb.201811131

Saito, T., Kuma, A., Sugiura, Y., Ichimura, Y., Obata, M., Kitamura, H., et al. (2019). Autophagy Regulates Lipid Metabolism through Selective Turnover of NCoR1. *Nat. Commun.* 10 (1). doi:10.1038/s41467-019-08829-3

Sarkar, S., Carroll, B., Buganim, Y., Maetzel, D., Ng, A. H. M., Cassady, J. P., et al. (2013). Impaired Autophagy in the Lipid-Storage Disorder Niemann-Pick Type C1 Disease. *Cel Rep.* 5 (5), 1302–1315. doi:10.1016/j.celrep.2013.10.042

Seppala-Lindroos, A. (2002). Fat Accumulation in the Liver Is Associated with Defects in Insulin Suppression of Glucose Production and Serum Free Fatty Acids Independent of Obesity in Normal Men. *J. Clin. Endocrinol. Metab.* 87 (7), 3023–3028. doi:10.1210/jcem.87.7.8638

Seranova, E., Connolly, K. J., Zatyka, M., Rosenstock, T. R., Barrett, T., Tuxworth, R. I., et al. (2017). Dysregulation of Autophagy as a Common Mechanism in Lysosomal Storage Diseases. *Essays Biochem.* 61 (6), 733–749. doi:10.1042/EBC20170055

Serrano-Puebla, A., and Boya, P. (2016). Lysosomal Membrane Permeabilization in Cell Death: New Evidence and Implications for Health and Disease. *Ann. N.Y. Acad. Sci.* 1371 (1), 30–44. doi:10.1111/nyas.12966

Shaikh, S. R., Haas, K. M., Beck, M. A., and Teague, H. (2015). The Effects of Diet-Induced Obesity on B Cell Function. *Clin. Exp. Immunol.* 179 (1), 90–99. doi:10.1111/cei.12444

Shi, L., Liu, J., Su, Qing., and Yang, Zhen. (2019). Glucose Metabolism Imaging. *Front. Endocrinol.* 10 (October), 1–10. doi:10.1007/978-3-319-48382-5_810.1007/978-981-13-7458-6_1

Showalter, M. R., Berg, A. L., Nagourney, A., Heil, H., Carraway, K. L., and Fiehn, O. (2020). The Emerging and Diverse Roles of Bis(Monoacylglycero) Phosphate Lipids in Cellular Physiology and Disease. *Ijms* 21 (21), 8067. doi:10.3390/ijms21218067

Silverstein, R. L., and Febbraio., M. (2009). CD36, a Scavenger Receptor Involved in Immunity, Metabolism, Angiogenesis, and Behavior. *Sci. Signal.* 2 (72). doi:10.1126/scisignal.272re3

Singh, R., and Cresswell, P. (2010). Defective Cross-Presentation of Viral Antigens in GILT-free Mice. *Science* 328 (5984), 1394–1398. doi:10.1126/science.1189176

Singh, R., Xiang, Y., Wang, Y., Baikati, K., Cuervo, A. M., Luu, Y. K., et al. (2009). Autophagy Regulates Adipose Mass and Differentiation in Mice. *J. Clin. Invest.* 119 (11), 3329–3339. doi:10.1172/JCI39228

Singhal, A., Krystofiak, E. S., Jerome, W. G., and Song, B. (2020). 2-Hydroxypropyl-Gamma-Cyclodextrin Overcomes NPC1 Deficiency by Enhancing Lysosome-ER Association and Autophagy. *Sci. Rep.* 10 (1), 1–14. doi:10.1038/s41598-020-65627-4

Singhal, A., Szente, L., Hildreth, J. E. K., and Song, B. (2018). Hydroxypropyl-beta and -gamma Cyclodextrins rescue Cholesterol Accumulation in Niemann-Pick C1 Mutant Cell via Lysosome-Associated Membrane Protein 1. *Cel Death Dis.* 9 (10), 1019. doi:10.1038/s41419-018-1056-1

Soccio, R. E., and Breslow, J. L. (2004). Intracellular Cholesterol Transport. *Atvb* 24 (7), 1150–1160. doi:10.1161/01.ATV.0000131264.66417.d5

Soussi, H., Clément, K., and Dugail, I. (2016). Adipose Tissue Autophagy Status in Obesity: Expression and Flux-Two Faces of the Picture. *Autophagy* 12 (3), 588–589. doi:10.1080/15548627.2015.1106667

Srikakulapu, P., and McNamara, C. A. (2020). B Lymphocytes and Adipose Tissue Inflammation. *Atvb* 40 (5), 1110–1122. doi:10.1161/ATVBAHA.119.312467

Starosta, R. T., Vairo, F. P. e., Dornelles, A. D., Basgalupp, S. P., Siebert, M., Pedroso, M. L. A., et al. (2020). Liver Involvement in Patients with Gaucher Disease Types I and III. *Mol. Genet. Metab. Rep.* 22 (September 2019), 100564. doi:10.1016/j.ymgmr.2019.100564

Stirnemann, J., Belmatoug, N., Camou, F., Serratrice, C., Froissart, R., Caillaud, C., et al. (2017). A Review of Gaucher Disease Pathophysiology, Clinical Presentation and Treatments. *Ijms* 18 (2), 441. doi:10.3390/ijms18020441

Sun, Y., Liou, B., Ran, H., Skelton, M. R., Williams, M. T., Vorhees, C. V., et al. (2010). Neuronopathic Gaucher Disease in the Mouse: Viable Combined Selective Saposin C Deficiency and Mutant Glucocerebrosidase (V394L) Mice with Glucosylsphingosine and Glucosylceramide Accumulation and Progressive Neurological Deficits. *Hum. Mol. Genet.* 19 (6), 1088–1097. doi:10.1093/hmg/ddp580

Tatti, M., Motta, M., Di bartolomeo, S., Scarpa, S., Cianfanelli, V., Cecconi, F., et al. (2012). Reduced Cathepsins B and D Cause Impaired Autophagic Degradation that Can Be Almost Completely Restored by Overexpression of These Two Proteases in Sap C-Deficient Fibroblasts. *Hum. Mol. Genet.* 21 (23), 5159–5173. doi:10.1093/hmg/dds367

te Vruchte, D., Jeans, A., Platt, F. M., and Sillence, D. J. (2010). Glycosphingolipid Storage Leads to the Enhanced Degradation of the B Cell Receptor in Sandhoff Disease Mice. *J. Inherit. Metab. Dis.* 33 (3), 261–270. doi:10.1007/s10545-010-9109-3

Tian, K., Xu, Y., Sahebkar, A., and Xu, S. (2020). CD36 in Atherosclerosis: Pathophysiological Mechanisms and Therapeutic Implications. *Curr. Atheroscler. Rep.* 22 (10). doi:10.1007/s11883-020-00870-8

Tong, L., Wang, L., Yao, S., Jin, L., Yang, J., Zhang, Y., et al. (2019). PPARδ Attenuates Hepatic Steatosis through Autophagy-Mediated Fatty Acid Oxidation. *Cel Death Dis.* 10 (3). doi:10.1038/s41419-019-1458-8

Tontonoz, P., and Spiegelman, B. M. (2008). Fat and beyond: The Diverse Biology of PPARγ. *Annu. Rev. Biochem.* 77, 289–312. doi:10.1146/annurev.biochem.77.061307.091829

Turcot, V., Bouchard, L., Faucher, G., Tchernof, A., Deshaies, Y., Pérusse, L., et al. (2012). A Polymorphism of the Interferon-Gamma-Inducible Protein 30 Gene Is Associated with Hyperglycemia in Severely Obese Individuals. *Hum. Genet.* 131 (1), 57–66. doi:10.1007/s00439-011-1043-4

Turk, V. (2001). New Embo Members' Review: Lysosomal Cysteine Proteases: Facts and Opportunities. *EMBO J.* 20 (17), 4629–4633. doi:10.1093/emboj/20.17.4629

Turk, V., Stoka, V., Vasiljeva, O., Renko, M., Sun, T., Turk, B., et al. (2012). Cysteine Cathepsins: From Structure, Function and Regulation to New

Frontiers. *Biochim. Biophys. Acta (Bba) - Proteins Proteomics* 1824 (1), 68–88. doi:10.1016/j.bbapap.2011.10.002

Uranga, R. M., and Keller, J. N. (2019). The Complex Interactions between Obesity, Metabolism and the Brain. *Front. Neurosci.* 13, 1–21. doi:10.3389/fnins.2019.00513

Urban, B. C., Willcox, N., and Roberts, D. J. (2001). A Role for CD36 in the Regulation of Dendritic Cell Function. *Proc. Natl. Acad. Sci.* 98 (15), 8750–8755. doi:10.1073/pnas.151028698

van der Lienden, M. J. C., Aten, J., Marques, A. R. A., Marques, I. S. E., Larsen, P. W. B., Claessen, N., et al. (2021). Gcase and Limp2 Abnormalities in the Liver of Niemann Pick Type C Mice. *Ijms* 22 (5), 2532. doi:10.3390/ijms22052532

Vanier, M., and Millat, G. (2003). Niemann-Pick Disease Type C. *Clin. Genet.* 64 (4), 269–281. doi:10.1034/j.1399-0004.2003.00147.x

Vázquez, M. C., del Pozo, T., Robledo, F. A., Carrasco, G., Pavez, L., Olivares, F., et al. (2011). Talía del Pozo, Fermín A. Robledo, Gonzalo Carrasco, Leonardo Pavez, Felipe Olivares, Mauricio González, and Silvana ZanlungoAlteration of Gene Expression Profile in Niemann-Pick Type C Mice Correlates with Tissue Damage and Oxidative Stress. *PLoS ONE* 6 (12), e28777. doi:10.1371/journal.pone.0028777

Vázquez-Vela, M. E. F., Torres, N., Tovar, A. R., and Tovar, A. R. (2008). White Adipose Tissue as Endocrine Organ and its Role in Obesity. *Arch. Med. Res.* 39 (8), 715–728. doi:10.1016/j.arcmed.2008.09.005

Vidal-Puig, A. J., Considine, R. V., Jimenez-Liñan, M., Werman, A., Pories, W. J., Caro, J. F., et al. (1997). Peroxisome Proliferator-Activated Receptor Gene Expression in Human Tissues. Effects of Obesity, Weight Loss, and Regulation by Insulin and Glucocorticoids. *J. Clin. Invest.* 99 (10), 2416–2422. doi:10.1172/JCI119424

Vitner, E. B., Dekel, H., Zigdon, H., Shachar, T., Farfel-Becker, T., Eilam, R., et al. (2010). Hani Dekel, Hila Zigdon, Tamar Shachar, Tamar Farfel-Becker, Raya Eilam, Stefan Karlsson, and Anthony H. FutermanAltered Expression and Distribution of Cathepsins in Neuronopathic Forms of Gaucher Disease and in Other Sphingolipidoses. *Hum. Mol. Genet.* 19 (18), 3583–3590. doi:10.1093/hmg/ddq273

Wang, F., Jia, J., and Rodrigues, B. (2017). Autophagy, Metabolic Disease, and Pathogenesis of Heart Dysfunction. *Can. J. Cardiol.* 33 (7), 850–859. doi:10.1016/j.cjca.2017.01.002

Wang, T., Wei, Q., Liang, L., Tang, X., Yao, J., Lu, Y., et al. (2020a). OSBPL2 Is Required for the Binding of COPB1 to ATGL and the Regulation of Lipid Droplet Lipolysis. *IScience* 23 (7), 101252. doi:10.1016/j.isci.2020.101252

Wang, Y., Nakajima, T., Gonzalez, F. J., and Tanaka, N. (2020b). PPARs as Metabolic Regulators in the Liver: Lessons from Liver-specific PPAR-Null Mice. *Ijms* 21 (6), 2061. doi:10.3390/ijms21062061

Weisberg, S. P., McCann, D., Desai, M., Rosenbaum, M., Leibel, R. L., and Ferrante, A. W. (2003). Daniel McCann, Manisha Desai, Michael Rosenbaum, Rudolph L. Leibel, and Anthony W. FerranteObesity Is Associated with Macrophage Accumulation in Adipose Tissue. *J. Clin. Invest.* 112 (12), 1796–1808. doi:10.1172/JCI1924610.1172/jci200319246

Winer, D. A., Winer, S., Shen, L., Wadia, P. P., Yantha, J., Paltser, G., et al. (2011). B Cells Promote Insulin Resistance through Modulation of T Cells and Production of Pathogenic IgG Antibodies. *Nat. Med.* 17 (5), 610–617. doi:10.1038/nm.2353

Won, W.-J., Bachmann, M. F., and Kearney, J. F. (2008). CD36 Is Differentially Expressed on B Cell Subsets during Development and in Responses to Antigen. *J. Immunol.* 180 (1), 230–237. doi:10.4049/jimmunol.180.1.230

Wraith, J. E., Baumgartner, M. R., Bembi, B., Covanis, A., Levade, T., Mengel, E., et al. (2009). Recommendations on the Diagnosis and Management of Niemann-Pick Disease Type C. *Mol. Genet. Metab.* 98 (1–2), 152–165. doi:10.1016/j.ymgme.2009.06.008

Wu, Z., Xu, J., Tan, J., Song, Y., Liu, L., Zhang, F., et al. (2019). Mesenteric Adipose Tissue B Lymphocytes Promote Local and Hepatic Inflammation in Non-alcoholic Fatty Liver Disease Mice. *J. Cel Mol. Med.* 23 (5), 3375–3385. doi:10.1111/jcmm.14232

Xie, C., Turley, S. D., and Dietschy, J. M. (2000). Centripetal Cholesterol Flow from the Extrahepatic Organs through the Liver Is Normal in Mice with Mutated Niemann-Pick Type C Protein (NPC1). *J. Lipid Res.* 41 (8), 1278–1289. PMID: 10946016. doi:10.1016/s0022-2275(20)33436-2

Xu, Q., Mariman, E. C. M., Goossens, G. H., Blaak, E. E., Jocken, J. W. E., and JohanJocken, W. E. (2020). Cathepsin Gene Expression in Abdominal Subcutaneous Adipose Tissue of Obese/Overweight Humans. *Adipocyte* 9 (1), 246–252. doi:10.1080/21623945.2020.1775035

Yadati, T., Houben, T., Bitorina, A., Oligschlaeger, Y., Gijbels, M. J., Mohren, R., et al. (2021). Inhibition of Extracellular Cathepsin D Reduces Hepatic Lipid Accumulation and Leads to Mild Changes in Inflammationin NASH Mice. *Front. Immunol.* 12 (July), 675535. doi:10.3389/fimmu.2021.675535

Yadati, T., Houben, T., Bitorina, A., and Shiri-Sverdlov, R. (2020). The Ins and Outs of Cathepsins: Physiological Function and Role in Disease Management. *Cells* 9 (7), 1679. doi:10.3390/cells9071679

Yañez, M. J., Marín, T., Balboa, E., Klein, A. D., Alvarez, A. R., and Zanlungo, S. (2020). Finding Pathogenic Commonalities between Niemann-Pick Type C and Other Lysosomal Storage Disorders: Opportunities for Shared Therapeutic Interventions. *Biochim. Biophys. Acta (Bba) - Mol. Basis Dis.* 1866 (10), 165875. doi:10.1016/j.bbadis.2020.165875

Yang, L., Li, P., Fu, S., Calay, E. S., and Hotamisligil, G. S. (2010). Defective Hepatic Autophagy in Obesity Promotes ER Stress and Causes Insulin Resistance. *Cel Metab.* 11 (6), 467–478. doi:10.1016/j.cmet.2010.04.005

Yazıcı, D., and Sezer, H. (2017). "Insulin Resistance, Obesity and Lipotoxicity," in *" in Vol. 960. Advances in Experimental Medicine and Biology*. Editors A. B. Engin and A. Engin (Cham: Springer International Publishing), 277–304. doi:10.1007/978-3-319-48382-5_12

You, Y., Bao, W.-L., Zhang, S.-L., Li, H.-D., Li, H., Dang, W.-Z., et al. (2020). Sorting Nexin 10 Mediates Metabolic Reprogramming of Macrophages in Atherosclerosis through the Lyn-dependent TFEB Signaling Pathway. *Circ. Res.* 127 (4), 534–549. doi:10.1161/CIRCRESAHA.119.315516

Yu, H., Yang, F., Zhong, W., Jiang, X., Zhang, F., Ji, X., et al. (2021). Secretory Galectin-3 Promotes Hepatic Steatosis via Regulation of the PPARγ/CD36 Signaling Pathway. *Cell Signal.* 84 (May), 110043. doi:10.1016/j.cellsig.2021.110043

Yu, W., Gong, J.-S., Ko, M., Garver, W. S., Yanagisawa, K., and Michikawa, M. (2005). Altered Cholesterol Metabolism in Niemann-Pick Type C1 Mouse Brains Affects Mitochondrial Function. *J. Biol. Chem.* 280 (12), 11731–11739. doi:10.1074/jbc.M412898200

Yuseff, M.-I., Lennon-DumÃ©nil, A. M., and Ana, M. L. (2015). B Cells Use Conserved Polarity Cues to Regulate Their Antigen Processing and Presentation Functions. *Front. Immunol.* 6 (4), 1–7. doi:10.3389/fimmu.2015.00251

Yuseff, M.-I., Reversat, A., Lankar, D., Diaz, J., Fanget, I., Pierobon, P., et al. (2011). Polarized Secretion of Lysosomes at the B Cell Synapse Couples Antigen Extraction to Processing and Presentation. *Immunity* 35 (3), 361–374. doi:10.1016/j.immuni.2011.07.008

Zhang, F., Jiang, W. W., Li, X., Qiu, X. Y., Wu, Z., Chi, Y. J., et al. (2016). Role of Intrahepatic B Cells in Non-alcoholic Fatty Liver Disease by Secreting Pro-inflammatory Cytokines and Regulating Intrahepatic T Cells. *J. Dig. Dis.* 17 (7), 464–474. doi:10.1111/1751-2980.12362

Zhang, X., Evans, T. D., Jeong, S.-J., and Razani, B. (2018b). Classical and Alternative Roles for Autophagy in Lipid Metabolism. *Curr. Opin. Lipidol.* 29 (3), 203–211. doi:10.1097/MOL.0000000000000509

Zhang, Y., Sowers, J. R., and Ren., J. (2018a). Targeting Autophagy in Obesity: From Pathophysiology to Management. *Nat. Rev. Endocrinol.* 14 (6), 356–376. doi:10.1038/s41574-018-0009-1

Zhao, L., Zhang, C., Luo, X., Wang, P., Zhou, W., Zhong, S., et al. (2018). CD36 Palmitoylation Disrupts Free Fatty Acid Metabolism and Promotes Tissue Inflammation in Non-alcoholic Steatohepatitis. *J. Hepatol.* 69 (3), 705–717. doi:10.1016/j.jhep.2018.04.006

Conflict of Interest: The authors declare that the research was conducted in the absence of any commercial or financial relationships that could be construed as a potential conflict of interest.

Publisher's Note: All claims expressed in this article are solely those of the authors and do not necessarily represent those of their affiliated organizations, or those of the publisher, the editors and the reviewers. Any product that may be evaluated in this article, or claim that may be made by its manufacturer, is not guaranteed or endorsed by the publisher.

frontiers in Cell and Developmental Biology

MINI REVIEW
published: 16 December 2021
doi: 10.3389/fcell.2021.813995

Weibel Palade Bodies: Unique Secretory Organelles of Endothelial Cells that Control Blood Vessel Homeostasis

*Johannes Naß†, Julian Terglane† and Volker Gerke**

Centre for Molecular Biology of Inflammation, Institute of Medical Biochemistry, University of Muenster, Muenster, Germany

Vascular endothelial cells produce and release compounds regulating vascular tone, blood vessel growth and differentiation, plasma composition, coagulation and fibrinolysis, and also engage in interactions with blood cells thereby controlling hemostasis and acute inflammatory reactions. These interactions have to be tightly regulated to guarantee smooth blood flow in normal physiology, but also allow specific and often local responses to blood vessel injury and infectious or inflammatory insults. To cope with these challenges, endothelial cells have the remarkable capability of rapidly changing their surface properties from non-adhesive (supporting unrestricted blood flow) to adhesive (capturing circulating blood cells). This is brought about by the evoked secretion of major adhesion receptors for platelets (von-Willebrand factor, VWF) and leukocytes (P-selectin) which are stored in a ready-to-be-used form in specialized secretory granules, the Weibel-Palade bodies (WPB). WPB are unique, lysosome related organelles that form at the trans-Golgi network and further mature by receiving material from the endolysosomal system. Failure to produce correctly matured VWF and release it through regulated WPB exocytosis results in pathologies, most importantly von-Willebrand disease, the most common inherited blood clotting disorder. The biogenesis of WPB, their intracellular motility and their fusion with the plasma membrane are regulated by a complex interplay of proteins and lipids, involving Rab proteins and their effectors, cytoskeletal components as well as membrane tethering and fusion machineries. This review will discuss aspects of WPB biogenesis, trafficking and exocytosis focussing on recent findings describing factors contributing to WPB maturation, WPB-actin interactions and WPB-plasma membrane tethering and fusion.

Keywords: calcium, exocytosis, lysosome-related organelle, secretory organelles, hemostasis

OPEN ACCESS

Edited by:
Mitsuo Tagaya,
Tokyo University of Pharmacy and Life Sciences, Japan

Reviewed by:
Ruben Bierings,
Erasmus Medical Center, Netherlands
Thomas Daniel Nightingale,
Queen Mary University of London, United Kingdom

****Correspondence:***
Volker Gerke
gerke@uni-muenster.de

†These authors have contributed equally to this work and share first authorship

Specialty section:
This article was submitted to Membrane Traffic, a section of the journal Frontiers in Cell and Developmental Biology

Received: *12 November 2021*
Accepted: *30 November 2021*
Published: *16 December 2021*

Citation:
Naß J, Terglane J and Gerke V (2021) Weibel Palade Bodies: Unique Secretory Organelles of Endothelial Cells that Control Blood Vessel Homeostasis. Front. Cell Dev. Biol. 9:813995. doi: 10.3389/fcell.2021.813995

INTRODUCTION

Endothelial cells comprise the inner lining of blood vessels and thus the first cellular barrier separating blood and tissue. They form single-layered epithelia that differ in morphology, molecular characteristics, physiology and function depending on the type of vascular bed. As such they seal blood vessels and control traffic of nutrients, hormones, growth and differentiation factors, particles and cells (immune cells, metastasizing tumor cells and even pathogens) to and from the vasculature. Moreover, through selective secretion and uptake as well as production and decoding of signaling

molecules they regulate blood vessel homeostasis including clotting and coagulation, fibrinolysis and thrombosis as well as vascular tone and local inflammatory reactions.

One striking characteristic of endothelial cells relates to the adhesive properties of their apical cell surface that faces the blood vessel lumen. In the normal physiological state this surface does not interact firmly with leukocytes, erythrocytes and platelets thereby permitting an unrestricted blood flow and blood cell circulation. However, upon insult and endothelial cell activation surface properties change rapidly allowing leukocytes and platelets to adhere to the vessel wall. These cell interactions are vital to ensure proper responses to blood vessel injury (platelet plug formation and initiation of coagulation) and inflammatory or infectious insult (recruitment of leukocytes to sites of tissue damage or infection). Endothelial cells can actively control these surface properties by the regulated presentation of specific adhesion molecules. To do so, vascular endothelial cells are equipped with unique secretory organelles that store among other things leukocyte and platelet adhesion receptors to be released on demand. In honor of their initial discovery by Ewald Weibel and George Palade in electron microscopic analyses of rat and human pulmonary arteries these organelles were termed Weibel-Palade bodies (WPB) (Weibel and Palade, 1964). Only later these peculiar membrane compartments were shown to contain the major platelet adhesion molecule von-Willebrand factor (VWF) and the leukocyte receptor P-selectin (Wagner et al., 1982; Bonfanti et al., 1989). The physiological and also pathophysiological importance of WPB and their principal cargo VWF is emphasized by the fact that failure to produce and release proper VWF results in von-Willebrand disease, the major inherited bleeding disorder (for reviews see Schneppenheim and Budde, 2011; Leebeek and Eikenboom, 2016). On the other hand, vascular occlusion is a consequence of highly elevated vascular VWF levels as for instance observed in thrombotic thrombocytopenic purpura. (for review see Sadler, 2008). Thus, WPB are pivotal components of the precisely tuned machinery that orchestrates blood vessel homeostasis. This mini review will highlight the unique features of WPB particularly emphasizing recent developments in the understanding of their maturation and secretion.

WPB Maturation

WPB are born at the trans-Golgi network (TGN) where they bud off in the form of discernible structures. Their dimensions and unique morphology are dictated by the main cargo VWF, a large glycoprotein synthesized and first processed in the ER (for references and recent crystal structure of the VWF D'D3 domains see Dong et al., 2019). VWF is then transported to the Golgi where it is assembled into defined quanta. A copacking of these quanta occurs in the TGN prior to or concomitant with the actual budding of immature WPB which can maintain connections to the Golgi for 2–4 h (Zenner et al., 2007; Ferraro et al., 2014; Mourik et al., 2015). These connections and the close proximity to the Golgi likely permit the further addition of VWF and possibly other cargo to the immature WPB (Mourik et al., 2015). The early WPB released from the TGN further mature to finally yield the highly elongated cigar-shaped organelles primarily found in the periphery of endothelial cells (for reviews see van Mourik et al., 2002; Michaux and Cutler, 2004; McCormack et al., 2017; Karampini et al., 2020). This maturation is driven on one hand by the continued multimerization and tight packing of VWF into a quasi-crystalline arrangement enwrapped by a membrane, which requires luminal acidification and reflects itself in the condensation of WPB from an electron lucent immature organelle to an electron dense mature structure. On the other hand, post-Golgi maturation is accompanied by acquisition of additional cytosolic and also endosomal/lysosomal components. They include the RabGTPase Rab27a and the tetraspanin CD63 identifying WPB as lysosome-related organelles (LRO) that share molecular features with pigment-storing melanosomes (for reviews see Raposo et al., 2007; Bowman et al., 2019). It is worth noting here that the net size of WPB is primarily determined at the level of the Golgi and that further maturation mainly leads to condensation and tubular elongation. Several aspects of WPB size control and maturation have been addressed recently revealing novel and exciting connections.

An interesting link between WPB size control and cell metabolism was discovered recently following the identification of the Arf guanine nucleotide exchange factor (GEF) GBF1 (a GEF for Arf1 and 4) as a factor promoting ER/Golgi trafficking of VWF. GBF1 can be activated by phosphorylation by AMP-activated protein kinase (AMPK), a key enzyme coupling metabolic changes to cellular signaling, and it was shown that low glucose levels and subsequent AMPK activation lead to GBF1 phosphorylation and a resulting upregulation of anterograde VWF trafficking. This in turn produces smaller WPB and reduces VWF secretion (Lopes-da-Silva et al., 2019) (**Figure 1**). Arf GTPase activating proteins (GAPs) that inactivate their cognate Arf proteins also appear to regulate WPB size as depletion in endothelial cells of the ArfGAP SMAP1 leads to a size reduction in the WPB that form (Watanabe et al., 2021). The SNARE Sec22b was recently identified as another factor controlling WPB morphology presumably also by affecting the ER/Golgi transport route of VWF. Depletion of Sec22b causes a loss of large, elongated WPB along with a dilation of ER cisternae that accumulate non-processed VWF (Karampini et al., 2020) (**Figure 1**). Thus, several factors regulating VWF maturation and packing into WPB and thereby affecting WPB size and morphology have been discovered and approaches to exploit these also in pathophysiological settings appear promising. Along these lines, Ferraro and coworkers developed a microscopic screening approach measuring WPB size that led to the identification of first candidate compounds that reduce WPB length. As a consequence, this also reduces the pro-thrombotic activity of secreted VWF as VWF secretion from shorter WPB significantly dampens its platelet adhesion capability (Ferraro et al., 2016, 2020).

Once early WPB have emerged from the Golgi they acquire additional proteins (and presumably also lipids) in the process of maturation that is accompanied by a microtubule-dependent movement to the cell periphery (for review see McCormack et al., 2017). Many of those additional WPB components have been identified, among other things through proteomic screens

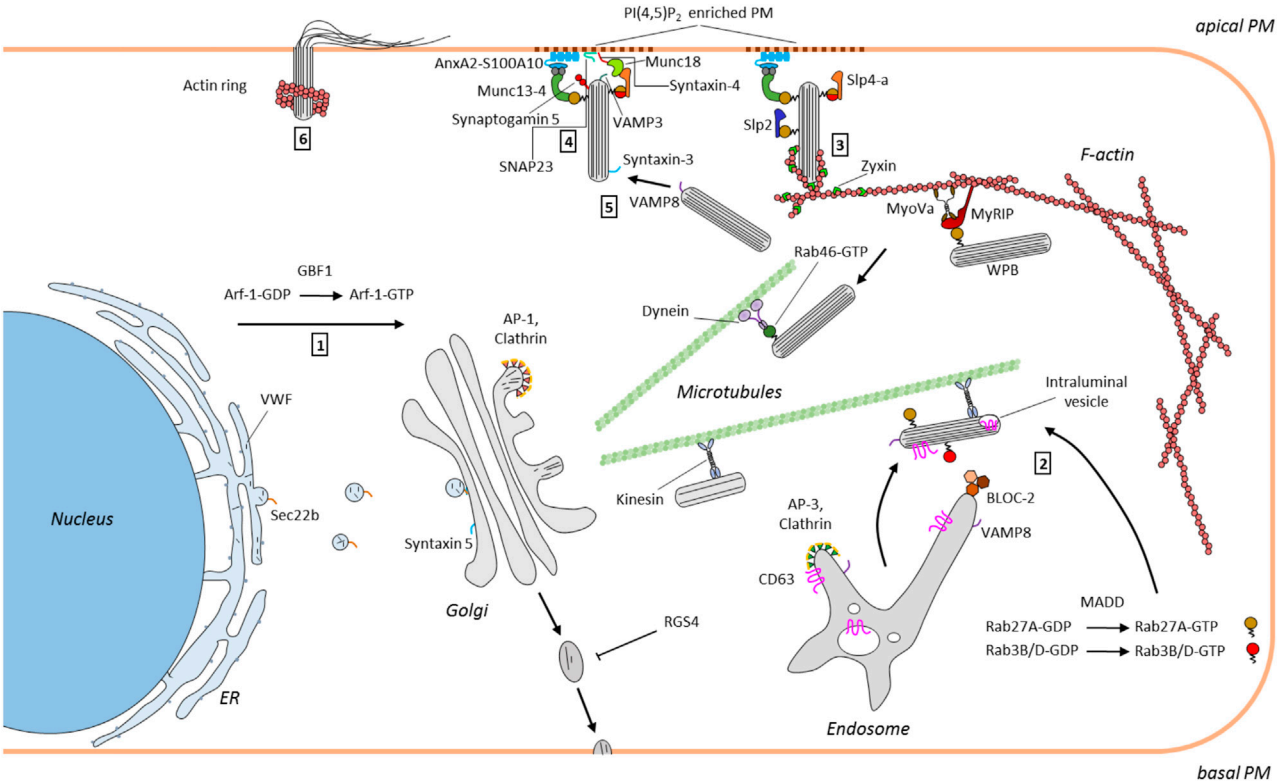

FIGURE 1 | Scheme depicting the WPB itinerary in endothelial cells. WPB formation is driven by VWF that is produced at the ER and trafficked to the Golgi (1). WPB that bud from the TGN in an AP-1 and clathrin dependent process are then transported to the cell periphery along microtubules. This is accompanied by the BLOC-2 and annexin A8 dependent transfer of endosomal components such as CD63 and VAMP8 to WPB (2). Maturing WPB acquire certain RabGTPases, e.g. Rab27A and Rab3B/D, the former required for linking WPB at the cortical actin cytoskeleton (via MyRIP/MyoVc) and supporting exocytosis (*via* Slp4-a) (3). Secretagogue induced tethering at and fusion with the PM requires docking factors, such as the annexin A2/S100A10/Munc13-4 complex and a SNARE-based fusion machinery and can also involve compound and cumulative events (3, 4 and 5). Finally, post fusion actin rings have been observed that support the full release of highly multimeric VWF (6). Mainly factors identified in the recent years have been included.

(van Breevoort et al., 2012; Holthenrich et al., 2019); however, their delivery to and association with the maturing organelle has only recently been characterized in a few cases. In line with WPB representing LRO, some proteins found on mature WPB are of late endosome/lysosome (LEL) origin (e.g. the tetraspanin and P selectin cofactor CD63) and most likely routed to the organelle by direct transport possibly involving tubular carriers. Whereas earlier studies had identified the Ca^{2+}/phospholipid-binding protein annexin A8 as a LEL-localized component of the machinery facilitating LEL-to-WPB delivery of CD63 (Poeter et al., 2014), Sharda and coworkers (Sharda et al., 2020) recently reported the participation of biogenesis of lysosome related organelle-2 (BLOC-2), a protein that can be mutated in the recessive bleeding disorder Hermansky-Pudlak syndrome. Among other things Hermansky-Pudlak syndrome is associated with platelet aggregation and pigmentation defects, the latter due to compromised maturation of melanosomes, LROs that show several parallels to WPB (for reviews see Raposo et al., 2007; Simons and Raposo, 2009). Depletion of BLOC-2 results in both, compromised LEL-to-WPB transport of CD63 and general WPB maturation defects with the WPB appearing round instead of elongated and clustered in the perinuclear region (**Figure 1**). As the immature organelles formed under these conditions failed to process VWF into the highly multimeric forms these were absent in the material secreted from BLOC-2 depleted endothelial cells following thrombin stimulation (and intracellular Ca^{2+} mobilization). Moreover, the exocyst complex was identified as a target of BLOC-2 in endothelial cells and exocyst depletion or inhibition phenocopied the WPB maturation defects seen in BLOC-2 deficient cells. In this study exocyst was also found to serve a second function in impeding WPB exocytosis at the PM (Sharda et al., 2020). The involvement of BLOC-2 in proper WPB maturation was also shown in the respective mutant mice that are characterized by impaired VWF tubulation (Ma et al., 2016). Another gene that can be mutated in Hermansky-Pudlak syndrome is *AP3B1* encoding the adaptor complex three β1 subunit. Blood outgrowth endothelial cells from Hermansky-Pudlak syndrome patients carrying the *AP3B1* mutation also lack CD63 in their WPB indicative of improper organelle maturation. Moreover, these cells are compromised in their evoked WPB exocytosis, most likely because they fail to recruit the v-SNARE VAMP8 to maturing WPB (Karampini et al., 2019) (**Figure 1**). While the above-mentioned studies identified maturation factors/pathways involved in the delivery of

transmembrane proteins (CD63, VAMP8) to maturing WPB, another hallmark of mature WPB are a specific subset of cytosolically associated RabGTPases, in particular Rab27a and the Rab3 isoforms b and d. Addressing this aspect of the maturation, Kat and coworkers (Kat et al., 2021) could recently identify MAP kinase-activating death domain (MADD) as a crucial component involved. MADD serves as a GEF for these Rabs and silencing of MADD through knockdown approaches markedly reduced the recruitment of Rab27a, Rab3b and Rab3d to maturing WPB (**Figure 1**). Finally, it should be noted that WPB maturation is not only accompanied by tubulation and tight packing of VWF and the acquisition of additional protein contents, it also generates other morphological characteristics typical for LRO. Specifically, vesicles inside the lumen of the organelle, a hallmark of many LRO, were observed recently in mature WPB of endothelial cells. Following WPB exocytosis these intraluminal vesicles which are positive for CD63 could also be released and possibly function in intercellular communication, again extending the similarity to other LROs (Streetley et al., 2019).

Thus, WPB maturation is a highly complex process involving *de novo* protein acquisition, LEL-to-WPB protein transport and morphological alterations that eventually generate the unique rod-shaped organelle containing the tubulated highly multimeric VWF.

WPB-Plasma Membrane Tethering and Secretion

The VWF stored in WPB can be released in different ways. Basal secretion, typically of less multimeric VWF, provides the circulation with low levels of these VWF species, and constitutive secretion, preferentially occurring at the basolateral membrane surface of endothelial cells, deposits VWF in the subendothelial matrix. Specific components regulating these secretory events have not been systematically investigated with the exception of a recent screen that identified the regulator of G protein signaling 4 (RGS4) as a negative regulator of the constitutive pathway (Patella and Cutler, 2020). The majority of fully matured WPB, however, is retained inside the cell to await secretagogue stimulation, for example following blood vessel injury or local inflammatory insults, to present highly multimeric VWF and P-selectin on the endothelial cell surface by regulated exocytosis. Retention is achieved by anchorage in the cortical actin cytoskeleton, which is mediated with help of a complex consisting of Rab27a, the Rab27a effector MyRIP and the actin binding myosin Va (Nightingale et al., 2009; Rojo Pulido et al., 2011; Conte et al., 2016) (**Figure 1**). Endothelial stimulation, which can be elicited by a plethora of agonists (Lowenstein et al., 2005; Schillemans et al., 2019b) and typically results in elevated intracellular Ca^{2+} or cAMP levels functioning as second messengers, mobilizes the cortically anchored WPB and initiates the tethering/docking at and fusion with the plasma membrane (PM). The detailed molecular mechanisms responsible for releasing WPB from the cortical anchorage and enabling their PM contact are largely unknown, but they are likely to involve WPB associated RabGTPases. A central role for Rab27a in this event has been shown by Bierings and coworkers (Bierings et al., 2012) who reported that the evoked release of mature WPB is regulated by the interaction of Rab27a with either MyRIP (supporting cortical anchorage) or synaptotagmin-like protein 4-a (Slp4-a) (promoting WPB exocytosis) (**Figure 1**). Rab46 was recently identified as another Rab regulating selective WPB trafficking in the cell cortex and thereby specific cargo release following histamine evoked and Ca^{2+} mediated exocytosis of WPB. Rab46, which harbors a Ca^{2+}-binding EF hand, localizes to only a subset of the peripheral WPB that are negative for the leukocyte receptor P-selectin but contain angiopoietin-2. It senses the Ca^{2+} elevation elicited by histamine stimulation and then triggers a retrograde, dynein-dependent transport of the associated peripheral WPB to the cell center. As the Rab46 negative, P-selectin containing WPB exocytose under these conditions, only a fraction of the WPB cargo, e.g. the proinflammatory P-selectin, is released (Miteva et al., 2019) (**Figure 1**). How and when such WPB diversification, i.e. a sorting of P-selectin to only some organelles, occurs and how Rab46 is recruited to only a subset of WPB is not known but these pose interesting and very central cell biological questions.

Following cortical release and in preparation of PM fusion, WPB are most likely tethered or docked at the membrane. Here, another Rab27a effector, the mammalian uncoordinated 13–4 (Munc13-4), has been shown to promote WPB exocytosis most likely by providing a link or tether between the organelle surface and a PM-bound complex consisting of annexin A2 (AnxA2) and S100A10 (Zografou et al., 2012; Chehab et al., 2017) (**Figure 1**). In this configuration the AnxA2/S100A10 complex most likely functions as a module binding Ca^{2+}-dependently to PM phospholipids [e.g. phosphatidylinositol 4,5-bisphosphate, $PI(4,5)P_2$] via its AnxA2 subunit and to WPB-bound Munc13-4 via its S100A10 subunit (Chehab et al., 2017). A special enrichment of certain PM phospholipids is indeed observed at WPB-PM fusion sites and inhibitor and depletion experiments suggest that $PI(4,5)P_2$ and the $PI(4,5)P_2$ producing PI4P 5-kinase are required for efficient histamine-evoked WPB exocytosis (Nguyen et al., 2020). In the course of regulated exocytosis tethered WPB are finally recognized by the membrane fusion machinery consisting of SNAREs and associated proteins. Several of the factors involved at this stage have been described over the years, including a trans-SNARE complex consisting of WPB-localized VAMP3 and PM-localized syntaxin-4 and SNAP23 as well as syntaxin-binding Munc18 proteins (Matsushita et al., 2003; Pulido et al., 2011; van Breevoort et al., 2014) (**Figure 1**). However, the picture is probably more complex as recent studies employing blood outgrowth endothelial cells which were isolated from a patient suffering from variant microvillus inclusion disease and shown to lack another SNARE, syntaxin-3, showed markedly impaired agonist-evoked VWF secretion. Syntaxin-3 interacts with VAMP8, another WPB-associated v-SNARE, but interestingly, was shown to localize mainly to WPB (Schillemans et al., 2018, 2019). This suggests that syntaxin-3, most likely pairing with VAMP8 on another WPB, supports homotypic fusions of WPB that could occur during compound or cumulative exocytosis (Zupančič et al., 2002; Valentijn et al., 2010; Kiskin et al., 2014; Stevenson et al., 2017) (**Figure 1**). Thus,

several SNARE complexes are likely to support heterotypic and homotypic WPB fusion events that characterize the final steps in regulated exocytosis. Common to these events is their regulation by signaling mediators, in the case of Ca^{2+}-dependent exocytosis the elevated Ca^{2+} concentrations. Several Ca^{2+} binding proteins have been implicated in coupling these Ca^{2+} signals to regulated WPB exocytosis, including the above-mentioned Slp4-a, AnxA2 and Munc13-4 as well as another Munc13 family member, Munc13-2 (Zhou et al., 2016; Holthenrich et al., 2019); however, the actual WPB-associated Ca^{2+} sensor that could directly activate the SNARE machinery most likely is a member of the synaptotagmin family. Synaptotagmin-5 has recently emerged as an interesting candidate as it localizes to WPB and is required for histamine evoked WPB exocytosis and VWF secretion. Importantly, a mutant synaptotagmin-5 lacking the Ca^{2+} coordinating asparagine residue in the C2A domain negatively interferes with histamine evoked WPB exocytosis directly showing the importance of synaptotagmin-5 Ca^{2+} binding (Lenzi et al., 2019). Thus, a complex interplay of Ca^{2+}-regulated proteins, also including the recently identified Slp2-a (Francis et al., 2021), likely transmits the rise in intracellular Ca^{2+} to WPB-PM docking and fusion in the course of regulated exocytosis.

The Link to Actin

While cargo release in many exocytotic events occurs automatically with completion of the granule-PM fusion, WPB and some other secretory organelles carrying large cargo, e.g. surfactant-loaded lamellar bodies of alveolar epithelial cells (Miklavc et al., 2015), most likely require mechanical forces for efficient cargo expulsion. This can be provided by rearrangements of the cortical actin cytoskeleton that first has to be weakened to allow granule penetration to the PM and then site-specifically repolymerizes to support cargo release. In the case of WPB, it was observed that rings of polymerized actin form at the distal end of WPB several seconds after the actual PM fusion event (**Figure 1**). Furthermore, it was shown that these structures, in an active myosin motor-dependent process, are required for the efficient release of highly multimeric VWF cargo from the fused WPB (Nightingale et al., 2011). In later studies it was observed that the formation of such actin rings at WPB-PM fusion sites probably is not obligatory for VWF release, at least in case of histamine stimulation and Ca^{2+}-dependent WPB exocytosis (Conte et al., 2015), and that the extent of actin ring formation at these fusion sites appears to depend on the type of stimulus (Nightingale et al., 2018; Mietkowska et al., 2019). Interestingly, a different actomyosin network that is also positive for the focal adhesion protein zyxin has been observed around peripheral WPB of endothelial cells stimulated with cAMP raising agonists. Here, actin framework formation occurs prior to the actual fusion event facilitating WPB exocytosis (Han et al., 2017; Li et al., 2018). Clearly, more work is required to establish a potential link between this zyxin/actomyosin network and the post-fusion actin rings, e.g. by identifying the factor(s) promoting actin polymerisation into the ring/coat-like structures at fused WPB. Moreover, the precise function of the actin structures also needs further attention. They could support exocytotic membrane fusion and VWF expulsion but potentially could also prevent fused WPB from fully collapsing into the PM, for example to permit rapid and spatially restricted compensatory endocytosis that has been shown to occur on the membrane of fused WPB (Stevenson et al., 2017). Another unresolved issue concerns the regulation of the spatially restricted changes in cortical actin architecture, in particular the questions whether certain membrane lipids enriched at WPB fusion sites such as $PI(4,5)P_2$ are involved and which molecular players organize the actin reorganization precisely at the sites where WPB fuse or have fused.

Concluding Remarks

WPB are unique secretory organelles that allow vascular endothelial cells to respond rapidly to environmental changes by the secretion of factors that control hemostasis and inflammation. Marked progress in understanding their biogenesis, intracellular transport and secretion has been made in the last decade revealing fascinating cell biological phenomena that drive the formation of the organelle and its many modes of exocytosis. However, our picture of the organelle is far from complete and important questions, e.g. concerning unique maturation steps, cargo selection and Rab recruitment and the involvement of different actin structures in VWF release, remain to be answered. Future research in this exciting topic of cell biology has to tell and will likely also benefit pharmacological interventions of the pathway that could help controlling vascular VWF (and P-selectin) levels in pathophysiological scenarios (Karampini et al., 2020; El-Mansi and Nightingale, 2021).

AUTHOR CONTRIBUTIONS

JN, JT, and VG contributed to writing of the manuscript and generating/editing the figure.

FUNDING

The authors research is supported by the 290 German Research Foundation (SFB1348/A04, SFB1009/A06, and GE514/6-3). JN is member of the joint graduate school Cells-in-Motion 292 (CiM)/ IMPRS, Münster, Germany.

REFERENCES

Bierings, R., Hellen, N., Kiskin, N., Knipe, L., Fonseca, A.-V., Patel, B., et al. (2012). The Interplay between the Rab27A Effectors Slp4-A and MyRIP Controls Hormone-Evoked Weibel-Palade Body Exocytosis. *Blood* 120, 2757–2767. doi:10.1182/blood-2012-05-429936

Bonfanti, R., Furie, B., Furie, B., and Wagner, D. (1989). PADGEM (GMP140) Is a Component of Weibel-Palade Bodies of Human Endothelial Cells. *Blood* 73, 1109–1112. doi:10.1182/blood.v73.5.1109.bloodjournal7351109

Bowman, S. L., Bi-Karchin, J., Le, L., and Marks, M. S. (2019). The Road to Lysosome-related Organelles: Insights from Hermansky-Pudlak Syndrome and Other Rare Diseases. *Traffic* 20, 404–435. doi:10.1111/tra.12646

Chehab, T., Santos, N. C., Holthenrich, A., Koerdt, S. N., Disse, J., Schuberth, C., et al. (2017). A Novel Munc13-4/S100A10/annexin A2 Complex Promotes Weibel-Palade Body Exocytosis in Endothelial Cells. *MBoC* 28, 1688–1700. doi:10.1091/mbc.e17-02-0128

Conte, I. L., Cookson, E., Hellen, N., Bierings, R., Mashanov, G., and Carter, T. (2015). Is There More Than One Way to Unpack a Weibel-Palade Body? *Blood* 126, 2165–2167. doi:10.1182/blood-2015-08-664961

Conte, I. L., Hellen, N., Bierings, R., Mashanov, G. I., Manneville, J.-B., Kiskin, N. I., et al. (2016). Interaction between MyRIP and the Actin Cytoskeleton Regulates Weibel-Palade Body Trafficking and Exocytosis. *J. Cel Sci.* 129, 592–603. doi:10.1242/jcs.178285

Dong, X., Leksa, N. C., Chhabra, E. S., Arndt, J. W., Lu, Q., Knockenhauer, K. E., et al. (2019). The von Willebrand factor D′D3 assembly and structural principles for factor VIII binding and concatemer biogenesis. *Blood* 133, 1523–1533. doi:10.1182/blood-2018-10-876300

El-Mansi, S., and Nightingale, T. D. (2021). Emerging Mechanisms to Modulate VWF Release from Endothelial Cells. *Int. J. Biochem. Cel Biol.* 131, 105900. doi:10.1016/j.biocel.2020.105900

Ferraro, F., da Silva, M. L., Grimes, W., Lee, H. K., Ketteler, R., Kriston-Vizi, J., et al. (2016). Weibel-Palade body size modulates the adhesive activity of its von Willebrand Factor cargo in cultured endothelial cells. *Sci. Rep.* 6, 32473. doi:10.1038/srep32473

Ferraro, F., Kriston-Vizi, J., Metcalf, D. J., Martin-Martin, B., Freeman, J., Burden, J. J., et al. (2014). A Two-Tier Golgi-Based Control of Organelle Size Underpins the Functional Plasticity of Endothelial Cells. *Develop. Cel* 29, 292–304. doi:10.1016/j.devcel.2014.03.021

Ferraro, F., Patella, F., Costa, J. R., Ketteler, R., Kriston-Vizi, J., and Cutler, D. F. (2020). Modulation of Endothelial Organelle Size as an Antithrombotic Strategy. *J. Thromb. Haemost.* 18, 3296–3308. doi:10.1111/jth.15084

Francis, C. R., Claflin, S., and Kushner, E. J. (2021).Synaptotagmin-Like Protein 2a Regulates Angiogenic Lumen Formation via Weibel-Palade Body Apical Secretion of Angiopoietin-2, *Atvb.* Arteriosclerosis, Thrombosis, and Vascular Biology, 41121., 2021 ATVBAHA, Dallas, USA, 1972–1986. doi:10.1161/ATVBAHA.121.316113

Han, X., Li, P., Yang, Z., Huang, X., Wei, G., Sun, Y., et al. (2017). Zyxin regulates endothelial von Willebrand factor secretion by reorganizing actin filaments around exocytic granules. *Nat. Commun.* 8, 14639. doi:10.1038/ncomms14639

Holthenrich, A., Drexler, H. C. A., Chehab, T., Naß, J., and Gerke, V. (2019). Proximity proteomics of endothelial Weibel-Palade bodies identifies novel regulator of von Willebrand factor secretion. *Blood* 134, 979–982. doi:10.1182/blood.2019000786

Karampini, E., Bierings, R., and Voorberg, J. (2020a). Orchestration of Primary Hemostasis by Platelet and Endothelial Lysosome-Related Organelles. *ATVB* 40, 1441–1453. doi:10.1161/ATVBAHA.120.314245

Karampini, E., Petra E. Bürgisser, P. E., Jenny Olins, J., Aat A. Mulder, A. A., Carolina R. Jost, C. R., Dirk Geerts, D., et al. (2020b). Sec22b Determines Weibel-Palade Body Length by Controlling Anterograde ER-Golgi Transport. *haematol* 106, 1138–1147. doi:10.3324/haematol.2019.242727

Karampini, E., Schillemans, M., Hofman, M., van Alphen, F., de Boer, M., Kuijpers, T. W., et al. (2019). Defective AP-3-dependent VAMP8 Trafficking Impairs Weibel-Palade Body Exocytosis in Hermansky-Pudlak Syndrome Type 2 Blood Outgrowth Endothelial Cells. *Haematologica* 104, 2091–2099. doi:10.3324/haematol.2018.207787

Kat, M., Bürgisser, P. E., Janssen, H., De Cuyper, I. M., Conte, I. L., Hume, A. N., et al. (2021). GDP/GTP Exchange Factor MADD Drives Activation and Recruitment of Secretory Rab GTPases to Weibel-Palade Bodies. *Blood Adv. Bloodadvances.* 2021. 202100482. doi:10.1182/bloodadvances.2021004827

Kiskin, N. I., Babich, V., Knipe, L., Hannah, M. J., and Carter, T. (2014). Differential Cargo Mobilisation within Weibel-Palade Bodies after Transient Fusion with the Plasma Membrane. *PLoS ONE* 9, e108093. doi:10.1371/journal.pone.0108093

Leebeek, F. W. G., and Eikenboom, J. C. J. (2016). Von Willebrand's Disease. *N. Engl. J. Med.* 375, 2067–2080. doi:10.1056/NEJMra1601561

Lenzi, C., Stevens, J., Osborn, D., Hannah, M. J., Bierings, R., and Carter, T. (2019). Synaptotagmin 5 Regulates Calcium-dependent Weibel-Palade Body Exocytosis in Human Endothelial Cells. *J. Cel Sci.*, 221952. doi:10.1242/jcs.221952

Li, P., Wei, G., Cao, Y., Deng, Q., Han, X., Huang, X., et al. (2018). Myosin IIa is critical for cAMP-mediated endothelial secretion of von Willebrand factor. *Blood* 131, 686–698. doi:10.1182/blood-2017-08-802140

Lopes-da-Silva, M., McCormack, J. J., Burden, J. J., Harrison-Lavoie, K. J., Ferraro, F., and Cutler, D. F. (2019). A GBF1-dependent Mechanism for Environmentally Responsive Regulation of ER-Golgi Transport. *Develop. Cel* 49, 786–801. e6. doi:10.1016/j.devcel.2019.04.006

Lowenstein, C. J., Morrell, C. N., and Yamakuchi, M. (2005). Regulation of Weibel-Palade Body Exocytosis. *Trends Cardiovasc. Med.* 15, 302–308. doi:10.1016/j.tcm.2005.09.005

Ma, J., Zhang, Z., Yang, L., Kriston-Vizi, J., Cutler, D. F., and Li, W. (2016). BLOC-2 subunit HPS6 deficiency affects the tubulation and secretion of von Willebrand factor from mouse endothelial cells. *J. Genet. Genomics* 43, 686–693. doi:10.1016/j.jgg.2016.09.007

Matsushita, K., Morrell, C. N., Cambien, B., Yang, S.-X., Yamakuchi, M., Bao, C., et al. (2003). Nitric Oxide Regulates Exocytosis by S-Nitrosylation of N-Ethylmaleimide-Sensitive Factor. *Cell* 115, 139–150. doi:10.1016/S0092-8674(03)00803-1

McCormack, J. J., Lopes da Silva, M., Ferraro, F., Patella, F., and Cutler, D. F. (2017). Weibel–Palade Bodies at a Glance. *J. Cel Sci.* 130, 3611–3617. doi:10.1242/jcs.208033

Michaux, G., and Cutler, D. F. (2004). How to Roll an Endothelial Cigar: The Biogenesis of Weibel-Palade Bodies. *Traffic* 5, 69–78. doi:10.1111/j.1600-0854.2004.00157.x

Mietkowska, M., Schuberth, C., Wedlich-Söldner, R., and Gerke, V. (20191866). Actin Dynamics during Ca2+-dependent Exocytosis of Endothelial Weibel-Palade Bodies. *Biochim. Biophys. Acta (Bba) - Mol. Cel Res.* 1866, 1218–1229. doi:10.1016/j.bbamcr.2018.11.010

Miklavc, P., Ehinger, K., Sultan, A., Felder, T., Paul, P., Gottschalk, K.-E., et al. (2015). Actin Depolymerisation and Crosslinking Join Forces with Myosin II to Contract Actin coats on Fused Secretory Vesicles. *J. Cel Sci.* 128, 1193–1203. doi:10.1242/jcs.165571

Miteva, K. T., Pedicini, L., Wilson, L. A., Jayasinghe, I., Slip, R. G., Marszalek, K., et al. (2019). Rab46 Integrates Ca2+ and Histamine Signaling to Regulate Selective Cargo Release from Weibel-Palade Bodies. *J. Cel Biol.* 218, 2232–2246. doi:10.1083/jcb.201810118

Mourik, M. J., Faas, F. G. A., Zimmermann, H., Voorberg, J., Koster, A. J., and Eikenboom, J. (2015). Content Delivery to Newly Forming Weibel-Palade Bodies Is Facilitated by Multiple Connections with the Golgi Apparatus. *Blood* 125, 3509–3516. doi:10.1182/blood-2014-10-608596

Nguyen, T. T. N., Koerdt, S. N., and Gerke, V. (2020). Plasma Membrane Phosphatidylinositol (4,5)-bisphosphate Promotes Weibel-Palade Body Exocytosis. *Life Sci. Alliance* 3, e202000788. doi:10.26508/lsa.202000788

Nightingale, T. D., McCormack, J. J., Grimes, W., Robinson, C., Lopes da Silva, M., White, I. J., et al. (2018). Tuning the Endothelial Response: Differential Release of Exocytic Cargos from Weibel-Palade Bodies. *J. Thromb. Haemost.* 16, 1873–1886. doi:10.1111/jth.14218

Nightingale, T. D., Pattni, K., Hume, A. N., Seabra, M. C., and Cutler, D. F. (2009). Rab27a and MyRIP Regulate the Amount and Multimeric State of VWF Released from Endothelial Cells. *Blood* 113, 5010–5018. doi:10.1182/blood-2008-09-181206

Nightingale, T. D., White, I. J., Doyle, E. L., Turmaine, M., Harrison-Lavoie, K. J., Webb, K. F., et al. (2011). Actomyosin II contractility expels von Willebrand factor from Weibel-Palade bodies during exocytosis. *J. Cel Biol.* 194, 613–629. doi:10.1083/jcb.201011119

Patella, F., and Cutler, D. F. (2020). Regulator of G protein signalling 4 controls secretion of von Willebrand factor to the subendothelial matrix. *J. Cel Sci.* 133. doi:10.1242/jcs.247312

Poeter, M., Brandherm, I., Rossaint, J., Rosso, G., Shahin, V., Skryabin, B. V., et al. (2014). Annexin A8 Controls Leukocyte Recruitment to Activated Endothelial Cells via Cell Surface Delivery of CD63. *Nat. Commun.* 5, 3738. doi:10.1038/ncomms4738

Pulido, I. R., Jahn, R., and Gerke, V. (2011). VAMP3 Is Associated with Endothelial Weibel-Palade Bodies and Participates in Their Ca2+-dependent Exocytosis. *Biochim. Biophys. Acta (Bba) - Mol. Cel Res.* 1813, 1038–1044. doi:10.1016/j.bbamcr.2010.11.007

Raposo, G., Marks, M. S., and Cutler, D. F. (2007). Lysosome-Related Organelles: Driving post-Golgi Compartments into Specialisation. *Curr. Opin. Cel Biol.* 19, 394–401. doi:10.1016/j.ceb.2007.05.001

Rojo Pulido, I., Nightingale, T. D., Darchen, F., Seabra, M. C., Cutler, D. F., and Gerke, V. (2011). Myosin Va Acts in Concert with Rab27a and MyRIP to Regulate Acute Von-Willebrand Factor Release from Endothelial Cells. *Traffic* 12, 1371–1382. doi:10.1111/j.1600-0854.2011.01248.x

Sadler, J. E. (2008). Von Willebrand Factor, ADAMTS13, and Thrombotic Thrombocytopenic Purpura. *Blood* 112, 11–18. doi:10.1182/blood-2008-02-078170

Schillemans, M., Karampini, E., Hoogendijk, A. J., Wahedi, M., van Alphen, F. P. J., van den Biggelaar, M., et al. (2019a). Interaction Networks of Weibel-Palade Body Regulators Syntaxin-3 and Syntaxin Binding Protein 5 in Endothelial Cells. *J. Proteomics* 205, 103417. doi:10.1016/j.jprot.2019.103417

Schillemans, M., Karampini, E., Kat, M., and Bierings, R. (2019b). Exocytosis of Weibel-Palade Bodies: How to Unpack a Vascular Emergency Kit. *J. Thromb. Haemost.* 17, 6–18. doi:10.1111/jth.14322

Schillemans, M., Karampini, E., van den Eshof, B. L., Gangaev, A., Hofman, M., van Breevoort, D., et al. (2018). Weibel-Palade Body Localized Syntaxin-3 Modulates Von Willebrand Factor Secretion from Endothelial Cells. *ATVB* 38, 1549–1561. doi:10.1161/ATVBAHA.117.310701

Schneppenheim, R., and Budde, U. (2011). von Willebrand factor: the complex molecular genetics of a multidomain and multifunctional protein. *J. Thromb. Haemost.* 9, 209–215. doi:10.1111/j.1538-7836.2011.04324.x

Sharda, A. V., Barr, A. M., Harrison, J. A., Wilkie, A. R., Fang, C., Mendez, L. M., et al. (2020). VWF Maturation and Release Are Controlled by 2 Regulators of Weibel-Palade Body Biogenesis: Exocyst and BLOC-2. *Blood* 136, 2824–2837. doi:10.1182/blood.2020005300

Simons, M., and Raposo, G. (2009). Exosomes - Vesicular Carriers for Intercellular Communication. *Curr. Opin. Cel Biol.* 21, 575–581. doi:10.1016/j.ceb.2009.03.007

Stevenson, N. L., White, I. J., McCormack, J. J., Robinson, C., Cutler, D. F., and Nightingale, T. D. (2017). Clathrin-mediated post-fusion Membrane Retrieval Influences the Exocytic Mode of Endothelial Weibel-Palade Bodies. *J. Cel Sci.* 130, 2591–2605. doi:10.1242/jcs.200840

Streetley, J., Fonseca, A.-V., Turner, J., Kiskin, N. I., Knipe, L., Rosenthal, P. B., et al. (2019). Stimulated Release of Intraluminal Vesicles from Weibel-Palade Bodies. *Blood* 133, 2707–2717. doi:10.1182/blood-2018-09-874552

Valentijn, K. M., van Driel, L. F., Mourik, M. J., Hendriks, G.-J., Arends, T. J., Koster, A. J., et al. (2010). Multigranular Exocytosis of Weibel-Palade Bodies in Vascular Endothelial Cells. *Blood* 116, 1807–1816. doi:10.1182/blood-2010-03-274209

van Breevoort, D., Snijders, A. P., Hellen, N., Weckhuysen, S., van Hooren, K. W. E. M., Eikenboom, J., et al. (2014). STXBP1 Promotes Weibel-Palade Body Exocytosis through its Interaction with the Rab27A Effector Slp4-A. *Blood* 123, 3185–3194. doi:10.1182/blood-2013-10-535831

van Breevoort, D., van Agtmaal, E. L., Dragt, B. S., Gebbinck, J. K., Dienava-Verdoold, I., Kragt, A., et al. (2012). Proteomic Screen Identifies IGFBP7 as a Novel Component of Endothelial Cell-specific Weibel-Palade Bodies. *J. Proteome Res.* 11, 2925–2936. doi:10.1021/pr300010r

van Mourik, J. A., Romani de Wit, T., and Voorberg, J. (2002). Biogenesis and Exocytosis of Weibel-Palade Bodies. *Histochem. Cel Biol* 117, 113–122. doi:10.1007/s00418-001-0368-9

Wagner, D. D., Olmsted, J. B., and Marder, V. J. (1982). Immunolocalization of von Willebrand protein in Weibel-Palade bodies of human endothelial cells. *J. Cel Biol.* 95, 355–360. doi:10.1083/jcb.95.1.355

Watanabe, A., Hataida, H., Inoue, N., Kamon, K., Baba, K., Sasaki, K., et al. (2021). Arf GTPase-activating proteins SMAP1 and AGFG2 regulate the size of Weibel-Palade bodies and exocytosis of von Willebrand factor. *Biol. Open* 10. doi:10.1242/bio.058789

Weibel, E. R., and Palade, G. E. (1964). New Cytoplasmic Components in Arterial Endothelia. *J. Cel Biol.* 23, 101–112. doi:10.1083/jcb.23.1.101

Zenner, H. L., Collinson, L. M., Michaux, G., and Cutler, D. F. (2007). High-pressure Freezing Provides Insights into Weibel-Palade Body Biogenesis. *J. Cel Sci.* 120, 2117–2125. doi:10.1242/jcs.007781

Zhou, H. J., Qin, L., Zhang, H., Tang, W., Ji, W., He, Y., et al. (2016). Endothelial Exocytosis of Angiopoietin-2 Resulting from CCM3 Deficiency Contributes to Cerebral Cavernous Malformation. *Nat. Med.* 22, 1033–1042. doi:10.1038/nm.4169

Zografou, S., Basagiannis, D., Papafotika, A., Shirakawa, R., Horiuchi, H., Auerbach, D., et al. (2012). Rab-genome Analysis Reveals Novel Insights in Weibel-Palade Body Exocytosis. *J. Cel Sci.* 125, 4780–4790. doi:10.1242/jcs.104174

Zupančič, G., Ogden, D., Magnus, C. J., Wheeler-Jones, C., and Carter, T. D. (2002). Differential Exocytosis from Human Endothelial Cells Evoked by High Intracellular Ca2+concentration. *J. Physiol.* 544, 741–755. doi:10.1113/jphysiol.2002.027490

Conflict of Interest: The authors declare that the research was conducted in the absence of any commercial or financial relationships that could be construed as a potential conflict of interest.

Publisher's Note: All claims expressed in this article are solely those of the authors and do not necessarily represent those of their affiliated organizations, or those of the publisher, the editors and the reviewers. Any product that may be evaluated in this article, or claim that may be made by its manufacturer, is not guaranteed or endorsed by the publisher.

frontiers in Cell and Developmental Biology

REVIEW
published: 24 December 2021
doi: 10.3389/fcell.2021.783857

OPEN ACCESS

Edited by:
Carlos Enrich,
University of Barcelona, Spain

Reviewed by:
Guillaume Drin,
UMR7275 Institut de Pharmacologie Moléculaire et Cellulaire (IPMC), France
Nobuhiro Nakamura,
Kyoto Sangyo University, Japan
Akihiko Nakano,
RIKEN, Japan

***Correspondence:**
Tomohiko Taguchi
tom_taguchi@tohoku.ac.jp

†Present address:
Junya Hasegawa, Department of Biochemical Pathophysiology, Medical Research Institute, Tokyo Medical and Dental University, Tokyo, Japan; Yasunori Uchida, Kojiro Mukai; Tomohiko Taguchi, Laboratory of Organelle Pathophysiology, Department of Integrative Life Sciences, Graduate School of Life Sciences, Tohoku University, Sendai, Japan; Shoken Lee, Department of Molecular Cellular and Developmental Biology, Yale University, New Haven, United States; Tatsuyuki Matsudaira, Department of Molecular Microbiology, Research Institute for Microbial Diseases(RIMD), Osaka University, Suita, Japan

‡These authors have contributed equally to the work

Specialty section:
This article was submitted to Membrane Traffic, a section of the journal Frontiers in Cell and Developmental Biology

Received: 27 September 2021
Accepted: 29 November 2021
Published: 24 December 2021

Citation:
Hasegawa J, Uchida Y, Mukai K, Lee S, Matsudaira T and Taguchi T (2021) A Role of Phosphatidylserine in the Function of Recycling Endosomes. Front. Cell Dev. Biol. 9:783857. doi: 10.3389/fcell.2021.783857

A Role of Phosphatidylserine in the Function of Recycling Endosomes

*Junya Hasegawa†‡, Yasunori Uchida†‡, Kojiro Mukai†‡, Shoken Lee‡, Tatsuyuki Matsudaira‡ and Tomohiko Taguchi *†*

Department of Health Chemistry, Graduate School of Pharmaceutical Sciences, University of Tokyo, Tokyo, Japan

Cells internalize proteins and lipids in the plasma membrane (PM) and solutes in the extracellular space by endocytosis. The removal of PM by endocytosis is constantly balanced by the replenishment of proteins and lipids to PM through recycling pathway. Recycling endosomes (REs) are specific subsets of endosomes. Besides the established role of REs in recycling pathway, recent studies have revealed unanticipated roles of REs in membrane traffic and cell signalling. In this review, we highlight these emerging issues, with a particular focus on phosphatidylserine (PS), a phospholipid that is highly enriched in the cytosolic leaflet of RE membranes. We also discuss the pathogenesis of Hermansky Pudlak syndrome type 2 (HPS2) that arises from mutations in the AP3B1 gene, from the point of view of dysregulated RE functions.

Keywords: phosphatidylserine, pleckstrin-homology domain, flippase, bioID proximity labeling, endosomes, membrane traffic

INTRODUCTION

Cells internalize proteins and lipids in the PM and solutes in the extracellular space by endocytosis. Internalized cargos are first transported to early endosomes (EEs). Cargos are further transported either to lysosomes through late endosomes for their degradation, or to the PM for their reuse. A direct route from EEs to the PM (the fast recycling pathway) and an indirect route through REs (the slow recycling pathway) are involved in the latter transport (Sheff et al., 1999; Sönnichsen et al., 2000). Alternatively, cargos can be transported to the Golgi by retrograde pathway (Bonifacino and Rojas, 2006; Johannes and Popoff, 2008). Some cargos bound to retrograde pathway pass through REs before reaching the Golgi (Mallet and Maxfield, 1999; Uchida et al., 2011; McKenzie et al., 2012). Furthermore, there is accumulating evidence that some exocytic cargos pass through REs before reaching the PM (Ang et al., 2004; Murray et al., 2005; Misaki et al., 2010). Thus, the classical view of REs, *i.e.*, the organelle for recycling traffic, has been challenged and revised to the one that REs function as a hub for a variety of membrane traffic (Taguchi, 2013) (**Figure 1**).

PS represents up to 10% of the total phospholipids in cells and is the most abundant negatively charged glycerophospholipids (Leventis and Grinstein, 2010; Kay and Fairn, 2019). PS has a phosphoserine headgroup attached to the *sn*-3 position of the glycerol backbone. In mammals, PS is synthesized by two distinct base-exchange enzymes, PS synthase-1 (PSS1) and PS synthase-2 (PSS2). PSS1 substitutes serine for choline of phosphatidylcholine, whereas PSS2 replaces ethanolamine of phosphatidylethanolamine for serine (Kuge and Nishijima, 1997; Vance, 2018). These enzymes localize in the mitochondria-associated membranes of the ER (Vance, 2018). PS is highly enriched in the cytosolic leaflet of the PM and participates in various physiological events such as the coagulation cascade, recruitment and activation of signalling molecules that include protein kinase C, and clearance of apoptotic cells (Leventis and Grinstein, 2010). PS is also found in the cytosolic leaflet of intracellular organelles including EEs and late endosomes (Yeung et al., 2008),

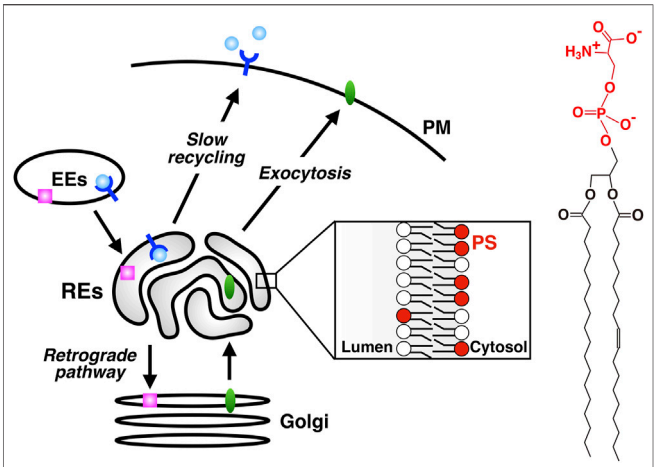

FIGURE 1 | PS is enriched in REs, an organelle that serves as a hub for a variety of membrane traffic. slow recycling: PM→ EEs→ REs→ PM; retrograde transport: PM→ EEs→ REs→ the Golgi; exocytic transport: ER→ the Golgi→ REs→ PM. PS is concentrated in the cytosolic leaflet of RE membranes. Chemical structure of PS is shown in the right. The headgroup of PS (phosphoserine, shown in red) has one net negative charge.

where its function has not been fully elucidated. Both vesicular membrane trafficking and non-vesicular transport by lipid transfer proteins appear to contribute to maintaining the subcellular PS distribution (Kay and Fairn, 2019).

Nearly a decade ago, we revealed that REs were enriched in PS. The finding was followed by a series of studies that identified the PS-specific protein domain, PS-effector RE proteins, and unanticipated roles of PS in the Hippo-YAP signalling. In this review, we summarize the role of PS in RE functions and discuss the pathogenesis of Hermansky Pudlak syndrome type 2 (HPS2) from the point of view of dysregulated PS/RE functions.

EVECTIN-2, A PS BINDING RE PROTEIN

Evectin-1 and -2 were identified as post-Golgi proteins of unknown function (Krappa et al., 1999). Evectin-1 is expressed specifically in the nervous system, whereas evectin-2 is ubiquitously expressed. Both proteins are predicted to have a type IV membrane topology, *i.e.*, the *N*-terminal part of the protein, which is anchored to the membrane by a *C*-terminal transmembrane domain, is oriented towards the cytosol (Krappa et al., 1999). They have a pleckstrin-homology (PH) domain at the *N*-terminus, which typically binds phosphoinositides (PIPs) (Lemmon, 2008). We showed that evectin-2 localized to REs and that evectin-2 PH was required for the localization of evectin-2 to REs (Uchida et al., 2011). Evectin-2 PH alone, expressed in the cytosol, localized to REs, indicating the presence of an RE-specific phospholipid.

The human proteome has about 300 proteins with PH domains. About 10% of these proteins were shown to bind specifically to PIPs through their PH domains (Lemmon, 2008). A number of PH domains did not bind lipids but protein partners (Wang et al., 1994; Scheffzek and Welti, 2012). We measured the binding of several negatively charged lipids on liposomes to recombinant evectin-2 PH. Contrary to what we expected, PS bound evectin-2 PH, but phosphatidic acid, phosphatidylinositol, sulfatide, and all PIPs did not (Uchida et al., 2011) (**Figure 2A**). Lys20 is highly conserved in other PH domains. evectin-2 PH (K20E) lost the ability to bind to PS.

A *Saccharomyces cerevisiae* mutant (*cho1Δ*) lacks *de novo* PS synthesis and is devoid of PS (Atkinson et al., 1980; Hikiji et al., 1988). We exploited this yeast strain to examine if evectin-2 PH bound PS *in vivo*. Given that a tandem fusion of lipid-binding domains, such as the FYVE domain of EEA1 and Hrs, increased the lipid-binding affinity of their FYVE domain (Gillooly et al., 2000), a tandem fusion of evectin-2 PH (2xPH, hereafter) was generated. 2xPH localized exclusively at the PM of the wild-type yeast, whereas it was cytosolic in *cho1Δ*, indicating that evectin-2 PH recognized PS *in vivo* (Uchida et al., 2011). These results also indicated that 1) the cytosolic leaflet of RE membranes was enriched in PS and 2) evectin-2 localized to REs by the recognition of the PS at REs with its PH domain.

EVECTIN-2 PH DOMAIN AS A PS PROBE

Since we reported that evectin-2 PH was highly specific to PS, this domain or the tandem fusion of evectin-2 PH (2xPH) has been widely used to examine the subcellular distribution of PS both in live and fixed cells (**Table 1**). If 2xPH tagged with a fluorescent protein, such as EGFP, is expressed in the cytosol, PS in the cytosolic leaflet of the PM and organelle membranes can be detected in live cells. If the recombinant 2xPH is used for fixed and permeabilized cells, PS in membranes, regardless of its transbilayer distribution, can be detected (**Figure 3**).

C2-domain of lactadherin (lact-C2, hereafter) has also been used to detect PS in cells (Yeung et al., 2008; Kay and Grinstein, 2011). Two papers used 2xPH and lact-C2 in the same cellular system: Platre et al. (Platre et al., 2018) found that the PM localization of lact-C2 was more pronounced than that of 2xPH; Chung et al. (Chung et al., 2015) reported that (total internal reflection fluorescence)/(epi fluorescence) with 2xPH was 0.1, whereas that with lact-C2 was 0.4. These results suggested that lact-C2 appeared more sensitive to detect PS in the PM than 2xPH. Intriguingly, Wen et al. (Wen et al., 2016) reported that 2xPH bound preferentially to PS in the liquid-disordered (Ld) phase, compared to PS in the liquid-ordered (Lo) phase using liposome reconstitution system. 2xPH, thus, may be susceptible to the lipid environment where PS is placed.

The crystal structure of evectin-2 PH with phosphoserine, the head group of PS, was solved (Uchida et al., 2011). By comparing the crystal structure of the apo-form of evectin-2 PH (Okazaki et al., 2012), Ile15 and Leu16 were found to be positioned closer to the PS-binding pocket upon PS binding (**Figures 2B,C**). The insertion of the hydrophobic side chains of Ile15 and Leu16 into densely packed lipid domains is expected to be energetically disfavored, which may account for the *in vitro* 2xPH preference for PS in the Ld phase rather than PS in the Lo phase.

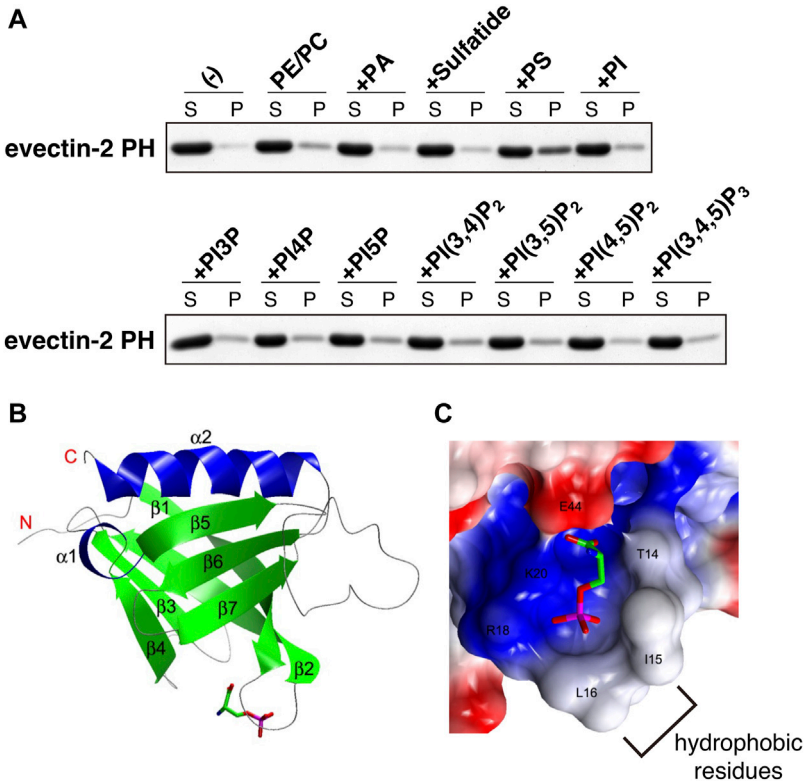

FIGURE 2 | evectin-2 PH specifically binds to PS **(A)** *In vitro* lipid-binding assays. His-tagged evectin-2 PH was mixed with liposomes composed of brain phosphatidylcholine (PC), brain phosphatidylethanolamine (PE), and the indicated negatively charged lipid (20% mol/mol of total lipids). The mixture was then spun at 100,000 *g*, and the resultant supernatant (S) and pellet (P) were subjected to SDS-PAGE, followed by Coomassie blue staining **(B)** Overall structure of human evectin-2 PH in complex with phosphoserine, the headgroup of PS **(C)** Charge distribution surface model of evectin-2 PH in complex with phosphoserine (stick model). The surface is colored according to the electrostatic potential of the residues (blue, positive; red, negative). Hydrophobic residues around the PS-binding pocket, which are expected to be inserted into the membrane, are indicated. Data were reproduced and modified from (Uchida et al., 2011).

TABLE 1 | Representative studies using 2xPH.

Model system	Purpose of using 2xPH	References
Mammalian cell line	Protein localization to PS-rich membranes	Chiba et al. (2013)
Mammalian cell line	PS transport to the PM	Chung et al. (2015)
Yeast	Change of PS distribution in genetic mutants	Hatakeyama et al. (2017)
Mammalian cell line	Identification of proteins in close proximity to PS	Matsudaira et al. (2017)
Plant	PS distribution in endosomal membrane	Platre (2018)
Plant	PS accumulation in nanodomains at the PM	Platre et al. (2019)
Yeast, mammalian cell line	Transbilayer PS distribution in organelle membranes	Tsuji et al. (2019)
Yeast	Change of PS distribution in genetic mutants	Kishimoto et al. (2021)
Mammalian cell line	PS levels in cellular membranes	Li et al. (2021)
Yeast	PS distribution in autophagosomes/autophagic bodies	Orii et al. (2021)

ATP8A1, AN RE-LOCALIZED PS FLIPPASE

Asymmetric distribution of phospholipids in the lipid bilayer is generated, in part, by the selective translocation of phospholipids across the membranes (Graham, 2004; Holthuis and Levine, 2005; Best et al., 2019). The P_4 subfamily of P-type ATPases (P_4-ATPases) flips phospholipids from the luminal leaflet (or extracellular leaflet) to the cytosolic leaflet of biomembranes (Sebastian et al., 2012; Coleman et al., 2013). Fourteen P_4-ATPases are encoded in human genome, and mutations in

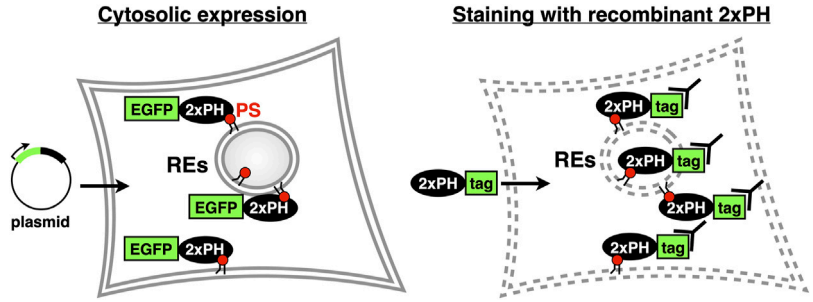

FIGURE 3 | Two methods to examine intracellular PS distribution with 2xPH (*Left*) 2xPH tagged with a fluorescent protein, such as EGFP, is expressed in the cytosol by plasmid transfection. In this case, 2xPH detects PS in the cytosolic leaflet of the PM and organelle membranes (*Right*) Recombinant 2xPH detects PS in both leaflets when applied to fixed and permeabilized cells. 2xPH can be detected by immunocytochemistry using antibodies against the tag attached to 2xPH.

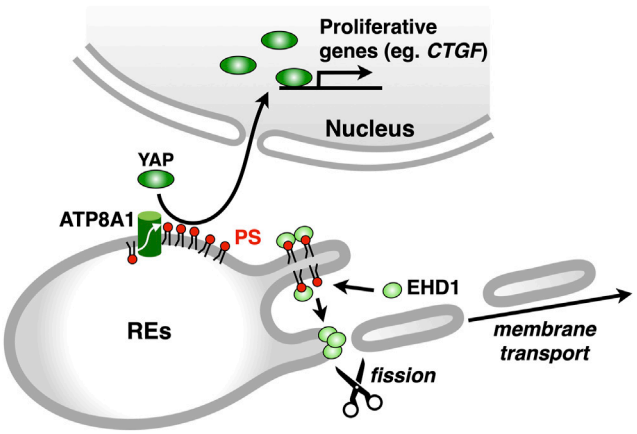

FIGURE 4 | ATP8A1 regulates membrane trafficking and signalling at REs. ATP8A1 flips PS to the cytosolic leaflet of RE membranes. The PS then recruits a membrane fission protein EHD1 from the cytosol to REs. The EHD1-mediated fission of RE membranes generates membrane transport carriers. PS in REs also facilitates the nuclear translocation of YAP, thereby promoting the transcription of YAP-target proliferative genes, such as CTGF (connective tissue growth factor).

some P_4-ATPases cause genetic diseases, such as intrahepatic cholestasis (Bull et al., 1998), B-cell deficiency syndrome (Siggs et al., 2011; Yabas et al., 2011), and neurodegenerative disorder (Onat et al., 2013). We sought to identify the P_4-ATPase that concentrates PS in the cytosolic leaflet of RE membranes. Four P_4-ATPases (ATP8A1, ATP9A, ATP11A, and ATP11B) are ubiquitously expressed and suggested to localize at endosomes (Takatsu et al., 2011; Kato et al., 2013). We found that ATP8A1 localized at REs and its knockdown resulted in an increase in PS levels in the luminal leaflet of RE membranes (Lee et al., 2015). Knockdown of ATP8A1 also impaired the recycling of transferrin (Tfn) and the retrograde traffic of cholera toxin B subunit (CTxB) at REs. Importantly, the rescue experiments with siRNA-resistant ATP8A1 E191Q (an ATPase-deficient variant) showed that ATPase activity of ATP8A1 was required for the recycling of Tfn from REs. These results suggested that PS in the cytosolic leaflet of RE membranes was essential for membrane traffic that passes through REs. Intriguingly, knockdown of ATP8A1 resulted in the generation of aberrant tubules that were positive with Tfn receptor (TfnR). PS in the cytosolic leaflet of RE membranes may function in the fission process of membrane carriers (**Figure 4**).

The function of PS flippases in endosomal membrane traffic appears to be evolutionally conserved. For example, a P_4-ATPase Drs2 in *Saccharomyces cerevisiae*, which flips PS, is essential for membrane traffic between the late Golgi compartment and endosomes (Best et al., 2019). Drs2 increases membrane curvature and anionic phospholipid levels by providing an excess of lipids in the cytosolic leaflet of the membrane, both of which are sensed by the Arf GTPase-activating protein (ArfGAP) Gcs1 through its +ALPS motif (Xu et al., 2013). By analogy, ATP8A1 may also contribute to membrane traffic through REs by creating positive membrane curvature, which is essential for generating membrane carriers. A P_4-ATPase TAT-1 in *Caenorhabditis elegans*, is most closely related to mammalian ATP8A1. The loss of *tat-1* leads to the generation of abnormal endo-lysosomal compartments, suggesting impaired endocytic traffic (Ruaud et al., 2009; Chen et al., 2010). Of note, ATP9A, another P4-ATPase that localizes at endosomes, is required for the efficient recycling of Tfn from endosomes to the PM (Tanaka et al., 2016). It is currently unclear whether ATP9A is involved in the enrichment of PS in the cytosolic leaflet of endosomal membranes.

ATP8A2, a paralogue of ATP8A1, is specifically expressed in brain, testis, and retina (Zhu et al., 2012). An ATP8A2 variant (I376M) is associated with a neurodegenerative disease (CAMRQ) characterized by cerebellar ataxia, mental retardation, and disequilibrium (Onat et al., 2013). We hypothesized that ATP8A2, like ATP8A1, was essential for endosomal traffic through REs. Thus, three human ATP8A2 variants [wild-type (WT), I376M, and E210Q deficient in flippase-activity] were examined if the expression of these could compensate for the loss of ATP8A1. All three ATP8A2 proteins localized at REs, however, only the expression of ATP8A2 (WT), in cells depleted of ATP8A1, resulted in the disappearance of aberrant TfnR-positive tubules and restored EHD1 localization to REs (Lee et al., 2015) (please see the

following section). These results suggested that ATP8A2 functioned in recycling endosomal traffic. The defect in recycling endosomal traffic in neurons may underlie the pathogenesis of CAMRQ.

EHD1, A PS-EFFECTOR RE PROTEIN

Eps15 homology domain-containing protein 1 (EHD1) is a member of the EHD (EH-domain containing) family, which contains four homologues in mammals designated EHD1, EHD2, EHD3, and EHD4. These proteins are highly conserved eukaryotic dynamin-like ATPases that mediate membrane remodeling (Daumke et al., 2007; Grant and Caplan, 2008). EHD1 facilitates tubulation or fission of liposomes containing anionic phospholipids, suggesting that EHD1 functions in the formation of membrane carriers *in vivo* (Pant et al., 2009). Knockdown of EHD1 impaired the recycling of Tfn from REs to the PM and the retrograde transport of CTxB from REs to the Golgi (McKenzie et al., 2012; Lee et al., 2015). Intriguingly, EHD1 knockdown, like ATP8A1 knockdown, resulted in the emergence of aberrant TfnR-positive tubules emanating from REs.

Given the similar phenotype of the distribution of TfnR between ATP8A1-and EHD1-depleted cells, we hypothesized that PS in the cytosolic leaflet of RE membranes regulated EHD1 function. Indeed, we found that EHD1 localized primarily at REs in WT cells, but not in ATP8A1-depleted cells. Furthermore, the RE localization of EHD1 in ATP8A1-depleted cells was restored by the expression of siRNA-resistant WT ATP8A1, but not by the expression of siRNA-resistant E191Q mutant deficient in ATPase activity (Lee et al., 2015). Co-sedimentation assays with recombinant EHD1 mixed with liposomes of increasing PS levels showed a sigmoidal increase in the EHD1 binding, with an EC50 of 40–50 mol% PS. This PS concentration matched well the concentration of PS in the cytosolic leaflet of RE membranes estimated with a method using recombinant 2xPH (Lee et al., 2015). Thus, PS in the cytosolic leaflet of RE membranes by itself may recruit EHD1 from the cytosol, thereby facilitating its function to generate membrane carriers for the PM and/or the Golgi (**Figure 4**).

REGULATION OF THE YAP SIGNALLING BY PS IN REs

Given the presence of RE proteins, such as evectin-2 and EHD1, the localization of which depends on the levels of PS in the cytosolic leaflet of RE membranes, we hypothesized that there were more PS-binding RE proteins. To identify these proteins, the proximity-dependent biotin identification (BioID) method was exploited. The BioID method is based on proximity-dependent cellular biotinylation by a promiscuous bacterial biotin ligase BirA* fused to a bait protein (Roux et al., 2012). Biotinylated proteins can be purified by avidin-coated beads, and subsequently identified using mass spectrometry analysis.

As the bait protein, we used 2xPH, expecting that RE proteins in close proximity to PS could be biotinylated. Among 400 biotinylated proteins identified, 113 proteins were annotated to "endosomes" in gene ontology in Uniprot. Several proteins that function in membrane trafficking at REs were identified, including EHD1, VAMP3 (McMahon et al., 1993), Rab11-FIP1 (Hales et al., 2001), MICAL-L1 (Sharma et al., 2009), and SMAP2 (Matsudaira et al., 2013; Matsudaira et al., 2015). Intriguingly, we found that YAP, a critical growth-promoting transcription coactivator, and a group of proteins associated with the YAP signalling pathway (the Hippo pathway) were biotinylated with BirA*-2xPH (Matsudaira et al., 2017). These results suggested that PS in the RE membranes was involved in the YAP signalling. Indeed, we found that YAP localized at REs in low-density proliferating cells, in addition to its expected localization of the nucleus, where YAP regulates target genes that are essential for cell proliferation (Zhao et al., 2007; Zhao et al., 2008). Knockdown of ATP8A1 reduced the nuclear/RE localization of YAP and the mRNA expression of CTGF, a YAP-regulated gene (Matsudaira et al., 2017). These results suggested that PS in REs had a role in the YAP activation (**Figure 4**). Whether YAP directly binds to PS at REs remains to be elucidated. Knockdown of evectin-2 also reduced the nuclear/RE localization of YAP and the mRNA expression of CTGF. The regulation of YAP by evectin-2 was suggested to be mediated through the direct activation of Nedd4 E3 ligases, such as Itch, WWP1, and WWP2, by evectin-2. These E3 ligases ubiquitinated Lats1 kinase, the critical negative regulator of YAP function, leading to proteasome degradation of Lats1.

HERMANSKY PUDLAK SYNDROME TYPE 2

Hermansky-Pudlak syndrome (HPS) is a rare, hereditary disorder characterized by decreased pigmentation (albinism) with visual impairment, blood platelet dysfunction with prolonged bleeding, and pulmonary fibrosis (Vicary et al., 2016; Bowman et al., 2019). The most lethal complication in HPS patients is pulmonary fibrosis. So far, human genetics identify more than 10 separate forms of HPS with mutations in different genes (Vicary et al., 2016). All HPS have defect in membrane trafficking and the biogenesis of lysosome-related organelles (LROs), including melanosomes and platelet dense granules (Bowman et al., 2019). Hermansky Pudlak syndrome type 2 (HPS2) is caused by mutations in AP3B1 gene, which encodes β1 subunit of the adaptor protein 3 (AP-3) complex (Dell'Angelica et al., 1999). AP-3 serves as a protein coat of membrane vesicles and mediates the transport of transmembrane proteins to lysosomes or LROs (Bowman et al., 2019). Although dysregulation of alveolar epithelial cells appears critical to the pathogenesis of HSP, the molecular mechanism by which the fibrosis proceeds is largely unknown.

Lamellar bodies (LBs) are LROs of surfactant-producing alveolar type 2 (AT2) cells of the distal lung epithelium (Weaver et al., 2002). A recent study showed that ATP8A1 in AT2 cells was constantly transported to LBs by AP-3 (Kook et al., 2021). Interestingly, instead of being transported to LBs, ATP8A1 in AP-3-depleted cells re-localized to REs, enhancing the cytosolic exposure of PS in REs, as we reported in other cell

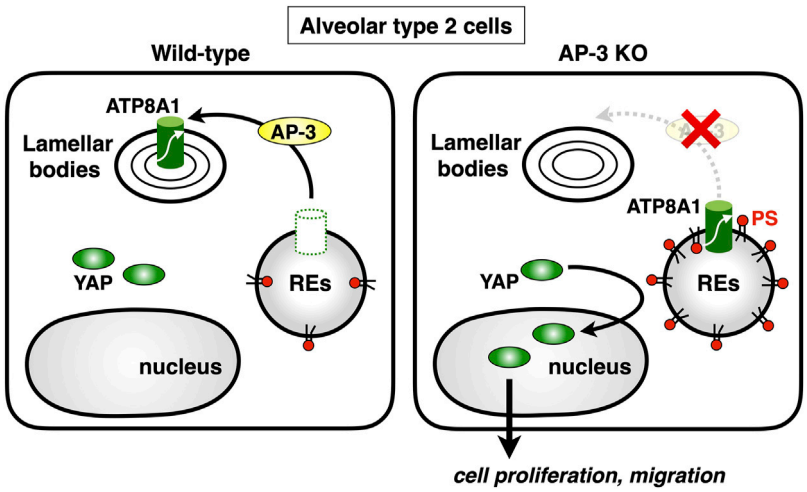

FIGURE 5 | Deficiency of AP-3 results in YAP activation. AP-3 mediates ATP8A1 transport from endosomes to lamella bodies in alveolar type 2 cells. In AP-3-knockout cells, because the trafficking of ATP8A1 from endosomes is impaired, ATP8A1 is forced to re-localize to REs, thereby increasing the levels of cytosolic PS in RE membranes. The PS enrichment in RE membranes promotes aberrant activation of YAP, which augments cell proliferation and migration.

lines (Lee et al., 2015). This, in turn, promoted activation of YAP, enhancing cell migration and AT2 cell numbers (Kook et al., 2021) (**Figure 5**). Thus, the dysregulated PS exposure in REs may in part contribute to the pathogenesis of HSP2.

CONCLUDING REMARKS

Nearly a decade ago when we investigated the mechanism by which evectin-2 localized at REs, we serendipitously found that the cytosolic leaflet of RE membranes were enriched in PS (Uchida et al., 2011). The enrichment of PS at the cytosolic leaflet of RE membranes highly contrasts with the specific expression of PIPs at the cytosolic leaflet of other membrane compartments, *e.g.*, PI(3)P at EEs and PI(4,5)P_2 at the PM (Schink et al., 2016). Given a variety of PIP effectors that regulate organelle function (Di Paolo and De Camilli, 2006), we reason that more PS effectors, in addition to evectin-2 and EHD1, exist and contribute to the function of REs. The BioID methods should help identify these.

Besides the classical roles of REs in endocytic recycling, we and others have shown that REs have a role in the exocytic and retrograde membrane traffic. These results raise a fundamental question how individual cargos are packaged into appropriate membrane carriers. *In vivo* imaging system to visualize the dynamics of multiple cargos for distinct destinations, and *in vitro* reconstitution system, such as those developed for the early secretory pathway (Kim et al., 2005; Kim et al., 2007), would greatly benefit in our understanding of the nature and regulators of membrane traffic at REs.

AUTHOR CONTRIBUTIONS

JH, YU, KM, SL, and TM gathered the information over the review's topics. YU prepared the figures. TT conceptualized the layout of the topics and wrote the review.

FUNDING

This work was supported by JSPS KAKENHI Grant Numbers JP19H00974 (TT), JP20H05307 (KM), JP20H03202 (KM), JP21K06153 (YU), and AMED-PRIME (17939604) (TT).

ACKNOWLEDGMENTS

All the authors used to be affiliated with Dr. Hiroyuki Arai's laboratory in Department of Pharmaceutical Sciences, University of Tokyo. We would like to thank Dr. Hiroyuki Arai for his consistent support, guidance, and enthusiasm during the running of the series of PS projects that were described in this review.

REFERENCES

Ang, A. L., Taguchi, T., Francis, S., Fölsch, H., Murrells, L. J., Pypaert, M., et al. (2004). Recycling Endosomes Can Serve as Intermediates during Transport from the Golgi to the Plasma Membrane of MDCK Cells. *J. Cel Biol* 167, 531–543. doi:10.1083/jcb.200408165

Atkinson, K. D., Jensen, B., Kolat, A. I., Storm, E. M., Henry, S. A., and Fogel, S. (1980). Yeast Mutants Auxotrophic for Choline or Ethanolamine. *J. Bacteriol.* 141, 558–564. doi:10.1128/jb.141.2.558-564.1980

Best, J. T., Xu, P., and Graham, T. R. (2019). Phospholipid Flippases in Membrane Remodeling and Transport Carrier Biogenesis. *Curr. Opin. Cel Biol* 59, 8–15. doi:10.1016/j.ceb.2019.02.004

Bonifacino, J. S., and Rojas, R. (2006). Retrograde Transport from Endosomes to the Trans-golgi Network. *Nat. Rev. Mol. Cel Biol* 7, 568–579. doi:10.1038/nrm1985

Bowman, S. L., Bi-Karchin, J., Le, L., and Marks, M. S. (2019). The Road to Lysosome-Related Organelles: Insights from Hermansky-Pudlak Syndrome and Other Rare Diseases. *Traffic* 20, 404–435. doi:10.1111/tra.12646

Bull, L. N., van Eijk, M. J., Pawlikowska, L., DeYoung, J. A., Juijn, J. A., Liao, M., et al. (1998). A Gene Encoding a P-type ATPase Mutated in Two Forms of Hereditary Cholestasis. *Nat. Genet.* 18, 219–224. doi:10.1038/ng0398-219

Chen, B., Jiang, Y., Zeng, S., Yan, J., Li, X., Zhang, Y., et al. (2010). Endocytic Sorting and Recycling Require Membrane Phosphatidylserine Asymmetry Maintained by TAT-1/CHAT-1. *Plos Genet.* 6, e1001235. doi:10.1371/journal.pgen.1001235

Chiba, S., Amagai, Y., Homma, Y., Fukuda, M., and Mizuno, K. (2013). NDR2-Mediated Rabin8 Phosphorylation is Crucial for Ciliogenesis by Switching Binding Specificity from Phosphatidylserine to Sec15. *EMBO J.* 32, 874–885.

Chung, J., Torta, F., Masai, K., Lucast, L., Czapla, H., Tanner, L. B., et al. (2015). PI4P/phosphatidylserine Countertransport at ORP5- and ORP8-Mediated ER-Plasma Membrane Contacts. *Science* 349, 428–432. doi:10.1126/science.aab1370

Coleman, J. A., Quazi, F., and Molday, R. S. (2013). Mammalian P4-ATPases and ABC Transporters and Their Role in Phospholipid Transport. *Biochim. Biophys. Acta* 1831, 555–574. doi:10.1016/j.bbalip.2012.10.006

Daumke, O., Lundmark, R., Vallis, Y., Martens, S., Butler, P. J., and McMahon, H. T. (2007). Architectural and Mechanistic Insights into an EHD ATPase Involved in Membrane Remodelling. *Nature* 449, 923–927. doi:10.1038/nature06173

Dell'Angelica, E. C., Shotelersuk, V., Aguilar, R. C., Gahl, W. A., and Bonifacino, J. S. (1999). Altered Trafficking of Lysosomal Proteins in Hermansky-Pudlak Syndrome Due to Mutations in the Beta 3A Subunit of the AP-3 Adaptor. *Mol. Cel* 3, 11–21.

Di Paolo, G., and De Camilli, P. (2006). Phosphoinositides in Cell Regulation and Membrane Dynamics. *Nature* 443, 651–657. doi:10.1038/nature05185

Gillooly, D. J., Morrow, I. C., Lindsay, M., Gould, R., Bryant, N. J., Gaullier, J. M., et al. (2000). Localization of Phosphatidylinositol 3-phosphate in Yeast and Mammalian Cells. *EMBO J.* 19, 4577–4588. doi:10.1093/emboj/19.17.4577

Graham, T. R. (2004). Flippases and Vesicle-Mediated Protein Transport. *Trends Cel Biol* 14, 670–677. doi:10.1016/j.tcb.2004.10.008

Grant, B. D., and Caplan, S. (2008). Mechanisms of EHD/RME-1 Protein Function in Endocytic Transport. *Traffic* 9, 2043–2052. doi:10.1111/j.1600-0854.2008.00834.x

Hales, C. M., Griner, R., Hobdy-Henderson, K. C., Dorn, M. C., Hardy, D., Kumar, R., et al. (2001). Identification and Characterization of a Family of Rab11-Interacting Proteins. *J. Biol. Chem.* 276, 39067–39075. doi:10.1074/jbc.m104831200

Hatakeyama, R., Kono, K., and Yoshida, S. (2017). Ypk1 and Ypk2 Kinases Maintain Rho1 at The Plasma Membrane by Flippase-Dependent Lipid Remodeling After Membrane Stresses. *J. Cell Sci.* 130, 1169–1178.

Hikiji, T., Miura, K., Kiyono, K., Shibuya, I., and Ohta, A. (1988). Disruption of the CHO1 Gene Encoding Phosphatidylserine Synthase in *Saccharomyces cerevisiae*. *J. Biochem.* 104, 894–900. doi:10.1093/oxfordjournals.jbchem.a122579

Holthuis, J. C., and Levine, T. P. (2005). Lipid Traffic: Floppy Drives and a Superhighway. *Nat. Rev. Mol. Cel Biol* 6, 209–220. doi:10.1038/nrm1591

Johannes, L., and Popoff, V. (2008). Tracing the Retrograde Route in Protein Trafficking. *Cell* 135, 1175–1187. doi:10.1016/j.cell.2008.12.009

Kato, U., Inadome, H., Yamamoto, M., Emoto, K., Kobayashi, T., and Umeda, M. (2013). Role for Phospholipid Flippase Complex of ATP8A1 and CDC50A Proteins in Cell Migration. *J. Biol. Chem.* 288, 4922–4934. doi:10.1074/jbc.m112.402701

Kay, J. G., and Fairn, G. D. (2019). Distribution, Dynamics and Functional Roles of Phosphatidylserine within the Cell. *Cell Commun Signal* 17, 126. doi:10.1186/s12964-019-0438-z

Kay, J. G., and Grinstein, S. (2011). Sensing Phosphatidylserine in Cellular Membranes. *Sensors (Basel)* 11, 1744–1755. doi:10.3390/s110201744

Kim, J., Hamamoto, S., Ravazzola, M., Orci, L., and Schekman, R. (2005). Uncoupled Packaging of Amyloid Precursor Protein and Presenilin 1 into Coat Protein Complex II Vesicles. *J. Biol. Chem.* 280, 7758–7768. doi:10.1074/jbc.m411091200

Kim, J., Kleizen, B., Choy, R., Thinakaran, G., Sisodia, S. S., and Schekman, R. W. (2007). Biogenesis of Gamma-Secretase Early in the Secretory Pathway. *J. Cel Biol* 179, 951–963. doi:10.1083/jcb.200709012

Kishimoto, T., Mioka, T., Itoh, E., Williams, D. E., Andersen, R. J., Tanaka, K., et al. (2021). Phospholipid Flippases and Sfk1 are Essential for the Retention of Ergosterol in the Plasma Membrane. *Mol. Biol. Cell.* 32, 1,374–1,392.

Kook, S., Wang, P., Meng, S., Jetter, C. S., Sucre, J. M. S., Benjamin, J. T., et al. (2021). AP-3-dependent Targeting of Flippase ATP8A1 to Lamellar Bodies Suppresses Activation of YAP in Alveolar Epithelial Type 2 Cells. *Proc. Natl. Acad. Sci. U S A.* 118, e2025208118. doi:10.1073/pnas.2025208118

Krappa, R., Nguyen, A., Burrola, P., Deretic, D., and Lemke, G. (1999). Evectins: Vesicular Proteins that Carry a Pleckstrin Homology Domain and Localize to post-Golgi Membranes. *Proc. Natl. Acad. Sci. U S A.* 96, 4633–4638. doi:10.1073/pnas.96.8.4633

Kuge, O., and Nishijima, M. (1997). Phosphatidylserine Synthase I and II of Mammalian Cells. *Biochim. Biophys. Acta* 1348, 151–156. doi:10.1016/s0005-2760(97)00137-9

Lee, S., Uchida, Y., Wang, J., Matsudaira, T., Nakagawa, T., Kishimoto, T., et al. (2015). Transport through Recycling Endosomes Requires EHD1 Recruitment by a Phosphatidylserine Translocase. *EMBO J.* 34, 669–688. doi:10.15252/embj.201489703

Lemmon, M. A. (2008). Membrane Recognition by Phospholipid-Binding Domains. *Nat. Rev. Mol. Cel Biol* 9, 99–111. doi:10.1038/nrm2328

Leventis, P. A., and Grinstein, S. (2010). The Distribution and Function of Phosphatidylserine in Cellular Membranes. *Annu. Rev. Biophys.* 39, 407–427. doi:10.1146/annurev.biophys.093008.131234

Li, Y. E., Wang, Y., Du, Z., Zhang, T., Mak, H. Y., Hancock, S. E., et al. (2021). TMEM41B and VMP1 are Scramblases and Regulate the Distribution of Cholesterol and Phosphatidylserine. *J. Cell Biol.* 220, e202103105.

Mallet, W. G., and Maxfield, F. R. (1999). Chimeric Forms of Furin and Tgn38 Are Transported from the Plasma Membrane to the Trans-golgi Network via Distinct Endosomal Pathways. *J. Cel Biol* 146, 345–360. doi:10.1083/jcb.146.2.345

Matsudaira, T., Mukai, K., Noguchi, T., Hasegawa, J., Hatta, T., Iemura, S. I., et al. (2017). Endosomal Phosphatidylserine Is Critical for the YAP Signalling Pathway in Proliferating Cells. *Nat. Commun.* 8, 1246. doi:10.1038/s41467-017-01255-3

Matsudaira, T., Niki, T., Taguchi, T., and Arai, H. (2015). Transport of the Cholera Toxin B-Subunit from Recycling Endosomes to the Golgi Requires Clathrin and AP-1. *J. Cel Sci* 128, 3131–3142. doi:10.1242/jcs.172171

Matsudaira, T., Uchida, Y., Tanabe, K., Kon, S., Watanabe, T., Taguchi, T., et al. (2013). SMAP2 Regulates Retrograde Transport from Recycling Endosomes to the Golgi. *PLoS One* 8, e69145. doi:10.1371/journal.pone.0069145

McKenzie, J. E., Raisley, B., Zhou, X., Naslavsky, N., Taguchi, T., Caplan, S., et al. (2012). Retromer Guides STxB and CD8-M6PR from Early to Recycling Endosomes, EHD1 Guides STxB from Recycling Endosome to Golgi. *Traffic* 13, 1140–1159. doi:10.1111/j.1600-0854.2012.01374.x

McMahon, H. T., Ushkaryov, Y. A., Edelmann, L., Link, E., Binz, T., Niemann, H., et al. (1993). Cellubrevin Is a Ubiquitous Tetanus-Toxin Substrate Homologous to a Putative Synaptic Vesicle Fusion Protein. *Nature* 364, 346–349. doi:10.1038/364346a0

Misaki, R., Morimatsu, M., Uemura, T., Waguri, S., Miyoshi, E., Taniguchi, N., et al. (2010). Palmitoylated Ras Proteins Traffic through Recycling Endosomes to the Plasma Membrane during Exocytosis. *J. Cel Biol* 191, 23–29. doi:10.1083/jcb.200911143

Murray, R. Z., Kay, J. G., Sangermani, D. G., and Stow, J. L. (2005). A Role for the Phagosome in Cytokine Secretion. *Science* 310, 1492–1495. doi:10.1126/science.1120225

Okazaki, S., Kato, R., Uchida, Y., Taguchi, T., Arai, H., and Wakatsuki, S. (2012). Structural Basis of the Strict Phospholipid Binding Specificity of the Pleckstrin Homology Domain of Human Evectin-2. *Acta Crystallogr. D Biol. Crystallogr.* 68, 117–123. doi:10.1107/s0907444911051626

Onat, O. E., Gulsuner, S., Bilguvar, K., Nazli Basak, A., Topaloglu, H., Tan, M., et al. (2013). Missense Mutation in the ATPase, Aminophospholipid Transporter

Protein ATP8A2 Is Associated with Cerebellar Atrophy and Quadrupedal Locomotion. *Eur. J. Hum. Genet.* 21, 281–285. doi:10.1038/ejhg.2012.170

Orii, M., Tsuji, T., Ogasawara, Y., and Fujimoto, T. (2021). Transmembrane Phospholipid Translocation Mediated by Atg9 is Involved in Autophagosome Formation. *J. Cell Biol.* 220, e202009194.

Pant, S., Sharma, M., Patel, K., Caplan, S., Carr, C. M., and Grant, B. D. (2009). AMPH-1/Amphiphysin/Bin1 Functions with RME-1/Ehd1 in Endocytic Recycling. *Nat. Cel Biol* 11, 1399–1410. doi:10.1038/ncb1986

Platre, M. P., Bayle, V., Armengot, L., Bareille, J., Marqués-Bueno, M. D. M., Creff, A., et al. (2019). Developmental Control of Plant Rho Gtpase Nano-Organization by the Lipid Phosphatidylserine. *Science* 364, 57–62.

Platre, M. P., Noack, L. C., Doumane, M., Bayle, V., Simon, M. L. A., Maneta-Peyret, L., et al. (2018). A Combinatorial Lipid Code Shapes the Electrostatic Landscape of Plant Endomembranes. *Dev. Cel* 45, 465–480. e11. doi:10.1016/j.devcel.2018.04.011

Roux, K. J., Kim, D. I., Raida, M., and Burke, B. (2012). A Promiscuous Biotin Ligase Fusion Protein Identifies Proximal and Interacting Proteins in Mammalian Cells. *J. Cel Biol* 196, 801–810. doi:10.1083/jcb.201112098

Ruaud, A. F., Nilsson, L., Richard, F., Larsen, M. K., Bessereau, J. L., and Tuck, S. (2009). The *C. elegans* P4-ATPase TAT-1 Regulates Lysosome Biogenesis and Endocytosis. *Traffic* 10, 88–100. doi:10.1111/j.1600-0854.2008.00844.x

Scheffzek, K., and Welti, S. (2012). Pleckstrin Homology (PH) like Domains - Versatile Modules in Protein-Protein Interaction Platforms. *FEBS Lett.* 586, 2662–2673. doi:10.1016/j.febslet.2012.06.006

Schink, K. O., Tan, K. W., and Stenmark, H. (2016). Phosphoinositides in Control of Membrane Dynamics. *Annu. Rev. Cel Dev Biol* 32, 143–171. doi:10.1146/annurev-cellbio-111315-125349

Sebastian, T. T., Baldridge, R. D., Xu, P., and Graham, T. R. (2012). Phospholipid Flippases: Building Asymmetric Membranes and Transport Vesicles. *Biochim. Biophys. Acta* 1821, 1068–1077. doi:10.1016/j.bbalip.2011.12.007

Sharma, M., Giridharan, S. S., Rahajeng, J., Naslavsky, N., and Caplan, S. (2009). MICAL-L1 Links EHD1 to Tubular Recycling Endosomes and Regulates Receptor Recycling. *Mol. Biol. Cel* 20, 5181–5194. doi:10.1091/mbc.e09-06-0535

Sheff, D. R., Daro, E. A., Hull, M., and Mellman, I. (1999). The Receptor Recycling Pathway Contains Two Distinct Populations of Early Endosomes with Different Sorting Functions. *J. Cel Biol* 145, 123–139. doi:10.1083/jcb.145.1.123

Siggs, O. M., Arnold, C. N., Huber, C., Pirie, E., Xia, Y., Lin, P., et al. (2011). The P4-type ATPase ATP11C Is Essential for B Lymphopoiesis in Adult Bone Marrow. *Nat. Immunol.* 12, 434–440. doi:10.1038/ni.2012

Sönnichsen, B., De Renzis, S., Nielsen, E., Rietdorf, J., and Zerial, M. (2000). Distinct Membrane Domains on Endosomes in the Recycling Pathway Visualized by Multicolor Imaging of Rab4, Rab5, and Rab11. *J. Cel Biol* 149, 901–914. doi:10.1083/jcb.149.4.901

Taguchi, T. (2013). Emerging Roles of Recycling Endosomes. *J. Biochem.* 153, 505–510. doi:10.1093/jb/mvt034

Takatsu, H., Baba, K., Shima, T., Umino, H., Kato, U., Umeda, M., et al. (2011). ATP9B, a P4-ATPase (A Putative Aminophospholipid Translocase), Localizes to the Trans-golgi Network in a CDC50 Protein-independent Manner. *J. Biol. Chem.* 286, 38159–38167. doi:10.1074/jbc.m111.281006

Tanaka, Y., Ono, N., Shima, T., Tanaka, G., Katoh, Y., Nakayama, K., et al. (2016). The Phospholipid Flippase ATP9A Is Required for the Recycling Pathway from the Endosomes to the Plasma Membrane. *Mol. Biol. Cel* 27, 3883–3893. doi:10.1091/mbc.e16-08-0586

Tsuji, T., Cheng, J., Tatematsu, T., Ebata, A., Kamikawa, H., Fujita, A., et al. (2019). Predominant Localization of Phosphatidylserine at the Cytoplasmic Leaflet of the ER, and its TMEM16K-Dependent Redistribution. *Proc. Natl. Acad. Sci. USA* 116, 13368–13373.

Uchida, Y., Hasegawa, J., Chinnapen, D., Inoue, T., Okazaki, S., and Kato, R., Intracellular Phosphatidylserine Is Essential for Retrograde Membrane Traffic through Endosomes. *Proc. Natl. Acad. Sci. U S A.* (2011) 108:15846–15851. doi:10.1073/pnas.1109101108

Vance, J. E. (2018). Historical Perspective: Phosphatidylserine and Phosphatidylethanolamine from the 1800s to the Present. *J. Lipid Res.* 59, 923–944. doi:10.1194/jlr.r084004

Vicary, G. W., Vergne, Y., Santiago-Cornier, A., Young, L. R., and Roman, J. (2016). Pulmonary Fibrosis in Hermansky-Pudlak Syndrome. *Ann. Am. Thorac. Soc.* 13, 1839–1846. doi:10.1513/AnnalsATS.201603-186FR

Wang, D. S., Shaw, R., Winkelmann, J. C., and Shaw, G. (1994). Binding of PH Domains of Beta-Adrenergic Receptor Kinase and Beta-Spectrin to WD40/beta-Transducin Repeat Containing Regions of the Beta-Subunit of Trimeric G-Proteins. *Biochem. Biophys. Res. Commun.* 203, 29–35. doi:10.1006/bbrc.1994.2144

Weaver, T. E., Na, C. L., and Stahlman, M. (2002). Biogenesis of Lamellar Bodies, Lysosome-Related Organelles Involved in Storage and Secretion of Pulmonary Surfactant. *Semin. Cel Dev Biol* 13, 263–270. doi:10.1016/s1084952102000551

Wen, Y., Dick, R. A., Feigenson, G. W., and Vogt, V. M. (2016). Effects of Membrane Charge and Order on Membrane Binding of the Retroviral Structural Protein Gag. *J. Virol.* 90, 9518–9532. doi:10.1128/jvi.01102-16

Xu, P., Baldridge, R. D., Chi, R. J., Burd, C. G., and Graham, T. R. (2013). Phosphatidylserine Flipping Enhances Membrane Curvature and Negative Charge Required for Vesicular Transport. *J. Cel Biol* 202, 875–886. doi:10.1083/jcb.201305094

Yabas, M., Teh, C. E., Frankenreiter, S., Lal, D., Roots, C. M., Whittle, B., et al. (2011). ATP11C Is Critical for the Internalization of Phosphatidylserine and Differentiation of B Lymphocytes. *Nat. Immunol.* 12, 441–449. doi:10.1038/ni.2011

Yeung, T., Gilbert, G. E., Shi, J., Silvius, J., Kapus, A., and Grinstein, S. (2008). Membrane Phosphatidylserine Regulates Surface Charge and Protein Localization. *Science* 319, 210–213. doi:10.1126/science.1152066

Zhao, B., Wei, X., Li, W., Udan, R. S., Yang, Q., Kim, J., et al. (2007). Inactivation of YAP Oncoprotein by the Hippo Pathway Is Involved in Cell Contact Inhibition and Tissue Growth Control. *Genes Dev.* 21, 2747–2761. doi:10.1101/gad.1602907

Zhao, B., Ye, X., Yu, J., Li, L., Li, W., Li, S., et al. (2008). TEAD Mediates YAP-dependent Gene Induction and Growth Control. *Genes Dev.* 22, 1962–1971. doi:10.1101/gad.1664408

Zhu, X., Libby, R. T., de Vries, W. N., Smith, R. S., Wright, D. L., Bronson, R. T., et al. (2012). Mutations in a P-type ATPase Gene Cause Axonal Degeneration. *Plos Genet.* 8, e1002853. doi:10.1371/journal.pgen.1002853

Conflict of Interest: The authors declare that the research was conducted in the absence of any commercial or financial relationships that could be construed as a potential conflict of interest.

Publisher's Note: All claims expressed in this article are solely those of the authors and do not necessarily represent those of their affiliated organizations, or those of the publisher, the editors and the reviewers. Any product that may be evaluated in this article, or claim that may be made by its manufacturer, is not guaranteed or endorsed by the publisher.

frontiers in Cell and Developmental Biology

MINI REVIEW
published: 06 January 2022
doi: 10.3389/fcell.2021.797949

Annexins Bridging the Gap: Novel Roles in Membrane Contact Site Formation

Carlos Enrich[1,2]*, *Albert Lu*[1,2], *Francesc Tebar*[1,2], *Carles Rentero*[1,2] and *Thomas Grewal*[3]

[1]Departament de Biomedicina, Unitat de Biologia Cel·lular, Facultat de Medicina i Ciències de la Salut, Universitat de Barcelona, Barcelona, Spain, [2]Centre de Recerca Biomèdica CELLEX, Institut d'Investigacions Biomèdiques August Pi i Sunyer (IDIBAPS), Barcelona, Spain, [3]School of Pharmacy, Faculty of Medicine and Health, University of Sydney, Sydney, NSW, Australia

Membrane contact sites (MCS) are specialized small areas of close apposition between two different organelles that have led researchers to reconsider the dogma of intercellular communication *via* vesicular trafficking. The latter is now being challenged by the discovery of lipid and ion transfer across MCS connecting adjacent organelles. These findings gave rise to a new concept that implicates cell compartments not to function as individual and isolated entities, but as a dynamic and regulated ensemble facilitating the trafficking of lipids, including cholesterol, and ions. Hence, MCS are now envisaged as metabolic platforms, crucial for cellular homeostasis. In this context, well-known as well as novel proteins were ascribed functions such as tethers, transporters, and scaffolds in MCS, or transient MCS companions with yet unknown functions. Intriguingly, we and others uncovered metabolic alterations in cell-based disease models that perturbed MCS size and numbers between coupled organelles such as endolysosomes, the endoplasmic reticulum, mitochondria, or lipid droplets. On the other hand, overexpression or deficiency of certain proteins in this narrow 10–30 nm membrane contact zone can enable MCS formation to either rescue compromised MCS function, or in certain disease settings trigger undesired metabolite transport. In this "*Mini Review*" we summarize recent findings regarding a subset of annexins and discuss their multiple roles to regulate MCS dynamics and functioning. Their contribution to novel pathways related to MCS biology will provide new insights relevant for a number of human diseases and offer opportunities to design innovative treatments in the future.

Keywords: annexins, membrane contact sites, endolysosomes, mitochondria, endoplasmic reticulum, cholesterol, calcium-binding proteins, lipid transport

OPEN ACCESS

Edited by:
Mitsuo Tagaya,
Tokyo University of Pharmacy and Life Sciences, Japan

Reviewed by:
Jyoti K. Jaiswal,
Children's National Hospital, United States

***Correspondence:**
Carlos Enrich
enrich@ub.edu

Specialty section:
This article was submitted to Membrane Traffic, a section of the journal Frontiers in Cell and Developmental Biology

Received: *19 October 2021*
Accepted: *16 December 2021*
Published: *06 January 2022*

Citation:
Enrich C, Lu A, Tebar F, Rentero C and Grewal T (2022) Annexins Bridging the Gap: Novel Roles in Membrane Contact Site Formation. Front. Cell Dev. Biol. 9:797949. doi: 10.3389/fcell.2021.797949

INTRODUCTION

Despite the identification of membrane contacts between neighbouring organelles in the early times of electron microscopy, these small microdomains only received greater attention in the last decade. Two findings prompted further research on the structure and function of membrane contact sites (MCS). Firstly, the endoplasmic reticulum (ER) representing a dynamic 3D network of cisternae and tubules, it fills the cytoplasm and is in physical contact with other organelles (Nixon-Abell et al., 2016). Secondly, the discovery of the physiological relevance of contacts between the ER and mitochondria (mitochondria-associated membranes, MAMs) in the synthesis and exchange of lipids and calcium (Ca^{2+}) homeostasis (Vance, 1990). Since then, the MCS-related Universe expanded

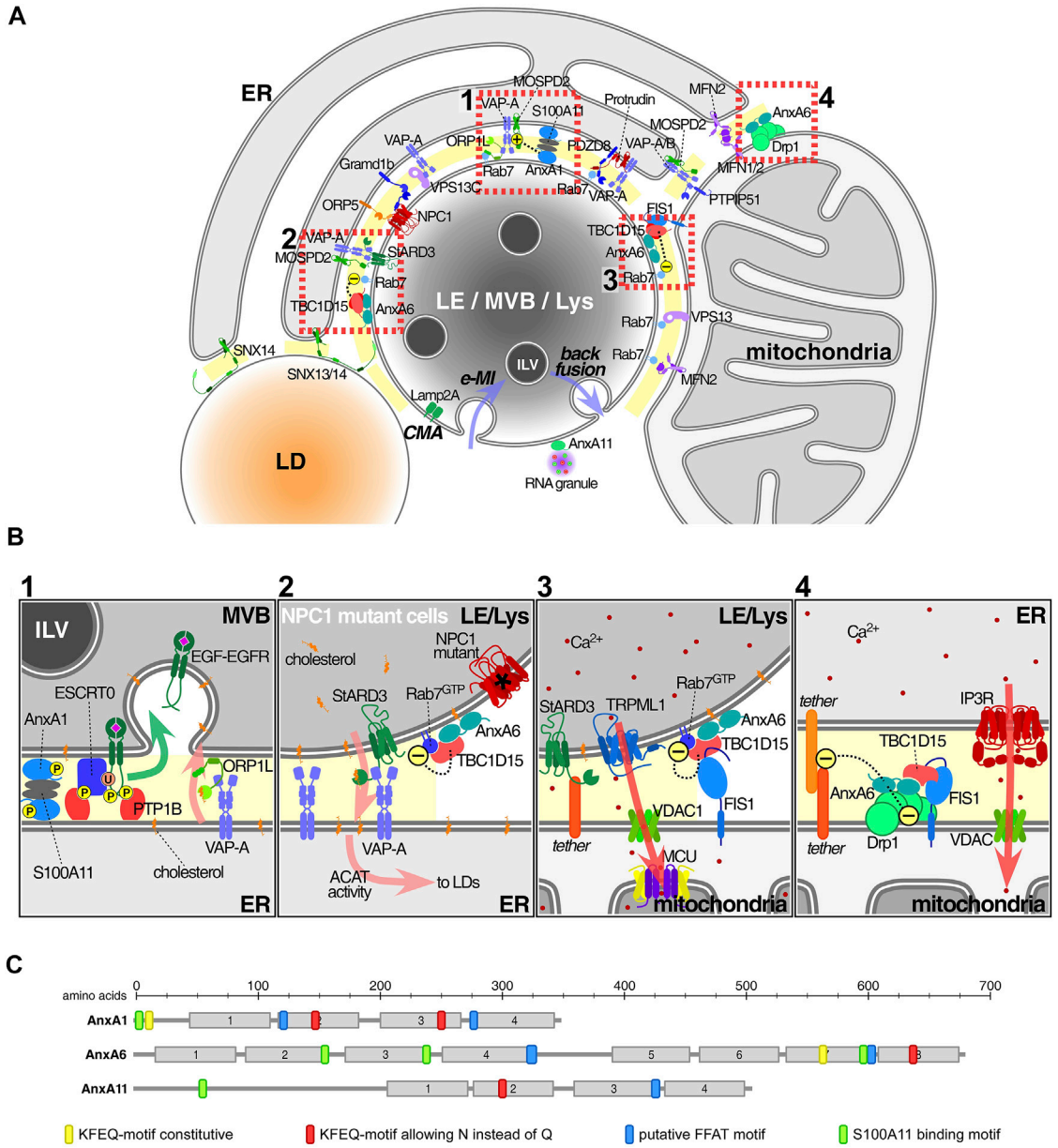

FIGURE 1 | Annexins and associated protein complexes at membrane contact sites. **(A)** Endolysosomes (LE/MVBs/Lys) establish multiple membrane contact sites (MCS) with a variety of other organelles, in particular the ER and mitochondria, but also peroxisomes and lipid droplets. Here we only illustrate a subset of contacts and contact site proteins. Lipid transfer, including cholesterol as well as Ca^{2+} mobilization and signalling are probably the most important MCS-associated functions. Annexins have been found in MCS connecting the ER with either LE or mitochondria (MAMs), as well as in LE-mitochondria contacts. Other proteins or protein complexes serve as tethers to ensure the formation of MCS, including several sorting nexins (Henne et al., 2015; Dong et al., 2016; Saric et al., 2021), VAP proteins, PTPIP51, PDZD8 or protrudin (Shirane et al., 2020; Neefjes and Cabukusta, 2021). Furthermore, ORP5/8 and NPC1/Gramd1 also translocate lipids including PS and cholesterol, across MCS between the ER and mitochondria and/or LE respectively (Galmes et al., 2016; Hoglinger et al., 2019). At the bottom of this endolysosome, we contemplate the possible recruitment of cytosolic annexins into ILV (see text for details) *via* two autophagic pathways. While chaperone-mediated and Lamp2a-dependent autophagy (CMA) may carry annexins into the lumen of MVBs or the outer membrane of ILVs, endosomal microautophagy (e-MI) may board annexins inside ILV (both routes *via* KFERQ-motif) (Tekirdag and Cuervo, 2018). In any case, whatever the topology, these proteins have to escape from lysosomal degradation (Meneses-Salas et al., 2020b). Then, ILV might undergo back fusion/retrofusion (Eden and Futter, 2021), delivering annexins and/or other cargo out of the MVB into the cytosol in the vicinity of MCS, where a suitable local Ca^{2+} and lipid microenvironment could then favour retention in MCS. Alternatively, MVB diversion to exocytosis could generate exosomes. This could be the destination of AnxA11, highly enriched in exosomes. Otherwise, cytosolic AnxA11 could be confined to PI(3,5)P2 at the endolysosomal cytosolic membrane to tether RNA granules (Liao et al., 2019). **(B) 1**: AnxA1, together with S100-A11 as a tetrameric complex, tethers MCS to mediate cholesterol transport from ER to LE/Lys *via* interaction of VAP-A with ORP1L (Eden et al., 2016). In this scenario, AnxA1 overexpression increases MCS between MVB and ER (Wong L. H. et al., 2018). **2**: AnxA6 overexpression decreased MCS numbers between ER and LE/Lys, whereas AnxA6 depletion in NPC1 mutant cells stimulated MCS formation. The underlying mechanism involves the recruitment of AnxA6 and TBC1D15 to Rab7-positive organelles and was associated with increased

(*Continued*)

FIGURE 1 | LE motility and LE-cholesterol release into the ER, through StARD3-VAP-A in MCS (Meneses-Salas et al., 2020b). **3**: TBC1D15 and Rab7 in complex with FIS1 between LE/Lys and mitochondria affects the fission of mitochondria (Wong Y. C. et al., 2018). **4**: AnxA6 interacts with Drp1 and FIS1 between ER and mitochondria to modulate Ca^{2+} dynamics and mitochondrial fission (Chlystun et al., 2013). In all settings shown in Insets 2-4 the presence of AnxA6 seems to cause MCS untethering. Arrows indicate the following: translocation of EGFR-EGF into ILV (green, inset 1), cholesterol flux (pink, insets 1-2), Ca^{2+} flux (red, insets 3-4). **(C)** Schematic representation of the domain structure of the three annexins found in MCS: Motifs that may be involved in the recruitment annexins to MCS are indicated and include the homology to FFAT motifs (blue), S100-binding sites (green) (Rety et al., 2000; Chang et al., 2007; Rintala-Dempsey et al., 2008) and KFERQ-motifs (yellow and red) (Cuervo et al., 2000). Abbreviations that do not appear in the text: ACAT, Acyl-CoA:cholesterol acyltransferase; MCU, mitochondrial calcium uniporter; FIS1, mitochondrial fission 1; IP3R, inositol 1,4,5-triphosphate receptor; TRPML1, transient receptor potential mucolipin 1; Vps13, Vacuolar protein sorting-associated protein 13; MFN1/2, mitofusin1/2; Gramd1b, GRAM domain containing 1B; VAP proteins, VAP-A, VAP-B; monomer specific d-peptide 1 (MOSD1, 2 and 3) and PS, phosphatidylserine.

rapidly and MCS are now considered metabolic platforms for the transport of small molecules such as lipids and ions (Prinz et al., 2020). In addition, MCS modulate various other functions, including organelle trafficking, endosome maturation and positioning, membrane dynamics, Ca^{2+} signalling, autophagy and membrane/vesicle/organelle fusion and fission (Friedman et al., 2013; van der Kant and Neefjes, 2014; Raiborg et al., 2015a; Raiborg et al., 2015b; Eisenberg-Bord et al., 2016; Abrisch et al., 2020; Silva et al., 2020). Membrane contacts also exist in organelles with internal membranes, including mitochondria, chloroplasts, and multivesicular bodies (MVBs) (Prinz et al., 2020). As MCS formation can be manipulated experimentally and is de-regulated in human disease models (Wu et al., 2018; Henne, 2019; Scorrano et al., 2019; Ballabio and Bonifacino, 2020; Martello et al., 2020; Petkovic et al., 2021), MCS have become attractive therapeutic targets.

MCS appear as small contact zones between neighbouring organelles, but contain a plethora of proteins and lipids. The biogenesis, maintenance, dynamics, and function of MCS rely on protein-protein interactions bridging apposed membranes to establish their communication. These proteins in MCS include numerous lipid and cholesterol transfer proteins, and a variety of tethers, sorting nexins, membrane channels, SNAREs, small Rab-GTPases and their regulators. In addition, as outlined in more detail below, several annexins are also found in MCS. It would go beyond the scope of this *Mini Review* to list all proteins and we recommend excellent articles and reviews on this topic (Alpy and Tomasetto, 2005; Eisenberg-Bord et al., 2016; Kentala et al., 2016; Atakpa et al., 2018; Hoyer et al., 2018; Kumar et al., 2018; Quon et al., 2018; Sandhu et al., 2018; Balla et al., 2019; Bohnert, 2019; Liao et al., 2019; Patel, 2019; Cremer et al., 2020; Islinger et al., 2020; Meneses-Salas et al., 2020b; Peng et al., 2020; Hewlett et al., 2021; Reinisch and Prinz, 2021; Saric et al., 2021; Wu and Voeltz, 2021).

Annexins—Novel Players in Intracellular Communication and Membrane Contact Sites

Annexins are characterized by a high structural homology that enables binding to acidic phospholipids in a Ca^{2+}-dependent manner. In fact, most annexin functions in cells are due to their dynamic and reversible binding to membranes (Gerke et al., 2005; Enrich et al., 2017). More recently, mouse models lacking individual annexins validated proposed functions in complex physiological processes *in vivo* (Alvarez-Guaita et al., 2020; Grewal et al., 2021). Annexins are present in multiple cellular compartments to regulate numerous functions, including membrane trafficking, cytoskeleton dynamics, ion channels, cell signalling, membrane repair and pro- or anti-inflammatory activities. Most relevant for this review, annexins (AnxA1, A6 and A11) are located in endolysosomes in the vicinity of the ER (**Figure 1A**) with novel MCS-related roles for these annexins in cell physiology (Pons et al., 2000; Eden et al., 2016; Liao et al., 2019).

AnxA1 is ubiquitously expressed and found at the plasma membrane, endo-/exocytic vesicles, the cytoskeleton and nucleus (Grewal et al., 2021). Moreover, AnxA1 acts as a tether connecting the ER and MVBs (Eden et al., 2010; Eden et al., 2016). Tyrosine phosphorylated AnxA1 together with its binding partner S100A11 provide a docking site for tyrosine phosphatase 1B (PTP1B), an enzyme localized in the ER, at MVB-ER contacts to enable sorting of ligand-stimulated epidermal growth factor receptor (EGFR) onto intraluminal vesicles (ILVs) (**Figure 1B1**). EGF-induced AnxA1 phosphorylation is crucial for the segregation of EGFR onto ILVs (White et al., 2006). It remains to be clarified if AnxA1 acts in concert with the ESCRT complex and associated proteins and lipids (Raiborg and Stenmark, 2009) to facilitate this indispensable step targeting EGFR to lysosomes for degradation. Thus, MVB-ER contacts may provide localized sites where the phosphorylation status of AnxA1 and MVB sorting machinery components could be tightly controlled (Futter et al., 1993; White et al., 2006; Du et al., 2012; Eden et al., 2016).

Importantly, the AnxA1 tethering function is also required for ER-derived cholesterol transport to MVBs, a critical step for ILV formation to spatially regulate EGFR signalling. When cholesterol levels are low due to reduced endocytosis of Low-density lipoproteins (LDL), AnxA1-regulated membrane contacts facilitate cholesterol transfer from the ER to MVBs *via* the interaction of ER-localized VAMP-associated proteins (VAPs) and the endosomal oxysterol-binding protein related protein 1L (ORP1L) (Eden et al., 2016).

Besides the AnxA1-S100A11 complex, other annexins also interact with S100 proteins, and may interact with two membranes simultaneously (Rescher and Gerke, 2004; Rintala-Dempsey et al., 2008). Hence, the reversible membrane binding capacity of annexins could establish initial protein-protein (or protein-phospholipid) interactions between LE/MVB and ER membranes to induce MCS formation and allow the exchange of ions and lipids, including cholesterol in other physiological settings (Miwa et al., 2008; Rintala-Dempsey et al., 2008).

AnxA6 has recently also been associated with MCS formation (Meneses-Salas et al., 2020b). Further to its association with the plasma membrane, endo-/exocytic vesicles, mitochondria and lipid droplets (Grewal et al., 2021), AnxA6 was additionally detected in MAMs (Sala-Vila et al., 2016), specialized membrane subdomains enriched in cholesterol and neutral lipids that permit the communication between the ER and mitochondria (Vance, 1990; Hayashi and Su, 2003).

Given the recently identified role of AnxA6 in cholesterol transfer across MCS (Meneses-Salas et al., 2020b) and its presence in MAMs (Sala-Vila et al., 2016), the control of cholesterol transfer across MAMs and its alignment with steroid, oxysterol and bile acid synthesis is decisive for proper mitochondrial homeostasis. Emerging molecular insights include the identification of the founder member of the START [(Steroidogenic Acute Regulatory protein) related lipid transfer] domain family, StAR, also known as StARD1, at the outer mitochondrial membrane (OMM) as part of a multi-protein complex, with the voltage-dependent anion-selective channel protein (VDAC) and phosphate carrier protein (PCP), involved in the import of cholesterol (Reitz et al., 2008; Alpy and Tomasetto, 2014; Elustondo et al., 2017). StARD1 first incorporates ER-derived cholesterol into OMM, and together with VDAC and the translocator protein (TSPO), interacts with ATPase family AAA domain containing 3A (ATAD3A) and cytochrome P450 family 11 subfamily A member 1 (CYP11A1) in the inner mitochondrial membrane (Rone et al., 2012), to move and then metabolize cholesterol (Elustondo et al., 2017). Yet, how the feedback loop that coordinates LDL-derived cholesterol uptake and *de novo* cholesterol synthesis links to tethering and untethering events between the ER or LE/Lys with mitochondria to prevent excessive cholesterol transfer across MAMs remains unclear. Despite regulatory roles for AnxA6 in cholesterol transfer across LE/Lys-ER contacts (see below), similar functions for AnxA6 in MAMs have yet to be identified.

This indicates that mechanisms are in place that keep alternative and NPC1-independent cholesterol transport in an inactive state and do not enable other transport machinery to overcome cholesterol accumulation caused by NPC1 deficiency. Therefore, the presence of yet unidentified inhibitory proteins that act as "gatekeepers" may control activation of alternative cholesterol transport routes exiting LE/Lys. Indeed, NPC1 deficiency was associated with downregulation of the GTPase Rab7, the master regulator of LE/Lys function. Inhibition of Rab7 activity was mediated by AnxA6, which recruited the Rab7-GTPase activating protein (Rab7-GAP) TBC1 domain family member 15 (TBC1D15) to cholesterol-rich LE, thereby lowering Rab7-GTP levels. Strikingly, AnxA6 depletion in NPC1 mutant cells and the concomitant loss of TBC1D15 membrane targeting elevated Rab7-GTP levels, leading to increased MCS formation between LE/Lys and the ER (**Figure 1B2**). This MCS restoration enabled cholesterol transfer across LE/Lys-ER contacts *via* the cholesterol transporter StARD3 for storage in lipid droplets. Hence, the AnxA6/TBC1D15 complex could become a potential therapeutic target to slow down the progressive neurodegeneration in NPC disease (Enrich et al., 2019; Meneses-Salas et al., 2020b).

Interestingly, loss of TBC1D15-mediated Rab7-GTP hydrolysis also inhibited the untethering of mitochondria-LE/Lys contacts, disrupting mitochondrial distribution and function in models mimicking Parkinson's disease pathophysiology (Wong Y. C. et al., 2018; Kim et al., 2021) (**Figure 1B3**). Similarly, Rab7 mutations with reduced GTPase activity in Charcot-Marie-Tooth type 2B (CMT2B) are linked to defective mitochondria-lysosome contact dynamics (Bucci and De Luca, 2012; Wong et al., 2019). Of note, in mitochondria, AnxA6 also interacts with dynamin-related protein 1 (Drp1) (Chlystun et al., 2013), a GTPase interconnected with Rab7-dependent mitochondrial-LE/Lys contact formation in CMT2B (Wong et al., 2019). Hence, one can envisage a scaffolding role for AnxA6 in Rab7/TBC1D15 and Drp1-dependent dynamics of mitochondria-LE/Lys contacts in these neurological diseases (**Figure 1B4**).

Studies described above suggest annexin levels to differentially impact on MCS numbers, composition and function. Indeed, AnxA1 depletion markedly reduced MCS connecting EGFR-containing MVBs and the ER, while MCS between EGFR-deficient MVBs and the ER remained unaffected (Eden et al., 2016). Likewise, MCS exist in NPC mutant cells, in particular between LE/Lys and mitochondria (Hoglinger et al., 2019), yet AnxA6 depletion and consequently, loss of TBC1D15 recruitment to LE/Lys in these cells, increased MCS numbers between LE/Lys and the ER for cholesterol transfer, requiring Rab7, and the cholesterol transporter StARD3. Hence, high/low annexin levels acting as tethers (AnxA1) or gatekeepers (AnxA6) will differentially influence MCS protein composition and functions, with consequences for cholesterol transport between organelles. This may extend to other annexins, including AnxA2, which together with S100A10, can bridge membranes (Illien et al., 2012; Grill et al., 2018; Berg Klenow et al., 2021), and bind to cholesterol-rich LE (Mayran et al., 2003). Similarly, AnxA8 is recruited to cholesterol-laden LE, and AnxA8 depletion caused LE/Lys cholesterol accumulation (Heitzig et al., 2018). Further examples of up- or downregulated tethers, with consequences for lipid- or ion-related MCS transfer, comprise phosphatase interacting protein 51 (PTPIP51, also called RMDN3) (Galmes et al., 2016), and PDZ domain-containing protein 8 (PDZD8) (Hirabayashi et al., 2017). Thus, manipulating the levels of tethers, untethers and lipid transporters (Galmes et al., 2016; Pulli et al., 2018) can offer therapeutic opportunities to modulate MCS formation in disease.

Protein Domains in Annexins That Could Modulate MCS Assembly

The potential involvement of annexins in MCS formation by means of interactions with FFAT motifs (two phenylalanines in an acidic tract) in MCS-associated proteins should also be considered. FFAT motifs were originally identified in late endosomal/lysosomal proteins, interacting with ER-associated VAPs. Several variations of the original FFAT motif exist (Mikitova and Levine, 2012; Murphy and Levine, 2016;

Cabukusta et al., 2020), including the Phospho-FFAT motif in AnxA5 and A8 (Di Mattia et al., 2020). Homologies to FFAT motifs were also located in AnxA1, A6 and A11 (**Figure 1C**) (Rentero et al., 2018). Given their association with the LE/Lys compartment and affinity for cholesterol (de Diego et al., 2002; Hulce et al., 2013), one could envisage MCS formation between the ER and LE/Lys being influenced by ER-associated VAPs or motile sperm domain-containing proteins (MOSPDs) recognizing FFAT-like motifs in these annexins.

Alternatively, post-translational modifications such as palmitoylation, which enables the targeting of cytosolic proteins to membranes, often modulating the activity of multiprotein complexes in specialized microdomains (Charollais and Van Der Goot, 2009). This is exemplified by palmitoylated caveolin-1 and its ability to bind cholesterol, thereby determining the cholesterol content of ER-mitochondria subdomains, linking organelle communication across MAMs with intracellular steroid and lipoprotein metabolism (Sala-Vila et al., 2016).

Likewise, palmitoylated cytoskeleton-associated protein 4 (CKAP4) interacts with VDAC2 at ER-mitochondrial contacts (Harada et al., 2020). This could impact on cholesterol transfer, as StARD1, which transfers ER-derived cholesterol to mitochondria, can form a complex with TOM22 and VDAC2 (see above) (Torres et al., 2017; Gordaliza-Alaguero et al., 2019).

Another example is the transmembrane protein 55B (TMEM55B), which interacts with the cytosolic scaffold protein JIP4 and dynein/dynactin in MCS to modulate the spatial distribution and positioning of lysosomes. TMEM55B palmitoylation was decisive for lysosomal positioning, implicating a critical role in determining the speed and location of MCS being formed, (Ballabio and Bonifacino, 2020; Rudnik et al., 2021; Saftig and Puertollano, 2021).

Interestingly, AnxA1 and AnxA6 were recently identified as palmitoylated substrates in extracellular vesicle fractions, including exosomes (Albacete-Albacete et al., 2020; Mariscal et al., 2020). The mechanisms that regulate this post-translational modification or whether this modification also applies for other annexins remains unknown. Hence, palmitoylated annexins may also contribute to MCS tethering. Exploring whether annexins establish palmitoylated links with perimeter LE/Lys membranes as well as mutational analysis of the FFAT-like motif in annexins will address the relevance and potential consequences of these proposed interactions.

AnxA11 is a Tether of Lysosomes and RNA Granules

Recently, AnxA11 was detected in lysosomes that connect with RNA granules (Liao et al., 2019). Alike AnxA1 and A6, AnxA11 is widely expressed with diverse, often Ca^{2+}- and S100A6 (calcyclin)-dependent functions in cytoplasmic and nuclear membrane locations, relevant for growth, cell cycle progression, differentiation, and exocytosis (Grewal et al., 2021).

Liao and coworkers identified AnxA11 as a tether mediating RNA granule association with lysosomes during their transport to distal regions of the axon (Liao et al., 2019). Strikingly, AnxA11 mutations associated with amyotrophic lateral sclerosis (ALS) disrupted docking between RNA granules and lysosomes, thus hampering neuronal RNA granule transport. Mutant analysis mapped the AnxA11 N-terminus as necessary for Ca^{2+}- and phospholipid-dependent lysosome-RNA granule interactions, which could be relevant for RNA granule microtubule-based transport in polarized epithelial cells or neurons, facilitating local protein translation at subcellular locations (Lee et al., 2020; Das et al., 2021). Hence, AnxA11 represents a novel mechanistic and structural link between lysosomes and a membraneless compartment in ALS pathogenesis. This observation might extend to other annexins, as the AnxA11 interactome included AnxA7 (Liao et al., 2019). Similarly, using AnxA6 as bait, we identified AnxA11 and AnxA7 as binding partners, indicating that interactions between multiple annexins, as proposed previously (Li et al., 2016), may contribute to the tethering of lysosomes to other organelles.

DISCUSSION

Since the discovery of the annexin domain structure (Geisow, 1986), annexins have been identified in many organisms, including humans (Moss and Morgan, 2004). The Ca^{2+}-inducible conformational change and differential preference for negatively charged phospholipids and other lipids, in particular cholesterol, can enhance membrane association of several annexins (Enrich et al., 2017). Furthermore, their promiscuous behaviour to differentially interact with other proteins together with their innate properties to "annex" membranes, make annexins suitable applicants for MCS appointments.

Annexins: Regulators of Cholesterol Trafficking, ILV Formation and MCS Association

As outlined above, AnxA1 and AnxA6 control cholesterol transport from the ER to LE/Lys and vice versa *via* MCS (Eden et al., 2016; Meneses-Salas et al., 2020b). This contribution to MCS functioning may assist to control cholesterol levels in MVBs to participate, together with other lipids and accessory proteins (Gruenberg, 2020), in ILV biogenesis. This might even create transport specificity, as AnxA1 only mediates MCS formation between the ER and EGFR-containing MVBs (Wong L. H. et al., 2018).

However, annexin recruitment to MCS remains to be clarified. Besides the potential contribution of FFAT motifs or palmitoylation listed above, this could occur *via* translocation of cytosolic annexin pools where local Ca^{2+}, cholesterol or annexin-binding proteins could contribute to their association with MCS. Alternatively, annexin pools inside ILVs could be released *via* back fusion, a constitutive process occurring in MVBs, where ILV fuse with the perimeter LE membrane leaving the cargo at cytosolic interfaces delimited by juxtaposed membranes of MVBs and other organelles (i.e., ER) (Gruenberg, 2020; Perrin et al., 2021). In this scenario, annexins could locally encounter a suitable Ca^{2+} and lipid microenvironment that would enable them to act as

interorganelle tethers. On the other hand, annexins on ILVs facing the lumen of MVBs might be part of the fusion machinery (including LBPA, cholesterol, Alix) for the back fusion process. In fact, some of the complex protein networks that interact with AnxA6 are also involved in ILV formation and may regulate back fusion (Enrich et al., 2017). The well-documented presence of annexins in exosomes provides credibility for mechanisms such as chaperone-mediated autophagy (CMA) or endosome microautophagy (e-MI) for annexin association with ILV, the latter having the ability to keep proteins inside ILV. This is supported by all annexins harbouring the KFERQ motif (**Figure 1C**) (Cuervo et al., 2000; Kaushik and Cuervo, 2018), which is considered responsible for the location of annexins inside ILV (White et al., 2006; Meneses-Salas et al., 2020a).

Overall, the evidence of annexins contributing to MCS formation and function in LE/Lys is growing, with consequences for membrane traffic, microdomain organization, interactions with the cytoskeleton, cholesterol homeostasis, tethering, Ca^{2+} signalling and positioning of acidic compartments, and likely relevant for many biological settings.

AUTHOR CONTRIBUTIONS

AL, inputs and discussion FT, reading, criticisms and discussion CR, art work and discussion TG, editing, discussion CE, write the manuscript and coordinate the review.

FUNDING

CR is supported by the Serra Húnter Programme (Generalitat de Catalunya). AL is supported by the Michael J Fox Foundation for Parkinson's Research. TG is supported by the University of Sydney, Sydney, Australia.

ACKNOWLEDGMENTS

CE and CR acknowledge the funding from Ministerio de Ciencia e Innovación (Spain, Grant PID 2020-115910RB-I00). CE is also thankful to the University of Barcelona (Grant AR0RM005) and UIU2019 fellowship.

REFERENCES

Abrisch, R. G., Gumbin, S. C., Wisniewski, B. T., Lackner, L. L., and Voeltz, G. K. (2020). Fission and Fusion Machineries Converge at ER Contact Sites to Regulate Mitochondrial Morphology. *J. Cel Biol* 219 (4), e201911122. doi:10.1083/jcb.201911122

Albacete-Albacete, L., Navarro-Lérida, I., López, J. A., Martín-Padura, I., Astudillo, A. M., Ferrarini, A., et al. (2020). ECM Deposition Is Driven by Caveolin-1-dependent Regulation of Exosomal Biogenesis and Cargo Sorting. *J. Cel Biol* 219 (11), e202006178. doi:10.1083/jcb.202006178

Alpy, F., and Tomasetto, C. (2005). Give Lipids a START: the StAR-related Lipid Transfer (START) Domain in Mammals. *J. Cel Sci* 118 (Pt 13), 2791–2801. doi:10.1242/jcs.02485

Alpy, F., and Tomasetto, C. (2014). START Ships Lipids across Interorganelle Space. *Biochimie* 96, 85–95. doi:10.1016/j.biochi.2013.09.015

Alvarez-Guaita, A., Blanco-Muñoz, P., Meneses-Salas, E., Wahba, M., Pollock, A. H., Jose, J., et al. (2020). Annexin A6 Is Critical to Maintain Glucose Homeostasis and Survival during Liver Regeneration in Mice. *Hepatology* 72 (6), 2149–2164. doi:10.1002/hep.31232

Atakpa, P., Thillaiappan, N. B., Mataragka, S., Prole, D. L., and Taylor, C. W. (2018). IP3 Receptors Preferentially Associate with ER-Lysosome Contact Sites and Selectively Deliver Ca2+ to Lysosomes. *Cel Rep.* 25 (11), 3180–3193.e7. doi:10.1016/j.celrep.2018.11.064

Balla, T., Kim, Y. J., Alvarez-Prats, A., and Pemberton, J. (2019). Lipid Dynamics at Contact Sites between the Endoplasmic Reticulum and Other Organelles. *Annu. Rev. Cel Dev. Biol.* 35, 85–109. doi:10.1146/annurev-cellbio-100818-125251

Ballabio, A., and Bonifacino, J. S. (2020). Lysosomes as Dynamic Regulators of Cell and Organismal Homeostasis. *Nat. Rev. Mol. Cel Biol* 21 (2), 101–118. doi:10.1038/s41580-019-0185-4

Berg Klenow, M., Iversen, C., Wendelboe Lund, F., Mularski, A., Busk Heitmann, A. S., Dias, C., et al. (2021). Annexins A1 and A2 Accumulate and Are Immobilized at Cross-Linked Membrane-Membrane Interfaces. *Biochemistry* 60 (16), 1248–1259. doi:10.1021/acs.biochem.1c00126

Bohnert, M. (2019). Organelle Contact Sites: Lipid Droplets Hooked by Metabolically Controlled Tethers. *Curr. Biol.* 29 (10), R375–R377. doi:10.1016/j.cub.2019.03.049

Bucci, C., and De Luca, M. (2012). Molecular Basis of Charcot-Marie-Tooth Type 2B Disease. *Biochem. Soc. Trans.* 40 (6), 1368–1372. doi:10.1042/BST20120197

Cabukusta, B., Berlin, I., van Elsland, D. M., Forkink, I., Spits, M., de Jong, A. W. M., et al. (2020). Human VAPome Analysis Reveals MOSPD1 and MOSPD3 as Membrane Contact Site Proteins Interacting with FFAT-Related FFNT Motifs. *Cel Rep.* 33 (10), 108475. doi:10.1016/j.celrep.2020.108475

Chang, N., Sutherland, C., Hesse, E., Winkfein, R., Wiehler, W. B., Pho, M., et al. (2007). Identification of a Novel Interaction between the Ca2+-Binding Protein S100A11 and the Ca2+- and Phospholipid-Binding Protein Annexin A6. *Am. J. Physiology-Cell Physiol.* 292 (4), C1417–C1430. doi:10.1152/ajpcell.00439.2006

Charollais, J., and Van Der Goot, F. G. (2009). Palmitoylation of Membrane Proteins (Review). *Mol. Membr. Biol.* 26 (1), 55–66. doi:10.1080/09687680802620369

Chlystun, M., Campanella, M., Law, A.-L., Duchen, M. R., Fatimathas, L., Levine, T. P., et al. (2013). Regulation of Mitochondrial Morphogenesis by Annexin A6. *PLoS One* 8 (1), e53774. doi:10.1371/journal.pone.0053774

Cremer, T., Neefjes, J., and Berlin, I. (2020). The Journey of Ca2+ through the Cell - Pulsing through the Network of ER Membrane Contact Sites. *J. Cel Sci* 133 (24), jcs249136. doi:10.1242/jcs.249136

Cuervo, A. M., Gomes, A. V., Barnes, J. A., and Dice, J. F. (2000). Selective Degradation of Annexins by Chaperone-Mediated Autophagy. *J. Biol. Chem.* 275 (43), 33329–33335. doi:10.1074/jbc.M005655200

Das, S., Vera, M., Gandin, V., Singer, R. H., and Tutucci, E. (2021). Intracellular mRNA Transport and Localized Translation. *Nat. Rev. Mol. Cel Biol* 22 (7), 483–504. doi:10.1038/s41580-021-00356-8

de Diego, I., Schwartz, F., Siegfried, H., Dauterstedt, P., Heeren, J., Beisiegel, U., et al. (2002). Cholesterol Modulates the Membrane Binding and Intracellular Distribution of Annexin 6. *J. Biol. Chem.* 277 (35), 32187–32194. doi:10.1074/jbc.M205499200

Di Mattia, T., Martinet, A., Ikhlef, S., McEwen, A. G., Nominé, Y., Wendling, C., et al. (2020). FFAT Motif Phosphorylation Controls Formation and Lipid Transfer Function of Inter-organelle Contacts. *EMBO J.* 39 (23), e104369. doi:10.15252/embj.2019104369

Dong, R., Saheki, Y., Swarup, S., Lucast, L., Harper, J. W., and De Camilli, P. (2016). Endosome-ER Contacts Control Actin Nucleation and Retromer Function through VAP-dependent Regulation of PI4P. *Cell* 166 (2), 408–423. doi:10.1016/j.cell.2016.06.037

Du, X., Kazim, A. S., Brown, A. J., and Yang, H. (2012). An Essential Role of Hrs/Vps27 in Endosomal Cholesterol Trafficking. *Cel Rep.* 1 (1), 29–35. doi:10.1016/j.celrep.2011.10.004

Eden, E. R., and Futter, C. E. (2021). Membrane Trafficking: Retrofusion as an Escape Route Out of the Endosome. *Curr. Biol.* 31 (17), R1037–R1040. doi:10.1016/j.cub.2021.07.055

Eden, E. R., Sanchez-Heras, E., Tsapara, A., Sobota, A., Levine, T. P., and Futter, C. E. (2016). Annexin A1 Tethers Membrane Contact Sites that Mediate ER to Endosome Cholesterol Transport. *Develop. Cel* 37 (5), 473–483. doi:10.1016/j.devcel.2016.05.005

Eden, E. R., White, I. J., Tsapara, A., and Futter, C. E. (2010). Membrane Contacts between Endosomes and ER Provide Sites for PTP1B-Epidermal Growth Factor Receptor Interaction. *Nat. Cel Biol* 12 (3), 267–272. doi:10.1038/ncb2026

Eisenberg-Bord, M., Shai, N., Schuldiner, M., and Bohnert, M. (2016). A Tether Is a Tether Is a Tether: Tethering at Membrane Contact Sites. *Develop. Cel* 39 (4), 395–409. doi:10.1016/j.devcel.2016.10.022

Elustondo, P., Martin, L. A., and Karten, B. (2017). Mitochondrial Cholesterol Import. *Biochim. Biophys. Acta (Bba) - Mol. Cel Biol. Lipids* 1862 (1), 90–101. doi:10.1016/j.bbalip.2016.08.012

Enrich, C., Rentero, C., Grewal, T., Futter, C. E., and Eden, E. R. (2019). Cholesterol Overload: Contact Sites to the Rescue!. *Contact* 2, 251525641989350. doi:10.1177/2515256419893507

Enrich, C., Rentero, C., Meneses-Salas, E., Tebar, F., and Grewal, T. (2017). Annexins: Ca2+ Effectors Determining Membrane Trafficking in the Late Endocytic Compartment. *Adv. Exp. Med. Biol.* 981, 351–385. doi:10.1007/978-3-319-55858-5_14

Friedman, J. R., Dibenedetto, J. R., West, M., Rowland, A. A., and Voeltz, G. K. (2013). Endoplasmic Reticulum-Endosome Contact Increases as Endosomes Traffic and Mature. *MBoC* 24 (7), 1030–1040. doi:10.1091/mbc.E12-10-0733

Futter, C. E., Felder, S., Schlessinger, J., Ullrich, A., and Hopkins, C. R. (1993). Annexin I Is Phosphorylated in the Multivesicular Body during the Processing of the Epidermal Growth Factor Receptor. *J. Cel Biol* 120 (1), 77–83. doi:10.1083/jcb.120.1.77

Galmes, R., Houcine, A., Vliet, A. R., Agostinis, P., Jackson, C. L., and Giordano, F. (2016). ORP5/ORP8 Localize to Endoplasmic Reticulum-Mitochondria Contacts and Are Involved in Mitochondrial Function. *EMBO Rep.* 17 (6), 800–810. doi:10.15252/embr.201541108

Geisow, M. J. (1986). Common Domain Structure of Ca2+and Lipid-Binding Proteins. *FEBS Lett.* 203 (1), 99–103. doi:10.1016/0014-5793(86)81445-4

Gerke, V., Creutz, C. E., and Moss, S. E. (2005). Annexins: Linking Ca2+ Signalling to Membrane Dynamics. *Nat. Rev. Mol. Cel Biol* 6 (6), 449–461. doi:10.1038/nrm1661

Gordaliza-Alaguero, I., Cantó, C., and Zorzano, A. (2019). Metabolic Implications of Organelle-Mitochondria Communication. *EMBO Rep.* 20 (9), e47928. doi:10.15252/embr.201947928

Grewal, T., Rentero, C., Enrich, C., Wahba, M., Raabe, C. A., and Rescher, U. (2021). Annexin Animal Models-From Fundamental Principles to Translational Research. *Int. J. Mol. Sci.* 22 (7), 3439. doi:10.3390/ijms22073439

Grill, D., Matos, A. L. L., de Vries, W. C., Kudruk, S., Heflik, M., Dörner, W., et al. (2018). Bridging of Membrane Surfaces by Annexin A2. *Sci. Rep.* 8 (1), 14662. doi:10.1038/s41598-018-33044-3

Gruenberg, J. (2020). Life in the Lumen: The Multivesicular Endosome. *Traffic* 21 (1), 76–93. doi:10.1111/tra.12715

Harada, T., Sada, R., Osugi, Y., Matsumoto, S., Matsuda, T., Hayashi-Nishino, M., et al. (2020). Palmitoylated CKAP4 Regulates Mitochondrial Functions through an Interaction with VDAC2 at ER-Mitochondria Contact Sites. *J. Cel Sci* 133 (21), jcs249045. doi:10.1242/jcs.249045

Hayashi, T., and Su, T.-P. (2003). σ-1 Receptors (σ1Binding Sites) Form Raft-like Microdomains and Target Lipid Droplets on the Endoplasmic Reticulum: Roles in Endoplasmic Reticulum Lipid Compartmentalization and Export. *J. Pharmacol. Exp. Ther.* 306 (2), 718–725. doi:10.1124/jpet.103.051284

Heitzig, N., Kühnl, A., Grill, D., Ludewig, K., Schloer, S., Galla, H.-J., et al. (2018). Cooperative Binding Promotes Demand-Driven Recruitment of AnxA8 to Cholesterol-Containing Membranes. *Biochim. Biophys. Acta (Bba) - Mol. Cel Biol. Lipids* 1863 (4), 349–358. doi:10.1016/j.bbalip.2018.01.001

Henne, M. (2019). And Three's a Party: Lysosomes, Lipid Droplets, and the ER in Lipid Trafficking and Cell Homeostasis. *Curr. Opin. Cel Biol.* 59, 40–49. doi:10.1016/j.ceb.2019.02.011

Henne, W. M., Zhu, L., Balogi, Z., Stefan, C., Pleiss, J. A., and Emr, S. D. (2015). Mdm1/Snx13 Is a Novel ER-Endolysosomal Interorganelle Tethering Protein. *J. Cel Biol* 210 (4), 541–551. doi:10.1083/jcb.201503088

Hewlett, B., Singh, N. P., Vannier, C., and Galli, T. (2021). ER-PM Contact Sites - SNARING Actors in Emerging Functions. *Front. Cel Dev. Biol.* 9, 635518. doi:10.3389/fcell.2021.635518

Hirabayashi, Y., Kwon, S.-K., Paek, H., Pernice, W. M., Paul, M. A., Lee, J., et al. (2017). ER-mitochondria Tethering by PDZD8 Regulates Ca2+dynamics in Mammalian Neurons. *Science* 358 (6363), 623–630. doi:10.1126/science.aan6009

Höglinger, D., Burgoyne, T., Sanchez-Heras, E., Hartwig, P., Colaco, A., Newton, J., et al. (2019). NPC1 Regulates ER Contacts with Endocytic Organelles to Mediate Cholesterol Egress. *Nat. Commun.* 10 (1), 4276. doi:10.1038/s41467-019-12152-2

Hoyer, M. J., Chitwood, P. J., Ebmeier, C. C., Striepen, J. F., Qi, R. Z., Old, W. M., et al. (2018). A Novel Class of ER Membrane Proteins Regulates ER-Associated Endosome Fission. *Cell* 175 (1), 254–265.e14. doi:10.1016/j.cell.2018.08.030

Hulce, J. J., Cognetta, A. B., Niphakis, M. J., Tully, S. E., and Cravatt, B. F. (2013). Proteome-wide Mapping of Cholesterol-Interacting Proteins in Mammalian Cells. *Nat. Methods* 10 (3), 259–264. doi:10.1038/nmeth.2368

Illien, F., Piao, H.-R., Coué, M., di Marco, C., and Ayala-Sanmartin, J. (2012). Lipid Organization Regulates Annexin A2 Ca2+-Sensitivity for Membrane Bridging and its Modulator Effects on Membrane Fluidity. *Biochim. Biophys. Acta (Bba) - Biomembranes* 1818 (11), 2892–2900. doi:10.1016/j.bbamem.2012.07.012

Islinger, M., Costello, J. L., Kors, S., Soupene, E., Levine, T. P., Kuypers, F. A., et al. (2020). The Diversity of ACBD Proteins - from Lipid Binding to Protein Modulators and Organelle Tethers. *Biochim. Biophys. Acta (Bba) - Mol. Cel Res.* 1867 (5), 118675. doi:10.1016/j.bbamcr.2020.118675

Kaushik, S., and Cuervo, A. M. (2018). The Coming of Age of Chaperone-Mediated Autophagy. *Nat. Rev. Mol. Cel Biol* 19 (6), 365–381. doi:10.1038/s41580-018-0001-6

Kentala, H., Weber-Boyvat, M., and Olkkonen, V. M. (2016). OSBP-related Protein Family: Mediators of Lipid Transport and Signaling at Membrane Contact Sites. *Int. Rev. Cel Mol Biol* 321, 299–340. doi:10.1016/bs.ircmb.2015.09.006

Kim, S., Wong, Y. C., Gao, F., and Krainc, D. (2021). Dysregulation of Mitochondria-Lysosome Contacts by GBA1 Dysfunction in Dopaminergic Neuronal Models of Parkinson's Disease. *Nat. Commun.* 12 (1), 1807. doi:10.1038/s41467-021-22113-3

Kumar, N., Leonzino, M., Hancock-Cerutti, W., Horenkamp, F. A., Li, P., Lees, J. A., et al. (2018). VPS13A and VPS13C Are Lipid Transport Proteins Differentially Localized at ER Contact Sites. *J. Cel Biol* 217 (10), 3625–3639. doi:10.1083/jcb.201807019

Lee, J. E., Cathey, P. I., Wu, H., Parker, R., and Voeltz, G. K. (2020). Endoplasmic Reticulum Contact Sites Regulate the Dynamics of Membraneless Organelles. *Science* 367 (6477), eaay7108. doi:10.1126/science.aay7108

Li, H.-D., Menon, R., Eksi, R., Guerler, A., Zhang, Y., Omenn, G. S., et al. (2016). A Network of Splice Isoforms for the Mouse. *Sci. Rep.* 6, 24507. doi:10.1038/srep24507

Liao, Y.-C., Fernandopulle, M. S., Wang, G., Choi, H., Hao, L., Drerup, C. M., et al. (2019). RNA Granules Hitchhike on Lysosomes for Long-Distance Transport, Using Annexin A11 as a Molecular Tether. *Cell* 179 (1), 147–164. doi:10.1016/j.cell.2019.08.050

Mariscal, J., Vagner, T., Kim, M., Zhou, B., Chin, A., Zandian, M., et al. (2020). Comprehensive Palmitoyl-proteomic Analysis Identifies Distinct Protein Signatures for Large and Small Cancer-derived Extracellular Vesicles. *J. Extracellular Vesicles* 9 (1), 1764192. doi:10.1080/20013078.2020.1764192

Martello, A., Platt, F. M., and Eden, E. R. (2020). Staying in Touch with the Endocytic Network: The Importance of Contacts for Cholesterol Transport. *Traffic* 21 (5), 354–363. doi:10.1111/tra.12726

Mayran, N., Parton, R. G., and Gruenberg, J. (2003). Annexin II Regulates Multivesicular Endosome Biogenesis in the Degradation Pathway of Animal Cells. *EMBO J.* 22 (13), 3242–3253. doi:10.1093/emboj/cdg321

Meneses-Salas, E., García-Melero, A., Blanco-Muñoz, P., Jose, J., Brenner, M.-S., Lu, A., et al. (2020a). Selective Degradation Permits a Feedback Loop Controlling Annexin A6 and Cholesterol Levels in Endolysosomes of NPC1 Mutant Cells. *Cells* 9 (5), 1152. doi:10.3390/cells9051152

Meneses-Salas, E., García-Melero, A., Kanerva, K., Blanco-Muñoz, P., Morales-Paytuvi, F., Bonjoch, J., et al. (2020b). Annexin A6 Modulates TBC1D15/Rab7/StARD3 axis to Control Endosomal Cholesterol export in NPC1 Cells. *Cell. Mol. Life Sci.* 77 (14), 2839–2857. doi:10.1007/s00018-019-03330-y

Mikitova, V., and Levine, T. P. (2012). Analysis of the Key Elements of FFAT-like Motifs Identifies New Proteins that Potentially Bind VAP on the ER, Including

Two AKAPs and FAPP2. *PLoS One* 7 (1), e30455. doi:10.1371/journal.pone.0030455

Miwa, N., Uebi, T., and Kawamura, S. (2008). S100-annexin Complexes - Biology of Conditional Association. *FEBS J.* 275 (20), 4945–4955. doi:10.1111/j.1742-4658.2008.06653.x

Moss, S. E., and Morgan, R. O. (2004). The Annexins. *Genome Biol.* 5 (4), 219. doi:10.1186/gb-2004-5-4-219

Murphy, S. E., and Levine, T. P. (2016). VAP, a Versatile Access Point for the Endoplasmic Reticulum: Review and Analysis of FFAT-like Motifs in the VAPome. *Biochim. Biophys. Acta (Bba) - Mol. Cel Biol. Lipids* 1861 (8 Pt B), 952–961. doi:10.1016/j.bbalip.2016.02.009

Neefjes, J., and Cabukusta, B. (2021). What the VAP: The Expanded VAP Family of Proteins Interacting with FFAT and FFAT-Related Motifs for Interorganellar Contact. *Contact* 4, 251525642110122. doi:10.1177/25152564211012246

Nixon-Abell, J., Obara, C. J., Weigel, A. V., Li, D., Legant, W. R., Xu, C. S., et al. (2016). Increased Spatiotemporal Resolution Reveals Highly Dynamic Dense Tubular Matrices in the Peripheral ER. *Science* 354 (6311), aaf3928. doi:10.1126/science.aaf3928

Patel, S. (2019). Getting Close. Lysosome-ER Contact Sites Tailor Ca2+ Signals. *Cell Calcium* 80, 194–196. doi:10.1016/j.ceca.2019.02.003

Peng, W., Wong, Y. C., and Krainc, D. (2020). Mitochondria-lysosome Contacts Regulate Mitochondrial Ca2+dynamics via Lysosomal TRPML1. *Proc. Natl. Acad. Sci. USA* 117 (32), 19266–19275. doi:10.1073/pnas.2003236117

Perrin, P., Janssen, L., Janssen, H., van den Broek, B., Voortman, L. M., van Elsland, D., et al. (2021). Retrofusion of Intralumenal MVB Membranes Parallels Viral Infection and Coexists with Exosome Release. *Curr. Biol.* 31 (17), 3884–3893.e4. doi:10.1016/j.cub.2021.06.022

Petkovic, M., O'Brien, C. E., and Jan, Y. N. (2021). Interorganelle Communication, Aging, and Neurodegeneration. *Genes Dev.* 35 (7-8), 449–469. doi:10.1101/gad.346759.120

Pons, M., Ihrke, G., Koch, S., Biermer, M., Pol, A., Grewal, T., et al. (2000). Late Endocytic Compartments Are Major Sites of Annexin VI Localization in NRK Fibroblasts and Polarized WIF-B Hepatoma Cells. *Exp. Cel Res.* 257 (1), 33–47. doi:10.1006/excr.2000.4861

Prinz, W. A., Toulmay, A., and Balla, T. (2020). The Functional Universe of Membrane Contact Sites. *Nat. Rev. Mol. Cel Biol* 21 (1), 7–24. doi:10.1038/s41580-019-0180-9

Pulli, I., Lassila, T., Pan, G., Yan, D., Olkkonen, V. M., and Törnquist, K. (2018). Oxysterol-binding Protein Related-Proteins (ORPs) 5 and 8 Regulate Calcium Signaling at Specific Cell Compartments. *Cell Calcium* 72, 62–69. doi:10.1016/j.ceca.2018.03.001

Quon, E., Sere, Y. Y., Chauhan, N., Johansen, J., Sullivan, D. P., Dittman, J. S., et al. (2018). Endoplasmic Reticulum-Plasma Membrane Contact Sites Integrate Sterol and Phospholipid Regulation. *Plos Biol.* 16 (5), e2003864. doi:10.1371/journal.pbio.2003864

Raiborg, C., and Stenmark, H. (2009). The ESCRT Machinery in Endosomal Sorting of Ubiquitylated Membrane Proteins. *Nature* 458 (7237), 445–452. doi:10.1038/nature07961

Raiborg, C., Wenzel, E. M., Pedersen, N. M., Olsvik, H., Schink, K. O., Schultz, S. W., et al. (2015a). Repeated ER-Endosome Contacts Promote Endosome Translocation and Neurite Outgrowth. *Nature* 520 (7546), 234–238. doi:10.1038/nature14359

Raiborg, C., Wenzel, E. M., and Stenmark, H. (2015b). ER -endosome Contact Sites: Molecular Compositions and Functions. *EMBO J.* 34 (14), 1848–1858. doi:10.15252/embj.201591481

Reinisch, K. M., and Prinz, W. A. (2021). Mechanisms of Nonvesicular Lipid Transport. *J. Cel Biol* 220 (3), e202012058. doi:10.1083/jcb.202012058

Reitz, J., Gehrig-Burger, K., Strauss, J. F., 3rd, and Gimpl, G. (2008). Cholesterol Interaction with the Related Steroidogenic Acute Regulatory Lipid-Transfer (START) Domains of StAR (STARD1) and MLN64 (STARD3). *FEBS J.* 275 (8), 1790–1802. doi:10.1111/j.1742-4658.2008.06337.x

Rentero, C., Blanco-Muñoz, P., Meneses-Salas, E., Grewal, T., and Enrich, C. (2018). Annexins-Coordinators of Cholesterol Homeostasis in Endocytic Pathways. *Int. J. Mol. Sci.* 19 (5), 1444. doi:10.3390/ijms19051444

Rescher, U., and Gerke, V. (2004). Annexins - Unique Membrane Binding Proteins with Diverse Functions. *J. Cel Sci* 117 (Pt 13), 2631–2639. doi:10.1242/jcs.01245

Réty, S., Osterloh, D., Arié, J.-P., Tabaries, S., Seeman, J., Russo-Marie, F., et al. (2000). Structural Basis of the Ca2+-dependent Association between S100C (S100A11) and its Target, the N-Terminal Part of Annexin I. *Structure* 8 (2), 175–184. doi:10.1016/s0969-2126(00)00093-9

Rintala-Dempsey, A. C., Rezvanpour, A., and Shaw, G. S. (2008). S100-annexin Complexes - Structural Insights. *FEBS J.* 275 (20), 4956–4966. doi:10.1111/j.1742-4658.2008.06654.x

Rone, M. B., Midzak, A. S., Issop, L., Rammouz, G., Jagannathan, S., Fan, J., et al. (2012). Identification of a Dynamic Mitochondrial Protein Complex Driving Cholesterol Import, Trafficking, and Metabolism to Steroid Hormones. *Mol. Endocrinol.* 26 (11), 1868–1882. doi:10.1210/me.2012-1159

Rudnik, S., Heybrock, S., Saftig, P., and Damme, M. (2021). S-palmitoylation Determines TMEM55B-dependent Positioning of Lysosomes. *J. Cel Sci* 135, jcs258566. doi:10.1242/jcs.258566

Saftig, P., and Puertollano, R. (2021). How Lysosomes Sense, Integrate, and Cope with Stress. *Trends Biochem. Sci.* 46 (2), 97–112. doi:10.1016/j.tibs.2020.09.004

Sala-Vila, A., Navarro-Lérida, I., Sánchez-Alvarez, M., Bosch, M., Calvo, C., López, J. A., et al. (2016). Interplay between Hepatic Mitochondria-Associated Membranes, Lipid Metabolism and Caveolin-1 in Mice. *Sci. Rep.* 6, 27351. doi:10.1038/srep27351

Sandhu, J., Li, S., Fairall, L., Pfisterer, S. G., Gurnett, J. E., Xiao, X., et al. (2018). Aster Proteins Facilitate Nonvesicular Plasma Membrane to ER Cholesterol Transport in Mammalian Cells. *Cell* 175 (2), 514–529. doi:10.1016/j.cell.2018.08.033

Saric, A., Freeman, S. A., Williamson, C. D., Jarnik, M., Guardia, C. M., Fernandopulle, M. S., et al. (2021). SNX19 Restricts Endolysosome Motility through Contacts with the Endoplasmic Reticulum. *Nat. Commun.* 12 (1), 4552. doi:10.1038/s41467-021-24709-1

Scorrano, L., De Matteis, M. A., Emr, S., Giordano, F., Hajnóczky, G., Kornmann, B., et al. (2019). Coming Together to Define Membrane Contact Sites. *Nat. Commun.* 10 (1), 1287. doi:10.1038/s41467-019-09253-3

Shirane, M., Wada, M., Morita, K., Hayashi, N., Kunimatsu, R., Matsumoto, Y., et al. (2020). Protrudin and PDZD8 Contribute to Neuronal Integrity by Promoting Lipid Extraction Required for Endosome Maturation. *Nat. Commun.* 11 (1), 4576. doi:10.1038/s41467-020-18413-9

Silva, B. S. C., DiGiovanni, L., Kumar, R., Carmichael, R. E., Kim, P. K., and Schrader, M. (2020). Maintaining Social Contacts: The Physiological Relevance of Organelle Interactions. *Biochim. Biophys. Acta (Bba) - Mol. Cel Res.* 1867 (11), 118800. doi:10.1016/j.bbamcr.2020.118800

Tekirdag, K., and Cuervo, A. M. (2018). Chaperone-mediated Autophagy and Endosomal Microautophagy: Jointed by a Chaperone. *J. Biol. Chem.* 293 (15), 5414–5424. doi:10.1074/jbc.R117.818237

Torres, S., Balboa, E., Zanlungo, S., Enrich, C., Garcia-Ruiz, C., and Fernandez-Checa, J. C. (2017). Lysosomal and Mitochondrial Liaisons in Niemann-Pick Disease. *Front. Physiol.* 8, 982. doi:10.3389/fphys.2017.00982

van der Kant, R., and Neefjes, J. (2014). Small Regulators, Major Consequences - Ca2+ and Cholesterol at the Endosome-ER Interface. *J. Cel Sci* 127 (Pt 5), 929–938. doi:10.1242/jcs.137539

Vance, J. E. (1990). Phospholipid Synthesis in a Membrane Fraction Associated with Mitochondria. *J. Biol. Chem.* 265 (13), 7248–7256. doi:10.1016/s0021-9258(19)39106-9

White, I. J., Bailey, L. M., Aghakhani, M. R., Moss, S. E., and Futter, C. E. (2006). EGF Stimulates Annexin 1-dependent Inward Vesiculation in a Multivesicular Endosome Subpopulation. *EMBO J.* 25 (1), 1–12. doi:10.1038/sj.emboj.7600759

Wong, L. H., Eden, E. R., and Futter, C. E. (2018). Roles for ER:endosome Membrane Contact Sites in Ligand-Stimulated Intraluminal Vesicle Formation. *Biochem. Soc. Trans.* 46 (5), 1055–1062. doi:10.1042/BST20170432

Wong, Y. C., Peng, W., and Krainc, D. (2019). Lysosomal Regulation of Inter-mitochondrial Contact Fate and Motility in Charcot-Marie-Tooth Type 2. *Develop. Cel* 50 (3), 339–354.e4. doi:10.1016/j.devcel.2019.05.033

Wong, Y. C., Ysselstein, D., and Krainc, D. (2018). Mitochondria-lysosome Contacts Regulate Mitochondrial Fission via RAB7 GTP Hydrolysis. *Nature* 554 (7692), 382–386. doi:10.1038/nature25486

Wu, H., Carvalho, P., and Voeltz, G. K. (2018). Here, There, and Everywhere: The Importance of ER Membrane Contact Sites. *Science* 361 (6401), eaan5835. doi:10.1126/science.aan5835

Wu, H., and Voeltz, G. K. (2021). Reticulon-3 Promotes Endosome Maturation at ER Membrane Contact Sites. *Develop. Cel* 56 (1), 52–66.e7. doi:10.1016/j.devcel.2020.12.014

Conflict of Interest: The authors declare that the research was conducted in the absence of any commercial or financial relationships that could be construed as a potential conflict of interest.

Publisher's Note: All claims expressed in this article are solely those of the authors and do not necessarily represent those of their affiliated organizations, or those of the publisher, the editors and the reviewers. Any product that may be evaluated in this article, or claim that may be made by its manufacturer, is not guaranteed or endorsed by the publisher.

frontiers in Cell and Developmental Biology

REVIEW
published: 01 February 2022
doi: 10.3389/fcell.2022.837406

Running 'LAPS' Around nLD: Nuclear Lipid Droplet Form and Function

Michael J. McPhee[1], Jayme Salsman[2], Jason Foster[1], Jordan Thompson[1], Sabateeshan Mathavarajah[2], Graham Dellaire[1,2] and Neale D. Ridgway[1,3]**

[1]Department of Biochemistry & Molecular Biology, Dalhousie University, Halifax, NS, Canada, [2]Department of Pathology, Dalhousie University, Halifax, NS, Canada, [3]Department of Pediatrics, Dalhousie University, Halifax, NS, Canada

The nucleus harbours numerous protein subdomains and condensates that regulate chromatin organization, gene expression and genomic stress. A novel nuclear subdomain that is formed following exposure of cells to excess fatty acids is the nuclear lipid droplet (nLD), which is composed of a neutral lipid core surrounded by a phospholipid monolayer and associated regulatory and lipid biosynthetic enzymes. While structurally resembling cytoplasmic LDs, nLDs are formed by distinct but poorly understood mechanisms that involve the emergence of lipid droplets from the lumen of the nucleoplasmic reticulum and *de novo* lipid synthesis. Luminal lipid droplets that emerge into the nucleoplasm do so at regions of the inner nuclear membrane that become enriched in promyelocytic leukemia (PML) protein. The resulting nLDs that retain PML on their surface are termed lipid-associated PML structures (LAPS), and are distinct from canonical PML nuclear bodies (NB) as they lack key proteins and modifications associated with these NBs. PML is a key regulator of nuclear signaling events and PML NBs are sites of gene regulation and post-translational modification of transcription factors. Therefore, the subfraction of nLDs that form LAPS could regulate lipid stress responses through their recruitment and retention of the PML protein. Both nLDs and LAPS have lipid biosynthetic enzymes on their surface suggesting they are active sites for nuclear phospholipid and triacylglycerol synthesis as well as global lipid regulation. In this review we have summarized the current understanding of nLD and LAPS biogenesis in different cell types, their structure and composition relative to other PML-associated cellular structures, and their role in coordinating a nuclear response to cellular overload of fatty acids.

Keywords: nuclear lipid droplets, PML, lipin, CCTalpha, phosphatidylcholine, fatty acid

OPEN ACCESS

Edited by:
Volker Gerke,
University of Münster, Germany

Reviewed by:
Mlke Henne,
University of Texas Southwestern Medical Center, United States
Tokuko Haraguchi,
Osaka University, Japan

****Correspondence:***
Neale D. Ridgway
nridgway@dal.ca
Graham Dellaire
dellaire@dal.ca

Specialty section:
This article was submitted to Membrane Traffic, a section of the journal Frontiers in Cell and Developmental Biology

Received: *16 December 2021*
Accepted: *10 January 2022*
Published: *01 February 2022*

Citation:
McPhee MJ, Salsman J, Foster J, Thompson J, Mathavarajah S, Dellaire G and Ridgway ND (2022) Running 'LAPS' Around nLD: Nuclear Lipid Droplet Form and Function. Front. Cell Dev. Biol. 10:837406. doi: 10.3389/fcell.2022.837406

Abbreviations: AGPAT, 1-acylglycerol 3-phosphate acyltransferases; ALT, alternative lengthening of telomeres; BLM, Bloom syndrome protein cLD, cytoplasmic lipid droplets; CEPT, choline/ethanolamine phosphotransferase; CPT, choline phosphotransferase; CRAG, CRMP-5-associated GTPase; CCTα, CTP:phosphocholine cytidylyltransferase α; DAG, diacylglycerol; DGAT, DAG acyltransferase; DAXX, Death domain-associated protein 6; ER, endoplasmic reticulum; eLD, ER luminal lipid droplets; GPAT; glycerol 3-phosphate acyltransferases; HGPS, Hutchinson-Gilford progeria syndrome INM, inner nuclear membrane; LAPS, lipid-associated PML structures; LD, lipid droplets; MAPP, mitotic accumulations of PML protein; MTP, microsomal triglyceride transfer protein; NAFLD, non-alcoholic fatty liver disease; NR, nucleoplasmic reticulum; NE, nuclear envelope; nLD, nuclear lipid droplets; PA, phosphatidic acid; PGC1A, PPARγ co-activator 1A; PML, promyelocytic leukemia; PPAR, peroxisome proliferator-activated receptors; RBCC, RING-B-box-coiled-coiled; SUMO, small-ubiquitin like modifier; SIM, SUM-interaction motif; SREBP, sterol regulatory element-binding protein; ring finger protein 4, RNF5; TAG, triacylglyceride; VLDL, very-low density lipoproteins.

INTRODUCTION

The lipid droplet (LD) is a unique cellular organelle composed of a surface monolayer of phospholipids and proteins surrounding a neutral lipid core containing triacylglycerides (TAG[1]) (Walther et al., 2017), steryl esters (Shen et al., 2016) and/or retinyl esters (Orban et al., 2011). Nutrient stress or excess fatty acids promote the storage of neutral lipids in LDs, which can be subsequently released by ester hydrolases to provide energy, lipid precursors for membrane biogenesis and signalling molecules (Henne et al., 2018). LDs therefore sequester essential biomaterials, while protecting the cell from the lipotoxic effects of excess fatty acids and cholesterol that can promote ER stress and mitochondrial dysfunction, which promote cell death (Olzmann and Carvalho, 2019). The defective storage of lipids in LDs has profound pathophysiological consequences. In the case of TAG, unilocular LDs in adipocytes are the primary storage depot but hepatocytes and other cells are also capable of short-term storage and release of fatty acids from LDs. However, chronic exposure of hepatocytes to fatty acids causes non-alcoholic fatty liver disease (NAFLD) (Diehl and Day, 2017), a common form of hepatic steatosis caused by fatty acid-induced ER and mitochondrial stress (Cazanave et al., 2010; Mantzaris et al., 2011), defective lipophagy of LDs (Singh et al., 2009) and lipid activation of pro-apoptotic transcriptional pathways (Barreyro et al., 2007). When combined with an inflammatory insult, NAFLD can progress to non-alcoholic steatohepatitis, which is associated with hepatic fibrosis and cirrhosis. NAFLD is a major risk factor for chronic liver disease and contributes to rising rates of liver transplantation in developed countries (Pais et al., 2016).

The lipid storage function of LDs relies on a complement of core proteins on their surface that regulate the storage and release of lipids in response to nutrient signaling. Proteomic analysis has revealed an expanded repertoire of associated proteins that suggest a wide-ranging role for LDs in cell physiology. These include the MAX dimerization (MLX) protein and related glucose-sensing transcription factors (Mejhert et al., 2020), histone storage (Cermelli et al., 2006), nuclear pore protein expression (Kumanski et al., 2021), clearance of misfolded and ubiquitinated proteins (Ohsaki et al., 2008; Moldavski et al., 2015) and immune responses to viral and bacterial infection (Bosch et al., 2021). Consequently, our understanding of LD biology has evolved from that of lipid storage depots to one of dynamic organelles that functionally intersect with many cellular metabolic and signalling activities. This has been further challenged by the discovery and characterization of nuclear lipid droplets (nLD) that share features with their cytosolic counterparts but are unique in terms of biogenesis, their associated proteins and lipids, and ultimately their cellular activities (Sołtysik et al., 2019).

nLDs were first characterized in normal and transformed hepatocytes (Layerenza et al., 2013; Uzbekov and Roingeard, 2013; Wang et al., 2013) and later Caco2 intestinal epithelial cells (Yue et al., 2020), reflecting their biogenesis from lipoprotein precursors (Soltysik et al., 2019). nLDs are rarely observed in common laboratory cell lines and tissues that do not secrete lipoproteins. An exception is U2OS osteosarcoma cells that contain abundant nLDs when incubated with oleate (Ohsaki et al., 2016). nLDs have been identified in yeast under nutrient stress conditions and certain mutational backgrounds (Romanauska and Kohler, 2018) and intestinal and germ cells of *Caenorhabditis elegans* (Mosquera et al., 2021). As will be discussed, the apparent restricted distribution of nLDs reflects both their unique biosynthetic origins and limited investigation in other cells and organisms.

Since cytoplasmic lipid droplets (cLD) are more abundant than their nuclear counterparts, nLDs visualized by wide-field microscopy could be cLDs trapped in invaginations of the nuclear envelope (NE). However, serial sections of human liver revealed that nLDs are not connected to the NE and associate with heterochromatin (Uzbekov and Roingeard, 2013). nLDs visualized by confocal microscopy of rat hepatocytes were not associated with nuclear lamina, and could be isolated from purified nuclei (Layerenza et al., 2013). A detailed lipidomic analysis of isolated nLDs is not available; however, lipid class analysis indicated they contain more cholesterol ester, cholesterol and phospholipids, less TAG, and a higher protein-to-lipid ratio relative to cLDs (Layerenza et al., 2013). These features reflect the smaller size and larger surface-to-volume ratio of nLDs. A proteomic analysis of purified nLDs from rat liver revealed a variety of cytoskeletal proteins, transcription and translation factors, histones and carboxyl esterase 1 (Lagrutta et al., 2021). Interestingly, the proteome of purified nLDs did not contain any nLD-associated proteins identified by microscopy-based methods (Ohsaki et al., 2016; Soltysik et al., 2019; Lee et al., 2020; Soltysik et al., 2021). These differences likely reflect the conditions used to isolate the nLDs, which could strip loosely associated proteins. As a result, to more fully assess the nLD proteome, gentler *in situ* methods are required that do not involve cellular disruption and biochemical purification, such as proximity labelling and mass spectrometry of *in vivo* labelled protein complexes. In the following sections, we will highlight our current understanding of the proteins and lipids involved in the biogenesis of nLDs at the inner nuclear membrane (INM) and potential functions in the nucleoplasm, with a focus on the association of nLDs with promyelocytic leukemia (PML) protein in lipid-associated PML structures (LAPS).

MECHANISMS OF NUCLEAR LIPID DROPLET BIOGENESIS

Nuclear Lipid Droplet Biogenesis on the Inner Nuclear Membrane

The immiscibility of hydrophobic neutral lipids in the cytosol is ultimately the key physical property driving nLD and cLD formation, growth and stability. Eukaryotic cells coordinate each of these processes through a dynamic, non-stochastic, and tightly regulated mechanism, allowing cells to effectively respond to changes in energy status, substrate availability and cellular stress. nLD biogenesis occurs by at least two known pathways: 1) *in situ* biogenesis at the INM and nLD budding into the nucleoplasm and 2) ER luminal lipid droplets (eLD) that

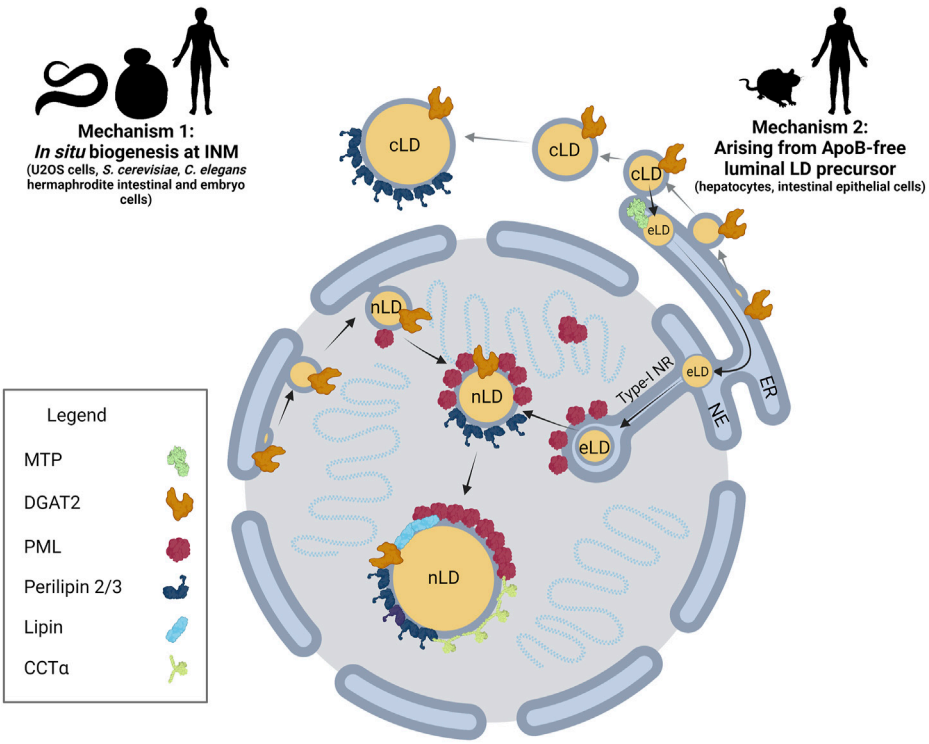

FIGURE 1 | nLD biogenesis in mammalian cells. Two mechanisms have been identified for nLD formation. Mechanism 1: Much like cLD biogenesis, nLD biogenesis in U2OS cells, *S. cerevisiae*, and *C. elegans* involves *in situ* TAG synthesis at the INM facilitated by lipid biosynthetic enzymes. nLD biogenesis is seipin-dependent in *S. cerevisiae*, whereas the process is seipin-independent in U2OS cells. Mechanism 2: In specialized lipoprotein-exporting mammalian cells like hepatocytes and intestinal epithelial cells, ApoB-free eLDs form in an MTP-dependent manner and subsequently migrate through the lumen of the ER into the lumen of the NE. Next, eLDs enter into type-I NR invaginations of the INM that extend into the nucleoplasm. PML-II localizes to INM at lamin-deficient regions, possibly facilitating translocation of the LD through ruptures of the INM into the nucleoplasm. In mammalian cells more generally, lipid biosynthetic enzymes DGAT2, Lipin-1 and CCTα**,** LD coat protein perilipin-3, and PML are all present at the surface of nLDs. The binding of lipid biosynthetic enzymes and the formation of LAPS are two commonalities of nLDs irrespective of their biogenesis in mammalian cells, suggesting a possible conserved function for these structures.

migrate into type-1 nucleoplasmic reticulum (NR) invaginations that rupture to release a nascent nLDs into the nucleoplasm (**Figure 1**).

In situ nLD biogenesis is documented in *Saccharomyces cerevisiae* (Romanauska and Kohler, 2018) as well as U2OS cells (Lee et al., 2020; Soltysik et al., 2021). While nLDs are particularly enriched in cholesterol esters (Layerenza et al., 2013), nLD biogenesis in most studies in mammalian cells is induced with exogenous oleate. The mechanism for formation of TAG-enriched nLDs appears to have many features in common with that for cLD formation in the ER (Thiam et al., 2013; Walther et al., 2017) (**Figure 2**). TAG is synthesized *de novo* from glycerol-3-phosphate and fatty acids by the concerted activity of glycerol 3-phosphate acyltransferases (GPAT) and 1-acylglycerol 3-phosphate acyltransferases (AGPAT) to produce phosphatidic acid (PA), which is dephosphorylated by Pah1 (*S. cerevisiae)* and Lipins (mammals) to produce diacylglycerol (DAG). Finally, DAG acyltransferases (DGAT) 1 and DGAT2 produce TAG (**Figure 2A**). These TAG lipid synthetic enzymes concentrate at specific sites of the endoplasmic reticulum (ER) membrane to facilitate the nucleation of *de novo* synthesized neutral lipid between leaflets of phospholipid bilayer (**Figure 2B**). These lens-like structures accumulate lipids and bud into the cytoplasm to produce nascent cytoplasmic LDs (cLD). cLDs continue to mature or 'ripen' through three mechanisms: 1) seipin-dependent membrane bridges that connect the cLD monolayer with the cytosolic leaflet of the ER, allowing the diffusion of proteins and lipids to the LD (Wang et al., 2016; Salo et al., 2019), 2) targeting of GPAT4, AGPAT4, and DGAT2 to the LD to facilitate *in situ* TAG synthesis (Wilfling et al., 2013; McFie et al., 2018; Olarte et al., 2022) and 3) coalescence of lipid droplets (Thiam et al., 2013).

In the case of oleate-treated U2OS cells, nLD biogenesis involves an *in situ* pathway. Similar to cLDs (**Figure 2**), AGPAT2, GPAT3/4, Lipin-1 and DGAT1/2 are localized to the INM of U2OS cells and required for nLD biogenesis (Lee et al., 2020; Soltysik et al., 2021). Acyl-CoA synthetase long chain family member 3 (ASCL3), lyso-phosphatidylcholine acyltransferase 1 (LPCAT1), GPAT3/4, Lipin-1β, and DGAT2 also localize to the surface of the nLD and could provide TAG and phosphatidylcholine (PC) for growth of the nLD after it buds into the nucleoplasm (Soltysik et al., 2021). mTORC1 inhibition promotes the nuclear translocation of Lipin-1β and increased nLDs (Soltysik et al., 2021). Lipin-1α and -1β are enriched on the

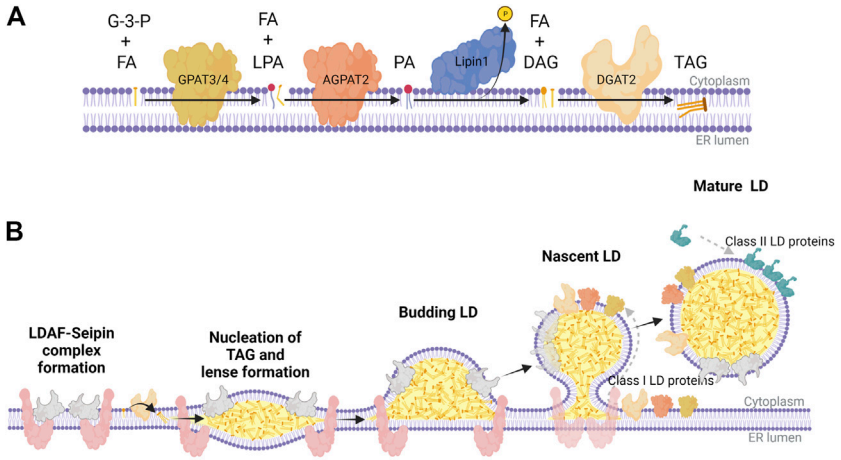

FIGURE 2 | The Kennedy pathway for TAG synthesis and LD biogenesis in mammalian cells. **(A)** Biosynthetic enzymes of the Kennedy pathway act sequentially to synthesize triacylglycerol (TAG) at the ER membrane; GPAT3/4 synthesizes lysophosphatidic acid (LPA) from glycerol 3-phosphate (G-3-P) and fatty acids (FA), AGPAT2 synthesizes phosphatidic acid (PA) from LPA and FA, Lipin-1 hydrolyzes PA to diacylglycerol (DAG), and DGAT2 catalyzes the final acylation to form TAG. **(B)** TAG nucleates between the two leaflets of the ER membrane bilayer, which is partly facilitated by a complex of LDAF and seipin at distinct domains throughout the ER. These points of TAG nucleation develop into lens-like structures that proceed to bud into the cytoplasm as a budding LD coated with LDAF as it dissociates from seipin. As seipin funnels TAG and DAG into nascent LDs, lipid biosynthetic enzymes (class I LD proteins) like GPAT3/4, AGPAT2, and DGAT2 transfer across membrane bridges to the surface monolayer, further facilitating the maturation of LDs. Once the mature LD separates from the ER, it recruits class II LD proteins like perilipin-2/3, which coat the surface to regulate access of LDs to lipases and autophagy proteins. This graphic was created with Biorender.com.

surface of a significant fraction of nLDs containing DAG suggesting they provide substrate for DGAT and TAG biosynthesis (Lee et al., 2020). nLDs in oleate-treated U2OS also serve as a platform for recruitment and activation of CTP: phosphocholine cytidylyltransferase α (CCTα), the rate-limiting enzyme in the CDP-choline pathway for PC synthesis (**Figure 1**) (Lee et al., 2020). Similar to the activation of CCT1 on cLDs in *Drosophila melanogaster* S2 cells (Krahmer et al., 2011), CCTα activation on nLDs increases cellular PC synthesis to expand the TAG storage capacity in cLDs, or to provide PC to reduce fatty acid-induced ER stress (Soltysik et al., 2019).

In contrast to cLD biogenesis in the ER (**Figure 2B**), the formation of nLDs in U2OS cells is seipin-independent (Soltysik et al., 2021). Seipin has a well-recognized role in the nucleation of cLD formation in the ER where it forms an oligomeric ring complex with lipid droplet assembly factor 1 (LDAF1) that acts to concentrate DAG and TAG, and facilitate protein and lipid transfer from the ER to nascent cLDs (**Figure 2B**) (Wang et al., 2016; Yan et al., 2018; Chung et al., 2019; Salo et al., 2019). Seipin also interacts with GPAT3/4, AGPAT2, and Lipin1 to concentrate the production of TAG at specific sites in the ER (Sim et al., 2012; Sim et al., 2020). Interestingly, RNAi-mediated seipin knockdown in U2OS cells promoted increased nLD formation by an ACSL3 and Lipin-1β-dependent mechanism (Soltysik et al., 2021). This correlated with reduced expression of the splicing factor TRA2B leading to increased expression and translocation of Lipin-1β into the nucleus. The mechanism for seipin induction of TRA2B is not clear but the resultant increase in Lipin-1β activity provides an explanation for the observed increase in nLDs. Since seipin establishes the site of cLD biogenesis and membrane tethers required for expansion, other factors at the INM must be responsible for nucleating and tethering nLDs in U2OS cells. While there is evidence for nLD biogenesis in the INM of U2OS cells, it is uncertain whether this pathway is responsible for formation of nLDs in other mammalian cells or works in conjunction with the eLD pathway for nLD formation in hepatocytes (see below).

nLDs form *in situ* at the INM of *S. cerevisiae* by a seipin-dependent mechanism that bares many of the features of cLD biogenesis (Romanauska and Kohler, 2018). Increased availability of PA resulting from genetic mutations of lipid biosynthetic enzymes facilitates DAG formation and nLD budding at the INM (Romanauska and Kohler, 2018). For example, a temperature-sensitive CDP-diacylglycerol synthase 1 (*Cds1*) mutant grown at the non-permissive temperature had a 6-fold increase in nLDs due to the shift toward TAG storage. Cds1 synthesizes CDP-DAG, the common substrate for synthesis of *S. cerevisiae* phospholipids, and is one of many lipogenic enzymes upregulated by the Ino2-Ino4 transcription factors (Carman and Han, 2011). *INO2-INO4* deletion or antagonism by its repressor Opi1 recapitulated a similar nLD phenotype as *Cds1* mutants (Romanauska and Kohler, 2018). Key enzymes in yeast TAG synthesis, Pah1, Dgk1 and Cds1, were localized to the INM, as were the substrates for TAG synthesis, PA and DAG. The TAG lipase Tgl5 was found on the surface of nLDs providing a plausible mechanism for nLD turnover. A recent study addressed how the lipid synthesis and storage capacity of the INM maintains an optimal lipid environment by overcoming unsaturated fatty acid-induced stress (Romanauska and Kohler, 2021). Membrane fluidity biosensors were used to identify a Mga1-Ole1 transcriptional circuit for unsaturated fatty acid synthesis that induced storage in cLDs and suppressed nLD formation by reducing seipin and PA levels in the INM. This mechanism

for unsaturated fatty acid detoxification would maintain the optimal phospholipid fluidity and packing in the INM.

Unlike mammalian cells, seipin is required for nLD formation in *S. cerevisiae* (Romanauska and Kohler, 2018). Seipin was found to localize to the INM using bimolecular fluorescence complementation with the nuclear pore protein Nup60, and ultrastructural analysis confirmed the presence of seipin-dependent bridges between the outer leaflet of the INM and the nLD monolayer. nLD biogenesis occurs in seipin-deficient *S. cerevisiae* but membrane bridges are notably absent and nLDs are mostly embedded within inclusions within the INM.

Some clues as to the evolutionary emergence of nLDs in eukaryotes are provided by comparing yeast and amoeba. *Dictyostelium discoideum* expresses a seipin homologue but nLDs have not been observed (Du et al., 2013). The localization of *D. discoideum* seipin was restricted to a subset of foci and rings co-localizing to the ER and cLDs at the edge of the plasma membrane (Kornke and Maniak, 2017). While the loss of seipin in amoebae resulted in fewer but larger cLDs, there was no change in overall TAG production (Kornke and Maniak, 2017). The lack of nuclear membrane localization of *D. discoideum* seipin may explain why the species lacks nLDs. A transition in seipin localization from the ER to the ER-INM during opisthokont evolution could contribute to the formation of nLDs that are observed in yeast.

Different classes of nLDs were identified in hermaphrodite intestinal and germ cell nuclei of *C. elegans* based on association with chromatin and the lamina (Mosquera et al., 2021). The frequency of nLDs in the nuclei of intestinal cells ranged from 5 to 20% and increased with developmental stage. Cells usually contained a single nLD that could, on occasion, occupy one-third the nuclear volume. Transmission electron microscopy imaging of intestinal nuclei revealed nLDs that were; 1) free within the nucleoplasm, 2) between the peripheral heterochromatin and nuclear lamina, 3) coated by heterochromatin, lamina and membrane, and 4) surrounded by double membrane due to in-pocketing in type-1 NR (Mosquera et al., 2021). Gonadal germ cells acquire lipid from intestinal lipoproteins for storage in cLDs during development, and a small population of these cells (<20%) also produced nLDs. Unlike intestinal cells, nLDs in germ cells did not have associated lamina, heterochromatin or surrounding membrane, and were associated with rapid oogenesis. While the function(s) of nLDs in *C. elegans* is unclear, it was observed that nLDs were frequently associated with sites of nuclear rupture and repair in intestinal cells, suggesting they may interfere with chromatin organization, lamina integrity and/or repair pathways. In contrast, nLDs were not associated with nuclear damage or cell survival in germ cells. Aside from a single report showing association of the hydroxysteroid reductase DHS-9 with intestinal nLDs by immunofluorescence microscopy (Liu et al., 2018), the proteome of *C. elegans* nLDs is unknown.

The close proximity of intestinal nLDs with the INM and type-I NR suggests they could originate by an *in situ* mechanism similar to that proposed for U2OS cells and yeast (**Figure 1**). However, intestinal cells of *C. elegans* produce a lipoprotein-like paralog of ApoB called vitellogenin, a yolk protein exported from intestinal cells into the coelom where it is taken up by the hermaphrodite gonads to support embryogenesis and fertility (Perez and Lehner, 2019). *C. elegans* also expresses an orthologue of MTP (Dsc4) that is targeted to the ER and supports lipoprotein secretion (Rava and Hussain, 2007). These findings indicate that nLD biogenesis could involve a TAG-rich lipoprotein precursor, as reported in hepatocytes (see below) (Soltysik et al., 2019).

In an effort to determine if *C. elegans* nLDs affect germ cell viability, a mutational screen was used to identify genes that regulated nLD abundance and size (Mosquera et al., 2021). Mutants of SEIP-1, NEMP-1 and the COPII coat proteins COPA-1 and COPB-2 increased nLD size and number in germ cells but did not affect viability. SEIP-1 encodes the *C. elegans* homologue of seipin, the absence of which caused the appearance of large nLDs in germ cells. This is similar to the effect of seipin knockdown in U2OS cells (Soltysik et al., 2021) and suggests an indirect role for SEIP-1 in nLD biogenesis in the cytoplasm. NEMP-1 is a poorly characterized integral membrane protein that localizes to the nuclear lamina and contains a RanGTP binding domain (Shibano et al., 2015). The loss of COPA-1 and COPB-2 coat proteins could increase nLD formation indirectly by promoting unfolded protein stress in the ER or by the delivery of enzymes that control TAG storage, as proposed for COPII vesicle transport of adipose triglyceride lipase and perilipin-2 to cLDs in mammalian cells (Soni et al., 2009).

Finally, it should be noted that neither the yeast or *C. elegans* genomes encode a PML ortholog. As such, these data indicate that nLD formation in these species does not strictly require PML, as is the case for mammalian cells (see below). However, it remains to be determined if a paralogous PML-like protein, for example containing the highly conserved tripartite motif (TRIM) domain found in PML and many E3 ubiquitin ligases (Gushchina et al., 2018), exists in these species in association with nLDs.

Nuclear Lipid Droplet Biogenesis From ER Luminal Lipid Droplet

Another pathway for nLD formation occurs in cells that secrete TAG-rich lipoproteins, such as hepatocytes (Ohsaki et al., 2016; Soltysik et al., 2019) and intestinal epithelial Caco2 cells (Yue et al., 2020) (**Figure 1**). Hepatocytes assemble TAG-rich ApoB-containing very low-density lipoproteins (VLDL) in the ER lumen from which they are exported to the *cis*-Golgi via COPII transport vesicles for eventual secretion into circulation. Microsomal triglyceride transfer protein (MTP) in the ER lumen transfers TAG and phospholipids to newly synthesized ApoB to form a VLDL precursor (Lehner et al., 2012). MTP also transfers lipids to eLDs that are ApoB-deficient and fuse with ApoB-containing precursors to produce VLDL. Under conditions of ER stress and increased TAG synthesis, a fraction of these eLDs traffic from the ER lumen into type-I NR invaginations of the INM (Soltysik et al., 2019) (**Figure 1**). eLDs containing ApoE and ApoCIII translocate into the nucleoplasm through regions of the inner leaflet of the INM enriched in PML-II but depleted of lamin A, lamin B receptor and SUN1/2 (Ohsaki et al., 2016; Soltysik et al., 2019). PML-II is the

only isoform involved in eLD egress into the nucleoplasm. Type-I NR seems to be dispensable for nLD formation since stimulation of NR formation by tunicamycin had no effect (Soltysik et al., 2019). Once in the nucleoplasm, nLDs can expand or mature by recruitment DGAT2 and CCTα to increase *de novo* synthesis of TAG and PC synthesis, respectively (Ohsaki et al., 2016; Soltysik et al., 2019).

FUNCTIONS OF NUCLEAR LIPID DROPLETS AND LIPID-ASSOCIATED PROMYELOCYTIC LEUKEMIA STRUCTURES

Platforms for the Regulation of Lipid Synthesis

nLDs represent <10% of the LD pool (Ohsaki et al., 2016; Lee et al., 2020), are TAG-poor relative to cLDs (Layerenza et al., 2013) and lack proximity to the mitochondria and ER, the primary loci of lipid oxidation and synthesis, respectively. Thus nLDs are unlikely to serve as energy storage reservoirs but could have additional functions related to cell signalling, protein storage and mitigation of ER stress. nLDs in hepatocytes and intestinal epithelial cells have an origin and functions that are linked to the absorption, repackaging and secretion of lipids in lipoproteins (Soltysik et al., 2019). During ER stress, ApoB is degraded co-translationally leading to accumulation of eLDs and release into the nucleoplasm through type-1 NR invaginations to form nLDs. The subsequent recruitment and activation of CCTα on nLDs increases PC synthesis, which is negatively regulated by displacement from nLDs by perilipin-3. Increased PC synthesis could mitigate ER stress by; 1) expanding the ER network to accommodate unfolded proteins and 2) providing surface monolayer phospholipids for the packaging of fatty acids into TAG for storage in cLDs and secretion in VLDL. It is notable that nLD formation did not occur in hepatocytes treated with tunacimycin alone; however, the unfolded protein response induced by tunicamycin enhanced nLD formation in response to oleate (Soltysik et al., 2019).

It is currently unknown why CCTα translocates to the surface of nLDs rather than the INM, which is commonly observed in oleate-treated cells that lack nLDs (Wang et al., 1995; Lagace and Ridgway, 2005; Gehrig et al., 2008) and during 3T3-L1 preadipocyte differentiation (Aitchison et al., 2015). The association of the domain M α-helix of CCTα with membranes is enhanced by low PC content and the presence of lipid activators, such as DAG, PA and fatty acids (Cornell and Ridgway, 2015). LAPS appear to be a preferred substrate for CCTα translocation as PML-knockout U2OS cells had a partial shift of CCTα to the NE (Lee et al., 2020). The preferred association of CCTα with nLDs could be driven by a unique protein and/or lipid composition. However, the eLD precursors of nLDs and LAPS have a similar lipid composition as cLDs (Wang et al., 2007), and the composition of hepatic nLDs does not indicate enrichment in CCTα activating lipids (Layerenza et al., 2013). Interestingly, LAPS are enriched in DAG, a known activator of CCTα; however, the DAG content of LAPS did not correlate with enrichment in CCTα (Lee et al., 2020). PA was only observed on nuclear puncta and infrequently on small nLD in U2OS cells and is also unlikely to be a factor in CCTα activation (Soltysik et al., 2021).

Nuclear CCTα controls the rate of PC synthesis by supplying CDP-choline to choline/ethanolamine phosphotransferase (CEPT) and choline phosphotransferase (CPT) in the ER and ER/Golgi, respectively (Henneberry et al., 2002). This cellular topology implies that CDP-choline synthesized by CCTα is transported to the cytoplasm for PC synthesis. However, a split-GFP reporter screen identified the yeast homologues of CPT and CEPT, Cpt1p and Ept1p, in the INM (Smoyer et al., 2016). In support of INM localization of CEPT, approximately 10% of the epitope-tagged enzyme was in the NE of CHO cells (Gehrig and Ridgway, 2011) and deuterated choline-labelled lipids were detected in the NE using nanoscale-secondary ion mass spectrometry (Drozdz et al., 2017). The last two studies do not preclude the possibility that CEPT is active on the outer nuclear membrane and newly synthesized PC undergoes lateral diffusion to the INM at nuclear pores (Barger et al., 2022).

Regulation of Chromatin Structure, Gene Expression and Cell Signalling

There is indirect evidence that nLDs could perturb chromatin structure and gene expression. nLD formation from eLDs occurs at sites of lamin depletion in the INM (Ohsaki et al., 2016), which could affect the interaction and organization of chromatin (Dechat et al., 2008). nLDs isolated from rat liver have associated histones, including variants of H2A, H2B, H3.3 and H4 (Lagrutta et al., 2021). Similarly, cLDs in a variety of eukaryotic species are high capacity storage sites for histones (Welte, 2007), both buffering the genotoxic effects of histone excess and increasing supply to match DNA replication, as demonstrated during *Drosophila* embryogenesis (Li et al., 2012). While the role of nLDs in histone regulation is less clear, the PML NB-associated protein death domain-associated protein 6 (DAXX) is a H3.3 chaperone (Drane et al., 2010), and H3.3 localization to PML-NB regulates its association with chromatin (Corpet et al., 2014). Whether this association with H3.3 also occurs on LAPS is unknown but supports the notion that nLDs and LAPS could modify chromatin and gene expression (next section). Studies in *C. elegans* have shown direct interaction between nLD and chromatin; however, it was not determined whether these interactions are facilitated by proteins or lipids, and if gene expression was altered (Mosquera et al., 2021). While not fully investigated, understanding the interplay between nLDs and LAPS with chromatin appears to be a promising way to better understand nLD function.

nLDs could also influence gene expression by providing the ligands for the activation of nuclear transcription factors. For example, nLDs could serve as a source of cholesterol, fatty acids and PC ligands and precursors for liver X receptor (Janowski et al., 1996), peroxisome proliferator-activated receptors (PPAR) (Tanaka et al., 2017) and LRH-1 (Musille et al., 2012). More

TABLE 1 | Nuclear structures containing PML.

PML structure	Description	Conditions/ Stimuli	Localization	Key components	Diagnostic criteria	References
PML NB	PML nuclear bodies	Normal cells	4–30 bodies per cell	SUMO, SP100, DAXX	SUMO, SP100, DAXX	Song et al. (2004), Cheng and Kao (2012), Banani et al. (2016), Hoischen et al. (2018), Corpet et al. (2020)
LAPS	Lipid-associated PML structures	Excess oleate	nLD	CCTα, Lipin1, DAG	Visualized with lipid dyes	Ohsaki et al. (2016), Lee et al. (2020)
APB	ALT-associated PML bodies	ALT-positive cancer cells	Telomere-associated PML bodies	SUMO, SP100, DAXX, BTR complex, TRF2, telomeric DNA	Co-localization withTRF2 in *tert-negative* cells	Chung et al. (2012), Loe et al. (2020)
MAPP	Mitotic accumulation of PML proteinsl	Mitosis	Endosome-associated	PML protein aggregates	Co-localization with EEA1, TfR	Dellaire et al. (2006b); Palibrk et al. (2014)
PML patches	Nuclear lamin-associated patches/ threads	Hutchinson-Gilford progeria cells; senescent cells	PML-II on nuclear lamina, type-1 NR	SUMO DAXX Progerin	Reduced associated with DNA repair proteins (γH2AX, RPA32, MRE11)	Wang et al. (2020)
Nucleolar caps	Senescence-associated PML-I caps	Senescent cells	surrounding nucleolar fragments and blebs	SUMO, DAXX, SP100,B23, DHX9,FBL	Co-localization with nucleolus-fibrillar center	Condemine et al. (2007), Imrichova et al. (2019)
PML clastosomes	PolyQ-associated PML rings at nuclear protein inclusions	Misfolded polyQ proteins, UV	Enlarged nuclear ring	CRAG RNF4 SUMO PML	Co-localization with ubiqutitin-positive inclusions; SUMO	Qin et al. (2006), Guo et al. (2014), Janer et al. (2006)

directly, the recruitment of the transcriptional co-activator Lipin-1 to nLDs in U2OS and HuH7 cells (Lee et al., 2020; Soltysik et al., 2021) could affect the expression of multiple genes involved in fatty acid catabolism and storage. Lipin-1 is a co-activator of PPARγ, which is also activated by fatty acid ligands (Tanaka et al., 2017). Mechanistically, this involves Lipin-1 activation of PPARγ co-activator 1A (PGC1A) to promote the transcription of fatty acid oxidation genes (Finck et al., 2006). Lipin-1 also influences expression of lipid catabolic genes through its direct interaction with hepatic nuclear factor 4α (Chen et al., 2012). Nuclear Lipin-1 is also a repressor of the lipogenic transcription factor sterol regulatory element binding protein (SREBP) 1c by a mechanism involving mTORC1 phosphorylation (Peterson et al., 2011). Lipin-1 phosphorylation by mTORC1 causes its retention in the cytoplasm, while dephosphorylation by the NE complex of C-terminal domain nuclear envelope protein (CTDNEP) and nuclear envelope protein 1 regulatory subunit 1 (NEP1R1) leads to nuclear import (Csaki et al., 2013). Treatment of U2OS cells with an mTORC1 inhibitor and oleate increased nLD formation, which was dependent on the catalytic and transcriptional co-activation activity of Lipin-1 (Soltysik et al., 2021). The AAA+ ATPase Torsin A is another important regulator of lipid metabolism via its inhibitory effects on Lipin activity in the nucleus (Grillet et al., 2016; Jacquemyn et al., 2021). In *Drosophila*, Torsin was shown to promote dissociation of the NEP1R1-CTDNEP1 phosphatase complex from the NE, resulting in Lipin exclusion from the nucleus (Jacquemyn et al., 2021). Torsin dysregulation was associated with nuclear pore assembly defects in *Drosophila* fat body cells. However, mice with an hepatic knockout of lamina-associated polypeptide 1 (LAP1), which is required for Torsin A activity, displayed impaired VLDL secretion, hepatic steatosis and nLD accumulation (Shin et al., 2019). This increased nLD phenotype could result from loss of negative regulation of Lipin-1 via Torsin A/NEP1R1-CTDNEP1 and increase eLD translocation into the nucleus due to inhibition of VLDL assembly. By virtue of its role as a key regulator of fatty acid incorporation into TAG, Lipin-1 has the potential to connect lipid metabolism on nLD to the transcriptional activation of pathways that control fatty acid homeostasis.

STRUCTURE AND FUNCTION OF PROMYELOCYTIC LEUKEMIA-ASSOCIATED SUB-CELLULAR DOMAINS AND LIPID-ASSOCIATED PML STRUCTURES

The Structure and Function of Classical Promyelocytic Leukemia Nuclear Bodies

As mentioned in previous sections, a defining feature of nLDs in mammalian cells is their association with PML to form lipid-associated PML structures called LAPS, one of numerous nuclear substructures containing PML that are summarized in **Table 1** and **Figure 3**. The PML gene contains 9 exons which are subjected to alternative mRNA splicing, resulting in at least 6

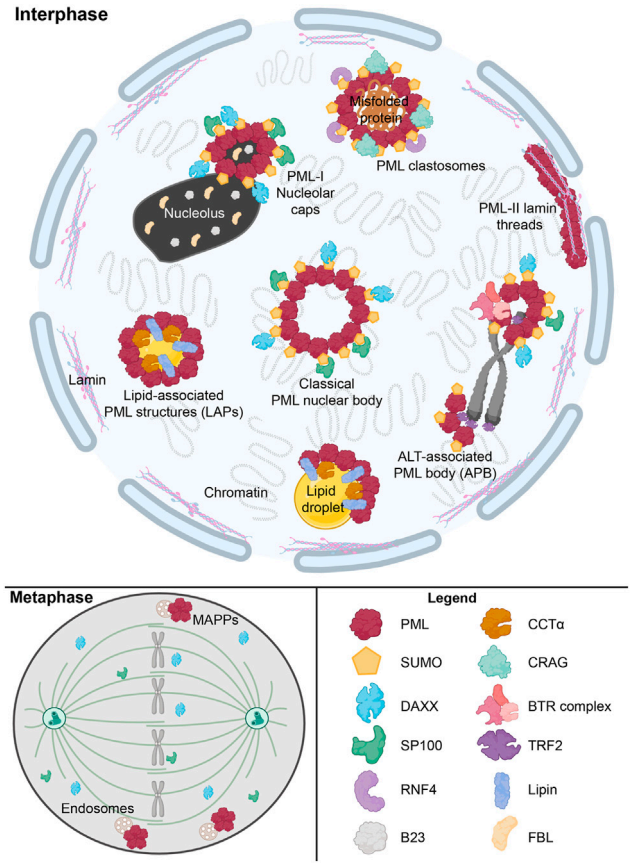

FIGURE 3 | Overview of nuclear PML structures and their interactors. The formation of canonical phase-separated spherical PML NB is driven by protein oligomerization and SUMO-SIM interactions, which also recruit other proteins such as DAXX and SP100. However, other novel PML structures form under specific stimuli. These include ALT-associated PML bodies (APB), PML-I nucleolar caps and PML clastosomes. SUMO-independent LAPS form on nLDs and host lipid biosynthetic enzymes such as Lipin1 and CCTα. During mitosis, SUMO-independent structure known as mitotic accumulations of PML protein (MAPP) form and are tethered to endosomes. In certain disease states such as with Hutchinson-Gilford progeria syndrome, PML-II lamin threads are formed. These aforementioned PML structures uniquely interact with a number of proteins, such as RNF4, CRAG, TRF2, and the BTR complex, to modulate normal cellular functions and the cell's response to stress states. This graphic was. created with Biorender.com.

nuclear isoforms containing a common N-terminal RING-B-box-coiled-coiled (RBCC) motif (also referred to as the TRIM domain) and variable C-terminal tails (Jensen et al., 2001; Nisole et al., 2013; Gushchina et al., 2018) Collectively, the PML isoforms form the molecular basis for the formation of PML NBs (**Figure 3**). These PML NBs are dynamic, heterogeneous sub-nuclear structures that serve as regulatory hubs for over 150 associated nuclear proteins, consisting primarily of transcription factors and chromatin remodeling protein (Van Damme et al., 2010). Thus PML NBs are implicated in a variety of key cell survival pathways, including the DNA damage response, senescence, gene expression regulation, apoptosis, nuclear proteolysis and the antiviral response (Pearson and Pelicci, 2001; Bischof et al., 2002; Dellaire and Bazett-Jones, 2004; Dellaire et al., 2006a; Villagra et al., 2006; Bernardi et al., 2008; Attwood et al., 2020). In addition, many components of the small-ubiquitin like modifier (SUMO) machinery, such as SUMO proteases (i.e., SENPs) and SUMO ligases (i.e., UBC9, PIAS), associate with PML NBs making these structures hubs for SUMO biology within the cell (Van Damme et al., 2010; Hattersley et al., 2011; Sahin et al., 2014; Brown et al., 2016; Barroso-Gomila et al., 2021).

PML NBs range in diameter from 0.1 to 1 μm, with mammalian cells hosting 4–30 bodies (**Table 1**) (Banani et al., 2016; Hoischen et al., 2018). Electron microscopy and super-resolution techniques revealed that PML NB typically form a phase-separated spherical shell that tethers to chromatin (Hoischen et al., 2018; Corpet et al., 2020). The PML NB shell results from self-oligomerization that occurs through two steps; 1) the N-terminal RBCC domain of PML primarily facilitates self-oligomerization between PML monomers (Sahin et al., 2014) and 2) further multimerization promoted by PML post-translational modification by SUMO (Hoischen et al., 2018). The PML protein contains at least seven validated SUMOylation sites and a C-terminal SUMO-interacting motif (SIM). This allows SUMO-modified PML proteins to homo-multimerize through their SIM motifs (Song et al., 2004; Cheng and Kao, 2012). Furthermore, many PML NB client proteins associate with PML NBs in a SUMOylation- and/or SIM-dependent manner. For example, two well established PML NB interactors that consistently localize and comprise the "classical" PML NBs are DAXX (via SIMs) and the SP100 (via SUMO) nuclear antigen (Szostecki et al., 1990; Khelifi et al., 2005) (**Figure 3**). Such SUMO-SIM interactions between partner proteins are fundamental to how classical PML NBs interact with other protein constituents, highlighting the importance of SUMO-SIM interactions in PML biology.

Novel Promyelocytic Leukemia Containing Nuclear Structures

Although the protein composition of PML NBs is dynamic, the PML NBs themselves are stable structures. However, PML NBs are more dynamic in stressed cells and can shift in morphology and function in the context of cell cycle progression, stressful stimuli and virus infection. There are several non-canonical PML structures that only occur in abnormal cells (**Table 1** and **Figure 3**). For example, in ~15% of all cancers, cells circumvent their rapid proliferation and eventual loss of telomeres through a pathway known as the alternative lengthening of telomeres (ALT) (Bryan et al., 1995). In ALT-positive cells, PML co-localizes with the telomere marker TRF2 and promotes ALT processes at the telomere (Loe et al., 2020). These novel PML structures, termed ALT-associated PML bodies, are essential for facilitating telomere lengthening by recruiting Bloom syndrome protein (BLM) via SUMO-SIM interactions, and ultimately promoting BLM-TOPO3a-RMI complex formation at telomeres (Zhu et al., 2008; Chung et al., 2012). Therefore, while ALT-associated PML bodies have novel functions, mechanistically their roles are driven by SUMO-SIM interactions as with classical PML NB.

Novel PML structures have also been linked to aging and disease. In senescent cells, PML can appear to form thread-like structures with the nuclear lamina and proteinaceous rings or caps around the nucleoli (**Figure 3**) (Condemine et al., 2007; Jul-Larsen et al., 2010; Stixova et al., 2012). These structures retain a similar composition to classical PML NBs, harboring DAXX and SP100 (Condemine et al., 2007; Jul-Larsen et al., 2010). Senescence-associated PML-lamina threads occur in Hutchinson-Gilford progeria syndrome (HGPS), a premature aging syndrome resulting from disruption of nuclear lamina integrity (Wang et al., 2020). PML-II is essential for the formation of these PML-lamina threads, which then contribute to the accelerated senescence in HGPS (Jul-Larsen et al., 2010).

While detrimental in HGPS, in other contexts, PML has been shown to help prevent human disease. Neurodegenerative polyglutamine (polyQ) diseases are caused by the expansion of polyQ repeats that are deleterious to neurons (Sato et al., 1999; Yoshizawa et al., 2000). A common pathological feature is the appearance of ubiquitin-positive nuclear inclusions (Qin et al., 2006). To prevent the occurrence of nuclear inclusions and maintain nuclear protein quality, the cell has quality control pathways which include the polyQ-associated PML bodies called PML clastosomes (**Figure 3**) (Gartner and Muller, 2014). PML is capable of selectively interacting with misfolded nuclear proteins via CRMP-5-associated GTPase (CRAG) through distinct conjugate sites (Guo et al., 2014). Once polyQ misfolded proteins interact with PML NBs, they are conjugated to SUMO, recognized by ring-finger protein 4 (RNF4) and ubiquitinated for degradation through the ubiquitin-proteasome system (Guo et al., 2014). Therefore, PML dynamics in human disease is complex, with novel PML NB structures both promoting and preventing pathologies.

During mitosis, PML proteins form a unique SUMO-negative structure known as mitotic accumulations of PML protein (MAPP) (**Figure 3**) (Dellaire et al., 2006b). MAPPs also lack DAXX and SP100, which diffuse into the mitotic cytoplasm from prophase to metaphase (Everett et al., 1999; Dellaire et al., 2006b; Chen et al., 2008). MAPPs form once PML NBs are untethered from chromatin during mitosis, and they appear to be bound to early endosomes in dividing cells (Chen et al., 2008; Palibrk et al., 2014). MAPPs remain in the cytoplasm until early G1 phase until the PML protein within them is imported in the nucleus to re-establish PML NBs after the NE reforms (Dellaire et al., 2006b; Chen et al., 2008).

Lipid-Associated Promyelocytic Leukemia Structures

The recently characterized LAPS represent a new PML subnuclear compartment that associates with nLDs. Most LAPS (~75%) share similarities to the MAPPs in the sense that they lack SUMO, DAXX and SP100 (Lee et al., 2020). However, LAPS appear to be sphere-like structures, much like classical PML NBs, that form in the nucleus during interphase in response to nLD accumulation. The sequence of events that lead to PML association with nLDs and formation of LAPS has not been fully elucidated. However, in the case of hepatocytes it is mediated by PML-II, which has a unique C-terminal nuclear periphery binding motif that facilitates association with the INM (**Figure 1**). It is not understood if the interaction of PML-II with the INM is direct, involves adaptor proteins or post-translational modifications (Jul-Larsen et al., 2010). In Huh7 cells, eLDs emerge into the nucleoplasm from the lumen of type-1 NR by membrane disruption at sites of PML-II enrichment and/or depletion of the nuclear lamina, SUN1 and LBR (**Figure 1**) (Ohsaki et al., 2016; Soltysik et al., 2019). Depletion of PML-II by siRNA knockdown reduced total nLDs by 30–50%, while knockdown of SUN1 and REEP3/4 increased nLDs. The result suggested a model in which PML-II links nLDs to chromatin and the INM that would be otherwise be removed by SUN1 and REEP3/4 (Ohsaki et al., 2016). However, it is unclear how eLDs break through the INM at PML-II patches, and how and when PML-II and other PML isoforms associate with the primordial nLD to form a LAPS.

RNA-mediated silencing of PML-II in U2OS cells did not significantly affect total nLD abundance and size (Soltysik et al., 2021) indicating that nLDs derive from the INM by a mechanism that does not involve PML-II. However, ablation of LAPS by CRISPR/Cas9-mediated PML knockout in U2OS cells significantly reduced nLD abundance by 50% and decreased nLD size (Lee et al., 2020). This discrepancy suggests that a total PML knockout places more stringent conditions on nLD formation and other PML isoforms are involved in LAPS formation. The association of PML with nLDs appears to be dynamic as well, with about 25% of the LAPS resembling classical PML NB containing SP100, SUMO, DAXX, with the remainder being devoid of these canonical partners (Lee et al., 2020). One interpretation is that classical PML NBs initially associate with newly forming nLDs and are gradually remodelled into LAPS as the nLD matures and grows. Most strikingly, this remodeling of PML NBs into LAPS involves loss of SUMO in the structure (Lee et al., 2020). Whether this loss of SUMOylation at LAPS is necessary for the maturation and processing of nLDs is not known, particularly as both yeast and worms form nLDs and lack a PML ortholog (as discussed previously). Since SUMO-SIM interactions play such an important role in PML NB-mediated gene regulation, it would be surprising if such gross reorganization of PML NBs into LAPS would not have some impact on the cell beyond nLD metabolism.

High resolution imaging of immunostained LAPS in U2OS cell revealed that CCTα and PML occupy different regions of the LAPS and have minimal overlap. Clues as to how CCTα and PML form this association with LAPS comes from HGPS fibroblasts in which CCTα is associated with nuclear lamina threads like those observed for PML (Gehrig and Ridgway, 2011). These thread-like PML-II and CCTα structures are likely formed at the type-I NR since CCTα forms foci at normal prelamin-A induced nucleoplasmic reticulum (Goulbourne et al., 2011). In the context of progeria where prelamin-A (progerin) accumulates, this shifts normal foci formation to thread-like structures containing CCTα and PML. Therefore, the prelamin-A type-I NR appears to be a key nucleation center for CCTα and PML foci

formation, which could contribute to how PML-coated nLDs are formed. The cell type- and context-specific association of PML-II with the INM supports the idea that additional lipid or protein factors are involved in regulating its membrane association.

The association of PML and nLDs represents a novel function for PML in regulating lipid metabolism through direct structural association with a LD. However, PML and PML NBs have been implicated in lipid metabolism through their more well-established role as gene regulators. PML has been implicated in SREBP signalling (Chen et al., 2018). SREBP-1 and -2, transcription factors that control the expression of genes involved in fatty acid and cholesterol synthesis, are proteolytically processed to their mature nuclear form in response to changes in ER lipid and cholesterol composition (Horton et al., 2003; Brown et al., 2018). In a mouse prostate cancer model, the deletion of *Pml* in *Pten*-null tumours resulted in the hyperactivation of SREBP and ultimately, in a SREBP-dependent aggressive metastatic phenotype (Chen et al., 2018). Mechanistically, this could be related to SREBP-2, which localized to classical PML NBs unlike the diffusely nuclear SREBP-1 (Zoumi et al., 2005). In contrast, PML has an uncharacteristic pro-tumor function in triple negative breast cancers by promoting fatty acid oxidation (Carracedo et al., 2012). Mechanistically, this is accomplished through negative regulation of PGC1A acetylation, likely at PML NBs, which in turn activates PPAR signaling and fatty acid oxidation (Carracedo et al., 2012). Given the ability of SREBP-2 and PGC1A to associate with PML NBs and the presence of Lipin-1— a SREBP repressor found at PML-containing LAPS— it seems plausible that LAPS might affect SREBP activity. Despite this intriguing hypothesis, to date SREBP-2 and PGC1A localization to LAPS has not been evaluated. Taken together, the results suggest that LAPS put PML as a physical interactor and contributor to nLD formation, and therefore lipid metabolism under conditions of fatty acid stress in mammals. However, there are also roles for the canonical PML structures in regulating lipid metabolism in other contexts via SREBPs and fatty acid oxidation that most likely contribute to lipid-stress responses.

CONCLUSION

nLDs are emerging as potentially important organelles in their capacity to; 1) store and supply lipid precursors for membrane biogenesis and signalling molecules in the nucleus, and 2) regulate the cellular response to fatty acid stress. Although two different pathways for nLD biogenesis have been identified, both involve maturation by the *de novo* synthesis of TAG at the INM or on nLDs. Regardless of the mechanism of biogenesis, newly formed nLDs are an important regulatory site for PC synthesis via recruitment and activation of CCTα to enhance the TAG storage capacity or relieve ER stress. However, many questions remain, such as why do nLDs only appear in certain cell types and species, how are lipids in nLDs degraded and/or redistributed in the nucleus, how are cytosolic lipid metabolic enzymes imported into the nucleus to make nLDs and how are these enzymes recruited to the INM and nLDs?

Studies of the nLD maturation process has also revealed an important role for PML, and particularly PML-II, in the formation of a discrete subset of nLDs called LAPS. LAPS represent a novel PML-containing subnuclear structure that adds to our understanding of how the PML protein responds to various cellular stresses and disease states by altering the structure, composition, and localization of PML NBs. In the case of LAPS, there is much work to be in done to fully elucidate what role(s) PML might play in LAPS biology beyond LAPS formation and the recruitment of CCTα and Lipin-1. The presence of these lipid enzymes and the concurrent loss of SUMO, SP100 and DAXX from LAPS indicates they are unique PML-containing structures specialized in regulating lipid metabolism. It will be important to identify the proteome of nLDs and the role that PML plays in the association of client proteins with LAPS. In the absence of SUMO-SIM interactions, which drive the majority of protein associations with PML NBs, one might expect a more limited and specific repertoire of LAPS-associated proteins that rely on conventional protein-protein or protein-lipid interactions to be recruited and retained at LAPS. In this situation it is possible that specific PML isoforms, through their unique C-terminal regions, could recruit LAPS-associated proteins in a more direct way. Alternatively, or in addition to, PML-containing portion of LAPS could retain the phase separation properties of PML NBs to recruit and retain proteins in liquid condensates. In addition, it is still unclear if LAPS are associated with chromatin regions or specific gene promoters in the same way as PML NBs, although we do know that nLDs can modify nuclear architecture and chromatin dynamics. Therefore, PML association with nLDs through LAPS formation might provide a mechanism for the cell to effect transcriptional changes as part of the lipid stress response in much the same way that PML NBs regulate gene expression through chromatin contacts as well as recruitment and modification of transcription factors and chromatin modifying enzymes. The lack of key PML NB components at LAPS would, however, indicate that the mechanism for gene regulation at LAPS involves a different complement of PML-associated proteins that do not interact with LAPS via SUMO-SIM interactions. Collectively, these findings usher in new paradigms for not only PML-based nuclear structures but also for nLD biology.

AUTHOR CONTRIBUTIONS

MM, JS, JF, JT and SM drafted individual sections and edited the final manuscript. MM and SM constructed figures. GD and NR compiled drafts and edited the final manuscript.

FUNDING

CIHR Project grant PJT162390.

REFERENCES

Aitchison, A. J., Arsenault, D. J., and Ridgway, N. D. (2015). Nuclear-localized CTP:phosphocholine Cytidylyltransferase α Regulates Phosphatidylcholine Synthesis Required for Lipid Droplet Biogenesis. *MBoC* 26, 2927–2938. doi:10.1091/mbc.e15-03-0159

Attwood, K. M., Salsman, J., Chung, D., Mathavarajah, S., Van Iderstine, C., and Dellaire, G. (2020). PML Isoform Expression and DNA Break Location Relative to PML Nuclear Bodies Impacts the Efficiency of Homologous Recombination. *Biochem. Cel Biol.* 98, 314–326. doi:10.1139/bcb-2019-0115

Banani, S. F., Rice, A. M., Peeples, W. B., Lin, Y., Jain, S., Parker, R., et al. (2016). Compositional Control of Phase-Separated Cellular Bodies. *Cell* 166, 651–663. doi:10.1016/j.cell.2016.06.010

Barger, S. R., Penfield, L., and Bahmanyar, S. (2022). Coupling Lipid Synthesis with Nuclear Envelope Remodeling. *Trends Biochem. Sci.* 47, 52–65. doi:10.1016/j.tibs.2021.08.009

Barreyro, F. J., Kobayashi, S., Bronk, S. F., Werneburg, N. W., Malhi, H., and Gores, G. J. (2007). Transcriptional Regulation of Bim by FoxO3A Mediates Hepatocyte Lipoapoptosis. *J. Biol. Chem.* 282, 27141–27154. doi:10.1074/jbc.m704391200

Barroso-Gomila, O., Trulsson, F., Muratore, V., Canosa, I., Merino-Cacho, L., Cortazar, A. R., et al. (2021). Identification of Proximal SUMO-dependent Interactors Using SUMO-ID. *Nat. Commun.* 12, 6671. doi:10.1038/s41467-021-26807-6

Bernardi, R., Papa, A., and Pandolfi, P. P. (2008). Regulation of Apoptosis by PML and the PML-NBs. *Oncogene* 27, 6299–6312. doi:10.1038/onc.2008.305

Bischof, O., Kirsh, O., Pearson, M., Itahana, K., Pelicci, P. G., and Dejean, A. (2002). Deconstructing PML-Induced Premature Senescence. *EMBO J.* 21, 3358–3369. doi:10.1093/emboj/cdf341

Bosch, M., Sweet, M. J., Parton, R. G., and Pol, A. (2021). Lipid Droplets and the Host-Pathogen Dynamic: FATal Attraction? *J. Cel Biol.* 220, e202104005. doi:10.1083/jcb.202104005

Brown, J. R., Conn, K. L., Wasson, P., Charman, M., Tong, L., Grant, K., et al. (2016). SUMO Ligase Protein Inhibitor of Activated STAT1 (PIAS1) Is a Constituent Promyelocytic Leukemia Nuclear Body Protein that Contributes to the Intrinsic Antiviral Immune Response to Herpes Simplex Virus 1. *J. Virol.* 90, 5939–5952. doi:10.1128/jvi.00426-16

Brown, M. S., Radhakrishnan, A., and Goldstein, J. L. (2018). Retrospective on Cholesterol Homeostasis: The Central Role of Scap. *Annu. Rev. Biochem.* 87, 783–807. doi:10.1146/annurev-biochem-062917-011852

Bryan, T. M., Englezou, A., Gupta, J., Bacchetti, S., and Reddel, R. R. (1995). Telomere Elongation in Immortal Human Cells without Detectable Telomerase Activity. *EMBO J.* 14, 4240–4248. doi:10.1002/j.1460-2075.1995.tb00098.x

Carman, G. M., and Han, G.-S. (2011). Regulation of Phospholipid Synthesis in the Yeast *Saccharomyces cerevisiae*. *Annu. Rev. Biochem.* 80, 859–883. doi:10.1146/annurev-biochem-060409-092229

Carracedo, A., Weiss, D., Leliaert, A. K., Bhasin, M., de Boer, V. C. J., Laurent, G., et al. (2012). A Metabolic Prosurvival Role for PML in Breast Cancer. *J. Clin. Invest.* 122, 3088–3100. doi:10.1172/jci62129

Cazanave, S. C., Elmi, N. A., Akazawa, Y., Bronk, S. F., Mott, J. L., and Gores, G. J. (2010). CHOP and AP-1 Cooperatively Mediate PUMA Expression during Lipoapoptosis. *Am. J. Physiol. Gastrointestinal Liver Physiol.* 299, G236–G243. doi:10.1152/ajpgi.00091.2010

Cermelli, S., Guo, Y., Gross, S. P., and Welte, M. A. (2006). The Lipid-Droplet Proteome Reveals that Droplets Are a Protein-Storage Depot. *Curr. Biol.* 16, 1783–1795. doi:10.1016/j.cub.2006.07.062

Chen, Y.-C. M., Kappel, C., Beaudouin, J., Eils, R., and Spector, D. L. (2008). Live Cell Dynamics of Promyelocytic Leukemia Nuclear Bodies upon Entry into and Exit from Mitosis. *MBoC* 19, 3147–3162. doi:10.1091/mbc.e08-01-0035

Chen, Z., Gropler, M. C., Mitra, M. S., and Finck, B. N. (2012). Complex Interplay between the Lipin 1 and the Hepatocyte Nuclear Factor 4 α (HNF4α) Pathways to Regulate Liver Lipid Metabolism. *PLoS One* 7, e51320. doi:10.1371/journal.pone.0051320

Chen, M., Zhang, J., Sampieri, K., Clohessy, J. G., Mendez, L., Gonzalez-Billalabeitia, E., et al. (2018). An Aberrant SREBP-dependent Lipogenic Program Promotes Metastatic Prostate Cancer. *Nat. Genet.* 50, 206–218. doi:10.1038/s41588-017-0027-2

Cheng, X., and Kao, H. Y. (2012). Post-translational Modifications of PML: Consequences and Implications. *Front. Oncol.* 2, 210. doi:10.3389/fonc.2012.00210

Chung, I., Osterwald, S., Deeg, K. I., and Rippe, K. (2012). PML Body Meets Telomere. *Nucleus* 3, 263–275. doi:10.4161/nucl.20326

Chung, J., Wu, X., Lambert, T. J., Lai, Z. W., Walther, T. C., and Farese, R. V., Jr. (2019). LDAF1 and Seipin Form a Lipid Droplet Assembly Complex. *Develop. Cel* 51, 551–563. doi:10.1016/j.devcel.2019.10.006

Condemine, W., Takahashi, Y., Le Bras, M., and de The´, H. (2007). A Nucleolar Targeting Signal in PML-I Addresses PML to Nucleolar Caps in Stressed or Senescent Cells. *J. Cel Sci.* 120, 3219–3227. doi:10.1242/jcs.007492

Cornell, R. B., and Ridgway, N. D. (2015). CTP:phosphocholine Cytidylyltransferase: Function, Regulation, and Structure of an Amphitropic Enzyme Required for Membrane Biogenesis. *Prog. Lipid Res.* 59, 147–171. doi:10.1016/j.plipres.2015.07.001

Corpet, A., Olbrich, T., Gwerder, M., Fink, D., and Stucki, M. (2014). Dynamics of Histone H3.3 Deposition in Proliferating and Senescent Cells Reveals a DAXX-dependent Targeting to PML-NBs Important for Pericentromeric Heterochromatin Organization. *Cell Cycle* 13, 249–267. doi:10.4161/cc.26988

Corpet, A., Kleijwegt, C., Roubille, S., Juillard, F., Jacquet, K., Texier, P., et al. (2020). PML Nuclear Bodies and Chromatin Dynamics: Catch Me if You Can! *Nucleic Acids Res.* 48, 11890–11912. doi:10.1093/nar/gkaa828

Csaki, L. S., Dwyer, J. R., Fong, L. G., Tontonoz, P., Young, S. G., and Reue, K. (2013). Lipins, Lipinopathies, and the Modulation of Cellular Lipid Storage and Signaling. *Prog. Lipid Res.* 52, 305–316. doi:10.1016/j.plipres.2013.04.001

Dechat, T., Pfleghaar, K., Sengupta, K., Shimi, T., Shumaker, D. K., Solimando, L., et al. (2008). Nuclear Lamins: Major Factors in the Structural Organization and Function of the Nucleus and Chromatin. *Genes Dev.* 22, 832–853. doi:10.1101/gad.1652708

Dellaire, G., and Bazett-Jones, D. P. (2004). PML Nuclear Bodies: Dynamic Sensors of DNA Damage and Cellular Stress. *Bioessays* 26, 963–977. doi:10.1002/bies.20089

Dellaire, G., Ching, R. W., Ahmed, K., Jalali, F., Tse, K. C. K., Bristow, R. G., et al. (2006a). Promyelocytic Leukemia Nuclear Bodies Behave as DNA Damage Sensors Whose Response to DNA Double-Strand Breaks Is Regulated by NBS1 and the Kinases ATM, Chk2, and ATR. *J. Cel Biol.* 175, 55–66. doi:10.1083/jcb.200604009

Dellaire, G., Eskiw, C. H., Dehghani, H., Ching, R. W., and Bazett-Jones, D. P. (2006b). Mitotic Accumulations of PML Protein Contribute to the Re-establishment of PML Nuclear Bodies in G1. *J. Cel Sci.* 119, 1034–1042. doi:10.1242/jcs.02817

Diehl, A. M., and Day, C. (2017). Cause, Pathogenesis, and Treatment of Nonalcoholic Steatohepatitis. *N. Engl. J. Med.* 377, 2063–2072. doi:10.1056/nejmra1503519

Drané, P., Ouararhni, K., Depaux, A., Shuaib, M., and Hamiche, A. (2010). The Death-Associated Protein DAXX Is a Novel Histone Chaperone Involved in the Replication-independent Deposition of H3.3. *Genes Dev.* 24, 1253–1265. doi:10.1101/gad.566910

Drozdz, M. M., Jiang, H., Pytowski, L., Grovenor, C., and Vaux, D. J. (2017). Formation of a Nucleoplasmic Reticulum Requires De Novo Assembly of Nascent Phospholipids and Shows Preferential Incorporation of Nascent Lamins. *Sci. Rep.* 7, 7454. doi:10.1038/s41598-017-07614-w

Du, X., Barisch, C., Paschke, P., Herrfurth, C., Bertinetti, O., Pawolleck, N., et al. (2013). Dictyostelium Lipid Droplets Host Novel Proteins. *Eukaryot. Cel* 12, 1517–1529. doi:10.1128/ec.00182-13

Everett, R. D., Lomonte, P., Sternsdorf, T., van Driel, R., and Orr, A. (1999). Cell Cycle Regulation of PML Modification and ND10 Composition. *J. Cel Sci.* 112 (Pt 24), 4581–4588. doi:10.1242/jcs.112.24.4581

Finck, B. N., Gropler, M. C., Chen, Z., Leone, T. C., Croce, M. A., Harris, T. E., et al. (2006). Lipin 1 Is an Inducible Amplifier of the Hepatic PGC-1α/PPARα Regulatory Pathway. *Cel Metab.* 4, 199–210. doi:10.1016/j.cmet.2006.08.005

Gärtner, A., and Muller, S. (2014). PML, SUMO, and RNF4: Guardians of Nuclear Protein Quality. *Mol. Cel* 55, 1–3. doi:10.1016/j.molcel.2014.06.022

Gehrig, K., and Ridgway, N. D. (2011). CTP:phosphocholine Cytidylyltransferase α (CCTα) and Lamins Alter Nuclear Membrane Structure without Affecting Phosphatidylcholine Synthesis. *Biochim. Biophys. Acta Mol. Cel Biol. Lipids* 1811, 377–385. doi:10.1016/j.bbalip.2011.04.001

Gehrig, K., Cornell, R. B., and Ridgway, N. D. (2008). Expansion of the Nucleoplasmic Reticulum Requires the Coordinated Activity of Lamins and CTP:Phosphocholine Cytidylyltransferase α. *MBoC* 19, 237–247. doi:10.1091/mbc.e07-02-0179

Goulbourne, C. N., Malhas, A. N., and Vaux, D. J. (2011). The Induction of a Nucleoplasmic Reticulum by Prelamin A Accumulation Requires CTP: phosphocholine Cytidylyltransferase-α. *J. Cel Sci.* 124, 4253–4266. doi:10.1242/jcs.091009

Grillet, M., Dominguez Gonzalez, B., Sicart, A., Pöttler, M., Cascalho, A., Billion, K., et al. (2016). Torsins Are Essential Regulators of Cellular Lipid Metabolism. *Develop. Cel* 38, 235–247. doi:10.1016/j.devcel.2016.06.017

Guo, L., Giasson, B. I., Glavis-Bloom, A., Brewer, M. D., Shorter, J., Gitler, A. D., et al. (2014). A Cellular System that Degrades Misfolded Proteins and Protects against Neurodegeneration. *Mol. Cel* 55, 15–30. doi:10.1016/j.molcel.2014.04.030

Gushchina, L. V., Kwiatkowski, T. A., Bhattacharya, S., and Weisleder, N. L. (2018). Conserved Structural and Functional Aspects of the Tripartite Motif Gene Family point towards Therapeutic Applications in Multiple Diseases. *Pharmacol. Ther.* 185, 12–25. doi:10.1016/j.pharmthera.2017.10.020

Hattersley, N., Shen, L., Jaffray, E. G., and Hay, R. T. (2011). The SUMO Protease SENP6 Is a Direct Regulator of PML Nuclear Bodies. *MBoC* 22, 78–90. doi:10.1091/mbc.e10-06-0504

Henne, W. M., Reese, M. L., and Goodman, J. M. (2018). The Assembly of Lipid Droplets and Their Roles in Challenged Cells. *EMBO J.* 37, e98947. doi:10.15252/embj.201898947

Henneberry, A. L., Wright, M. M., and McMaster, C. R. (2002). The Major Sites of Cellular Phospholipid Synthesis and Molecular Determinants of Fatty Acid and Lipid Head Group Specificity. *MBoC* 13, 3148–3161. doi:10.1091/mbc.01-11-0540

Hoischen, C., Monajembashi, S., Weisshart, K., and Hemmerich, P. (2018). Multimodal Light Microscopy Approaches to Reveal Structural and Functional Properties of Promyelocytic Leukemia Nuclear Bodies. *Front. Oncol.* 8, 125. doi:10.3389/fonc.2018.00125

Horton, J. D., Shah, N. A., Warrington, J. A., Anderson, N. N., Park, S. W., Brown, M. S., et al. (2003). Combined Analysis of Oligonucleotide Microarray Data from Transgenic and Knockout Mice Identifies Direct SREBP Target Genes. *Proc. Natl. Acad. Sci.* 100, 12027–12032. doi:10.1073/pnas.1534923100

Imrichova, T., Hubackova, A., Kucerova, A., Kosla, J., Bartek, Z., Hodny, J., et al. (2019). Dynamic PML Protein Nucleolar Associations With Persistent DNA Damage Lesions in Response to Nucleolar Stress and Senescence-Inducing Stimuli. *Aging* 11, 7206–7235.

Jacquemyn, J., Foroozandeh, J., Vints, K., Swerts, J., Verstreken, P., Gounko, N. V., et al. (2021). Torsin and NEP1R1-CTDNEP1 Phosphatase Affect Interphase Nuclear Pore Complex Insertion by Lipid-dependent and Lipid-independent Mechanisms. *EMBO J.* 40, e106914. doi:10.15252/embj.2020106914

Janer, A., Martin, E., Muriel, M. P., Latouche, M., Fujigasaki, H., Ruberg, M., et al. (2006). PML Clastosomes Prevent Nuclear Accumulation of Mutant Ataxin-7 and Other Polyglutamine Proteins. *J. Cell Biol.* 174, 65–76.

Janowski, B. A., Willy, P. J., Devi, T. R., Falck, J. R., and Mangelsdorf, D. J. (1996). An Oxysterol Signalling Pathway Mediated by the Nuclear Receptor LXRα. *Nature* 383, 728–731. doi:10.1038/383728a0

Jensen, K., Shiels, C., and Freemont, P. S. (2001). PML Protein Isoforms and the RBCC/TRIM Motif. *Oncogene* 20, 7223–7233. doi:10.1038/sj.onc.1204765

Jul-Larsen, A., Grudic, A., Bjerkvig, R., and Bøe, S. O. (2010). Subcellular Distribution of Nuclear Import-Defective Isoforms of the Promyelocytic Leukemia Protein. *BMC Mol. Biol.* 11, 89. doi:10.1186/1471-2199-11-89

Khelifi, A. F., D'Alcontres, M. S., and Salomoni, P. (2005). Daxx Is Required for Stress-Induced Cell Death and JNK Activation. *Cell Death Differ.* 12, 724–733. doi:10.1038/sj.cdd.4401559

Kornke, J. M., and Maniak, M. (2017). Fat-containing Cells Are Eliminated during Dictyostelium Development. *Biol. Open* 6, 1294–1304. doi:10.1242/bio.025478

Krahmer, N., Guo, Y., Wilfling, F., Hilger, M., Lingrell, S., Heger, K., et al. (2011). Phosphatidylcholine Synthesis for Lipid Droplet Expansion Is Mediated by Localized Activation of CTP:phosphocholine Cytidylyltransferase. *Cel Metab.* 14, 504–515. doi:10.1016/j.cmet.2011.07.013

Kumanski, S., Viart, B., Kossida, S., and Moriel-Carretero, M. (2021). Lipid Droplets Are a Physiological Nucleoporin Reservoir. *Cells* 10, 472–481. doi:10.3390/cells10020472

Lagace, T. A., and Ridgway, N. D. (2005). The Rate-Limiting Enzyme in Phosphatidylcholine Synthesis Regulates Proliferation of the Nucleoplasmic Reticulum. *MBoC* 16, 1120–1130. doi:10.1091/mbc.e04-10-0874

Lagrutta, L. C., Layerenza, J. P., Bronsoms, S., Trejo, S. A., and Ves-Losada, A. (2021). Nuclear-lipid-droplet Proteome: Carboxylesterase as a Nuclear Lipase Involved in Lipid-Droplet Homeostasis. *Heliyon* 7, e06539. doi:10.1016/j.heliyon.2021.e06539

Layerenza, J. P., González, P., García de Bravo, M. M., Polo, M. P., Sisti, M. S., and Ves-Losada, A. (2013). Nuclear Lipid Droplets: a Novel Nuclear Domain. *Biochim. Biophys. Acta Mol. Cel Biol. Lipids* 1831, 327–340. doi:10.1016/j.bbalip.2012.10.005

Lee, J., Salsman, J., Foster, J., Dellaire, G., and Ridgway, N. D. (2020). Lipid-associated PML Structures Assemble Nuclear Lipid Droplets Containing CCTα and Lipin1. *Life Sci. Alliance* 3, e202000751. doi:10.26508/lsa.202000751

Lehner, R., Lian, J., and Quiroga, A. D. (2012). Lumenal Lipid Metabolism. *Arterioscler Thromb. Vasc. Biol.* 32, 1087–1093. doi:10.1161/atvbaha.111.241497

Li, Z., Thiel, K., Thul, P. J., Beller, M., Kühnlein, R. P., and Welte, M. A. (2012). Lipid Droplets Control the Maternal Histone Supply of Drosophila Embryos. *Curr. Biol.* 22, 2104–2113. doi:10.1016/j.cub.2012.09.018

Liu, Y., Xu, S., Zhang, C., Zhu, X., Hammad, M. A., Zhang, X., et al. (2018). Hydroxysteroid Dehydrogenase Family Proteins on Lipid Droplets through Bacteria, *C. elegans*, and Mammals. *Biochim. Biophys. Acta Mol. Cel Biol. Lipids* 1863, 881–894. doi:10.1016/j.bbalip.2018.04.018

Loe, T. K., Li, J. S. Z., Zhang, Y., Azeroglu, B., Boddy, M. N., and Denchi, E. L. (2020). Telomere Length Heterogeneity in ALT Cells Is Maintained by PML-dependent Localization of the BTR Complex to Telomeres. *Genes Dev.* 34, 650–662. doi:10.1101/gad.333963.119

Mantzaris, M. D., Tsianos, E. V., and Galaris, D. (2011). Interruption of Triacylglycerol Synthesis in the Endoplasmic Reticulum Is the Initiating Event for Saturated Fatty Acid-Induced Lipotoxicity in Liver Cells. *FEBS J.* 278, 519–530. doi:10.1111/j.1742-4658.2010.07972.x

McFie, P. J., Banman, S. L., and Stone, S. J. (2018). Diacylglycerol Acyltransferase-2 Contains a C-Terminal Sequence that Interacts with Lipid Droplets. *Biochim. Biophys. Acta Mol. Cel Biol. Lipids* 1863, 1068–1081. doi:10.1016/j.bbalip.2018.06.008

Mejhert, N., Kuruvilla, L., Gabriel, K. R., Elliott, S. D., Guie, M.-A., Wang, H., et al. (2020). Partitioning of MLX-Family Transcription Factors to Lipid Droplets Regulates Metabolic Gene Expression. *Mol. Cel* 77, 1251–1264. doi:10.1016/j.molcel.2020.01.014

Moldavski, O., Amen, T., Levin-Zaidman, S., Eisenstein, M., Rogachev, I., Brandis, A., et al. (2015). Lipid Droplets Are Essential for Efficient Clearance of Cytosolic Inclusion Bodies. *Develop. Cel* 33, 603–610. doi:10.1016/j.devcel.2015.04.015

Mosquera, J. V., Bacher, M. C., and Priess, J. R. (2021). Nuclear Lipid Droplets and Nuclear Damage in *Caenorhabditis elegans*. *Plos Genet.* 17, e1009602. doi:10.1371/journal.pgen.1009602

Musille, P. M., Pathak, M. C., Lauer, J. L., Hudson, W. H., Griffin, P. R., and Ortlund, E. A. (2012). Antidiabetic Phospholipid-Nuclear Receptor Complex Reveals the Mechanism for Phospholipid-Driven Gene Regulation. *Nat. Struct. Mol. Biol.* 19, 532–537. doi:10.1038/nsmb.2279

Nisole, S., Maroui, M. A., Mascle, X. H., Aubry, M., and Chelbi-Alix, M. K. (2013). Differential Roles of PML Isoforms. *Front. Oncol.* 3, 125. doi:10.3389/fonc.2013.00125

Ohsaki, Y., Cheng, J., Suzuki, M., Fujita, A., and Fujimoto, T. (2008). Lipid Droplets Are Arrested in the ER Membrane by Tight Binding of Lipidated Apolipoprotein B-100. *J. Cel Sci.* 121, 2415–2422. doi:10.1242/jcs.025452

Ohsaki, Y., Kawai, T., Yoshikawa, Y., Cheng, J., Jokitalo, E., and Fujimoto, T. (2016). PML Isoform II Plays a Critical Role in Nuclear Lipid Droplet Formation. *J. Cel Biol.* 212, 29–38. doi:10.1083/jcb.201507122

Olarte, M.-J., Swanson, J. M. J., Walther, T. C., and Farese, R. V., Jr. (2022). The CYTOLD and ERTOLD Pathways for Lipid Droplet-Protein Targeting. *Trends Biochem. Sci.* 47, 39–51. doi:10.1016/j.tibs.2021.08.007

Olzmann, J. A., and Carvalho, P. (2019). Dynamics and Functions of Lipid Droplets. *Nat. Rev. Mol. Cel Biol.* 20, 137–155. doi:10.1038/s41580-018-0085-z

Orban, T., Palczewska, G., and Palczewski, K. (2011). Retinyl Ester Storage Particles (Retinosomes) from the Retinal Pigmented Epithelium Resemble

Lipid Droplets in Other Tissues. *J. Biol. Chem.* 286, 17248–17258. doi:10.1074/jbc.m110.195198

Pais, R., Barritt, A. S., Calmus, Y., Scatton, O., Runge, T., Lebray, P., et al. (2016). NAFLD and Liver Transplantation: Current burden and Expected Challenges. *J. Hepatol.* 65, 1245–1257. doi:10.1016/j.jhep.2016.07.033

Palibrk, V., Lång, E., Lång, A., Schink, K. O., Rowe, A. D., and Bøe, S. O. (2014). Promyelocytic Leukemia Bodies Tether to Early Endosomes during Mitosis. *Cell Cycle* 13, 1749–1755. doi:10.4161/cc.28653

Pearson, M., and Pelicci, P. G. (2001). PML Interaction with P53 and its Role in Apoptosis and Replicative Senescence. *Oncogene* 20, 7250–7256. doi:10.1038/sj.onc.1204856

Perez, M. F., and Lehner, B. (2019). Vitellogenins - Yolk Gene Function and Regulation in *Caenorhabditis elegans*. *Front. Physiol.* 10, 1067. doi:10.3389/fphys.2019.01067

Peterson, T. R., Sengupta, S. S., Harris, T. E., Carmack, A. E., Kang, S. A., Balderas, E., et al. (2011). mTOR Complex 1 Regulates Lipin 1 Localization to Control the SREBP Pathway. *Cell* 146, 408–420. doi:10.1016/j.cell.2011.06.034

Qin, Q., Inatome, R., Hotta, A., Kojima, M., Yamamura, H., Hirai, H., et al. (2006). A Novel GTPase, CRAG, Mediates Promyelocytic Leukemia Protein-Associated Nuclear Body Formation and Degradation of Expanded Polyglutamine Protein. *J. Cel Biol.* 172, 497–504. doi:10.1083/jcb.200505079

Rava, P., and Hussain, M. M. (2007). Acquisition of Triacylglycerol Transfer Activity by Microsomal Triglyceride Transfer Protein during Evolution. *Biochemistry* 46, 12263–12274. doi:10.1021/bi700762z

Romanauska, A., and Köhler, A. (2018). The Inner Nuclear Membrane Is a Metabolically Active Territory that Generates Nuclear Lipid Droplets. *Cell* 174, 700–715. doi:10.1016/j.cell.2018.05.047

Romanauska, A., and Köhler, A. (2021). Reprogrammed Lipid Metabolism Protects Inner Nuclear Membrane against Unsaturated Fat. *Develop. Cel* 56, 2562–2578. doi:10.1016/j.devcel.2021.07.018

Sahin, U., Ferhi, O., Jeanne, M., Benhenda, S., Berthier, C., Jollivet, F., et al. (2014). Oxidative Stress-Induced Assembly of PML Nuclear Bodies Controls Sumoylation of Partner Proteins. *J. Cel Biol.* 204, 931–945. doi:10.1083/jcb.201305148

Salo, V. T., Li, S., Vihinen, H., Hölttä-Vuori, M., Szkalisity, A., Horvath, P., et al. (2019). Seipin Facilitates Triglyceride Flow to Lipid Droplet and Counteracts Droplet Ripening via Endoplasmic Reticulum Contact. *Develop. Cel* 50, 478–493. doi:10.1016/j.devcel.2019.05.016

Sato, A., Shimohata, T., Koide, R., Takano, H., Sato, T., Oyake, M., et al. (1999). Adenovirus-mediated Expression of Mutant DRPLA Proteins with Expanded Polyglutamine Stretches in Neuronally Differentiated PC12 Cells. Preferential Intranuclear Aggregate Formation and Apoptosis. *Hum. Mol. Genet.* 8, 997–1006. doi:10.1093/hmg/8.6.997

Shen, W.-J., Azhar, S., and Kraemer, F. B. (2016). Lipid Droplets and Steroidogenic Cells. *Exp. Cel Res.* 340, 209–214. doi:10.1016/j.yexcr.2015.11.024

Shibano, T., Mamada, H., Hakuno, F., Takahashi, S.-I., and Taira, M. (2015). The Inner Nuclear Membrane Protein Nemp1 Is a New Type of RanGTP-Binding Protein in Eukaryotes. *PLoS One* 10, e0127271. doi:10.1371/journal.pone.0127271

Shin, J.-Y., Hernandez-Ono, A., Fedotova, T., Östlund, C., Lee, M. J., Gibeley, S. B., et al. (2019). Nuclear Envelope-Localized torsinA-LAP1 Complex Regulates Hepatic VLDL Secretion and Steatosis. *J. Clin. Invest.* 129, 4885–4900. doi:10.1172/jci129769

Sim, M. F., Dennis, R. J., Aubry, E. M., Ramanathan, N., Sembongi, H., Saudek, V., et al. (2012). The Human Lipodystrophy Protein Seipin Is an ER Membrane Adaptor for the Adipogenic PA Phosphatase Lipin 1. *Mol. Metab.* 2, 38–46. doi:10.1016/j.molmet.2012.11.002

Sim, M. F. M., Persiani, E., Talukder, M. M. U., McIlroy, G. D., Roumane, A., Edwardson, J. M., et al. (2020). Oligomers of the Lipodystrophy Protein Seipin May Co-ordinate GPAT3 and AGPAT2 Enzymes to Facilitate Adipocyte Differentiation. *Sci. Rep.* 10, 3259. doi:10.1038/s41598-020-59982-5

Singh, R., Kaushik, S., Wang, Y., Xiang, Y., Novak, I., Komatsu, M., et al. (2009). Autophagy Regulates Lipid Metabolism. *Nature* 458, 1131–1135. doi:10.1038/nature07976

Smoyer, C. J., Katta, S. S., Gardner, J. M., Stoltz, L., McCroskey, S., Bradford, W. D., et al. (2016). Analysis of Membrane Proteins Localizing to the Inner Nuclear Envelope in Living Cells. *J. Cel Biol* 215, 575–590. doi:10.1083/jcb.201607043

Sołtysik, K., Ohsaki, Y., and Fujimoto, T. (2019). Duo in a Mystical Realm-Nuclear Lipid Droplets and the Inner Nuclear Membrane. *Contact* 2, 251525641989696. doi:10.1177/2515256419896965

Soltysik, K., Ohsaki, Y., Tatematsu, T., Cheng, J., and Fujimoto, T. (2019). Nuclear Lipid Droplets Derive from a Lipoprotein Precursor and Regulate Phosphatidylcholine Synthesis. *Nat. Commun.* 10, 473. doi:10.1038/s41467-019-08411-x

Soltysik, K., Ohsaki, Y., Tatematsu, T., Cheng, J., Maeda, A., Morita, S. Y., et al. (2021). Nuclear Lipid Droplets Form in the Inner Nuclear Membrane in a Seipin-independent Manner. *J. Cel Biol.* 220, e202005026. doi:10.1083/jcb.202005026

Song, J., Durrin, L. K., Wilkinson, T. A., Krontiris, T. G., and Chen, Y. (2004). Identification of a SUMO-Binding Motif that Recognizes SUMO-Modified Proteins. *Proc. Natl. Acad. Sci.* 101, 14373–14378. doi:10.1073/pnas.0403498101

Soni, K. G., Mardones, G. A., Sougrat, R., Smirnova, E., Jackson, C. L., and Bonifacino, J. S. (2009). Coatomer-dependent Protein Delivery to Lipid Droplets. *J. Cel Sci.* 122, 1834–1841. doi:10.1242/jcs.045849

Stixová, L., Matula, P., Kozubek, S., Gombitová, A., Cmarko, D., Raška, I., et al. (2012). Trajectories and Nuclear Arrangement of PML Bodies Are Influenced by A-type Lamin Deficiency. *Biol. Cel* 104, 418–432. doi:10.1111/boc.201100053

Szostecki, C., Guldner, H. H., Netter, H. J., and Will, H. (1990). Isolation and Characterization of cDNA Encoding a Human Nuclear Antigen Predominantly Recognized by Autoantibodies from Patients with Primary Biliary Cirrhosis. *J. Immunol.* 145, 4338–4347.

Tanaka, N., Aoyama, T., Kimura, S., and Gonzalez, F. J. (2017). Targeting Nuclear Receptors for the Treatment of Fatty Liver Disease. *Pharmacol. Ther.* 179, 142–157. doi:10.1016/j.pharmthera.2017.05.011

Thiam, A. R., Farese Jr, R. V., Jr., and Walther, T. C. (2013). The Biophysics and Cell Biology of Lipid Droplets. *Nat. Rev. Mol. Cel Biol.* 14, 775–786. doi:10.1038/nrm3699

Uzbekov, R., and Roingeard, P. (2013). Nuclear Lipid Droplets Identified by Electron Microscopy of Serial Sections. *BMC Res. Notes* 6, 386. doi:10.1186/1756-0500-6-386

Van Damme, E., Laukens, K., Dang, T. H., and Van Ostade, X. (2010). A Manually Curated Network of the PML Nuclear Body Interactome Reveals an Important Role for PML-NBs in SUMOylation Dynamics. *Int. J. Biol. Sci.* 6, 51–67. doi:10.7150/ijbs.6.51

Villagra, N. T., Navascues, J., Casafont, I., Val-Bernal, J. F., Lafarga, M., and Berciano, M. T. (2006). The PML-Nuclear Inclusion of Human Supraoptic Neurons: a New Compartment with SUMO-1- and Ubiquitin-Proteasome-Associated Domains. *Neurobiol. Dis.* 21, 181–193. doi:10.1016/j.nbd.2005.07.003

Walther, T. C., Chung, J., and Farese, R. V., Jr. (2017). Lipid Droplet Biogenesis. *Annu. Rev. Cel Dev. Biol.* 33, 491–510. doi:10.1146/annurev-cellbio-100616-060608

Wang, Y., MacDonald, J. I. S., and Kent, C. (1995). Identification of the Nuclear Localization Signal of Rat Liver CTP:phosphocholine Cytidylyltransferase. *J. Biol. Chem.* 270, 354–360. doi:10.1074/jbc.270.1.354

Wang, H., Gilham, D., and Lehner, R. (2007). Proteomic and Lipid Characterization of Apolipoprotein B-free Luminal Lipid Droplets from Mouse Liver Microsomes. *J. Biol. Chem.* 282, 33218–33226. doi:10.1074/jbc.m706841200

Wang, L., Wang, Y., Liang, Y., Li, J., Liu, Y., Zhang, J., et al. (2013). Specific Accumulation of Lipid Droplets in Hepatocyte Nuclei of PFOA-Exposed BALB/c Mice. *Sci. Rep.* 3, 2174. doi:10.1038/srep02174

Wang, H., Becuwe, M., Housden, B. E., Chitraju, C., Porras, A. J., Graham, M. M., et al. (2016). Seipin Is Required for Converting Nascent to Mature Lipid Droplets. *Elife* 5, e16582. doi:10.7554/eLife.16582

Wang, M., Wang, L., Qian, M., Tang, X., Liu, Z., Lai, Y., et al. (2020). PML2-mediated Thread-like Nuclear Bodies Mark Late Senescence in Hutchinson-Gilford Progeria Syndrome. *Aging Cell* 19, e13147. doi:10.1111/acel.13147

Welte, M. A. (2007). Proteins under New Management: Lipid Droplets Deliver. *Trends Cel Biol.* 17, 363–369. doi:10.1016/j.tcb.2007.06.004

Wilfling, F., Wang, H., Haas, J. T., Krahmer, N., Gould, T. J., Uchida, A., et al. (2013). Triacylglycerol Synthesis Enzymes Mediate Lipid Droplet Growth by Relocalizing from the ER to Lipid Droplets. *Develop. Cel* 24, 384–399. doi:10.1016/j.devcel.2013.01.013

Yan, R., Qian, H., Lukmantara, I., Gao, M., Du, X., Yan, N., et al. (2018). Human SEIPIN Binds Anionic Phospholipids. *Develop. Cel* 47, 248–256. doi:10.1016/j.devcel.2018.09.010

Yoshizawa, T., Yamagishi, Y., Koseki, N., Goto, J., Yoshida, H., Shibasaki, F., et al. (2000). Cell Cycle Arrest Enhances the *In Vitro* Cellular Toxicity of the Truncated Machado-Joseph Disease Gene Product with an Expanded Polyglutamine Stretch. *Hum. Mol. Genet.* 9, 69–78. doi:10.1093/hmg/9.1.69

Yue, L., McPhee, M. J., Gonzalez, K., Charman, M., Lee, J., Thompson, J., et al. (2020). Differential Dephosphorylation of CTP:phosphocholine Cytidylyltransferase upon Translocation to Nuclear Membranes and Lipid Droplets. *MBoC* 31, 1047–1059. doi:10.1091/mbc.e20-01-0014

Zhu, J., Zhu, S., Guzzo, C. M., Ellis, N. A., Sung, K. S., Choi, C. Y., et al. (2008). Small Ubiquitin-Related Modifier (SUMO) Binding Determines Substrate Recognition and Paralog-Selective SUMO Modification. *J. Biol. Chem.* 283, 29405–29415. doi:10.1074/jbc.m803632200

Zoumi, A., Datta, S., Liaw, L.-H. L., Wu, C. J., Manthripragada, G., Osborne, T. F., et al. (2005). Spatial Distribution and Function of Sterol Regulatory Element-Binding Protein 1a and 2 Homo- and Heterodimers by *In Vivo* Two-Photon Imaging and Spectroscopy Fluorescence Resonance Energy Transfer. *Mol. Cel Biol.* 25, 2946–2956. doi:10.1128/mcb.25.8.2946-2956.2005

Conflict of Interest: The authors declare that the research was conducted in the absence of any commercial or financial relationships that could be construed as a potential conflict of interest.

Publisher's Note: All claims expressed in this article are solely those of the authors and do not necessarily represent those of their affiliated organizations, or those of the publisher, the editors and the reviewers. Any product that may be evaluated in this article, or claim that may be made by its manufacturer, is not guaranteed or endorsed by the publisher.

frontiers in Cell and Developmental Biology

REVIEW
published: 07 February 2022
doi: 10.3389/fcell.2021.826248

Biogenesis and Breakdown of Lipid Droplets in Pathological Conditions

Claudio M. Fader Kaiser[1†], Patricia S. Romano[1†], M. Cristina Vanrell[1], Cristian A. Pocognoni[1], Julieta Jacob[1], Benjamín Caruso[2] and Laura R. Delgui[1]**

[1]CONICET Dr. Mario H. Burgos Institute of Histology and Embryology (IHEM), Mendoza, Argentina, [2]Instituto de Investigaciones Biologicas y Tecnologicas, Facultad de Ciencias Exactas, Físicas y Naturales, Universidad Nacional de Cordoba, Cordoba, Argentina

Lipid droplets (LD) have long been considered as mere fat drops; however, LD have lately been revealed to be ubiquitous, dynamic and to be present in diverse organelles in which they have a wide range of key functions. Although incompletely understood, the biogenesis of eukaryotic LD initiates with the synthesis of neutral lipids (NL) by enzymes located in the endoplasmic reticulum (ER). The accumulation of NL leads to their segregation into nanometric nuclei which then grow into lenses between the ER leaflets as they are further filled with NL. The lipid composition and interfacial tensions of both ER and the lenses modulate their shape which, together with specific ER proteins, determine the proneness of LD to bud from the ER toward the cytoplasm. The most important function of LD is the buffering of energy. But far beyond this, LD are actively integrated into physiological processes, such as lipid metabolism, control of protein homeostasis, sequestration of toxic lipid metabolic intermediates, protection from stress, and proliferation of tumours. Besides, LD may serve as platforms for pathogen replication and defense. To accomplish these functions, from biogenesis to breakdown, eukaryotic LD have developed mechanisms to travel within the cytoplasm and to establish contact with other organelles. When nutrient deprivation occurs, LD undergo breakdown (lipolysis), which begins with the LD-associated members of the perilipins family PLIN2 and PLIN3 chaperone-mediated autophagy degradation (CMA), a specific type of autophagy that selectively degrades a subset of cytosolic proteins in lysosomes. Indeed, PLINs CMA degradation is a prerequisite for further true lipolysis, which occurs via cytosolic lipases or by lysosome luminal lipases when autophagosomes engulf portions of LD and target them to lysosomes. LD play a crucial role in several pathophysiological processes. Increased accumulation of LD in non-adipose cells is commonly observed in numerous infectious diseases caused by intracellular pathogens including viral, bacterial, and parasite infections, and is gradually recognized as a prominent characteristic in a variety of cancers. This review discusses current evidence related to the modulation of LD biogenesis and breakdown caused by intracellular pathogens and cancer.

Keywords: lipid droplet (LD), LD breakdown, LD biogenesis, protozoans, viral infection, cancer

OPEN ACCESS

Edited by:
Carlos Enrich,
University of Barcelona, Spain

Reviewed by:
Jesús Balsinde,
Instituto de Biología y Genética Molecular (CSIC), Spain
Stéphanie Lebreton,
Institut Pasteur, France

****Correspondence:***
Benjamín Caruso
bcaruso@unc.edu.ar
Laura R. Delgui
ldelgui@mendoza-conicet.gob.ar

†These authors share first authorship

Specialty section:
This article was submitted to Membrane Traffic, a section of the journal Frontiers in Cell and Developmental Biology

Received: *30 November 2021*
Accepted: *22 December 2021*
Published: *07 February 2022*

Citation:
Fader Kaiser CM, Romano PS, Vanrell MC, Pocognoni CA, Jacob J, Caruso B and Delgui LR (2022) Biogenesis and Breakdown of Lipid Droplets in Pathological Conditions. Front. Cell Dev. Biol. 9:826248. doi: 10.3389/fcell.2021.826248

INTRODUCTION

Lipid droplets (LD) are multi-functional and highly connected organelles with a central role in cellular metabolism and homeostasis (Farese and Walther, 2009; Walther and Farese, 2012; Thiam et al., 2013b; Gao and Goodman, 2015; Welte and Gould, 2017; Olzmann and Carvalho, 2019; Beller et al., 2020). LD are ubiquitous in nature as regards cell and organism types. They present a wide range of sizes (from the nanometer order up to microns) and composition (Thiam and Beller, 2017), and have a simple and conserved particular structure consisting of a core of neutral lipids, primarily triacylglycerols (TAG), and sterolesters (SE) and are stabilized by a coating monolayer of phospholipids (PL) and specific proteins (Zhang and Liu, 2017). The mobilization of fat stores from LD is regulated by the metabolic and energy demands of the cell. When the energy demand increases, TAGs are broken down into fatty acids (FA) and the glycerol backbone, and the former enter cellular energy production pathways in the mitochondria. LD are also highly dynamic as their size, shape, and composition can vary under stress conditions, such as viral and microbial infections (Roingeard and Melo, 2017; Martins et al., 2018). Like other cell organelles, LD follow a biogenesis and degradation cycle, which contributes to LD homeostasis. In this review, we present an overview of the LD biogenesis and degradation processes as well as the mechanisms modulating their functioning in pathological conditions such as viral and protozoan infections and cancer.

Biogenesis

The mechanism of formation and growth of LD has been considered a fundamental question in LD biology (Ohsaki et al., 2014), and their biogenesis and modulating factors have become a research special focus over the last years (Thiam and Forêt, 2016; Walther et al., 2017; Chorlay and Thiam, 2018; Chapman et al., 2019; Jackson, 2019; Zoni et al., 2019, Zoni et al., 2021; Nettebrock and Bohnert, 2020; Santinho et al., 2020). LD are closely associated to the endoplasmic reticulum (ER), where the enzymes catalyzing the last step of TAG and SE synthesis are located (Pol et al., 2014). Several LD biogenesis models have been described, which differ from each other in the way that the protuberance of non-polar molecules located inside the bilayer is detached from the ER membrane (Brasaemle and Wolins, 2012; Thiam et al., 2013b; Thiam and Forêt, 2016; Jackson, 2019). In some models, the detachment process is driven by proteins whereas in others, the PL demixing driven by the membrane curvature plays a fundamental role (Zanghellini et al., 2010). The first step of an initial protuberance formation has been studied in depth by molecular dynamics (MD) simulations, which demonstrated that triolein blisters form inside PL bilayers (Khandelia et al., 2010; Zoni et al., 2019, Zoni et al., 2020, Zoni et al., 2021), and by mathematical models describing their shape using mechanical constraints (i.e., parameters determining elastic free energies of the bilayer and the monolayers coating the LD) (Zanghellini et al., 2010; Deslandes et al., 2017; Choudhary et al., 2018). Some factors that have been considered for the formation of an initial droplet are the TAG lateral solubility in bilayers, the mechanical constraints of the bilayer for deformation and the wettability of the bilayer with TAG. Solubility is referred as the maximum amount of TAG molecules that can be arranged in parallel to PL molecules (with the glycerol backbone facing the water phase), which is known to be 3–4% at most (Hamilton, 1989; Li et al., 2003). At higher contents, TAG molecules, like other NL may segregate into the intrabilayer space (Hauß et al., 2002; Corvalán and Perillo, 2020; Zoni et al., 2021). However, the nucleation process is poorly understood (Santinho et al., 2020) and there is a lack of experimental approaches that can address this issue, as at this stage LD are below optical resolution. Although some studies (Hamilton, 1989; Li et al., 2003; Duelund et al., 2013) have clearly demonstrated the presence of a segregated TAG phase somehow incorporated inside multilamellar vesicles at a TAG content slightly above 3%, the methods employed in those studies did not allow to draw any conclusion about the distribution of the TAG domains. Recently, Caruso et al. have used phosphatidylcholine (PC)/TAG Langmuir films to describe the segregation of TAG as a function of the packing and the composition of the membrane. This approach supports the assumption that TAG molecules segregate into discrete TAG lenses, whose shape is determined by the interfacial tensions through the contact angle between the lenses and their surrounding membrane, that is, its wettability (Caruso et al., 2021). Other authors have previously shown that the subsequent steps in the biogenesis process (budding and protrusion) are determined by physics of wetting. Thiam et al. have proposed and examined how bilayers interfacial tensions (and PL composition) affect the contact angles of apolar droplets introduced into the intrabilayer space (Thiam and Forêt, 2016). It has been observed that a system with a lower wettability (lower bilayer interfacial tension) forms more marked protrusions and thus a higher tendency to budding (Ben M'barek et al., 2017). Furthermore, the authors described that the compositional asymmetry of the bilayer determines the direction of budding in experimental systems (Chorlay and Thiam, 2018). In the cell, budding is expected to occur towards the cytoplasm, with this process being determined by ER membrane asymmetry.

Considering this evidence, LD formation can be described as a four-step process, comprising nucleation, growth, budding and detachment. Besides, the modulation of this process by proteins is currently being studied considering this differentiation. The first two steps are strongly modulated by the ER membrane protein seipin, which is more abundant in tubules than in the rest of the ER. Furthermore, the initial stage of LD biogenesis is most frequent in ER tubules. Seipin is known to stabilize TAG clusters and promotes the recruitment of TAG into them, whereas mutated forms give rise to aberrant LD shape and number (Cartwright et al., 2015; Wang et al., 2016; Santinho et al., 2020). However, the mechanism underlying TAG recruitment and nascent LD stabilization remains unclear. Similarly, the fat storage-inducing transmembrane protein 2 (FIT2) drives the LD biogenesis by interacting with ER tubule-forming proteins and septins (Chen et al., 2021). The lipase phosphatase activity of FIT2 has been recently described suggesting a role in the maintenance of the phospholipid

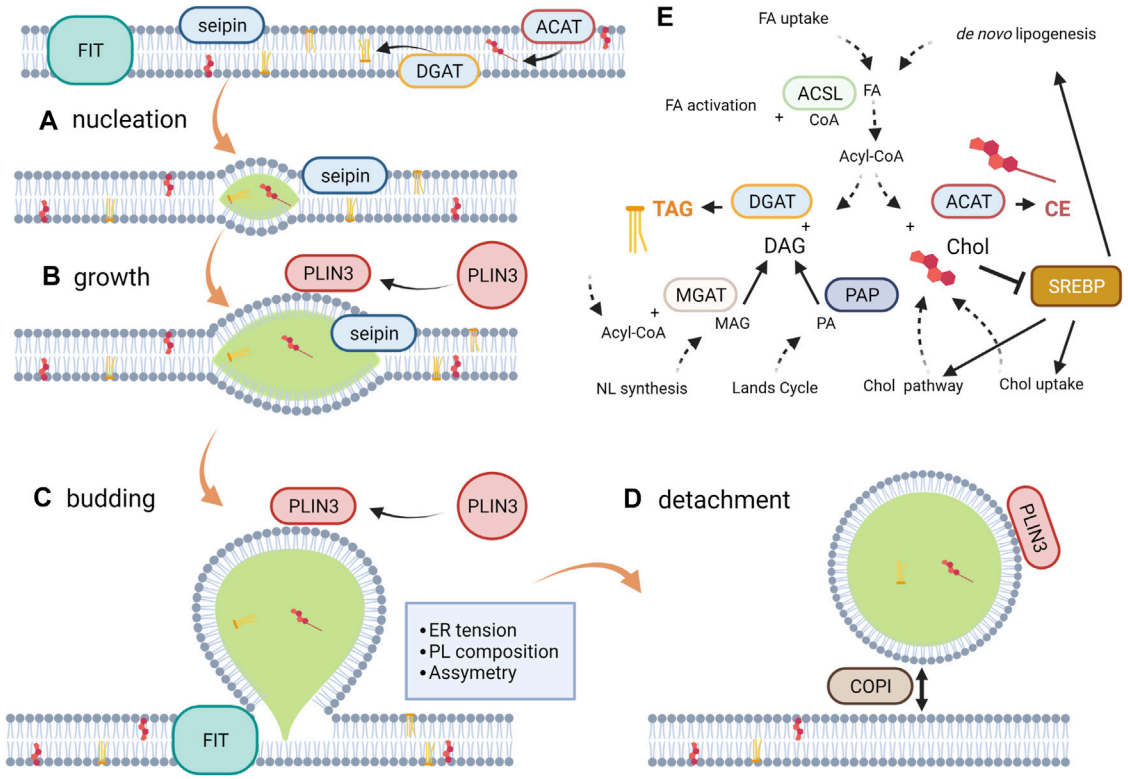

FIGURE 1 | LD Biogenesis. From a biophysical perspective, LD biogenesis can be described as a four-step process. **(A)** Nucleation occurs when the ER bilayer saturates with NL, reaching a concentration in the bilayer to form lenses of the size in the order of nanometers. The PL composition and seipin among other proteins modulates this process through bilayer hydration, bending and curvature. **(B)** The individual lens growth takes place as newly synthesized NL are incorporated and by ripening and fusion between lenses; seipin prevents NL from shedding. **(C)** Budding is a spontaneous process (dewetting) driven by the interfacial tensions that come into play surrounding the droplet. The bilayer tension and the phospholipid asymmetry determine the sphericity and direction of budding, respectively. FIT has been recently proposed to be involved in the maintenance of the appropriate PL composition in each ER hemi-layer. **(D)** Although detachment is not to be expected for all LD, it is a reversible process. COPI has been proposed to be involved in the detachment/re-attachment process to the ER membrane. **(E)** Metabolic reactions more closely affecting NL synthesis and its modulating pathway SREBP. Note: the scheme represents a simplification of the metabolic vias according to the available evidence regarding the revised pathologies. For a more detailed description, see Pol et al. (2014).

balance between the cytosol and the lumen facing the ER hemi-layers (Becuwe et al., 2020). Another protein that participates in the first stages of the synthesis of LD, ubiquitously distributed, is perilipin 3 (PLIN3), which protects TAG aggregates from lipolysis. This protein, present in the cytoplasm, accumulates in nascent LD immediately after TAG nucleation (Pol et al., 2014). This recruitment has been postulated to be controlled by a hydrophobic pocket of the protein (Ohsaki et al., 2006). Finally, not all LD detach from the ER (Mishra et al., 2016; Valm et al., 2017) and although the detachment mechanism remains to be elucidated, indirect evidences suggest a role of complex protein I, COPI; i.e., detachment is reversible, with the re-attachment requiring the COPI coatomer complex (Thiam et al., 2013a; Wilfling et al., 2014).

The mechanisms for protein targeting to LD are currently the focus of an expanding research field, although some underlying mechanisms have already been elucidated (Dhiman et al., 2020). Proteins that are targeted to LD are divided into class I and class II, according to where they come from, i.e., the ER bilayer surrounding the attached LD or the cytosol, respectively. Thus, seipin and PLIN3 are examples of each class of proteins playing a role in the initial instances of LD biogenesis. Targeting membrane proteins from ER bilayer to LD surface is a logistical challenge for cells (Dhiman et al., 2020). The biophysical properties of ER (bilayer) and LD (monolayer + inner TG) membranes would be a first selection barrier controlling what type of proteins will partition between both structures (Thiam et al., 2013b; Kory et al., 2016). In this sense, LD cannot accommodate proteins with transmembrane regions that span the thickness of a bilayer.

The above considerations describe LD biogenesis mainly from a biophysical perspective. However, to determine the factors modulating this process, cell metabolism pathways must also be considered. For instance, the *de novo* lipogenesis is regulated by the intracellular concentrations of glucose and sterol via the carbohydrate responsive element binding protein (ChREBP) and the sterol regulatory element binding protein (SREBP). In the latter, a decrease in cholesterol levels and polyunsaturated FA (PUFA) facilitates the proteolysis of SREBP yielding transcription factors that activate the expression of components of the lipogenic pathway and cholesterol metabolism in a species-specific

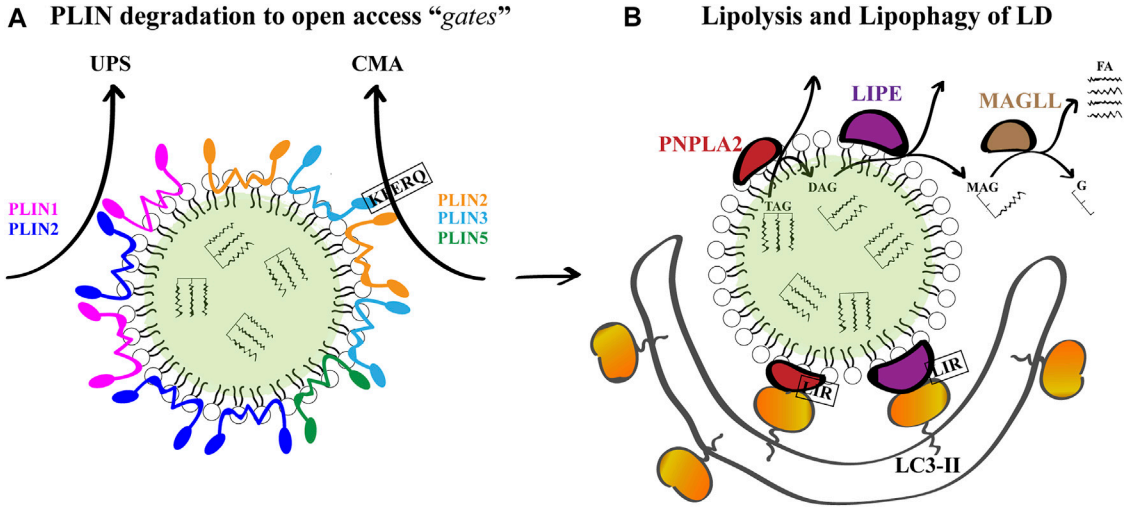

FIGURE 2 | LD Breakdown. **(A)** Given that PLINs are gatekeepers of LD breakdown and further lipolysis, they must be degraded for breakdown to proceed. PLIN1 and PLIN2 are substrates of the ubiquitin-proteasome system (UPS), and PLIN2, PLIN3 and PLIN5 are substrates of chaperone mediated autophagy (CMA) under conditions of lipid demand. For PLIN2 and PLIN3, a KFERQ peptide has been demonstrated to mediate CMA. **(B)** The degradation of LD TAG and SE occurs by the sequential action of PNPLA2, LIPE and MGLL to produce glycerol (G) and free FA for further β-oxidation. Concomitantly, PNPLA2 and LIPE located on the LD surface can interact with LC3-II on phagophore membranes through their LC3 interacting regions (LIR) to promote lipophagy-mediated LD breakdown.

manner (Shimano and Sato, 2017). The *de novo* lipogenesis generates FA, which subsequently esterify the glycerol backbone in a series of steps shared by the phospholipid and neutral lipid synthetic pathways. The branching-off point between these pathways is the dephosphorylation of phosphatidic acid into diacylglycerol (DAG) by phosphatidate phosphatases (Zhang and Reue, 2017; Petan, 2020). Finally, other enzymes located in the ER membrane, namely diacylglycerol acyltransferase (DGAT) and acyl-CoA cholesterol transferases (ACAT) catalyze the last steps of TAG and cholesterol esters synthesis, respectively. The regulation of these pathways has been shown to be modulated both in infections and cancer. All these evidences have been incorporated into **Figure 1**.

Breakdown

The catabolism of LD is regulated by the protein composition of the organelle surface and occurs by two mechanisms: lipolysis and lipophagy. As mentioned, LD have many different structural and functional proteins on its surface. In mammalian LD, the predominant proteins are the PLIN/adipose differentiation-related protein (ADRP)/tail-interacting protein of 47 kDa (TIP47) and their orthologs (grouped as the PAT family) (Miura et al., 2002; Bickel et al., 2009; Thiam et al., 2013b; Kory et al., 2016). In mammals, there are 5 different PLIN (PLIN1 to 5), among which PLIN1 and PLIN2 are exclusively associated with LD. The expression of PLIN1 is restricted to adipocytes and steroidogenic cells, while the expression of PLIN2 and PLIN3 are ubiquitously distributed (Sztalryd and Brasaemle, 2017). Among these proteins, PLIN regulate lipase access to the LD core; increased lipolysis in adipocytes was observed in their absence (Tansey et al., 2004). A general idea is that PLIN are needed to be somehow removed from the LD surface to "open a gate" for lipases to access the TAG (Brasaemle, 2013; Schweiger and Zechner, 2015).

Several LD proteins are degraded by the ubiquitin-proteasome system (UPS) under conditions of lipid starvation (e.g., cells cultured in the absence of FA supplementation), among which are PLIN1 (Xu et al., 2006) and PLIN2 (Xu et al., 2005; Takahashi et al., 2016). Lipolysis begins with the phosphorylation of PLIN1 by cAMP-dependent protein kinase A (PKA). Phosphorylated PLIN1 is then removed from the surface of LD for further proteasomal degradation, leading to the direct activation of LD-associated lipases: 1) patatin-like phospholipase domain containing 2 (PNPLA2/ATGL), which catalyzes the hydrolysis of TAG into DAG; 2) lipase E, hormone sensitive type (LIPE/HSL), which mediates the breakdown of DAG into MAG, and the hydrolysis of the ester bonds of other lipids such as SE, and 3) monoglyceride lipase (MGLL/MGL), which catalyzes the hydrolysis of MAG into glycerol and FA, which together with regulatory protein factors constitute the basis for this process (Zechner et al., 2012). The sequential action of the three lipases results in glycerol and FA generation. The products of lipolysis secreted from the adipose tissue are transported to other tissues and used for β-oxidation and ATP production. In non-adipose tissues, FA can enter the mitochondria directly for ATP production (D'Andrea, 2016).

Alternatively, PLIN2 and PLIN3, and more-recently described PLIN5, are substrates of lysosomal-degradation through a pathway named chaperone mediated autophagy (CMA) (Kaushik and Cuervo, 2015; Ma et al., 2020). CMA mediates the delivery of a subset of proteins exposing a pentapeptide motif (KFERQ or a related sequence) to the lysosome for proteolysis. In this process, heat shock cognate protein of 70 kDa (hsc70) recognizes, binds and delivers the protein to the lysosome-associated membrane protein 2A (LAMP-2A) within the lysosomal membrane, which forms a multimeric complex that translocates unfolded KFERQ-containing proteins into the

lysosome lumen for degradation (Kaushik and Cuervo, 2018). CMA related-pentapeptides were identified in PLIN-2 (LDRLQ) and PLIN-3 (SLKVQ), and their degradation by CMA precedes ATGL-dependent lipolysis and lipophagy. Therefore, CMA is a crucial process in the degradation of LD (Schneider et al., 2014; Kaushik and Cuervo, 2015; Ma et al., 2020).

Macroautophagy, another autophagy-related pathway, constitutes an alternative route for the breaking-down of intracellular LDs and mobilization of lipid storage. In general, autophagy is one of the major degradation pathways that enables the cell to survive under stress conditions by recycling metabolic components with an especially relevant role in the degradation of hepatocellular LD (Singh et al., 2009; Van Zutphen et al., 2014). First described in mouse hepatocytes under starvation, a selective form of LD-targeting macroautophagy known as lipophagy is thought to involve the recognition of LD to promote the localized assembly and extension of a sequestering phagophore around the perimeter of the LD and their subsequent delivery to lysosomes for turnover (Singh et al., 2009; Singh and Cuervo, 2012; Schulze et al., 2017; Filali-Mouncef et al., 2021). How this phagophore is targeted to (and extended around) the LD surface to facilitate lipophagy remains unclear. However, it has been demonstrated that both ATGL and HSL, localized on the phospholipid monolayer limiting LD, contain several putative LC3-the major autophagosome marker-interacting regions (LIR) motifs. Co-immunoprecipitation experiments have revealed that these proteins interact with the microtubule associated protein 1 light chain 3 (MAP1LC3/LC3), and therefore could dock LD onto the cytoplasmic surface of phagophores (Martinez-Lopez et al., 2016). Once fully enclosed, the double-membrane vesicle named autophagosome undergoes fusion with the lysosome to form a degradative organelle known as an autolysosome. Lysosomal lipases within the autolysosome are then ultimately responsible for the acid hydrolysis of the LD-stored NL and subsequent release of free FA (Warner et al., 1981; Liu and Czaja, 2013; Gatica et al., 2018). Degradation products are then released back into the cytosol and can be reused by the cell for synthesis processes. The two pathways of lipolysis and lipophagy likely work in tandem as coordinated processes (Martinez-Lopez et al., 2016). Indeed, a different possible scenario is that lipolysis can act to rapidly reduce the size of large LD to diameters more appropriate in size for engulfment by lipophagic vesicles (Schott et al., 2019).

Among the vast repertoire of components that exquisitely regulate the autophagy pathway, Rab proteins, a family of small GTPases, act as important mediators of endosomal tracking events. Cycling between active GTP- and inactive GDP-bound states, Rab proteins regulate the vesicular tracking network within the cell (Stenmark, 2009). Numerous Rab proteins have been identified on LD, and changes in members of the Rab proteins family have deleterious effects on LD turnover in response to classical lipophagy-inducing stimuli (Kiss and Nilsson, 2014). The most conspicuous case is the presence of Rab7 on the LD surface. Rab7 is a well-characterized member involved in the control of late endocytic membrane trafficking (Vitelli et al., 1997), assisting the regulation of lysosome–autophagosome interaction (Gutierrez et al., 2004; Jäger et al., 2004). Moreover, Rab7 decorates the surface of LD and regulates macrolipophagy in mammalian cells (Schroeder et al., 2015). The Rab7 GTPase located on the surface of LD becomes activated upon nutrient deprivation, resulting in its increased activity for GTP over GDP. Such activated state promotes the recruitment of lysosomes near LD and their target degradation via lipophagy (Carmona-Gutierrez et al., 2015). All these evidences have been incorporated into **Figure 2**.

LIPID DROPLETS AND PROTOZOANS

Protists are a heterogeneous group of ancient unicellular or pluricellular eukaryotes that can be divided into free living organisms and pathogenic parasites. The latter group encompasses organisms of Apicomplexa (*Toxoplasma gondii* and *Plasmodium falciparum*) and Kinetoplastida (*Trypanosoma cruzi*, *Trypanosoma brucei* and species of *Leishmania*) orders that infect humans causing the named Neglected Tropical Diseases (NTD), which are highly spread worldwide. These organisms possess the metabolic pathways for the production and breakdown of LD, like other higher eukaryotic cells. In the past, pathogen-derived LD were mostly considered as lipid deposits with low turnover rates (Murphy, 2012). In recent years, there has been an increasing interest in the study of these lipid-rich organelles present in pathogenic prokaryotes and lower eukaryotes. In this context, evidence begins to accumulate demonstrating that cytosolic LD of parasitic protozoans bear more dynamic roles in both, mammalian and non-mammalian stages of the parasite's life cycle. Furthermore, they can interact with the LD of mammalian cells for their own benefit. In this section we present recent data demonstrating the role of LD during the biological cycle of protozoan pathogens (including the stages living inside and outside the host cells) and suggest the relevance of these compartments as targets of antiparasitic drugs.

Lipid Inclusions of Reservosomes and Cytoplasmic LD are Key Components During *Trypanosoma cruzi* Differentiation and Host Cell Infection

T. cruzi, the etiological agent of Chagas disease, is one of the main causes of morbidity and mortality in Latin America. The life cycle of *T. cruzi* comprises three stages; epimastigotes and amastigotes are the replicative forms found in the intestine of the insect vector and in the cytoplasm of host cells, respectively; and the infective forms, metacyclic trypomastigotes and blood-stream trypomastigotes, which transmit the infection from the insect to mammals and *vice versa*. Two main compartments for lipid storage have been described in epimastigotes: the reservosome lipid inclusions and the cytoplasmic LD. The accumulation of cholesterol and SE within the reservosomes, the lysosome-like organelle of this parasite, is directly related to the host's serum concentration of these metabolites (Pereira et al., 2011). Although *T. cruzi* cannot synthesize cholesterol, this compound is acquired through the uptake of low density lipoprotein (LDL) particles

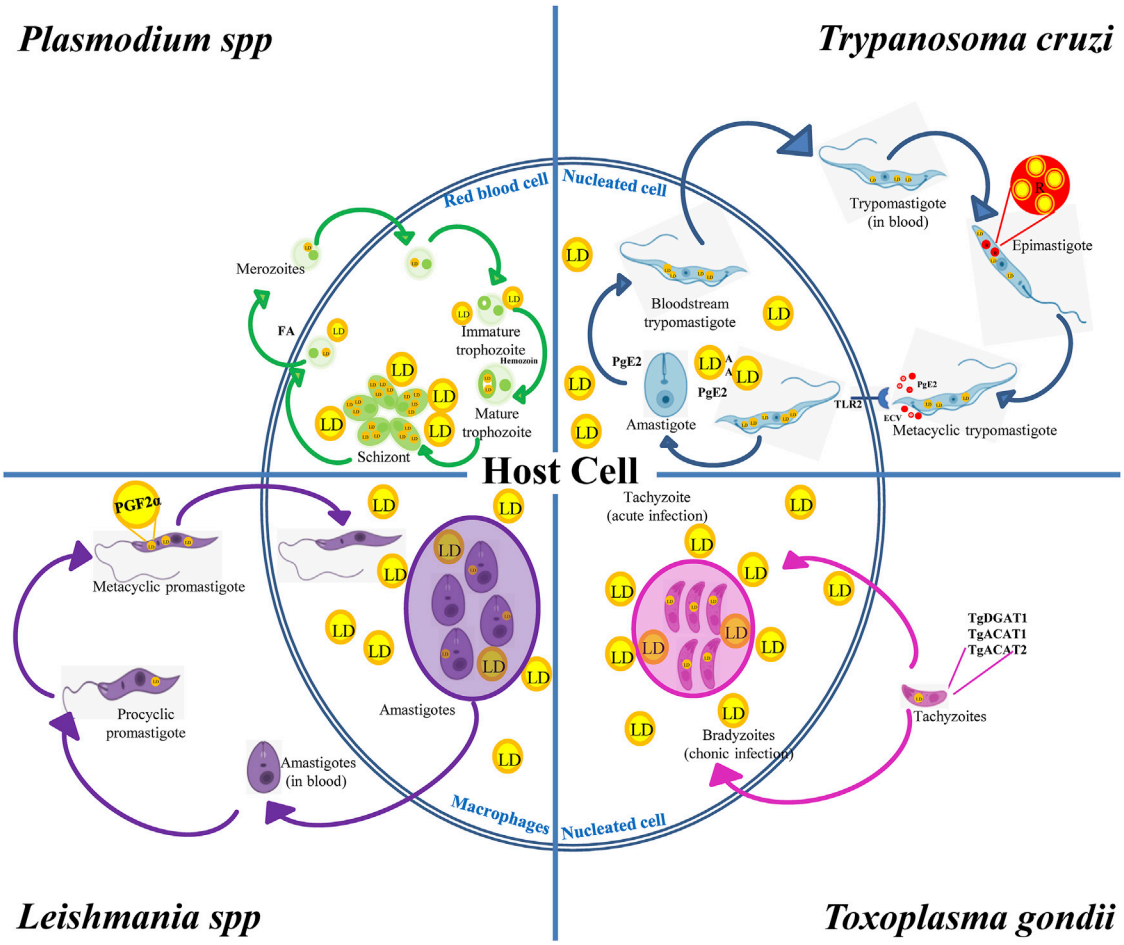

FIGURE 3 | LD in the biological cycles of protozoan parasites. *Trypanosoma cruzi* displays reservosomes (R) in epimastigotes and cytoplasmic LD in metacyclic trypomastigotes (MT) that mainly store cholesterol and SE, respectively. While degradation of R occurs during metacyclogenesis, the contact with the host cell induces the production of LD and PGE2 in MT and in the host cell favoring *T. cruzi* infection and replication. *Toxoplasma gondii* expresses TgDGAT1, TgACAT1 and TgACAT2, which are the enzymes responsible for the LD synthesis in the parasite. An increased number of host LD was observed in cells containing vacuoles with tachyzoites, which is the characteristic parasite stage of the acute infection. These LD are also observed in the vacuole lumen and inside the parasite cytoplasm, thus evidencing the transport of host lipids to the parasite. *Leishmania* spp. increases the LD number during the evolution from procyclic to metacyclic promastigotes, which also contain PGF2α, suggesting a role of this eicosanoid as a parasite virulence factor. Host's LD are also increased in macrophages infected with *Leishmania*. Like *T. gondii*, these host LD have been observed inside the *Leishmania* vacuole and even in the parasite's cytoplasm. *Plasmodium* was found to store NL in the food vacuole. NL are important to prevent heme toxicity by production of the malaria pigment hemozoin. Infected red-blood cells increase the number and size of LD when they evolve from the trophozoite to squizont form, whereas LD breakdown characterizes merozoite maturation and release together with FA.

from the hematophagous insect diet (José Soares and de Souza, 1991). LDL are then transported in endocytic vesicles and delivered to reservosomes (Pereira et al., 2018). Inside the reservosome, LD are surrounded by a PL monolayer and display disk or rod-like shapes. Crystals of cholesterol were observed when cholesterol and SE masses reach a critical point, in a process that resembles the formation of foam cells in mammals (Varsano et al., 2018). In contrast, serum deprivation results in the consumption of the cholesterol storage of reservosomes (Pereira et al., 2015). Interestingly, it has been observed that as in higher eukaryotes, autophagy in *T. cruzi* is induced in response to nutrient starvation, leading to metacyclogenesis, the process of differentiation of epimastigotes to metacyclic trypomastigotes (Vanrell et al., 2017). This process is characterized by a dramatic reduction in the number of reservosomes, indicating that degradation of the reservosome content is a key step during differentiation, probably as an energy source (Cunha-e-Silva et al., 2002). Furthermore, it has been demonstrated that the induction of autophagy during metacyclogenesis increases the proteolytic activity of reservosomes, mainly due to cruzipain, which is the major cysteine-protease of *T. cruzi* and also an important virulence and immune evasion factor (Losinno et al., 2021). Therefore, it is reasonable to hypothesize that the degradation of LD in reservosomes could also be important during metacyclogenesis as an energy, cholesterol and other precursors source to generate the membranes of metacyclic trypomastigotes. *T. cruzi* also presents many uncharacterized LD distributed throughout its

cytoplasm. During lipid starvation, cholesterol of reservosomes is mobilized and inserted into the membranes to maintain parasite proliferation, whereas under normal conditions, esterification reactions predominate, most likely to remove the excess of free cholesterol, leading to the formation of cytoplasmic LD (Pereira et al., 2015). The finding of enzymes involved in lipid metabolism, methyltransferases, reductases, lipases, and proteins like Rab18, and the ATP-binding cassette transporter 1, associated with the cholesterol efflux in humans, in reservosomes supports this hypothesis (Torres et al., 2004; Sant'Anna et al., 2009). The activity of an ACAT sensitive to avasimibe was also found in *T. cruzi* (Pereira et al., 2015). ACAT most likely function is to remove the excess of free cholesterol of reservosomes, leading to the formation of LD in *T. cruzi*. Aspartyl-like peptidases and cruzipain are also involved in cholesterol mobilization as shown by the accumulation of rod-shaped and droplet-shaped LD in reservosomes when the parasites are incubated with pepstatin-A, a typical aspartyl-peptidase inhibitor (Sangenito et al., 2021). Interestingly, this effect is imitated by lopinavir and nelfinavir, two Human Immunodeficiency Virus peptidase inhibitors with a high impact in *T. cruzi* viability (Sangenito et al., 2021). Although the connection between these peptidases and lipid accumulation is poorly understood, some authors have postulated that aspartyl-like peptidases present in the reservosomes could be directly and/or indirectly linked to the process of cholesterol mobilization by the endocytic pathway in the protozoan (Lechuga et al., 2020). *T. cruzi* trypomastigotes and amastigotes also have LD. In trypomastigotes, LD increase after both host interaction and exogenous arachidonic acid (AA) stimulation. Notably, AA-stimulated trypomastigotes release high amounts of prostaglandin E2 (PGE2) and show PGE2 synthase expression (Toledo et al., 2016). Although PGE2 actions are mainly proinflammatory, different authors propose an immunomodulatory effect that could contribute to the immunosuppression observed during *T. cruzi* infection, thus risking the survival of the parasite within its host. On the other hand, it is known that the *T. cruzi* trypomastigotes release extracellular vesicles with different functions, favoring the biosynthesis of LD and PGE2 in the host cell and reducing the production of inflammatory cytokines and trypanocide molecules such as nitric oxide, thus making the environment more favorable for the infection (Lovo-Martins et al., 2018). There is evidence showing that the infection of macrophages with trypomastigotes causes an increase in LD biogenesis in a Toll-like receptor (TLR) 2-dependent mechanism, since this process is not observed in bone marrow macrophages derived from C57BL/6 TLR2 knock out mice (TLR2−/−). D'Avila et al. (2011) have demonstrated that Toll-like receptor 4 does not participate in this process. It is known that TLR2, TLR3, TLR4 and TLR7 agonists increase the levels of proteins that are crucial for LD biogenesis (PLIN2 or DGAT2); however, in *T. cruzi* infected macrophages this effect is elicited only by TLR2, which, together with TLR9, plays a role in the immune recognition of this parasite (Tarleton, 2007). Interestingly, in contrast to LD from other host cells, LD from macrophages contain AA which is used to produce eicosanoids that are used in *T. cruzi* metabolism (den Brok et al., 2018). Thus, the treatment of macrophages with C75 (a FA synthase inhibitor) inhibits LD biogenesis and also induces a downregulation of eicosanoid production and replication of the parasite (de Almeida et al., 2018).

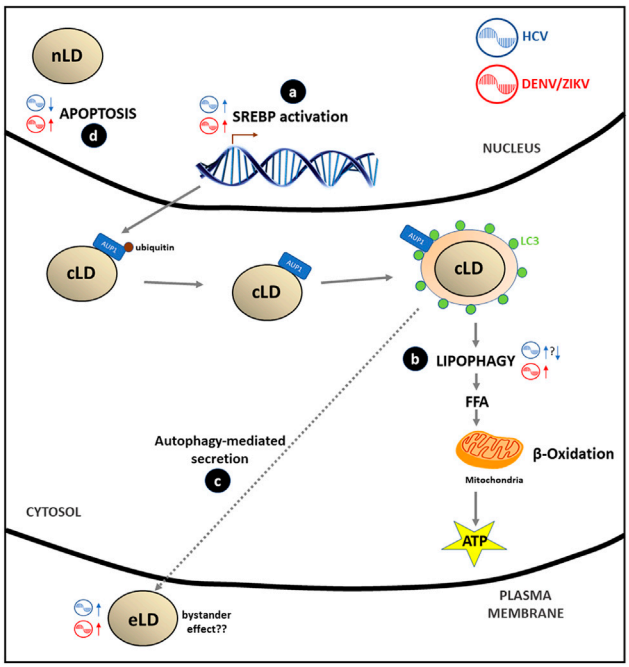

FIGURE 4 | *Flaviviridae* effects in LD metabolism: **(A)** HCV, ZIKV/DENV stimulate the SREBP pathway through the transcription of genes involved in LD and lipids biosynthesis in order to cover the extra membrane requirement that virus replication generates. **(B)** DENV/ZIKV stimulates lipophagy by recruitment of deubiquitinated AUP1 from LD membrane to the LC3-positive autophagosome; this process generates FA that after catabolism inside the mitochondria (β-oxidation) produce energy (ATP) to accomplish viral replication. Data on the HCV effect on lipophagy are controversial: some authors report a stimulation of this process while other suggest that inhibition of lipophagy may occur. **(C)** Some authors hypothesize that there is a putative secretion of HCV or DENV/ZIKV virions, viral proteins or infectious viral RNA mediated by autophagy of LC3-positive LD vesicles (eLD) to spread the infection. This phenomenon may support the bystander effect proposed for DENV/ZIKV infections. **(D)** Apoptosis is inhibited (HCV) or stimulated (DENV/ZIKV) by viral and nLD interaction with PML nuclear bodies.

Trypanosoma brucei Replication Requires the Rapid Turnover of Parasite LD

T. brucei is the causative agent of sleeping sickness or African trypanosomiasis, a disease characterized by behavioral abnormalities such as somnolence during daytime. Unlike all other pathogenic trypanosomatids which have an intracellular life-stage, *T. brucei* infection takes place in the bloodstream of mammalian hosts. After a blood feed of the tse-tse vector fly, metacyclic trypomastigotes reach the bloodstream of mammals and differentiate into long-slender trypomastigotes with high replicative capacity, followed by a second differentiation step into non-replicative short-stumpy forms when parasite density increases. The cycle is completed when blood trypomastigotes

ingested by flies transform into procyclic trypomastigotes which migrate from the midgut to the salivary gland of the insect where they undergo differentiation to infective metacyclic trypomastigotes. The biogenesis of LD in *T. brucei* depends on the activity of a novel LD Kinase (LDK). The association of LDK with LD is apparently mediated by its hydrophobic domain that allows the insertion into the membrane monolayer of the organelles. The loss of this enzyme dramatically decreases the abundance of LD and affects the growth of parasites in delipidated serum (Flaspohler et al., 2010). It has been postulated that the function of FA storage in LD is to enable the adaptation of procyclic trypomastigotes to nutritional challenges during the development and migration inside the tse-tse fly. Under physiological conditions, FA (oleate) are taken from the medium and incorporated to TAG in the LD of procyclic trypomastigotes (Allmann et al., 2014). Plasma membrane PL provide the precursor DAG for esterification. Nejad et al. have shown that the *T. brucei* lipin homolog TbLpn is essential for parasite survival in culture. Lipins are a family of phosphatidic acid phosphatases that catalyze the dephosphorylation of PA to DAG. It has been demonstrated that the inducible downregulation of TbLpn decreases the number of LD and reduces TAG steady-state levels (Dawoody Nejad et al., 2018). These authors hypothesized that the rapid lipid turnover observed in their experiments could be required for the synthesis or remodeling of membrane lipids during cell proliferation, or for energy supply under limited nutrient availability. Apart from TAG, *T. brucei* also produces SE. Although a putative gene for the ACAT enzyme has not been found in *T. brucei*, its presence was evidenced by the production of SE from host LDL particles and subsequent accumulation in parasite LD, as it occurs in *T. cruzi* (Coppens et al., 1995).

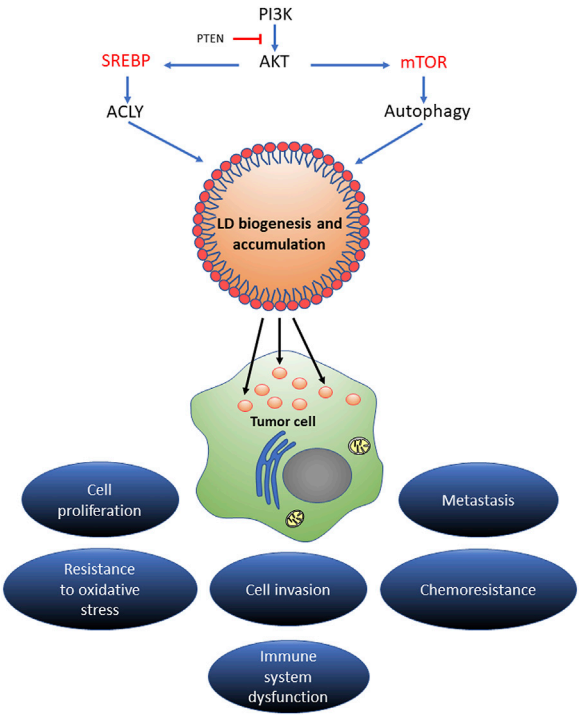

FIGURE 5 | The regulatory mechanism of LD in cancer progression. Different signaling pathways of lipid acquisition may drive LD biogenesis in stressed cancer cells. Increased LD contents could expand the source of lipid substrates and energy to meet the metabolic needs of proliferating cancer cells. In the tumor microenvironment, LD could act as an energy reservoir for an aggressive cancer to trigger metastatic cloning. LD accumulation extensively mediates proliferation, invasion, metastasis, and oxidative stress and chemotherapy resistance in multiple types of cancers.

LD Biogenesis Increases During *Leishmania* Metacyclogenesis and Contributes to the Infection Process

Leishmaniasis is a disease caused by more than twenty species of the *Leishmania* genus. Distributed worldwide, this disease can be found in three clinical forms: visceral leishmaniasis, the most severe illness, is highly endemic in the Indian subcontinent and East Africa; cutaneous leishmaniasis, which occurs in the Americas, the Mediterranean basin, the Middle East and Central Asia; and mucocutaneous leishmaniasis, mainly occurring in Brazil, Bolivia, Ethiopia and Peru. The infection is transmitted to mammals by metacyclic promastigotes present in the proboscis of sandflies, which are the vectors of the disease. Metacyclic promastigotes are phagocytized by macrophages and differentiate into amastigotes that replicate in phagolysosomal compartments, releasing the parasite after macrophage lysis, a process that causes tissue damage (Pace, 2014). After a blood feed, amastigotes are taken by the vector and differentiate in procyclic promastigotes which proliferate in the insect gut and then migrate to the proboscis where they differentiate into metacyclic promastigotes. It has been demonstrated that LD numbers increase during *Leishmania* metacyclogenesis, i.e., the transformation of procyclic to metacyclic promastigotes. LD from metacyclic forms contain PGF2α synthase (PGFS) and release PGF2α in higher quantities than in other procyclic or amastigote forms, suggesting a role of PGF2α in parasite virulence (Araújo-Santos et al., 2014). On the other hand, the cholesterol supply is assured by the uptake and retention of LDL particles in *L. amazonensis* lipid membrane microdomains. BODIPY-labeled LDL is distributed in large compartments along the parasite body. These compartments also contain SE, suggesting the presence of an ACAT enzyme similar to *T. cruzi* and *T. brucei* (De Cicco et al., 2012). Furthermore, when metacyclic promastigotes of *Leishmania major* infect the bone marrow-derived macrophages (BMM), an increase in the LD biogenesis in these host cells is observed as a function of time. This increase is due to an induction of the expression of genes involved in cholesterol uptake and *de novo* synthesis of TAG in BMM infected with *L. major*. By a microarray assay, the authors demonstrated the transcriptional activation of several genes of BMM such as *DGAT2*. This host cell response occurs regardless of the viability of the parasites, as it occurs in either living or dead parasites and even in uninfected neighboring cells, although at a lesser extent than in infected cells, which would indicate that the phagocytosis of this parasite further increases the biogenesis of LD (Rabhi et al., 2016).

Toxoplasma gondii Incorporates Host LD in its Parasitophorous Vacuole Favoring Parasite Replication

T. gondii is the etiological agent of toxoplasmosis, a severe disease in individuals with an impaired immune system, mainly producing neurological complications, and in the fetus that becomes infected by vertical transmission during pregnancy. In the latter case, *T. gondii* can cause severe neurological, ocular and cardiac disorders (Paquet et al., 2013; Laboudi, 2017; Fard et al., 2020). *T. gondii* is an obligate intracellular parasite with a complex life cycle involving one feline host, where the parasite sexual phase occurs, and intermediate hosts including humans. In humans, parasite transmission occurs through the ingestion of either raw or undercooked meat containing tissue cysts with bradyzoites; the ingestion of water and food contaminated with feline feces containing oocysts with sporozoites; and through transplacental transmission of tachyzoites during pregnancy. After ingestion, bradyzoites and sporozoites invade intestinal epithelial cells and differentiate into the fast-replicating tachyzoites inside a parasitophorous vacuole. In the acute infection, tachyzoites exit the cells, reach the bloodstream, and disseminate throughout the body. In healthy adults, cysts containing slow-replicating bradyzoites are located in the eyes, brain and muscles in the chronic phase of the disease, while in immunocompromised patients, the infection becomes severe and even fatal, as mentioned above (Attias et al., 2020). A DGAT1-like enzyme, required for the synthesis of NL, was characterized in *T. gondii* (TgDGAT1). This enzyme, localized in the parasite cortical and perinuclear ER, synthesizes TAG and generates cytosolic LD (Quittnat et al., 2004). As in other pathogenic protozoans, cholesterol is incorporated in *T. gondii* from the host environment. In this sense, two ACAT-related enzymes were identified and characterized in this parasite, TgACAT1α and TgACAT1β (also named TgACAT1 and TgACAT2). These enzymes localize to the ER and participate in the SE and LD synthesis (Nishikawa et al., 2005; Lige et al., 2013). Genetic ablation of each individual ACAT results in impairment of parasite growth, whereas dual ablation is not tolerated by *T. gondii*, thus highlighting the key role of cholesterol storages and LD in this organism and the possibility to consider this system as a target for new antitoxoplasmosis drugs (Lige et al., 2013). As for host cell stages, an increase was observed in the synthesis and accumulation of TAG when skeletal muscle cells (SkMC) are infected with *T. gondii* tachyzoites (Hu et al., 2017; Nolan et al., 2017), which is related to an increase in the number and size of LD in the host cells (Gomes et al., 2014; Nolan et al., 2017). There is evidence indicating that effectors synthesized by the parasites and exported from the PV to the host cell cytosol are responsible for the increase in the number of LD, since the knockout of the MYR1 protein (involved in the export of other PV effectors to the cytosol) is necessary for the accumulation of LD induced by this parasite. Other authors have demonstrated a role of the c-Jun kinase and the mammalian target of rapamycin (mTOR) signaling pathways in the modulation of parasite-induced generation of LD, which were supposed to provide nutrients to the parasite, since the pharmacological inhibition of these pathways did not produce an accumulation of LD during infection (Hu et al., 2017). Accordingly, it has been shown that the replication of *T. gondii* decreases when host cell LD are scarce, for example when the enzyme DGAT is inhibited (Nolan et al., 2017). It has also been observed that these LD were in contact with the ER and with the PV containing the parasite (Gomes et al., 2014). Other authors have described the presence of host LD within the PV and even in the parasite's cytoplasm, suggesting that *T. gondii* can access and incorporate host lipids to its own membranes and LD (Nolan et al., 2017). Interestingly, although the increase in LD numbers is beneficial for the parasite as a nutrient source, LD serve as substrate for the production of PGE2, which is a crucial metabolite for the synthesis of interleukin-12 and interferons that participate in the repair and homeostasis of SkMC after the injury caused by the parasite, and contributing to the establishment of the chronic phase of infection (Gomes et al., 2014). Other parasites of the same family (*Sarcoystidae*) also induce the formation of host LD, like *Neospora caninum*, an Apicomplexa parasite of livestock and domestic animals, which is known to increase the levels of TAG and LD in human fibroblasts after infection (Hu et al., 2017).

Biogenesis and Breakdown of Host LD are Required During the Intraerythrocytic Development of *Plasmodium*

Plasmodium species are the causative agents of malaria, the illness with the highest morbidity rates among human parasitic diseases. Currently, five identified species of *Plasmodium* infect humans, with *P. falciparum* being the most lethal. *Anopheles* spp. mosquitoes are the host that transmit the infection to humans (intermediary hosts) through the inoculation of sporozoites which migrate and develop in the liver. After invasion of hepatocytes, infective elongated sporozoites start the asexual multiplication and form the squizont. Sporozoites inside the squizont then form daughter cells called merozoites which, after maturation, are released from hepatocytes enclosed in a membrane (merosome). After merosome lysis, free merozoites invade red blood cells and transform into round proliferative trophozoites that mature into an erythrocytic schizont, which in turn rupture and release merozoites (Maier et al., 2019). A proportion of parasites differentiate into gametocytes (sexual forms) which are taken up by a mosquito when it feeds on human blood. Gametocytes undergo sexual reproduction in the midgut of the mosquito and develop into sporozoites, which migrate to the salivary glands to start a new cycle. The metabolism and trafficking of TAG and host LD in infected erythrocytes varies in a specific way during the intraerythrocytic cycle of this parasite. Increased DGAT activity and accumulation of TAG was observed during the development of *Plasmodium* from the trophozoite to squizont form, whereas TAG degradation was induced during the fragmentation of the squizont, with FA being released to the medium together with merozoites (Palacpac et al., 2004). In line with these observations, LD within red blood cells increase in size and number during the intraerythrocytic development, reaching a maximum number in the segmented schizonts stage. Interestingly, in the intraerythrocytic stage of *P. falciparum*, a population of Nile Red-positive particles was

observed within the digestive vacuole of the parasite. These particles are composed of NL. These NL-rich particles, which may have originated from the digestion of previously internalized PL by the food vacuole (Jackson et al., 2004), have a key role in heme detoxification through the formation of the insoluble malaria pigment hemozoin (Hoang et al., 2010). These findings support the hypothesis that the storage and degradation of TAG are important processes during merozoite maturation and that NL present in the parasite food vacuole prevent heme toxicity. In contrast to the described role of LD in the erythrocytic cycle of *Plasmodium*, there is no evidence supporting the existence of a metabolism and trafficking of LD in the intrahepatic infection that occurs before intraerythrocytic phase.

In summary, pathogenic protozoans can produce and degrade their own LD and interact with the host's LD throughout their biological cycle. While parasite LD favor stage differentiation and infection stages, host LD are nutritional sources during their intracellular replication. Like in mammalian cells, parasite LD are distributed in the cell cytoplasm, although in some cases they are present inside other organelles such as lipid inclusions inside reservosomes of *T. cruzi* or NL particles in the *Plasmodium* food vacuole. LD biogenesis is induced after the acquisition of lipids (e.g., cholesterol and FA) from the external environment, blood of mammalian hosts or insect vectors mainly by endocytosis. DGAT and ACAT present in protozoans then lead to DAG and cholesterol esterification for final storage in LD. A few studies have addressed the catabolism of LD in these parasites; however, this process is known to be induced at specific developmental stages during the differentiation from a parasitic form to another, suggesting a role of LD in the energy supply required for the process. Interestingly, many of the enzymes involved in LD metabolism in protozoan parasites are vital for the organism, for they are unique, unlike their mammalian counterparts (Lige et al., 2013; Dawoody Nejad et al., 2018). Therefore, specific inhibitors of these enzymes could be interesting targets of drugs to interrupt the biological cycle of pathogenic protozoa, mainly in the mammalian stages. On the other hand, *T. cruzi*, *Leishmania* spp., *T. gondii* and *Plasmodium* spp., have intracellular stages that generate changes in the number and size of the LD of the host cell. It has been shown that LD increase in number and size when these intracellular parasites interact with the host cell. There is increasing evidence that protozoan parasites may target these host-derived LD to obtain nutrients for growth. However, host cells use the lipids stored in LD to produce inflammatory mediators against these parasites (Melo et al., 2003; D'Avila et al., 2012; Gomes et al., 2014; de Almeida et al., 2018). Due to the modulation of LD number by intracellular forms of protozoans that can determine the success or failure of the infection, the parasite/host LD interplay might be an attractive target to exploit in the future. All these evidences have been incorporated into **Figure 3**.

FLAVIVIRIDAE AND LIPID DROPLETS

Flaviviridae is a large group of enveloped viruses, with a positive sense single strand RNA genome. The *Flaviviridae* family includes several viruses that cause high clinical impact diseases in humans: hepatitis C virus (HCV) of the *Hepacivirus* genus, yellow fever virus (YFV), West Nile virus (WNV), dengue virus (DENV) and Zika virus (ZIKV) belonging to the *Flavivirus* genus (Wu et al., 2015). Several studies have shown that members of the *Flaviviridae* virus family hijack the LD machinery for the replication and production of new mature viral particles. So far, the *Hepacivirus* HCV, and the *Flavivirus* DENV and ZIKV, are the most studied viruses as regard as LD usurpation (Filipe and McLauchlan, 2015; Sun et al., 2017; Cloherty et al., 2020).

Hepacivirus and *Flavivirus* genera share almost the same number and structural distribution of their proteins: a capsid protein (*Core* for HCV and *C* for *Flavivirus*), two envelope proteins (E1 and E2 for HCV, and prM and E for *Flavivirus*) and several non-structural proteins (NS) (Neufeldt et al., 2018). On the other hand, their replication cycle are quite similar: they first interact and enter the target cell by receptor mediated endocytosis, and after fusion with the lysosomes and acidification they uncoat and release their genome for translation of the viral polyprotein. At this point, the LD and ER play a key role as a scaffold for the newly synthetized virus assembly. Afterwards, the virion moves into the ER-Golgi lumen for proper assembly and maturation, and the final mature viruses are released through the secretory pathway to the extracellular space to start a new infective cycle (Zeisel et al., 2013; Guzman and Harris, 2015; Musso and Gubler, 2016).

HCV and DENV/ZIKV Hijack the SREBP Pathway to Accomplish Viral Replication

The SREBP pathway is a key regulator of cholesterol/lipid levels, and therefore a key pathway for LD homeostasis (Eberle et al., 2004; Moon, 2017). Several studies have shown that some members of the *Flaviviridae* family hijack SREBP for their own benefit. Particularly, it has been shown that HCV and DENV/ZIKV trigger SREBP activation in order to fulfil the extra-membrane requirements during the cellular infection, replication and production of new virions (Randall, 2018; Meng et al., 2019; Yuan et al., 2019; Cloherty et al., 2020; Raini et al., 2021).

HCV is the most studied flavivirus hijacking the SREBP pathway. In this regard, HCV usurps and stimulates SREBP by disruption of the lipid homeostasis, generating a membranous web and activating the transcription of SREBP target genes for the final release of lipid-coated lipoviroparticles (LVPs) (Waris et al., 2007). In fact, clinical studies have shown that patients with chronic HCV infection resulted in a reduction of their circulating lipid levels (lower LDL and total cholesterol levels) as compared to patients developing a sustained virologic response (SVR) (patients with non-detectable HCV RNA after the completion of the antiviral therapy). This phenomenon might be explained by the extra lipid consumption that the HCV infection generates, re-routing the circulating lipids for the formation of LVPs (Corey et al., 2009). LVPs are hybrid particles composed of viral components (E1, E2, core protein and HCV RNA) and apolipoproteins (ApoE, ApoB, ApoCI, ApoCII and ApoCIII) (Scholtes et al., 2012). The presence of these apolipoproteins

on the HCV surface has been proposed as a viral strategy to hijack neutralizing antibodies (Vercauteren et al., 2014). Particularly, the HCV core protein, the non-structural proteins NS4B, NS5A and the 3′ untranslated region (UTR) increase the activation of both SREBP-1 and SREBP-2, stimulating the synthesis of cholesterol and membrane lipids. In addition, it has been reported that HCV infection induces SREBPs cleavage and phosphorylation. In this regard, HCV core and NS4B proteins can induce the proteolytic cleavage of SREBP and oxidative stress by activating the phosphatidylinositol 3-kinase (PI3-K)-protein kinase B (PKB, also known as AKT) pathway, increasing phosphorylation and transactivation of SREBPs (Waris et al., 2007).

As mentioned, AMPK is an important sensor for cellular energy levels and has been demonstrated to be involved in lipid metabolism regulation. In a recent publication, HCV NS5A was shown to inhibit AMPK phosphorylation *in vivo* and *in vitro*, resulting in an increase of SREBP-1c expression levels, acetyl-coenzyme A carboxylase 1 (ACC1) and FA synthase (FASN) via the AMPK/SREBP-1c pathway, generating at the same time, higher numbers of LD (Meng et al., 2019).

The ATP-dependent RNA helicase DEAD-box helicase 3 X (DDX3X) is involved in cellular processes that are different from those involved in innate immunity. DDX3X is required for the replication of many viruses including HCV (He et al., 2021; Winnard et al., 2021). DDX3X has been shown to colocalize with LD, HCV core and NS proteins. However, DDX3X specifically recognizes the HCV 3′ untranslated region (UTR) in the cytosol and after cross-activation of IκB kinase-α (IKKα), it translocates to the nucleus and activates SREBPs. Thus, the LD biogenesis and HCV viral assembly are stimulated (Li et al., 2013; Pene et al., 2015). In summary, these findings highlight that LD are necessary and that their synthesis is stimulated during the HCV infection lifecycle.

The role of the SREBP pathway in *Flaviviridae* infection has been determined in several studies, in which different inhibitors of this pathway were used. In the case of the HCV infection, the SK1-1/S1P pathway was blocked with PF-429242 (a small, site-directed, competitive inhibitor of SKI-1/S1P). The treatment with PF-429242 led to a reduction of LD formation and an impairment in the early steps of HCV lifecycle was shown at all the inhibitor concentrations employed (Olmstead et al., 2012; Blanchet et al., 2015). PF-429242 showed a similar inhibitory profile for DENV and ZIKV, causing a marked reduction in the number of LD and LD-positive areas and a significant reduction in the viral titer in all the treated cell lines (Hyrina et al., 2017; Raini et al., 2021). In accordance, the AM580 (a retinoic acid receptor α selective agonist) binds SREBP1/2, showing an antiviral effect against a wide range of viruses including ZIKV. AM580 would then block the interaction between SREBP and the sterol regulatory elements (SREs) of the genes involved in lipid biosynthesis. Therefore, gene transcription is inhibited, with the consequent inhibition of ZIKV replication (Yuan et al., 2019). In a follow-up study, a link between the SREBP pathway and the antiviral protein STING (stimulator of interferon (IFN) genes) was proposed in DENV infection (Liu et al., 2017). In that work, the protein SCAP (SREBP member) was shown to bind and block the DENV protease NS2B3, thus inhibiting the cleavage of STING and impairing DENV infection. Interestingly, the authors also found that the ectopic expression of SCAP inhibited DENV infection, whereas the knockdown of this protein did not cause any effect on DENV lifecycle (Liu et al., 2017).

In conclusion, these facts highlight the importance of SREBP upregulation in HCV and DENV/ZIKV replication. During these infections an extramembrane and LD requirement appears to be crucial for the viral lifecycle. However, a better understanding of this pathway is necessary to provide a more detailed description of the molecular interactions between LD and some *Flaviviridae* members.

Nuclear Lipid Droplets and HCV or the DENV/ZIKV Interaction May Contribute to the Viral Hijacking Process

Although initially LD were proposed to localize only to the cytoplasm of eukaryotic cells, later reports confirmed that these structures can also be found in the nucleus (nuclear lipid droplets, nLD). Nuclear LD are dynamic organelles storing neutral lipids originated from the inner nuclear membrane (INM). Nuclear LD have been proposed to act as an endonuclear buffer system, either providing or accepting lipids and proteins in different signaling pathways (Lagrutta et al., 2021). However, they can also be found attached to the INM in some processes by the transmembrane protein seipin (Romanauska and Kohler, 2018). Because nLDs have been described recently, very little is known about their role in the *Flaviviridae* replication cycle. Several studies indicate that HCV and DENV/ZIKV capsid and NS proteins may localize to the nucleus in infected cells (Majumder et al., 2001; Falcon et al., 2005; Netsawang et al., 2010; Garcia et al., 2020). It has been suggested that these viral proteins might interact with nLD, thus prolonging the interaction time and permanency with different host nuclear proteins. In turn, this phenomenon may allow an extended viral hijacking time of cellular metabolic pathways (Cloherty et al., 2020). In fact, recent publications suggest that the co-localization of nLD with *Flaviviridae* core proteins and the non-structural proteins NS5A (HCV) or NS5 (DENV/ZIKV) may represent a novel way to either induce (DENV/ZIKV) or inhibit (HCV) host cell apoptosis, as well as to create a link with viral release, carcinogenesis induction or impairment of the cellular interferon response (Ng et al., 2003; Herzer et al., 2005, Herzer et al., 2012; Heaton and Randall, 2010; Zhang and Wang, 2012; Liang et al., 2016; Wu et al., 2021).

Summarizing, the targeting of some *Flaviviridae* components to nLD may represent a novel understudied viral hijacking mechanism, in which apoptosis might also be involved. However, further studies assessing the interaction of nLD with *Flaviviridae* proteins may contribute to the understanding of the mechanisms by which viral infections progress to apoptosis, cancer or even steatosis in different cell types.

Role of Lipophagy During HCV and DENV/ZIKV Infection

According to many authors, lipophagy refers to the catabolic process by which internal cell lipids stored in LD can be directed

to lysosomes for final degradation by autophagy to release FA, and subsequently be processed via β-oxidation to provide energy for viral infection and replication processes (Singh et al., 2009). In fact, it has been reported that some of the *Flaviviridae* members may alter the autophagy degradative process to their advantage (Liang et al., 2016; Chan and Ou, 2017; Zhang et al., 2018). For instance, HCV, hijacks autophagy in order to promote the translation of its RNA and allow viral replication (Dreux et al., 2009). In addition, the proteins Beclin1and ATG7, involved in the autophagosome biogenesis, have been shown to be crucial for the release of mature HCV particles in Huh-7 infected cells, since the knocking down of Beclin1 or ATG7 causes a marked accumulation of HCV viral particles inside infected cells (Shrivastava et al., 2016). In a follow-up study, it was demonstrated that HCV infection upregulated autophagy at early steps of the infection cycle (Chan and Ou, 2017).

However, there are few studies showing contradictory results regarding how HCV may modulate lipophagy. On one hand, it has been reported that HCV core and NS5A proteins would generate LD aggregation (lipophagy inhibition), contributing to liver steatosis (fat accumulation) by a mechanism not fully understood (Mancone et al., 2011). Another study reported that the HCV core protein downregulates lipophagy in a model requiring DGAT1 for access to LD. Furthermore, the LD-localized core is consequently able to impair lipophagy, allowing LD accumulation and facilitating HCV assembly and steatosis (Harris et al., 2011). On the other hand, increased lipophagy was observed in HCV-infected HuH7 cells, suggesting a protective role for autophagy, as an inverse correlation between liver steatosis and lipophagy rates was found (Vescovo et al., 2012). Moreover, an induction of lipophagy during HCV infection is necessary and may contribute to the high ATP levels required for viral replication (Bose and Ray, 2014; Meyers et al., 2016).

Taken together, these findings allow hypothesizing the existence of an additional mechanism contributing to the release of HCV virions. This mechanism proposes the generation of extracellular LD (eLD) (positive for LC3) as a result of autophagy-mediated secretion. These eLD have been described to carry HCV infective RNA and HCV core and NS5A viral proteins. In fact, this mechanism may represent way to facilitate the spread of infectious HCV material from the host infected cell (Cloherty et al., 2020).

Several studies have confirmed that autophagy plays an important role in DENV/ZIKV infection; in fact, the blocking the autophagy pathway leads to a significant reduction in the viral replication rate (Heaton and Randall, 2010; Mateo et al., 2013; Jordan and Randall, 2017). In addition, an initial LD biogenesis upregulation has also been proposed, followed by an increase in lipophagy to drive virus production (Heaton and Randall, 2010; Cloherty et al., 2020). In this sense, a reduction in LD size was observed in DENV infected Huh-7.5 cells by electron microscopy (Heaton and Randall, 2010). Similar findings were reported in Huh-7 ZIKV infected cells in which a reduction in the LD numbers and total volume were observed, confirming an overall consumption of these organelles (Garcia et al., 2020). AUP1(ancient ubiquitous protein 1) is a multifunctional type III membrane protein that localizes predominantly to the ER and LD surface. AUP1 is involved in the LD accumulation and ER protein quality control, and has been proposed to act as a lipophagy-specific factor (Klemm et al., 2011). Specifically, DENV infection induces AUP1 deubiquitylation through a not fully understood mechanism. DENV NS4A and NS4B proteins bind and translocate AUP1 from the LD membrane to the LC3-decorated autophagosome surface, consequently upregulating lipophagy possibly through the AMPK/mTOR pathway (Randall, 2018; Wu et al., 2021). In this sense, the ZIKV proteins NS4A and NS4B have been found to bind and inhibit the Akt-mTOR pathway leading to lipophagy induction and defective neurogenesis in human neural stem cells (Liang et al., 2016). In addition, the knockout of AUP1 in HeLa and HepG2 cells leads to a decreased generation of infective DENV particles (Zhang et al., 2018).

It is suggested that eLD are also generated during DENV/ZIKV infection. In fact, it has been shown that cells infected by DENV/ZIKV were able to release LD inside secretory LC3-positive autophagosome structures, suggesting the existence of eLD originated from LD. Notably, DENV antigens, infective DENV RNA and LD have been found in secreted autophagosomes by Huh-7 infected cells (Wu et al., 2016). Besides, it has been hypothesized that for placental transmission. ZIKV would use a mechanism involving eLD through secretory autophagy (Zhang et al., 2016). Similarly, the bystander effect refers as a number of different not fully understood mechanisms allowing many viruses to establish intercellular communication in order to promote viral spreading (Palmer et al., 2005; Kofahi et al., 2016). In a recent study, an increase in the LD number and size in uninfected neighboring placental cells was found, suggesting a putative role for eLD bystander effect in the transmission of ZIKV infective components (Chen et al., 2020).

In summary, it is now clear that HCV and DENV/ZIKV take advantage of lipophagy as a source of energy for replication and for a possible extracellular spreading of the infective viral content through the generation of eLD. The detailed understanding of the molecular mechanism of lipophagy and its relationship with different *Flaviviridae* still needs further study and may set the scene for the development of novel antiviral treatments. All these evidences have been incorporated into **Figure 4**.

LIPID DROPLETS IN CANCER

In general, tumor cells are nutritionally challenged due to poor vascularization (Wellen and Thompson, 2010). Under deficient nutrient conditions, cells display a remarkable adaptability that is critical for survival, migration and invasion of other tissues (Pavlova and Thompson, 2016). In this context, tumor cells require energy suppliers to adapt to oxidative and nutritional stress conditions, allowing a rapid proliferation and progression of cancer. Lipids are an important energy reservoir that cancer cells can acquire from both exogenous and endogenous pools. Exogenous lipids are obtained from blood or from the tumoral microenvironment. On the other hand, the endogenous lipid availability depends on biosynthetic pathways, hydrolysis of

membrane PL, autophagy, and LD (Petan et al., 2018). In addition to the capacity to obtain extracellular lipids, cancer cells have an efficient machinery to recycle intracellular lipids, which gives them a significantly higher probability of survival during hypoxia and starvation (Petan et al., 2018). Actually, some aggressive types of tumors have an increased capacity to accumulate FA in LD to resist nutrient and oxidative stress (Kamphorst et al., 2013; Padanad et al., 2016; Jarc et al., 2018; Kim et al., 2018). LD accumulation has been observed in many cancer cells such as colorectal, breast, prostate, hepatocellular carcinoma, renal carcinoma, and glioblastoma, suggesting that this organelle serves as a substrate for cell survival when the glucose levels decrease [recently reviewed in (Li et al., 2020)].

Several works have suggested that the accumulation of LD has a pro-tumoral role acting as sites of PGE2 synthesis (a suppressant of the immune system), in the polarization of tumor-associated macrophages in myeloid-derived cells, and on the dysfunctional antigen presentation by dendritic cells [recently reviewed in (Cruz et al., 2020)]. Recent studies suggest that these organelles suppress nutrient and oxidative stress and contribute to cancer cell survival and growth, metastasis, and resistance to chemotherapeutic and pharmacological treatments (Przybytkowski et al., 2007; Pucer et al., 2013; Bensaad et al., 2014; Welte and Gould, 2017; Cotte et al., 2018; Henne et al., 2018; Jarc et al., 2018; Pizato et al., 2019), suggesting that an in-depth study of LD metabolism could be an attractive target for reducing cancer cell resistance to stress. For this reason, LD accumulation in non-adipose tissues has been proposed as a new hallmark of cancer (Cotte et al., 2018).

Lipid Droplet Biogenesis is Highly Regulated in Tumor Cells

Through tumorigenesis, cancer cells acquire different metabolic alterations to overcome the energetic requirement related to the accelerated proliferation under unfavorable conditions. Several studies have shown that some of these changes include the reprogramming of lipid metabolism such as *de novo* lipogenesis (Menendez and Lupu, 2007; Carracedo et al., 2013; Currie et al., 2013; Röhrig and Schulze, 2016). In contrast to normal cells, which preferentially use extracellular lipids for the synthesis of new structural lipids, cancer cells stimulate *de novo* FA synthesis to satisfy their requirements for lipids (Menendez and Lupu, 2007; Röhrig and Schulze, 2016). During *de novo* lipogenesis, saturated and monounsaturated FA are synthesized; nonetheless mammalian cells lack an enzyme capable of converting monounsaturated to polyunsaturated FA. This makes cancer cells more resistant to death from oxidative stress as well as drug therapy (Ameer et al., 2014). Even lipid-rich tumors have been associated with a high aggressive potential and an unfavorable clinical outcome (de Gonzalo-Calvo et al., 2015; Guillaumond et al., 2015).

As mentioned, SREBPs belong to a family of transcription factors bound to the ER membrane and, together with the mTOR, they act as key positive regulators of lipogenesis (Cruz et al., 2020). SREBPs have been shown to promote tumor growth as well as the accumulation of LD and the overexpression of the enzymes involved in lipogenesis. In addition, the SREBP cleavage-activating protein acts as a sensor for available glucose levels. It has been observed that the dysregulation of SREBPs occurs in several metabolic syndromes and cancers (Cheng et al., 2018). Moreover, SREBP as well as ATP Citrate Lyase (ACLY), a downstream target of SREBP, have been found to be upregulated in glioblastoma, colorectal cancer, breast cancer, non-small cell lung cancer, and hepatocellular carcinoma (de Gonzalo-Calvo et al., 2015; Guillaumond et al., 2015).

In mice with lung, prostate, or ovarian cancer xenografts, either the genetic or the pharmacological inhibition of SREBP and ACLY has been shown to significantly suppress tumor growth and induce cancer cell death (Hatzivassiliou et al., 2005; Hanai et al., 2013; Cheng et al., 2018), making SREBP and/or ACLY promising therapeutic targets (Infantino et al., 2007; Guo et al., 2009; Williams et al., 2013; Li et al., 2014; Geng et al., 2016). Interestingly, pre-clinical studies have demonstrated that some SREBP inhibitors such as fatostatin, botulin, and PF-429242 have promising anti-tumor effects (Kamisuki et al., 2009; Li et al., 2014, Li et al., 2015; Król et al., 2015; Gholkar et al., 2016; Shao et al., 2016). In addition, through the quantification of the mRNA expression levels, it has been demonstrated that LD coat proteins (PLIN) (Wang et al., 2018) and FA-binding proteins (FABP) are also involved in the regulation of LD formation and trafficking in cancer cells (Senga et al., 2018).

On the other hand, mTOR acts as a detector for the availability of extracellular nutrients, stimulating the activation of anabolic pathways such as protein translation and nucleotide synthesis. The PI3K/AKT/mTOR pathway regulates SREBP levels by promoting the synthesis of FA, cholesterol, and glycerolipids and is associated with an increase in the density of LD in tumor cells (Petan et al., 2018; Li et al., 2020).

Moreover, during starvation, the mTOR pathway is inhibited and the cell resorts to autophagy as a mechanism for the degradation of cytosolic components and membranous organelles to obtain FA available for LD biogenesis (Petan et al., 2018).

Under excess conditions, intracellular lipids are converted to TAG and SE in the ER, leading to the formation of LD (Fei et al., 2011; Walther and Farese, 2012). These structures have been visualized in several types of tumors including glioblastoma, renal clear cell carcinoma, and prostate, colon, or pancreas cancer (Accioly et al., 2008; Yue et al., 2014; Geng et al., 2016; Koizume and Miyagi, 2016). While in normal tissues SE are usually undetectable, they are abundant in the tumor tissue (Bemlih et al., 2010). Sterol *O*-acyltransferase 1 (SOAT1), also known as acyl-CoA acyltransferase 1 (ACAT1), converts cholesterol to SE for storage in LD. Interestingly, glioblastomas and prostate and pancreas cancers express high levels of this enzyme, being its expression level inversely correlated with patient survival (Bemlih et al., 2010; Saraon et al., 2014; Ohmoto et al., 2015; Geng et al., 2016, Geng et al., 2020; LaPensee et al., 2016; Li et al., 2016). The genetic silencing of SOAT1/ACAT1 or the pharmacologic blocking of its activity suppresses tumor growth in several cancer xenograft models (Bemlih et al., 2010; Ohmoto et al., 2015; Geng et al., 2016; LaPensee et al., 2016). These results suggest that SOAT1 and the synthesis of SE are two possible targets in the development of antitumor strategies.

Colorectal cancer (CRC) is one of the most common forms of cancer, in which the accumulation of LD appears to be a common

feature (Tirinato et al., 2015; Kawasaki et al., 2017). The binding of the epidermal growth factor (EGF) to its receptor induces its activation, enabling downstream signaling pathways, including the PI3K/mTOR pathway, to induce cell proliferation and tumorigenesis, promoting the synthesis and accumulation of LD (Guri et al., 2017). Some authors postulate the existence of a negative regulatory loop between LD, the forkhead box transcription factor O-3 (FOXO3), and sirtuin 6 (a negative regulator of lipid biosynthesis) since the silencing of FOXO3 would promote the down-regulation of sirtuin 6 to increase LD levels (Penrose et al., 2016).

Breast cancer (BC) is the leading cause of cancer-associated death in women and the most common cancer worldwide (Bray et al., 2015). Several epidemiological studies have revealed that adipose tissue dysfunction appears to be one of the risk factors that contributes to the development and progression of BC. Given that aggressive BC cells have been shown to have a higher number of LD, and that obesity is a risk factor for breast cancer, some authors suggested an association between the alteration of LD homeostasis of the cancer cells and obesity (Wölwer et al., 2016; Blücher and Stadler, 2017).

Prostate cancer (PC) is the second leading cause of cancer-related death in men (Boettcher et al., 2019). PC cells can incorporate either circulating lipids or lipids from the adipose microenvironment to promote PC invasiveness through oxidative stress and the secretion of the hypoxia-inducible factor 1α (HIF-1α) (Diedrich et al., 2016; Victor, 2019). On the other hand, the *de novo* lipogenesis is also upregulated in PC cells and its inhibition suppresses PC growth both *in vitro* and *in vivo* (Yoshii et al., 2013). Cancer aggressiveness is positively correlated with LD density and LD movement speed during the transport of cargo proteins along microtubules (Yue et al., 2014). In addition, it has recently been described that autophagy and lipophagy are also associated with the aggressiveness and progression of PC, possibly through a mechanism that leads to the exploitation of a lipid-rich microenvironment by tumor cells (Panda et al., 2020).

Hepatocellular carcinoma (HCC) is the most common and aggressive liver cancer. One of the main pathological features of HCC is steatosis, which generally leads to an increase in the number of LD. PTEN (the phosphatase and tensin homologue on chromosome ten) has also been shown to be a negative regulator of the PI3K/AKT pathway and a classic tumor gene suppressor due to its lipid and protein phosphatase activity. The deletion of PTEN along with the overexpression of the *NRAS* proto-oncogene (RAS neuroblastoma) synergistically leads to a metabolic disorder that increases the LD content and promotes the appearance of HCC (Gao and Liu, 2017). Therefore, the accumulation of LD induced by the activation of oncogenic pathways could contribute to the development and progression of HCC. On the other hand, it is well known that SREBP1 plays a fundamental role in the progression of HCC as it promotes cancer cell growth and metastasis. It has recently been shown that Acyl-CoA Synthetase Long Chain 4 (ACSL4) enhances the expression of lipogenic enzymes through the *c-Myc/SREBP1* oncogene signaling; however more studies are needed to determine the association between ACSL4, metabolism and tumor lipid abnormalities (Chen et al., 2021).

Renal cell carcinoma (RCC) is one of the most common malignant tumors of the urinary system (Dutta et al., 2016). Among them, clear cell RCC (ccRCC) is the most common RCC subtype featured by an accumulation of LD. This carcinoma has a high risk of metastasis and a poor response to radiotherapy and chemotherapy (Gong et al., 2016). Patients with ccRCC display a high expression of PLIN3, and this phenomenon is closely correlated with clinicopathological features. Furthermore, the high expression of PLIN3 suggests a poor clinical prognosis (Wang et al., 2018). On the other hand, HIF2α promotes lipid storage, ER homeostasis, and cell viability in ccRCC through upregulation of the LD PLIN2 envelope protein. In conclusion, the study of the members of the perilipins family and the possible suppression of HIF2α/PLIN2 could be a useful tool for the development of therapeutic strategies in this common renal malignant neoplasm.

Glioblastoma (GBM) is a malignant tumor with lipid metabolism dysfunction (Guo et al., 2013; Cheng et al., 2015). Large amounts of LD are observed in tumor tissues of GBM patients that are not detectable in low-grade gliomas (Geng et al., 2016). Therefore, LD could be used as a diagnostic biomarker for GBM. When glucose supply decreases in GBM cells, LD are hydrolyzed by autophagy, thus explaining the survival of GBM cells in situations of energy stress (Geng et al., 2020). In addition, SREBP-1 has a high activity in GBM (Guo et al., 2011). The inhibition of SOAT1 down-regulates SREBP-1, resulting in a decrease in SE synthesis. Meanwhile, SOAT1 suppression reduces LD formation and consequently blocks GBM growth (Geng et al., 2016). Therefore, blocking the degradation of LD or the SREBP1/SOAT1 pathway would be a suitable therapeutic strategy to increase the sensitivity of GBM to treatments and overcome resistance.

To summarize, the accumulation of LD in cancer cells depends on the activation of SREBP and mTOR pathways, suggesting that both pathways are important in cancer development and progression.

Lipolysis and Lipophagy in Cancer

As mentioned above, the energy demand can drive the degradation of accumulated LD in the cell, mainly by two mechanisms, lipolysis or lipophagy. Although several authors have shown that lipophagy has pro-tumoral effects (Kaini et al., 2012; Assumpção et al., 2017), most studies performed so far suggest that lipophagy restricts tumorigenesis (Xu et al., 2016; Mukhopadhyay et al., 2017). Moreover, it has been shown that the overexpression of ATG14, a member of the ATG proteins, induces LD breakdown in Hela cells (a cervical cancer cell line) and stimulates free FA accumulation. This process leads to ER stress and reactive oxygen species-mediated apoptosis, whereas the inhibition of lipophagy or the inhibition of lysosomal acid lipases (LAL) reverts these effects (Mukhopadhyay et al., 2017). LAL plays a tumor suppressor role and its deficiency in mice has been linked with spontaneous tumorigenesis. In contrast, the re-expression of LAL prevents liver metastases (Du et al., 2015) and reduces inflammation and metastasis in lung cancer (Zhao et al., 2016). On the other hand, it has been shown that when autophagy is inhibited in adipocytes, LD clearance is slowed down and consequently the effects that promote adipocyte growth are

attenuated. In other words, in this cell type, lipophagy is activated in order to promote the production of energy and the survival of cancer cells (Petan et al., 2018). It has been demonstrated that abhydrolase domain-containing protein 5, a cellular lipolytic activator, which functions as a tumor suppressor in CRC, binds and prevents the cleavage of the essential autophagy regulator beclin 1, thus stimulating autophagy, reducing colon cancer tumorigenesis (Peng et al., 2016). Additionally, it has been demonstrated that ATGL promotes the autophagic flux and the interactions between LC3 and LD (Drizyte-Miller et al., 2020). In turn, LC3 depletion results in reduced LD accumulation in various cancer cell lines such as HeLa, HepG2, and PC12 (Shibata et al., 2010). Together, these results suggest an important role for LC3 in the formation of LD. Interestingly, rapamycin-induced autophagy leads to TAG synthesis in yeast (Madeira et al., 2015), and autophagy is necessary for TAG accumulation under nitrogen-deprived conditions in this microorganism. In conclusion, autophagy-driven LD synthesis is helpful for the progression of a variety of cancer cells. Further studies should confirm whether LD biogenesis is a protective response to high levels of autophagy. All these evidences have been incorporated into **Figure 5**.

CONCLUDING REMARKS

As mentioned, the biology of LD has recently received the attention of multiple research fields, opening a wide window of knowledge in science. Given that LD are conserved structures in prokaryotic and eukaryotic cells (Walther et al., 2017; Zhang and Liu, 2017; Lupette and Maréchal, 2020), a role in every studied biological process should not be surprising. Pathogen invasion, as well as the unlimited proliferation of cancer cells, are processes that impose a huge cellular remodeling, with a consequent energy demand satisfied by LD metabolism.

In general, studies describing LD changes during infections and cancer focus on metabolic aspects and organelle patterns at the cellular level (LD size and number) associated with different disease stages. The bridge between these approaches is currently being disentangled as considerable advances have been done in the study of the LD biogenesis and degradation processes. Some of these metabolic aspects are: 1) the increase in TAG levels, which leads to an increase of DGAT activity (parasitic protozoans), *de novo* FA synthesis, (e.g., SREBP upregulation in HCV and DENV/ZIKV replication and cancer cells), and increase in FA uptake (cancer cells), and 2) the free cholesterol/SE balance, which is modulated by SREBP (cancer) or aspartyl-like peptidase (e.g., *T. cruzi*) and the enzyme ACAT, which might display a key role in the parasite's survival (e.g., *T. gondii*).

In cancer cells, *de novo* lipogenesis enhancement leads to the generation of cell membranes that are enriched in saturated and/or mono-unsaturated FA (as polyunsaturated FAs cannot be synthesized by this pathway) (Ameer et al., 2014). In turn, NL saturation has been observed to respond to demands of unsaturated species in the cell (providing a homeostasis mechanism of membrane saturation by "buffering" specific FA). For instance, the TAG saturation index increases as a consequence of the liberation of unsaturated FA to counteract their esterification and transformation into phospholipids when cancer cells are subjected to nutrient stress (Lisec et al., 2019) or inhibition of the *de novo* desaturation pathway through hypoxia (Ackerman et al., 2018).

Tumor tissues contain abnormal levels of SE (Nygren et al., 2009; Bemlih et al., 2010). In *T. cruzi*, the cholesterol content variation leads to morphological changes (on both reservosomes and cytosolic LD) arising from NL crystallization in the core of these structures. This suggests that significant biophysical differences between the stages of LD biogenesis as well as on protein targeting to LD surface could be taking place. The latter findings deserve further exploration. The requirement of sterols for the coordinated assembly of LD seems to be universal. Recently, this aspect has been studied in *Arabidopsis* developing seeds to find that the mutations of proteins of the sterol pathway account for the different LD number, size and oil content phenotypes (Yu et al., 2021) and some interesting comparisons with cholesterol effects arise. For instance, cholesterol generates lipid packing defects and increases the surface tension of membranes synergistically with DAG (Coorssen and Rand, 2011; Alwarawrah et al., 2012; Subczynski et al., 2017), which has been suggested to be critical for neutral lipid nucleation and LD budding (Adeyo et al., 2011; Choudhary et al., 2018). In this sense, in a study that combined molecular simulations, yeast genetics, and fluorescence microscopy (Zoni et al., 2021), it has been recently demonstrated that cholesterol promotes LD nucleation and the packaging of TG into LD.

Taking into account the above considerations, current experimental models using biophysical approaches may help address the following questions that arise from metabolic observations: how NL composition (cholesterol:cholesterol-esters:triglyceride proportions) affect the biogenesis process? How do properties (unsaturation and carbon length) of FA constituting neutral lipids affect biogenesis?

Regarding protein targeting to LD, a putative effect of the LD core composition has also been considered. The interaction of amphipatic helices (AH) to LD model surface was sensitive to the core composition (Dhiman et al., 2020). Surprisingly, this effect was independent of the phospholipid monolayer packing. On the other hand, cholesterol has been demonstrated to affect the physical properties of the LD surface and hence the targeting of TG-synthesizing enzymes to LD (Wilfling et al., 2014). In this sense, PLIN4 has served as an interesting model protein due to its exceptional length and repetitiveness that confers it versatility to compensate between those properties (AH length, hydrophobicity, and charge) targeting it to the LD surface, although with a loss of specificity (Čopič et al., 2018). How changes in the NL composition of LD, promoted in infections and cancer, can impact on their interaction with AH containing proteins remains to be assessed.

Finally, LD degradation helps cells coping with the high energy demands in pathological processes; therefore, this process could serve as a target for the development of novel therapeutic approaches.

AUTHOR CONTRIBUTIONS

CK and PR contributed to the manuscript writing and supervising it. CV, JJ, and CP were contributors. LD had the idea and coordinated the whole work, together with BC.

FUNDING

This work was financed by grants from CONICET (PIP 11220200101585CO to C.F.K. and 11220200103139CO to L.R.D. and PUE 2016-22920160100059). All authors are Research Career Members from CONICET.

REFERENCES

Abbasi Fard, S., Khajeh, A., Khosravi, A., Mirshekar, A., Masoumi, S., Tabasi, F., et al. (2020). Fulminant and Diffuse Cerebral Toxoplasmosis as the First Manifestation of Hiv Infection: A Case Presentation and Review of the Literature. *Am. J. Case Rep.* 21, 1. doi:10.12659/AJCR.919624

Accioly, M. T., Pacheco, P., Maya-Monteiro, C. M., Carrossini, N., Robbs, B. K., Oliveira, S. S., et al. (2008). Lipid Bodies Are Reservoirs of Cyclooxygenase-2 and Sites of Prostaglandin-E2Synthesis in Colon Cancer Cells. *Cancer Res.* 68, 1732–1740. doi:10.1158/0008-5472.CAN-07-1999

Ackerman, D., Tumanov, S., Qiu, B., Michalopoulou, E., Spata, M., Azzam, A., et al. (2018). Triglycerides Promote Lipid Homeostasis during Hypoxic Stress by Balancing Fatty Acid Saturation. *Cell Rep.* 24, 2596–2605. e5. doi:10.1016/J.CELREP.2018.08.015

Adeyo, O., Horn, P. J., Lee, S., Binns, D. D., Chandrahas, A., Chapman, K. D., et al. (2011). The Yeast Lipin Orthologue Pah1p Is Important for Biogenesis of Lipid Droplets. *J. Cell Biol.* 192, 1043–1055. doi:10.1083/JCB.201010111/VIDEO-2

Allmann, S., Mazet, M., Ziebart, N., Bouyssou, G., Fouillen, L., Dupuy, J.-W., et al. (2014). Triacylglycerol Storage in Lipid Droplets in Procyclic Trypanosoma Brucei. *PLoS One* 9, e114628. doi:10.1371/journal.pone.0114628

Almeida, P. E. d., Toledo, D. A. M., Rodrigues, G. S. C., and D'Avila, H. (2018). Lipid Bodies as Sites of Prostaglandin E2 Synthesis during Chagas Disease: Impact in the Parasite Escape Mechanism. *Front. Microbiol.* 9, 1. doi:10.3389/fmicb.2018.00499

Alwarawrah, M., Dai, J., and Huang, J. (2012). Modification of Lipid Bilayer Structure by Diacylglycerol: A Comparative Study of Diacylglycerol and Cholesterol. *J. Chem. Theor. Comput.* 8, 749–758. doi:10.1021/ct200790q

Ameer, F., Scandiuzzi, L., Hasnain, S., Kalbacher, H., and Zaidi, N. (2014). De Novo lipogenesis in Health and Disease. *Metabolism* 63, 895–902. doi:10.1016/J.METABOL.2014.04.003

Araújo-Santos, T., Prates, D. B., França-Costa, J., Luz, N. F., Andrade, B. B., Miranda, J. C., et al. (2014). Prostaglandin E2/Leukotriene B4 Balance Induced by Lutzomyia Longipalpis Saliva Favors Leishmania Infantum Infection. *Parasites Vectors* 7, 1. doi:10.1186/s13071-014-0601-8

Assumpção, J. A. F., Magalhães, K. G., and Corrêa, J. R. (2017). The Role of Pparγ and Autophagy in Ros Production, Lipid Droplets Biogenesis and its Involvement with Colorectal Cancer Cells Modulation. *Cancer Cell Int* 17, 1–12. doi:10.1186/s12935-017-0451-5

Attias, M., Teixeira, D. E., Benchimol, M., Vommaro, R. C., Crepaldi, P. H., and De Souza, W. (2020). The Life-Cycle of Toxoplasma Gondii Reviewed Using Animations. *Parasites Vectors* 13, 1. doi:10.1186/s13071-020-04445-z

Becuwe, M., Bond, L. M., Pinto, A. F. M., Boland, S., Mejhert, N., Elliott, S. D., et al. (2020). FIT2 Is an Acyl-Coenzyme A Diphosphatase Crucial for Endoplasmic Reticulum Homeostasis. *J. Cell Biol.* 219, 1. doi:10.1083/JCB.202006111

Beller, M., Herker, E., and Füllekrug, J. (2020). Grease On-Perspectives in Lipid Droplet Biology. *Semin. Cell Dev. Biol.* 108, 94–101. doi:10.1016/J.SEMCDB.2020.06.017

Bemlih, S., Poirier, M.-D., and Andaloussi, A. E. (2010). Acyl-coenzyme A: Cholesterol Acyltransferase Inhibitor Avasimibe Affect Survival and Proliferation of Glioma Tumor Cell Lines. *Cancer Biol. Ther.* 9, 1025–1032. doi:10.4161/cbt.9.12.11875

Ben M'barek, K., Ajjaji, D., Chorlay, A., Vanni, S., Forêt, L., and Thiam, A. R. (2017). ER Membrane Phospholipids and Surface Tension Control Cellular Lipid Droplet Formation. *Dev. Cell* 41, 591–604. e7. doi:10.1016/J.DEVCEL.2017.05.012

Bensaad, K., Favaro, E., Lewis, C. A., Peck, B., Lord, S., Collins, J. M., et al. (2014). Fatty Acid Uptake and Lipid Storage Induced by HIF-1α Contribute to Cell Growth and Survival after Hypoxia-Reoxygenation. *Cell Rep.* 9, 349–365. doi:10.1016/j.celrep.2014.08.056

Bickel, P. E., Tansey, J. T., and Welte, M. A. (2009). PAT Proteins, an Ancient Family of Lipid Droplet Proteins that Regulate Cellular Lipid Stores. *Biochim. Biophys. Acta (Bba) - Mol. Cell Biol. Lipids* 1791, 419–440. doi:10.1016/j.bbalip.2009.04.002

Blanchet, M., Sureau, C., Guévin, C., Seidah, N. G., and Labonté, P. (2015). SKI-1/S1P Inhibitor PF-429242 Impairs the Onset of HCV Infection. *Antiviral Res.* 115, 94–104. doi:10.1016/j.antiviral.2014.12.017

Blücher, C., and Stadler, S. C. (2017). Obesity and Breast Cancer: Current Insights on the Role of Fatty Acids and Lipid Metabolism in Promoting Breast Cancer Growth and Progression. *Front. Endocrinol.* 8, 1–7. doi:10.3389/fendo.2017.00293

Boettcher, A. N., Usman, A., Morgans, A., VanderWeele, D. J., Sosman, J., and Wu, J. D. (2019). Past, Current, and Future of Immunotherapies for Prostate Cancer. *Front. Oncol.* 9, 1–12. doi:10.3389/fonc.2019.00884

Bose, S. K., and Ray, R. (2014). Hepatitis C Virus Infection and Insulin Resistance. *Wjd* 5, 52–58. doi:10.4239/wjd.v5.i1.52

Brasaemle, D. L. (2013). Perilipin 5: Putting the Brakes on Lipolysis. *J. Lipid Res.* 54, 876–877. doi:10.1194/JLR.E036962

Brasaemle, D. L., and Wolins, N. E. (2012). Packaging of Fat: An Evolving Model of Lipid Droplet Assembly and Expansion. *J. Biol. Chem.* 287, 2273–2279. doi:10.1074/JBC.R111.309088

Bray, F., Ferlay, J., Laversanne, M., Brewster, D. H., Gombe Mbalawa, C., Kohler, B., et al. (2015). Cancer Incidence in Five Continents: Inclusion Criteria, Highlights from Volume X and the Global Status of Cancer Registration. *Int. J. Cancer* 137, 2060–2071. doi:10.1002/ijc.29670

Carmona-Gutierrez, D., Zimmermann, A., and Madeo, F. (2015). A Molecular Mechanism for Lipophagy Regulation in the Liver. *Hepatology* 61, 1781–1783. doi:10.1002/HEP.27738

Carracedo, A., Cantley, L. C., and Pandolfi, P. P. (2013). Cancer Metabolism: Fatty Acid Oxidation in the Limelight. *Nat. Rev. Cancer* 13, 227–232. doi:10.1038/nrc3483

Cartwright, B. R., Binns, D. D., Hilton, C. L., Han, S., Gao, Q., and Goodman, J. M. (2015). Seipin Performs Dissectible Functions in Promoting Lipid Droplet Biogenesis and Regulating Droplet Morphology. *MBoC* 26, 726–739. doi:10.1091/MBC.E14-08-1303

Caruso, B., Wilke, N., and Perillo, M. A. (2021). Triglyceride Lenses at the Air-Water Interface as a Model System for Studying the Initial Stage in the Biogenesis of Lipid Droplets. *Langmuir* 37, 10958–10970. doi:10.1021/ACS.LANGMUIR.1C01359

Chan, S., and Ou, J.-h. (2017). Hepatitis C Virus-Induced Autophagy and Host Innate Immune Response. *Viruses* 9, 224. doi:10.3390/v9080224

Chapman, K. D., Aziz, M., Dyer, J. M., and Mullen, R. T. (2019). Mechanisms of Lipid Droplet Biogenesis. *Biochem. J.* 476, 1929–1942. doi:10.1042/BCJ20180021

Chen, F., Yan, B., Ren, J., Lyu, R., Wu, Y., Guo, Y., et al. (2021a). FIT2 Organizes Lipid Droplet Biogenesis with ER Tubule-Forming Proteins and Septins. *J. Cell Biol.* 220, 1. doi:10.1083/JCB.201907183/VIDEO-4

Chen, J., Ding, C., Chen, Y., Hu, W., Yu, C., Peng, C., et al. (2021b). ACSL4 Reprograms Fatty Acid Metabolism in Hepatocellular Carcinoma via C-Myc/SREBP1 Pathway. *Cancer Lett.* 502, 154–165. doi:10.1016/j.canlet.2020.12.019

Chen, Q., Gouilly, J., Ferrat, Y. J., Espino, A., Glaziou, Q., Cartron, G., et al. (2020). Metabolic Reprogramming by Zika Virus Provokes Inflammation in Human Placenta. *Nat. Commun.* 11, 2967. doi:10.1038/s41467-020-16754-z

Cheng, C., Geng, F., Cheng, X., and Guo, D. (2018). Lipid Metabolism Reprogramming and its Potential Targets in Cancer. *Cancer Commun.* 38, 27. doi:10.1186/s40880-018-0301-4

Cheng, C., Ru, P., Geng, F., Liu, J., Yoo, J. Y., Wu, X., et al. (2015). Glucose-Mediated N-Glycosylation of SCAP Is Essential for SREBP-1 Activation and Tumor Growth. *Cancer Cell* 28, 569–581. doi:10.1016/j.ccell.2015.09.021

Chorlay, A., and Thiam, A. R. (2018). An Asymmetry in Monolayer Tension Regulates Lipid Droplet Budding Direction. *Biophysical J.* 114, 631–640. doi:10.1016/J.BPJ.2017.12.014

Choudhary, V., Golani, G., Joshi, A. S., Cottier, S., Schneiter, R., Prinz, W. A., et al. (2018). Architecture of Lipid Droplets in Endoplasmic Reticulum Is Determined by Phospholipid Intrinsic Curvature. *Curr. Biol.* 28, 915–926. e9. doi:10.1016/J.CUB.2018.02.020

Cloherty, A. P. M., Olmstead, A. D., Ribeiro, C. M. S., and Jean, F. (2020). Hijacking of Lipid Droplets by Hepatitis C, Dengue and Zika Viruses-From Viral Protein Moonlighting to Extracellular Release. *Ijms* 21, 7901. doi:10.3390/ijms21217901

Coorssen, J. R., and Rand, R. P. (1990). Effects of Cholesterol on the Structural Transitions Induced by Diacylglycerol in Phosphatidylcholine and Phosphatidylethanolamine Bilayer Systems. *Biochem. Cell Biol.* 68, 65–69. doi:10.1139/O90-008

Čopič, A., Antoine-Bally, S., Giménez-Andrés, M., La Torre Garay, C., Antonny, B., Manni, M. M., et al. (20182018). A Giant Amphipathic helix from a Perilipin that Is Adapted for Coating Lipid Droplets. *Nat. Commun.* 9 (9), 1–16. doi:10.1038/s41467-018-03717-8

Coppens, I., Levade, T., and Courtoy, P. J. (1995). Host Plasma Low Density Lipoprotein Particles as an Essential Source of Lipids for the Bloodstream Forms of Trypanosoma Brucei. *J. Biol. Chem.* 270, 5736–5741. doi:10.1074/jbc.270.11.5736

Corey, K. E., Kane, E., Munroe, C., Barlow, L. L., Zheng, H., and Chung, R. T. (2009). Hepatitis C Virus Infection and its Clearance Alter Circulating Lipids: Implications for Long-Term Follow-Up. *Hepatology* 50, 1030–1037. doi:10.1002/hep.23219

Corvalán, N. A., and Perillo, M. A. (2020). Probing Thermotropic Phase Behavior of Dipalmitoylphosphatidylcholine Bilayers from Electrical and Topographic Data in a Horizontal Black Lipid Membrane Model. *Langmuir* 36, 1083–1093. doi:10.1021/ACS.LANGMUIR.9B02854

Cotte, A. K., Aires, V., Fredon, M., Limagne, E., Derangère, V., Thibaudin, M., et al. (2018). Lysophosphatidylcholine Acyltransferase 2-mediated Lipid Droplet Production Supports Colorectal Cancer Chemoresistance. *Nat. Commun.* 9. doi:10.1038/s41467-017-02732-5

Cruz, A. L. S., Barreto, E. d. A., Fazolini, N. P. B., Viola, J. P. B., and Bozza, P. T. (2020). Lipid Droplets: Platforms with Multiple Functions in Cancer Hallmarks. *Cell Death Dis* 11, 1. doi:10.1038/s41419-020-2297-3

Cunha-e-Silva, N. L., Atella, G. C., Porto-Carreiro, I. A., Morgado-Diaz, J. A., Pereira, M. G., and Souza, W. (2002). Isolation and Characterization of a Reservosome Fraction fromTrypanosoma Cruzi. *FEMS Microbiol. Lett.* 214, 7–12. doi:10.1111/j.1574-6968.2002.tb11317.x

Currie, E., Schulze, A., Zechner, R., Walther, T. C., and Farese, R. V. (2013). Cellular Fatty Acid Metabolism and Cancer. *Cell Metab.* 18, 153–161. doi:10.1016/j.cmet.2013.05.017

D'Andrea, S. (2016). Lipid Droplet Mobilization: The Different Ways to Loosen the Purse Strings. *Biochimie* 120, 17–27. doi:10.1016/j.biochi.2015.07.010

D'Avila, H., Toledo, D. A. M., and Melo, R. C. N. (2012). Lipid Bodies: Inflammatory Organelles Implicated in Host-Trypanosoma cruziInterplay during Innate Immune Responses. *Mediators Inflamm.* 2012, 1–11. doi:10.1155/2012/478601

D'Avila, H., Freire-de-Lima, C. G., Roque, N. R., Teixeira, L., Barja-Fidalgo, C., Silva, A. R., et al. (2011). Host Cell Lipid Bodies Triggered by Trypanosoma Cruzi Infection and Enhanced by the Uptake of Apoptotic Cells Are Associated with Prostaglandin E2 Generation and Increased Parasite Growth. *J. Infect. Dis.* 204, 951–961. doi:10.1093/INFDIS/JIR432

Dawoody Nejad, L., Serricchio, M., Jelk, J., Hemphill, A., and Bütikofer, P. (2018). TbLpn, a Key Enzyme in Lipid Droplet Formation and Phospholipid Metabolism, Is Essential for Mitochondrial Integrity and Growth ofTrypanosoma Brucei. *Mol. Microbiol.* 109, 105–120. doi:10.1111/mmi.13976

De Cicco, N. N. T., Pereira, M. G., Corrêa, J. R., Andrade-Neto, V. V., Saraiva, F. B., Chagas-Lima, A. C., et al. (2012). LDL Uptake by Leishmania Amazonensis: Involvement of Membrane Lipid Microdomains. *Exp. Parasitol.* 130, 330–340. doi:10.1016/j.exppara.2012.02.014

de Gonzalo-Calvo, D., López-Vilaró, L., Nasarre, L., Perez-Olabarria, M., Vázquez, T., Escuin, D., et al. (2015). Intratumor Cholesteryl Ester Accumulation Is Associated with Human Breast Cancer Proliferation and Aggressive Potential: A Molecular and Clinicopathological Study. *BMC Cancer* 15, 1. doi:10.1186/s12885-015-1469-5

den Brok, M. H., Raaijmakers, T. K., Collado-Camps, E., and Adema, G. J. (2018). Lipid Droplets as Immune Modulators in Myeloid Cells. *Trends Immunol.* 39, 380–392. doi:10.1016/J.IT.2018.01.012

Deslandes, F., Thiam, A. R., and Forêt, L. (2017). Lipid Droplets Can Spontaneously Bud off from a Symmetric Bilayer. *Biophysical J.* 113, 15–18. doi:10.1016/J.BPJ.2017.05.045

Dhiman, R., Caesar, S., Thiam, A. R., and Schrul, B. (2020). Mechanisms of Protein Targeting to Lipid Droplets: A Unified Cell Biological and Biophysical Perspective. *Semin. Cell Dev. Biol.* 108, 4–13. doi:10.1016/J.SEMCDB.2020.03.004

Diedrich, J. D., Rajagurubandara, E., Herroon, M. K., Mahapatra, G., Hüttemann, M., and Podgorski, I. (2016). Bone Marrow Adipocytes Promote the Warburg Phenotype in Metastatic Prostate Tumors via HIF-1α Activation. *Oncotarget* 7, 64854–64877. doi:10.18632/oncotarget.11712

Dreux, M., Gastaminza, P., Wieland, S. F., and Chisari, F. V. (2009). The Autophagy Machinery Is Required to Initiate Hepatitis C Virus Replication. *Proc. Natl. Acad. Sci.* 106, 14046–14051. doi:10.1073/pnas.0907344106

Drizyte-Miller, K., Schott, M. B., and McNiven, M. A. (2020). Lipid Droplet Contacts with Autophagosomes, Lysosomes, and Other Degradative Vesicles. *Contact* 3, 251525642091089. doi:10.1177/2515256420910892

Du, H., Zhao, T., Ding, X., and Yan, C. (2015). Hepatocyte-Specific Expression of Human Lysosome Acid Lipase Corrects Liver Inflammation and Tumor Metastasis in Lal Mice. *Am. J. Pathol.* 185, 2379–2389. doi:10.1016/j.ajpath.2015.05.021

Duelund, L., Jensen, G. V., Hannibal-Bach, H. K., Ejsing, C. S., Pedersen, J. S., Pakkanen, K. I., et al. (2013). Composition, Structure and Properties of POPC-Triolein Mixtures. Evidence of Triglyceride Domains in Phospholipid Bilayers. *Biochim. Biophys. Acta (Bba) - Biomembranes* 1828, 1909–1917. doi:10.1016/J.BBAMEM.2013.03.020

Dutta, P., Haller, E., Sharp, A., and Nanjundan, M. (2016). MIR494 Reduces Renal Cancer Cell Survival Coinciding with Increased Lipid Droplets and Mitochondrial Changes. *BMC Cancer* 16, 1–14. doi:10.1186/s12885-016-2053-3

Eberlé, D., Hegarty, B., Bossard, P., Ferré, P., and Foufelle, F. (2004). SREBP Transcription Factors: Master Regulators of Lipid Homeostasis. *Biochimie* 86, 839–848. doi:10.1016/j.biochi.2004.09.018

Falcón, V., Acosta-Rivero, N., Shibayama, M., Chinea, G., Gavilondo, J. V., de la Rosa, M. C., et al. (2005). HCV Core Protein Localizes in the Nuclei of Nonparenchymal Liver Cells from Chronically HCV-Infected Patients. *Biochem. Biophysical Res. Commun.* 329, 1320–1328. doi:10.1016/j.bbrc.2005.02.107

Farese, R. V., and Walther, T. C. (2009). Lipid Droplets Finally Get a Little R-E-S-P-E-C-T. *Cell* 139, 855–860. doi:10.1016/J.CELL.2009.11.005

Fei, W., Shui, G., Zhang, Y., Krahmer, N., Ferguson, C., Kapterian, T. S., et al. (2011). A Role for Phosphatidic Acid in the Formation of "Supersized" Lipid Droplets. *Plos Genet.* 7, e1002201. doi:10.1371/journal.pgen.1002201

Filali-Mouncef, Y., Hunter, C., Roccio, F., Zagkou, S., Dupont, N., Primard, C., et al. (2021). The ménage à trois of autophagy, lipid droplets and liver disease. *Autophagy* 2021, 1–24. doi:10.1080/15548627.2021.1895658

Filipe, A., and McLauchlan, J. (2015). Hepatitis C Virus and Lipid Droplets: Finding a Niche. *Trends Mol. Med.* 21, 34–42. doi:10.1016/j.molmed.2014.11.003

Flaspohler, J. A., Jensen, B. C., Saveria, T., Kifer, C. T., and Parsons, M. (2010). A Novel Protein Kinase Localized to Lipid Droplets Is Required for Droplet Biogenesis in Trypanosomes. *Eukaryot. Cell* 9, 1702–1710. doi:10.1128/EC.00106-10

Gao, M., and Liu, D. (2017). CRISPR/Cas9-based Pten Knock-Out and Sleeping Beauty Transposon-Mediated Nras Knock-In Induces Hepatocellular Carcinoma and Hepatic Lipid Accumulation in Mice. *Cancer Biol. Ther.* 18, 505–512. doi:10.1080/15384047.2017.1323597

Gao, Q., and Goodman, J. M. (2015). The Lipid Droplet-A Well-Connected Organelle. *Front. Cell Dev. Biol.* 3, 1. doi:10.3389/FCELL.2015.00049

García, C. C., Vázquez, C. A., Giovannoni, F., Russo, C. A., Cordo, S. M., Alaimo, A., et al. (2020). Cellular Organelles Reorganization during Zika Virus Infection of Human Cells. *Front. Microbiol.* 11, 1558. doi:10.3389/fmicb.2020.01558

Gatica, D., Lahiri, V., and Klionsky, D. J. (2018). Cargo Recognition and Degradation by Selective Autophagy. *Nat. Cell Biol.* 20, 233–242. doi:10.1038/S41556-018-0037-Z

Geng, F., Cheng, X., Wu, X., Yoo, J. Y., Cheng, C., Guo, J. Y., et al. (2016). Inhibition of SOAT1 Suppresses Glioblastoma Growth via Blocking SREBP-1-Mediated

Lipogenesis. *Clin. Cancer Res.* 22, 5337–5348. doi:10.1158/1078-0432.CCR-15-2973

Gholkar, A. A., Cheung, K., Williams, K. J., Lo, Y.-C., Hamideh, S. A., Nnebe, C., et al. (2016). Fatostatin Inhibits Cancer Cell Proliferation by Affecting Mitotic Microtubule Spindle Assembly and Cell Division. *J. Biol. Chem.* 291, 17001–17008. doi:10.1074/jbc.C116.737346

Gomes, A. F., Magalhães, K. G., Rodrigues, R. M., De Carvalho, L., Molinaro, R., Bozza, P. T., et al. (2014). Toxoplasma Gondii- Skeletal Muscle Cells Interaction Increases Lipid Droplet Biogenesis and Positively Modulates the Production of IL-12, IFN-G and PGE2. *Parasites Vectors* 7, 1. doi:10.1186/1756-3305-7-47

Gong, J., Maia, M. C., Dizman, N., Govindarajan, A., and Pal, S. K. (2016). Metastasis in Renal Cell Carcinoma: Biology and Implications for Therapy. *Asian J. Urol.* 3, 286–292. doi:10.1016/j.ajur.2016.08.006

Guillaumond, F., Bidaut, G., Ouaissi, M., Servais, S., Gouirand, V., Olivares, O., et al. (2015). Cholesterol Uptake Disruption, in Association with Chemotherapy, Is a Promising Combined Metabolic Therapy for Pancreatic Adenocarcinoma. *Proc. Natl. Acad. Sci. USA* 112, 2473–2478. doi:10.1073/pnas.1421601112

Guo, D., Bell, E. H., and Chakravarti, A. (2013). Lipid Metabolism Emerges as a Promising Target for Malignant Glioma Therapy. *CNS Oncol.* 2, 289–299. doi:10.2217/cns.13.20

Guo, D., Prins, R. M., Dang, J., Kuga, D., Iwanami, A., Soto, H., et al. (2009). EGFR Signaling through an Akt-SREBP-1-dependent, Rapamycin-Resistant Pathway Sensitizes Glioblastomas to Antilipogenic Therapy. *Sci. Signal.* 2, 1–12. doi:10.1126/scisignal.2000446

Guo, D., Reinitz, F., Youssef, M., Hong, C., Nathanson, D., Akhavan, D., et al. (2011). An LXR Agonist Promotes Glioblastoma Cell Death through Inhibition of an EGFR/AKT/SREBP-1/LDLR-Dependent Pathway. *Cancer Discov.* 1, 442–456. doi:10.1158/2159-8290.CD-11-0102

Guri, Y., Colombi, M., Dazert, E., Hindupur, S. K., Roszik, J., Moes, S., et al. (2017). mTORC2 Promotes Tumorigenesis via Lipid Synthesis. *Cancer Cell* 32, 807–823. e12. doi:10.1016/j.ccell.2017.11.011

Gutierrez, M. G., Munafo´, D. B., Bero´n, W., and Colombo, M. I. (2004). Rab7 Is Required for the normal Progression of the Autophagic Pathway in Mammalian Cells. *J. Cell Sci.* 117, 2687–2697. doi:10.1242/JCS.01114

Guzman, M. G., and Harris, E. (2015). Dengue. *The Lancet* 385, 453–465. doi:10.1016/S0140-6736(14)60572-9

Hamilton, J. A. (1989). Interactions of Triglycerides with Phospholipids: Incorporation into the Bilayer Structure and Formation of Emulsions. *Biochemistry* 28, 2514–2520. doi:10.1021/BI00432A025

Hanai, J.-i., Doro, N., Seth, P., and Sukhatme, V. P. (2013). ATP Citrate Lyase Knockdown Impacts Cancer Stem Cells *In Vitro*. *Cell Death Dis* 4, e696. doi:10.1038/cddis.2013.215

Harris, C., Herker, E., Farese, R. V., Jr., and Ott, M. (2011). Hepatitis C Virus Core Protein Decreases Lipid Droplet Turnover. *J. Biol. Chem.* 286, 42615–42625. doi:10.1074/jbc.M111.285148

Hatzivassiliou, G., Zhao, F., Bauer, D. E., Andreadis, C., Shaw, A. N., Dhanak, D., et al. (2005). ATP Citrate Lyase Inhibition Can Suppress Tumor Cell Growth. *Cancer Cell* 8, 311–321. doi:10.1016/j.ccr.2005.09.008

Hauß, T., Dante, S., Dencher, N. A., and Haines, T. H. (2002). Squalane Is in the Midplane of the Lipid Bilayer: Implications for its Function as a Proton Permeability Barrier. *Biochim. Biophys. Acta (Bba) - Bioenerg.* 1556, 149–154. doi:10.1016/S0005-2728(02)00346-8

He, X., Li, T., Qin, K., Luo, S., Li, Z., Ji, Q., et al. (2021). Demalonylation of DDX3 by Sirtuin 5 Promotes Antiviral Innate Immune Responses. *Theranostics* 11, 7235–7246. doi:10.7150/thno.52934

Heaton, N. S., and Randall, G. (2010). Dengue Virus-Induced Autophagy Regulates Lipid Metabolism. *Cell Host & Microbe* 8, 422–432. doi:10.1016/j.chom.2010.10.006

Henne, W. M., Reese, M. L., and Goodman, J. M. (2018). The Assembly of Lipid Droplets and Their Roles in Challenged Cells. *EMBO J.* 37, 1. doi:10.15252/embj.201898947

Herzer, K., Carbow, A., Sydor, S., Sowa, J.-P., Biesterfeld, S., Hofmann, T.-G., et al. (2012). Deficiency of the Promyelocytic Leukemia Protein Fosters Hepatitis C-Associated Hepatocarcinogenesis in Mice. *PLoS One* 7, e44474. doi:10.1371/JOURNAL.PONE.0044474

Herzer, K., Weyer, S., Krammer, P. H., Galle, P. R., and Hofmann, T. G. (2005). Hepatitis C Virus Core Protein Inhibits Tumor Suppressor Protein Promyelocytic Leukemia Function in Human Hepatoma Cells. *Cancer Res.* 65, 10830–10837. doi:10.1158/0008-5472.CAN-05-0880

Hoang, A. N., Sandlin, R. D., Omar, A., Egan, T. J., and Wright, D. W. (2010). The Neutral Lipid Composition Present in the Digestive Vacuole of Plasmodium Falciparum Concentrates Heme and Mediates β-Hematin Formation with an Unusually Low Activation Energy. *Biochemistry* 49, 10107–10116. doi:10.1021/BI101397U

Hu, X., Binns, D., and Reese, M. L. (2017). The Coccidian Parasites Toxoplasma and Neospora Dysregulate Mammalian Lipid Droplet Biogenesis. *J. Biol. Chem.* 292, 11009–11020. doi:10.1074/jbc.M116.768176

Hyrina, A., Meng, F., McArthur, S. J., Eivemark, S., Nabi, I. R., and Jean, F. (2017). Human Subtilisin Kexin Isozyme-1 (SKI-1)/Site-1 Protease (S1P) Regulates Cytoplasmic Lipid Droplet Abundance: A Potential Target for Indirect-Acting Anti-dengue Virus Agents. *PLoS One* 12, e0174483. doi:10.1371/journal.pone.0174483

Infantino, V., Iacobazzi, V., Santis, F. D., Mastrapasqua, M., and Palmieri, F. (2007). Transcription of the Mitochondrial Citrate Carrier Gene: Role of SREBP-1, Upregulation by Insulin and Downregulation by PUFA. *Biochem. Biophysical Res. Commun.* 356, 249–254. doi:10.1016/j.bbrc.2007.02.114

Jackson, C. L. (2019). Lipid Droplet Biogenesis. *Curr. Opin. Cell Biol.* 59, 88–96. doi:10.1016/J.CEB.2019.03.018

Jackson, K. E., Klonis, N., Ferguson, D. J. P., Adisa, A., Dogovski, C., and Tilley, L. (2004). Food Vacuole-Associated Lipid Bodies and Heterogeneous Lipid Environments in the Malaria Parasite, Plasmodium Falciparum. *Mol. Microbiol.* 54, 109–122. doi:10.1111/j.1365-2958.2004.04284.x

Jarc, E., Kump, A., Malavašič, P., Eichmann, T. O., Zimmermann, R., and Petan, T. (2018). Lipid Droplets Induced by Secreted Phospholipase A2 and Unsaturated Fatty Acids Protect Breast Cancer Cells from Nutrient and Lipotoxic Stress. *Biochim. Biophys. Acta (Bba) - Mol. Cell Biol. Lipids* 1863, 247–265. doi:10.1016/j.bbalip.2017.12.006

Jäger, S., Bucci, C., Tanida, I., Ueno, T., Kominami, E., Saftig, P., et al. (2004). Role for Rab7 in Maturation of Late Autophagic Vacuoles. *J. Cell Sci.* 117, 4837–4848. doi:10.1242/JCS.01370

Jordan, T. X., and Randall, G. (2017). Dengue Virus Activates the AMP Kinase-mTOR Axis to Stimulate a Proviral Lipophagy. *J. Virol.* 91, 1. doi:10.1128/JVI.02020-16

José Soares, M., and de Souza, W. (1991). Endocytosis of Gold-Labeled Proteins and LDL byTrypanosoma Cruzi. *Parasitol. Res.* 77, 461–468. doi:10.1007/BF00928410

Kaini, R. R., Sillerud, L. O., Zhaorigetu, S., and Hu, C.-A. A. (2012). Autophagy Regulates Lipolysis and Cell Survival through Lipid Droplet Degradation in Androgen-Sensitive Prostate Cancer Cells. *Prostate* 72, 1412–1422. doi:10.1002/pros.22489

Kamisuki, S., Mao, Q., Abu-Elheiga, L., Gu, Z., Kugimiya, A., Kwon, Y., et al. (2009). A Small Molecule that Blocks Fat Synthesis by Inhibiting the Activation of SREBP. *Chem. Biol.* 16, 882–892. doi:10.1016/j.chembiol.2009.07.007

Kamphorst, J. J., Cross, J. R., Fan, J., De Stanchina, E., Mathew, R., White, E. P., et al. (2013). Hypoxic and Ras-Transformed Cells Support Growth by Scavenging Unsaturated Fatty Acids from Lysophospholipids. *Proc. Natl. Acad. Sci.* 110, 8882–8887. doi:10.1073/pnas.1307237110

Kaushik, S., and Cuervo, A. M. (2015). Degradation of Lipid Droplet-Associated Proteins by Chaperone-Mediated Autophagy Facilitates Lipolysis. *Nat. Cell Biol.* 17, 759–770. doi:10.1038/ncb3166

Kaushik, S., and Cuervo, A. M. (2018). The Coming of Age of Chaperone-Mediated Autophagy. *Nat. Rev. Mol. Cell Biol.* 19, 365–381. doi:10.1038/s41580-018-0001-6

Kawasaki, K., Eizuka, M., Nakamura, S., Endo, M., Yanai, S., Akasaka, R., et al. (2017). Association between white Opaque Substance under Magnifying Colonoscopy and Lipid Droplets in Colorectal Epithelial Neoplasms. *Wjg* 23, 8367–8375. doi:10.3748/wjg.v23.i47.8367

Khandelia, H., Duelund, L., Pakkanen, K. I., and Ipsen, J. H. (2010). Triglyceride Blisters in Lipid Bilayers: Implications for Lipid Droplet Biogenesis and the Mobile Lipid Signal in Cancer Cell Membranes. *PLoS One* 5, e12811. doi:10.1371/JOURNAL.PONE.0012811

Kim, S. M., Nguyen, T. T., Ravi, A., Kubiniok, P., Finicle, B. T., Jayashankar, V., et al. (2018). PTEN Deficiency and AMPK Activation Promote Nutrient Scavenging and Anabolism in Prostate Cancer Cells. *Cancer Discov.* 8, 866–883. doi:10.1158/2159-8290.CD-17-1215

Kiss, R., and Nilsson, T. (2014). Rab Proteins Implicated in Lipid Storage and Mobilization. *J. Biomed. Res.* 28, 169–177. doi:10.7555/JBR.28.20140029

Klemm, E. J., Spooner, E., and Ploegh, H. L. (2011). Dual Role of Ancient Ubiquitous Protein 1 (AUP1) in Lipid Droplet Accumulation and Endoplasmic Reticulum (ER) Protein Quality Control. *J. Biol. Chem.* 286, 37602–37614. doi:10.1074/jbc.M111.284794

Kofahi, H. M., Taylor, N. G. A., Hirasawa, K., Grant, M. D., and Russell, R. S. (2016). Hepatitis C Virus Infection of Cultured Human Hepatoma Cells Causes Apoptosis and Pyroptosis in Both Infected and Bystander Cells. *Sci. Rep.* 6, 37433. doi:10.1038/srep37433

Koizume, S., and Miyagi, Y. (2016). Lipid Droplets: A Key Cellular Organelle Associated with Cancer Cell Survival under Normoxia and Hypoxia. *Ijms* 17 (9), 1–23. doi:10.3390/ijms17091430

Kory, N., Farese, R. V., and Walther, T. C. (2016). Targeting Fat: Mechanisms of Protein Localization to Lipid Droplets. *Trends Cell Biol.* 26, 535–546. doi:10.1016/J.TCB.2016.02.007

Król, S. K., Kiełbus, M., Rivero-Müller, A., and Stepulak, A. (2015). Comprehensive Review on Betulin as a Potent Anticancer Agent. *Biomed. Res. Int.* 2015, 1–11. doi:10.1155/2015/584189

Laboudi, M. (2017). Review of Toxoplasmosis in Morocco: Seroprevalence and Risk Factors for Toxoplasma Infection Among Pregnant Women and HIV-Infected Patients. *Pan Afr. Med. J.* 27, 1. doi:10.11604/pamj.2017.27.269.11822

Lagrutta, L. C., Layerenza, J. P., Bronsoms, S., Trejo, S. A., and Ves-Losada, A. (2021). Nuclear-lipid-droplet Proteome: Carboxylesterase as a Nuclear Lipase Involved in Lipid-Droplet Homeostasis. *Heliyon* 7, e06539. doi:10.1016/j.heliyon.2021.e06539

LaPensee, C. R., Mann, J. E., Rainey, W. E., Crudo, V., Hunt, S. W., and Hammer, G. D. (2016). ATR-101, a Selective and Potent Inhibitor of Acyl-CoA Acyltransferase 1, Induces Apoptosis in H295R Adrenocortical Cells and in the Adrenal Cortex of Dogs. *Endocrinology* 157, 1775–1788. doi:10.1210/en.2015-2052

Laurent, V., Toulet, A., Attané, C., Milhas, D., Dauvillier, S., Zaidi, F., et al. (2019). Periprostatic Adipose Tissue Favors Prostate Cancer Cell Invasion in an Obesity-dependent Manner: Role of Oxidative Stress. *Mol. Cancer Res.* 17, 821–835. doi:10.1158/1541-7786.MCR-18-0748

Lechuga, G. C., Napoleão-Pêgo, P., Bottino, C. C. G., Pinho, R. T., Provance-Jr, D. W., and De-Simone, S. G. (2020). Trypanosoma Cruzi Presenilin-like Transmembrane Aspartyl Protease: Characterization and Cellular Localization. *Biomolecules* 10, 1564–1620. doi:10.3390/BIOM10111564

Li, J., Gu, D., Lee, S. S.-Y., Song, B., Bandyopadhyay, S., Chen, S., et al. (2016). Abrogating Cholesterol Esterification Suppresses Growth and Metastasis of Pancreatic Cancer. *Oncogene* 35, 6378–6388. doi:10.1038/onc.2016.168

Li, Q., Pène, V., Krishnamurthy, S., Cha, H., and Liang, T. J. (2013). Hepatitis C Virus Infection Activates an Innate Pathway Involving IKK-α in Lipogenesis and Viral Assembly. *Nat. Med.* 19, 722–729. doi:10.1038/nm.3190

Li, R., Schmidt, W., Rankin, S., Walzem, R. L., and Boyle-Roden, E. (2003). Solubilization of Acyl Heterogeneous Triacylglycerol in Phosphatidylcholine Vesicles. *J. Agric. Food Chem.* 51, 477–482. doi:10.1021/JF025676N

Li, X., Chen, Y.-T., Hu, P., and Huang, W.-C. (2014). Fatostatin Displays High Antitumor Activity in Prostate Cancer by Blocking SREBP-Regulated Metabolic Pathways and Androgen Receptor Signaling. *Mol. Cancer Ther.* 13, 855–866. doi:10.1158/1535-7163.MCT-13-0797

Li, X., Wu, J. B., Chung, L. W. K., and Huang, W.-C. (2015). Anti-cancer Efficacy of SREBP Inhibitor, Alone or in Combination with Docetaxel, in Prostate Cancer Harboring P53 Mutations. *Oncotarget* 6, 41018–41032. doi:10.18632/oncotarget.5879

Li, Z., Liu, H., and Luo, X. (2020). Lipid Droplet and its Implication in Cancer Progression. *Am. J. Cancer Res.* 10, 4112–4122.

Liang, Q., Luo, Z., Zeng, J., Chen, W., Foo, S.-S., Lee, S.-A., et al. (2016). Zika Virus NS4A and NS4B Proteins Deregulate Akt-mTOR Signaling in Human Fetal Neural Stem Cells to Inhibit Neurogenesis and Induce Autophagy. *Cell Stem Cell* 19, 663–671. doi:10.1016/j.stem.2016.07.019

Lige, B., Sampels, V., and Coppens, I. (2013). Characterization of a Second Sterol-Esterifying Enzyme inToxoplasmahighlights the Importance of Cholesterol Storage Pathways for the Parasite. *Mol. Microbiol.* 87, 951–967. doi:10.1111/mmi.12142

Lisec, J., Jaeger, C., Rashid, R., Munir, R., and Zaidi, N. (2019). Cancer Cell Lipid Class Homeostasis Is Altered under Nutrient-Deprivation but Stable under Hypoxia. *BMC Cancer* 19, 501–511. doi:10.1186/S12885-019-5733-Y/FIGURES/5

Liu, H., Zhang, L., Sun, J., Chen, W., Li, S., Wang, Q., et al. (2017). Endoplasmic Reticulum Protein SCAP Inhibits Dengue Virus NS2B3 Protease by Suppressing its K27-Linked Polyubiquitylation. *J. Virol.* 91, 1. doi:10.1128/JVI.02234-16

Liu, K., and Czaja, M. J. (2013). Regulation of Lipid Stores and Metabolism by Lipophagy. *Cell Death Differ* 20, 3–11. doi:10.1038/CDD.2012.63

Losinno, A. D., Martínez, S. J., Labriola, C. A., Carrillo, C., and Romano, P. S. (2021). Induction of Autophagy Increases the Proteolytic Activity of Reservosomes during Trypanosoma Cruzi Metacyclogenesis. *Autophagy* 17, 439–456. doi:10.1080/15548627.2020.1720428

Lovo-Martins, M. I., Malvezi, A. D., Zanluqui, N. G., Lucchetti, B. F. C., Tatakihara, V. L. H., Mörking, P. A., et al. (2018). Extracellular Vesicles Shed by Trypanosoma Cruzi Potentiate Infection and Elicit Lipid Body Formation and PGE2 Production in Murine Macrophages. *Front. Immunol.* 9, 1. doi:10.3389/fimmu.2018.00896

Lupette, J., and Maréchal, E. (2020). The Puzzling Conservation and Diversification of Lipid Droplets from Bacteria to Eukaryotes. *Results Probl. Cell Differ.* 69, 281–334. doi:10.1007/978-3-030-51849-3_11

Ma, S. Y., Sun, K. S., Zhang, M., Zhou, X., Zheng, X. H., Tian, S. Y., et al. (2020). Disruption of Plin5 Degradation by CMA Causes Lipid Homeostasis Imbalance in NAFLD. *Liver Int.* 40, 2427–2438. doi:10.1111/LIV.14492

Madeira, J. B., Masuda, C. A., Maya-Monteiro, C. M., Matos, G. S., Montero-Lomelí, M., and Bozaquel-Morais, B. L. (2015). TORC1 Inhibition Induces Lipid Droplet Replenishment in Yeast. *Mol. Cell. Biol.* 35, 737–746. doi:10.1128/mcb.01314-14

Maier, A. G., Matuschewski, K., Zhang, M., and Rug, M. (2019). Plasmodium Falciparum. *Trends Parasitol.* 35, 481–482. doi:10.1016/j.pt.2018.11.010

Majumder, M., Ghosh, A. K., Steele, R., Ray, R., and Ray, R. B. (2001). Hepatitis C Virus NS5A Physically Associates with P53 and Regulates P21/waf1 Gene Expression in a P53-dependent Manner. *J. Virol.* 75, 1401–1407. doi:10.1128/JVI.75.3.1401-1407.2001

Mancone, C., Steindler, C., Santangelo, L., Simonte, G., Vlassi, C., Longo, M. A., et al. (2011). Hepatitis C Virus Production Requires Apolipoprotein A-I and Affects its Association with Nascent Low-Density Lipoproteins. *Gut* 60, 378–386. doi:10.1136/gut.2010.211292

Martinez-Lopez, N., Garcia-Macia, M., Sahu, S., Athonvarangkul, D., Liebling, E., Merlo, P., et al. (2016). Autophagy in the CNS and Periphery Coordinate Lipophagy and Lipolysis in the Brown Adipose Tissue and Liver. *Cell Metab.* 23, 113–127. doi:10.1016/J.CMET.2015.10.008

Martins, A. S., Martins, I. C., and Santos, N. C. (2018). Methods for Lipid Droplet Biophysical Characterization in Flaviviridae Infections. *Front. Microbiol.* 9, 1951. doi:10.3389/fmicb.2018.01951

Mateo, R., Nagamine, C. M., Spagnolo, J., Méndez, E., Rahe, M., Gale, M., Jr., et al. (2013). Inhibition of Cellular Autophagy Deranges Dengue Virion Maturation. *J. Virol.* 87, 1312–1321. doi:10.1128/JVI.02177-12

Melo, R. C. N., D'Ávila, H., Fabrino, D. L., Almeida, P. E., and Bozza, P. T. (2003). Macrophage Lipid Body Induction by Chagas Disease *In Vivo*: Putative Intracellular Domains for Eicosanoid Formation during Infection. *Tissue and Cell* 35, 59–67. doi:10.1016/S0040-8166(02)00105-2

Menendez, J. A., and Lupu, R. (2007). Fatty Acid Synthase and the Lipogenic Phenotype in Cancer Pathogenesis. *Nat. Rev. Cancer* 7, 763–777. doi:10.1038/nrc2222

Meng, Z., Liu, Q., Sun, F., and Qiao, L. (2019). Hepatitis C Virus Nonstructural Protein 5A Perturbs Lipid Metabolism by Modulating AMPK/SREBP-1c Signaling. *Lipids Health Dis.* 18, 191. doi:10.1186/s12944-019-1136-y

Meyers, N. L., Fontaine, K. A., Kumar, G. R., and Ott, M. (2016). Entangled in a Membranous Web: ER and Lipid Droplet Reorganization during Hepatitis C Virus Infection. *Curr. Opin. Cell Biol.* 41, 117–124. doi:10.1016/j.ceb.2016.05.003

Mishra, S., Khaddaj, R., Cottier, S., Stradalova, V., Jacob, C., and Schneiter, R. (2016). Mature Lipid Droplets Are Accessible to ER Luminal Proteins. *J. Cell Sci.* 129, 3803–3815. doi:10.1242/jcs.189191

Miura, S., Gan, J.-W., Brzostowski, J., Parisi, M. J., Schultz, C. J., Londos, C., et al. (2002). Functional Conservation for Lipid Storage Droplet Association Among Perilipin, ADRP, and TIP47 (PAT)-related Proteins in Mammals, Drosophila, and Dictyostelium. *J. Biol. Chem.* 277, 32253–32257. doi:10.1074/jbc.M204410200

Moon, Y.-A. (2017). The SCAP/SREBP Pathway: A Mediator of Hepatic Steatosis. *Endocrinol. Metab.* 32, 6–10. doi:10.3803/EnM.2017.32.1.6

Mukhopadhyay, S., Schlaepfer, I. R., Bergman, B. C., Panda, P. K., Praharaj, P. P., Naik, P. P., et al. (2017). ATG14 Facilitated Lipophagy in Cancer Cells Induce ER Stress Mediated Mitoptosis through a ROS Dependent Pathway. *Free Radic. Biol. Med.* 104, 199–213. doi:10.1016/j.freeradbiomed.2017.01.007

Murphy, D. J. (2012). The Dynamic Roles of Intracellular Lipid Droplets: From Archaea to Mammals. *Protoplasma* 249, 541–585. doi:10.1007/s00709-011-0329-7

Musso, D., and Gubler, D. J. (2016). Zika Virus. *Clin. Microbiol. Rev.* 29, 487–524. doi:10.1128/CMR.00072-15

Netsawang, J., Noisakran, S., Puttikhunt, C., Kasinrerk, W., Wongwiwat, W., Malasit, P., et al. (2010). Nuclear Localization of Dengue Virus Capsid Protein Is Required for DAXX Interaction and Apoptosis. *Virus. Res.* 147, 275–283. doi:10.1016/j.virusres.2009.11.012

Nettebrock, N. T., and Bohnert, M. (2020). Born This Way - Biogenesis of Lipid Droplets from Specialized ER Subdomains. *Biochim. Biophys. Acta (Bba) - Mol. Cell Biol. Lipids* 1865, 158448. doi:10.1016/j.bbalip.2019.04.008

Neufeldt, C. J., Cortese, M., Acosta, E. G., and Bartenschlager, R. (2018). Rewiring Cellular Networks by Members of the Flaviviridae Family. *Nat. Rev. Microbiol.* 16, 125–142. doi:10.1038/nrmicro.2017.170

Ng, K. H., Lim, B. G., and Wong, K. P. (2003). Sulfate Conjugating and Transport Functions of MDCK Distal Tubular Cells. *Kidney Int.* 63, 976–986. doi:10.1046/j.1523-1755.2003.00818.x

Nishikawa, Y., Quittnat, F., Stedman, T. T., Voelker, D. R., and Choi, J.-Y. (2005). Host Cell Lipids Control Cholesteryl Ester Synthesis and Storage in Intracellular Toxoplasma. *Cell. Microbiol.* 7, 849–867. doi:10.1111/J.1462-5822.2005.00518.X

Nolan, S. J., Romano, J. D., and Coppens, I. (2017). Host Lipid Droplets: An Important Source of Lipids Salvaged by the Intracellular Parasite Toxoplasma Gondii. *Plos Pathog.* 13, e1006362. doi:10.1371/journal.ppat.1006362

Nygren, H., Von Holst, J-E., Mansson1, C., Von Holst, H., Månsson, J. E., and Fredman, P. (2009). Increased Levels of Cholesterol Esters in Glioma Tissue and Surrounding Areas of Human Brain. *Br. J. Neurosurg.* 11, 216–220. doi:10.1080/02688699746276

Ohmoto, T., Nishitsuji, K., Yoshitani, N., Mizuguchi, M., Yanagisawa, Y., Saito, H., et al. (2015). K604, a Specific Acyl-CoA:cholesterol Acyltransferase 1 Inhibitor, Suppresses Proliferation of U251-MG Glioblastoma Cells. *Mol. Med. Rep.* 12, 6037–6042. doi:10.3892/mmr.2015.4200

Ohsaki, Y., Maeda, T., Maeda, M., Tauchi-Sato, K., and Fujimoto, T. (2006). Recruitment of TIP47 to Lipid Droplets Is Controlled by the Putative Hydrophobic Cleft. *Biochem. Biophysical Res. Commun.* 347, 279–287. doi:10.1016/J.BBRC.2006.06.074

Ohsaki, Y., Suzuki, M., and Fujimoto, T. (2014). Open Questions in Lipid Droplet Biology. *Chem. Biol.* 21, 86–96. doi:10.1016/J.CHEMBIOL.2013.08.009

Olmstead, A. D., Knecht, W., Lazarov, I., Dixit, S. B., and Jean, F. (2012). Human Subtilase SKI-1/S1P Is a Master Regulator of the HCV Lifecycle and a Potential Host Cell Target for Developing Indirect-Acting Antiviral Agents. *Plos Pathog.* 8, e1002468. doi:10.1371/journal.ppat.1002468

Olzmann, J. A., and Carvalho, P. (2019). Dynamics and Functions of Lipid Droplets. *Nat. Rev. Mol. Cell Biol.* 20, 137–155. doi:10.1038/s41580-018-0085-z

Pace, D. (2014). Leishmaniasis. *J. Infect.* 69, S10–S18. doi:10.1016/j.jinf.2014.07.016

Padanad, M. S., Konstantinidou, G., Venkateswaran, N., Melegari, M., Rindhe, S., Mitsche, M., et al. (2016). Fatty Acid Oxidation Mediated by Acyl-CoA Synthetase Long Chain 3 Is Required for Mutant KRAS Lung Tumorigenesis. *Cell Rep.* 16, 1614–1628. doi:10.1016/j.celrep.2016.07.009

Palacpac, N. M. Q., Hiramine, Y., Seto, S., Hiramatsu, R., Horii, T., and Mitamura, T. (2004). Evidence that Plasmodium Falciparum Diacylglycerol Acyltransferase Is Essential for Intraerythrocytic Proliferation. *Biochem. Biophysical Res. Commun.* 321, 1062–1068. doi:10.1016/j.bbrc.2004.07.070

Palmer, D. R., Sun, P., Celluzzi, C., Bisbing, J., Pang, S., Sun, W., et al. (2005). Differential Effects of Dengue Virus on Infected and Bystander Dendritic Cells. *J. Virol.* 79, 2432–2439. doi:10.1128/JVI.79.4.2432-2439.2005

Panda, P. K., Patra, S., Naik, P. P., Praharaj, P. P., Mukhopadhyay, S., Meher, B. R., et al. (2020). Deacetylation of LAMP1 Drives Lipophagy-dependent Generation of Free Fatty Acids by Abrus Agglutinin to Promote Senescence in Prostate Cancer. *J. Cell. Physiol.* 235, 2776–2791. doi:10.1002/jcp.29182

Paquet, C., Yudin, M. H., Yudin, M. H., Allen, V. M., Bouchard, C., Boucher, M., et al. (2013). Toxoplasmosis in Pregnancy: Prevention, Screening, and Treatment. *J. Obstet. Gynaecol. Can.* 35, 78–79. doi:10.1016/S1701-2163(15)31053-7

Pavlova, N. N., and Thompson, C. B. (2016). The Emerging Hallmarks of Cancer Metabolism. *Cell Metab.* 23, 27–47. doi:10.1016/j.cmet.2015.12.006

Pène, V., Li, Q., Sodroski, C., Hsu, C.-S., and Liang, T. J. (2015). Dynamic Interaction of Stress Granules, DDX3X, and IKK-α Mediates Multiple Functions in Hepatitis C Virus Infection. *J. Virol.* 89, 5462–5477. doi:10.1128/JVI.03197-14

Peng, Y., Miao, H., Wu, S., Yang, W., Zhang, Y., Xie, G., et al. (2016). ABHD5 Interacts with BECN1 to Regulate Autophagy and Tumorigenesis of colon Cancer Independent of PNPLA2. *Autophagy* 12, 2167–2182. doi:10.1080/15548627.2016.1217380

Penrose, H., Heller, S., Cable, C., Makboul, R., Chadalawada, G., Chen, Y., et al. (2016). Epidermal Growth Factor Receptor Mediated Proliferation Depends on Increased Lipid Droplet Density Regulated via a Negative Regulatory Loop with FOXO3/Sirtuin6. *Biochem. Biophysical Res. Commun.* 469, 370–376. doi:10.1016/j.bbrc.2015.11.119

Pereira, M. G., Nakayasu, E. S., Sant'Anna, C., de Cicco, N. N. T., Atella, G. C., de Souza, W., et al. (2011). Trypanosoma Cruzi Epimastigotes Are Able to Store and Mobilize High Amounts of Cholesterol in Reservosome Lipid Inclusions. *PLoS One* 6, e22359. doi:10.1371/journal.pone.0022359

Pereira, M. G., Visbal, G., Costa, T. F. R., Frases, S., de Souza, W., Atella, G., et al. (2018). Trypanosoma Cruzi Epimastigotes Store Cholesteryl Esters in Lipid Droplets after Cholesterol Endocytosis. *Mol. Biochem. Parasitol.* 224, 6–16. doi:10.1016/j.molbiopara.2018.07.004

Pereira, M. G., Visbal, G., Salgado, L. T., Vidal, J. C., Godinho, J. L. P., De Cicco, N. N. T., et al. (2015). Trypanosoma Cruzi Epimastigotes Are Able to Manage Internal Cholesterol Levels under Nutritional Lipid Stress Conditions. *PLoS One* 10, e0128949. doi:10.1371/journal.pone.0128949

Petan, T., Jarc, E., and Jusović, M. (2018). Lipid Droplets in Cancer: Guardians of Fat in a Stressful World. *Molecules* 23 (8), 11–15. doi:10.3390/molecules23081941

Petan, T. (2020). Lipid Droplets in Cancer. *Rev. Physiol. Biochem. Pharmacol.* 2020, 1–34. doi:10.1007/112_2020_51

Pizato, N., Kiffer, L. F. M. V., Luzete, B. C., Assumpção, J. A. F., Correa, L. H., Melo, H. A. B., et al. (2019). Omega 3-DHA and delta-tocotrienol Modulate Lipid Droplet Biogenesis and Lipophagy in Breast Cancer Cells: The Impact in Cancer Aggressiveness. *Nutrients* 11 (6), 1–18. doi:10.3390/nu11061199

Pol, A., Gross, S. P., and Parton, R. G. (2014). Biogenesis of the Multifunctional Lipid Droplet: Lipids, Proteins, and Sites. *J. Cell Biol.* 204, 635–646. doi:10.1083/JCB.201311051

Przybytkowski, E., Joly, É., Nolan, C. J., Hardy, S., Francoeur, A.-M., Langelier, Y., et al. (2007). Upregulation of Cellular Triacylglycerol - Free Fatty Acid Cycling by Oleate Is Associated with Long-Term Serum-free Survival of Human Breast Cancer Cells. *Biochem. Cell Biol.* 85, 301–310. doi:10.1139/O07-001

Pucer, A., Brglez, V., Payré, C., Pungerčar, J., Lambeau, G., and Petan, T. (2013). Group X Secreted Phospholipase A2 Induces Lipid Droplet Formation and Prolongs Breast Cancer Cell Survival. *Mol. Cancer* 12, 1–23. doi:10.1186/1476-4598-12-111

Quittnat, F., Nishikawa, Y., Stedman, T. T., Voelker, D. R., Choi, J.-Y., Zahn, M. M., et al. (2004). On the Biogenesis of Lipid Bodies in Ancient Eukaryotes: Synthesis of Triacylglycerols by a Toxoplasma DGAT1-Related Enzyme. *Mol. Biochem. Parasitol.* 138, 107–122. doi:10.1016/j.molbiopara.2004.08.004

Rabhi, S., Rabhi, I., Trentin, B., Piquemal, D., Regnault, B., Goyard, S., et al. (2016). Lipid Droplet Formation, Their Localization and Dynamics during Leishmania Major Macrophage Infection. *PLoS One* 11, e0148640. doi:10.1371/journal.pone.0148640

Raini, S. K., Takamatsu, Y., Dumre, S. P., Urata, S., Mizukami, S., Moi, M. L., et al. (2021). The Novel Therapeutic Target and Inhibitory Effects of PF-429242 against Zika Virus Infection. *Antiviral Res.* 192, 105121. doi:10.1016/j.antiviral.2021.105121

Randall, G. (2018). Lipid Droplet Metabolism during Dengue Virus Infection. *Trends Microbiol.* 26, 640–642. doi:10.1016/j.tim.2018.05.010

Röhrig, F., and Schulze, A. (2016). The Multifaceted Roles of Fatty Acid Synthesis in Cancer. *Nat. Rev. Cancer* 16, 732–749. doi:10.1038/nrc.2016.89

Roingeard, P., and Melo, R. C. N. (2017). Lipid Droplet Hijacking by Intracellular Pathogens. *Cell Microbiol.* 19, e12688. doi:10.1111/cmi.12688

Romanauska, A., and Köhler, A. (2018). The Inner Nuclear Membrane Is a Metabolically Active Territory that Generates Nuclear Lipid Droplets. *Cell* 174, 700–715. doi:10.1016/j.cell.2018.05.047

Sangenito, L. S., Pereira, M. G., Souto-Padron, T., Branquinha, M. H., and Santos, A. L. S. (2021). Lopinavir and Nelfinavir Induce the Accumulation of Crystalloid Lipid Inclusions within the Reservosomes of Trypanosoma Cruzi and Inhibit Both Aspartyl-type Peptidase and Cruzipain Activities Detected in These Crucial Organelles. *TropicalMed* 6, 120. doi:10.3390/tropicalmed6030120

Sant'Anna, C., Nakayasu, E. S., Pereira, M. G., Lourenço, D., De Souza, W., Almeida, I. C., et al. (2009). Subcellular Proteomics ofTrypanosoma Cruzireservosomes. *Proteomics* 9, 1782–1794. doi:10.1002/pmic.200800730

Santinho, A., Salo, V. T., Chorlay, A., Li, S., Zhou, X., Omrane, M., et al. (2020). Membrane Curvature Catalyzes Lipid Droplet Assembly. *Curr. Biol.* 30, 2481–2494. doi:10.1016/j.cub.2020.04.066

Saraon, P., Trudel, D., Kron, K., Dmitromanolakis, A., Trachtenberg, J., Bapat, B., et al. (2014). Evaluation and Prognostic Significance of ACAT1 as a Marker of Prostate Cancer Progression. *Prostate* 74, 372–380. doi:10.1002/pros.22758

Schneider, J. L., Suh, Y., and Cuervo, A. M. (2014). Deficient Chaperone-Mediated Autophagy in Liver Leads to Metabolic Dysregulation. *Cell Metab.* 20, 417–432. doi:10.1016/J.CMET.2014.06.009

Scholtes, C., Ramière, C., Rainteau, D., Perrin-Cocon, L., Wolf, C., Humbert, L., et al. (2012). High Plasma Level of Nucleocapsid-free Envelope Glycoprotein-Positive Lipoproteins in Hepatitis C Patients. *Hepatology* 56, 39–48. doi:10.1002/hep.25628

Schott, M. B., Weller, S. G., Schulze, R. J., Krueger, E. W., Drizyte-Miller, K., Casey, C. A., et al. (2019). Lipid Droplet Size Directs Lipolysis and Lipophagy Catabolism in Hepatocytes. *J. Cell Biol.* 218, 3320–3335. doi:10.1083/JCB.201803153

Schroeder, B., Schulze, R. J., Weller, S. G., Sletten, A. C., Casey, C. A., and McNiven, M. A. (2015). The Small GTPase Rab7 as a central Regulator of Hepatocellular Lipophagy. *Hepatology* 61, 1896–1907. doi:10.1002/HEP.27667

Schulze, R. J., Drižytė, K., Casey, C. A., and McNiven, M. A. (2017). Hepatic Lipophagy: New Insights into Autophagic Catabolism of Lipid Droplets in the Liver. *Hepatol. Commun.* 1, 359–369. doi:10.1002/hep4.1056

Schweiger, M., and Zechner, R. (2015). Breaking the Barrier-Chaperone-Mediated Autophagy of Perilipins Regulates the Lipolytic Degradation of Fat. *Cell Metab.* 22, 60–61. doi:10.1016/j.cmet.2015.06.017

Senga, S., Kobayashi, N., Kawaguchi, K., Ando, A., and Fujii, H. (2018). Fatty Acid-Binding Protein 5 (FABP5) Promotes Lipolysis of Lipid Droplets, De Novo Fatty Acid (FA) Synthesis and Activation of Nuclear Factor-Kappa B (NF-Kb) Signaling in Cancer Cells. *Biochim. Biophys. Acta (Bba) - Mol. Cell Biol. Lipids* 1863, 1057–1067. doi:10.1016/j.bbalip.2018.06.010

Shao, W., Machamer, C. E., and Espenshade, P. J. (2016). Fatostatin Blocks ER Exit of SCAP but Inhibits Cell Growth in a SCAP-independent Manner. *J. Lipid Res.* 57, 1564–1573. doi:10.1194/jlr.M069583

Shibata, M., Yoshimura, K., Tamura, H., Ueno, T., Nishimura, T., Inoue, T., et al. (2010). LC3, a Microtubule-Associated protein1A/B Light Chain3, Is Involved in Cytoplasmic Lipid Droplet Formation. *Biochem. Biophysical Res. Commun.* 393, 274–279. doi:10.1016/j.bbrc.2010.01.121

Shimano, H., and Sato, R. (2017). SREBP-regulated Lipid Metabolism: Convergent Physiology - Divergent Pathophysiology. *Nat. Rev. Endocrinol.* 13, 710–730. doi:10.1038/NRENDO.2017.91

Shrivastava, S., Devhare, P., Sujijantarat, N., Steele, R., Kwon, Y.-C., Ray, R., et al. (2016). Knockdown of Autophagy Inhibits Infectious Hepatitis C Virus Release by the Exosomal Pathway. *J. Virol.* 90, 1387–1396. doi:10.1128/JVI.02383-15

Singh, R., and Cuervo, A. M. (2012). Lipophagy: Connecting Autophagy and Lipid Metabolism. *Int. J. Cell Biol.* 2012, 282041. doi:10.1155/2012/282041

Singh, R., Kaushik, S., Wang, Y., Xiang, Y., Novak, I., Komatsu, M., et al. (2009). Autophagy Regulates Lipid Metabolism. *Nature* 458, 1131–1135. doi:10.1038/nature07976

Stenmark, H. (2009). Rab GTPases as Coordinators of Vesicle Traffic. *Nat. Rev. Mol. Cell Biol.* 10, 513–525. doi:10.1038/nrm2728

Subczynski, W. K., Pasenkiewicz-Gierula, M., Widomska, J., Mainali, L., and Raguz, M. (2017). High Cholesterol/Low Cholesterol: Effects in Biological Membranes: A Review. *Cell Biochem. Biophys.* 75, 369–385. doi:10.1007/S12013-017-0792-7

Sun, H.-Y., Lin, C.-C., Tsai, P.-J., Tsai, W.-J., Lee, J.-C., Tsao, C.-W., et al. (2017). Lipoprotein Lipase Liberates Free Fatty Acids to Inhibit HCV Infection and Prevent Hepatic Lipid Accumulation. *Cell Microbiol.* 19, e12673. doi:10.1111/cmi.12673

Sztalryd, C., and Brasaemle, D. L. (2017). The Perilipin Family of Lipid Droplet Proteins: Gatekeepers of Intracellular Lipolysis. *Biochim. Biophys. Acta (Bba) - Mol. Cell Biol. Lipids* 1862, 1221–1232. doi:10.1016/j.bbalip.2017.07.009

Takahashi, Y., Shinoda, A., Kamada, H., Shimizu, M., Inoue, J., and Sato, R. (2016). Perilipin2 Plays a Positive Role in Adipocytes during Lipolysis by Escaping Proteasomal Degradation. *Sci. Rep.* 6, 1–14. doi:10.1038/srep20975

Tansey, J., Sztalryd, C., Hlavin, E., Kimmel, A., and Londos, C. (2004). The central Role of Perilipin a in Lipid Metabolism and Adipocyte Lipolysis. *IUBMB Life (International Union Biochem. Mol. Biol. Life)* 56, 379–385. doi:10.1080/15216540400009968

Tarleton, R. L. (2007). Immune System Recognition of Trypanosoma Cruzi. *Curr. Opin. Immunol.* 19, 430–434. doi:10.1016/J.COI.2007.06.003

Thiam, A. R., Antonny, B., Wang, J., Delacotte, J., Wilfling, F., Walther, T. C., et al. (2013a). COPI Buds 60-nm Lipid Droplets from Reconstituted Water-Phospholipid-Triacylglyceride Interfaces, Suggesting a Tension Clamp Function. *Proc. Natl. Acad. Sci.* 110, 13244–13249. doi:10.1073/PNAS.1307685110/-/DCSUPPLEMENTAL

Thiam, A. R., and Beller, M. (2017). The Why, when and How of Lipid Droplet Diversity. *J. Cell Sci.* 130, 315–324. doi:10.1242/JCS.192021

Thiam, A. R., Farese Jr, R. V., and Walther, T. C. (2013b). The Biophysics and Cell Biology of Lipid Droplets. *Nat. Rev. Mol. Cell Biol.* 14, 775–786. doi:10.1038/nrm3699

Thiam, A. R., and Forêt, L. (2016). The Physics of Lipid Droplet Nucleation, Growth and Budding. *Biochim. Biophys. Acta (Bba) - Mol. Cell Biol. Lipids* 1861, 715–722. doi:10.1016/J.BBALIP.2016.04.018

Tirinato, L., Liberale, C., Di Franco, S., Candeloro, P., Benfante, A., La Rocca, R., et al. (2015). Lipid Droplets: A New Player in Colorectal Cancer Stem Cells Unveiled by Spectroscopic Imaging. *Stem Cells* 33, 35–44. doi:10.1002/stem.1837

Toledo, D. A. M., Roque, N. R., Teixeira, L., Milán-Garcés, E. A., Carneiro, A. B., Almeida, M. R., et al. (2016). Lipid Body Organelles within the Parasite Trypanosoma Cruzi: A Role for Intracellular Arachidonic Acid Metabolism. *PLoS One* 11, e0160433. doi:10.1371/journal.pone.0160433

Torres, C., Pérez-Victoria, F. J., Parodi-Talice, A., Castanys, S., and Gamarro, F. (2004). Characterization of an ABCA-like Transporter Involved in Vesicular Trafficking in the Protozoan Parasite Trypanosoma Cruzi. *Mol. Microbiol.* 54, 632–646. doi:10.1111/j.1365-2958.2004.04304.x

Valm, A. M., Cohen, S., Legant, W. R., Melunis, J., Hershberg, U., Wait, E., et al. (2017). Applying Systems-Level Spectral Imaging and Analysis to Reveal the Organelle Interactome. *Nature* 546, 162–167. doi:10.1038/nature22369

Van Zutphen, T., Todde, V., De Boer, R., Kreim, M., Hofbauer, H. F., Wolinski, H., et al. (2014). Lipid Droplet Autophagy in the Yeast *Saccharomyces cerevisiae*. *MBoC* 25, 290–301. doi:10.1091/MBC.E13-08-0448

Vanrell, M. C., Losinno, A. D., Cueto, J. A., Balcazar, D., Fraccaroli, L. V., Carrillo, C., et al. (2017). The Regulation of Autophagy Differentially Affects Trypanosoma Cruzi Metacyclogenesis. *Plos Negl. Trop. Dis.* 11, e0006049. doi:10.1371/journal.pntd.0006049

Varsano, N., Beghi, F., Elad, N., Pereiro, E., Dadosh, T., Pinkas, I., et al. (2018). Two Polymorphic Cholesterol Monohydrate crystal Structures Form in Macrophage Culture Models of Atherosclerosis. *Proc. Natl. Acad. Sci. USA* 115, 7662–7669. doi:10.1073/PNAS.1803119115/-/DCSUPPLEMENTAL

Vercauteren, K., Mesalam, A. A., Leroux-Roels, G., and Meuleman, P. (2014). Impact of Lipids and Lipoproteins on Hepatitis C Virus Infection and Virus Neutralization. *Wjg* 20, 15975–15991. doi:10.3748/wjg.v20.i43.15975

Vescovo, T., Romagnoli, A., Perdomo, A. B., Corazzari, M., Ciccosanti, F., Alonzi, T., et al. (2012). Autophagy Protects Cells from HCV-Induced Defects in Lipid Metabolism. *Gastroenterology* 142, 644–653. e3. doi:10.1053/j.gastro.2011.11.033

Vitelli, R., Santillo, M., Lattero, D., Chiariello, M., Bifulco, M., Bruni, C. B., et al. (1997). Role of the Small GTPase Rab7 in the Late Endocytic Pathway. *J. Biol. Chem.* 272, 4391–4397. doi:10.1074/jbc.272.7.4391

Walther, T. C., Chung, J., and Farese, R. V. (2017). Lipid Droplet Biogenesis. *Annu. Rev. Cell Dev. Biol.* 33, 491–510. doi:10.1146/ANNUREV-CELLBIO-100616-060608

Walther, T. C., and Farese, R. V. (2012). Lipid Droplets and Cellular Lipid Metabolism. *Annu. Rev. Biochem.* 81, 687–714. doi:10.1146/annurev-biochem-061009-102430

Wang, H., Becuwe, M., Housden, B. E., Chitraju, C., Porras, A. J., Graham, M. M., et al. (2016). Seipin Is Required for Converting Nascent to Mature Lipid Droplets. *Elife* 5, 1. doi:10.7554/ELIFE.16582

Wang, K., Ruan, H., Song, Z., Cao, Q., Bao, L., Liu, D., et al. (2018). PLIN3 Is Up-Regulated and Correlates with Poor Prognosis in clear Cell Renal Cell Carcinoma. *Urol. Oncol. Semin. Original Invest.* 36, e9–343. doi:10.1016/j.urolonc.2018.04.006

Waris, G., Felmlee, D. J., Negro, F., and Siddiqui, A. (2007). Hepatitis C Virus Induces Proteolytic Cleavage of Sterol Regulatory Element Binding Proteins and Stimulates Their Phosphorylation via Oxidative Stress. *J. Virol.* 81, 8122–8130. doi:10.1128/JVI.00125-07

Warner, T. G., Dambach, L. M., Shin, J. H., and O'Brien, J. S. (1981). Purification of the Lysosomal Acid Lipase from Human Liver and its Role in Lysosomal Lipid Hydrolysis. *J. Biol. Chem.* 256, 2952–2957. doi:10.1016/s0021-9258(19)69707-3

Wellen, K. E., and Thompson, C. B. (2010). Cellular Metabolic Stress: Considering How Cells Respond to Nutrient Excess. *Mol. Cell* 40, 323–332. doi:10.1016/j.molcel.2010.10.004

Welte, M. A., and Gould, A. P. (2017). Lipid Droplet Functions beyond Energy Storage. *Biochim. Biophys. Acta (Bba) - Mol. Cell Biol. Lipids* 1862, 1260–1272. doi:10.1016/j.bbalip.2017.07.006

Wilfling, F., Thiam, A. R., Olarte, M.-J., Wang, J., Beck, R., Gould, T. J., et al. (2014). Arf1/COPI Machinery Acts Directly on Lipid Droplets and Enables Their Connection to the ER for Protein Targeting. *Elife* 3, 1. doi:10.7554/ELIFE.01607

Williams, K. J., Argus, J. P., Zhu, Y., Wilks, M. Q., Marbois, B. N., York, A. G., et al. (2013). An Essential Requirement for the SCAP/SREBP Signaling axis to Protect Cancer Cells from Lipotoxicity. *Cancer Res.* 73, 2850–2862. doi:10.1158/0008-5472.CAN-13-0382-T

Winnard, P. T., Raman, V., and Raman, V. (2021). Targeting Host DEAD-Box RNA Helicase DDX3X for Treating Viral Infections. *Antiviral Res.* 185, 104994. doi:10.1016/j.antiviral.2020.104994

Wölwer, C. B., Pase, L. B., Russell, S. M., and Humbert, P. O. (2016). Calcium Signaling Is Required for Erythroid Enucleation. *PLoS One* 11, e0146201–12. doi:10.1371/journal.pone.0146201

Wu, J., Liu, W., and Gong, P. (2015). A Structural Overview of RNA-dependent RNA Polymerases from the Flaviviridae Family. *Ijms* 16, 12943–12957. doi:10.3390/ijms160612943

Wu, K., Fan, S., Zou, L., Zhao, F., Ma, S., Fan, J., et al. (2021). Molecular Events Occurring in Lipophagy and its Regulation in Flaviviridae Infection. *Front. Microbiol.* 12, 651952. doi:10.3389/fmicb.2021.651952

Wu, X., Geng, F., Cheng, X., Guo, Q., Zhong, Y., Cloughesy, T. F., et al. (2020). Lipid Droplets Maintain Energy Homeostasis and Glioblastoma Growth via Autophagic Release of Stored Fatty Acids. *ISCIENCE* 23, 101569. doi:10.1016/j.isci.2020.101569

Wu, Y.-W., Mettling, C., Wu, S.-R., Yu, C.-Y., Perng, G.-C., Lin, Y.-S., et al. (2016). Autophagy-associated Dengue Vesicles Promote Viral Transmission Avoiding Antibody Neutralization. *Sci. Rep.* 6, 32243. doi:10.1038/srep32243

Xu, G., Jiang, Y., Xiao, Y., Liu, X.-D., Yue, F., Li, W., et al. (2016). Fast Clearance of Lipid Droplets through MAP1S-Activated Autophagy Suppresses clear Cell Renal Cell Carcinomas and Promotes Patient Survival. *Oncotarget* 7, 6255–6265. doi:10.18632/oncotarget.6669

Xu, G., Sztalryd, C., and Londos, C. (2006). Degradation of Perilipin Is Mediated through Ubiquitination-Proteasome Pathway. *Biochim. Biophys. Acta (Bba) - Mol. Cell Biol. Lipids* 1761, 83–90. doi:10.1016/J.BBALIP.2005.12.005

Xu, G., Sztalryd, C., Lu, X., Tansey, J. T., Gan, J., Dorward, H., et al. (2005). Post-translational Regulation of Adipose Differentiation-Related Protein by the Ubiquitin/proteasome Pathway. *J. Biol. Chem.* 280, 42841–42847. doi:10.1074/JBC.M506569200

Yoshii, Y., Furukawa, T., Oyama, N., Hasegawa, Y., Kiyono, Y., Nishii, R., et al. (2013). Fatty Acid Synthase Is a Key Target in Multiple Essential Tumor Functions of Prostate Cancer: Uptake of Radiolabeled Acetate as a Predictor of the Targeted Therapy Outcome. *PLoS One* 8, 1. doi:10.1371/journal.pone.0064570

Yu, L., Fan, J., Zhou, C., and Xu, C. (2021). Sterols Are Required for the Coordinated Assembly of Lipid Droplets in Developing Seeds. *Nat. Commun.* 121 12, 1–14. doi:10.1038/s41467-021-25908-6

Yuan, S., Chu, H., Chan, J. F., Ye, Z. W., Wen, L., Yan, B., et al. (2019). SREBP-dependent Lipidomic Reprogramming as a Broad-Spectrum Antiviral Target. *Nat. Commun.* 10, 120. doi:10.1038/s41467-018-08015-x

Yue, S., Li, J., Lee, S. Y., Lee, H. J., Shao, T., Song, B., et al. (2014). Cholesteryl Ester Accumulation Induced by PTEN Loss and PI3K/AKT Activation Underlies Human Prostate Cancer Aggressiveness. *Cell Metab* 19, 393–406. doi:10.1016/j.cmet.2014.01.019

Zanghellini, J., Wodlei, F., Von Grünberg, H. H., and Grünberg, G. (2010). Phospholipid Demixing and the Birth of a Lipid Droplet. *J. Theor. Biol.* 264 (3), 952–961. doi:10.1016/j.jtbi.2010.02.025

Zechner, R., Zimmermann, R., Eichmann, T. O., Kohlwein, S. D., Haemmerle, G., Lass, A., et al. (2012). FAT SIGNALS-Llipases and Lipolysis in Lipid Metabolism and Signaling. *Cell Metab* 15, 279–291. doi:10.1016/J.CMET.2011.12.018

Zeisel, M. B., Felmlee, D. J., and Baumert, T. F. (2013). Hepatitis C Virus Entry. *Curr. Top. Microbiol. Immunol.* 369, 87–112. doi:10.1007/978-3-642-27340-7_4

Zhang, C., and Liu, P. (2017). The Lipid Droplet: A Conserved Cellular Organelle. *Protein Cell* 8, 796. doi:10.1007/S13238-017-0467-6

Zhang, J., Lan, Y., Li, M. Y., Lamers, M. M., Fusade-Boyer, M., Klemm, E., et al. (2018). Flaviviruses Exploit the Lipid Droplet Protein AUP1 to Trigger Lipophagy and Drive Virus Production. *Cell Host Microbe* 23, 819–831. e5. doi:10.1016/j.chom.2018.05.005

Zhang, L., and Wang, A. (2012). Virus-induced ER Stress and the Unfolded Protein Response. *Front. Plant Sci.* 3, 293. doi:10.3389/fpls.2012.00293

Zhang, P., and Reue, K. (2017). Lipin Proteins and Glycerolipid Metabolism: Roles at the ER Membrane and beyond. *Biochim. Biophys. Acta. Biomembr.* 1859, 1583–1595. doi:10.1016/J.BBAMEM.2017.04.007

Zhang, Z. W., Li, Z. L., and Yuan, S. (2016). The Role of Secretory Autophagy in Zika Virus Transfer through the Placental Barrier. *Front Cell Infect Microbiol* 6, 206. doi:10.3389/fcimb.2016.00206

Zhao, T., Ding, X., Du, H., and Yan, C. (2016). Lung Epithelial Cell–specific Expression of Human Lysosomal Acid Lipase Ameliorates Lung Inflammation and Tumor Metastasis in Lipa−/− Mice. *Am. J. Pathol.* 186, 2183–2192. doi:10.1016/j.ajpath.2016.04.014

Zoni, V., Khaddaj, R., Campomanes, P., Thiam, A. R., Schneiter, R., and Vanni, S. (2021). Pre-existing Bilayer Stresses Modulate Triglyceride Accumulation in the Er versus Lipid Droplets. *Elife* 10, 1–24. doi:10.7554/ELIFE.62886

Zoni, V., Khaddaj, R., Campomanes, P., Thiam, R., Schneiter, R., and Vanni, S. (2020). Lipid Droplet Biogenesis Is Driven by Liquid-Liquid Phase Separation. *SSRN Electron. J.* 2020, 1. doi:10.2139/SSRN.3526890

Zoni, V., Nieto, V., Endter, L. J., Risselada, H. J., Monticelli, L., and Vanni, S. (2019). To Bud or Not to Bud: A Perspective on Molecular Simulations of Lipid Droplet Budding. *Front. Mol. Biosci.* 0, 124. doi:10.3389/FMOLB.2019.00124

Conflict of Interest: The authors declare that the research was conducted in the absence of any commercial or financial relationships that could be construed as a potential conflict of interest.

frontiers in Cell and Developmental Biology

ORIGINAL RESEARCH
published: 17 February 2022
doi: 10.3389/fcell.2021.743124

HPS6 Regulates the Biogenesis of Weibel–Palade Body in Endothelial Cells Through Trafficking v-ATPase to Its Limiting Membrane

Jiran Lu†, *Jing Ma*†, *Zhenhua Hao and Wei Li**

Beijing Key Laboratory for Genetics of Birth Defects, MOE Key Laboratory of Major Diseases in Children, Rare Disease Center, National Center for Children's Health, Beijing Children's Hospital, Beijing Pediatric Research Institute, Capital Medical University, Beijing, China

The Weibel–Palade body (WPB) is one of the lysosome-related organelles (LROs) in endothelial cells, whose main content is von Willebrand factor (vWF). The biogenesis of LROs is regulated by the Hermansky–Pudlak syndrome (HPS) protein-associated complexes through transporting cargo proteins to WPBs. Our previous studies have shown that HPS6, a subunit of BLOC-2 complex, is likely involved in the maturation of WPBs. However, the underlying mechanism remains unknown. In this study, we found that the knockdown of *HPS6* in human umbilical vein endothelial cells (HUVECs) resulted in misshaped WPBs, decreased WPB number, and impaired vWF tubulation, which are similar to the characteristics of HPS6-deficient mouse endothelial cells. We observed similar morphological changes of WPBs in HUVECs after the knockdown of *ATP6V0D1* (a subunit of v-ATPase). Furthermore, we found that HPS6 interacted with ATP6V0D1, suggesting that HPS6 transports ATP6V0D1 to the WPB limiting membrane for the assembly of the v-ATPase complex to maintain its acidic luminal pH, which is critical for the formation of vWF tubules during WPB maturation. In conclusion, HPS6 likely regulates the biogenesis of WPBs by participating in the trafficking of v-ATPase to the WPB membrane.

Keywords: Weibel–Palade body, von Willebrand factor, lysosome-related organelle, Hermansky–Pudlak syndrome, HPS6, v-ATPase

OPEN ACCESS

Edited by:
Carlos Enrich, University of Barcelona, Spain

Reviewed by:
Vas Ponnambalam, University of Leeds, United Kingdom
Duarte C. Barral, Universidade Nova de Lisboa, Portugal

***Correspondence:**
Wei Li
liwei@bch.com.cn

†*These authors have contributed equally to this work*

Specialty section:
This article was submitted to Membrane Traffic, a section of the journal Frontiers in Cell and Developmental Biology

Received: *17 July 2021*
Accepted: *22 December 2021*
Published: *17 February 2022*

Citation:
Lu J, Ma J, Hao Z and Li W (2022) HPS6 Regulates the Biogenesis of Weibel–Palade Body in Endothelial Cells Through Trafficking v-ATPase to Its Limiting Membrane. Front. Cell Dev. Biol. 9:743124. doi: 10.3389/fcell.2021.743124

INTRODUCTION

Endothelial cells (ECs) form a layer of flat and polygonal cells that line the vascular wall, which is the biological barrier between the circulating blood and the blood vessel wall and is of great significance to maintain vascular homeostasis (Aird, 2007). The Weibel–Palade body (WPB) is a type of lysosome-related organelles (LROs) (Marks et al., 2013), which was discovered in 1964 by Ewald Weibel and George Palade in rat and human ECs (Weibel and Palade, 1964; Warhol and Sweet, 1984). As a morphological marker of ECs, WPBs are rod-shaped granules with a diameter of 0.1–0.3 μm and a length of 1–5 μm (Arribas and Cutler, 2000; Michaux and Cutler, 2004; Valentijn et al., 2008). WPBs contain various bioactive molecules, such as von Willebrand factor (vWF), angiopoietin-2, interleukin-6 and -8, monocyte chemoattractant protein-1, and P-selectin, which are released in response to the activation of ECs (Schillemans et al., 2019). ECs play an important role in numerous physiological activities that include hemostasis, inflammation, angiogenesis, and wound

healing. The main luminal content of WPB is vWF. vWF forms a highly multimerized tubular structure that is closely related to the shape and size of WPBs (Wagner et al., 1982; Karampini et al., 2020). Upon release into the plasma, the vWF tubules will unfurl into long strings that recruit platelets to prevent bleeding (Savage et al., 2002).

As a member of LROs, WPB biogenesis is likely regulated by Hermansky–Pudlak syndrome (HPS) protein-associated complexes (HPACs), which includes the biogenesis of lysosome-related organelles complex (BLOC)-1, -2, and -3, adaptor protein complex-3 (AP-3), and homotypic fusion and protein sorting complex (Wei and Li, 2013). It has been shown that AP-1/clathrin coat plays an essential role in forming WPBs in endothelial cells (Lui-Roberts et al., 2005) and that the recruitment of CD63 is dependent on AP-3 complex during the biogenesis of WPBs (Harrison-Lavoie et al., 2006). However, the functions of other HPACs in WPB biogenesis are unknown yet.

In our previous study (Ma et al., 2016), we compared the phenotypes of WPBs and the secretion of vWF multimers in various HPAC mutant mice, including *pa* (HPS9 deficiency in BLOC-1), *ru* (HPS6 deficiency in BLOC-2), and *ep* (HPS1 deficiency in BLOC-3). We found that the regulated secretion of vWF in *ru* mice was the most significantly reduced, and the maturation of WPBs in *ru* mice was impaired significantly compared with that in wild-type (WT) mice. Therefore, we hypothesized that HPS6 may be required to deliver cargo proteins necessary for the biogenesis of WPBs.

In this study using *ru* ECs and human umbilical vein endothelial cells (HUVECs), we firstly confirmed the impairments of WPB biogenesis and maturation due to HPS6 deficiency. Considering that neutralization treatment does not alter the elongated shape of WPBs in *ru* ECs and vacuolar-type H^+-ATPase (v-ATPase) is the primary proton pump for H^+ homeostasis in organelles, we further found that HPS6 is required for the trafficking of subunit d1 in the V0 domain (ATP6V0D1) to WPBs to maintain the acidic luminal environment. Thus, HPS6 likely regulates the biogenesis of WPBs by transporting ATP6V0D1 to the WPB membrane to form highly ordered vWF tubules in the acidic lumen.

RESULTS

Mutation of the *Hps6* Gene in Mice Impairs WPB Biogenesis and Maturation

Our previous study showed that WPBs in *ru*/*Hps6* mutant mice lose their classical "cigar" shape and do not release enough vWF multimers into the plasma after desmopressin stimulation (Ma et al., 2016). It is unknown whether these abnormities occur in the biogenesis stage or in the release stage. Therefore, we compared the shape and number of WPBs at various time points during their biogenesis between the primary ECs of WT and *ru* mice. The cells were treated with phorbol-12-myristate-13-acetate (PMA) to release existing mature WPBs. After washing out, the newly generated WPBs were examined at various time points (0, 2, 4, and 8 h). Immunofluorescence staining and statistical analysis showed that the average number of WPBs per cell in *ru* mice was higher than that in WT mice at 0-h time point after PMA treatment (**Figures 1A,E**) because there may be more immature WPBs that have not been released completely in *ru* mice compared with WT mice. When treated for a longer time, more WPBs that represented nascent WPBs were seen in WT cells than in *ru* cells. At 2 h, the number of WPBs in WT and *ru* ECs reached almost the same amount ($p > 0.05$). However, the number of WPBs in *ru* ECs was significantly reduced at 8-h time point compared with WT ECs (**Figures 1B–E**). The results of Feret's diameter of WPBs in WT and *ru* mice showed a large cluster of WPBs in *ru* mice whose Feret's diameter was concentrated at 0.5 μm and then reached the highest percentage (nearly 30%) at 2 h after PMA treatment. However, with the prolongation of time, WPBs in *ru* cells with Feret's diameter of ≥1.3 μm were rarely seen and WPBs with Feret's diameter of ≥1.8 μm were only seen in WT cells (**Figure 1F**), which indicated less mature WPBs in *ru* cells. Taken together, HPS6 deficiency may affect WPB biogenesis and maturation, which is consistent with our previous report (Ma et al., 2016).

Biogenesis and Maturation of WPBs Are Compromised in *HPS6* Knockdown HUVECs

We further investigated the effects of HPS6 deficiency by siRNA knockdown of *HPS6* (KD-HPS6) in HUVECs (**Figure 2C**). Immunofluorescence staining of vWF revealed more round-shaped WPBs in KD-HPS6 cells compared with negative control (NC) cells (**Figures 2A,B**). Moreover, the number of WPBs was significantly reduced in KD-HPS6 cells compared with NC cells (**Figure 2D**). These features resembled the changes in *ru* mouse ECs as we reported previously (Ma et al., 2016).

Similarly, we observed the newly formed WPBs in HUVECs at various time points (2, 4, 8, and 16 h) after PMA treatment (**Figure 2E**). Immunofluorescence staining and statistical analysis showed that the average number of WPBs per cell was significantly reduced in KD-HPS6 HUVECs at 4, 8, and 16 h after PMA treatment compared with the NC HUVECs (**Figures 2E,F**). In terms of the Feret's diameter of WPBs in these two groups, the statistical results showed that the distribution of Feret's diameter of WPBs in KD-HPS6 cells began to shift to small values from 4 h onward. At 16 h, there were significantly more WPBs with a Feret's diameter of ≤1.5 μm in KD-HPS6 cells, while many rod-shaped WPBs of ≥2.5 μm were seen in NC cells (**Figure 2G**). These results confirmed that HPS6 deficiency affected the *de novo* production and maturation of WPBs.

Regulated Secretion and Tubulation of vWF Are Compromised in *HPS6* Knockdown HUVECs

The existence of regular tubules of ultra-large vWF is an indicator of WPB maturation that is a driving force to form rod-shaped WPBs (McCormack et al., 2017; Tiemeier et al., 2020). Studies

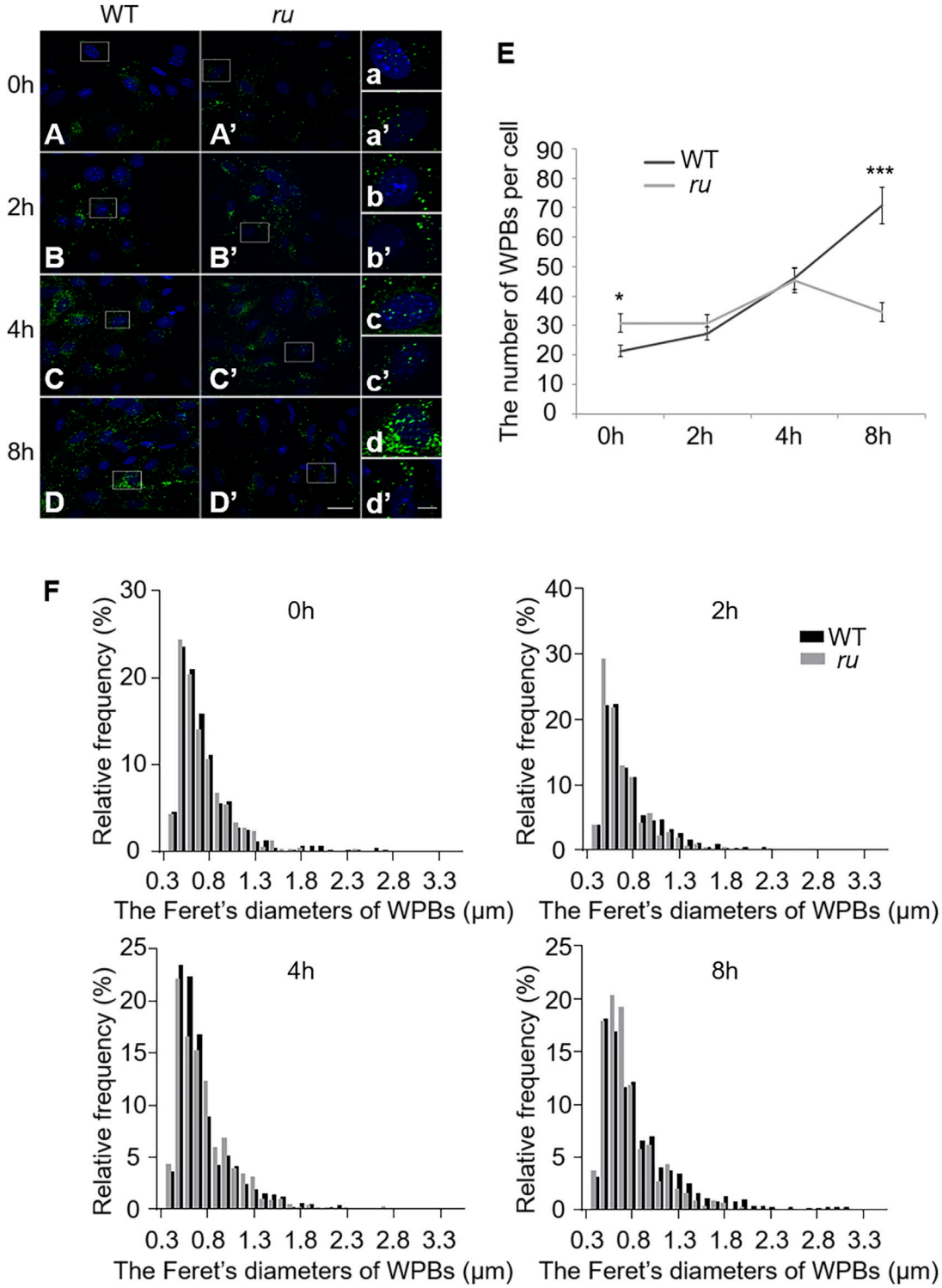

FIGURE 1 | The number and the elongated shape of newly formed Weibel–Palade bodies (WPBs) are affected in *ru* endothelial cells (ECs). Primary endothelial cells were isolated from 4-week-old male WT and *ru* mice and cultured for 10 days, then 80 nM PMA was added to each dish to stimulate WPB secretion for 30 min, and the cells were fixed at 0, 2, 4, and 8 h after washing out. (**A**–**D**) (**A′**–**D′**) Immunofluorescence images of primary endothelial cells at different time points labeled against vWF (green) and nucleus (DAPI, blue). Scale bar, 20 μm. The boxed square in (**A**–**D**) and (**A′**–**D′**) was magnified as (a–d) and (a′-d′), respectively. Scale bar, 5 μm. (**E**) Quantitative analysis of the number of WPBs in each cell of WT and *ru* mice at different time points ($n = 20$, $^{*}p < 0.05$, $^{***}p < 0.001$). (**F**) Feret's diameter distribution of WPBs at each time point in WT and *ru* mice was analyzed quantitatively (WT_{0h}: 428 WPBs, ru_{0h}: 616 WPBs, WT_{2h}: 545 WPBs, ru_{2h}: 612 WPBs, WT_{4h}: 921 WPBs, ru_{4h}: 903 WPBs, WT_{8h}: 1,412 WPBs, and ru_{8h}: 692 WPBs). All the images were analyzed by the NIH ImageJ software. Data were expressed as mean ± SEM. Two independent experiments were performed.

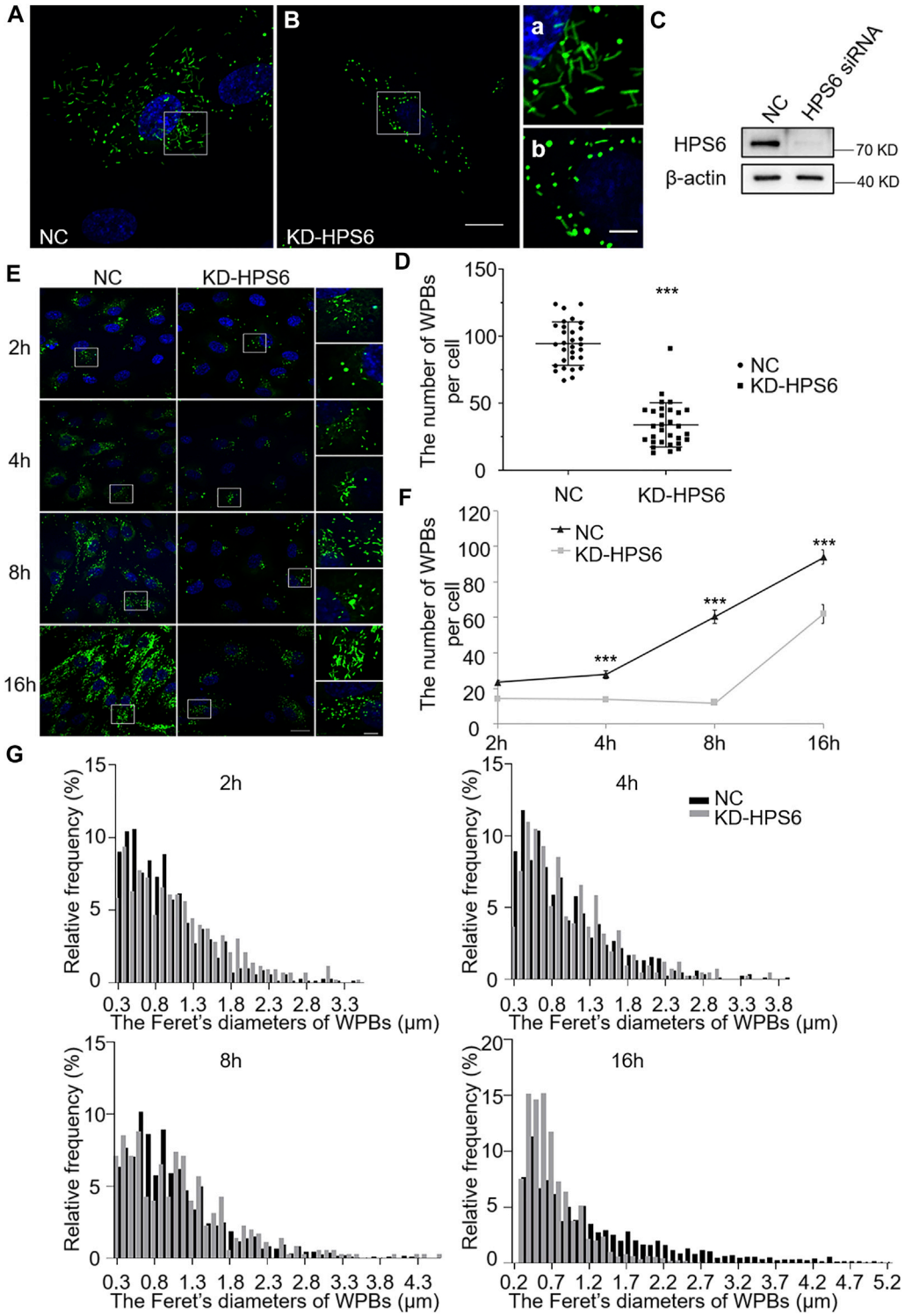

FIGURE 2 | The number and the elongated shape of newly formed Weibel–Palade bodies (WPBs) are affected in KD-HPS6 human umbilical vein endothelial cells (HUVECs). (**A**, **B**) Immunofluorescence images of negative control (NC; **A**) and HPS6 (KD-HPS6; **B**) siRNA-mediated knockdown in HUVECs labeled against vWF (green) and nucleus (DAPI, blue). Moreover, 80 nM PMA was added to each dish to stimulate WPB secretion for 30 min, and the cells were fixed at 2, 4, 8, and 16 h after washing out. Scale bar, 20 μm. The boxed square in (**A**, **B**) was magnified as (a, b) respectively. Scale bar, 5 μm. (**C**) Western blotting analysis of the detection of *HPS6* knockdown. (**D**) Quantitative analysis of the number of WPBs per cell of NC and KD-HS6 HUVECs ($n = 30$, $^{***}p < 0.001$). (**E**) Both NC and KD-HPS6 HUVECs were exposed to 80 nM PMA for 30 min to stimulate WPB secretion, and the cells were fixed at 2, 4, 8, and 16 h, respectively, after washing out. Immunofluorescence images

(*Continued*)

FIGURE 2 | showed the HUVECs at different time points labeled against vWF (green) and nucleus (DAPI, blue). Scale bar, 20 μm. The boxed square was magnified, respectively. Scale bar, 5 μm. (**F**) Quantitative analysis of the number of WPBs per cell of NC and KD-HPS6 HUVECs (n = 20, ***p < 0.001). (**G**) Feret's diameter distribution of WPBs at each time point in NC and KD-HPS6 HUVECs was analyzed quantitatively (NC_{2h}: 700 WPBs, KD-$HPS6_{2h}$: 427 WPBs, NC_{4h}: 831 WPBs, KD-$HPS6_{4h}$: 410 WPBs, NC_{8h}: 812 WPBs, KD-$HPS6_{8h}$: 352 WPBs, NC_{16h}: 2,816 WPBs, and KD-$HPS6_{16h}$: 1,862 WPBs). Data were expressed as mean ± SEM. Two independent experiments were performed.

have shown that vWF is released by regulated secretion and unfurls into long strings that are highly efficient in recruiting platelets under flow in neutral plasma (Michaux et al., 2006; Ferraro et al., 2014; El-Mansi and Nightingale, 2021). However, string formation is also dependent on the initial coiling of vWF into tubules. Disruption of coiling impairs orderly unfurling and generates tangles of multimers, which fail to be released into the plasma. WPBs lose their classical rod shapes after the knockdown of *HPS6*. We speculated that this might result in failure of vWF multimerization.

We used PMA as a stimulus to compare the regulated secretion of vWF multimers between NC and KD-HPS6 HUVECs. The deficiency of HPS6 was confirmed by Western blotting analysis in KD-HPS6 HUVECs (**Figure 3A**). Western blotting with an anti-vWF antibody was used to analyze the culture supernatant that was subjected to SDS-agarose gel electrophoresis. The results showed apparently regulated secretion in NC cells after PMA stimulation, but not in KD-HPS6 cells (**Figures 3B,E**). These results suggested that HPS6 deficiency may lead to the failure of stimulated secretion of WPBs.

In general, VWF is secreted *via* three pathways. Regulated and basal secretion both occur from WPBs to transport highly multimerized VWF. Regulated secretion is triggered by agonist-mediated activation of the endothelium. In contrast, basal secretion occurs constitutively. The third pathway occurs by the constitutive release of VWF that has not been sorted into WPBs which is not subject to high multimerization. In **Figure 3B**, there was no difference between lane 1 (NC) and lane 3 (KD-HPS6), which can be explained by the fact that the constitutive release and the basal secretion of vWF did not seem affected after KD-HPS6. However, the comparison of lanes 1 and 2 *vs*. lanes 3 and 4 showed that the regulated secretion of vWF was compromised. Decreased vWF secretion is also one of the reasons why HPS6 deficiency leads to coagulation disorders.

To analyze the tubulation of vWF, the ability to form vWF strings in NC and KD-HPS6 HUVECs was assessed after treatment with Triton X-100. Triton X-100 destroys cell membranes and WPB membranes, which exposed vWF to neutral pH *in situ* (Michaux et al., 2006), thereby causing *in situ* diffusion to form vWF strings. Immunofluorescence staining showed vWF strings in NC cells, but very rarely in KD-HPS6 cells (**Figures 3C,D**). In addition, we measured the length of vWF strings in each group of HUVECs and found that the vWF strings were much shorter in KD-HPS6 cells than in WT cells (**Figure 3F**). This suggests that vWF multimers failed to unfurl into the plasma from KD-HPS6 HUVECs after stimulation, indicating failure of tubule formation in these cells. Thus, HPS6 plays an important role in the tubulation and secretion of vWF multimers in WPBs.

Steady-State Levels of Several Subunits of v-ATPase Complex Are Decreased in HPS6 Knockdown Cells

As vWF tubulation requires an appropriate acidic environment, we reason that the misshaped WPBs and abnormal release of WPBs in KD-HPS6 HUVECs might be due to a change of the pH value in the lumen of WPBs. It is well known that v-ATPase is the primary proton pump for H^+ homeostasis in organelles, which consists of two multi-subunit domains, V1 and V0. The V1 domain consists of A, B, C, D, E, F, G, and H subunits, while the V0 domain consists of a, d, c, c″, e, and Ac45 subunits. It binds and hydrolyzes ATP for active intermembrane transport of protons (Futai et al., 2019). Therefore, we treated HUVECs with bafilomycin A1 (Baf A1), a v-ATPase inhibitor (Tang et al., 2019), to observe whether the WPB shape and Feret's diameter changed accordingly. Our results showed that most WPBs in the Baf A1 group lost their elongated phenotype (**Figure 4B**), which was consistent with the phenotype of the KD-HPS6 group (**Figure 2B**), whereas no obvious abnormality was found in the DMSO control group (**Figure 4A**). The Feret's diameter distribution of WPBs in these two groups showed that more WPBs in the Baf A1 group had a Feret's diameter of ≤0.8 μm (**Figure 4C**), which indicated that v-ATPase inhibition significantly compromised the size of WPBs.

To further explore the effect of HPS6 on v-ATPase, the steady-state levels of several subunits of v-ATPase were examined in KD-HPS6 HUVECs by Western blotting. We found that the expression levels of ATP6V0D1, ATP6V1H, and ATP6V1B2 in the KD-HPS6 group were significantly lower than those in the NC group (**Figures 4D–I**). Similarly, these changes were observed in HPS3 (another BLOC-2 subunit) knockdown HUVECs (data not shown). These results suggest that HPS6 deficiency may destabilize the v-ATPase complex in KD-HPS6 HUVECs, which likely results in a higher pH in the lumen of WPBs and disrupts vWF tubule formation.

HPS6 Interacts With ATP6V0D1 for Its Trafficking to WPBs

We next investigated whether v-ATPase subunits localized to WPBs. We observed a partial co-localization of the WPB marker vWF with Myc-tagged ATP6V0D1 (**Figure 5A**). To verify the subcellular localization, an Optiprep continuous density gradient was applied to examine the distribution of ATP6V0D1 and vWF in each fraction. The results showed that the main peak of vWF distribution was in the fractions 10–12, which may be the position of the mature WPBs, while the low-density fraction may represent the vWF in the ER, Golgi, and immature WPB. A proportion of ATP6V0D1 existed in the fractions 10–12,

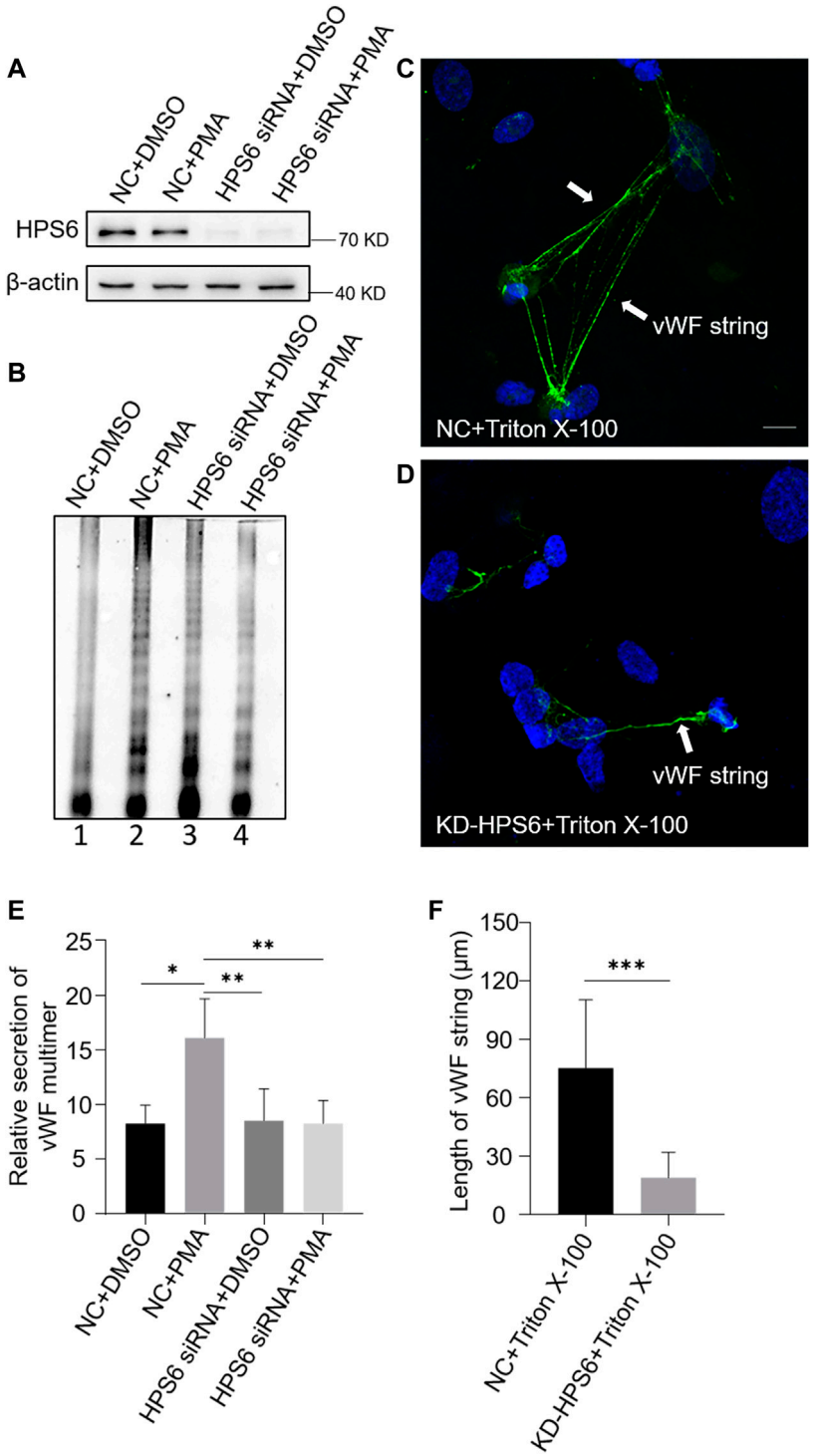

FIGURE 3 | von Willebrand factor (vWF) secretion and the ability to generate surface strings are compromised in KD-HPS6 human umbilical vein endothelial cells (HUVECs). The negative control (NC) and HPS6 siRNA were transfected into two groups of HUVECs, respectively. At 72 h later, one group of NC and KD-HPS6 cells was exposed to 80 nM PMA for 30 min to stimulate WPB secretion, and the other groups were exposed to 0.1% DMSO instead. (**A**) Western blotting analysis of the detection of HPS6 knockdown in cell lysate collection. (**B**, **E**) Western blotting analysis of vWF multimer secretion in supernatant. The multimer gels were analyzed using the NIH ImageJ software. The quantification of supernatant vWF multimers was carried out based on the normalization of the β-actin protein level of the cells in each well. $n = 5$, $^{*}p < 0.05$,$^{**}p < 0.01$. (**C**, **D**) Moreover, 1% Triton X-100 was added into the culture medium of NC and KD-HPS6 HUVECs and cultured at 37°C for 1 h. Immunofluorescence images of two groups of HUVECs labeled against vWF (green) and nucleus (DAPI, blue) were shown. Scale bar, 10 μm. (**F**) The length of vWF strings at each group of HUVECs was measured by the NIH ImageJ software ($n = 30$ per group, $^{***}p < 0.001$). Data were expressed as mean ± SEM. Three independent experiments were performed.

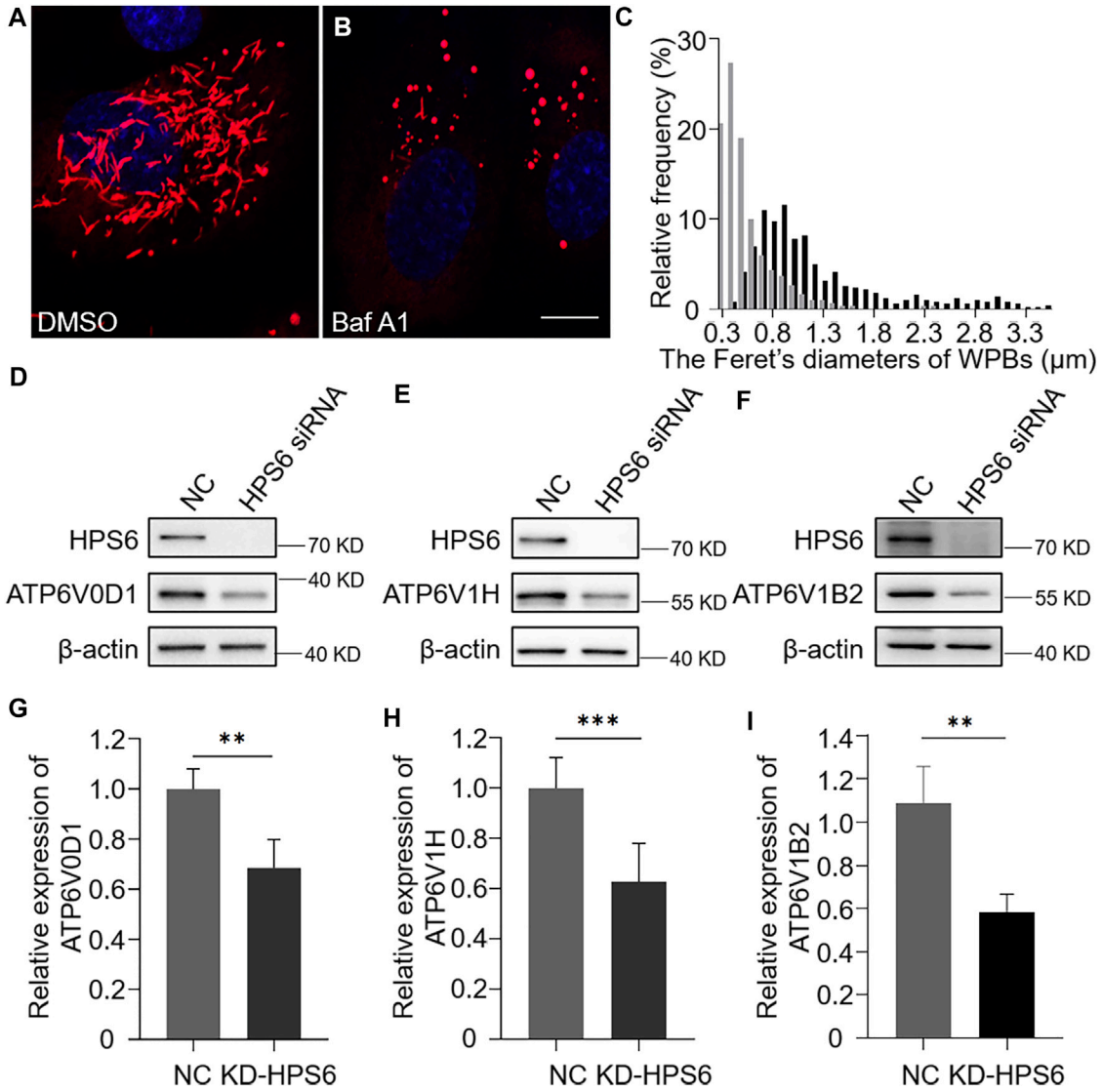

FIGURE 4 | v-ATPase is compromised in KD-HPS6 human umbilical vein endothelial cells (HUVECs). Pharmacological inhibition of the v-ATPase caused the Weibel–Palade bodies (WPBs) to lose their elongated shapes. DMSO or v-ATPase inhibitor, Baf A1 (200 nM), was administered 1 h before cell fixation by 4% PFA ($n = 20$ per group). (**A**, **B**) Immunofluorescence images of DMSO-treated (**A**) and Baf A1-treated cells labeled against vWF (red) and nucleus (DAPI, blue). Scale bar, 10 μm. (**C**) Feret's diameter of WPBs at each group of HUVECs was analyzed quantitatively (DMSO: 502 WPBs, gray; Baf A1: 300 WPBs, black). (**D–I**) siRNA-mediated HPS6 knockdown suppressed the expression of ATP6V0D1, ATP6V1H, and ATP6V1B2, three subunits of v-ATPase ($n = 8$ per group, $^{**}p < 0.01$,$^{***}p < 0.001$). Data were expressed as mean ± SEM. Three independent experiments were performed.

indicating that ATP6V0D1 is partially co-localized with mature WPBs. Part of ATP6V0D1 (fractions 5–8) was co-localized with late endosome/lysosome marker LAMP1 (**Figure 5B**). Furthermore, a co-immunoprecipitation analysis verified the interaction between Myc-tagged ATP6V0D1 and Flag-tagged HPS6 in 293 T cells (**Figure 5C**). Our endogenous immunoprecipitation (IP) also showed that HPS6 immunoprecipitated ATP6V0D1 (data not shown). These data suggest that ATP6V0D1 is likely transported to WPBs as a cargo of HPS6 or BLOC-2.

In order to compare the v-ATPase subunits on WPB after the knockdown of *HPS6*, we performed the Optiprep continuous density gradient experiment and took the same amount of fractions 10–12 that mainly represented the mature WPBs in NC and KD-HPS6 cells for Western blotting. The results showed that the protein levels of ATP6V0D1, ATP6V1H, and ATP6V1B2 were decreased in fractions 10–12 (**Figure 5D**). These results suggested that ATP6V0D1 could not be transported to the WPB membrane correctly after HPS6 deficiency, which likely affects the assembly of the v-ATPase complex and results in disrupted WPB acidification.

To explore whether the decrease in the protein level of ATP6V0D1 after *HPS6* knockdown is due to the degradation of the mis-localized protein, we treated NC and KD-HPS6

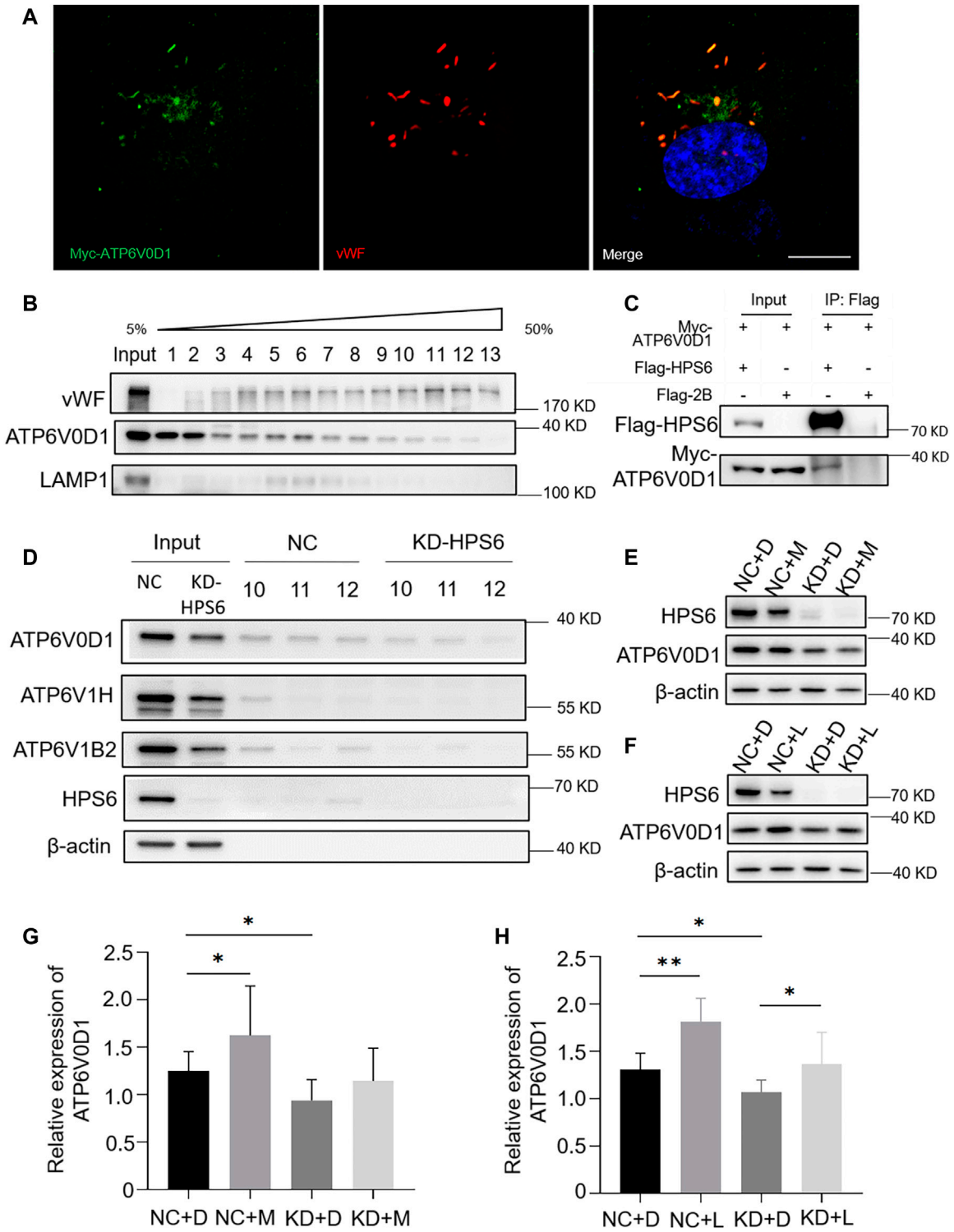

FIGURE 5 | HPS6 interacts with ATP6V0D1 and mediates its trafficking to the Weibel–Palade body (WPB). (**A**) Immunofluorescence images of Myc-ATP6V0D1 plasmid-transfected human umbilical vein endothelial cells (HUVECs) labeled against Myc (green), vWF (red), and nucleus (DAPI, blue). Scale bar, 10 μm. (**B**) Separation of organelles and proteins by Optiprep density gradient. The final organelles and protein pellets were placed onto 50–5% sucrose gradient layers and then centrifuged for 30,000 rpm for 16 h at 4°C. A total of 13 fractions were collected from the top to the bottom of the gradient for further Western blotting experiments to test the distribution of vWF and ATP6V0D1. (**C**) A total of 293 T cells were transfected with Flag-HPS6 and Myc-ATP6V0D1 plasmids, and the cell lysates were co-immunoprecipitated by anti-Flag M2 affinity gel. Western blotting analysis of detection of Flag and Myc bands. (**D**) NC and HPS6 siRNA were transfected into two groups

(*Continued*)

FIGURE 5 | of HUVECs, respectively. At 72 h later, the organelles and proteins were separated by Optiprep density gradient. The input and fractions 10–12 of each group were analyzed by Western blotting. (**E**–**H**) The negative control (NC) and HPS6 siRNA were transfected into two groups of HUVECs, respectively. At 72 h later, one group of NC and KD-HPS6 cells was exposed to 0.25 μM MG132 (M) or 20 μM Leupeptin (L), and the other groups were exposed to 0.1% DMSO (**D**) instead. (**E**, **G**) Western blotting analysis of detection of ATP6V0D1 in KD + M cells. (**F**, **H**) Western blotting analysis of detection of ATP6V0D1 in KD + L cells. $n = 7$, $^{*}p < 0.05$,$^{**}p < 0.01$. Data were expressed as mean ± SEM. Two independent experiments were performed.

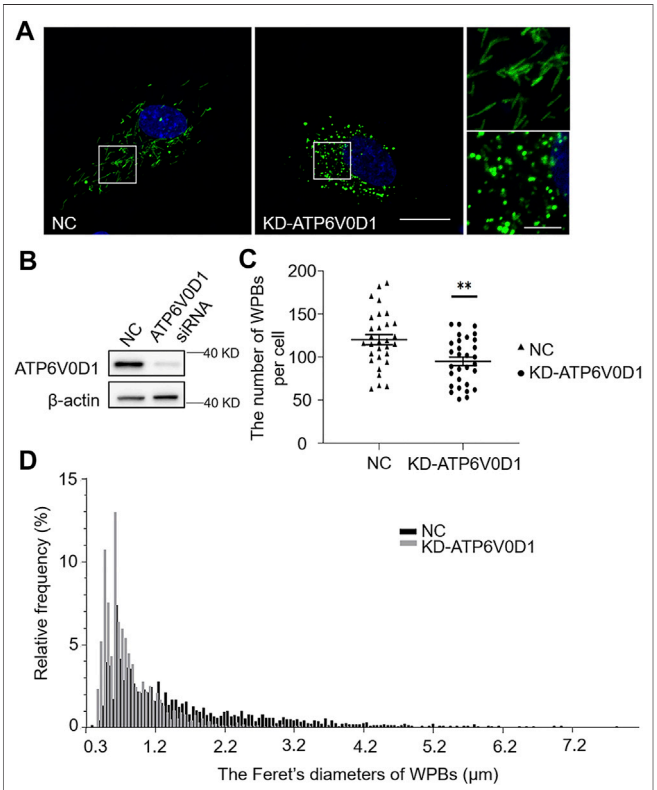

FIGURE 6 | Knockdown of ATP6V0D1 in human umbilical vein endothelial cells (HUVECs) phenocopies the abnormalities of Weibel–Palade bodies (WPBs) KD-HPS6 HUVECs. (**A**) Immunofluorescence images of negative control (NC) and ATP6V0D1 siRNA (KD-ATP6V0D1)-mediated knockdown in HUVECs labeled against vWF (green) and nucleus (DAPI, blue). Scale bar, 20 μm. The boxed squares were magnified, respectively. Scale bar, 5 μm. (**B**) Western blotting analysis of the detection of ATP6V0D1 knockdown. (**C**) Quantitative analysis of the number of WPBs per cell of NC and KD-ATP6V0D1 HUVECs ($n = 30$, $^{**}p < 0.01$). (**D**) Feret's diameter distribution of WPBs at each group of HUVECs was analyzed quantitatively (NC: 3,608 WPBs, black; KD-ATP6V0D1: 2,852 WPBs, gray). Data were expressed as mean ± SEM. Three independent experiments were performed.

HUVECs with a proteasome inhibitor MG132 (M) (Mazzotta et al., 2020; Olmedo et al., 2020) and a lysosome inhibitor leupeptin (L) (Mazzotta et al., 2020), respectively. We optimized the concentration of 0.25 μM MG132 and 20 μM leupeptin as the experimental conditions. Our results showed that, although ATP6V0D1 was increased significantly in the NC + M and NC + L groups compared with that in the NC + D (DMSO) group (**Figures 5E–H**), a significant increase of ATP6V0D1 was found only in the KD + L group and not in the KD + M group compared with the KD + D group (**Figures 5E–H**). These results suggest that, although a portion of ATP6V0D1 may be degraded by the proteosome, ATP6V0D1 is mainly subjected to lysosomal degradation, indicating that mis-targeted ATP6V0D1 is likely degraded *via* the lysosomal pathway that results in a decrease of the steady-state level of ATP6V0D1.

ATP6V0D1 Knockdown Phenocopies the Abnormalities of WPBs in *ru* Mouse Cells and in KD-HPS6 HUVECs

We next investigated the changes of WPBs in HUVECs after the knockdown of the *ATP6V0D1* gene (KD-ATP6V0D1). We found that the changes in shape, number, and size of WPBs in KD-ATP6V0D1 HUVECs were similar to those in *ru* mouse ECs and KD-HPS6 HUVECs (**Figures 6A–D**). The off-target effects of both *siHPS6* and *siATP6V0D1* were excluded by three different target siRNAs (data not shown). Additionally, the regulated secretion and ability to unfurl into the plasma of vWF multimers were impaired in KD-ATP6V0D1 HUVECs (**Figure 7**). These results further confirmed that HPS6 is likely involved in the trafficking of ATP6V0D1 to the WPB membrane for the assembly of v-ATPase to maintain the acidic pH in its lumen. This highlights the importance of H^+ homeostasis in the lumen of WPBs during their biogenesis and release.

DISCUSSION

The BLOC-2 complex functions in transporting cargos from endosomes to lysosomes or lysosome-related organelles in cells. Many studies have shown that the BLOC-2 complex plays an important role in the biogenesis of melanosomes (Dennis et al., 2015). As one of the subunits of the BLOC-2 complex, HPS6 has been reported to be involved in lysosome positioning and maturation in HeLa cells (Li et al., 2014). In this study, we found that HPS6 is involved in the trafficking of ATP6V0D1, a subunit of v-ATPase complex, to the WPB membrane for its assembly into v-ATPase complex to maintain the acidic state of the WPB lumen, which is essential for vWF tubulation and the formation of elongated mature WPBs. When HPS6 is deficient, ATP6V0D1 is missorted and likely subjected to lysosomal degradation, which increases the pH in the lumen of WPBs and ultimately disrupts WPB biogenesis and secretion. This result explains one of the molecular mechanisms by which HPS6 participates in the biogenesis and maturation of WPBs.

Additionally, we revealed that the protein level of ATP6V1H and ATP6V1B2, two other subunits of v-ATPase, was significantly reduced in KD-HPS6 cells. v-ATPase is a macro-

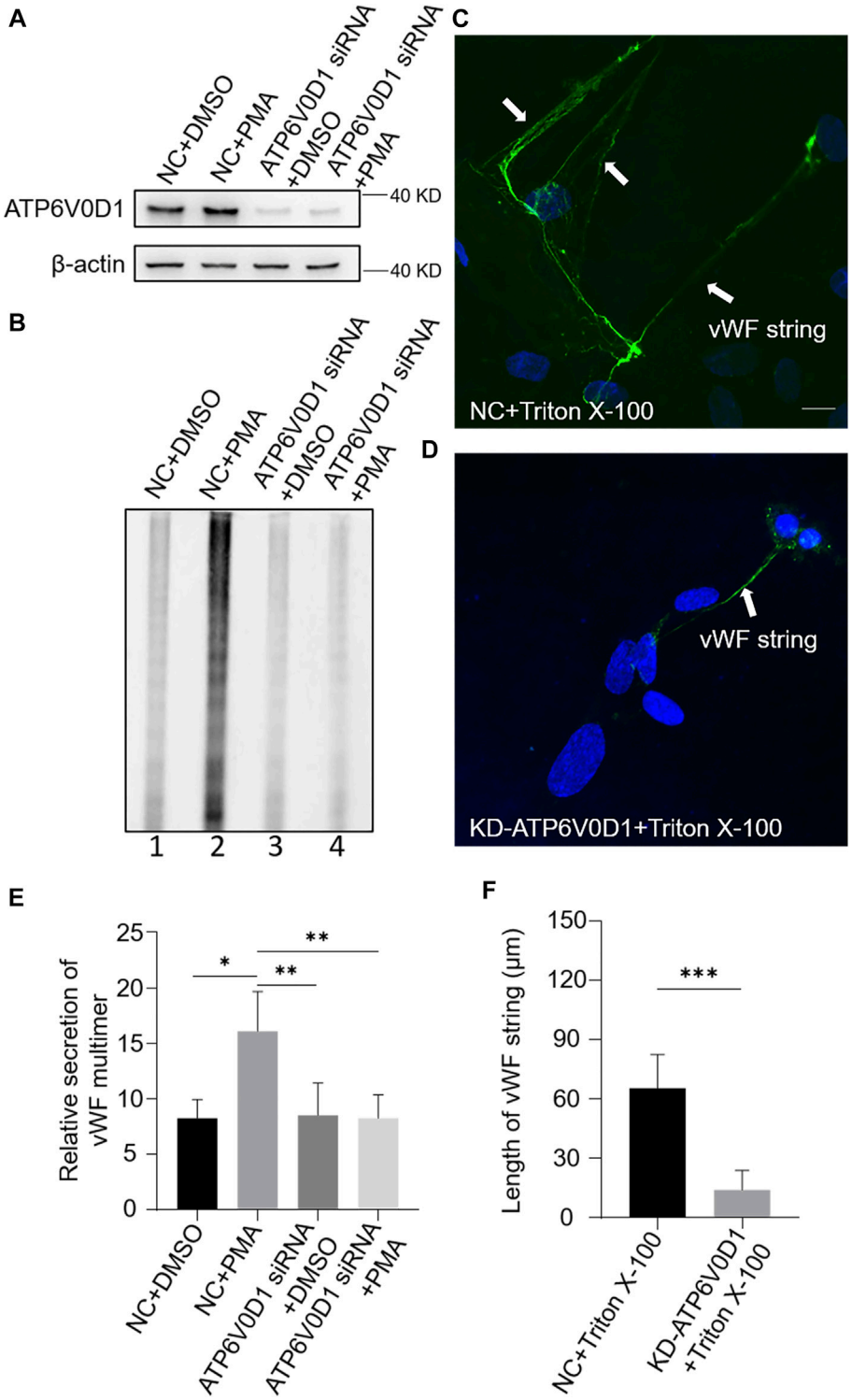

FIGURE 7 | vWF secretion and the ability to generate surface strings are also compromised in KD-ATP6V0D1 human umbilical vein endothelial cells (HUVECs). Negative control (NC) and ATP6V0D1 siRNA were transfected into two groups of HUVECs, respectively. At 72 h later, one group of NC and KD-ATP6V0D1 cells was exposed to 80 nM PMA for 30 min to stimulate Weibel–Palade body secretion, and the other groups were exposed to DMSO (0.1%) instead. (**A**) Western blotting analysis of the detection of ATP6V0D1 knockdown in cell lysate collection. (**B**, **E**) Western blotting analysis of the detection of vWF multimer secretion in supernatant. Multimer gels were analyzed using the NIH ImageJ software. The quantification of supernatant vWF multimers was carried out based on the normalization of the β-actin protein level of the cells in each well. $n = 5$, $^{*}p < 0.05$,$^{**}p < 0.01$. (**C**, **D**) 1% Triton X-100 was added into the culture medium of NC and KD-ATP6V0D1 HUVECs and cultured at 37°C for 1 h. Immunofluorescence images of two groups of HUVECs labeled against vWF (green) and nucleus (DAPI, blue) were shown. Scale bar, 10 μm. (**F**) The length of vWF strings at each group of HUVECs was measured by the NIH ImageJ software ($n = 30$ per group, $^{***}p < 0.001$). Data were expressed as mean ± SEM. Three independent experiments were performed.

complex that consists of two domains with 14 subunits. Except for the ATP6V0D1 subunit, HPS6 or BLOC-2 complex may be similarly involved in the trafficking of other v-ATPase subunits to WPBs. Because of the lack of available antibodies, the interactions between HPS6 and other v-ATPase subunits require further investigation. Another explanation is that the lack of one subunit destabilizes the other subunits in a heterogeneous complex. This is evident in the HPS mutants of BLOC-1/-2/-3, *i.e.*, one subunit deficiency destabilizes the other subunits (Wei and Li, 2013).

During WPB maturation, the luminal pH value is not constant, but it decreases gradually as the WPB matures. The direct correlation between this pH change and the shape of WPBs is evident by vWF multimerization and the assembly of the tubular structures. Mayadas *et al.* found that vWF dimers form multimers when the pH value is between 4.0 and 6.2, and the highest efficiency of multimerization occurs at 5.8 (Mayadas and Wagner, 1989). However, vWF multimers are no longer detectable when pH >6.2. Using compounds such as monensin, NH_4Cl, and chloroquine to increase the pH in the medium, obvious phenotypic changes are visible under an electron microscope, and WPBs showed a significantly round shape (Michaux et al., 2006), which are consistent with the phenotypic changes of WPBs in KD-HPS6 HUVECs. This agrees with the notion that the luminal pH of WPBs is important for their maturation. Unfortunately, we have tested several dyes or tools to monitor the luminal pH changes but failed. A sensitive tool for this measurement needs to be developed.

It is known that the highly polymerized vWF polymers are stored in mature WPBs, which dock near the plasma membrane and release their contents into the blood after stimulation. Both in the endothelial cells of *ru* mice and HUVEC cells, HPS6 deficiency not only changed the classic long rod shape of WPB but also led to a significant reduction in the number of newly generated WPBs. One possible explanation is that HPS6 may also participate in the process of WPB budding from TGN, which awaits further investigation.

In summary, we have revealed that HPS6 or BLOC-2 is involved in the trafficking of v-ATPase subunits to maintain the acidic lumen of LROs. This provides more insights into the underlying mechanism of LRO defects and the pathogenesis of HPS.

MATERIALS AND METHODS

Antibodies

Antibodies Used in Immunofluorescence

The mouse monoclonal antibodies anti-vWF antibodies (1:500, ab201336) were purchased from Abcam (United Kingdom). The rabbit polyclonal anti-human vWF antibodies (1:2,000, A0082) were purchased from Dako (Denmark). The rabbit polyclonal anti-c-Myc antibodies (1:500, C3956) were purchased from Sigma-Aldrich (United States). The goat anti-rabbit IgG (H + L) Highly Cross-Adsorbed Secondary Antibody, Alexa Fluor 488 (1:2,000, CA11008s) or Alexa Fluor 594 (1:2,000, CA11012s) and goat anti-mouse IgG (H + L) Highly Cross-Adsorbed Secondary Antibody, Alexa Fluor Plus 488 (1:2,000, CA11001s) were purchased from Invitrogen (United States).

Antibodies used in Western blotting

The rabbit polyclonal anti-human vWF antibodies (1:10,000, A0082) were purchased from Dako (Denmark). The rabbit polyclonal antibodies against human HPS6 (1:1,000, NBP2-14,100) were from Novus Biologicals (United States). The rabbit polyclonal antibodies against human ATP6V1B2 (1:500, ab73404), ATP6V1H (1:500, ab187706), and ATP6V0D1 (1:1,000, ab202899) were all from Abcam (United Kingdom). The mouse monoclonal antibodies anti-human β-actin (1:100,000, A5441), rabbit polyclonal anti-c-Myc antibodies (1:1,000, C3956), and rabbit polyclonal anti-LAMP1 antibodies (1:2,000, L1418) were purchased from Sigma-Aldrich (United States). The mouse monoclonal anti-Flag tag (1:1,000, MA1-91878) were purchased from Invitrogen (United States). The peroxidase-conjugated secondary anti-rabbit antibodies and anti-mouse antibodies (both 1:5,000, ZB2301 and ZB2305) were all purchased from ZSGB-bio (China).

Animals

Male WT or ruby-eye (*ru*) mutant (HPS6 deficiency in BLOC-2) mice (4 weeks of age) were used for the experiments. They were originally obtained from The Jackson Laboratory (Maine, United States) and maintained in the laboratory of Dr. Richard T. Swank. All these mutant mice arose from spontaneous mutations in C57BL/6J background. The mutation of the *Hps6* gene was confirmed by PCR analysis of tail DNA (data not shown). The animal experiments were carried out in accordance with institutional guidelines for animal experimentation, and the procedures were approved by the Institutional Animal Care and Use Committee of the Institute of Genetics and Developmental Biology, Chinese Academy of Sciences (mouse protocol # AP2021028).

Cell Culture

Primary mouse heart endothelial cells were isolated by magnetic activated cell sorting method as previously described (Ma et al., 2016). The human umbilical vein endothelial cells were obtained from Dr. Qiang Wang's Laboratory (Institute of Zoology, Chinese Academy of Sciences) and maintained in EGM-2 medium (Lonza, cc-3162) at 37°C and 5% CO_2.

ru EC Treatments

Phorbol-12-myristate-13-acetate (Sigma, P1585) in DMSO was added into the EGM-2 medium with 80 nmol/L final concentration. The cells were washed with the growth medium twice after 30 min, changing to fresh growth medium, and then fixed with 4% paraformaldehyde at 0, 2, 4, and 8 h later, respectively.

HUVEC Treatments

PMA in 80 nM final concentration or 0.1% DMSO was added into the EGM-2 medium (respectively) after 30 min. The cells were washed with growth medium twice, changing to fresh growth medium, and then fixed with 4% PFA after 2, 4, 8, and 16 h, respectively, or the supernatant was collected

directly. Triton X-100 (Sigma-Aldrich, T8787) was used at 1% in phosphate-buffered saline (PBS) after pH adjustment. The Triton X-100-treated cells were applied at 37°C for 1 h. All the procedures were followed as described (Michaux et al., 2006). The v-ATPase inhibitor, bafilomycin A1 (Abcam, ab120497), in 200 nM final concentration or 0.1% DMSO was added into the growth medium, respectively, washing the cells with growth medium twice after 1 h and then fixing them with 4% PFA immediately.

RNA Interference

HPS6 expression was suppressed with a siRNA (5′-GCUGGA GAGGAAGGUCCUATT-3′). *ATP6V0D1* expression was suppressed with a siRNA (5′-GCA CUG AUU AUG GUA ACU UTT-3′). The results were compared with a non-targeting NC siRNA (5′-UUCUCCGAACGUGUCACGUTT-3′). A total of 120 nM siRNAs were introduced into HUVECs using Lipofectamine RNAiMAX transfection reagent (Thermo Fisher Scientific, 2103411) according to the protocol of the manufacturer. After transfection (72 h), the cells were treated as needed.

Western Blotting

Cells were lysed with cell lysis buffer for Western and IP [Beyotime, P0013, 20 mM Tris (pH 7.5), 150 mM NaCl, 1% Triton X-100] supplemented with protease inhibitor mixture (Solarbio Life Science, P6730) on ice for 1 h. The lysates were separated in sodium dodecyl sulfate (SDS)-PAGE gels [30% acrylamide, 1.5 M Tris-HCl (pH 8.8), 1.0 M Tris-HCl (pH 6.8), 10% SDS, 10% ammonium persulfate, and TEMED] and then transferred to a polyvinylidene difluoride membrane (Millipore, IPVH00010), which was blocked with 5% non-fat milk in Tris-buffered saline and 0.2% Tween-20 (TBST) for 1 h at room temperature, followed by overnight incubation at 4°C with primary antibodies. After three washes with TBST, the membrane was incubated with appropriate horseradish peroxidase-conjugated secondary antibodies for 1 h at room temperature. The antigen was detected with Mini Chemiluminescent Imaging and Analysis System (MiniChemi) according to the instructions of the manufacturer. The procedures were repeated with the same samples more than twice to react with each primary antibody.

Immunochemistry

Cultured cells were washed once with PBS and fixed in 4% PFA. The cells were permeabilized with 0.4% Triton X-100 in PBS for 20 min and then blocked with 1% bovine serum albumin (BSA) in PBS for 2 h at room temperature. After blocking, the cells were incubated overnight at 4°C with primary antibodies against vWF (diluted 1:2,000 in 3% BSA) and Myc tag (diluted 1:1,000 in 3% BSA). Alexa red- or green-labeled secondary antibodies (1:2,000) were used for signal detection. To stain the nucleus, the cells were incubated with DAPI (ZSGB-BIO, ZLI-9557) before mounting. The labeled cells were observed with a confocal laser scanning microscope (ZEISS, LSM880) equipped with 405-, 488-, and 561-nm excitation laser. Images were taken with ×100 oil objective lens (Zeiss) using ZEN-Black (Zeiss).

vWF Multimer Analysis

Samples were gained from the supernatant after PMA stimulation as described above. In this experiment, the same amount of cells was seeded into each well of the 24-well plate, and the same volume of medium (200 μl) was used during the PMA stimulation. After treating with 80 nM PMA in each well for 1 h, the supernatant samples (150 μl) were loaded in 50 mmol/L Tris, pH 8.0, 1% SDS, 5% glycerol, and 0.002% bromophenol blue. The vWF multimer analysis was as previously described (Ma et al., 2016). Then, 1.2% agarose gels were prepared by dissolving Seakem high-gelling-temperature agarose (Lonza, 50,041) in 0.375 mol/L Tris (pH 8.8), with SDS added to a final concentration of 0.1%. The gels were run at 30 V for 16 h (Tanon, EPS600) before transferring to a nitrocellulose membrane labeled with rabbit anti-vWF antibody (1:10,000), followed by horseradish peroxidase-conjugated anti-rabbit secondary antibody (1: 5,000), and developed by chemiluminescence (Meilunbio, MA0186). The multimers of each lane on the same gel were arranged according to their molecular weight. The multimer gels were analyzed using the NIH ImageJ software. The quantification of supernatant vWF multimers was carried out based on the normalization of the β-actin protein level of the cells in each well.

Plasmid Transfection

The coding sequence of *ATP6V0D1* was amplified by PCR from human cDNA and cloned into the pCDNA3.1 Myc HisB vector, generating *ATP6V0D1* constructs tagged with Myc at the C-terminus. The Flag-HPS6 was obtained from the lab of Jiajia Liu (Li et al., 2014). The plasmids were transfected into 293 T cells with Lipofectamine 2000 (Invitrogen, 11,668) according to the protocol of the manufacturer. The plasmids were transfected into HUVECs with Lipofectamine 3000 (Invitrogen, L3000-015) according to the protocol of the manufacturer.

Co-immunoprecipitation Assay

Co-IP assays were performed as described by Zhang *et al.* (2014). The transfected 293 T cells were harvested and lysed with lysis buffer (1 M Tris-HCl, pH 7.4, 5 M NaCl, 0.5 M EDTA, 1% Triton X-100, and protease inhibitors). The cell lysates were centrifuged at 12,000 rpm for 5 min, and the supernatant was collected and incubated overnight with anti-FLAG M2 affinity antibody (Sigma-Aldrich, A2220) at 4°C and washed 4 times with ice-cold lysis buffer. The samples were eluted with protein loading buffer (Solarbio, P1040) and subjected to SDS-PAGE and Western blotting with anti-Myc antibody (1:1,000) or anti-Flag tag antibody (1:1,000).

OptiPrep Continuous Density Gradient Centrifugation

The fractionation assay was performed using the OptiPrep gradient method as described by Zhang *et al.* (2014). The HUVECs were washed once with PBS and transferred to a 15-ml centrifuge tube after digestion with trypsin. The supernatant

was discarded after centrifugation at 1,000 rpm for 3 min. The sample was resuspended and transferred to a 1.5-ml Eppendorf tube. The supernatant was discarded again after centrifugation. The sample was immediately homogenized with 250 µl HB lysis buffer (250 mM sucrose, 20 mM Tris-HCl, pH 7.4, and 1 mM EDTA) and ground. The sample was placed onto the top of a 12.4-ml continuous 5–50% OptiPrep (Axis-Shield, 1,114,542) gradient in HB buffer. The gradient was centrifuged at 30,000 g for 16 h in a Beckman SW41 rotor at 4°C. Thirteen fractions (900 µl each) were collected from the top. Equal aliquots from each fraction were analyzed for Western blotting.

Statistical Analysis

The NIH ImageJ software was used for the quantitative analysis of Western blotting, determining the number of WPBs in a single cell, and the measurement of Feret's diameter. All results were independently repeated at least three times. All the histograms were plotted using GraphPad Prism software. Student's *t*-test was used as the statistical method, and mean ± standard error (SEM) was used to represent the data. $*p < 0.05$ indicated that there were significant differences in the data. $**p < 0.01$ and $***p < 0.001$ indicated that there was a very significant difference in the data, while NS indicates that there is no significant difference in the data.

DATA AVAILABILITY STATEMENT

The raw data supporting the conclusion of this article will be made available by the authors without undue reservation.

AUTHOR CONTRIBUTIONS

WL and JM designed the study and administrated the whole study. JL and JM conducted the experiments, collected the data, and drafted the manuscript. ZH was involved in methodology and statistical analysis. All authors gave final approval of the version to be published and agreed to be responsible for all aspects of this work.

FUNDING

This work was supported by grants from the Ministry of Science and Technology of China (2019YFA0802104 to WL), from the National Natural Science Foundation of China (91854110 to ZH and 31830054 to WL), from Beijing Natural Science Foundation (5192008 to JM), and from Beijing Municipal Hospitals Scientific Research and Cultivation Program (PX2018048 to JM).

REFERENCES

Aird, W. C. (2007). Phenotypic Heterogeneity of the Endothelium. *Circ. Res.* 100 (2), 158–173. doi:10.1161/01.RES.0000255691.76142.4a

Arribas, M., and Cutler, D. F. (2000). Weibel-Palade Body Membrane Proteins Exhibit Differential Trafficking after Exocytosis in Endothelial Cells. *Traffic* 1 (10), 783–793. doi:10.1034/j.1600-0854.2000.011005.x

Dennis, M. K., Mantegazza, A. R., Snir, O. L., Tenza, D., Acosta-Ruiz, A., Delevoye, C., et al. (2015). BLOC-2 Targets Recycling Endosomal Tubules to Melanosomes for Cargo Delivery. *J. Cel Biol.* 209 (4), 563–577. doi:10.1083/jcb.201410026

El-Mansi, S., and Nightingale, T. D. (2021). Emerging Mechanisms to Modulate VWF Release from Endothelial Cells. *Int. J. Biochem. Cel Biol.* 131, 105900. doi:10.1016/j.biocel.2020.105900

Ferraro, F., Kriston-Vizi, J., Metcalf, D. J., Martin-Martin, B., Freeman, J., Burden, J. J., et al. (2014). A Two-Tier Golgi-Based Control of Organelle Size Underpins the Functional Plasticity of Endothelial Cells. *Develop. Cel* 29 (3), 292–304. doi:10.1016/j.devcel.2014.03.021

Futai, M., Sun-Wada, G.-H., Wada, Y., Matsumoto, N., and Nakanishi-Matsui, M. (2019). Vacuolar-Type ATPase: A Proton Pump to Lysosomal Trafficking. *Proc. Jpn. Acad. Ser. B: Phys. Biol. Sci.* 95 (6), 261–277. doi:10.2183/pjab.95.018

Harrison-Lavoie, K. J., Michaux, G., Hewlett, L., Kaur, J., Hannah, M. J., Lui-Roberts, W. W. Y., et al. (2006). P-Selectin and CD63 Use Different Mechanisms for Delivery to Weibel-Palade Bodies. *Traffic* 7 (6), 647–662. doi:10.1111/j.1600-0854.2006.00415.x

Karampini, E., Bierings, R., and Voorberg, J. (2020). Orchestration of Primary Hemostasis by Platelet and Endothelial Lysosome-Related Organelles. *Arterioscler Thromb. Vasc. Biol.* 40 (6), 1441–1453. doi:10.1161/ATVBAHA.120.314245

Li, K., Yang, L., Zhang, C., Niu, Y., Li, W., and Liu, J.-J. (2014). HPS6 Interacts with Dynactin p150Glued to Mediate Retrograde Trafficking and Maturation of Lysosomes. *J. Cel Sci.* 127 (21), 4574–4588. doi:10.1242/jcs.141978

Lui-Roberts, W. W. Y., Collinson, L. M., Hewlett, L. J., Michaux, G., and Cutler, D. F. (2005). An AP-1/Clathrin Coat Plays a Novel and Essential Role in Forming the Weibel-Palade Bodies of Endothelial Cells. *J. Cel Biol.* 170 (4), 627–636. doi:10.1083/jcb.200503054

Ma, J., Zhang, Z., Yang, L., Kriston-Vizi, J., Cutler, D. F., and Li, W. (2016). BLOC-2 subunit HPS6 deficiency affects the tubulation and secretion of von Willebrand factor from mouse endothelial cells. *J. Genet. Genomics* 43 (12), 686–693. doi:10.1016/j.jgg.2016.09.007

Marks, M. S., Heijnen, H. F., and Raposo, G. (2013). Lysosome-Related Organelles: Unusual Compartments Become Mainstream. *Curr. Opin. Cel Biol.* 25 (4), 495–505. doi:10.1016/j.ceb.2013.04.008

Mayadas, T. N., and Wagner, D. D. (1989). *In Vitro* Multimerization of von Willebrand Factor is Triggered by Low pH. *J. Biol. Chem.* 264 (23), 13497–13503. doi:10.1016/s0021-9258(18)80024-2

Mazzotta, C., Marden, G., Farina, A., Bujor, A., Trojanowski, M. A., and Trojanowska, M. (2020). FLI1 and ERG Protein Degradation Is Regulated via Cathepsin B Lysosomal Pathway in Human Dermal Microvascular Endothelial Cells. *Microcirculation* 28 (1), e12660. doi:10.1111/micc.12660

McCormack, J. J., Lopes Da Silva, M., Ferraro, F., Patella, F., and Cutler, D. F. (2017). Weibel–Palade Bodies at a Glance. *J. Cel Sci.* 130 (21), 3611–3617. doi:10.1242/jcs.208033

Michaux, G., Abbitt, K. B., Collinson, L. M., Haberichter, S. L., Norman, K. E., and Cutler, D. F. (2006). The Physiological Function of von Willebrand's Factor Depends on its Tubular Storage in Endothelial Weibel-Palade Bodies. *Develop. Cel* 10 (2), 223–232. doi:10.1016/j.devcel.2005.12.012

Michaux, G., and Cutler, D. F. (2004). How to Roll an Endothelial Cigar: The Biogenesis of Weibel-Palade Bodies. *Traffic* 5 (2), 69–78. doi:10.1111/j.1600-0854.2004.00157.x

Olmedo, I., Pino, G., Riquelme, J. A., Aranguiz, P., Díaz, M. C., López-Crisosto, C., et al. (2020). Inhibition of the Proteasome Preserves Mitofusin-2 and Mitochondrial Integrity, Protecting Cardiomyocytes during Ischemia-Reperfusion Injury. *Biochim. Biophys. Acta (Bba) - Mol. Basis Dis.* 1866 (5), 165659. doi:10.1016/j.bbadis.2019.165659

Savage, B., Sixma, J. J., and Ruggeri, Z. M. (2002). Functional Self-Association of von Willebrand Factor during Platelet Adhesion under Flow. *Proc. Natl. Acad. Sci.* 99 (1), 425–430. doi:10.1073/pnas.012459599

Schillemans, M., Karampini, E., Kat, M., and Bierings, R. (2019). Exocytosis of Weibel-Palade Bodies: How to Unpack a Vascular Emergency Kit. *J. Thromb. Haemost.* 17 (1), 6–18. doi:10.1111/jth.14322

Tang, T., Xu, W., Ma, J., Wang, H., Cui, Z., Jiang, T., et al. (2019). Inhibitory Mechanisms of DHA/CQ on pH and Iron Homeostasis of Erythrocytic Stage

Growth of Plasmodium Falciparum. *Molecules* 24 (10), 1941. doi:10.3390/molecules24101941

Tiemeier, G. L., Koning, R., Wang, G., Kostidis, S., Rietjens, R. G. J., Sol, W. M. P. J., et al. (2020). Lowering the Increased Intracellular pH of Human-Induced Pluripotent Stem Cell-derived Endothelial Cells Induces Formation of Mature Weibel-Palade Bodies. *STEM CELLS Transl Med.* 9 (7), 758–772. doi:10.1002/sctm.19-0392

Valentijn, K. M., Valentijn, J. A., Jansen, K. A., and Koster, A. J. (2008). A New Look at Weibel-Palade Body Structure in Endothelial Cells Using Electron Tomography. *J. Struct. Biol.* 161 (3), 447–458. doi:10.1016/j.jsb.2007.08.001

Wagner, D. D., Olmsted, J. B., and Marder, V. J. (1982). Immunolocalization of von Willebrand protein in Weibel-Palade bodies of human endothelial cells. *J. Cel Biol.* 95 (1), 355–360. doi:10.1083/jcb.95.1.355

Warhol, M. J., and Sweet, J. M. (1984). The ultrastructural localization of von Willebrand factor in endothelial cells. *Am. J. Pathol.* 117 (2), 310–315.

Wei, A.-H., and Li, W. (2013). Hermansky-Pudlak Syndrome: Pigmentary and Non-Pigmentary Defects and Their Pathogenesis. *Pigment Cel Melanoma Res* 26 (2), 176–192. doi:10.1111/pcmr.12051

Weibel, E. R., and Palade, G. E. (1964). New Cytoplasmic Components in Arterial Endothelia. *J. Cel Biol.* 23 (1), 101–112. doi:10.1083/jcb.23.1.101

Zhang, Z., Hao, C.-J., Li, C.-G., Zang, D.-J., Zhao, J., Li, X.-N., et al. (2014). Mutation of SLC35D3 Causes Metabolic Syndrome by Impairing Dopamine Signaling in Striatal D1 Neurons. *Plos Genet.* 10 (2), e1004124. doi:10.1371/journal.pgen.1004124

Conflict of Interest: The authors declare that the research was conducted in the absence of any commercial or financial relationships that could be construed as a potential conflict of interest.

Publisher's Note: All claims expressed in this article are solely those of the authors and do not necessarily represent those of their affiliated organizations or those of the publisher, the editors, and the reviewers. Any product that may be evaluated in this article or claim that may be made by its manufacturer is not guaranteed or endorsed by the publisher.

frontiers in Cell and Developmental Biology

REVIEW
published: 01 March 2022
doi: 10.3389/fcell.2022.834408

Pathways and Mechanisms of Cellular Cholesterol Efflux—Insight From Imaging

*Alice Dupont Juhl and Daniel Wüstner**

Department of Biochemistry and Molecular Biology, PhyLife, Physical Life Sciences, University of Southern Denmark, Odense, Denmark

Cholesterol is an essential molecule in cellular membranes, but too much cholesterol can be toxic. Therefore, mammalian cells have developed complex mechanisms to remove excess cholesterol. In this review article, we discuss what is known about such efflux pathways including a discussion of reverse cholesterol transport and formation of high-density lipoprotein, the function of ABC transporters and other sterol efflux proteins, and we highlight their role in human diseases. Attention is paid to the biophysical principles governing efflux of sterols from cells. We also discuss recent evidence for cholesterol efflux by the release of exosomes, microvesicles, and migrasomes. The role of the endo-lysosomal network, lipophagy, and selected lysosomal transporters, such as Niemann Pick type C proteins in cholesterol export from cells is elucidated. Since oxysterols are important regulators of cellular cholesterol efflux, their formation, trafficking, and secretion are described briefly. In addition to discussing results obtained with traditional biochemical methods, focus is on studies that use established and novel bioimaging approaches to obtain insight into cholesterol efflux pathways, including fluorescence and electron microscopy, atomic force microscopy, X-ray tomography as well as mass spectrometry imaging.

Keywords: cholesterol, oxysterol, HDL, LDL, ABC transporter, extracellular vesicles, niemann pick disease, apoprotein A1 (Apo A1)

OPEN ACCESS

Edited by:
Emily Eden,
University College London,
United Kingdom

Reviewed by:
Frederick Maxfield,
Cornell University, United States
Neale David Ridgway,
Dalhousie University, Canada

****Correspondence:***
Daniel Wüstner
wuestner@bmb.sdu.dk

Specialty section:
This article was submitted to Membrane Traffic, a section of the journal Frontiers in Cell and Developmental Biology

Received: *13 December 2021*
Accepted: *04 February 2022*
Published: *01 March 2022*

Citation:
Juhl AD and Wüstner D (2022) Pathways and Mechanisms of Cellular Cholesterol Efflux—Insight From Imaging. Front. Cell Dev. Biol. 10:834408. doi: 10.3389/fcell.2022.834408

1 CHOLESTEROL–AN IMPORT LIPID CONSTITUENT OF CELLULAR MEMBRANES

Cholesterol is a small lipid molecule consisting of a steroid ring system, a short alkyl-chain and a hydroxy group at position 3 as the only polar constituent. These properties, together with the asymmetric orientation of its methyl groups, give cholesterol a unique ability to interact with phospholipids in cellular membranes. Cholesterol reduces the propensity of gauche configurations in carbon chains, thereby ordering the fatty acid acyl chains, decreasing the distance between phospholipid head groups and condensing the lipid bilayer (Mouritsen and Zuckermann, 2004). This ability critically depends on both, the steroid back bone and the aliphatic side chain of cholesterol (Ipsen et al., 1990; Henriksen et al., 2006; Scheidt et al., 2013). As a result of this interaction, membrane permeability and bending flexibility are reduced, while lateral lipid diffusion is largely preserved (Ipsen et al., 1990). Thus, cholesterol has the ability to maintain lipid and protein mobility in a membrane, while controlling membrane thickness and flexibility as well as the membrane barrier function to metabolites, ions, and signaling molecules. Its presence creates free energy penalties for conformational transitions of proteins in cholesterol-containing membranes,

e.g., due to hydrophobic mismatch or bending resistance in curved membrane regions and during vesicle formation (Lundbæck and Andersen, 2012). Energy barriers to be overcome by proteins during their catalytic cycle in membranes containing cholesterol compared to cholesterol-free membranes can be as high as 45 kJ/mol. This corresponds to 18 times the thermal energy and almost as much as hydrolysis of one ATP molecule (54 kJ/mol) (Lundbæck and Andersen, 2012). In addition, cholesterol can specifically interact with membrane proteins, thereby regulating their function. Prominent examples for regulation of protein function by cholesterol as allosteric ligand are G-protein coupled receptors or ligand-gated ion channels (de Almeida et al., 2004; Chattopadhyay et al., 2005). Cholesterol can also directly control signaling cascades, as shown by its specific binding to components of the Hedgehog pathway, such as Smoothened or Patched (Huang et al., 2016; Gong et al., 2018). Finally, cholesterol can be covalently attached to signaling proteins of the Hedgehog pathway, i.e., as a membrane anchor for Hedgehog and as a sensor to locate Smoothened to primary cilia (Garcia et al., 2001; Xiao et al., 2017). These diverse functions of cholesterol necessitate a tight control of its abundance in cellular membranes. We will start this review by introducing, how cholesterol synthesis and uptake are regulated before discussing mechanisms of cellular efflux of excess cholesterol.

2 CHOLESTEROL HOMEOSTASIS BY FEEDBACK-REGULATED *DE NOVO* SYNTHESIS AND CELLULAR UPTAKE

2.1 A Short Detour Into Cholesterol Synthesis

All carbon atoms in cholesterol originate from acetate, and cholesterol-specific biosynthesis starts with the reduction of the activated ketone body hydroxymethylglutaryl-Coenzyme A into mevalonate by the cytoplasmic enzyme hydroxymethylglutaryl-Coenzyme A reductase (HMG-CoA reductase) (Bloch, 1965). This is followed by a sequential synthesis of five-carbon isoprene units, which can condense to form geranyl- and from there farnesyl-pyrophosphate (a 15-carbon isoprene), which condenses in a head-to-tail-manner to form squalene. Upon oxygen-dependent epoxide formation to activate squalene, cyclization into the steroid backbone to form lanosterol is catalyzed by oxidosqualene cyclase. From lanosterol to cholesterol, either the Bloch or the Kandutsch-Russel pathway are used, which involve an additional 8-9 reaction steps to finally form cholesterol (Cerqueira et al., 2016). Thus, the biosynthesis of cholesterol is very complex, leading also to other important biomolecules, which are either needed in oxidative phosphorylation, such as ubiquinone, for glycosylation reactions, for example, dolichol, or for hydrophobic anchoring of peripheral membrane proteins (e.g. via farnesylations) (Cerqueira et al., 2016). Statins, which are used to lower blood cholesterol levels for the prevention of atherosclerosis, are competitive inhibitors of HMG-CoA reductase, resulting not only in inhibition of synthesis of cholesterol but also of such important isoprene derivatives (Cerqueira et al., 2016).

2.2 Cellular Uptake and Intracellular Fate of Low Density Lipoprotein

Low density lipoprotein (LDL) provides cholesterol for uptake into cells. Upon binding to the LDL-receptor at the plasma membrane (PM), the LDL/LDL receptor complex can be internalized by clathrin-dependent endocytosis (Iaea and Maxfield, 2015; Pfisterer et al., 2016). Adaptor proteins, such as autosomal recessive hypercholesterolemia (ARH) protein are essential for endocytosis of the LDL/LDL receptor complex, and mutations in ARH or the LDL receptor can lead to inherited forms of hypercholesterolemia (Garcia et al., 2001). Upon endocytosis, newly formed endosomes, containing both LDL and its receptor, will release the clathrin coat and start to fuse with pre-existing sorting/early endosomes located in the cellular periphery. Due to a slight drop in pH in the sorting endosomes compared to the cell surface, the LDL-receptor undergoes a conformational change and releases the LDL particle. The free LDL-receptor will subsequently recycle back to the cell surface, either directly from sorting endosomes or via the endocytic recycling compartment (ERC) (Maxfield and Mcgraw, 2004). Exit of the LDL receptor from the sorting endosomes takes place primarily by narrow diameter tubules ensuring a high surface-to-volume ratio for efficient membrane recycling. The released LDL is retained in the lumen of sorting endosomes, which slowly mature into late endosomes, thereby losing their fusion capacity for incoming vesicles and acquiring acid hydrolases from the trans-Golgi network (TGN) for degradation of luminal cargo (Maxfield and Mcgraw, 2004). The LDL particles will be degraded in late endosome and lysosomes (LE/LYSs) where LDL-associated cholesteryl esters (CEs) will be hydrolyzed by acid lipase to unesterified (free) cholesterol and free fatty acids (Chao et al., 1992; Ameis et al., 1994). Some of the liberated cholesterol can be re-esterified by acyl-Coenzyme A acyl transferase (ACAT) in the endoplasmic reticulum (ER) and stored as CEs in lipid droplets (LDs).

2.3 Regulation of Cholesterol Synthesis and Uptake

Since several important regulators of cholesterol homeostasis reside in the ER and the sterol concentration in this organelle is low under physiological conditions, the ER is an excellent control center for cholesterol homeostasis. Cells respond to a drop in cholesterol levels with increased expression of HMG-CoA reductase and other biosynthetic enzymes, which is an important feedback mechanism. (Istvan and Deisenhofer, 2001). This feedback is based on the ER-resident sterol regulatory binding protein (SREBP). SREBP is retained in the ER together with the cholesterol-sensing protein (SCAP), and the two ER retention proteins Insig-1 or -2, during cholesterol replete conditions (Iaea and Maxfield, 2015). Under such condition, cholesterol will bind to SCAP, causing it to bind to Insig (Adams et al., 2004), while oxysterols will bind to Insig promoting it to bind and

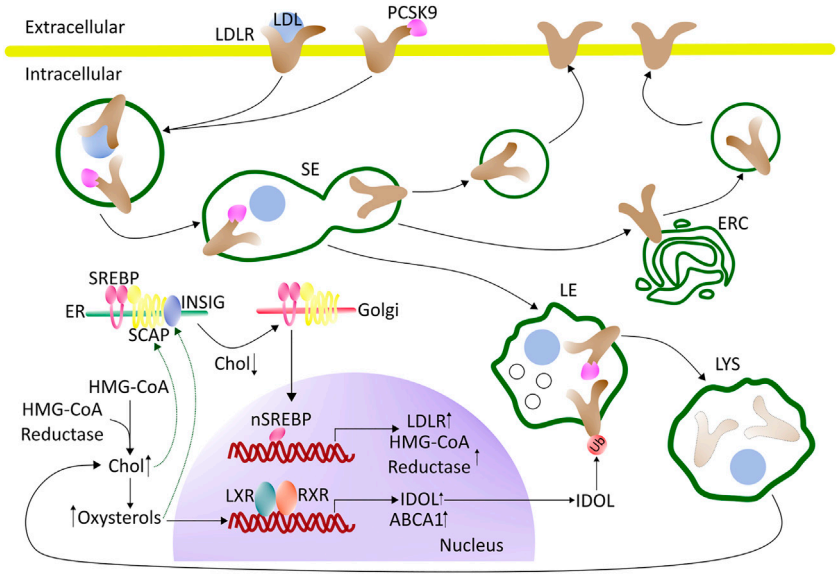

FIGURE 1 | Regulation of cholesterol synthesis and uptake - an overview. LDL binds to the LDL receptor (LDLR) at the cell surface and becomes internalized by clathrin-mediated endocytosis. Upon arrival in the sorting endosomes (SE), LDL dissociates from the LDLR and is retained in the lumen of SE which gradually mature into late endosomes (LE). The LDLR recycles back to the cell surface, either directly from the SE or by passing through the endocytic recycling compartment (ERC). The maturation process of SE into LE, and the further conversion of LE into lysosomes (LYS), involves the formation of internal vesicles in LE, acquisition of LBPA, a drop in pH, and import of proteases, lipases, and other lysosomal enzymes from the Golgi. When the cell is rich in cholesterol, SREBP will be retained in the ER by SCAP and Insig. Cholesterol will bind to SCAP, whereas oxysterol will bind to Insig (green arrows). LXR will be activated by oxysterols, which together with RXR can induce the transcription of genes involved in protecting the cells from becoming overloaded with cholesterol. During low cholesterol conditions, the SCAP-SREBP complex will be released from Insig in the ER and move to the Golgi for cleavage and activation (nSREBP). In the nucleus, nSREBP can activate the transcription of genes involved in cholesterol biosynthesis and uptake. The expression of PCSK9, which promotes the degradation of the LDL-receptor by interfering with its recycling, is also under the control of the nSREBP system. Intracellular degradation of LDLR is promoted by the E3 ubiquitin ligase IDOL, whose expression is stimulated by LXR under conditions of high cellular cholesterol. See the text for more details. ABAC1 (ATP-binding cassette A1), Chol (cholesterol), ER (endoplasmic reticulum), ERC (endocytic recycling compartment), HMG-CoA (3-hydroxy-3-methylglutaryl-Coenzyme A), IDOL (inducible degrader of the LDL receptor), LDL (low-density lipoprotein), LDLR (LDL-receptor), LXR (liver-X receptor), PCSK9 (proprotein convertase substilisin/kexin type 9), RXR (retinoid X receptor) SCAP (SREBP-Cleavage-Activating protein), SE (sorting endosomes), SREBP (sterol regulatory element-binding protein), Ub (ubiquitin).

retain SCAP in the ER (Radhakrishnan et al., 2007; Luo et al., 2020). Once the ER cholesterol level drops below 5 mol% SCAP will undergo a conformational change that will cause the SCAP-SREBP complex to be released from Insig (Radhakrishnan et al., 2008). The SCAP-SREBP complex can then be transferred in COPII coated vesicles to the Golgi apparatus, where SREBP will be activated by cleavage and release of its N-terminal transcription factor (nSREBP). In the nucleus, nSREBP can activate the transcription of genes involved in cholesterol metabolism, synthesis, and uptake such as the HMG-CoA reductase and the LDL-receptor (Horton et al., 2003; Yang et al., 2020). Remarkably, nSREBP controls both LDL endocytosis, by activating the transcription of LDL-receptor, and at the same time down-regulation of the same receptor by inducing the transcription of the Proprotein convertase subtilisin/kexin type 9 (PCSK9; **Figure 1**). PCSK9 is a secreted protein, which binds to the extracellular site of LDL-receptor on the PM and becomes internalized together with the LDL-receptor. Once inside early endosomes, PCSK9 prevents the pH-dependent conformational change of the LDL-receptor, which is necessary for its recycling, promoting receptor degradation in the LE/LYSs (McNutt et al., 2007; Mousavi et al., 2009; Zhang et al., 2012). Upon nSREBP-stimulated synthesis, LDL receptor can also be escorted by PCSK on the secretory pathway from the TGN directly to LE/LYSs for degradation (Schilling et al., 2004). This complex control mechanism of LDL receptor synthesis and degradation by sterol-induced regulation of nSREBP activity shows the importance of tight surveillance of LDL uptake into cells for overall cholesterol homeostasis.

In addition to the SREBP/SCAP/Insig system, nuclear receptors play a major role in cholesterol regulation. For example, the liver X receptors (LXRs) function as complementary and independent sterols sensors, which are particularly important for the control of cellular cholesterol efflux. LXRs are activated by oxysterols, which are generated when cellular cholesterol levels are high (Luu et al., 2016). Upon activation LXRs together with isomers of retinoid X receptors (RXRs) will bind as heterodimers to their DNA response element (**Figure 1**) (Zhao and Dahlman-Wright, 2010). This will induce the transcription of genes that are involved in protecting the cell from becoming overloaded with cholesterol, including the ATP-binding cassette transporter A1 (ABCA1) which mediates the egress of phospholipids and cholesterol to acceptor proteins, such as apolipoprotein A-1 (apoA1) (Venkateswaran et al., 2000). To prevent a futile cycle of cellular cholesterol uptake via endocytosis of LDL and cholesterol efflux by ABC transporters, the inducible

degrader of LDL-receptor (IDOL), an E3 ubiquitin ligase, is also regulated by the LXR pathway (Zhang et al., 2012; Scotti et al., 2013). The function of IDOL is to ubiquitinate the LDL-receptor, which leads to its association with components of the endosomal sorting complex required for transport (ESCRT) (Scotti et al., 2013). As a consequence, the LDL-receptor is retained in LE/LYSs and degraded. ESCRT is not only essential for the degradation of endosomal cargo but also for the formation of cholesterol-rich intraluminal vesicles (ILVs), which accumulate in late endosomes, as they mature (Gruenberg, 2020). By ubiquitinating the LDL receptor and thereby stimulating its lysosomal degradation, IDOL limits the uptake of cholesterol when cellular cholesterol levels are high (Zelcer et al., 2009; Scotti et al., 2011; Zhang et al., 2012) (**Figure 1**). How precisely IDOL mediates degradation of the LDL receptor is not known, but it seems to be unaffected by proteasome blockers, suggesting that it takes place in endo-lysosomes (Zelcer et al., 2009). Additional regulatory mechanisms for LDL-receptor recycling versus degradation have been discovered and are discussed in a recent dedicated review (Vos and van de Sluis, 2021). Ubiquitination followed by proteasomal degradation is another important regulatory mechanism, which controls the abundance of SREBPs, LXRs, the LDL-receptor, and ATP-binding cassette (ABC) transporters, such as ABCA1 (Sharpe et al., 2014). The ubiquitin proteasome system (UPS) also limits the abundance of enzymes for cholesterol biosynthesis, thereby controlling the overall flux through this pathway (Heinrich and Schuster, 1996; Sharpe et al., 2014).

3 CHOLESTEROL DISTRIBUTION IN CELLS AND THE CHEMICAL POTENTIAL OF CHOLESTEROL IN CELLULAR MEMBRANES

3.1 Cholesterol Distribution Between Subcellular Membranes

Cholesterol is most abundant in the PM, the endocytic pathway, and the TGN with lower concentrations in the ER, mitochondria, and other organelles. Since cholesterol can exchange between organelle membranes by non-vesicular transport without apparent free energy consumption, a homogeneous distribution would be expected, if the chemical potential of cholesterol in all membranes would be equal (Maxfield and Menon, 2006; Wüstner and Solanko, 2015). To prevent that, cells seem to use the free energy gained from ATP-hydrolysis to generate different phospho- and sphingolipid compositions of subcellular organelles. This creates characteristic conditions for the specific interaction of cholesterol in each organelle, which, in turn, indirectly affects the distribution of cholesterol between cellular membranes. Lipid gradients could be maintained by active phospholipid transport, for example via ABC transporters or by enzyme-catalyzed phospholipid modifications, e.g., phosphorylation and dephosphorylation of phosphatidyl inositol species at the ER-Golgi interface (Mesmin and Antonny, 2016). As a consequence, the chemical potential of cholesterol between different organelle membranes could be the same, despite quite different concentrations.

3.2 Active Cholesterol as a Useful Thermodynamic Concept to Rationalize Non-vesicular Transport

Biophysical studies in binary and ternary model membranes have shown that cholesterol can cause the formation of a liquid-ordered phase coexisting with a fluid lipid phase at physiologically relevant temperatures (Ipsen et al., 1987). Above a critical sterol mole fraction, cholesterol can also precipitate from membranes as aggregates and even form cholesterol monohydrate crystals. This pure cholesterol phase forms when the capacity of phospholipids to interact with and thereby solubilize cholesterol in the bilayer is exceeded (Huang. et al., 1999; Bach and Wachtel, 2003). Thus, the chemical potential of cholesterol is assumed to rise abruptly beyond this threshold concentration, leading to free cholesterol, which is not bound to phospholipids (Radhakrishnan and McConnell, 2000). This pool is often popularized as "active cholesterol" and assumed to play an important role in determining inter-organelle sterol fluxes for feedback regulation (Steck and Lange, 2010). For example, if the cholesterol concentration in the PM is raised beyond its physiological set point, non-vesicular transport of this excess cholesterol termed "active cholesterol" back to the ER could reestablish a steady state by shutting off cholesterol synthesis and LDL-mediated uptake via inhibition of the aforementioned SREBP/SCAP/Insig receptor system (Radhakrishnan et al., 2008; Sokolov and Radhakrishnan, 2010; Das et al., 2014). Since membrane cholesterol beyond a critical concentration is often detected using fluorescence labeled bacterial toxin derivatives, such as perifringolysin O (PFO), "active" cholesterol is sometimes also termed "accessible cholesterol" (Das et al., 2013). Concentration-dependent non-vesicular cholesterol transport from the PM to the ER and other organelles, such as LDs, could be mediated by the recently discovered GramD1/Aster proteins (Sandhu et al., 2018; Ferrari et al., 2020; Ercan et al., 2021), by oxysterol binding protein related protein 2 (ORP2) (Wang et al., 2019) or the steroid acute regulatory protein D4 (StARD4) (Mesmin et al., 2011; Iaea et al., 2020). Most of such lipid transfer proteins function at membrane contact sites, where membranes are tethered in close proximity, usually in the range of 5–50 nm, but never fully fuse (Scorrano et al., 2019). The reason for that could be to ensure increased efficiency of cholesterol flux between membranes when cholesterol's chemical potential changes abruptly, since for large changes of the chemical potential, the flux-force relationship between the inter-membrane cholesterol flux and the chemical potential difference can become non-linear (Wüstner and Solanko, 2015). Thus, membrane contact sites might be necessary to enable rapid non-vesicular sterol fluxes when the cholesterol gradient between organelles increases beyond a critical set point.

3.3 Specific Interactions of Cholesterol With Phospholipids Might Determine Its Distribution in Cells

A variety of mechanisms including the formation of stoichiometric complexes, specific hydrogen bonding and

lipid-specific shielding of cholesterol underneath phospholipid headgroups have been invoked to explain specific interactions of cholesterol with other lipids in cellular membranes (Huang. and Feigenson, 1999; Ohvo-Rekila et al., 2002; McConnell and Radhakrishnan, 2003). Notably, fluorescent analogues of cholesterol which have been added to cells in trace amounts or in exchange for some cholesterol have a homogeneous lateral distribution in the PM at least down to an accessible scale of 80 nm and diffuse faster than comparable phospholipid analogues (Wüstner et al., 2016; Pinkwart et al., 2019). These observations indicate that stoichiometric complexes of cholesterol with phospholipids would form only transiently in the PM. On the other hand, phospholipid-specific affinity of cholesterol could not only determine its distribution between cellular membranes at steady state (Wüstner and Solanko, 2015), but also dictate the transbilayer orientation and dynamics of cholesterol in the PM and other membranes. Both, preferred interactions of cholesterol with sphingolipids, like sphingomyelin (SM) and with phosphatidylserine (PS) compared to phosphatidylcholine (PC) or phosphatidylethanolamine (PE) have been described (Niu and Litman, 2002; Ohvo-Rekila et al., 2002; Nyholm et al., 2019). Recent studies in yeast and mammalian cells indicate that the majority of ergosterol and cholesterol reside in the cytoplasmic leaflet of the PM, which is rich in PS but not sphingolipids (Mondal et al., 2009; Maekawa and Fairn, 2015; Courtney et al., 2017; Solanko et al., 2018). Still, in both yeast and mammalian cells, sphingolipids, and PS asymmetry control sterol enrichment in the inner leaflet (Maekawa and Fairn, 2015; Courtney K. C. et al., 2018; Solanko et al., 2018). We will discuss the implications of these observations in the context of cholesterol efflux mechanisms from the PM below.

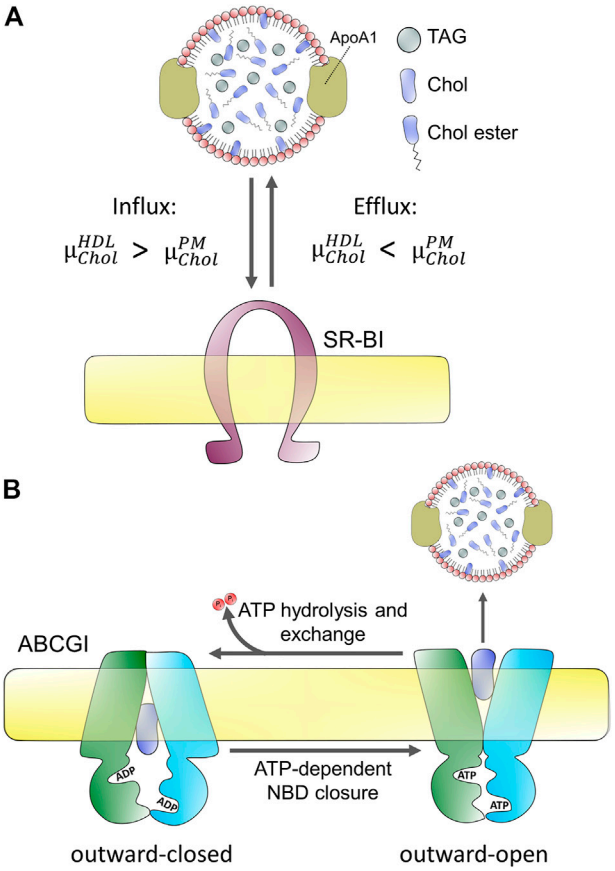

FIGURE 2 | Passive and active protein-mediated cholesterol efflux from mammalian cells. **(A)** passive efflux does not require hydrolysis of ATP but depends on the difference of chemical potentials of cholesterol in the acceptor, here HDL (μ_{Chol}^{HDL}) and PM (μ_{Chol}^{PM}). Cholesterol efflux requires, that $\mu_{Chol}^{HDL} < \mu_{Chol}^{PM}$, and is shown here for scavenger receptor BI (SR-BI). **(B)** Active efflux, illustrated here for the ABC transporter ABCG1, depends on the binding of two ATP molecules, which stabilize an outward-open conformation for efflux of cholesterol and phospholipids to e.g., HDL. ATP-hydrolysis causes the transition of the protein two an outward-closed conformation, allowing for entrance of new substrate on the cytosolic side of the PM. The full cycle is more complex and involves at least four steps; see (Skarda et al., 2021).

4 CELLULAR EFFLUX OF CHOLESTEROL AND FORMATION OF HIGH-DENSITY LIPOPROTEINS

4.1 Cell-type Dependent Efflux of Cholesterol and Formation of High-Density Lipoprotein

Early observations made more than 50 years ago showed that cholesterol can be partly removed from mammalian cells by incubation with serum and particularly the high-density lipoprotein (HDL) fraction of serum (Bailey, 1965; Rothblat et al., 1999). Later studies showed that the half-time of cholesterol efflux is cell-type dependent, being about 4 h in rat hepatoma cells but more than 1 day in human fibroblasts (reviewed in Rothblat et al. (1999)). Cells can efflux cholesterol to the HDL apoprotein apoA1, to lipid vesicles, and to serum albumin (Rothblat et al., 1999; Sankaranarayanan et al., 2013). Additionally, cyclodextrins have been shown to be efficient efflux acceptors, often employed as research tools to study kinetic pools of cellular cholesterol efflux (Kilsdonk E. P. C. et al., 1995; Yancey et al., 1996; Haynes et al., 2000). While the kinetics of cholesterol efflux differs between sterol acceptors, the overall rank order of efflux between cell types does not, and only the abundance of phospholipids in acceptor particles seem to dictate the net efflux capacity (Rothblat et al., 1999). To a large extent, the formation of nascent HDL takes place at the cell surface. However, HDL can also receive cholesterol upon endocytosis of the lipoprotein, its passage through early endosomes, and recycling back to the cell surface, as shown for mature HDL and apoprotein E (Heeren et al., 2003; Heeren et al., 2004). This so-called retroendocytosis can also deliver cholesterol from HDL to cells as shown in fibroblasts and hepatocytes by biochemical methods and quantitative imaging, respectively (Webb et al., 2004; Wüstner et al., 2004; Wüstner, 2005; Sun et al., 2006; Röhrl et al., 2012). It appears that net cholesterol efflux is only possible if the chemical potential of cholesterol in the acceptor

particles, for example HDL, μ_{Chol}^{HDL}, is lower than in the donor membrane, which could be the PM, μ_{Chol}^{PM}, (Yancey et al., 1996; Rothblat et al., 1999). In the opposite case, cholesterol will be delivered to cells, and if the chemical potentials are equal, i.e., $\mu_{Chol}^{HDL} = \mu_{Chol}^{PM}$, cholesterol will passively exchange between donor and acceptor without net efflux from or net influx into cells (**Figure 2**).

4.2 Cells Regulate Cholesterol Efflux by Setting its Chemical Potential in Membranes and Lipoproteins

How can cells regulate the efflux of cholesterol based on this physicochemical principle? There are primarily two mechanisms mammalian cells use to ensure efflux of cholesterol by lowering its chemical potential in the acceptor particles; 1) the fraction of phospholipids in acceptor particles is increased, providing interaction partners for cholesterol, thereby lowering its chemical potential, and 2) by preventing cholesterol from being recaptured by cells via its esterification in the acceptor particle (Fielding, 2009). Both processes are widely implemented and—in fact—tightly regulated, as will be discussed in more detail below. First, the efflux efficiency of sera is strongly correlated with HDL phospholipid levels and many efflux transporters, such as ABC transporters either co-transport phospholipids with cholesterol or even have certain phospholipid species as primary substrate (Rothblat et al., 1999; Coleman et al., 2013). Second, Lecithin:cholesterol acyltransferase (LCAT) catalyzes the transfer of an acyl chain from PC, the main phospholipid in cell membranes and lipoproteins, to the released cholesterol, thereby creating CEs and lysolecithin in the acceptor particle (Fielding and Fielding, 1971; Fielding, 1985). Conversion of cholesterol into CEs in HDL lowers its chemical potential, μ_{Chol}^{HDL}, ensuring that the condition for efflux of cholesterol from cells along its chemical potential gradient (i.e., $\mu_{Chol}^{HDL} < \mu_{Chol}^{PM}$) is maintained (**Figure 2**). Electron microscopy (EM) combined with cross-linking and deuterium exchange mass spectrometry has been used to show that LCAT directly binds to nascent, discoidal HDL particles via interaction with the protein belt formed by helix 5 and 6 of apoA1 (Nakamura et al., 2004; Manthei et al., 2020). Importantly, the activity of the enzyme is highest for lipid-poor apoA1 containing 2–3 PC and cholesterol molecules compared to mature HDL and ceases, as HDL particles mature (Nakamura et al., 2004; Fielding, 2009). This is likely, because a lid at the LCAT surface, which is necessary to allow for substrate entrance and activation by lipid-free apoA1, is prevented from opening in mature HDL particles but not in nascent HDL (Manthei et al., 2017; Manthei et al., 2020). Thus, biochemical feedback ensures that lipoprotein-associated cholesterol esterification ceases, when HDL has matured, and efflux stops (i.e. $\mu_{Chol}^{HDL} \approx \mu_{Chol}^{PM}$). Subsequently, the sterol-loaded HDL particle can return to the liver for transfer of CEs into hepatocytes followed by cholesterol secretion into bile or incorporation of cholesterol into very low density lipoproteins (VLDL) (Robins and Fasulo, 1997; Wanon et al., 1998; Robins and Fasulo, 1999). A third possible mechanism to maintain a chemical gradient of non-esterified cholesterol between cells and efflux acceptors, such as HDL is to remove some of the generated CEs in exchange for PC with other lipoproteins. This process is catalyzed by cholesteryl ester transfer protein (CETP), which exchanges CEs for PC molecules in a 1:1 fashion between HDL and apoprotein B containing lipoproteins, such as VLDL and LDL (Tall, 1993; Barter et al., 2003). Unfortunately, enrichment of these lipoproteins with CEs has a proatherogenic effect, which made inhibitors of CETP an attractive target for drug development (Ferri et al., 2018). However, despite several promising drug candidates as CETP inhibitors, none have been approved (Sheridan, 2016). Anacetrapib, developed by Merck, showed particularly promising results but was in the end not submitted for regulatory approval, as the drug had a very long half-life (Nissen, 2017). Other drugs, such as torcetrapib developed by Pfizer and Dalcetrapib developed by Roche, also raised plasma HDL levels but did not show any benefit in preventing cardiovascular disease (Sheridan, 2016). Based on these outcomes, it is unlikely that developing CETP inhibitors is a useful strategy for treatment of arteriosclerosis and cardiovascular disease in the near future (Swain, 2017). In some cases, HDL might also directly receive cholesterol from other lipoproteins, for example from aggregated LDL during contact with activated macrophages in the intima of the vessel wall (Singh et al., 2019).

5 STRUCTURE, MEMBRANE DYNAMICS, AND MOLECULAR FUNCTION OF CHOLESTEROL EFFLUX TRANSPORTERS

5.1 Transporters for Active Versus Passive Efflux of Cholesterol From Cells

Since cholesterol is very hydrophobic its water solubility is very low (i.e., below 30 nM), and there is a high free energy cost of moving it between membranes through the water phase (Rothblat et al., 1999; Wüstner and Solanko, 2015). Consequently, cholesterol exchange between membranes is very slow in the absence of proteins, and mammalian cells use a variety of transporters to facilitate cholesterol efflux to lipoproteins. Energy-dependent efflux of cholesterol from cells is mediated by ABC transporters, primarily ABCA1, ABCG1, and ABCG4 (Tall et al., 2002; Phillips, 2014). Passive cholesterol exchange between cells and mature HDL is facilitated by scavenger receptors, especially scavenger receptor BI (SR-BI; **Figure 2**), but results concerning the quantitative contribution of each of these transporters are not without contradiction (Wang et al., 2001; Thuahnai et al., 2003; Peng et al., 2004; Wang et al., 2004; Yancey et al., 2004a; Yancey et al., 2004b; Vedhachalam et al., 2007; Wang et al., 2007b; Pagler et al., 2011). Cell-type specific differences reflected in different tissue expression of these transporters contribute to disparate findings concerning their precise role in cholesterol efflux. In addition, they might have a varying affinity to nascent versus mature HDL. For example, while ABCG1/4 and SR-BI preferentially transfer cholesterol to mature HDL, ABCA1 plays a major role in the initial lipidation of ApoA1 to form nascent HDL particles (Liu et al., 2003; Thuahnai et al., 2003; Wang et al., 2004; Vaughan and Oram, 2006; Adorni et al., 2007). Also, ATP-dependent efflux by ABC transporters, such as ABCA1 and exchangers, like SR-BI seems to be inversely regulated (Chen et al., 2000). Based on these and other findings, a model has been proposed according to which the specific interaction between ApoA1 and ABCA1 creates nascent

HDL particles which become transformed into mature HDL, increasingly receiving cholesterol from efflux by ABCG1 and ABCG4 (Vaughan and Oram, 2006; Wang et al., 2008). SR-BI is a bi-directional transporter with regulated and cell-type dependent endocytosis and recycling (Silver et al., 2001; Eckhardt et al., 2004; Webb et al., 2004; Wüstner, 2005; Shetty et al., 2006; Sun et al., 2006; Marques et al., 2019). Most cholesterol transfer between HDL and SR-BI seems to take place at the cell surface, but some cholesterol exchange can also happen in endosomes (Wüstner et al., 2004; Wüstner, 2005; Sun et al., 2006; Marques et al., 2019). The direction of net cholesterol flux between subcellular membranes is also dictated by the sterol gradient, such that cholesterol moves from membranes where its chemical potential is high to membranes, where its chemical potential is low (see above and **Figure 2**). Therefore, efflux of cholesterol to an acceptor lowers the chemical potential of cholesterol in the donating membrane (e.g., the PM), which, in turn, stimulates replenishment of cholesterol from intracellular sites. Vice versa, selective uptake of cholesterol from HDL will increase the chemical potential of cholesterol in the PM, thereby stimulating non-vesicular sterol transfer to intracellular sites. SR-BI also mediates selective uptake of cholesterol and CEs from HDL into hepatocytes, which plays an important role in cholesterol clearance into bile during reverse cholesterol transport (Kozarsky et al., 1997; Robins and Fasulo, 1997; Robins and Fasulo, 1999). Similarly, SR-BI mediates selective uptake of CEs into steroid hormone-producing cells. Based on the crystal structure of LIMP-2, which is a related member of the CD36 superfamily of scavenger receptors, a large hydrophobic cavity acting as a tunnel for transfer of CEs has been proposed for SR-BI (Neculai et al., 2013). Bidirectional lipid transfer between membranes and HDL or other lipoproteins can also be induced as a passive process upon contact, as shown by combined fluorescence correlation spectroscopy and high-speed atomic force microscopy (AFM) (Plochberger et al., 2017). Thus, the function of SR-BI and other scavenger receptors might be primarily to bring lipoprotein and PM into close enough contact, such that hydrophobic lipid transfer can take place. Alternatively, the hydrophobic channel formed by SR-BI is needed for sterol exchange. Future studies are needed to clarify this issue.

5.2 ATP-Binding Cassette Transporter A1 is a Prototype Efflux Transporter for Cholesterol

Mutations in ABCA1 have been associated with Tangier disease, a rare genetic disorder characterized by very low levels of HDL and apoA1 and high accumulation of CEs, primarily in blood-derived macrophages but also in tissue macrophages in various organs, such as tonsils, liver, spleen, and lymph nodes (Tall and Wang, 2000; Quazi and Molday, 2011). Additionally, patients have lipid deposits in other cell types, such as fibroblasts, Schwann cells, or smooth muscle cells (Oram, 2000). Symptoms of Tangier disease include coronary artery disease, neuropathies, splenomegaly, and hepatomegaly (i.e., enlargement of spleen and liver) (Oram, 2000). A recently reported cryo-electron microscopy structure of ABCA1 with 4.1 Å resolution revealed the symmetric nature of the protein, in which the two transmembrane domains with the connected nucleotide-binding domains and the two large extracellular domains form a hydrophobic tunnel for lipid translocation (Qian et al., 2017). A lateral access model for lipid substrates has been proprosed and Tangier disease mutations could be mapped to the structure of the protein (Qian et al., 2017). Interestingly, monomeric ABCA1 has significant sequence identity and similarity with ABCG5/8, a heterodimer of ABC transporters, which is responsible for the excretion of cholesterol from the apical canalicular membrane of hepatocytes into bile (Yu et al., 2002; Qian et al., 2017). Both ABC structures can be superimposed revealing close structural similarity despite the fact, that they belong to different ABC transporter subfamilies (Qian et al., 2017). ABCA1 might act in concert with other ABC transporters, such as ABCG transporters, but also with ABCA8 and ABCA12, as shown in macrophages during reverse cholesterol transport (Fu et al., 2013; Trigueros-Motos et al., 2017). More information about the structure, regulatory sequences, such as phosphorylation and ubiquitination sites, as well as substrate specificity of ABCA1 and other ABC transporters involved in cholesterol transport can be found in comprehensive recent reviews (Phillips, 2018; Kerr et al., 2021).

5.3 Quantitative Imaging of Membrane Transporters for Cholesterol Efflux

Live-cell imaging and correlative microscopy have contributed greatly to our current understanding of proteins involved in cholesterol export from cells. For example, by combining EM with light microscopy using diaminobenzidine induced photooxidation, Stangl and co-workers studied subcellular trafficking of SR-BI and its lipid substrates with high resolution (Röhrl et al., 2012). Recent single-molecule tracking and Förster resonance energy transfer (FRET) imaging experiments in living cells revealed that SR-BI is primarily organized in dimers and fails to enter clathrin-coated pits for endocytosis (Sahoo et al., 2007; Marques et al., 2019). This underlines its importance in exchange of cholesterol and CEs at the cell surface. Green fluorescent protein-tagged ABCA1 (GFP-ABCA1) traffics very dynamically between PM, endo-lysosomes, and the Golgi apparatus in cells (Neufeld et al., 2001; Neufeld et al., 2004). GFP-ABCA1 diffuses apparently freely in the PM, but its lateral dynamics depends on its ATPase activity and binding to apoA1, as shown by spot variation fluorescence correlation spectroscopy (Raducka-Jaszul et al., 2021). Similarly, the ATPase activity of ABCA1 affects the diffusion of other membrane proteins, such as the transferrin receptor and fluorescent lipid analogues, as shown in fluorescence recovery after photobleaching experiments (Zarubica et al., 2009). GFP-ABCA1 resides in liquid-disordered domains in formaldehyde-induced giant plasma membrane vesicles (GPMVs), suggesting that it prefers a fluid lipid environment (Zarubica et al., 2009). Single-molecule tracking found GFP-ABCA1 in largely immobile spots at the PM, and its confinement depended on its ATPase activity, somehow contradicting the findings made by fluorescence correlation spectroscopy (Nagata et al., 2013; Raducka-Jaszul et al., 2021). Photobleaching of GFP-ABCA1 occurred primarily in two discrete steps, indicating that the protein forms dimers in the

PM, supporting an earlier study based on FRET imaging and native PAGE analysis (Trompier et al., 2006; Nagata et al., 2013). Both studies found that apoA1 stabilizes dimers or oligomers, suggesting that ABCA1 is not able to transfer lipids to apoproteins in its monomeric state. These and similar studies show the power of sensitive fluorescence imaging to reveal the molecular function and dynamics of ABC transporters in cholesterol efflux from cells (Wong et al., 2016). But it remains an important challenge to validate results of membrane receptor dynamics with different imaging approaches.

6 MECHANISMS OF LIPID EFFLUX TO APOA1—WHICH STRUCTURES ARE FORMED AT THE CELL SURFACE?

6.1 ATP-Binding Cassette Transporter A1 Transports a Variety of Phospholipids Across Lipid Membranes

Several hypotheses have been put forward to explain the molecular mechanisms underlying ABCA1's function: 1) ABCA1 acts as a receptor for apoA1 on the cell surface thereby catalyzing the direct transfer of lipids onto apoA1 (Wang et al., 2001; Fitzgerald et al., 2004). 2) ABCA1, which follows a complex intracellular trafficking scheme (Neufeld et al., 2002; Zha et al., 2003; Neufeld et al., 2004), mediates lipidation of apoA1 during its passage through the cell, likely by a retroendocytic pathway (Denis et al., 2008). 3) ABCA1 acts as a pump for lipids, like the aminophospholipid PS, or other hydrophobic substances at the cell surface, which is supported by its intrinsic ATPase activity and substrate specificity (Wang et al., 2001; Tall et al., 2002; Alder-Baerens et al., 2005; Linsel-Nitschke and Tall, 2005; Quazi and Molday, 2013), 4) ABCA1 acts as cholesterol floppase, i.e. actively moving cholesterol from the inner to the outer PM leaflet for pick up by apoA1 (Ogasawara et al., 2019; Okamoto et al., 2020). In fact, ABCA1 translocates analogues of PC, SM, and PS across membranes in a reconstituted system and PE and PS to the outer leaflet of mammalian cells, and it seems to bind and transport even phosphatidylinositol-bisphosphate (Alder-Baerens et al., 2005; Quazi and Molday, 2013; Gulshan et al., 2016). Whether ABCA1 directly binds cholesterol, a precondition for its translocation by this ABC transporter, is debated (Reboul et al., 2013; Dergunov et al., 2019).

6.2 ATP-Binding Cassette Transporter A1 Controls the Transbilayer Distribution of Lipids in the Plasma Membrane

Phospholipid asymmetry in the PM has a regulatory function in cholesterol efflux, and there is a large body of evidence that ABCA1 affects the transverse distribution of phospholipids and cholesterol in the PM, thereby increasing the propensity of these lipids to efflux from cells. Translocation of negatively charged phospholipids to the outer PM leaflet by ABCA1 causes altered surface membrane potential and reduced rate of endocytosis (Zha et al., 2001; Alder-Baerens et al., 2005; Zarubica et al., 2009). Exposing more PS to the outer leaflet by other mechanisms, for example by inhibiting the synthesis of sphingolipids with myriocin, causes increased ABCA1-independent cholesterol efflux in RAW macrophages (Gulshan et al., 2013). The same treatment increased the ergosterol content in the outer PM leaflet of yeast cells and long-chain sphingolipids in the outer leaflet regulate cholesterol asymmetry in the PM of mammalian cells (Courtney K. C. et al., 2018; Solanko et al., 2018). Thus, it is likely that altering the transbilayer distribution of PS and abundance of sphingolipids can indirectly cause an increased availability of cholesterol for efflux from the outer PM leaflet. Interestingly, the expression of ABCA1 shifts the steady state distribution of not only PS but also of fluorescent cholesterol analogues towards the outer leaflet, from which apoA1 can directly access the sterols for efflux (Alder-Baerens et al., 2005; Pagler et al., 2011; Gulshan et al., 2013). Since the transbilayer dynamics of cholesterol in model membranes and likely the PM of living cells is very high, with flip-flop time constants in the msec-sec range, any actively generated cholesterol gradient across the PM bilayer would equilibrate rapidly (John et al., 2002; Steck et al., 2002; Bennett et al., 2009). Measured hydrolytic activity of ABCA1 and other ABC transporters for ATP is too slow to maintain a transbilayer cholesterol asymmetry by directly pumping sterol to the outer leaflet in the presence of such high rates for passive sterol flip-flop (Quazi and Molday, 2013; Skarda et al., 2021). This is in contrast to the much slower passive flip-flop of phospholipids across membranes (Coleman et al., 2013). Thus, instead of directly transporting cholesterol, it is more likely that active translocation of PS by ABCA1 indirectly increases cholesterol availability in the outer half of the bilayer for efflux to acceptor proteins. Supporting that notion are observations in yeast and mammalian cells, which found that loss of PS asymmetry or abundance in the inner leaflet increases cholesterol availability in the outer leaflet of the PM (Maekawa and Fairn, 2015; Solanko et al., 2018). Together, these results suggest that ABCA1 alters the lipid composition and transbilayer orientation of lipids in the PM, which can facilitate phospholipid and cholesterol efflux from cells to apoA1.

6.3 Does ATP-Binding Cassette Transporter A1 Facilitate Protrusion of Cholesterol From the Bilayer or Bending of the Plasma Membrane?

Binding experiments with fluorescence-labeled PFO, which detects membrane cholesterol above a characteristic threshold concentration, found strong binding in cells expressing ABCA1 (Ogasawara et al., 2019; Okamoto et al., 2020). The cholesterol pool detectable by PFO domain D4 and similar reporters, such as the cholesterol-binding domain 4 of anthrolysin O (ALO-D4), has often been associated with "accessible" or "active" cholesterol (see **Section 3**, above) (Courtney K. C. et al., 2018). The increased chemical potential of "active cholesterol" implies, that it might have an elevated propensity to protrude from the membrane, but whether this sterol pool is entirely available for efflux from cells remains to be shown. It also remains an open question whether the ATPase activity of ABCA1 is only used to translocate PS and

other phospholipids to the outer PM leaflet, or also to decrease the energy barrier for partial cholesterol protrusion from the bilayer, which could facilitate sterol transfer to an acceptor particle, such as apoA1 (Small, 2003; Van Meer et al., 2006; Phillips, 2014; Plummer et al., 2021). Zha and co-workers have shown that expression of ABCA1 without any addition of apoA1 changes the organization of proteins and lipids in the PM and causes the release of apoA1-free microparticles with a size of >20 nm (Landry et al., 2006; Nandi et al., 2009). RAW macrophages express ABCA1 only when preincubated in the presence of cAMP to activate protein kinase A, and expression of functional ABCA1 in the absence of apoA1 triggers cellular excretion of apoA1-free microparticles (Liu et al., 2003; Nandi et al., 2009). Vice versa, deletion of ABCA1 and ABCG1 resulted in increased cholesterol content of the PM and impaired migration of macrophages due to increased Rac signaling (Pagler et al., 2011). Morphological analysis of EM images of baby hamster kidney (BHK) cells with inducible expression of ABCA1 revealed disc-like HDL particles with a diameter < 20 nm and additionally larger vesicular structures secreted from cells with a diameter of 50–150 nm and up to 500 nm (Hafiane and Genest, 2017). Such microparticles were also secreted by THP1 macrophages in an ABCA1 and ApoA1 dependent manner (Hafiane and Genest, 2017). Could such particles be vesicles which form at the PM and if so, how do they form? When apoA1 inserts into the lipid bilayer, formation of an "activated lipid domain" has been proposed, which can lead to outward-directed vesiculation of the PM (Vedhachalam et al., 2007; Phillips, 2014). Such a mechanism could be supported by ABCA1-mediated translocation of phospholipids to the outer PM leaflet, creating increased lateral pressure in this monolayer thereby facilitating membrane bending (Coleman et al., 2013; Phillips, 2014). Active lipid flipping has been proposed as a mechanism for the regulation of endocytosis by aminophopholipid translocases, which catalyze ATP-dependent flipping of PS and PE to the inner PM leaflet (Pomorski et al., 2003; Hirama et al., 2017). Since ABC transporters, such as ABCA1 transport phospholipids in the opposite direction, they can create an excess area in the outer PM monolayer, and this asymmetric membrane stress can be relieved by bending the bilayer outwards, eventually leading to the formation of exovesicles and/or nanodiscs (Coleman et al., 2013). Such a monolayer pleating effect of phospholipid flopping to the outer leaflet is supported by molecular dynamics simulations (Segrest et al., 2015). This study suggests that ABCA1 forms an extracellular reservoir containing an isolated squeezed monolayer, which triggers the release of membrane particles from the PM. In the presence of apoA1, such particles are primarily membrane discs, with a majority of lipids originating from the outer PM leaflet, while in the absence of ApoA1, the disks transform into unilamellar vesicles (Segrest et al., 2015). In this model, tight packing of membrane helices of ABCA1 in dimers could control access of cholesterol to prevent it from counterbalancing the outward bending of the bilayer. The latter is needed since fast passive flipping of cholesterol to the inner leaflet was found to relax bending energies of membranes, both in experiments and simulations (Bruckner et al., 2009; Choubey et al., 2013; Segrest et al., 2015). Whether ABCA1 controls access of cholesterol to the forming membrane protrusions, as suggested in simulations (Segrest et al., 2015), or eventually reduces its flipping to the inner leaflet during membrane bending by a cholesterol floppase activity remains to be determined (Okamoto et al., 2020). In our view, the latter is unlikely due to the high passive flip-flop rates of cholesterol and the comparably slow ATPase activity of ABC transporters (see above).

6.4 Biliary Lipid Secretion as a Model for Exo-vesiculation of the Plasma Membrane by ATP-Binding Cassette Transporters

Interestingly, a very similar vesiculation mechanism to that described above has been proposed to mediate biliary secretion of cholesterol and PC. This process depends on the ABCG5/8 heterodimer and the PC-translocating ABC transporter ABCB4, also named multidrug resistance protein 2 (MDR2), which are both expressed in the canalicular membrane of hepatocytes (Yu et al., 2002). ABCG5/8 mediate the secretion of cholesterol and plant sterols, such as sitosterol, into bile and intestine, and mutations in these transporters lead to sitosterolemia, an inherited accumulation of plant sterols in various tissues (Plummer et al., 2021). Loss of functional ABCG5/8 or ABCB4 leads to defective lipid secretion into the bile, which is the major pathway for cholesterol clearance from the human body (Small, 2003). In mice, about 55% of cholesterol is excreted as fecal neutral sterols, with the remainder being secreted as bile acids (Dietschy and Turley, 2002). However, these values can change dramatically in animals with defective sterol transporters. EM of rapidly frozen liver sections, has provided evidence that the initial event of biliary secretion of PC and cholesterol takes place as small vesicles, shed directly from the canalicular membrane (Crawford et al., 1995). This process is facilitated by the aforementioned ABC transporters and by bile acids, cholesterol-derived detergents, which contribute to lipid solubilization in the bile fluid (Crawford, 1996; Crawford et al., 1997; Small, 2003). Bile acids intercalate into the outer leaflet of the PM, from which they can solubilize phospholipids, either as mixed micelles or as microvesicles, and independent of phospholipid head group composition (Kuipers et al., 1997; Wüstner et al., 1998; Wüstner et al., 2000). Thus, a preferred vesiculation of the outer leaflet of the canalicular membrane was proposed to result in specific enrichment of PC and cholesterol in the bile fluid (Crawford et al., 1995; Small, 2003). Monomeric bile acids can also directly stimulate the ATPase activity of ABCB4/MDR2 (Kroll et al., 2021). Active translocation of PC to the outer leaflet by ABCA4 as well as of aminophospholipids to the inner leaflet of the canalicular membrane by the P-type ATPase ATP8B are required to prevent membrane damage and to ensure specific enrichment of PC, bile acids, and cholesterol in the bile (Tannert et al., 2003; Cai et al., 2009; Groen et al., 2011). This conclusion is supported by clinical manifestations of cholestasis and liver damage when either ABC4 or ATP8B are mutated and dysfunctional, as observed in progressive familial intrahepatic cholestasis (Cai et al., 2009; Groen et al., 2011). Another example

for cooperation between ABC transporters in lipid secretion is that of ABC4 and ABCG5/8, which are both required for release of cholesterol into the bile (Langheim et al., 2005). Interestingly, while apoA1 secreted into bile can assist in solubilizing cholesterol and preventing gallstone formation (Secknus et al., 1999), the ABCA1/apoA1 system is not directly involved in cholesterol secretion from hepatocytes into bile. In fact, ABCA1 resides in the basolateral but not in the canalicular membrane in cultured polarized hepatocytes (Neufeld et al., 2002). ABCA1 is also enriched in a subapical endocytic compartment in such hepatocytes, an organelle which is known to be rich in free cholesterol and accessible to HDL from the basolateral cell surface during endocytic recycling (Silver et al., 2001; Neufeld et al., 2002; Wüstner et al., 2002; Wüstner et al., 2004). Consequently, ABCA1 is likely involved in regulating intracellular hepatic cholesterol and plasma HDL levels (Neufeld et al., 2002).

7 ORIGIN, STRUCTURE, AND FUNCTION OF CHOLESTEROL-CONTAINING EXTRACELLULAR VESICLES AND PARTICLES

7.1 The Diversity of Extracellular Vesicles and the Challenge of Their Classification

Extracellular vesicles formed independently of the HDL/ABC transporter system have started to be recognized as cholesterol efflux routes, eventually complementing the classical efflux pathways (Pfrieger and Vitale, 2018). Based on their size and origins, extracellular vesicles have roughly been divided into exosomes and microvesicles. Exosomes originate from ILVs inside multivesicular bodies which can fuse with the PM during lysosomal exocytosis (Gruenberg, 2020). They are typically in the size range of 30–150 nm, and their secretion contributes to the efflux of excess cholesterol in lysosomal storage disorders (see below, 8.) (Strauss et al., 2010; Vacca et al., 2019; Ilnytska et al., 2021a). Microvesicles, also called ectosomes, are generated by outward budding of the PM and tend to be more heterogeneous in their morphology and content compared to exosomes (Cocucci et al., 2009). Microvesicles tend to be larger, normally around 100–1,000 nm in size, but have been reported to be up to 8–10 μm in size (Falchi et al., 2013). However, the classification of extracellular vesicles should be taken with some caution, as no standard approaches for their characterization have yet been defined (Cocucci et al., 2009; Van Niel et al., 2018). Several methods and approaches are being used to examine extracellular vesicles. One way is to first isolate the vesicles, and subsequently analyze them. The isolation of cell-derived vesicles can be done by several methods including centrifugation, filtration, and aqueous two-phase systems, and the analysis can be carried out with techniques such as immunoblotting, dynamic light scattering, and microscopy (Kim et al., 2015; Shin et al., 2015; Pollet et al., 2018; Hartjes et al., 2019; Kırbaş et al., 2019; Mondal et al., 2019). Another approach is to study the biology of extracellular vesicles directly by microscopy as discussed below and recently reviewed by Verweij et al. (2021). He et al. (2018) used a combination of scanning electron microscopy (SEM) and nanoscale secondary ion mass spectrometry (nanoSIMS) to study PM-derived particles secreted from macrophages upon loading with acetylated LDL (He et al., 2018). Their findings confirm and extend earlier observations made by EM and particle size analysis (Hafiane and Genest, 2017). SEM allowed He et al., 2018) to visualize the formation and release of the particles, whereas nanoSIMS enabled them to obtain high-resolution images of the particle's cholesterol content (**Figure 3**). With this approach, the authors found that the cholesterol content of such released particles varies depending on the cholesterol loading condition (He et al., 2018). By growing the macrophages in the presence of fetal bovine serum and by activating cholesterol efflux via stimulation of LXRs and RXR complexes with agonists, He et al. found that the particles became enriched with cholesterol accessible to ALO-D4, and that this cholesterol pool could be transferred to HDL (He et al., 2018).

7.2 Does Cholesterol Aggregate During its Efflux From Cells?

Using an antibody named mAb 58B1, which is supposed to bind specifically to two-dimensional arrays of 10–20 cholesterol molecules, Jin et al. (2018) reported that macrophages remove excess cholesterol by shedding of cholesterol microdomains (**Figure 3A**) (Jin et al., 2018). This "type" of shedded cholesterol, was different from the one described by He et al. (2018), as particles tended to be larger, up to several hundred nm, and irregularly shaped rather than spherical, like vesicles. The authors of this study found that the cholesterol-binding polyene filipin does not label the cholesterol microdomains detected with mAb 58B1, and they speculated that filipin cannot intercalate into the supposed two-dimensional arrays of cholesterol in the PM of cholesterol-loaded macrophages (Jin et al., 2018). An alternative explanation would be that the primary IgM antibody used in this study cross-links membrane-dispersed cholesterol due to its multivalency, which could be further enhanced by the use of secondary antibodies, employed for detection. Thus, lateral cholesterol clustering could be induced by the antibody treatment, and there is no evidence for naturally occurring cholesterol microdomains. Ample evidence obtained by fluorescence imaging of fluorescent cholesterol analogues shows that sterols move rapidly and freely in the PM of living cells and do not form clusters detectable by light microscopy and super-resolution microscopy (Wüstner et al., 2016; Pinkwart et al., 2019). Even in cholesterol-loaded cells, such as macrophage foam cells, in which ACAT was inhibited, fluorescent cholesterol analogues did not cluster in the PM (Wüstner, 2008). On the other hand, Kruth, Addadi and co-workers found by super-resolution fluorescence microscopy of antibody-treated cells and by X-ray microscopy that microcrystals can form in macrophages under prolonged excess cholesterol loading conditions in the absence of sterol acceptors (Addadi et al., 2003; Varsano et al., 2016). Formation of cholesterol crystals in macrophages after extended incubation with excess cholesterol or atherogenic lipoproteins has been shown previously by EM, and this might be related to the occurrence of cholesterol crystals in the intima of the vessel wall in patients suffering from myocardial infarction

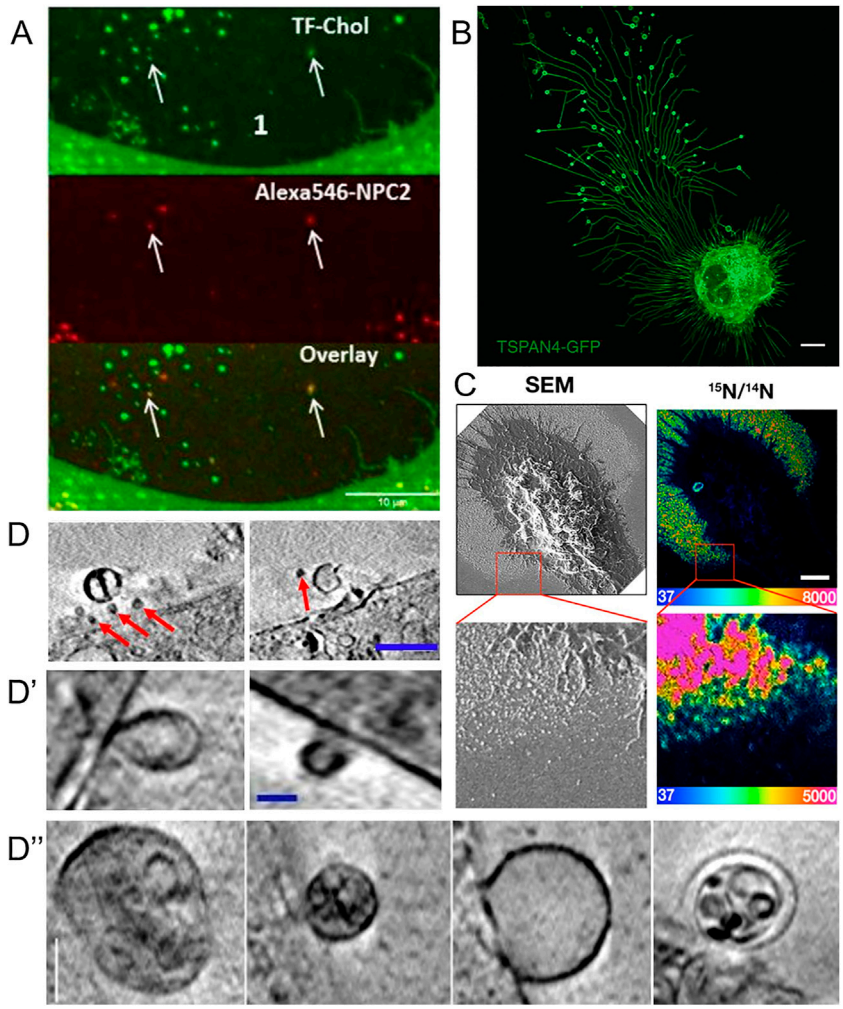

FIGURE 3 | Visualization of extracellular vesicles and particles during cholesterol efflux. **(A)** Spinning disk microscopy image of extracellular vesicles from a NPC2-deficient fibroblasts treated with NPC2 protein, tagged with a red Alexa546 fluorophore (red), and labeled additionally with TopFluor-cholesterol (green) (Juhl et al., 2021). **(B)** Confocal microscopy image of migrasomes from L929 cell transfected with TSPAN4-GFP (Chen et al., 2018). Scalebar 10 µm. **(C)** SEM of nanoSIMS of macrophage after incubation with [^{15}N]ALO-D4. Scalebar 2 µm (He et al., 2018). **(D,D′,D′′)** examples of extracellular vesicles from NPC2 deficient and healthy fibroblasts imaged with cryo-SXT. Scalebar 0.5 µm for **(D)** and 0.15 µm in **(D′,D′′)** (Juhl et al., 2021). Red arrows point to microvesicles.

(Tangirala et al., 1994; Kellner-Weibel et al., 1999; Janoudi et al., 2016). It is possible, that excess cholesterol precipitates from the membrane to form cell-adhered crystals, if cholesterol efflux mechanisms fail. Release of cholesterol in microparticles, as reported by Kruth and co-workers depended on ABCA1, as the authors found no, or very few, microparticles released from macrophages treated with the ABCA1 inhibitor, probucol (Jin et al., 2018). Future studies are needed to clarify the nature of different microparticles released from macrophages during cholesterol efflux.

7.3 Is Shedding of Cholesterol-Rich Microvesicles Coupled to Cell Migration?

Using a combination of proteomics, tracer experiments, super-resolution microscopy, SEM, live cells imaging, and nanoSIMS, Young and co-workers showed that the membrane-derived particles, they described earlier, were released from the macrophages during cell migration (He et al., 2018; Hu et al., 2019). The authors also showed that the released particles were enriched with ALO-D4 accessible cholesterol, but not sphingolipid-sequestered cholesterol (**Figure 3**) (Hu et al., 2019). Interestingly, Das et al. showed that the cholesterol content of the plasma membrane can be divided into three distinct pools: a pool accessible to bacterial toxins, a pool sequestered by sphingomyelin, and an essential pool (Das et al., 2014). The accessible pool was found to be connected with the cholesterol levels in the ER and thus is involved in cellular cholesterol homeostasis (Das et al., 2014; Infante and Radhakrishnan, 2017). Hu et al. suggested that the sphingolipid-sequestered cholesterol, located in the outer leaflet of the PM, is more likely to remain in the membrane during movement as it is indirectly associated with the actin cytoskeleton (Raghupathy et al., 2015;

Hu et al., 2019). The toxin-accessible cholesterol pool of the PM could be more prone to be released from cells during migration (Infante and Radhakrishnan, 2017; Hu et al., 2019). Thus, it is likely that the movement of cells, and thereby the release of cholesterol-rich particles contributes to cellular cholesterol efflux. Supporting that notion, the release of membrane fragments in the form of vesicles and nanotubes during cell migration has been known for decades (Huttenlocher et al., 1995; Fuhr et al., 1998). Such cell traces have been visualized by a variety of imaging techniques, including confocal, interference reflection, and total internal reflection microscopy as well as by AFM and EM (Fuhr et al., 1998). Support for cholesterol efflux from cells in surface-shed vesicles during migration comes from other recent imaging studies; using an elegant mixture of live-cell imaging, EM, and mass spectrometry, Ma et al. described a migration-dependent mechanism of vesicle release from cells, named migracytosis (Ma et al., 2015). During migration, the cell will leave retraction fibers behind on which vesicles up to 3 μm in size can grow, either at the fiber tips or at fiber intersections (**Figure 3B**). These vesicles, named migrasomes, will eventually detach from the fibers and be released. The migrasomes contain a varying number of smaller vesicles and during their growth, they are actively receiving content from the main cell body (Huang et al., 2019). They contain increased amounts of the protein tetraspanin 4 (TSPAN4) and more cholesterol than the retraction fibers, and both, cholesterol and TSPAN4, were necessary and sufficient for migrasome formation (Huang et al., 2019). The primary function of migrasomes has been suggested to be in cell-cell communication (Ma et al., 2015). But due to their relatively high content of cholesterol, their detachment from the cell could be another indirect way for the cell to release cholesterol. Excess cholesterol can also be transferred to co-cultured smooth muscle cells in the absence of HDL or serum (He et al., 2020). Using nanoSIMS, Young and co-workers showed that this pathway is substantially contributing to cholesterol efflux from macrophages and does not depend on ABCA1 (He et al., 2020). Whether it relies on shedding of microvesicles from the donor cells, remains to be determined in future studies. Another recent study reported shedding of large GPMVs containing the cholesterol markers TopFluor-cholesterol or filipin, in human fibroblasts upon induction of membrane vesiculation using dithiotreitol (Sedgwick et al., 2018). Formation of such GPMVs was enhanced upon cyclodextrin treatment to remove cholesterol and upon microtubule stabilization and required actin polymerization (Sedgwick et al., 2018). However, GPMVs are often employed as a model system for the PM, and their chemical-induced formation does not resemble natural vesiculation processes taking place in intact and healthy cells (Sezgin et al., 2012). **Table 1** gives an overview of described extracellular cholesterol-rich particles, their size, cellular origin, and method of detection with focus on various imaging studies.

7.4 Ultrastructure of Released Vesicles–do Cells Shed Entire Endo-Lysosomes Containing Cholesterol?

Using a combination of fluorescence and cryo-soft X-ray tomography (cryo-SXT), we have recently shown that human fibroblasts can shed cholesterol-rich microvesicles from the cell surface without chemical pretreatment (Juhl et al., 2021). These vesicles contained several fluorescent cholesterol markers, such as TopFluor-cholesterol or dehydroergosterol, and they could be labeled with filipin. Additionally, some of the microvesicles did contain lysosomal content including NPC2 protein tagged with a red fluorophore and Lysotracker, a content marker for lysosomes (**Figure 3A**) (Juhl et al., 2021). NPC2 has been shown to be secreted from primary astrocytes independently of secreted cholesterol-rich exosomes, suggesting that the NPC2 containing vesicles we observed in fibroblasts are not exosomes (Mutka et al., 2004; Juhl et al., 2021). Cryo-SXT is a comparably fast 3D ultrastructural microscopy technique, that allows imaging of fully hydrated cryo-fixed cells in less than 1 hour. As an energy source, it typically relies on synchrotron radiation in the energy range between the K-edge absorption of carbon (284 eV) and oxygen (543 eV), also known as the water window (Schneider et al., 2010). Additional staining is not required when imaging biological samples within this water window, since a natural absorption contrast will emerge from the carbon-rich structures. The resolution is down to a few tens of nanometers, and due to the relatively high penetration depth of up to several microns, sectioning of cells is not needed. To obtain 3D tomograms, the sample is tilted around a rotation axis while acquiring single images, that can be aligned and reconstructed (McDermott et al., 2009; Harkiolaki et al., 2018). With cryo-SXT, we were able to resolve the delicate ultrastructure of the shed microvesicles, which revealed internal vesicles in some of them (**Figure 3D**). Based on these observations of extracellular vesicles containing lysosomal cargo and internal vesicles, we suggest the release of entire LE/LYSs as a new mechanism for cholesterol release (Juhl et al., 2021). This process might be reminiscent of cellular release of melanosomes, which are lysosome-related organelles containing melanin for skin pigmentation (Wu and Hammer, 2014). Transfer of melanosomes from melanocytes to skin keratinocytes involves surface shedding of melanosomes and/or melanosome exocytosis, similar to our observed lysosomal efflux of cholesterol (Wu and Hammer, 2014). Shedding of melanosomes takes place preferentially at sites of surface protrusions, such as filopodia and dendrites, to which melanosomes are reallocated in a Myosin-V and actin-dependent process (Wu and Hammer, 2014). Membrane shedding of entire organelles is likely not related to the formation of apoptotic bodies since it has been observed in other cell types under various conditions, including astrocytes, which were found to release lipid droplets and mitochondria together with ATP (Falchi et al., 2013). Extracellular release of mitochondria could be triggered by CD38-mediated synthesis of the calcium messenger cyclic ADP-ribose in astrocytes and serves a role in protecting neurons after stroke (Hayakawa et al., 2016). Vesicular shedding of lysosome-related organelles has also been identified as a mechanism of drug disposal in brain endothelial cells (Noack et al., 2018). Future studies should be directed towards determining the molecular mechanisms, cells use to shed vesicles containing endo-lysosomes and other organelles, and how such mechanisms could be utilized to secrete lipids, such as cholesterol. A summary of the discussed mechanisms for efflux of cellular cholesterol is shown in **Figure 4**, below.

TABLE 1 | Overview of reported extracellular non-lipoprotein particles rich in cholesterol.

Particle type	Size	Method	Cell type	Reference
Membrane-derived particles	30–250 nm	SEM, TEM, nanoSIMS	Macrophages	Vedhachalam et al. (2007), Nandi et al. (2009), Hafiane and Genest (2017), He et al. (2018)
Migrasomes	0.5–3 μm	SEM, TEM, confocal fluorescence microscopy	NRK cells, MEF, NIH3T3, HaCaT, MGC803, SKOV-3, B16, MDA-MB231, HCT116, SW480	Ma et al. (2015), Huang et al. (2019)
Irregular shaped, crystal-like deposits	<<0.5 μm	STED, AFM, SEM	Macrophages	Jin et al. (2018)
Membrane-derived small vesicles	30–700 nm	SXT, confocal fluorescence microscopy	Primary human fibroblasts	Juhl et al. (2021)
Membrane-derived multivesicular structures	0.5–2.0 μm	SXT, confocal fluorescence microscopy	Primary human fibroblasts	Juhl et al. (2021)
Exosomes	30–150 nm	TEM	Oligondendrocytes, Astrocytes, Primary human fibroblasts	Mutka et al. (2004), Strauss et al. (2010), Ilnytska et al. (2021a)

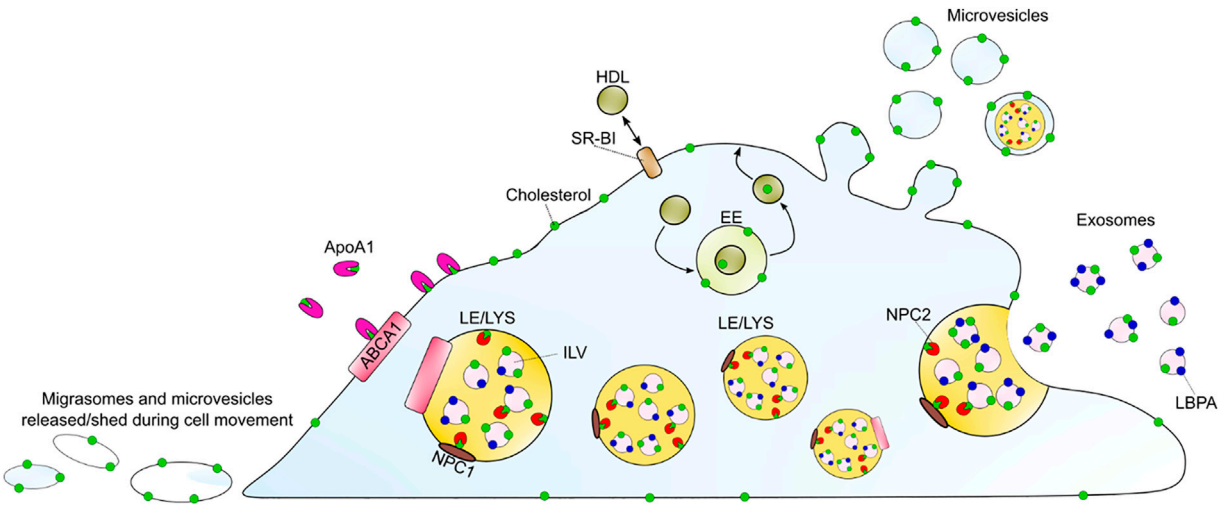

FIGURE 4 | Summary of discussed cholesterol efflux mechanisms. ABCA1 can efflux cholesterol to ApoA1 as the main sterol acceptor. Passive cholesterol exchange between the cell and HDL is mediated by SR-BI. HDL can also gain cholesterol upon endocytosis, passage through endosomes and recycling back to the PM. Additionally, cholesterol might leave the cell by the release of exosomes, upon LE/LYSs fusion with the plasma membrane, or by shedding as microvesicles and/or as migrasomes during cell migration. The LE/LYSs are drawn in different sizes to show the proteins and intraluminal organelles and not to illustrate different populations. ABAC1 (ATP-binding cassette A1), ApoA1 (apolipoprotein A1), EE (early endosomes), HDL (high density lipoprotein), ILV (intraluminal vesicle), LBPA (lysobisphosphatidic acid), LE/LYS (late endosome/lysosome), SR-BI (scavenger receptor BI).

8 EFFLUX OF CHOLESTEROL DERIVED FROM LATE ENDOSOMES AND LYSOSOMES

8.1 The Role of Niemann Pick Type C Proteins in Export of Cholesterol From Endo-lysosomes

Several organelles can provide cholesterol for efflux, including the cholesterol-rich recycling endosomes, LE/LYSs, the Golgi apparatus, and LDs (Neufeld et al., 2001; Neufeld et al., 2004; Denis et al., 2008; Ouimet et al., 2011; Phillips, 2014). Since most cells receive the majority of their cholesterol from endocytosis of LDL, the export of LDL-cholesterol from endo-lysosomes is closely linked to cholesterol efflux, for example to ABCA1, which resides to some extent in LE/LYSs at steady state (Neufeld et al., 2001). For cholesterol to leave LE/LYSs, the tandem action of the two Niemann Pick type C proteins, NPC1 and NPC2, is crucial. NPC1 is located in the lysosomal membrane and consists of 13 transmembrane helices, containing a sterol-sensing domain, and three luminal domains, a sterol-binding N-terminal domain, a middle luminal domain, and a C-terminal domain (Peake and Vance, 2010; Qian et al., 2020). NPC2 functions in the lumen of the LE/LYSs and is relatively small, consisting of 132 amino acids in its active form, and an additional 19 amino acids signal peptide (Storch and Xu, 2009; Qian et al., 2020). NPC2 binds to and buries the hydrocarbon chain of cholesterol deep into its hydrophobic pocket, in an orientation opposite to that of NPC1 (Infante et al., 2008; Kwon et al., 2009). In 2008, the group of Goldstein and Brown showed that NPC2 was required for the transfer of cholesterol from NPC1 to liposomes, although the transfer mechanism between the two

proteins could not be determined from these experiments (Infante et al., 2008). Based on biochemical assays, structural data, and mutagenesis experiments, a model was suggested in which unesterified cholesterol is first bound by NPC2 that hands it over to NPC1 (Infante et al., 2009). Deffieu and Pfeffer, 2011) found that at low pH, NPC2 binds to the second luminal domain of NPC1 and that the strength of the interaction increases in the presence of cholesterol (Deffieu and Pfeffer, 2011). From this study, it was suggested that NPC2 carrying cholesterol would bind to the second luminal loop of NPC1, which would bring the proteins in proximity and mediate the transfer of cholesterol from NPC2 to the N-terminal domain of NPC1. NPC2 would be released from the NPC1, once the latter has accepted the cholesterol, and finally, the cholesterol would be inserted into the membrane of LE/LYSs (Deffieu and Pfeffer, 2011). In support of this model, the crystal structure of an NPC1-NPC2 complex showed that the middle luminal domain of NPC1 binds to the top of NPC2, and revealed a putative cholesterol transfer tunnel between the binding pockets of the two proteins (Li et al., 2016). Moreover, recent studies found an internal tunnel in the structure of yeast and mammalian NPC1 homologs, through which sterols can be transferred to the lysosomal membrane (Winkler et al., 2019; Long et al., 2020). The importance of the NPC proteins is evident from the rare neurogenerative disorder (~1:120.000 birth) Niemann Pick Type C disease that is caused by lack of functional NPC1 or NPC2 protein. In NPC disease, unesterified cholesterol accumulates in the LE/LYSs together with other lipids such as gangliosides, sphingomyelin, and sphingosine. About 95% of the clinical cases are due to dysfunctional NPC1, however, independent of which protein is disabled, the clinical phenotypes appear similar (Peake and Vance, 2010).

8.2 Lipids, NPC Proteins, and ATP-Binding Cassette Transporters Control Cholesterol Efflux From Endo-lysosomes

Vesicles inside the LE/LYSs, known as ILVs, are enriched with cholesterol and lysobisohosphatidic acid (LBPA) (Kobayashi et al., 1999; Möbius et al., 2003; Gruenberg, 2020). LBPA is important for forming the membranes of ILVs and for controlling the cholesterol capacity of LE/LYSs. By treating cells lacking functional NPC1 with LBPA, or treating with its biosynthetic precursor phophatidylglycerol (PG), lysosomal cholesterol clearance was enhanced (McCauliff et al., 2019). Such LBPA/PG mediated cholesterol egress occurrs through increased exosomal secretion (Ilnytska et al., 2021a) and by enhancing the autophagic flux in cells lacking functional NPC1 (Ilnytska et al., 2021b). Interestingly, LBPA is not able to reduce cholesterol levels in cells expressing NPC2 protein mutated in the hydrophobic knob domain, which has been shown to directly interact with LBPA (McCauliff et al., 2019). Additionally, the efficiency of NPC2 to transfer cholesterol between membranes was found to be enhanced in the presence of LBPA, and inhibited by anti-LBPA antibodies (Xu et al., 2008). It is likely that NPC2 shuttles cholesterol from ILV membranes to the limiting LE/LYS membrane, making it available for other sterol transfer proteins (Storch and Xu, 2009). Dysfunction of NPC1, the cholesterol export protein in the endo-lysosomal limiting membrane, but not the absence of NPC2, can be rescued by overexpression of ABCA1 (Choi et al., 2003; Boadu et al., 2012). These important observations suggest that NPC2 is needed to solubilize cholesterol inside of the lysosome and donate it to different transporters including NPC1 and ABCA1 for export from this compartment. In line with this conclusion is our recent observation that treating NPC2-deficient human fibroblasts with purified NPC2 mobilized cholesterol from endo-lysosomes towards the PM, which was paralleled by reallocation of endo-lysosomes to the periphery and direct sterol transfer to the PM (Juhl et al., 2021). The latter could be shown by bleaching TopFluor-cholesterol in a portion of the PM and measuring a decrease in fluorescence of this sterol probe in nearby LE/LYSs underneath the PM (Juhl et al., 2021). Using kinetic modeling of such a fluorescence loss in photobleaching (FLIP) experiment, we inferred a dynamic pool of sterol in endo-lysosomes in exchange with the PM, which has a residence time in LE/LYSs of about 40 s (Juhl et al., 2021). Subsequent cholesterol efflux from the PM was independent of NPC2 but stimulated by LXR agonists and apoA1, suggesting that both pathways work in tandem (Juhl et al., 2021). Reallocation of endo-lysosomes to the cell periphery and reduction of the cholesterol storage phenotype was also found in fibroblasts lacking functional NPC1 upon treatment with PG (Ilnytska et al., 2021a). Some of those LE/LYSs might release their cholesterol content as exosomes, i.e., by lysosomal exocytosis, while vesicular shedding of lysosomal cargo from the PM could contribute as well. Interestingly, macrophages from NPC1 knockout ($NPC1^{-/-}$) mice have reduced cholesterol efflux capacity, which could be overcome by stimulating ABCA1 transporters with LXR agonists. Heterozygous $NPC1^{+/-}$ mice show less apoptosis and lesional necrosis, likely because cholesterol transport from lysosomes to the ER is impaired, as this pathway is essential for inflammosome activation and the UPR stress response (Feng et al., 2003; De la Roche et al., 2018). Similarly, incorporation of fatty acids derived from atherogenic LDL into phospholipids is impaired in NPC1-deficient macrophages (Leventhal et al., 2004). Together, these studies suggest that NPC1 and NPC2 provide cholesterol and phospholipids from LE/LYSs for efflux from cells.

8.3 The Connection Between Endo-lysosomes and Lipid Droplets in Cellular Cholesterol Efflux

To understand the role of lysosomes in the trafficking of lipoprotein-derived cholesterol, it is important to realize that cellular efflux of LDL-derived cholesterol differs between native LDL and oxidized, acetylated, or aggregated LDL, as such atherogenic LDL is differently processed in endo-lysosomes (Dhaliwal and Steinbrecher, 2000; Wang M.-D. et al., 2007; Haka et al., 2009). For example, aggregated and matrix-retained LDL in the intima of the vessel wall gets attacked by macrophages, which attempt to engulf the aggregated LDL, thereby triggering secretion of hydrolytic enzymes including acid lipase from lysosomes (Haka et al., 2009). This, in turn,

hydrolyzes CEs residing in aggregated LDL. To prevent a collapse of the pH gradient needed for optimal function of these enzymes, macrophages secrete lysosomal acid lipase into the contact area, thereby forming a tightly sealed so-called "lysosomal synapse" allowing for extracellular degradation of LDL's sterol esters (Singh et al., 2016). Upon uptake into the cells, the excess cholesterol is re-esterified and stored in LDs, whose abundant appearance converts those macrophages into foam cells. Thus, stored CEs in LDs represent another major intracellular source of cholesterol for efflux (Ouimet et al., 2011). CEs can be re-hydrolyzed for sterol mobilization via cytoplasmic cholesteryl ester hydrolase (Brown et al., 1979). Ingestion of LDs into lysosomes, so-called lipophagy, and hydrolysis of stored CEs by acid lipase provides significant amounts of cholesterol for efflux from macrophage foam cells (Ouimet et al., 2011; Robichaud et al., 2021). Lipophagy and likely other forms of autophagy are impaired in mammalian cells, lacking functional NPC1 or NPC2, suggesting that these sterol transporters play an important role in the efflux of droplet-derived sterols from lysosomes (Sarkar et al., 2013; Guo et al., 2016; Robichaud et al., 2021). This is likely an evolutionary ancient function of these proteins since impaired lipophagy is also observed in yeast Saccharomyces cerevisiae lacking functional NPC homologs, NCR1 or Npc2 (Tsuji et al., 2017; Winkler et al., 2019). Since these cells lack a lipoprotein pathway, yeast relies on sterol mobilization from LDs in the vacuole during starvation.

9 FORMATION AND EFFLUX OF OXYSTEROLS

9.1 Oxysterols as Polar Derivatives of Cholesterol Which Regulate Sterol Homeostasis and Efflux

Oxysterols are oxidized derivatives of cholesterol bearing additional hydroxy-, keto- or epoxy groups which significantly increase their water solubility compared to the parent cholesterol molecule (Luu et al., 2016). Since increased polarity results in lower membrane retention and higher inter-membrane transfer, oxysterols move very fast through cells and are more efficiently removed from cells compared to cholesterol (Sinensky, 1981; Lange et al., 1995; Morel et al., 1996). For example, the transfer from red blood cells to plasma lipoproteins is about 2000-fold faster for 25-hydroxycholesterol than for cholesterol (Lange et al., 1995). Sidechain oxidized cholesterol derivatives, such as 25-or 27-hydroxycholesterol, can form from LDL-derived cholesterol upon export from endo-lysosomes and transport to the ER or mitochondria, respectively (Axelson and Larsson, 1995; Frolov et al., 2003). Export of these oxysterols from endo-lysosomes depends on NPC1, and to a lower extent on NPC2 (Frolov et al., 2003; Abi-Mosleh et al., 2009; Petersen et al., 2020). 25-hydroxycholesterol can activate LXRs to stimulate ABCA1 mediated cholesterol efflux, and this oxysterol is itself efficiently removed from cells by ABCA1 (Venkateswaran et al., 2000; Tam et al., 2006). Therefore, impaired oxysterol formation in NPC1-deficient cells will likely contribute to the reduced efflux capacity and reduced HDL formation in NPC1 disease (Choi et al., 2003). The same is probably the case for Wolman disease and cholesteryl ester hydrolase deficiency, which both lead to accumulation of CEs in endo-lysosomes due to defective or absent acid lipase and thereby impaired ABCA1 mediated cholesterol efflux (Bowden et al., 2011). NPC2 binds 25-hydroxycholesterol with a much lower affinity than cholesterol and is probably less important for the export of oxysterols from endo-lysosomes because the water solubility of 25- and 27-hydroxycholesterol is sufficient for spontaneous transfer (Frolov et al., 2003; Petersen et al., 2020). Sidechain oxidized cholesterol derivatives move rapidly across membranes and can increase the permeability of lipid membranes to small molecules and ions, which could contribute to lysosome destabilization by oxysterols (Yuan et al., 2000; Kulig et al., 2018). In parallel, these oxysterols cannot order membranes as much as cholesterol does, and they might increase the propensity of cholesterol to partially protrude from the bilayer, thereby increasing the pool size of "accessible" cholesterol for efflux to acceptors (Bielska et al., 2014). However, there is also evidence that oxysterols, such as 25-hydroxycholesterol, actually lower cellular cholesterol efflux capacity (Kilsdonk E. P. et al., 1995; Luu et al., 2016). This could be due to stimulation of ACAT resulting in cholesterol esterification and storage in LDs.

9.2 Analysis of Oxysterol Trafficking and Efflux by Fluorescence Microscopy

The lack of appropriate tools to follow oxysterol transport in living cells has limited our knowledge about intracellular trafficking of oxysterols. Given that oxysterols, such as 25- or 27-hydroxycholesterol, differ from cholesterol only by having one additional hydroxy group, additional modifications to introduce fluorescent moieties for live-cell imaging must be kept to an absolute minimum. One approach is two add an alkyne group to the oxysterol, load this analogue into cells and covalently link it to a fluorescent group by click chemistry (Nedelcu et al., 2013; Peyrot et al., 2014). This approach allows for high-resolution imaging of oxysterol distribution, but it cannot be ruled out that either the click reaction or the attached dye molecule have an impact on this distribution. Also, imaging of the fluorescent construct is not possible in living cells. In a pioneering study, Iaea et al. (2015) presented a novel intrinsically fluorescent analogue of 25-hydroxycholesterol, which contains only two additional double bonds in the ring system compared to the parent oxysterol (Iaea et al., 2015). This analogue named 25-hydroxycholestatrienol can suppress cholesterol synthesis, activate ACAT for sterol esterification, be esterified in cells and stimulate expression of ABCA1 via activation of LXRs (Iaea et al., 2015). Its export from lysosomes depends on NPC1 and to a lower extent on NPC2 (Iaea et al., 2015; Petersen et al., 2020). Based on the same design strategy, we have recently developed a novel derivative of 27-hydroxycholesterol, 27-hydroxycholestatrienol (27-OH-CTL), which differs from 27-hydroxycholesterol only by two additional double bonds in the steroid ring system (**Figure 5**), allowing for spectroscopic analysis and live-cell imaging by

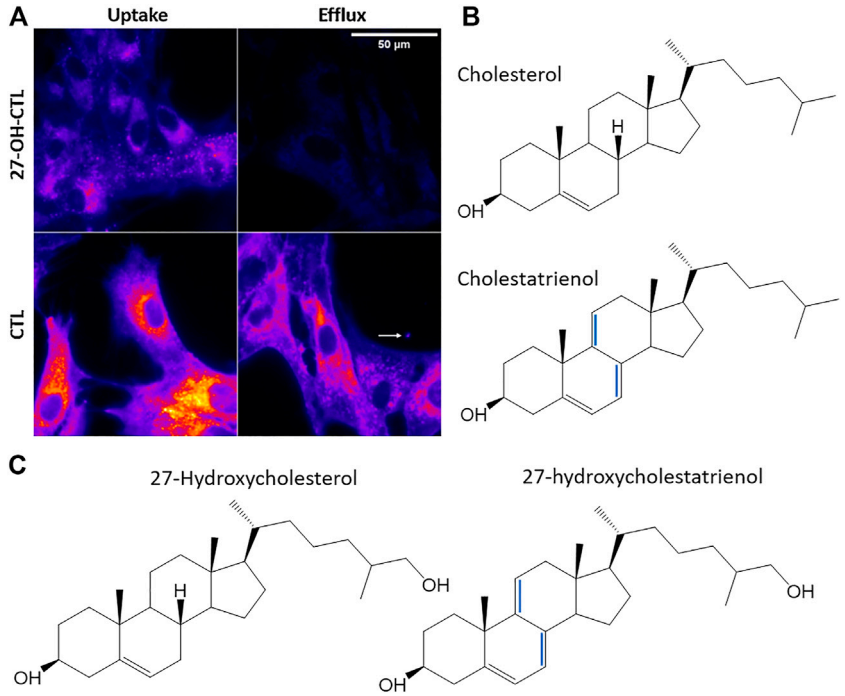

FIGURE 5 | Uptake and efflux of fluorescent oxysterols in human fibroblasts. **(A)** uptake and efflux of cholestatrienol (CTL) and 27-hydroxycholestatrienol (27-OH-CTL) in human fibroblasts studied by UV-sensitive fluorescence microscopy. **(B)** structures of cholesterol and its fluorescent analogue CTL. **(C)** 27-hydroxycholesterol and its fluorescent analogue 27-OH-CTL. Extra double bonds in the fluorescent analogs are the only modifications compared to the natural sterols and are shown in blue. Figure adapted and reproduced from (Szomek et al., 2020) with permission.

ultraviolet-sensitive microscopy, similar to 25-hydroxycholestatrienol (Szomek et al., 2020). We compared the intracellular trafficking of 27-OH-CTL with that of cholestatrienol (CTL), which has identical photophysical properties and just two additional double bonds compared to cholesterol (**Figure 5**). Thus, the difference between 27-OH-CTL and CTL is only one extra hydroxy group at carbon 27, exactly as the difference between 27-hydroxycholesterol and cholesterol (**Figure 5**). This enabled us to study the effect of one additional hydroxy group in the steroid side chain on intracellular sterol trafficking and efflux. We found that 27-OH-CTL and CTL show a similar extent of non-vesicular transport, as measured by fluorescence recovery after photobleaching (not shown but see Szomek et al. (2020)). However, 27-OH-CTL was much more efficiently effluxed from cells than CTL (**Figure 5A**) and 27-OH-CTL but not CTL accumulated a lot in LDs in human fibroblasts (Szomek et al., 2020). Comparable intracellular transport kinetics but more rapid and extensive efflux, as well as the metabolic conversion, was also found for 25-hydroxycholesterol compared to cholesterol in macrophages using radioactive sterol probes (Morel et al., 1996). Thus, cells can sensitively adapt transport and efflux to even minor structural changes of sterol molecules, and these processes can be studied using radioactive tracers but also directly observed in cells using intrinsically fluorescent analogues.

10 CONCLUSION AND OUTLOOK

Since mammalian cells cannot degrade cholesterol, they have developed intricate mechanisms for its disposal. Here, we have summarized our current understanding of the cellular mechanisms of cholesterol efflux. A particular challenge is the extremely low water solubility of cholesterol, which cells overcome by employing several mechanisms. In this review we discussed in detail; 1) how cells use a variety of transporters to shuttle cholesterol between membrane and lipoproteins; 2) how cells generate close protein-mediated membrane contacts to accelerate sterol exchange and 3) how they couple cholesterol export to the formation of extracellular carrier vesicles and lipoproteins. In addition to the classical pathways of reverse cholesterol transport and formation of HDL, we highlighted novel findings of the concerted action and molecular function of a variety of ABC transporters. We also provided an overview of recently described vesicular secretion pathways for cholesterol, ranging from the secretion of exosomes over shedding of ectosomes from the PM to the formation of migrasomes, and we explained, how those mechanisms might contribute to net cholesterol efflux from cells. A particular focus was set on human diseases related to disturbed cholesterol efflux, either at the cell surface or due to defective mobilization from intracellular sites, such as endo-lysosomes and LDs. Finally, we explained the important link between cholesterol efflux and the formation

and export of oxysterols from cells. However, many questions remain and future studies could focus on the following:

- What is the nature of active cholesterol, and how is the cholesterol pool accessible to bacterial toxins related to cholesterol efflux and precipitation from membranes? While being a powerful concept, the molecular picture of "active cholesterol" is very vague at the moment. New techniques, including novel biophysical and imaging approaches, are required to substantiate this concept in living cells. Also, a better understanding of the molecular mechanisms underlying the binding of bacterial toxins to cellular membranes is needed to ensure that the observed threshold phenomena indeed solely reflect different cholesterol pools in the membrane.
- Are there other mechanisms of controlling the chemical potential of cholesterol and thereby its fugacity in cellular membranes and lipoproteins? Our current understanding of the mechanisms regulating cholesterol's chemical potential in cellular membranes and lipoproteins are based on a large body of physico-chemical data about specific phospholipid-cholesterol interactions in model membrane systems. Such systems are necessarily much simpler than cellular membranes, and we might miss an important piece of the puzzle by relying too much on model membrane studies. Thus, more biophysical studies in living cells and development of more realistic model systems are needed to answer this question.
- How important are membrane contact sites for cellular efflux of cholesterol? It is well known that close, protein-mediated contact between organelles are involved in intracellular cholesterol transport, but it is little understood about whether the organelle interactome also regulates cellular cholesterol efflux and how sterol transporters, such as GramD1/Aster or oxysterol binding proteins function at those sites during export of excess cholesterol from cells.
- What are the molecular mechanisms underlying shedding of cholesterol-rich vesicles from the PM? Secretion of micro-vesicles as an export mode for cholesterol from cells is an exciting new field that will complement and expand our understanding of cholesterol efflux in the future. Understanding the underlying mechanisms of vesicle secretion and their regulation will be possible by combining live-cell and correlative super-resolution microscopy with genetic knockdown techniques in different cell types and under various cholesterol loading conditions.
- How is the recruitment of endo-lysosomes to the PM for cholesterol efflux regulated at a molecular level? Exciting new findings have revealed the importance of intracellular location and dynamics for lysosome function, and lysosomal cholesterol appears to be an important regulating factor in this context. Reallocation of LE/LYSs to the PM has been found to be linked to cholesterol efflux, and determining the underlying molecular mechanisms will enable us to understand, how intracellular cholesterol is mobilized for efflux from cells.
- Is there a quantitative contribution of the release of entire LE/LYSs to net cholesterol efflux, and if so, what are the underlying mechanisms? Shedding of vesicles containing entire endo-lysosomes and other organelles has been observed during cholesterol efflux, but also in other cellular processes and various cell types. Whether this indeed plays a physiological role or is exaggerated under cell culture conditions needs to be explored in the future.
- What are the molecular mechanisms and biophysical principles of oxysterol transport and efflux from cells and how can oxysterols control cholesterol efflux at the cellular and molecular level? Oxysterols play an important role in cholesterol efflux; they are efficiently exported from cells due to their higher water solubility compared to cholesterol, and they regulate cellular cholesterol efflux as ligands of sterol-metabolizing enzymes and transcription factors. Future studies could combine novel imaging technologies with analytical approaches, such as mass spectrometry to study trafficking and metabolism of oxysterols at a cellular and tissue level.

In the past, mechanisms of cellular cholesterol efflux were explored primarily by biochemical approaches, and this has generated a large amount of data on the formation and clearance of HDL. With the increasing use of quantitative live-cell imaging, super-resolution microscopy and correlative imaging, elucidation of the spatiotemporal orchestration of cholesterol efflux at a subcellular level becomes possible. We expect this trend to continue in the future with novel imaging technologies further contributing to our understanding of this important process.

AUTHOR CONTRIBUTIONS

AJ and DW researched and referenced current literature on cholesterol transport and efflux, wrote the individual sections of the manuscript, and created the figures.

FUNDING

We acknowledge funding from the Lundbeck foundation (grant no. R366-2021-226).

ACKNOWLEDGMENTS

The authors thank the Danish Molecular Bioimaging Center (DaMBIC) for providing microscope equipment for some of the published data shown in **Figure 3**.

REFERENCES

Abi-Mosleh, L., Infante, R. E., Radhakrishnan, A., Goldstein, J. L., and Brown, M. S. (2009). Cyclodextrin Overcomes Deficient Lysosome-To-Endoplasmic Reticulum Transport of Cholesterol in Niemann-Pick Type C Cells. *Proc. Natl. Acad. Sci.* 106, 19316–19321. doi:10.1073/pnas.0910916106

Adams, C. M., Reitz, J., De Brabander, J. K., Feramisco, J. D., Li, L., Brown, M. S., et al. (2004). Cholesterol and 25-hydroxycholesterol Inhibit Activation of SREBPs by Different Mechanisms, Both Involving SCAP and Insigs. *J. Biol. Chem.* 279, 52772–52780. doi:10.1074/jbc.m410302200

Addadi, L., Geva, M., and Kruth, H. S. (2003). Structural Information about Organized Cholesterol Domains from Specific Antibody Recognition. *Biochim. Biophys. Acta (Bba) - Biomembranes* 1610, 208–216. doi:10.1016/s0005-2736(03)00019-1

Adorni, M. P., Zimetti, F., Billheimer, J. T., Wang, N., Rader, D. J., Phillips, M. C., et al. (2007). The Roles of Different Pathways in the Release of Cholesterol from Macrophages. *J. Lipid Res.* 48, 2453–2462. doi:10.1194/jlr.m700274-jlr200

Alder-Baerens, N., Müller, P., Pohl, A., Korte, T., Hamon, Y., Chimini, G., et al. (2005). Headgroup-specific Exposure of Phospholipids in ABCA1-Expressing Cells. *J. Biol. Chem.* 280, 26321–26329. doi:10.1074/jbc.M413993200

Ameis, D., Merkel, M., Eckerskorn, C., and Greten, H. (1994). Purification, Characterization and Molecular Cloning of Human Hepatic Lysosomal Acid Lipase. *Eur. J. Biochem.* 219, 905–914. doi:10.1111/j.1432-1033.1994.tb18572.x

Axelson, M., and Larsson, O. (1995). Low Density Lipoprotein (LDL) Cholesterol Is Converted to 27-hydroxycholesterol in Human Fibroblasts. Evidence that 27-hydroxycholesterol Can Be an Important Intracellular Mediator between LDL and the Suppression of Cholesterol Production. *J. Biol. Chem.* 270, 15102–15110. doi:10.1074/jbc.270.25.15102

Bach, D., and Wachtel, E. (2003). Phospholipid/cholesterol Model Membranes: Formation of Cholesterol Crystallites. *Biochim. Biophys. Acta (Bba) - Biomembranes* 1610, 187–197. doi:10.1016/s0005-2736(03)00017-8

Bailey, J. M. (1965). Lipid Metabolism in Cultured Cells. *Exp. Cel Res.* 37, 175–182. doi:10.1016/0014-4827(65)90168-0

Barter, P. J., Brewer, H. B., Jr., Chapman, M. J., Hennekens, C. H., Rader, D. J., and Tall, A. R. (2003). Cholesteryl Ester Transfer Protein. *Atvb* 23, 160–167. doi:10.1161/01.atv.0000054658.91146.64

Bennett, W. F. D., Maccallum, J. L., Hinner, M. J., Marrink, S. J., and Tieleman, D. P. (2009). Molecular View of Cholesterol Flip-Flop and Chemical Potential in Different Membrane Environments. *J. Am. Chem. Soc.* 131, 12714–12720. doi:10.1021/ja903529f

Bielska, A. A., Olsen, B. N., Gale, S. E., Mydock-Mcgrane, L., Krishnan, K., Baker, N. A., et al. (2014). Side-chain Oxysterols Modulate Cholesterol Accessibility through Membrane Remodeling. *Biochemistry* 53, 3042–3051. doi:10.1021/bi5000096

Bloch, K. (1965). The Biological Synthesis of Cholesterol. *Science* 150, 19–28. doi:10.1126/science.150.3692.19

Boadu, E., Nelson, R. C., and Francis, G. A. (2012). ABCA1-dependent Mobilization of Lysosomal Cholesterol Requires Functional Niemann-Pick C2 but Not Niemann-Pick C1 Protein. *Biochim. Biophys. Acta (Bba) - Mol. Cel Biol. Lipids* 1821, 396–404. doi:10.1016/j.bbalip.2011.11.013

Bowden, K. L., Bilbey, N. J., Bilawchuk, L. M., Boadu, E., Sidhu, R., Ory, D. S., et al. (2011). Lysosomal Acid Lipase Deficiency Impairs Regulation of ABCA1 Gene and Formation of High Density Lipoproteins in Cholesteryl Ester Storage Disease. *J. Biol. Chem.* 286, 30624–30635. doi:10.1074/jbc.m111.274381

Brown, M. S., Goldstein, J. L., Krieger, M., Ho, Y. K., and Anderson, R. G. (1979). Reversible Accumulation of Cholesteryl Esters in Macrophages Incubated with Acetylated Lipoproteins. *J. Cel Biol.* 82, 597–613. doi:10.1083/jcb.82.3.597

Bruckner, R. J., Mansy, S. S., Ricardo, A., Mahadevan, L., and Szostak, J. W. (2009). Flip-flop-induced Relaxation of Bending Energy: Implications for Membrane Remodeling. *Biophysical J.* 97, 3113–3122. doi:10.1016/j.bpj.2009.09.025

Cai, S. Y., Gautam, S., Nguyen, T., Soroka, C. J., Rahner, C., and Boyer, J. L. (2009). ATP8B1 Deficiency Disrupts the Bile Canalicular Membrane Bilayer Structure in Hepatocytes, but FXR Expression and Activity Are Maintained. *Gastroenterology* 136, 1060–1069. doi:10.1053/j.gastro.2008.10.025

Cerqueira, N. M. F. S. A., Oliveira, E. F., Gesto, D. S., Santos-Martins, D., Moreira, C., Moorthy, H. N., et al. (2016). Cholesterol Biosynthesis: A Mechanistic Overview. *Biochemistry* 55, 5483–5506. doi:10.1021/acs.biochem.6b00342

Chao, F. F., Blanchette-Mackie, E. J., Tertov, V. V., Skarlatos, S. I., Chen, Y. J., and Kruth, H. S. (1992). Hydrolysis of Cholesteryl Ester in Low Density Lipoprotein Converts This Lipoprotein to a Liposome. *J. Biol. Chem.* 267, 4992–4998. doi:10.1016/s0021-9258(18)42929-8

Chattopadhyay, A., Jafurulla, M., Kalipatnapu, S., Pucadyil, T. J., and Harikumar, K. G. (2005). Role of Cholesterol in Ligand Binding and G-Protein Coupling of serotonin1A Receptors Solubilized from Bovine hippocampus. *Biochem. Biophysical Res. Commun.* 327, 1036–1041. doi:10.1016/j.bbrc.2004.12.102

Chen, W., Silver, D. L., Smith, J. D., and Tall, A. R. (2000). Scavenger Receptor-BI Inhibits ATP-Binding Cassette Transporter 1- Mediated Cholesterol Efflux in Macrophages. *J. Biol. Chem.* 275, 30794–30800. doi:10.1074/jbc.m004552200

Chen, Y., Li, Y., Ma, L., and Yu, L. (2018). "Detection of Migrasomes," in *In Cell Migration: Methods and Protocols*. Editor A. Gautreau. (New York, NY: Springer New York), 43–49. doi:10.1007/978-1-4939-7701-7_5:

Choi, H. Y., Karten, B., Chan, T., Vance, J. E., Greer, W. L., Heidenreich, R. A., et al. (2003). Impaired ABCA1-dependent Lipid Efflux and Hypoalphalipoproteinemia in Human Niemann-Pick Type C Disease. *J. Biol. Chem.* 278, 32569–32577. doi:10.1074/jbc.m304553200

Choubey, A., Kalia, R. K., Malmstadt, N., Nakano, A., and Vashishta, P. (2013). Cholesterol Translocation in a Phospholipid Membrane. *Biophysical J.* 104, 2429–2436. doi:10.1016/j.bpj.2013.04.036

Cocucci, E., Racchetti, G., and Meldolesi, J. (2009). Shedding Microvesicles: Artefacts No More. *Trends Cel Biol.* 19, 43–51. doi:10.1016/j.tcb.2008.11.003

Coleman, J. A., Quazi, F., and Molday, R. S. (2013). Mammalian P4-ATPases and ABC Transporters and Their Role in Phospholipid Transport. *Biochim. Biophys. Acta (Bba) - Mol. Cel Biol. Lipids* 1831, 555–574. doi:10.1016/j.bbalip.2012.10.006

Courtney, K. C., Fung, K. Y., Maxfield, F. R., Fairn, G. D., and Zha, X. (2018a). Comment on 'Orthogonal Lipid Sensors Identify Transbilayer Asymmetry of Plasma Membrane Cholesterol'. *Elife* 7.

Courtney, K. C., Pezeshkian, W., Raghupathy, R., Zhang, C., Darbyson, A., Ipsen, J. H., et al. (2018b). C24 Sphingolipids Govern the Transbilayer Asymmetry of Cholesterol and Lateral Organization of Model and Live-Cell Plasma Membranes. *Cel Rep.* 24, 1037–1049. doi:10.1016/j.celrep.2018.06.104

Courtney, K., Pezeshkian, W., Raghupathy, R., Zhang, G., Darbyson, A., Ipsen, J. H., et al. (2017). C24 Sphingolipids Play a Surprising and central Role in Governing Cholesterol and Lateral Organization of the Live Cell Plasma Membrane. *bioRxiv*.

Crawford, A. R., Smith, A. J., Hatch, V. C., Oude Elferink, R. P., Borst, P., and Crawford, J. M. (1997). Hepatic Secretion of Phospholipid Vesicles in the Mouse Critically Depends on Mdr2 or MDR3 P-Glycoprotein Expression. Visualization by Electron Microscopy. *J. Clin. Invest.* 100, 2562–2567. doi:10.1172/jci119799

Crawford, J. M., Möckel, G. M., Crawford, A. R., Hagen, S. J., Hatch, V. C., Barnes, S., et al. (1995). Imaging Biliary Lipid Secretion in the Rat: Ultrastructural Evidence for Vesiculation of the Hepatocyte Canalicular Membrane. *J. Lipid Res.* 36, 2147–2163.

Crawford, J. (1996). Role of Vesicle-Mediated Transport Pathways in Hepatocellular Bile Secretion. *Semin. Liver Dis.* 16, 169–189. doi:10.1055/s-2007-1007230

Das, A., Brown, M. S., Anderson, D. D., Goldstein, J. L., and Radhakrishnan, A. (2014). Three Pools of Plasma Membrane Cholesterol and Their Relation to Cholesterol Homeostasis. *Elife* 3, e02882. doi:10.7554/elife.02882

Das, A., Goldstein, J. L., Anderson, D. D., Brown, M. S., and Radhakrishnan, A. (2013). Use of Mutant 125I-Perfringolysin O to Probe Transport and Organization of Cholesterol in Membranes of Animal Cells. *Proc. Natl. Acad. Sci.* 110, 10580–10585. doi:10.1073/pnas.1309273110

De Almeida, R. F. M., Loura, L. M. S., Prieto, M., Watts, A., Fedorov, A., and Barrantes, F. J. (2004). Cholesterol Modulates the Organization of the γM4 Transmembrane Domain of the Muscle Nicotinic Acetylcholine Receptor. *Biophysical J.* 86, 2261–2272. doi:10.1016/s0006-3495(04)74284-8

De La Roche, M., Hamilton, C., Mortensen, R., Jeyaprakash, A. A., Ghosh, S., and Anand, P. K. (2018). Trafficking of Cholesterol to the ER Is Required for NLRP3 Inflammasome Activation. *J. Cel Biol* 217, 3560–3576. doi:10.1083/jcb.201709057

Deffieu, M. S., and Pfeffer, S. R. (2011). Niemann-Pick Type C 1 Function Requires Lumenal Domain Residues that Mediate Cholesterol-dependent NPC2 Binding. *Proc. Natl. Acad. Sci.* 108, 18932–18936. doi:10.1073/pnas.1110439108

Denis, M., Landry, Y. D., and Zha, X. (2008). ATP-binding Cassette A1-Mediated Lipidation of Apolipoprotein A-I Occurs at the Plasma Membrane and Not in the Endocytic Compartments. *J. Biol. Chem.* 283, 16178–16186. doi:10.1074/jbc.m709597200

Dergunov, A. D., Savushkin, E. V., Dergunova, L. V., and Litvinov, D. Y. (2019). Significance of Cholesterol-Binding Motifs in ABCA1, ABCG1, and SR-B1 Structure. *J. Membr. Biol* 252, 41–60. doi:10.1007/s00232-018-0056-5

Dhaliwal, B. S., and Steinbrecher, U. P. (2000). Cholesterol Delivered to Macrophages by Oxidized Low Density Lipoprotein Is Sequestered in Lysosomes and Fails to Efflux Normally. *J. Lipid Res.* 41, 1658–1665. doi:10.1016/s0022-2275(20)31999-4

Dietschy, J. M., and Turley, S. D. (2002). Control of Cholesterol Turnover in the Mouse. *J. Biol. Chem.* 277, 3801–3804. doi:10.1074/jbc.r100057200

Eckhardt, E. R. M., Cai, L., Sun, B., Webb, N. R., and Van Der Westhuyzen, D. R. (2004). High Density Lipoprotein Uptake by Scavenger Receptor SR-BII. *J. Biol. Chem.* 279, 14372–14381. doi:10.1074/jbc.m313793200

Ercan, B., Naito, T., Koh, D. H. Z., Dharmawan, D., and Saheki, Y. (2021). Molecular Basis of Accessible Plasma Membrane Cholesterol Recognition by the GRAM Domain of GRAMD1b. *EMBO J.* 40, e106524. doi:10.15252/embj.2020106524

Falchi, A. M., Sogos, V., Saba, F., Piras, M., Congiu, T., and Piludu, M. (2013). Astrocytes Shed Large Membrane Vesicles that Contain Mitochondria, Lipid Droplets and ATP. *Histochem. Cel Biol* 139, 221–231. doi:10.1007/s00418-012-1045-x

Feng, B., Zhang, D., Kuriakose, G., Devlin, C. M., Kockx, M., and Tabas, I. (2003). Niemann-Pick C Heterozygosity Confers Resistance to Lesional Necrosis and Macrophage Apoptosis in Murine Atherosclerosis. *Proc. Natl. Acad. Sci.* 100, 10423–10428. doi:10.1073/pnas.1732494100

Ferrari, A., He, C., Kennelly, J. P., Sandhu, J., Xiao, X., Chi, X., et al. (2020). Aster Proteins Regulate the Accessible Cholesterol Pool in the Plasma Membrane. *Mol. Cel Biol 40*. doi:10.1128/mcb.00255-20

Ferri, N., Corsini, A., Sirtori, C. R., and Ruscica, M. (2018). Present Therapeutic Role of Cholesteryl Ester Transfer Protein Inhibitors. *Pharmacol. Res.* 128, 29–41. doi:10.1016/j.phrs.2017.12.028

Fielding, C. J. (1985). [12] Lecithin-Cholesterol Acyltransferase and Cholesterol Transport. *Methods Enzymol.* 111, 267–274. doi:10.1016/s0076-6879(85)11014-1

Fielding, C. J. (2009). "Cellular Cholesterol Transport-Microdomains, Molecular Acceptors and Mechanisms,". Editor C. Ehnholm (Springer press.), 301–313. doi:10.1007/978-3-642-00300-4_12

Fielding, C. J., and Fielding, P. E. (1971). Purification and Substrate Specificity of Lecithin-Cholesterol Acyl Transferase from Human Plasma. *FEBS Lett.* 15, 355–358. doi:10.1016/0014-5793(71)80333-2

Fitzgerald, M. L., Morris, A. L., Chroni, A., Mendez, A. J., Zannis, V. I., and Freeman, M. W. (2004). ABCA1 and Amphipathic Apolipoproteins Form High-Affinity Molecular Complexes Required for Cholesterol Efflux. *J. Lipid Res.* 45, 287–294. doi:10.1194/jlr.m300355-jlr200

Frolov, A., Zielinski, S. E., Crowley, J. R., Dudley-Rucker, N., Schaffer, J. E., and Ory, D. S. (2003). NPC1 and NPC2 Regulate Cellular Cholesterol Homeostasis through Generation of Low Density Lipoprotein Cholesterol-Derived Oxysterols. *J. Biol. Chem.* 278, 25517–25525. doi:10.1074/jbc.m302588200

Fu, Y., Mukhamedova, N., Ip, S., D'Souza, W., Henley, K. J., Ditommaso, T., et al. (2013). ABCA12 Regulates ABCA1-dependent Cholesterol Efflux from Macrophages and the Development of Atherosclerosis. *Cel Metab.* 18, 225–238. doi:10.1016/j.cmet.2013.07.003

Fuhr, G., Richter, E., Zimmermann, H., Hitzler, H., Niehus, H., and Hagedorn, R. (1998). Cell Traces - Footprints of Individual Cells during Locomotion and Adhesion. *Biol. Chem.* 379, 1161–1173. doi:10.1515/bchm.1998.379.8-9.1161

Garcia, C. K., Wilund, K., Arca, M., Zuliani, G., Fellin, R., Maioli, M., et al. (2001). Autosomal Recessive Hypercholesterolemia Caused by Mutations in a Putative LDL Receptor Adaptor Protein. *Science* 292, 1394–1398. doi:10.1126/science.1060458

Gong, X., Qian, H., Cao, P., Zhao, X., Zhou, Q., Lei, J., et al. (2018). Structural Basis for the Recognition of Sonic Hedgehog by Human Patched1. *Sci. 361*. doi:10.1126/science.aas8935

Groen, A., Romero, M. R., Kunne, C., Hoosdally, S. J., Dixon, P. H., Wooding, C., et al. (2011). Complementary Functions of the Flippase ATP8B1 and the Floppase ABCB4 in Maintaining Canalicular Membrane Integrity. *Gastroenterology* 141, 1927–1937.e1–e4. doi:10.1053/j.gastro.2011.07.042

Gruenberg, J. (2020). Life in the Lumen: the Multivesicular Endosome. *Traffic* 21, 76–93. doi:10.1111/tra.12715

Gulshan, K., Brubaker, G., Conger, H., Wang, S., Zhang, R., Hazen, S. L., et al. (2016). PI(4,5)P2 Is Translocated by ABCA1 to the Cell Surface where it Mediates Apolipoprotein A1 Binding and Nascent HDL Assembly. *Circ. Res.* 119, 827–838. doi:10.1161/circresaha.116.308856

Gulshan, K., Brubaker, G., Wang, S., Hazen, S. L., and Smith, J. D. (2013). Sphingomyelin Depletion Impairs Anionic Phospholipid Inward Translocation and Induces Cholesterol Efflux. *J. Biol. Chem.* 288, 37166–37179. doi:10.1074/jbc.m113.512244

Guo, H., Zhao, M., Qiu, X., Deis, J. A., Huang, H., Tang, Q.-Q., et al. (2016). Niemann-Pick Type C2 Deficiency Impairs Autophagy-Lysosomal Activity, Mitochondrial Function, and TLR Signaling in Adipocytes. *J. Lipid Res.* 57, 1644–1658. doi:10.1194/jlr.m066522

Hafiane, A., and Genest, J. (2017). ATP Binding Cassette A1 (ABCA1) Mediates Microparticle Formation during High-Density Lipoprotein (HDL) Biogenesis. *Atherosclerosis* 257, 90–99. doi:10.1016/j.atherosclerosis.2017.01.013

Haka, A. S., Grosheva, I., Chiang, E., Buxbaum, A. R., Baird, B. A., Pierini, L. M., et al. (2009). Macrophages Create an Acidic Extracellular Hydrolytic Compartment to Digest Aggregated Lipoproteins. *MBoC* 20, 4932–4940. doi:10.1091/mbc.e09-07-0559

Harkiolaki, M., Darrow, M. C., Spink, M. C., Kosior, E., Dent, K., and Duke, E. (2018). Cryo-soft X-ray Tomography: Using Soft X-Rays to Explore the Ultrastructure of Whole Cells. *Emerging Top. Life Sci.* 2, 81–92. doi:10.1042/etls20170086

Hartjes, T., Mytnyk, S., Jenster, G., Van Steijn, V., and Van Royen, M. (2019). Extracellular Vesicle Quantification and Characterization: Common Methods and Emerging Approaches. *Bioengineering* 6, 7. doi:10.3390/bioengineering6010007

Hayakawa, K., Esposito, E., Wang, X., Terasaki, Y., Liu, Y., Xing, C., et al. (2016). Transfer of Mitochondria from Astrocytes to Neurons after Stroke. *Nature* 535, 551–555. doi:10.1038/nature18928

Haynes, M. P., Phillips, M. C., and Rothblat, G. H. (2000). Efflux of Cholesterol from Different Cellular Pools. *Biochemistry* 39, 4508–4517. doi:10.1021/bi992125q

He, C., Hu, X., Weston, T. A., Jung, R. S., Sandhu, J., Huang, S., et al. (2018). Macrophages Release Plasma Membrane-Derived Particles Rich in Accessible Cholesterol. *Proc. Natl. Acad. Sci. USA* 115, E8499–E8508. doi:10.1073/pnas.1810724115

He, C., Jiang, H., Song, W., Riezman, H., Tontonoz, P., Weston, T. A., et al. (2020). Cultured Macrophages Transfer Surplus Cholesterol into Adjacent Cells in the Absence of Serum or High-Density Lipoproteins. *Proc. Natl. Acad. Sci. USA* 117, 10476–10483. doi:10.1073/pnas.1922879117

Heeren, J., Grewal, T., Laatsch, A., Becker, N., Rinninger, F., Rye, K.-A., et al. (2004). Impaired Recycling of Apolipoprotein E4 Is Associated with Intracellular Cholesterol Accumulation. *J. Biol. Chem.* 279, 55483–55492. doi:10.1074/jbc.m409324200

Heeren, J., Grewal, T., Laatsch, A., Rottke, D., Rinninger, F., Enrich, C., et al. (2003). Recycling of Apoprotein E Is Associated with Cholesterol Efflux and High Density Lipoprotein Internalization. *J. Biol. Chem.* 278, 14370–14378. doi:10.1074/jbc.m209006200

Heinrich, R., and Schuster, S. (1996). The Regulation of Cellular Processes. *Chapman & Hall, New York, USA*, 123–134.

Henriksen, J., Rowat, A. C., Brief, E., Hsueh, Y. W., Thewalt, J. L., Zuckermann, M. J., et al. (2006). Universal Behavior of Membranes with Sterols. *Biophysical J.* 90, 1639–1649. doi:10.1529/biophysj.105.067652

Hirama, T., Lu, S. M., Kay, J. G., Maekawa, M., Kozlov, M. M., Grinstein, S., et al. (2017). Membrane Curvature Induced by Proximity of Anionic Phospholipids Can Initiate Endocytosis. *Nat. Commun.* 8, 1393. doi:10.1038/s41467-017-01554-9

Hjort Ipsen, J., Karlström, G., Mourtisen, O. G., Wennerström, H., and Zuckermann, M. J. (1987). Phase Equilibria in the Phosphatidylcholine-Cholesterol System. *Biochim. Biophys. Acta (Bba) - Biomembranes* 905, 162–172. doi:10.1016/0005-2736(87)90020-4

Horton, J. D., Shah, N. A., Warrington, J. A., Anderson, N. N., Park, S. W., Brown, M. S., et al. (2003). Combined Analysis of Oligonucleotide Microarray Data

from Transgenic and Knockout Mice Identifies Direct SREBP Target Genes. *Proc. Natl. Acad. Sci.* 100, 12027–12032. doi:10.1073/pnas.1534923100

Hu, X., Weston, T. A., He, C., Jung, R. S., Heizer, P. J., Young, B. D., et al. (2019). Release of Cholesterol-Rich Particles from the Macrophage Plasma Membrane during Movement of Filopodia and Lamellipodia. *Elife* 8, e50231. doi:10.7554/eLife.50231

Huang, J., Buboltz, J. T., and Feigenson, G. W. (1999). Maximum Solubility of Cholesterol in Phosphatidylcholine and Phosphatidylethanolamine Bilayers. *Biochim. Biophys. Acta (Bba) - Biomembranes* 1417, 89–100. doi:10.1016/s0005-2736(98)00260-0

Huang, J., and Feigenson, G. W. (1999). A Microscopic Interaction Model of Maximum Solubility of Cholesterol in Lipid Bilayers. *Biophysical J.* 76, 2142–2157. doi:10.1016/s0006-3495(99)77369-8

Huang, P., Nedelcu, D., Watanabe, M., Jao, C., Kim, Y., Liu, J., et al. (2016). Cellular Cholesterol Directly Activates Smoothened in Hedgehog Signaling. *Cell* 166, 1176–1187. doi:10.1016/j.cell.2016.08.003

Huang, Y., Zucker, B., Zhang, S., Elias, S., Zhu, Y., Chen, H., et al. (2019). Migrasome Formation Is Mediated by Assembly of Micron-Scale Tetraspanin Macrodomains. *Nat. Cel Biol* 21, 991–1002. doi:10.1038/s41556-019-0367-5

Huttenlocher, A., Sandborg, R. R., and Horwitz, A. F. (1995). Adhesion in Cell Migration. *Curr. Opin. Cel Biol* 7, 697–706. doi:10.1016/0955-0674(95)80112-x

Iaea, D. B., Gale, S. E., Bielska, A. A., Krishnan, K., Fujiwara, H., Jiang, H., et al. (2015). A Novel Intrinsically Fluorescent Probe for Study of Uptake and Trafficking of 25-hydroxycholesterol. *J. Lipid Res.* 56, 2408–2419. doi:10.1194/jlr.d064287

Iaea, D. B., and Maxfield, F. R. (2015). Cholesterol Trafficking and Distribution. *Essays Biochem.* 57, 43–55. doi:10.1042/bse0570043

Iaea, D. B., Spahr, Z. R., Singh, R. K., Chan, R. B., Zhou, B., Bareja, R., et al. (2020). Stable Reduction of STARD4 Alters Cholesterol Regulation and Lipid Homeostasis. *Biochim. Biophys. Acta (Bba) - Mol. Cel Biol. Lipids* 1865, 158609. doi:10.1016/j.bbalip.2020.158609

Ilnytska, O., Jeziorek, M., Lai, K., Altan-Bonnet, N., Dobrowolski, R., and Storch, J. (2021a). Lysobisphosphatidic Acid (LBPA) Enrichment Promotes Cholesterol Egress via Exosomes in Niemann Pick Type C1 Deficient Cells. *Biochim. Biophys. Acta (Bba) - Mol. Cel Biol. Lipids* 1866, 158916. doi:10.1016/j.bbalip.2021.158916

Ilnytska, O., Lai, K., Gorshkov, K., Schultz, M. L., Tran, B. N., Jeziorek, M., et al. (2021b). Enrichment of NPC1-Deficient Cells with the Lipid LBPA Stimulates Autophagy, Improves Lysosomal Function, and Reduces Cholesterol Storage. *J. Biol. Chem.* 100813. doi:10.1016/j.jbc.2021.100813

Infante, R., Brown, M., and Goldstein, J. (2009). NPC2 Facilitates Bidirectional Transfer of Cholesterol between NPC1 and Lipid Bilayers, a Potential Step in Cholesterol Egress from Lysosomes. *FASEB J.* 23, 521–525. doi:10.1096/fasebj.23.1_supplement.521.5

Infante, R. E., and Radhakrishnan, A. (2017). Continuous Transport of a Small Fraction of Plasma Membrane Cholesterol to Endoplasmic Reticulum Regulates Total Cellular Cholesterol. *Elife* 6, e25466. doi:10.7554/eLife.25466

Infante, R. E., Wang, M. L., Radhakrishnan, A., Kwon, H. J., Brown, M. S., and Goldstein, J. L. (2008). NPC2 Facilitates Bidirectional Transfer of Cholesterol between NPC1 and Lipid Bilayers, a Step in Cholesterol Egress from Lysosomes. *Pnas* 105, 15287–15292. doi:10.1073/pnas.0807328105

Ipsen, J. H., Mouritsen, O. G., and Bloom, M. (1990). Relationships between Lipid Membrane Area, Hydrophobic Thickness, and Acyl-Chain Orientational Order. The Effects of Cholesterol. *Biophysical J.* 57, 405–412. doi:10.1016/s0006-3495(90)82557-1

Istvan, E. S., and Deisenhofer, J. (2001). Structural Mechanism for Statin Inhibition of HMG-CoA Reductase. *Science* 292, 1160–1164. doi:10.1126/science.1059344

Janoudi, A., Shamoun, F. E., Kalavakunta, J. K., and Abela, G. S. (2016). Cholesterol crystal Induced Arterial Inflammation and Destabilization of Atherosclerotic Plaque. *Eur. Heart J.* 37, 1959–1967. doi:10.1093/eurheartj/ehv653

Jin, X., Dimitriadis, E. K., Liu, Y., Combs, C. A., Chang, J., Varsano, N., et al. (2018). Macrophages Shed Excess Cholesterol in Unique Extracellular Structures Containing Cholesterol Microdomains. *Atvb* 38, 1504–1518. doi:10.1161/atvbaha.118.311269

John, K., Kubelt, J., Müller, P., Wüstner, D., and Herrmann, A. (2002). Rapid Transbilayer Movement of the Fluorescent Sterol Dehydroergosterol in Lipid Membranes. *Biophysical J.* 83, 1525–1534. doi:10.1016/s0006-3495(02)73922-2

Juhl, A. D., Lund, F. W., Jensen, M. L. V., Szomek, M., Heegaard, C. W., Guttmann, P., et al. (2021). Niemann Pick C2 Protein Enables Cholesterol Transfer from Endo-Lysosomes to the Plasma Membrane for Efflux by Shedding of Extracellular Vesicles. *Chem. Phys. Lipids* 235, 105047. doi:10.1016/j.chemphyslip.2020.105047

Kellner-Weibel, G., Yancey, P. G., Jerome, W. G., Walser, T., Mason, R. P., Phillips, M. C., et al. (1999). Crystallization of Free Cholesterol in Model Macrophage Foam Cells. *Atvb* 19, 1891–1898. doi:10.1161/01.atv.19.8.1891

Kerr, I. D., Hutchison, E., Gerard, L., Aleidi, S. M., and Gelissen, I. C. (2021). Mammalian ABCG-Transporters, Sterols and Lipids: To Bind Perchance to Transport? *Biochim. Biophys. Acta (Bba) - Mol. Cel Biol. Lipids* 1866, 158860. doi:10.1016/j.bbalip.2020.158860

Kilsdonk, E. P. C., Yancey, P. G., Stoudt, G. W., Bangerter, F. W., Johnson, W. J., Phillips, M. C., et al. (1995b). Cellular Cholesterol Efflux Mediated by Cyclodextrins. *J. Biol. Chem.* 270, 17250–17256. doi:10.1074/jbc.270.29.17250

Kilsdonk, E. P., Morel, D. W., Johnson, W. J., and Rothblat, G. H. (1995a). Inhibition of Cellular Cholesterol Efflux by 25-hydroxycholesterol. *J. Lipid Res.* 36, 505–516. doi:10.1016/s0022-2275(20)39884-9

Kim, J., Shin, H., Kim, J., Kim, J., and Park, J. (2015). Isolation of High-Purity Extracellular Vesicles by Extracting Proteins Using Aqueous Two-phase System. *PloS one* 10, e0129760. doi:10.1371/journal.pone.0129760

Kırbaş, O. K., Bozkurt, B. T., Asutay, A. B., Mat, B., Ozdemir, B., Öztürkoğlu, D., et al. (2019). Optimized Isolation of Extracellular Vesicles from Various Organic Sources Using Aqueous Two-phase System. *Sci. Rep.* 9, 19159. doi:10.1038/s41598-019-55477-0

Kobayashi, T., Beuchat, M.-H., Lindsay, M., Frias, S., Palmiter, R. D., Sakuraba, H., et al. (1999). Late Endosomal Membranes Rich in Lysobisphosphatidic Acid Regulate Cholesterol Transport. *Nat. Cel Biol* 1, 113–118. doi:10.1038/10084

Kozarsky, K. F., Donahee, M. H., Rigotti, A., Iqbal, S. N., Edelman, E. R., and Krieger, M. (1997). Overexpression of the HDL Receptor SR-BI Alters Plasma HDL and Bile Cholesterol Levels. *Nature* 387, 414–417. doi:10.1038/387414a0

Kroll, T., Smits, S. H. J., and Schmitt, L. (2021). Monomeric Bile Acids Modulate the ATPase Activity of Detergent-Solubilized ABCB4/MDR3. *J. Lipid Res.* 62, 100087. doi:10.1016/j.jlr.2021.100087

Kuipers, F., Oude Elferink, R. P., Verkade, H. J., and Groen, A. K. (1997). Mechanisms and (Patho)physiological Significance of Biliary Cholesterol Secretion. *Subcell. Biochem.* 28, 295–318. doi:10.1007/978-1-4615-5901-6_11

Kulig, W., Mikkolainen, H., Olżyńska, A., Jurkiewicz, P., Cwiklik, L., Hof, M., et al. (2018). Bobbing of Oxysterols: Molecular Mechanism for Translocation of Tail-Oxidized Sterols through Biological Membranes. *J. Phys. Chem. Lett.* 9, 1118–1123. doi:10.1021/acs.jpclett.8b00211

Kwon, H. J., Abi-Mosleh, L., Wang, M. L., Deisenhofer, J., Goldstein, J. L., Brown, M. S., et al. (2009). Structure of N-Terminal Domain of NPC1 Reveals Distinct Subdomains for Binding and Transfer of Cholesterol. *Cell* 137, 1213–1224. doi:10.1016/j.cell.2009.03.049

Landry, Y. D., Denis, M., Nandi, S., Bell, S., Vaughan, A. M., and Zha, X. (2006). ATP-binding Cassette Transporter A1 Expression Disrupts Raft Membrane Microdomains through its ATPase-Related Functions. *J. Biol. Chem.* 281, 36091–36101. doi:10.1074/jbc.m602247200

Lange, Y., Ye, J., and Strebel, F. (1995). Movement of 25-hydroxycholesterol from the Plasma Membrane to the Rough Endoplasmic Reticulum in Cultured Hepatoma Cells. *J. Lipid Res.* 36, 1092–1097. doi:10.1016/s0022-2275(20)39867-9

Langheim, S., Yu, L., Von Bergmann, K., Lütjohann, D., Xu, F., Hobbs, H. H., et al. (2005). ABCG5 and ABCG8 Require MDR2 for Secretion of Cholesterol into Bile. *J. Lipid Res.* 46, 1732–1738. doi:10.1194/jlr.m500115-jlr200

Leventhal, A. R., Leslie, C. C., and Tabas, I. (2004). Suppression of Macrophage Eicosanoid Synthesis by Atherogenic Lipoproteins Is Profoundly Affected by Cholesterol-Fatty Acyl Esterification and the Niemann-Pick C Pathway of Lipid Trafficking. *J. Biol. Chem.* 279, 8084–8092. doi:10.1074/jbc.m310672200

Li, X., Saha, P., Li, J., Blobel, G., and Pfeffer, S. R. (2016). Clues to the Mechanism of Cholesterol Transfer from the Structure of NPC1 Middle Lumenal Domain Bound to NPC2. *Proc. Natl. Acad. Sci. USA* 113, 10079–10084. doi:10.1073/pnas.1611956113

Linsel-Nitschke, P., and Tall, A. R. (2005). HDL as a Target in the Treatment of Atherosclerotic Cardiovascular Disease. *Nat. Rev. Drug Discov.* 4, 193–205. doi:10.1038/nrd1658

Liu, L., Bortnick, A. E., Nickel, M., Dhanasekaran, P., Subbaiah, P. V., Lund-Katz, S., et al. (2003). Effects of Apolipoprotein A-I on ATP-Binding Cassette Transporter A1-Mediated Efflux of Macrophage Phospholipid and Cholesterol. *J. Biol. Chem.* 278, 42976–42984. doi:10.1074/jbc.m308420200

Long, T., Qi, X., Hassan, A., Liang, Q., De Brabander, J. K., and Li, X. (2020). Structural Basis for Itraconazole-Mediated NPC1 Inhibition. *Nat. Commun.* 11, 152. doi:10.1038/s41467-019-13917-5

Lundbæck, J. A., and Andersen, O. S. (2012). "Cholesterol Regulation of Membrane Protein Function by Changes in Bilayer Physical Properties - an Energetic Perspective," in *Cholesterol Regulation of Ion Channels and Receptors*. Editors I. A. B. Levitan and F. John (Wiley & Sons Inc), 27–44.

Luo, J., Yang, H., and Song, B.-L. (2020). Mechanisms and Regulation of Cholesterol Homeostasis. *Nat. Rev. Mol. Cel Biol* 21, 225–245. doi:10.1038/s41580-019-0190-7

Luu, W., Sharpe, L. J., Capell-Hattam, I., Gelissen, I. C., and Brown, A. J. (2016). Oxysterols: Old Tale, New Twists. *Annu. Rev. Pharmacol. Toxicol.* 56, 447–467. doi:10.1146/annurev-pharmtox-010715-103233

Ma, L., Li, Y., Peng, J., Wu, D., Zhao, X., Cui, Y., et al. (2015). Discovery of the Migrasome, an Organelle Mediating Release of Cytoplasmic Contents during Cell Migration. *Cell Res* 25, 24–38. doi:10.1038/cr.2014.135

Maekawa, M., and Fairn, G. D. (2015). Complementary Probes Reveal that Phosphatidylserine Is Required for the Proper Transbilayer Distribution of Cholesterol. *J. Cel Sci.* 128, 1422–1433. doi:10.1242/jcs.164715

Manthei, K. A., Ahn, J., Glukhova, A., Yuan, W., Larkin, C., Manett, T. D., et al. (2017). A Retractable Lid in Lecithin:cholesterol Acyltransferase Provides a Structural Mechanism for Activation by Apolipoprotein A-I. *J. Biol. Chem.* 292, 20313–20327. doi:10.1074/jbc.m117.802736

Manthei, K. A., Patra, D., Wilson, C. J., Fawaz, M. V., Piersimoni, L., Shenkar, J. C., et al. (2020). Structural Analysis of Lecithin:cholesterol Acyltransferase Bound to High Density Lipoprotein Particles. *Commun. Biol.* 3, 28. doi:10.1038/s42003-019-0749-z

Marques, P. E., Nyegaard, S., Collins, R. F., Troise, F., Freeman, S. A., Trimble, W. S., et al. (2019). Multimerization and Retention of the Scavenger Receptor SR-B1 in the Plasma Membrane. *Developmental Cel* 50, 283–295. doi:10.1016/j.devcel.2019.05.026

Maxfield, F. R., and Mcgraw, T. E. (2004). Endocytic Recycling. *Nat. Rev. Mol. Cel Biol* 5, 121–132. doi:10.1038/nrm1315

Maxfield, F. R., and Menon, A. K. (2006). Intracellular Sterol Transport and Distribution. *Curr. Opin. Cel Biol.* 18, 379–385. doi:10.1016/j.ceb.2006.06.012

McCauliff, L. A., Langan, A., Li, R., Ilnytska, O., Bose, D., Waghalter, M., et al. (2019). Intracellular Cholesterol Trafficking Is Dependent upon NPC2 Interaction with Lysobisphosphatidic Acid. *Elife* 8, e50832. doi:10.7554/eLife.50832

McConnell, H. M., and Radhakrishnan, A. (2003). Condensed Complexes of Cholesterol and Phospholipids. *Biochim. Biophys. Acta (Bba) - Biomembranes* 1610, 159–173. doi:10.1016/s0005-2736(03)00015-4

Mcdermott, G., Le Gros, M. A., Knoechel, C. G., Uchida, M., and Larabell, C. A. (2009). Soft X-ray Tomography and Cryogenic Light Microscopy: the Cool Combination in Cellular Imaging. *Trends Cell Biology* 19, 587–595. doi:10.1016/j.tcb.2009.08.005

Mcnutt, M. C., Lagace, T. A., and Horton, J. D. (2007). Catalytic Activity Is Not Required for Secreted PCSK9 to Reduce Low Density Lipoprotein Receptors in HepG2 Cells. *J. Biol. Chem.* 282, 20799–20803. doi:10.1074/jbc.c700095200

Mesmin, B., and Antonny, B. (2016). The Counterflow Transport of Sterols and PI4P. *Biochim. Biophys. Acta (Bba) - Mol. Cel Biol. Lipids* 1861, 940–951. doi:10.1016/j.bbalip.2016.02.024

Mesmin, B., Pipalia, N. H., Lund, F. W., Ramlall, T. F., Sokolov, A., Eliezer, D., et al. (2011). STARD4 Abundance Regulates Sterol Transport and Sensing. *MBoC* 22, 4004–4015. doi:10.1091/mbc.e11-04-0372

Möbius, W., Van Donselaar, E., Ohno-Iwashita, Y., Shimada, Y., Heijnen, H. F. G., Slot, J. W., et al. (2003). Recycling Compartments and the Internal Vesicles of Multivesicular Bodies Harbor Most of the Cholesterol Found in the Endocytic Pathway. *Traffic* 4, 222–231. doi:10.1034/j.1600-0854.2003.00072.x

Mondal, A., Ashiq, K. A., Phulpagar, P., Singh, D. K., and Shiras, A. (2019). Effective Visualization and Easy Tracking of Extracellular Vesicles in Glioma Cells. *Biol. Proced.* 21, 4–12. doi:10.1186/s12575-019-0092-2

Mondal, M., Mesmin, B., Mukherjee, S., and Maxfield, F. R. (2009). Sterols Are Mainly in the Cytoplasmic Leaflet of the Plasma Membrane and the Endocytic Recycling Compartment in CHO Cells. *MBoC* 20, 581–588. doi:10.1091/mbc.e08-07-0785

Morel, D. W., Edgerton, M. E., Warner, G. E., Johnson, W. J., Phillips, M. C., and Rothblat, G. H. (1996). Comparison of the Intracellular Metabolism and Trafficking of 25-hydroxycholesterol and Cholesterol in Macrophages. *J. Lipid Res.* 37, 2041–2051. doi:10.1016/s0022-2275(20)37568-4

Mouritsen, O. G., and Zuckermann, M. J. (2004). What's So Special about Cholesterol? *Lipids* 39, 1101–1113. doi:10.1007/s11745-004-1336-x

Mousavi, S. A., Berge, K. E., and Leren, T. P. (2009). The Unique Role of Proprotein Convertase Subtilisin/kexin 9 in Cholesterol Homeostasis. *J. Intern. Med.* 266, 507–519. doi:10.1111/j.1365-2796.2009.02167.x

Mutka, A.-L., Lusa, S., Linder, M. D., Jokitalo, E., Kopra, O., Jauhiainen, M., et al. (2004). Secretion of Sterols and the NPC2 Protein from Primary Astrocytes. *J. Biol. Chem.* 279, 48654–48662. doi:10.1074/jbc.m405345200

Nagata, K. O., Nakada, C., Kasai, R. S., Kusumi, A., and Ueda, K. (2013). ABCA1 Dimer-Monomer Interconversion during HDL Generation Revealed by Single-Molecule Imaging. *Proc. Natl. Acad. Sci.* 110, 5034–5039. doi:10.1073/pnas.1220703110

Nakamura, Y., Kotite, L., Gan, Y., Spencer, T. A., Fielding, C. J., and Fielding, P. E. (2004). Molecular Mechanism of Reverse Cholesterol Transport: Reaction of Pre-β-migrating High-Density Lipoprotein with Plasma Lecithin/Cholesterol Acyltransferase. *Biochemistry* 43, 14811–14820. doi:10.1021/bi0485629

Nandi, S., Ma, L., Denis, M., Karwatsky, J., Li, Z., Jiang, X.-C., et al. (2009). ABCA1-mediated Cholesterol Efflux Generates Microparticles in Addition to HDL through Processes Governed by Membrane Rigidity. *J. Lipid Res.* 50, 456–466. doi:10.1194/jlr.m800345-jlr200

Neculai, D., Schwake, M., Ravichandran, M., Zunke, F., Collins, R. F., Peters, J., et al. (2013). Structure of LIMP-2 Provides Functional Insights with Implications for SR-BI and CD36. *Nature* 504, 172–176. doi:10.1038/nature12684

Nedelcu, D., Liu, J., Xu, Y., Jao, C., and Salic, A. (2013). Oxysterol Binding to the Extracellular Domain of Smoothened in Hedgehog Signaling. *Nat. Chem. Biol.* 9, 557–564. doi:10.1038/nchembio.1290

Neufeld, E. B., Demosky, S. J., Jr., Stonik, J. A., Combs, C., Remaley, A. T., Duverger, N., et al. (2002). The ABCA1 Transporter Functions on the Basolateral Surface of Hepatocytes. *Biochem. Biophysical Res. Commun.* 297, 974–979. doi:10.1016/s0006-291x(02)02274-x

Neufeld, E. B., Remaley, A. T., Demosky, S. J., Stonik, J. A., Cooney, A. M., Comly, M., et al. (2001). Cellular Localization and Trafficking of the Human ABCA1 Transporter. *J. Biol. Chem.* 276, 27584–27590. doi:10.1074/jbc.m103264200

Neufeld, E. B., Stonik, J. A., Demosky, S. J., Jr., Knapper, C. L., Combs, C. A., Cooney, A., et al. (2004). The ABCA1 Transporter Modulates Late Endocytic Trafficking. *J. Biol. Chem.* 279, 15571–15578. doi:10.1074/jbc.m314160200

Nissen, S. E. (2017). Merck Halts Development of Anacetrapib. *Cardiol. Today*.

Niu, S.-L., and Litman, B. J. (2002). Determination of Membrane Cholesterol Partition Coefficient Using a Lipid Vesicle-Cyclodextrin Binary System: Effect of Phospholipid Acyl Chain Unsaturation and Headgroup Composition. *Biophysical J.* 83, 3408–3415. doi:10.1016/s0006-3495(02)75340-x

Noack, A., Gericke, B., von Köckritz-Blickwede, M., Menze, A., Noack, S., Gerhauser, I., et al. (2018). Mechanism of Drug Extrusion by Brain Endothelial Cells via Lysosomal Drug Trapping and Disposal by Neutrophils. *Proc. Natl. Acad. Sci. USA* 115, E9590–E9599. doi:10.1073/pnas.1719642115

Nyholm, T. K. M., Jaikishan, S., Engberg, O., Hautala, V., and Slotte, J. P. (2019). The Affinity of Sterols for Different Phospholipid Classes and its Impact on Lateral Segregation. *Biophysical J.* 116, 296–307. doi:10.1016/j.bpj.2018.11.3135

Ogasawara, F., Kano, F., Murata, M., Kimura, Y., Kioka, N., and Ueda, K. (2019). Changes in the Asymmetric Distribution of Cholesterol in the Plasma Membrane Influence Streptolysin O Pore Formation. *Sci. Rep.* 9, 4548. doi:10.1038/s41598-019-39973-x

Ohvo-RekilÃ¤, H., Ramstedt, B., Leppimaki, P., and Slotte, J. P. (2002). Cholesterol Interactions with Phospholipids in Membranes. *Prog. Lipid Res.* 41, 66–97. doi:10.1016/s0163-7827(01)00020-0

Okamoto, Y., Tomioka, M., Ogasawara, F., Nagaiwa, K., Kimura, Y., Kioka, N., et al. (2020). C-terminal of ABCA1 Separately Regulates Cholesterol Floppase Activity and Cholesterol Efflux Activity. *Biosci. Biotechnol. Biochem.* 84, 764–773. doi:10.1080/09168451.2019.1700775

Oram, J. (2000). Tangier Disease and ABCA1. *Biochim. Biophys. Acta* 1529, 321–330. doi:10.1016/s1388-1981(00)00157-8

Ouimet, M., Franklin, V., Mak, E., Liao, X., Tabas, I., and Marcel, Y. L. (2011). Autophagy Regulates Cholesterol Efflux from Macrophage Foam Cells via Lysosomal Acid Lipase. *Cel Metab.* 13, 655–667. doi:10.1016/j.cmet.2011.03.023

Pagler, T. A., Wang, M., Mondal, M., Murphy, A. J., Westerterp, M., Moore, K. J., et al. (2011). Deletion of ABCA1 and ABCG1 Impairs Macrophage Migration Because of Increased Rac1 Signaling. *Circ. Res.* 108, 194–200. doi:10.1161/circresaha.110.228619

Peake, K. B., and Vance, J. E. (2010). Defective Cholesterol Trafficking in Niemann-Pick C-Deficient Cells. *FEBS Lett.* 584, 2731–2739. doi:10.1016/j.febslet.2010.04.047

Peng, Y., Akmentin, W., Connelly, M. A., Lund-Katz, S., Phillips, M. C., and Williams, D. L. (2004). Scavenger Receptor BI (SR-BI) Clustered on Microvillar Extensions Suggests that This Plasma Membrane Domain Is a Way Station for Cholesterol Trafficking between Cells and High-Density Lipoprotein. *MBoC* 15, 384–396. doi:10.1091/mbc.e03-06-0445

Petersen, D., Reinholdt, P., Szomek, M., Hansen, S. K., Poongavanam, V., Dupont, A., et al. (2020). Binding and Intracellular Transport of 25-hydroxycholesterol by Niemann-Pick C2 Protein. *Biochim. Biophys. Acta (Bba) - Biomembranes* 1862, 183063. doi:10.1016/j.bbamem.2019.183063

Peyrot, S. M., Nachtergaele, S., Luchetti, G., Mydock-Mcgrane, L. K., Fujiwara, H., Scherrer, D., et al. (2014). Tracking the Subcellular Fate of 20(s)-Hydroxycholesterol with Click Chemistry Reveals a Transport Pathway to the Golgi. *J. Biol. Chem.* 289, 11095–11110. doi:10.1074/jbc.m113.540351

Pfisterer, S. G., Peränen, J., and Ikonen, E. (2016). LDL-cholesterol Transport to the Endoplasmic Reticulum. *Curr. Opin. Lipidol.* 27, 282–287. doi:10.1097/mol.0000000000000292

Pfrieger, F. W., and Vitale, N. (2018). Cholesterol and the Journey of Extracellular Vesicles. *J. Lipid Res*.

Phillips, M. C. (2018). Is ABCA1 a Lipid Transfer Protein? *J. Lipid Res.* 59, 749–763. doi:10.1194/jlr.r082313

Phillips, M. C. (2014). Molecular Mechanisms of Cellular Cholesterol Efflux. *J. Biol. Chem.* 289, 24020–24029. doi:10.1074/jbc.r114.583658

Pinkwart, K., Schneider, F., Lukoseviciute, M., Sauka-Spengler, T., Lyman, E., Eggeling, C., et al. (2019). Nanoscale Dynamics of Cholesterol in the Cell Membrane. *J. Biol. Chem.* 294, 12599–12609. doi:10.1074/jbc.ra119.009683

Plochberger, B., Röhrl, C., Preiner, J., Rankl, C., Brameshuber, M., Madl, J., et al. (2017). HDL Particles Incorporate into Lipid Bilayers - a Combined AFM and Single Molecule Fluorescence Microscopy Study. *Sci. Rep.* 7, 15886. doi:10.1038/s41598-017-15949-7

Plummer, A. M., Culbertson, A. T., and Liao, M. (2021). The ABCs of Sterol Transport. *Annu. Rev. Physiol.* 83, 153–181. doi:10.1146/annurev-physiol-031620-094944

Pollet, H., Conrard, L., Cloos, A.-S., and Tyteca, D. (2018). Plasma Membrane Lipid Domains as Platforms for Vesicle Biogenesis and Shedding? *Biomolecules* 8, 94. doi:10.3390/biom8030094

Pomorski, T., Lombardi, R., Riezman, H., Devaux, P. F., Van Meer, G., and Holthuis, J. C. M. (2003). Drs2p-related P-type ATPases Dnf1p and Dnf2p Are Required for Phospholipid Translocation across the Yeast Plasma Membrane and Serve a Role in Endocytosis. *MBoC* 14, 1240–1254. doi:10.1091/mbc.e02-08-0501

Qian, H., Wu, X., Du, X., Yao, X., Zhao, X., Lee, J., et al. (2020). Structural Basis of Low-pH-dependent Lysosomal Cholesterol Egress by NPC1 and NPC2. *Cell* 182, 98–111. doi:10.1016/j.cell.2020.05.020

Qian, H., Zhao, X., Cao, P., Lei, J., Yan, N., and Gong, X. (2017). Structure of the Human Lipid Exporter ABCA1. *Cell* 169, 1228–1239. doi:10.1016/j.cell.2017.05.020

Quazi, F., and Molday, R. S. (2013). Differential Phospholipid Substrates and Directional Transport by ATP-Binding Cassette Proteins ABCA1, ABCA7, and ABCA4 and Disease-Causing Mutants. *J. Biol. Chem.* 288, 34414–34426. doi:10.1074/jbc.m113.508812

Quazi, F., and Molday, R. S. (2011). Lipid Transport by Mammalian ABC Proteins. *Essays Biochem.* 50, 265–290. doi:10.1042/bse0500265

Radhakrishnan, A., Goldstein, J. L., Mcdonald, J. G., and Brown, M. S. (2008). Switch-like Control of SREBP-2 Transport Triggered by Small Changes in ER Cholesterol: a Delicate Balance. *Cel Metab.* 8, 512–521. doi:10.1016/j.cmet.2008.10.008

Radhakrishnan, A., Ikeda, Y., Kwon, H. J., Brown, M. S., and Goldstein, J. L. (2007). Sterol-regulated Transport of SREBPs from Endoplasmic Reticulum to Golgi: Oxysterols Block Transport by Binding to Insig. *Proc. Natl. Acad. Sci.* 104, 6511–6518. doi:10.1073/pnas.0700899104

Radhakrishnan, A., and Mcconnell, H. M. (2000). Chemical Activity of Cholesterol in Membranes. *Biochemistry* 39, 8119–8124. doi:10.1021/bi0005097

Raducka-Jaszul, O., Wojtowicz, K., Sikorski, A. F., Chimini, G., Hamon, Y., and Trombik, T. (2021). Molecular Diffusion of ABCA1 at the Cell Surface of Living Cells Assessed by svFCS. *Membranes (Basel)* 11. doi:10.3390/membranes11070498

Raghupathy, R., Anilkumar, A. A., Polley, A., Singh, P. P., Yadav, M., Johnson, C., et al. (2015). Transbilayer Lipid Interactions Mediate Nanoclustering of Lipid-Anchored Proteins. *Cell* 161, 581–594. doi:10.1016/j.cell.2015.03.048

Reboul, E., Dyka, F. M., Quazi, F., and Molday, R. S. (2013). Cholesterol Transport via ABCA1: New Insights from Solid-phase Binding Assay. *Biochimie* 95, 957–961. doi:10.1016/j.biochi.2012.11.009

Robichaud, S., Fairman, G., Vijithakumar, V., Mak, E., Cook, D. P., Pelletier, A. R., et al. (2021). Identification of Novel Lipid Droplet Factors that Regulate Lipophagy and Cholesterol Efflux in Macrophage Foam Cells. *Autophagy* 17, 3671–3689. doi:10.1080/15548627.2021.1886839

Robins, S. J., and Fasulo, J. M. (1999). Delineation of a Novel Hepatic Route for the Selective Transfer of Unesterified Sterols from High-Density Lipoproteins to Bile: Studies Using the Perfused Rat Liver. *Hepatology* 29, 1541–1548. doi:10.1002/hep.510290518

Robins, S. J., and Fasulo, J. M. (1997). High Density Lipoproteins, but Not Other Lipoproteins, Provide a Vehicle for Sterol Transport to Bile. *J. Clin. Invest.* 99, 380–384. doi:10.1172/jci119170

Röhrl, C., Meisslitzer-Ruppitsch, C., Bittman, R., Li, Z., Pabst, G., Prassl, R., et al. (2012). Combined Light and Electron Microscopy Using Diaminobenzidine Photooxidation to Monitor Trafficking of Lipids Derived from Lipoprotein Particles. *Cpb* 13, 331–340. doi:10.2174/138920112799095338

Rothblat, G. H., De La Llera-Moya, M., Atger, V., Kellner-Weibel, G., Williams, D. L., and Phillips, M. C. (1999). Cell Cholesterol Efflux: Integration of Old and New Observations Provides New Insights. *J. Lipid Res.* 40, 781–796. doi:10.1016/s0022-2275(20)32113-1

Sahoo, D., Peng, Y., Smith, J. R., Darlington, Y. F., and Connelly, M. A. (2007). Scavenger Receptor Class B, Type I (SR-BI) Homo-Dimerizes via its C-Terminal Region: Fluorescence Resonance Energy Transfer Analysis. *Biochim. Biophys. Acta (Bba) - Mol. Cel Biol. Lipids* 1771, 818–829. doi:10.1016/j.bbalip.2007.04.019

Sandhu, J., Li, S., Fairall, L., Pfisterer, S. G., Gurnett, J. E., Xiao, X., et al. (2018). Aster Proteins Facilitate Nonvesicular Plasma Membrane to ER Cholesterol Transport in Mammalian Cells. *Cell*. doi:10.1016/j.cell.2018.08.033

Sankaranarayanan, S., De La Llera-Moya, M., Drazul-Schrader, D., Phillips, M. C., Kellner-Weibel, G., and Rothblat, G. H. (2013). Serum Albumin Acts as a Shuttle to Enhance Cholesterol Efflux from Cells. *J. Lipid Res.* 54, 671–676. doi:10.1194/jlr.m031336

Sarkar, S., Carroll, B., Buganim, Y., Maetzel, D., Ng, A. H. M., Cassady, J. P., et al. (2013). Impaired Autophagy in the Lipid-Storage Disorder Niemann-Pick Type C1 Disease. *Cel Rep.* 5, 1302–1315. doi:10.1016/j.celrep.2013.10.042

Scheidt, H. A., Meyer, T., Nikolaus, J., Baek, D. J., Haralampiev, I., Thomas, L., et al. (2013). Cholesterol's Aliphatic Side Chain Modulates Membrane Properties. *Angew. Chem. Int. Ed.* 52, 12848–12851. doi:10.1002/anie.201306753

Schilling, G., Savonenko, A. V., Klevytska, A., Morton, J. L., Tucker, S. M., Poirier, M., et al. (2004). Nuclear-targeting of Mutant Huntingtin Fragments Produces Huntington's Disease-like Phenotypes in Transgenic Mice. *Hum. Mol. Genet.* 13, 1599–1610. doi:10.1093/hmg/ddh175

Schneider, G., Guttmann, P., Heim, S., Rehbein, S., Mueller, F., Nagashima, K., et al. (2010). Three-dimensional Cellular Ultrastructure Resolved by X-ray Microscopy. *Nat. Methods* 7, 985–987. doi:10.1038/nmeth.1533

Scorrano, L., De Matteis, M. A., Emr, S., Giordano, F., Hajnóczky, G., Kornmann, B., et al. (2019). Coming Together to Define Membrane Contact Sites. *Nat. Commun.* 10, 1287. doi:10.1038/s41467-019-09253-3

Scotti, E., Calamai, M., Goulbourne, C. N., Zhang, L., Hong, C., Lin, R. R., et al. (2013). IDOL Stimulates Clathrin-independent Endocytosis and Multivesicular Body-Mediated Lysosomal Degradation of the Low-Density Lipoprotein Receptor. *Mol. Cell Biol.* 33, 1503–1514. doi:10.1128/mcb.01716-12

Scotti, E., Hong, C., Yoshinaga, Y., Tu, Y., Hu, Y., Zelcer, N., et al. (2011). Targeted Disruption of the Idol Gene Alters Cellular Regulation of the Low-Density Lipoprotein Receptor by Sterols and Liver X Receptor Agonists. *Mol. Cel Biol* 31, 1885–1893. doi:10.1128/mcb.01469-10

Secknus, R., Darby, G. H., Chernosky, A., Juvonen, T., Moore, E. W., and Holzbach, R. T. (1999). Apolipoprotein A-I in Bile Inhibits Cholesterol Crystallization and Modifies Transcellular Lipid Transfer through Cultured Human Gall-Bladder Epithelial Cells. *J. Gastroenterol. Hepatol.* 14, 446–456. doi:10.1046/j.1440-1746.1999.01881.x

Sedgwick, A., Olivia Balmert, M., and D'Souza-Schorey, C. (2018). The Formation of Giant Plasma Membrane Vesicles Enable New Insights into the Regulation of Cholesterol Efflux. *Exp. Cel Res.* 365, 194–207. doi:10.1016/j.yexcr.2018.03.001

Segrest, J. P., Jones, M. K., Catte, A., Manchekar, M., Datta, G., Zhang, L., et al. (2015). Surface Density-Induced Pleating of a Lipid Monolayer Drives Nascent High-Density Lipoprotein Assembly. *Structure* 23, 1214–1226. doi:10.1016/j.str.2015.05.010

Sezgin, E., Kaiser, H.-J., Baumgart, T., Schwille, P., Simons, K., and Levental, I. (2012). Elucidating Membrane Structure and Protein Behavior Using Giant Plasma Membrane Vesicles. *Nat. Protoc.* 7, 1042–1051. doi:10.1038/nprot.2012.059

Sharpe, L. J., Cook, E. C. L., Zelcer, N., and Brown, A. J. (2014). The UPS and downs of Cholesterol Homeostasis. *Trends Biochem. Sci.* 39, 527–535. doi:10.1016/j.tibs.2014.08.008

Sheridan, C. (2016). CETP Inhibitors Boost 'good' Cholesterol to No Avail. *Nat. Biotechnol.* 34.

Shetty, S., Eckhardt, E. R. M., Post, S. R., and Van Der Westhuyzen, D. R. (2006). Phosphatidylinositol-3-kinase Regulates Scavenger Receptor Class B Type I Subcellular Localization and Selective Lipid Uptake in Hepatocytes. *Atvb* 26, 2125–2131. doi:10.1161/01.atv.0000233335.26362.37

Shin, H., Han, C., Labuz, J. M., Kim, J., Kim, J., Cho, S., et al. (2015). High-yield Isolation of Extracellular Vesicles Using Aqueous Two-phase System. *Sci. Rep.* 5, 13103–13111. doi:10.1038/srep13103

Silver, D. L., Wang, N., Xiao, X., and Tall, A. R. (2001). High Density Lipoprotein (HDL) Particle Uptake Mediated by Scavenger Receptor Class B Type 1 Results in Selective Sorting of HDL Cholesterol from Protein and Polarized Cholesterol Secretion. *J. Biol. Chem.* 276, 25287–25293. doi:10.1074/jbc.m101726200

Sinensky, M. (1981). A Comparison of Solution Properties of Cholesterol and 25-hydroxycholesterol. *Arch. Biochem. Biophys.* 209, 321–324. doi:10.1016/0003-9861(81)90287-3

Singh, R. K., Barbosa-Lorenzi, V. C., Lund, F. W., Grosheva, I., Maxfield, F. R., and Haka, A. S. (2016). Degradation of Aggregated LDL Occurs in Complex Extracellular Sub-compartments of the Lysosomal Synapse. *J. Cel Sci* 129, 1072–1082. doi:10.1242/jcs.181743

Singh, R. K., Lund, F. W., Haka, A. S., and Maxfield, F. R. (2019). High-density Lipoprotein or Cyclodextrin Extraction of Cholesterol from Aggregated LDL Reduces Foam Cell Formation. *J. Cel Sci* 132. doi:10.1242/jcs.237271

Skarda, L., Kowal, J., and Locher, K. P. (2021). Structure of the Human Cholesterol Transporter ABCG1. *J. Mol. Biol.* 433, 167218. doi:10.1016/j.jmb.2021.167218

Small, D. M. (2003). Role of ABC Transporters in Secretion of Cholesterol from Liver into Bile. *Proc. Natl. Acad. Sci.* 100, 4–6. doi:10.1073/pnas.0237205100

Sokolov, A., and Radhakrishnan, A. (2010). Accessibility of Cholesterol in Endoplasmic Reticulum Membranes and Activation of SREBP-2 Switch Abruptly at a Common Cholesterol Threshold. *J. Biol. Chem.* 285, 29480–29490. doi:10.1074/jbc.m110.148254

Solanko, L. M., Sullivan, D. P., Sere, Y. Y., Szomek, M., Lunding, A., Solanko, K. A., et al. (2018). Ergosterol Is Mainly Located in the Cytoplasmic Leaflet of the Yeast Plasma Membrane. *Traffic* 19, 198–214. doi:10.1111/tra.12545

Steck, T. L., and Lange, Y. (2010). Cell Cholesterol Homeostasis: Mediation by Active Cholesterol. *Trends Cel Biol.* 20, 680–687. doi:10.1016/j.tcb.2010.08.007

Steck, T. L., Ye, J., and Lange, Y. (2002). Probing Red Cell Membrane Cholesterol Movement with Cyclodextrin. *Biophysical J.* 83, 2118–2125. doi:10.1016/s0006-3495(02)73972-6

Storch, J., and Xu, Z. (2009). Niemann-Pick C2 (NPC2) and Intracellular Cholesterol Trafficking. *Biochim. Biophys. Acta (Bba) - Mol. Cel Biol. Lipids* 1791, 671–678. doi:10.1016/j.bbalip.2009.02.001

Strauss, K., Goebel, C., Runz, H., Möbius, W., Weiss, S., Feussner, I., et al. (2010). Exosome Secretion Ameliorates Lysosomal Storage of Cholesterol in Niemann-Pick Type C Disease. *J. Biol. Chem.* 285, 26279–26288. doi:10.1074/jbc.m110.134775

Sun, B., Eckhardt, E. R. M., Shetty, S., Van Der Westhuyzen, D. R., and Webb, N. R. (2006). Quantitative Analysis of SR-BI-dependent HDL Retroendocytosis in Hepatocytes and Fibroblasts. *J. Lipid Res.* 47, 1700–1713. doi:10.1194/jlr.m500450-jlr200

Swain, E. (2017). Performance of CETP Inhibitors Vexing. *Cardiol. Today*.

Szomek, M., Moesgaard, L., Reinholdt, P., Haarhøj Hald, S. B., Petersen, D., Krishnan, K., et al. (2020). Membrane Organization and Intracellular Transport of a Fluorescent Analogue of 27-hydroxycholesterol. *Chem. Phys. Lipids* 233, 105004. doi:10.1016/j.chemphyslip.2020.105004

Tall, A. (1993). Plasma Cholesteryl Ester Transfer Protein. *J. Lipid Res.* 34, 1255–1274. doi:10.1016/s0022-2275(20)36957-1

Tall, A. R., Costet, P., and Wang, N. (2002). Regulation and Mechanisms of Macrophage Cholesterol Efflux. *J. Clin. Invest.* 110, 899–904. doi:10.1172/jci0216391

Tall, A. R., and Wang, N. (2000). Tangier Disease as a Test of the Reverse Cholesterol Transport Hypothesis. *J. Clin. Invest.* 106, 1205–1207. doi:10.1172/jci11538

Tam, S.-P., Mok, L., Chimini, G., Vasa, M., and Deeley, R. G. (2006). ABCA1 Mediates High-Affinity Uptake of 25-hydroxycholesterol by Membrane Vesicles and Rapid Efflux of Oxysterol by Intact Cells. *Am. J. Physiology-Cell Physiol.* 291, C490–C502. doi:10.1152/ajpcell.00055.2006

Tangirala, R. K., Jerome, W. G., Jones, N. L., Small, D. M., Johnson, W. J., Glick, J. M., et al. (1994). Formation of Cholesterol Monohydrate Crystals in Macrophage-Derived Foam Cells. *J. Lipid Res.* 35, 93–104. doi:10.1016/s0022-2275(20)40131-2

Tannert, A., Wüstner, D., Bechstein, J., Müller, P., Devaux, P. F., and Herrmann, A. (2003). Aminophospholipids Have No Access to the Luminal Side of the Biliary Canaliculus. *J. Biol. Chem.* 278, 40631–40639. doi:10.1074/jbc.m302131200

Thuahnai, S. T., Lund-Katz, S., Anantharamaiah, G. M., Williams, D. L., and Phillips, M. C. (2003). A Quantitative Analysis of Apolipoprotein Binding to SR-BI: Multiple Binding Sites for Lipid-free and Lipid-Associated Apolipoproteins. *J. Lipid Res.* 44, 1132–1142. doi:10.1194/jlr.m200429-jlr200

Trigueros-Motos, L., Van Capelleveen, J. C., Torta, F., Castaño, D., Zhang, L.-H., Chai, E. C., et al. (2017). ABCA8 Regulates Cholesterol Efflux and High-Density Lipoprotein Cholesterol Levels. *Atvb* 37, 2147–2155. doi:10.1161/atvbaha.117.309574

Trompier, D., Alibert, M., Davanture, S., Hamon, Y., Pierres, M., and Chimini, G. (2006). Transition from Dimers to Higher Oligomeric Forms Occurs during the ATPase Cycle of the ABCA1 Transporter. *J. Biol. Chem.* 281, 20283–20290. doi:10.1074/jbc.m601072200

Tsuji, T., Fujimoto, M., Tatematsu, T., Cheng, J., Orii, M., Takatori, S., et al. (2017). Niemann-Pick Type C Proteins Promote Microautophagy by Expanding Raft-like Membrane Domains in the Yeast Vacuole. *Elife* 6. doi:10.7554/elife.25960

Vacca, F., Vossio, S., Mercier, V., Moreau, D., Johnson, S., Scott, C. C., et al. (2019). Cyclodextrin Triggers MCOLN1-dependent Endo-Lysosome Secretion in Niemann-Pick Type C Cells. *J. Lipid Res.* 60, 832–843. doi:10.1194/jlr.m089979

Van Meer, G., Halter, D., Sprong, H., Somerharju, P., and Egmond, M. R. (2006). ABC lipid transporters. ABC Lipid Transporters: Extruders, Flippases, or Flopless Activators? *FEBS Lett.* 580, 1171–1177. doi:10.1016/j.febslet.2005.12.019

Van Niel, G., D'angelo, G., and Raposo, G. (2018). Shedding Light on the Cell Biology of Extracellular Vesicles. *Nat. Rev. Mol. Cel Biol* 19, 213–228. doi:10.1038/nrm.2017.125

Varsano, N., Dadosh, T., Kapishnikov, S., Pereiro, E., Shimoni, E., Jin, X., et al. (2016). Development of Correlative Cryo-Soft X-ray Tomography and Stochastic Reconstruction Microscopy. A Study of Cholesterol Crystal Early Formation in Cells. *J. Am. Chem. Soc.* 138, 14931–14940. doi:10.1021/jacs.6b07584

Vaughan, A. M., and Oram, J. F. (2006). ABCA1 and ABCG1 or ABCG4 Act Sequentially to Remove Cellular Cholesterol and Generate Cholesterol-Rich HDL. *J. Lipid Res.* 47, 2433–2443. doi:10.1194/jlr.m600218-jlr200

Vedhachalam, C., Duong, P. T., Nickel, M., Nguyen, D., Dhanasekaran, P., Saito, H., et al. (2007). Mechanism of ATP-Binding Cassette Transporter A1-Mediated Cellular Lipid Efflux to Apolipoprotein A-I and Formation of High Density Lipoprotein Particles. *J. Biol. Chem.* 282, 25123–25130. doi:10.1074/jbc.m704590200

Venkateswaran, A., Laffitte, B. A., Joseph, S. B., Mak, P. A., Wilpitz, D. C., Edwards, P. A., et al. (2000). Control of Cellular Cholesterol Efflux by the Nuclear Oxysterol Receptor LXRalpha. *Proc. Natl. Acad. Sci.* 97, 12097–12102. doi:10.1073/pnas.200367697

Verweij, F. J., Balaj, L., Boulanger, C. M., Carter, D. R., Compeer, E. B., D'angelo, G., et al. (2021). The Power of Imaging to Understand Extracellular Vesicle Biology *In Vivo*. *Nat. Methods*, 1–14. doi:10.1038/s41592-021-01206-3

Vos, D. Y., and Van De Sluis, B. (2021). Function of the Endolysosomal Network in Cholesterol Homeostasis and Metabolic-Associated Fatty Liver Disease (MAFLD). *Mol. Metab.* 50, 101146. doi:10.1016/j.molmet.2020.101146

Wang, H., Ma, Q., Qi, Y., Dong, J., Du, X., Rae, J., et al. (2019). ORP2 Delivers Cholesterol to the Plasma Membrane in Exchange for Phosphatidylinositol 4, 5-Bisphosphate (PI(4,5)P2). *Mol. Cel* 73, 458–473. doi:10.1016/j.molcel.2018.11.014

Wang, M.-D., Kiss, R. S., Franklin, V., Mcbride, H. M., Whitman, S. C., and Marcel, Y. L. (2007a). Different Cellular Traffic of LDL-Cholesterol and Acetylated LDL-Cholesterol Leads to Distinct Reverse Cholesterol Transport Pathways. *J. Lipid Res.* 48, 633–645. doi:10.1194/jlr.m600470-jlr200

Wang, N., Lan, D., Chen, W., Matsuura, F., and Tall, A. R. (2004). ATP-binding Cassette Transporters G1 and G4 Mediate Cellular Cholesterol Efflux to High-Density Lipoproteins. *Proc. Natl. Acad. Sci.* 101, 9774–9779. doi:10.1073/pnas.0403506101

Wang, N., Silver, D. L., Thiele, C., and Tall, A. R. (2001). ATP-binding Cassette Transporter A1 (ABCA1) Functions as a Cholesterol Efflux Regulatory Protein. *J. Biol. Chem.* 276, 23742–23747. doi:10.1074/jbc.m102348200

Wang, N., Yvan-Charvet, L., Lütjohann, D., Mulder, M., Vanmierlo, T., Kim, T. W., et al. (2008). ATP-binding Cassette Transporters G1 and G4 Mediate Cholesterol and Desmosterol Efflux to HDL and Regulate Sterol Accumulation in the Brain. *FASEB J.* 22, 1073–1082. doi:10.1096/fj.07-9944com

Wang, X., Collins, H. L., Ranalletta, M., Fuki, I. V., Billheimer, J. T., Rothblat, G. H., et al. (2007b). Macrophage ABCA1 and ABCG1, but Not SR-BI, Promote Macrophage Reverse Cholesterol Transport *In Vivo*. *J. Clin. Invest.* 117, 2216–2224. doi:10.1172/jci32057

Wanon, J., Guertin, F., Brunet, S., Delvin, E., Gavino, V., Bouthillier, D., et al. (1998). The Effects of Cholesterol Uptake from High-Density Lipoprotein Subfractions on Biliary Sterol Secretion in Rats with Essential Fatty-Acid Deficiency. *Hepatology* 27, 779–786. doi:10.1002/hep.510270320

Webb, N. R., De Beer, M. C., Asztalos, B. F., Whitaker, N., Van Der Westhuyzen, D. R., and De Beer, F. C. (2004). Remodeling of HDL Remnants Generated by Scavenger Receptor Class B Type I. *J. Lipid Res.* 45, 1666–1673. doi:10.1194/jlr.m400026-jlr200

Winkler, M. B. L., Kidmose, R. T., Szomek, M., Thaysen, K., Rawson, S., Muench, S. P., et al. (2019). Structural Insight into Eukaryotic Sterol Transport through Niemann-Pick Type C Proteins. *Cell* 179, 485–497. e418. doi:10.1016/j.cell.2019.08.038

Wong, K., Briddon, S. J., Holliday, N. D., and Kerr, I. D. (2016). Plasma Membrane Dynamics and Tetrameric Organisation of ABCG2 Transporters in Mammalian Cells Revealed by Single Particle Imaging Techniques. *Biochim. Biophys. Acta (Bba) - Mol. Cel Res.* 1863, 19–29. doi:10.1016/j.bbamcr.2015.10.002

Wu, X., and Hammer, J. A. (2014). Melanosome Transfer: it Is Best to Give and Receive. *Curr. Opin. Cel Biol.* 29, 1–7. doi:10.1016/j.ceb.2014.02.003

Wüstner, D., and Solanko, K. (2015). How Cholesterol Interacts with Proteins and Lipids during its Intracellular Transport. *Biochim. Biophys. Acta* 1848, 1908–1926. doi:10.1016/j.bbamem.2015.05.010

Wüstner, D. (2008). Free-cholesterol Loading Does Not Trigger Phase Separation of the Fluorescent Sterol Dehydroergosterol in the Plasma Membrane of Macrophages. *Chem. Phys. Lipids* 154, 129–136. doi:10.1016/j.chemphyslip.2008.04.009

Wüstner, D., Herrmann, A., Hao, M., and Maxfield, F. R. (2002). Rapid Nonvesicular Transport of Sterol between the Plasma Membrane Domains of Polarized Hepatic Cells. *J. Biol. Chem.* 277, 30325–30336. doi:10.1074/jbc.m202626200

Wüstner, D., Herrmann, A., and Müller, P. (2000). Head Group-independent Interaction of Phospholipids with Bile Salts: a Fluorescence and EPR Study. *J. Lipid Res.* 41, 395–404. doi:10.1016/s0022-2275(20)34478-3

Wüstner, D. (2005). Mathematical Analysis of Hepatic High Density Lipoprotein Transport Based on Quantitative Imaging Data. *J. Biol. Chem.* 280, 6766–6779. doi:10.1074/jbc.m413238200

Wüstner, D., Modzel, M., Lund, F. W., and Lomholt, M. A. (2016). Imaging Approaches for Analysis of Cholesterol Distribution and Dynamics in the Plasma Membrane. *Chem. Phys. Lipids* 199, 106–135. doi:10.1016/j.chemphyslip.2016.03.003

Wüstner, D., Mondal, M., Huang, A., and Maxfield, F. R. (2004). Different Transport Routes for High Density Lipoprotein and its Associated Free Sterol in Polarized Hepatic Cells. *J. Lipid Res.* 45, 427–437. doi:10.1194/jlr.m300440-jlr200

Wüstner, D., Pomorski, T., Herrmann, A., and Müller, P. (1998). Release of Phospholipids from Erythrocyte Membranes by Taurocholate Is Determined by Their Transbilayer Orientation and Hydrophobic Backbone. *Biochemistry* 37, 17093–17103. doi:10.1021/bi981608b

Xiao, X., Tang, J.-J., Peng, C., Wang, Y., Fu, L., Qiu, Z.-P., et al. (2017). Cholesterol Modification of Smoothened Is Required for Hedgehog Signaling. *Mol. Cel* 66, 154–162. doi:10.1016/j.molcel.2017.02.015

Xu, Z., Farver, W., Kodukula, S., and Storch, J. (2008). Regulation of Sterol Transport between Membranes and NPC2. *Biochemistry* 47, 11134–11143. doi:10.1021/bi801328u

Yancey, P. G., Asztalos, B. F., Stettler, N., Piccoli, D., Williams, D. L., Connelly, M. A., et al. (2004a). SR-BI- and ABCA1-Mediated Cholesterol Efflux to Serum from Patients with Alagille Syndrome. *J. Lipid Res.* 45, 1724–1732. doi:10.1194/jlr.m400133-jlr200

Yancey, P. G., Kawashiri, M.-a., Moore, R., Glick, J. M., Williams, D. L., Connelly, M. A., et al. (2004b). *In Vivo* modulation of HDL Phospholipid Has Opposing Effects on SR-BI- and ABCA1-Mediated Cholesterol Efflux. *J. Lipid Res.* 45, 337–346. doi:10.1194/jlr.m300231-jlr200

Yancey, P. G., Rodrigueza, W. V., Kilsdonk, E. P. C., Stoudt, G. W., Johnson, W. J., Phillips, M. C., et al. (1996). Cellular Cholesterol Efflux Mediated by Cyclodextrins. *J. Biol. Chem.* 271, 16026–16034. doi:10.1074/jbc.271.27.16026

Yang, H.-x., Zhang, M., Long, S.-y., Tuo, Q.-h., Tian, Y., Chen, J.-x., et al. (2020). Cholesterol in LDL Receptor Recycling and Degradation. *Clinica Chim. Acta* 500, 81–86. doi:10.1016/j.cca.2019.09.022

Yu, L., Li-Hawkins, J., Hammer, R. E., Berge, K. E., Horton, J. D., Cohen, J. C., et al. (2002). Overexpression of ABCG5 and ABCG8 Promotes Biliary Cholesterol Secretion and Reduces Fractional Absorption of Dietary Cholesterol. *J. Clin. Invest.* 110, 671–680. doi:10.1172/jci0216001

Yuan, X. M., Li, W., Brunk, U. T., Dalen, H., Chang, Y. H., and Sevanian, A. (2000). Lysosomal Destabilization during Macrophage Damage Induced by Cholesterol Oxidation Products. *Free Radic. Biol. Med.* 28, 208–218. doi:10.1016/s0891-5849(99)00220-8

Zarubica, A., Plazzo, A. P., Stöckl, M., Trombik, T., Hamon, Y., MÜller, P., et al. (2009). Functional Implications of the Influence of ABCA1 on Lipid Microenvironment at the Plasma Membrane: a Biophysical Study. *FASEB J.* 23, 1775–1785. doi:10.1096/fj.08-122192

Zelcer, N., Hong, C., Boyadjian, R., and Tontonoz, P. (2009). LXR Regulates Cholesterol Uptake through Idol-dependent Ubiquitination of the LDL Receptor. *Science* 325, 100–104. doi:10.1126/science.1168974

Zha, X., Gauthier, A., Genest, J., and Mcpherson, R. (2003). Secretory Vesicular Transport from the Golgi Is Altered during ATP-Binding Cassette Protein A1 (ABCA1)-Mediated Cholesterol Efflux. *J. Biol. Chem.* 278, 10002–10005. doi:10.1074/jbc.c300024200

Zha, X., Genest, J., and Mcpherson, R. (2001). Endocytosis Is Enhanced in Tangier Fibroblasts. *J. Biol. Chem.* 276, 39476–39483. doi:10.1074/jbc.m105067200

Zhang, L., Reue, K., Fong, L. G., Young, S. G., and Tontonoz, P. (2012). Feedback Regulation of Cholesterol Uptake by the LXR-IDOL-LDLR axis. *Atvb* 32, 2541–2546. doi:10.1161/atvbaha.112.250571

Zhao, C., and Dahlman-Wright, K. (2010). Liver X Receptor in Cholesterol Metabolism. *J. Endocrinol.* 204, 233–240. doi:10.1677/joe-09-0271

Conflict of Interest: The authors declare that the research was conducted in the absence of any commercial or financial relationships that could be construed as a potential conflict of interest.

Publisher's Note: All claims expressed in this article are solely those of the authors and do not necessarily represent those of their affiliated organizations, or those of the publisher, the editors and the reviewers. Any product that may be evaluated in this article, or claim that may be made by its manufacturer, is not guaranteed or endorsed by the publisher.

frontiers in Cell and Developmental Biology

ORIGINAL RESEARCH
published: 02 March 2022
doi: 10.3389/fcell.2022.743287

Negative Modulation of Macroautophagy by Stabilized HERPUD1 is Counteracted by an Increased ER-Lysosomal Network With Impact in Drug-Induced Stress Cell Survival

Gabriela Vargas[1‡], Omar Cortés[1‡], Eloisa Arias-Muñoz[1,2], Sergio Hernández[1], Cristobal Cerda-Troncoso[1], Laura Hernández[1], Alexis E. González[3†], Michael H. Tatham[4], Hianara A. Bustamante[5], Claudio Retamal[1], Jorge Cancino[1], Manuel Varas-Godoy[1], Ronald T. Hay[4], Alejandro Rojas-Fernández[4,6], Viviana A. Cavieres[1,2] and Patricia V. Burgos[1,2,7]**

[1]Centro de Biología Celular y Biomedicina (CEBICEM), Facultad de Medicina y Ciencia, Universidad San Sebastián, Santiago, Chile, [2]Centro de Envejecimiento y Regeneración (CARE-UC), Facultad de Ciencias Biológicas, Pontificia Universidad Católica, Santiago, Chile, [3]Facultad de Medicina, Instituto de Fisiología, Universidad Austral de Chile, Valdivia, Chile, [4]Center for Gene Regulation and Expression, College of Life Sciences, University of Dundee, Dundee, United Kingdom, [5]Facultad de Medicina, Instituto de Microbiología Clínica, Universidad Austral de Chile, Valdivia, Chile, [6]Instituto de Medicina & Centro Interdisciplinario de Estudios del Sistema Nervioso (CISNe), Universidad Austral de Chile, Valdivia, Chile, [7]Centro Ciencia & Vida, Fundación Ciencia & Vida, Santiago, Chile

Macroautophagy and the ubiquitin proteasome system work as an interconnected network in the maintenance of cellular homeostasis. Indeed, efficient activation of macroautophagy upon nutritional deprivation is sustained by degradation of preexisting proteins by the proteasome. However, the specific substrates that are degraded by the proteasome in order to activate macroautophagy are currently unknown. By quantitative proteomic analysis we identified several proteins downregulated in response to starvation independently of ATG5 expression. Among them, the most significant was HERPUD1, an ER membrane protein with low expression and known to be degraded by the proteasome under normal conditions. Contrary, under ER stress, levels of HERPUD1 increased rapidly due to a blockage in its proteasomal degradation. Thus, we explored whether HERPUD1 stability could work as a negative regulator of autophagy. In this work, we expressed a version of HERPUD1 with its ubiquitin-like domain (UBL) deleted, which is known to be crucial for its proteasome degradation. In comparison to HERPUD1-WT, we found the UBL-deleted version caused a negative role on basal and induced macroautophagy. Unexpectedly, we found stabilized HERPUD1 promotes ER remodeling independent of unfolded protein response activation observing an increase in stacked-tubular structures resembling previously described tubular ER rearrangements. Importantly, a phosphomimetic S59D mutation within the UBL mimics the phenotype observed with the UBL-deleted version including an increase in HERPUD1 stability and ER remodeling together with a negative role on autophagy. Moreover, we found UBL-deleted version and

OPEN ACCESS

Edited by:
Emily Eden, University College London, United Kingdom

Reviewed by:
Caroline Mauvezin, University of Barcelona, Spain
Jieqiong Tan, Central South University, China

***Correspondence:**
Viviana A. Cavieres
vcavieresr@docente.uss.cl
Patricia V. Burgos
patricia.burgos@uss.cl

[†]Present address: Institute of Biochemistry II, School of Medicine, Goethe University Frankfurt, Frankfurt, Germany

[‡]These authors contributed equally to this work

Specialty section:
This article was submitted to Membrane Traffic, a section of the journal Frontiers in Cell and Developmental Biology

Received: *18 July 2021*
Accepted: *27 January 2022*
Published: *02 March 2022*

Citation:
Vargas G, Cortés O, Arias-Muñoz E, Hernández S, Cerda-Troncoso C, Hernández L, González AE, Tatham MH, Bustamante HA, Retamal C, Cancino J, Varas-Godoy M, Hay RT, Rojas-Fernández A, Cavieres VA and Burgos PV (2022) Negative Modulation of Macroautophagy by Stabilized HERPUD1 is Counteracted by an Increased ER-Lysosomal Network With Impact in Drug-Induced Stress Cell Survival. Front. Cell Dev. Biol. 10:743287. doi: 10.3389/fcell.2022.743287

HERPUD1-S59D trigger an increase in cellular size, whereas HERPUD1-S59D also causes an increased in nuclear size. Interestingly, ER remodeling by the deletion of the UBL and the phosphomimetic S59D version led to an increase in the number and function of lysosomes. In addition, the UBL-deleted version and phosphomimetic S59D version established a tight ER-lysosomal network with the presence of extended patches of ER-lysosomal membrane-contact sites condition that reveals an increase of cell survival under stress conditions. Altogether, we propose stabilized HERPUD1 downregulates macroautophagy favoring instead a closed interplay between the ER and lysosomes with consequences in drug-cell stress survival.

Keywords: HERPUD1, ubiquitin-like (UBL) domain, organelle network, lysosomal function, proteostais, MCSs, ERAD (ER associated protein degradation)

INTRODUCTION

Macroautophagy (from here referred to as autophagy) is a catabolic pathway that mediates the engulfment of aberrant or damaged cytoplasmic constituents into double-membrane autophagosomes that subsequently fuse with lysosomes to form a hybrid organelle called the autolysosome that mediates the degradation of the cargo by acid hydrolases (Mizushima et al., 2008; Khaminets et al., 2016). Autophagy is also implicated in the degradation of cellular constituents under basal conditions, playing an essential role in the maintenance of cellular homeostasis upon a variety of environmental conditions such as nutrient restriction or other stressors (Murrow and Debnath, 2013). Autophagy is highly inducible by environmental changes being a very dynamic process that resolves a variety of cellular demands (Murrow and Debnath, 2013). In fact, increased autophagy is protective in different cells and organisms, playing a crucial role in cell maintenance and survival under different insults (Moreau et al., 2010). On the other hand, defects in autophagy enhance cell vulnerability under harmful conditions such as those present in the tumor microenvironment (Camuzard et al., 2020).

Although initially autophagy was thought to work independently of the ubiquitin proteasome system (UPS), increasing evidence shows many layers of both negative and positive regulation (Bustamante et al., 2018), revealing an interconnected network with important roles in cellular homeostasis and maintenance (Korolchuk et al., 2010). Inhibitors of the proteasome 20S catalytic core with the use of β-subunits blockers triggers an enhancement in the biogenesis of autophagosomes (Zhu et al., 2010). In contrast, impairment of the proteasome 19S regulatory particle with an inhibitor of PSMD14, a proteasomal deubiquitinating enzyme, blocks the biogenesis of autophagosomes (Demishtein et al., 2017; Bustamante et al., 2020). To date a limited number of substrates of the UPS system are known to play a regulatory role in autophagy (Jia and Bonifacino, 2019; Thayer et al., 2020) and many aspects about the functional role of this interconnected network between autophagy and UPS remain elusive.

To identify UPS substrates that could act as negative regulators of autophagy, we conducted a quantitative SILAC proteomic analysis in cells stably depleted of ATG5 by shRNA-mediated knockdown. ATG5 protein is part of a complex with ATG12 and ATG16L that controls an essential step in the autophagosome formation (Walczak and Martens, 2013). We focused on proteins downregulated in response to nutrient deprivation, but not because of autophagy activation. The protein with the most significant downregulation, in wild type and ATG5 depleted cells was the Homocysteine-responsive endoplasmic reticulum-resident ubiquitin-like domain (UBL) member 1 protein named as HERPUD1. This protein is a transmembrane ER-resident protein with low levels of expression due to its short half-life by rapid proteasomal degradation (Kokame et al., 2000; Sai et al., 2003).

Here, we found that stabilized HERPUD1 through the deletion of its UBL domain causes a decrease in basal and induced autophagy. Additionally, it promotes an ER remodeling independent of the unfolded protein response activation into stacked tubular structures resembling previously described tubular ER rearrangements. Furthermore, we uncovered that higher HERPUD1 stability has a positive impact in lysosomal function, promoting an expanded ER-lysosomal network. Further, combining bioinformatics and site-directed mutagenesis we found the phosphomimetic S59D mutant within the UBL domain of HERPUD1 mimics the effect of the UBL deletion. In fact, we observed the phosphomimetic S59D mutant reduces basal and induced autophagy and remodeling of the ER-lysosomal network with the presence of ER-lysosomal membrane-contact sites, together promoting drug-stress cell survival. These findings thus identify HERPUD1 as a hotspot platform to promote stress cell survival by inducing the remodeling of the ER-lysosomal network when autophagy slows down.

MATERIALS AND METHODS

Reagents

Bafilomycin A1 (BafA1, cat#B1793), tunicamycin (Tun, cat#T7765), thapsigargin (Tg, cat#T9033), cisplatin (CDDP, cat#479306), Sulforhodamine B (SRB, cat#230162), Earle's balanced salt solution (EBSS, Cat#E2888), puromycin dihydrochloride (cat#P8833), and protease inhibitors cocktail (cat#P8340) were purchased from Sigma-Aldrich (St. Louis,

MO, United States). MG132 (cat#474790) was purchased from Merck Millipore (Burlington, MA, United States). LysoTracker™ Red DND-99 (cat#L7528), 4′,6-diamidino-2-phenylindole (DAPI) (cat#D-1306) and TRIzol™ (cat#15596018) were purchased from ThermoFisher Scientific (Waltham, MA, United States), Magic Red® (cat#6133) was purchased from Immunochemistry Technologies, LLC (Bloomington, IN, United States). The QuikChange II XL direct-mutagenesis kit was obtained from Stratagene (cat#200522, La Jolla, CA, United States) and the Vybrant Apoptosis Pacific Blue-annexin V kit and 7AAD from Invitrogen (cat#A35122). The siRNA against human HERPUD1 (cat#SASI_Hs01_00185592) was purchased from Sigma Aldrich. The siRNA control corresponded to a custom non-target sequence UUCUCCGAACGUGUCACGUUU purchased from Dharmacon.

Antibodies

The following monoclonal antibodies were used: mouse anti-β-ACTIN clone BA3R (cat# MA5-15739, Thermo Fisher Scientific), mouse anti-XBP-1S clone E7M5C (cat#47134S, Cell Signaling Technology, Danvers, MA, United States), mouse anti-FLAG clone M2 (cat#F1804, Sigma Aldrich), mouse anti-VAP-A clone 4C12 (cat#sc-293278, Santa Cruz Biotechnology, INC), mouse anti-GRP78/BiP clone 40/BiP (cat# 610978, BD Biosciences, San Jose, CA, United States), mouse anti-LAMP1 clone H4A3 (cat# 610978, Developmental Studies Hybridoma Bank, Iowa City, IA, United States), rabbit monoclonal anti-CALNEXIN clone C5C9 (cat#2679S, Cell Signaling Technologies), rabbit monoclonal anti-ATF4 clone D4B8 (cat#11815S, Cell Signaling Technologies), rabbit monoclonal anti-HERPUD1 clone EPR9649 (cat#ab150424, Abcam), rat monoclonal anti-GRP94 clone SPM249 (cat#ab233979, Abcam, Cambridge, United Kingdom). We used the following polyclonal antibodies: rabbit anti-LC3 (cat#2775S, Cell Signaling Technology), rabbit anti-PERK (cat#P0074, Sigma-Aldrich), rabbit anti-STARD3 (cat#ab3478, Abcam, Cambridge, United Kingdom), goat anti-CATHEPSIN-D (cat#AF1014, R&D Systems, Minneapolis, MN, United States), rabbit anti-TFEB (cat#4240, Cell Signaling Technologies), rabbit anti-HERPUD1 (cat#BML-PW9705, ENZO Life Sciences, Farmingdale, NY, United States). Horseradish peroxidase-conjugated secondary antibodies were purchased from Jackson ImmunoResearch Laboratories (West Grove, PA, United States), Alexa fluorophore-conjugated secondary antibodies were purchased from Thermo Fisher Scientific.

Mass Spectrometry Based Proteomics and Statistical Analysis

Human H4 neuroglioma cells stably expressing shLuc and shATG5 were grown in Dulbecco's modified Eagle's medium lacking all amino acids except L-lysine and L-arginine, which were replaced with either unlabelled amino-acids (Lys0 and Arg0) or stable isotopic forms 13C6 15N2-lysine (Lys8) and 13C6 15N4-arginine (Arg10) (Cambridge Isotope Laboratories). The medium was supplemented with 10% dialyzed FBS using previous published methods (Golebiowski et al., 2009; Yin et al., 2012). Two separate cultures of each shLuc and shATG5 cells were grown in light amino acids (Lys0 + Arg0) or heavy amino acids (Lys8 + Arg10) over nine replication cycles to achieve over 96% incorporation and similar cell counts per culture. Both cell cultures were divided in two, and cells were grown under control conditions in DMEM + 10% FBS or starvation in EBSS media for 4 h so that each cell type grown with each label were treated with both conditions (8 cultures in total). Cells were washed and lysed in 1.2 × LDS sample buffer with reducing agent, obtaining crude cell extracts at approximately 1 mg/ml. To allow all experimental conditions to be compared with one another a light reference mix was obtained by combining all four light amino acid conditions in a 1:1:1:1 ratio by volume. This was then mixed 1:1 ratio (v:v) with each heavy amino acid extract. The same comparisons were made in reverse by combining all heavy amino acid samples into a reference mix and combining this 1:1 (v:v) with each of the four individual light amino acid conditions. All eight mixes were fractionated by SDS-PAGE and stained gels were cut into three slices per lane before tryptic peptides were extracted. The resultant 24 samples of dried down peptides were resuspended in 35 µl 0.1% TFA 0.5% acetic acid. Peptide samples were analyzed by LC-MS/MS twice; the first using 9 µl peptide sample run over a 90 min peptide fractionation gradient, and the second using 18 µl peptide sample run over a 240 min fractionation gradient. Peptides were analyzed using a Q exactive mass spectrometer (Thermo Scientific) coupled to an EASY-nLC 1,000 liquid chromatography system (Thermo Scientific), using an EASY-Spray ion source (Thermo Scientific), running a 75 µm × 500 mm EASY-Spray column at 45°C. A top 10 data-dependent method was applied. Full scan spectra (m/z 300–1,800) were acquired with resolution R = 70,000 at m/z 200 (after accumulation to a target value of 1,000,000 with maximum injection time of 20 ms). The most intense ions were fragmented by HCD and measured with a resolution of R = 17,500 at m/z 200 (target value of 500,000 maximum injection time of 60 ms) and intensity threshold of 2.1×10^4. Peptide match was set to "preferred", a 40 s dynamic exclusion list was applied, and ions were ignored if they had an assigned charge state of 1, 8 or >8. All 48 data files were analyzed simultaneously in MaxQuant (v1.5.2.8) using default parameters excepting the selection of SILAC labels, activation of 'requantify' and 'match between runs', using a uniport 'HUMAN' proteome database (downloaded 24/02/2015- 73920 entries) as search space. Raw files derived from the same mix were grouped under the 'Experiment' heading as Mix01-Mix08. Raw files were given MaxQuant experimental design 'fraction' numbers such that spectra derived from the same HPLC gradient and from the equivalent gel slices across different lanes would be matched, as well as one sliced either side. 4,395 protein groups were listed as informed in the **Suppplementary File S1**, proteinGroups.txt sheet. This list was edited to leave 3,911 protein groups by removing decoy proteins, protein listed as potential contaminants, proteins identified only by modified peptides, and proteins without a H/L ratio reported for any comparison (see **Suppplementary File S1**, accepted sheet). The average of normalized forward and reverse ratios of starvation/control were

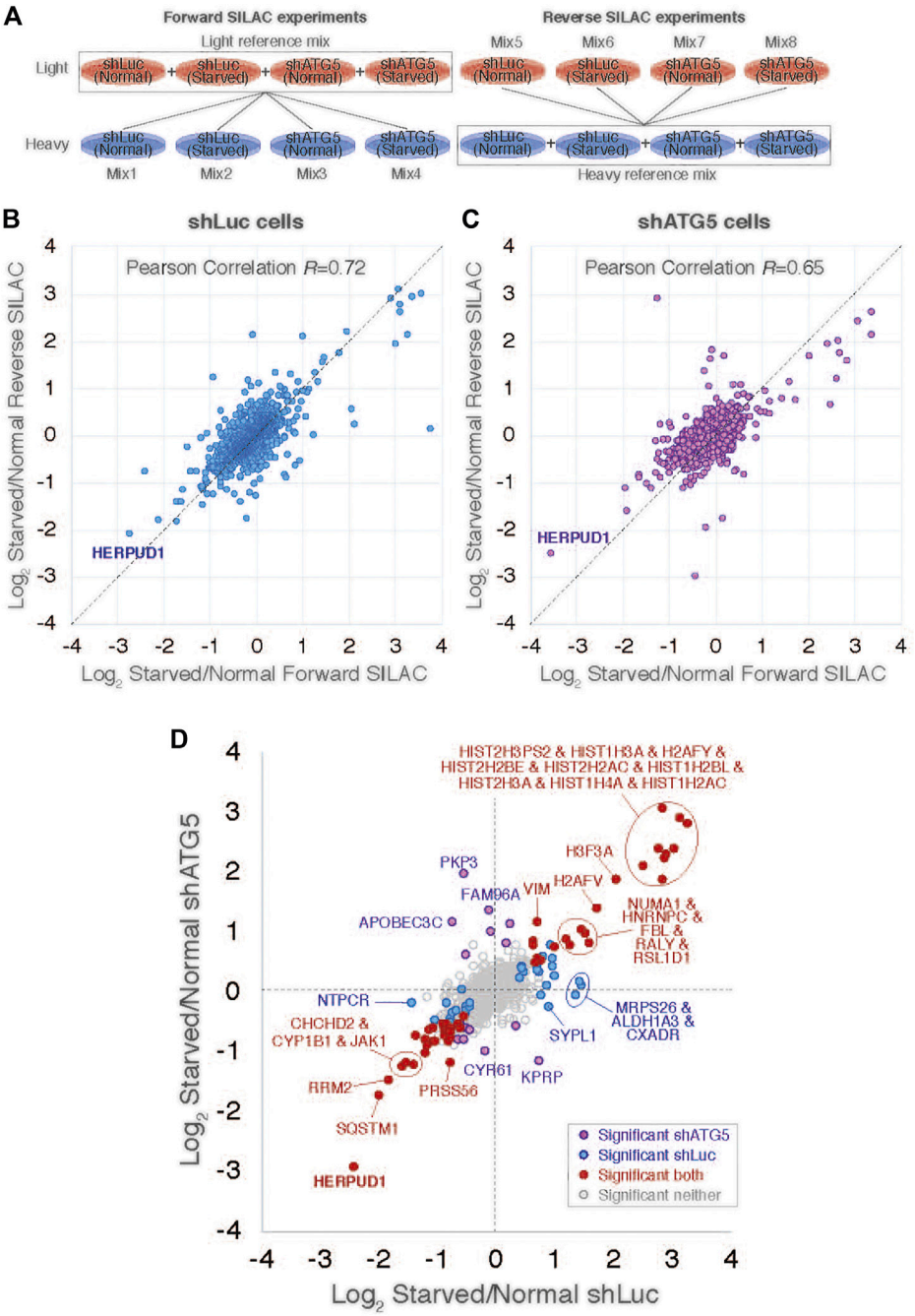

FIGURE 1 | SILAC-based proteomic study reveals HERPUD1 as a possible modulator of autophagy. **(A)**. Design of the SILAC experiment to monitor changes of the cellular proteome of H4 cells during starvation and shRNA-mediated knockdown of ATG5 (shATG5) or shRNA against the luciferase gene (shLuc). 'Reference' mixes of all cell extracts were prepared for light and heavy conditions for 'forward' and 'reverse' SILAC experiments and were mixed 1:1 with individual cell extracts, giving a total of eight mixes. **(B,C)** Scatter plot comparing 'Forward' and 'Reverse' Log2 Starvation/Normal ratio data for cells shLuc **(B)** and shATG5 **(C)**. **(D)** Comparison of average Log_2 Starvation/Normal ratios in shLuc (*x*-axis) and shATG5 (*y*-axis). Protein outliers under either or both knockdown conditions are colored as indicated.

carried forward for statistical analysis, but only for those with H/L ratios reported for both. These values along with average log_{10} protein intensities were used in Perseus to calculate Significance B values to identify statistical outliers (SigB < 0.001) for the three ratios. Data for these shortlisted proteins are summarized in **Suppplementary File S1**, shortlisted sheet. Data is available via

ProteomeXchange with identifier PXD024486. Reviewer account details: Username: reviewer pxd024486@ebi.ac.uk Password: ibjQUyjo.

Plasmids and Site-Directed Mutagenesis

For all HERPUD1 constructs generated in this study, previously described cDNAs encoding either the full-length or the ΔUBL deletion mutant human HERPUD1, both with a C-terminal FLAG-tag, were used as templates (Sai et al., 2003). pCI-HERPUD1-FLAG and pCI-ΔUBL-FLAG were digested with EcoRI and NotI restriction enzymes to obtain an insert, which was sub-cloned to a lentiviral pLVX-IRES-Puro vector (Takara Bio Inc., CA, United States) containing a puromycin resistance gene. The substitution S59D and S59A were introduced into the pLVX-IRES-FLAG-tagged HERPUD1 vector using the QuikChange II XL direct-mutagenesis kit (Stratagene, cat#200522) and the mutagenesis service of GenScript (Hong Kong, China).

Cell Culture and Generation of Stable Cell Lines

Maintenance of H4 human neuroglioma cells stably expressing either shRNAs against ATG5 or luciferase genes was performed as previously described (González et al., 2017). HeLa cells were obtained from the American Type Culture Collection (Manassas, VA, United States). HeLa-derived cell lines were cultured in Dulbecco's modified Eagle's medium (DMEM; Thermo Fisher Scientific) supplemented with 10% (vol/vol) heat-inactivated fetal bovine serum (FBS; Thermo Fisher Scientific), and 100 U/ml penicillin/100 mg/ml streptomycin (Thermo Fisher Scientific), in a 5% CO_2 atmosphere at 37°C. The generation of HeLa stable cell lines expressing all different variants of FLAG-tagged HERPUD1 cloned in the pLVX-IRES-Puro vector were generated by transfection with Lipofectamine 2000 (Invitrogen) according to manufacturer's instructions. After 24 h the cells were selected and maintained with 2 μg/ml of puromycin.

Preparation of Protein Extracts, Electrophoresis, SDS-PAGE and Western Blot Analysis

Cells were washed with ice-cold phosphate buffered saline (PBS) and lysed in Radioimmunoprecipitation assay buffer (RIPA lysis buffer) [50 mM Tris-HCl , 150 mM NaCl, 5 mM EDTA, 1% NP-40, 1% sodium deoxycholate, 0.1% SDS, pH 7.4], supplemented with a cocktail of protease inhibitors [416 μM 4-(2-Aminoethyl) benzenesulfonyl fluoride, 0.32 μM Aprotinin, 16 μM Bestatin, 5.6 μM E-64, 8 μM Leupeptin and 6 μM Pepstatin A; Sigma-Aldrich] and phosphatase inhibitors (1 mM NaF, 0,3 mM $Na_2P_2O_7$ and 1 mM Na_3VO_4; Sigma-Aldrich). Cell lysates were collected and lysed for 30 min at 4°C in rotation. Then, extracts were sonicated with ultrasonic power three times on ice with pulses of 2–3 s at 40 mA using a tip sonicator system. Extracts were further centrifuged for 20 min at 13.000×g at 4°C. The supernatants were collected, and protein concentration was quantified using the BCA assay (ThermoFisher Scientific). The protein extracts were denatured at 65°C for 5 min and analyzed using our previous described methods (González et al., 2017; Bustamante et al., 2020).

Transmission Electron Microscopy

HeLa cells were fixed for 16 h by immersion in 2.5% glutaraldehyde in 0.1 M cacodylate buffer (pH 7.0) at room temperature, and then washed three times with a cacodylate buffer for 2 h. Cells were post-fixed with 1% osmium tetroxide (OsO_4) for 2 h and washed three times with double distilled water. Then, the cells were treated with 1% aqueous uranyl for 90 min, and sequentially dehydrated through an acetone battery 50, 70, 95, and 100% for 20 min each. Cells were pre-embedded in epon/acetone 1:1 overnight and then in pure epon for 4 h. Finally, cells were embedded in fresh resin and polymerized in an oven at 60°C for 48 h. Ultrafine sections (80 nm) were obtained using an ultramicrotome Leica Ultracut R. The sections were incubated with 4% uranyl acetate in methanol for 2 min and lead citrate for 5 min. The grids were visualized using a Philips Tecnai 12 electron microscope (Eindhoven, Netherlands) at 80 kV. This work was performed in the Advanced Microscopy Facility of the Faculty of Biological Sciences at Pontificia Universidad Católica de Chile.

Fluorescence Microscopy, Data Acquisition, Quantification and High-Resolution Analysis

Cells grown on glass coverslips were washed with PBS-Ca^{2+}/Mg^{2+} and then fixed, permeabilized and stained using our published protocols (Bustamante et al., 2020; Cavieres et al., 2020). The images were acquired using a TCS SP8 laser-scanning confocal microscope (Leica Microsystems, Wetzlar, Germany) equipped with a ×63 oil immersion objective (1.4 NA), photomultipliers (PMT), hybrid detectors (HyD) system using 405 nm, 488 nm, 561 nm and 643 nm laser lines for excitation running the LASX Leica software. For image quantification, 16-bit (1024 × 1024) images were acquired under identical settings avoiding signal saturation. Cell and nucleus area measurements were performed by using ICY software (Quantitative Image Analysis Unit, Institut Pasteur, http://icy.bioimageanalysis.org/). A pipeline was created to completely automate image analysis by using the following sequential plugins: active contours (cell segmentation), hk-means (threshold detection), wavelet spot detector (spot detection) and studio (colocalization). Total Fluorescence Integrated intensity measurement was performed by using ImageJ (FIJI) (Schindelin et al., 2012). The number of dots (lysosomes) was performed by using the LOG detector algorithm available on the TrackMate plugin (FIJI). For live cell imaging assays, HeLa cells were grown in glass bottom culture dishes (MatTek Corporation, Ashland, MA, United States) and labeled with the following Invitrogen probes: ER-Tracker™ Blue-White DPX (E12353), LysoTracker™ Red DND-99 (L7528, Invitrogen) and Magic-red (Immunochemistry Technologies, LLC) according to the manufacturer's protocol. Before image acquisition, culture medium was replaced with phenol red-free DMEM supplemented with HEPES (10 mM, pH 7.4), and images were

acquired with the ×63 oil immersion objective (1.4 NA) of the TCS SP8 laser-scanning confocal microscope, running the Leica Application Suite LAS X software, coupled to a controlled temperature chamber (UNO-temp controller, OKOLAB) acquiring 16-bit images at 37°C (488 laser for excitation; HyD: 510–550 nm; 1,024 × 1,024 pixels; frame average 2). For volume analysis, z-stack (0.3 µm z-interval, 1024 × 1024, 180 µm pixel size) images were quantified using 3D analysis plugin by using ICY software. Total fluorescence integrated intensity and dots number were measured using ImageJ. High Resolution Analysis: Colocalization analysis of ER/lysosomes contacts was performed using Huygens software (SVI, Netherlands). Briefly, images were acquired as described above but oversampling upon Nyquist parameters (Nyquist Calculator). Images were then deconvolved (CMLE blind deconvolution) and 3D rendered with Surface Render plugin. Colocalization volumes were quantified using the advanced particle analyzer and colocalization plugin. Only colocalization patches bigger than 0,5 mm^3 and smaller than 10 mm^3 were counted.

RNA Isolation and RT-PCR Analysis

Total RNA extraction from HeLa cells, oligo-dT and MMLV reverse transcriptase and quantitative reverse transcription PCR of the cDNA template (RT-PCR) was carried out as previously described (Bustamante et al., 2020). The specific primer pairs used for CYCLOPHILIN-A, CYCA (NM_001300981.2) and XBP1 (NM_001079539.2) were the following: CYCA-F TCG AGTTGTCCACAGTCAGC, CYCA-R TTCATCTGCACTGCC AAGAC, XBP1-F CGCTTGGGGATGGATGCCCTG and XBP1-R CCTGCACCTGCTGCGGACT.

Cell Viability Assays

Exponentially growing cells stably expressing either FLAG-tagged HERPUD1-WT or HERPUD1-S59D were trypsinized and seeded at 20,000 cells per well in 96-well microplates and allowed to attach for 6 h at 37°C and 5% CO_2. Then, cells were incubated with CDDP in serial dilutions from 1 mM to 1 µM in 2% FBS medium and were incubated for 24 h at 37°C and 5% CO_2. After drug incubation, the IC50 was obtained using the Sulforhodamine B (SRB) cell cytotoxicity assay (Blois et al., 2011). Briefly, cells were fixed (10% trichloroacetic acid, 4°C, 1 h), water washed, dried and stained (0.4% SRB v/v in 0.1% acetic acid, 1 h at RT), and then washed four times (1% acetic acid). Dissolved SRB (10 mM Tris-base, pH 10) was quantified (564 nm, Synergy HT BioTek reader). CDDP treatments were done in quadruplicate in at least three independent experiments. The IC50 values associated with the cytotoxic effects of CDDP were calculated using GraphPad Prism software (version 8.2; GraphPad Software, San Diego, CA, United States) using non-linear regression model and dose-response equations (log(inhibitor) vs. normalized response). After drug incubation, apoptotic cells were analyzed with the commercial kit Vybrant Apoptosis Pacific Blue-annexin V (cat#A35122, Invitrogen) using the protocol provided by the manufacturer. Briefly, cells stably expressing either FLAG-tagged HERPUD1-WT or HERPUD1-S59D were treated with 10 µM CDDP for 24 h. Cells were harvested and centrifuged at 800 × g for 5 min at room temperature and washed with cold PBS 1X. Cells were re-centrifuged, and the pellet resuspended in 100 µl annexin-binding buffer. Then, 5 µl of the annexin V conjugate was added to the cell suspension and incubated for 15 min at room temperature. After, 400 µl of annexin-binding buffer was added, gently mixed, and maintained on ice for later analysis in a BD FACSCanto II flow cytometer (Flow Cytometer Facility of Cell 4 Cell, Santiago, Chile), with a previous incubation with 3 µl of 7-Amino-Actinomycin D (7AAD) to exclude non-viable cells (included in the kit).

Densitometric Quantification and Statistical Analysis

The amount of immunoblot signal was estimated using Image J software version 1.48v (Wayne Rasband, NIH, http://imagej.nih.gov). For each condition, protein bands were quantified from at least three independent experiments in order to ensure adequate statistical power. Data analysis was performed using Microsoft Excel 2013 for Windows (Redmond, WA, United States) or GraphPad Prism 6. Results are represented in graphs depicting the mean ± standard deviation. Statistical significance of data comparisons from two groups comparisons was determined with two-tailed unpaired Student's *t*-test for parametric data. Values of $p < 0.05$ (*), $p < 0.01$ (**), $p < 0.001$ (***) were regarded as statistically significant and are indicated in the figures.

RESULTS

HERPUD1 is a Regulator of Autophagy Under the Control of its UBL Domain

Previous reports have demonstrated a close interplay between autophagy and the Ubiquitin-Proteasome System (Bustamante et al., 2018), however, to date, few proteasomal substrates are known as modulators of autophagy (Jia and Bonifacino, 2019; Guarascio et al., 2020; Thayer et al., 2020). To search for potential novel candidates that could be downregulated by the proteasome in order to activate autophagy, we performed a SILAC-based proteomic study to quantitatively determine the proteome of H4 neuroglioma cells under basal and induced autophagy by EBSS starvation conditions. To eliminate all proteins downregulated because of autophagy activation, we compared the proteome of H4 cells where autophagy is inhibited by stable depletion of ATG5 by shRNA-mediated knockdown (shATG5) respect to control H4 cells expressing an shRNA against the luciferase gene (shLuc), both cell lines previously characterized (González et al., 2017; Tapia et al., 2019; **Figure 1A**). ATG5 protein is part of a complex with ATG12 and ATG16L that controls an essential step in the autophagosome formation (Walczak and Martens 2013). Silencing of ATG5 causes a strong inhibition in LC3B-positive autophagosomes, a phenotype also previously confirmed in our H4 cell lines (González et al., 2017). Among all the proteins downregulated by EBSS starvation, we found that in both H4 cell lines, shLuc (**Figure 1B**) and shATG5 (**Figure 1C**) the most significantly

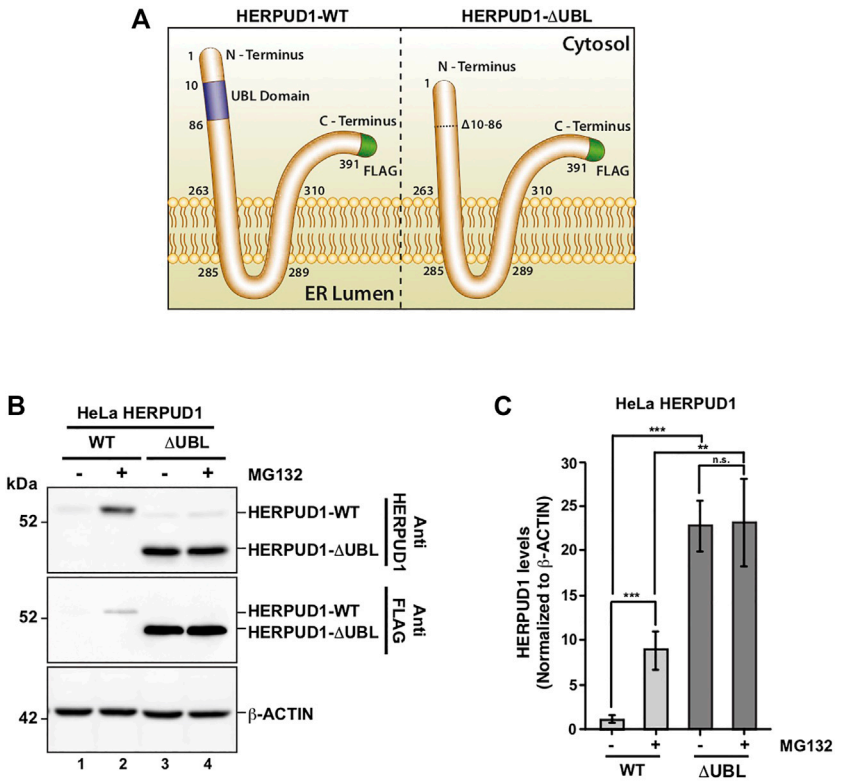

FIGURE 2 | Deletion of UBL domain increases HERPUD1 protein levels. **(A)** Schematic representation HERPUD1-WT (left image) and ΔUBL (right image) at the ER membrane, both FLAG-tagged at the carboxyl-terminus (shown in green). The Ubiquitin-Like domain (UBL, amino acids 10–86) are represented in purple. **(B)** HeLa cells stably expressing the WT or ΔUBL versions of HERPUD1 were not treated (lanes 1 and 3) or treated with 20 μM of MG132 for 4 h (lanes 2 and 4). Detergent-soluble protein extracts were analyzed by western blot with anti-HERPUD1 and anti-FLAG antibodies. β-ACTIN was used as loading control. Image is representative of three independent experiments. Position of molecular mass markers is indicated on the left. **(C)** Densitometry quantification of HERPUD1 protein levels from images as those shown in **B**. Bars represent the mean ± standard deviation of western blot signal normalized with β-ACTIN. Statistical analysis was performed using two-tailed unpaired Student's *t*-test ($n = 3$ n.s not statistically significant, $^{**}p < 0.01$ and $^{***}p < 0.001$.

downregulated protein was HERPUD1, a protein originally identified as a homocysteine-inducible gene, that is also upregulated by endoplasmic reticulum (ER) stress (Kokame et al., 2000; Kokame et al., 2001). Importantly, HERPUD1 is an ER-stress membrane protein whose levels under non-stressful conditions are low due to proteasome degradation (Kokame et al., 2000; Sai et al., 2003). Indeed, pharmacological inhibition of the proteasome leads to a rapid increase of HERPUD1 levels (Sai et al., 2003; Miura et al., 2010). In addition to HERPUD1, we found several other proteins significantly down- or up-regulated by EBSS treatment (**Figure 1D**). However, while some proteins were down- or up-regulated by EBSS treatment in both, shLuc and shATG5 stable expressing cell lines (**Figure 1D**, red dots), many other hits were only down or up-regulated dependent on ATG5 protein expression (**Figure 1D**, purple dots). The complete list of proteins that responded significantly to EBSS treatment in both cell lines is shown in **Supplementary Figure S1**. Here, we focus on the characterization of HERPUD1, the hit with the highest score of downregulation in both cell lines, working with the hypothesis that its reduction by EBSS treatment could be indicative of its role as negative regulator of autophagy activity. Previous studies had shown that silencing HERPUD1 triggers the autophagic flux (Quiroga et al., 2013). Therefore, in this study, and considering that HERPUD1 levels are increased under ER stress, we study the cellular consequences of HERPUD1 stability on autophagy function. HERPUD1 is an integral membrane protein with both termini facing the cytoplasm, with the ubiquitin-like domain (UBL) located in its N-terminus (**Figure 2A**; UBL: purple color, left side). Here, we cloned full-length HERPUD1 into the pLVX-IRES-Puro vector with a FLAG-tagged in its C-terminal end (**Figure 2A**; FLAG: green color) designed as HERPUD1-WT. In addition, we cloned a FLAG-tagged HERPUD1 version lacking the residues between Val^{10}-Cys^{86} designed as HERPUD1-ΔUBL (**Figure 2A**; right side), as previously reported (Sai et al., 2003). Further, we generated puromycin-resistant HeLa cells stably expressing either HERPUD1-WT or HERPUD1-ΔUBL, considering that previous characterization of HERPUD1 in HeLa cells was done only by transient transfection (Sai et al., 2003). Western blot analysis using either anti-HERPUD1and anti-FLAG antibodies showed higher levels of HERPUD1-ΔUBL compared to HERPUD1-WT (**Figure 2B**, lane 1 and lane 3). In fact, we found a significant increase in the levels of HERPUD1-ΔUBL (22.83 ± 2.90) compared to HERPUD1-WT (1.00 ± 0.49)

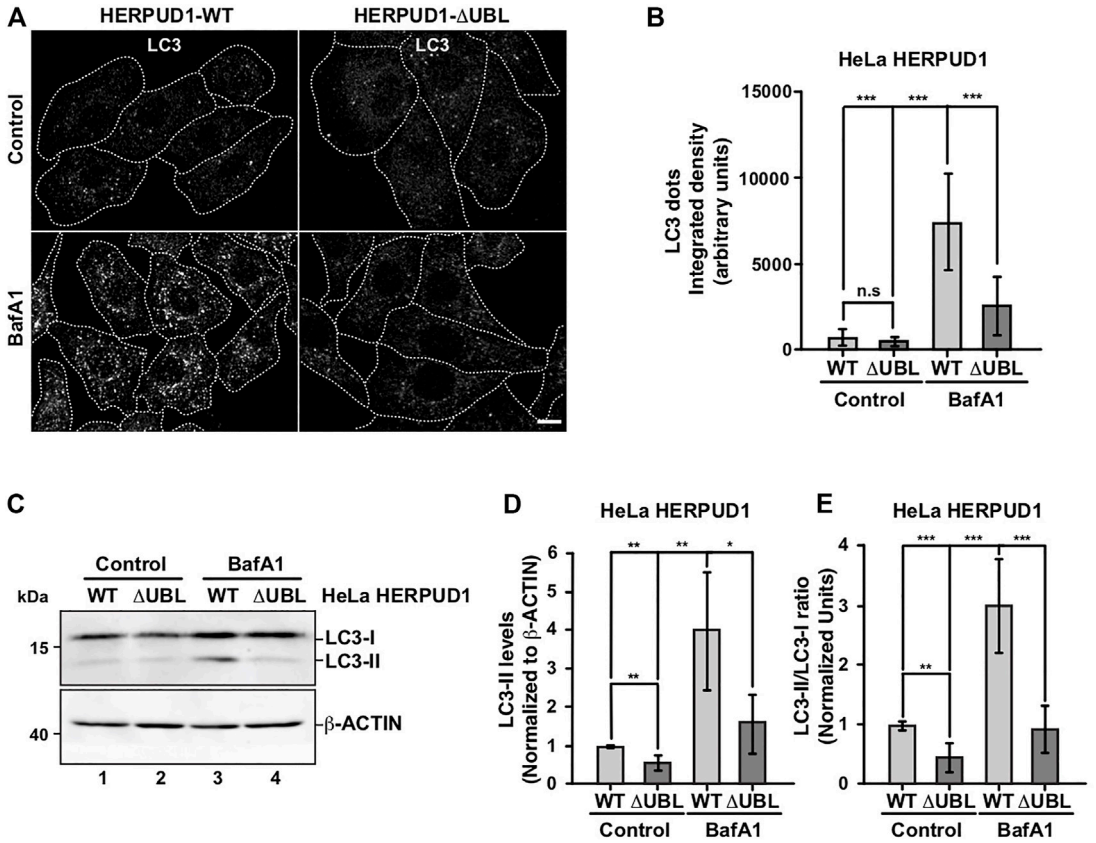

FIGURE 3 | The stabilization of HERPUD1 by its UBL deletion negatively regulates autophagy. **(A)** HeLa cells stably expressing HERPUD1-WT-FLAG or HERPUD1-ΔUBL-FLAG were grown in glass coverslips and were treated or not with 100 nM BafA1 for 4 h. Cells were fixed and incubated with an antibody to LC3 followed by incubation with Alexa-488-conjugated donkey anti-rabbit IgG. Stained cells were examined by confocal microscopy. Scale bar 10 μm. **(B)** Quantification of integrated density of LC3 puncta per cell under treatment with 100 nM BafA1 for 4 h. Bars represent the mean ± standard deviation ($n = 30$). **(C)** HeLa cells stably expressing HERPUD1-WT-FLAG or HERPUD1-ΔUBL-FLAG untreated (lanes 1 and 2) or treated with 100 nM BafA1 for 4 h (lanes 3 and 4). Detergent-soluble protein extracts were analyzed by western blot with a rabbit polyclonal antibody against LC3. Monoclonal antibody against β-ACTIN (clone BA3R) was used as loading control. Position of molecular mass markers is indicated on the left. **(D)** Densitometry quantification of LC3-II protein levels normalized with β-ACTIN. Bars represent the mean ± standard deviation. Statistical analysis was performed using two-tailed unpaired Student's t-test ($n = 3$ $^{*}p < 0.05$, $^{**}p < 0.01$). **(E)** Densitometry quantification of LC3-I and LC3-II protein levels from images as those shown in C. Relative levels are expressed as the ratio of LC3-II to LC3-I. Bars represent the mean ± standard deviation. Statistical analysis was performed using two-tailed unpaired Student's t-test ($n = 3$ $^{**}p < 0.01$, $^{***}p < 0.001$).

under basal conditions (**Figure 2C**). The UBL is a domain that resembles ubiquitin in terms of their primary sequence and three-dimensional structure, considered a general interaction motif with the proteasome particularly with the 19S regulatory particle of the 26S proteasome (Hartmann-Petersen and Gordon, 2004a). Interestingly, it has been previously shown that deletion of UBL in HERPUD1 abolishes its proteasomal degradation (Sai et al., 2003). To confirm this, we treated the cells during 4 h with 20 μM MG132, a potent blocker of the proteasome activity (Tsubuki et al., 1996; Lee, 1998). As expected, we observed that this treatment caused an increase in the levels of overexpressed HERPUD1-WT (9.00 ± 2.90) in comparisson to untreated cells (1.00 ± 0.49) (**Figure 2B**, lane 1 and 2) and **Figure 2C**. In contrast, HERPUD1-ΔUBL did not respond to this treatment, observing similar levels in the absence or presence of MG132 (22.83 ± 2.90 vs. 23.24 ± 4.89) (**Figure 2B**, lane 3 and 4) and **Figure 2C**, confirming previous findings (Sai et al., 2003). Together, these results confirmed HERPUD1-ΔUBL is a tool to explore the effect of HERPUD1 stability on autophagy.

Therefore, we investigated the effect of HERPUD1-ΔUBL stable expression by analyzing the subcellular distribution of the microtubule-associated protein 1 light chain 3B (LC3B), a classical marker of autophagy, from here referred for simplicity as LC3 (Tanida et al., 2008). Immunofluorescence analysis of LC3 in cells expressing HERPUD1-WT and HERPUD1-ΔUBL showed basal autophagy represented by LC3-positive membrane dots that correspond to autophagosomes decorated with lipidated LC3 (LC3-II) observing no significant differences between cell lines (**Figures 3A,B**). Because autophagosomes are constantly forming autolysosomes through the fusion with acidic lysosomes for degradation, we tested the effect of BafA1, a drug that raises the lysosomal pH resulting in the perturbation of the autophagic flux (González et al., 2017). Upon BafA1 treatment we found HERPUD1-WT cells showed a significant increase in the interated density of LC3 dots fluorescence (7046.4 ± 3223.2)

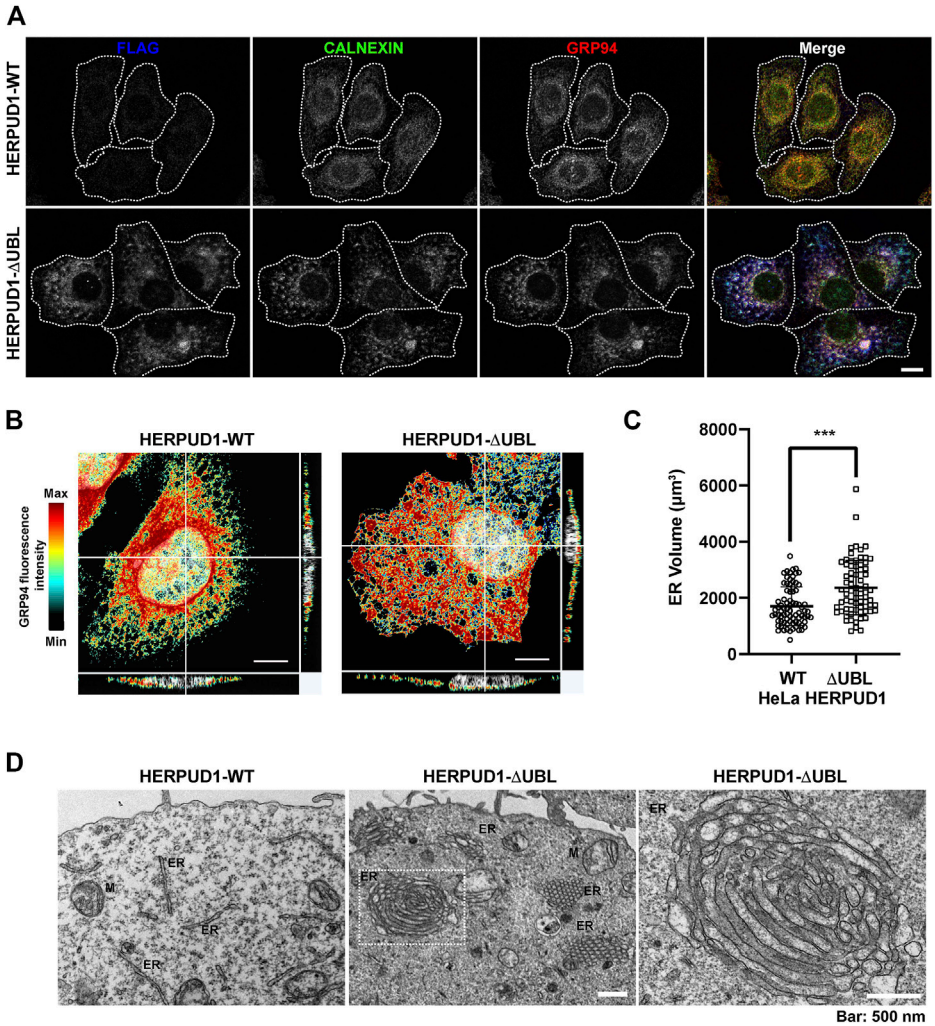

FIGURE 4 | HERPUD1-ΔUBL stabilization alters the ER morphology. **(A)** HeLa cells stably expressing HERPUD1-WT-FLAG or HERPUD1-ΔUBL-FLAG grown in glass coverslips were fixed, permeabilized and triple-labeled with a mouse monoclonal antibody against FLAG, with a rabbit monoclonal antibody against CALNEXIN and with a rat monoclonal antibody against GRP94 followed by incubation with Alexa-488-conjugated donkey anti-rabbit IgG (green channel), Alexa-594-conjugated donkey anti-rat IgG (red channel) and Alexa-647-conjugated donkey anti-mouse IgG (blue channel). Images were acquired using a TCS SP8 laser-scanning confocal microscope. The fourth image on each row is the merge of blue, green and red channels; yellow indicates colocalization of the red and green channels, cyan indicates colocalization of the green and blue channels, magenta indicates colocalization of the red and blue channels, and white indicates colocalization of all three channels. Scale bar, 10 μm. **(B)** HeLa cells stably expressing HERPUD1-WT-FLAG or HERPUD1-ΔUBL-FLAG grown in glass coverslips were fixed, permeabilized and labeled with rat monoclonal antibody against GRP94 followed by incubation with Alexa-594-conjugated donkey anti-rat IgG. Stained cells were examined by fluorescence microscopy. Images were acquired using a TCS SP8 laser-scanning confocal microscope. Pseudocolor image was created using all the serial confocal sections of HeLa HERPUD1-WT-FLAG (left image) and HERPUD1-ΔUBL-FLAG (right image). The scale on the right represents the maximum (red) to minimum (black) intensity measured for GPR94. **(C)** Quantification of ER-volume obtained from serial image reconstruction (z-stack 0.3 μm z-interval, 1024 × 1024, 180 μm pixel size). Volume is depicted in a scatter plot; open circles represent HeLa HERPUD1-WT-FLAG ($n = 79$) and open squares HERPUD1-ΔUBL-FLAG ($n = 72$). Statistical analysis was performed using two-tailed unpaired Student's t-test (***$p < 0.001$). **(D)** TEM micrograph shows HeLa HERPUD1-WT-FLAG or HERPUD1-ΔUBL-FLAG (left and center images, respectively) at a lower magnification. Crystalloid ER structure is visible as a honeycomb in HERPUD1-ΔUBL (central image). An ER crystalloid structure from HERPUD1-ΔUBL-FLAG at a higher magnification is shown (right image from dashed square in the center image, ER, endoplasmic reticulum; M, mitochondria). Scale bar 500 nm.

compared to HERPUD1-ΔUBL cells (2409.6 ± 1517.5) (**Figure 3A**, left, BafA1) and **Figure 3B**. Next, by western blot analysis we found that HERPUD1-ΔUBL caused a decrease in LC3-II levels under basal conditions (0.56 ± 0.21), in comparison to HERPUD1-WT expressing cells (1.00 ± 0.03) (**Figure 3C**, lane 1 and 2) and **Figure 3D**. Similar results in HERPUD1-ΔUBL were observed regarding the LC3-II/LC3-I ratio (0.47 ± 0.22), respect to control cells (1.00 ± 0.05) (**Figure 3E**) and in the presence of BafA1 treatment, observing in HERPUD1-ΔUBL cells a significant decrease in LC3-II levels (1.63 ± 0.85), respect to control cells (4.03 ± 1.61) (**Figure 3C**, lane 3 and 4) and **Figure 3D**. Same differences were observed analyzing the

LC3-II/LC3-I ratio in HERPUD1-ΔUBL cells treated with BafA1 (0.94 ± 0.37), respect control cells (3.01 ± 0.78) (**Figure 3E**). Importantly, similar findings were obtained under induced autophagy by EBSS starvation medium (**Supplementary Figure S2**). We observed that the LC3-II/LC3-I ratio in HERPUD1-ΔUBL cells in the presence of EBSS plus BafA1 was diminished with respect HERPUD1-WT cells (**Supplementary Figure S2A**, line 5 and 6 and **Supplementary Figure S2B**). Altogether, these findings strongly indicate that increased stability of HERPUD1 plays a negative effect on autophagy.

Increased Stability of HERPUD1 by the Deletion of its UBL Domain Triggers Remodeling of the ER in Stacked Tubular Structures Resembling Crystalloid ER-Like Structures in the Absence of ER Stress

Because previous reports have shown that defective autophagy leads to ER expansion (Ou et al., 1995; Jung et al., 2008) we investigated whether HERPUD1 stability could be linked with ER remodeling. In contrast to previous studies where only transient expression of HERPUD1-ΔUBL was characterized (Sai et al., 2003), we investigated the subcellular distribution of FLAG-tagged HERPUD1-ΔUBL but in stable HeLa cell lines, in comparison with its wild type version. Immunofluorescence analysis with an anti-FLAG antibody showed a stronger signal for HERPUD1 in the absence of its UBL domain (**Figure 4A**, FLAG, lower left panel) in comparison to HERPUD1-WT (**Figure 4A**, upper left panel). A similar result was also observed with an anti-HERPUD1 antibody (**Supplementary Figure S3A**). To unveil if this phenotype was affecting the ER in general, we analyzed by immunofluorescence the distribution of endogenous ER proteins markers. First, we tested endogenous CALNEXIN, an ER membrane resident protein that acts as a molecular chaperone of glycoproteins (Ou et al., 1995) and GRP94, an ER resident membrane protein of the Heat-Shock Protein (HSP) 90 family (Marzec et al., 2012). We found profound changes in the distribution of both proteins showing a similar pattern to anti-FLAG in HERPUD1-ΔUBL cells (**Figure 4A**, CALNEXIN and GRP94, lower panel), compared to HERPUD1-WT where a characteristic ER pattern is observed. Indeed, HERPUD1-ΔUBL shows a nice colocalization with CALNEXIN and GRP94 (**Figure 4A**, lower merge). In addition, and to exclude the possibility that this phenotype was specific to CALNEXIN and GRP94, we analyzed the ER pattern using an ER-tracker probe in live cells, observing clear changes in the morphology of the ER respect to HERPUD1-WT (**Supplementary Figure S3B**). We noticed that in comparison to HERPUD1-ΔUBL, HERPUD1-WT did not show a high colocalization with CALNEXIN and GRP94 (**Figure 4A**, upper merge), which can be explained by the low levels of HERPUD1-WT expression due to its constant degradation by the proteasome under basal conditions (Sai et al., 2003). In this regard, localization of HERPUD1 at the ER has been well documented (Kokame et al., 2000). Whereas HERPUD1-ΔUBL did not cause an increase in the levels of CALNEXIN and GRP94 measured by Western blot analysis (**Supplementary Figure S3C** y 3D), we concluded that HERPUD1 stability by the deletion of its UBL domain causes an ER-like expansion phenomena that does not involve the increase in the levels of CALNEXIN and GRP94. HERPUD1 is known to be upregulated under ER stress, a condition reported to cause ER membrane expansion and remodeling to alleviate this condition (Schuck et al., 2009). Therefore, we studied whether HERPUD1-ΔUBL could be causing ER proliferation. To assess this, we performed immunofluorescence analysis with an anti-GRP94 antibody. Interestingly, we observed that HERPUD1-ΔUBL expressing cells present a large and dense ER network extending throughout the entire cytoplasm including the periphery of the cell, compared to the less extended ER network observed in HERPUD1-WT cells (**Figure 4B**, left and right panel). To gain a more comprehensive understanding of the ER differences between HERPUD1-WT and HERPUD1-ΔUBL expressing cells, we measured the ER volume using 3D images at high magnification taken with a z-interval of 0.3 μm followed by a z-stack maximum intensity projection. For visualization, we analyzed the distribution of GRP94 in the whole cell using a heat map gradient ranging from non-intensity (black color) to the higher intensity (red color) (**Figure 4B**, left and right panel). This analysis confirmed HERPUD1-ΔUBL increases the volume of the ER and the ER remodeling, compared to the expression of HERPUD1-WT. Indeed, quantitative analysis showed a significant increase in the ER volume with the expression of HERPUD1-ΔUBL (2361 ± 967), compared to HERPUD1-WT (1700 ± 689) (**Figure 4C**). The ER morphological changes observed by confocal microscopy prompted us to perform ultra-structural analysis by transmission electron microscopy (TEM). While cells expressing HERPUD1-WT showed the common ER cytoplasmic structures (**Figure 4D** left panel [ER]), unexpectedly HERPUD1-ΔUBL showed a high number of stacked tubular structures that resemble tubular ER structures that were oriented in a hexagonal spatial distribution (**Figure 4D** center panel [ER]). Others have referred to these structures as energetically stable structures formed by a remarkable proliferation of smooth ER, resembling crystalloid structures of ER (Chin et al., 1982; Anderson et al., 1983; Pathak et al., 1986; Borgese et al., 2006), which in appearance can be compared with "honeycomb like-structures" (**Figure 4D** center panel [ER]). Additionally, a higher magnification (**Figure 4D**, right panel), strongly indicates these structures resemble crystalloid structures with the absence of attached ribosome structures.

To gain insights whether the ER proliferation triggered by the expression of HERPUD1-ΔUBL was the result of an ER stress response, we studied X-box binding protein 1 (XBP1) as a reporter of ER stress and the unfolded protein response (UPR). First, we analyzed by RT-PCR the XBP1 mRNA processing, from the unspliced inactive XBP1 mRNA (u*XBP1*) form to the spliced active XBP1 mRNA (s*XBP1*) form (**Figure 5A**), which is considered a hallmark of the UPR response (Yoshida et al., 2001). RT-PCR analysis of mRNA from HeLa WT untreated cells showed a single band as expected (**Figure 5A**, lane 1). The same analysis including tunicamycin (Tun) (inhibitor of N-linked glycosylation (Heifetz et al., 1979) and thapsigargin (Tg) (blocker of ER

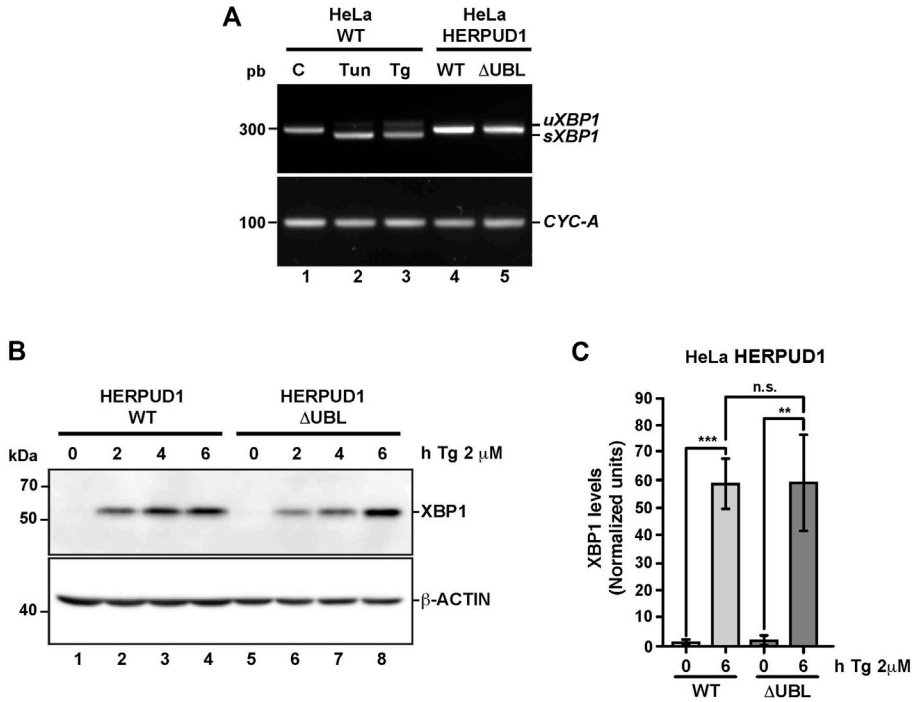

FIGURE 5 | The stability of HERPUD1 by the deletion of its UBL domain does not trigger endoplasmic reticulum stress. **(A)** Splicing of *XBP1* was analyzed by RT-PCR. Total RNAs were obtained from HeLa cells stably expressing HERPUD1-WT-FLAG or HERPUD1-ΔUBL-FLAG, additionally, total RNA was obtained from HeLa WT cells untreated or treated with 2 μM Thapsigargin (Tg) or 5 μg/ml Tunicamycin (Tun) for 4 h as a control of XBP1 splicing. Then, cDNA was synthesized and mRNA expression of XBP1 was analyzed using specific primers. (*uXBP1*: unspliced form, *sXBP1*: spliced form). CYCLOPHILIN-A (CYC-A) was used as an internal control. **(B)** HeLa cells stably expressing HERPUD1-WT-FLAG or HERPUD1-ΔUBL-FLAG were treated with 2 μM Thapsigargin (Tg) for different timepoints (0, 2, 4, and 6 h). Detergent-soluble protein extracts were analyzed by western blot with a monoclonal antibody against XBP1. Monoclonal antibody against β-ACTIN was used as loading control. Position of molecular mass markers is indicated on the left. **(C)** Densitometry quantification of XBP1 protein levels from images as those shown in **B**. Bars represent the mean ± standard deviation. Statistical analysis was performed using two-tailed unpaired Student's *t*-test ($n = 3$ n.s not statistically significant, $^{**}p < 0.01$, $^{***}p < 0.001$).

Ca2+ import (Thastrup et al., 1990)) as positive inducers of ER stress, produced the appearance of two bands in HeLa-WT cells, indicating the s*XBP1* form in response to ER stress (**Figure 5A**, lane 2 and 3). In contrast, a stable expression of either HERPUD1-WT or HERPUD1-ΔUBL showed no detection of s*XBP1,* observing only the expression of the u*XBP1* form (**Figure 5A**, lane 4 and 5), similar to untreated control HeLa WT untreated cells (**Figure 5A**, lane 1). Analysis of PCR bands relative to *CYCLOPHILIN A (CYC-A)* as a housekeeping control showed no difference between cells expressing either HERPUD1-WT or HERPUD1-ΔUBL proteins (**Figure 5A**, lane 4 and 5). Similar findings were observed by western blot analysis (**Figure 5B**). s*XBP1* is rapidly translated to a highly active transcription factor, known as XBP1, responsible for the upregulation of a variety of UPR genes (Yoshida et al., 2001). To examine the significance of the UBL domain of HERPUD1 in the response to ER stress induction, HERPUD1-WT cells and HERPUD1-ΔUBL cells were treated with 2 μM Tg for 2, 4, and 6 h and we performed western blot analysis for XBP1 detection. We observed XBP1 protein was almost undetectable in both cell lines in the absence of a stressor (**Figure 5B**, lane 1 and 5). In contrast, we observed a robust induction of XBP1 in both cell lines upon treatment for 2, 4, and 6 h with 2 μM Tg, observing similar XBP1 expression levels after 6 h of treatment in both cell lines (**Figure 5B**, lane 4 and 8). Quantitative analysis confirmed this conclusion, observing no significant differences between HERPUD1 WT (58.99 ± 9.18) and HERPUD1-ΔUBL (59.59 ± 17.49) expressing cells (**Figure 5C**). In addition to XBP1, we tested by western blot analysis the ER resident transmembrane protein PERK, a kinase that undergoes hyperphosphorylation in response to ER stress shown as a shift in its mobility during SDS-polyacrylamide gel electrophoresis (Bertolotti et al., 2000). This kinase mediates the attenuation of the global translation by the phosphorylation of eIF2α (Bertolotti et al., 2000; Harding and Zhang, 2000). In contrast to its differential electrophoretic migration with Tun and Tg (**Supplementary Figure S4**, lane 2 and 3), no changes in

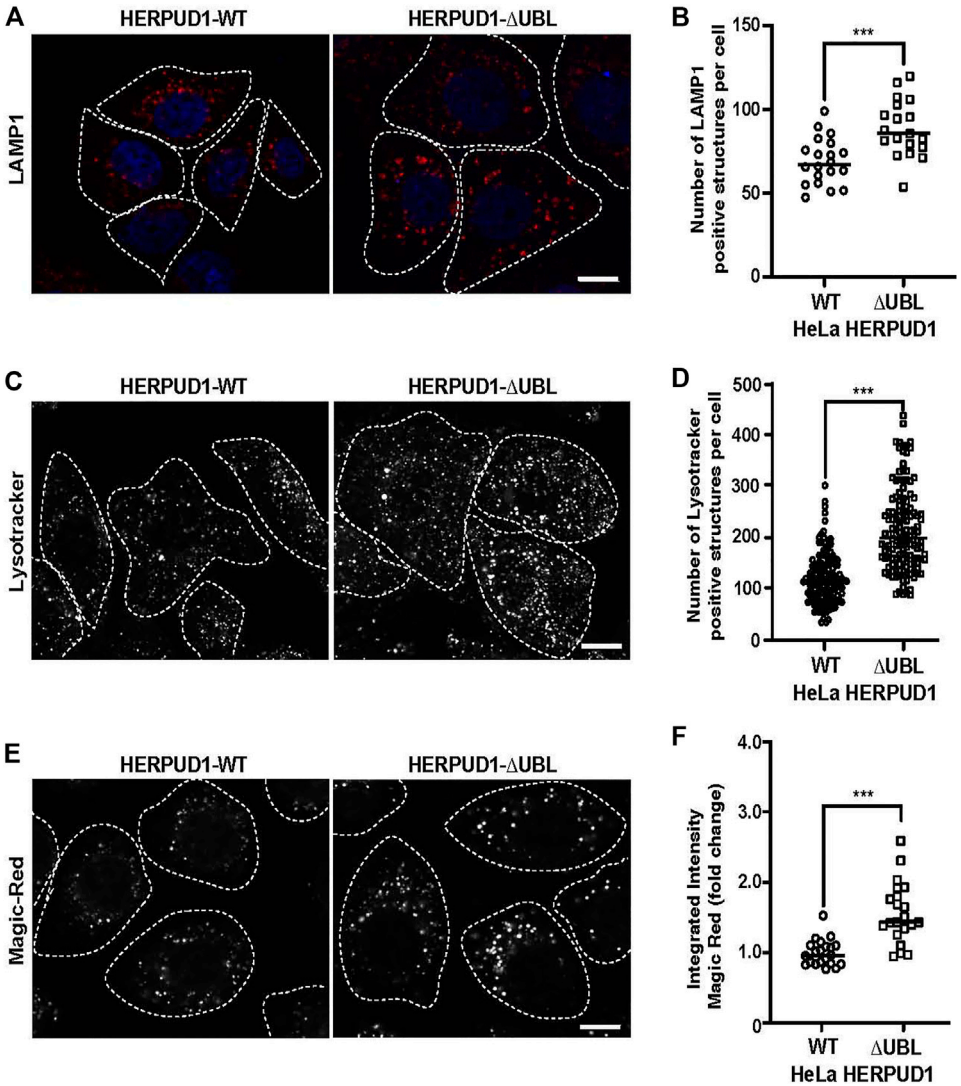

FIGURE 6 | Expression of HERPUD1-ΔUBL increases lysosomal number and function. **(A)** HeLa cells stably expressing HERPUD1-WT-FLAG or HERPUD1-ΔUBL-FLAG grown in glass coverslips were fixed, permeabilized and labeled with a mouse monoclonal antibody against LAMP1 followed by incubation with Alexa-594-conjugated donkey anti-mouse IgG, and DAPI for nuclei staining. Stained cells were examined by fluorescence microscopy. Images were acquired using a TCS SP8 laser-scanning confocal microscope. Scale bar 10 μm. **(B)** Quantification of LAMP1 positive structures per cell. In the scatter plot each circle and square represents the average of positive LAMP1 dots per cell from a frame of HeLa HERPUD1-WT (n = 559) or HERPUD1-ΔUBL (n = 700) respectively. The quantified cells were from three independent experiments. **(C,E)** HeLa cells stably expressing HERPUD1-WT-FLAG or HERPUD1-ΔUBL-FLAG were grown in glass bottom culture dishes and labeled with **(C)** LysoTracker™ Red DND-99 or **(E)** Magic Red®. For live cell imaging analysis, culture medium was replaced with phenol red-free DMEM supplemented with HEPES (10 mM, pH 7.4) and images were acquired with TCS SP8 laser-scanning confocal microscope at 37°C. Scale bar 10 μm. **(D)** Quantification of LysoTracker™ dots per cell. Open circles and open squares represent the average of fluorescence signals for each cell of HeLa HERPUD1-WT-FLAG (n = 139) or HERPUD1-ΔUBL-FLAG (n = 138) respectively. **(F)** Quantification of Magic Red® positive structures. In the scatter plot each circle and square represents the average of positive dots for Magic Red per cell from a frame of HeLa HERPUD1-WT-FLAG (n = 1,279) or HERPUD1-ΔUBL-FLAG (n = 984) respectively. The quantified cells were from three independent experiments. Statistical analysis was performed using two-tailed unpaired Student's t-test (***$p < 0.001$).

PERK migration were observed in HERPUD1-WT or HERPUD1-ΔUBL cells (**Supplementary Figure S4**, lane 4 and 5). Analysis of the activating transcription factor 4 (ATF4), a protein highly expressed upon UPR response (Harding and Novoa, 2000) showed again no changes in ATF4 levels in either cell line (**Supplementary Figure S4**, lane 4 and 5). In contrast, a robust detection of ATF4 was found upon the addition of Tun and Tg (**Supplementary**

Figure S4, lane 2 and 3). Altogether, our findings strongly indicate that ER remodeling triggered by HERPUD1 stability is not the consequence of ER stress.

Increased HERPUD1 Stability by the Deletion of its UBL Domain Leads to a Remarkable Increase in Lysosomal Number and Function

ER proliferation that excludes ribosomes is able to regulate ER contacts with lysosomes (Friedman et al., 2013; Lee and Craig, 2020). Lysosomes are an important catabolic organelle of eukaryotic cells, containing a diverse repertoire of acidic hydrolases (luminal pH of 4.5–5.0) that can digest macromolecules such as sugars, lipids and proteins and even entire organelles (Xu and Ren, 2015). We asked whether expanded ER by increased HERPUD1 stability could have an impact on endolysosomal organelles. To visualize these compartments, HERPUD1-WT and HERPUD1-ΔUBL expressing HeLa cells were stained with an antibody against the endogenous lysosomal-associated membrane protein 1 (LAMP1), a membrane protein found on late endosomes and lysosomes (Griffiths et al., 1988). Unexpectedly, we observed a robust increase in LAMP1 positive structures located around the entire cytoplasm (**Figure 6A**). In agreement with this finding, quantification analysis showed a significant increase in the number of LAMP1 positive structures in HERPUD1-ΔUBL (88.72 ± 16.77) respect to control cells (69.03 ± 13.79) (**Figure 6B**). To determine if the increase in LAMP1 structures corresponded to lysosome organelles, we performed co-staining of LAMP1 with CATHEPSIN-D (CAT-D), a luminal hydrolytic lysosomal enzyme (Benes et al., 2008), observing several LAMP1 positive structures positive to CAT-D (**Supplementary Figure S5A**, lower merge). In addition, we noticed a significant increase in the integrated fluorescence intensity of CAT-D in HERPUD1-ΔUBL (1.47 ± 0.88), compared to HERPUD1-WT expressing cells (1.00 ± 0.20) (**Supplementary Figure S5B**). Considering this increase in CAT-D fluorescence we evaluated if HERPUD1-ΔUBL also impacts lysosomal activity, as assessed by measuring lysosomal acidity and activity in live cells. We first measured if HERPUD1 stability affects the range of lysosomal pH, using the pH-sensitive lysosomal dye LysoTracker Red, which accumulates and emits red fluorescence in acidic compartments with pH < 6.5 (De Duve and Christian, 1974; Chou et al., 2001). Then, we measured CATHEPSIN-B activity using the Magic Red assay (Boonacker et al., 2003). As shown in **Figure 6C**, expression of HERPUD1-ΔUBL causes a significant increase in the number of LysoTracker positive structures (211.95 ± 78.90), compared to control cells (117.85 ± 48.97) (**Figures 6C,D**). Similarly, we found an increase in the number of structures positive to Magic Red fluorescence (**Figure 6E**). This was confirmed by measuring the integrated fluorescence intensity, which revealed a significant increase of this parameter in HERPUD1-ΔUBL cells (1.56 ± 0.43), compared to control cells (1.00 ± 0.19) (**Figure 6F**). Altogether, these findings show that ER remodeling triggered by HERPUD1 increased stability is a potent strategy to promote lysosomal function.

The Phosphomimetic Mutant S59D in the UBL Domain Promotes HERPUD1 Stability Mimicking the Effects of UBL Deletion on the ER and Autophagy

Further, we searched for a mechanism that could mimic the phenotype observed by the deletion of UBL on HERPUD1. As shown by the analysis with PyMOL molecular graphics system (**Supplementary Figure S6A**), the UBL domain of HERPUD1 (PDB 1WGD; green color) resembles UBIQUITIN (PDB 2MSG; purple color) in terms of their three-dimensional structure. UBIQUITIN as well as UBL domains are known targets of phosphorylation under cellular stress (Kondapalli et al., 2012; Swaney et al., 2015; Sauvé et al., 2018). In fact, oxidative stress promotes phosphorylation of UBIQUITIN at Ser65 causing the accumulation of ubiquitylated proteins due to a reduction in global protein turnover rates (Koyano et al., 2014; Swaney et al., 2015). In the same line, it is known that the UBL domain on PARKIN is phosphorylated by PINK1 and is responsible for the activation of its E3 ubiquitin-ligase activity (Sauvé et al., 2018), both essential players of mitochondria quality control by mitophagy (Jin and Youle 2012). Thereby, we searched for Ser residues as possible candidates of phosphorylation in the UBL domain of HERPUD1 using the KinasePhos2.0 web tool. Five residues were predicted in position Ser16, Ser27, Ser33, Ser59, and Ser90 (**Supplementary Figure S6B**, Ser residues in red color). For all these five Ser residues, we generated phosphoinert (substitutions to alanine) and phosphomimetic (substitutions to aspartic acid) mutant versions. Stably transfected HeLa cells were generated for each mutant. Among all mutations tested, the substitution S59D, but not the S59A, showed the strongest increase in HERPUD1 signal, as is shown by immunofluorescence with an anti-FLAG antibody (**Figures 7A,B**). Importantly, we found that the phosphomimetic S59D mutant presents an ER pattern very similar to HERPUD1-ΔUBL cells, confirmed by co-staining with GRP94 (**Figure 7A**, right panel merge). Moreover, to evaluate the specificity of the ER remodeling phenotype in HERPUD1-ΔUBL and HERPUD1-S59D expressing cells, we performed silencing of HERPUD1 with a specific siRNA. In both cell lines we observed a robust rescue of the ER pattern positive to CALNEXIN, compared to the siControl (**Supplementary Figure S7A**). Silencing of HERPUD1-ΔUBL and HERPUD1-S59D with the siRNA was confirmed by western blot (**Supplementary Figure S7B**). Also, no changes with the phosphoinert S59A mutant were observed, showing a similar phenotype than HERPUD1-WT (**Figures 7A,B**). Thus, further characterization included the comparison between HERPUD1-WT and HERPUD1-S59D. In this regard, under basal conditions western blot analysis using anti-HERPUD1 and anti-FLAG antibodies showed higher levels of HERPUD1-S59D (40.09 ± 5.31) compared to either HERPUD1-WT (1.00 ± 0.53) or HERPUD1-S59A (2.88 ± 1.76) (**Figure 7C**, lane 5 compared to lane 1 and 3 and **Figure 7D**). We also measured the levels of these versions upon treatment for 4 h with 20 mM MG132, which is a proteasomal inhibitor, known to abolish HERPUD1 proteasomal degradation (Yan et al., 2014). As expected, MG132 treatment caused a significant increase in HERPUD1-WT (16.55 ± 7.13) (**Figure 7C**, lane 1 compared to lane 2 and **Figure 7D**). A similar result was obtained with HERPUD1-S59A (20.36 ± 9.65) (**Figure 7C**, lane 3

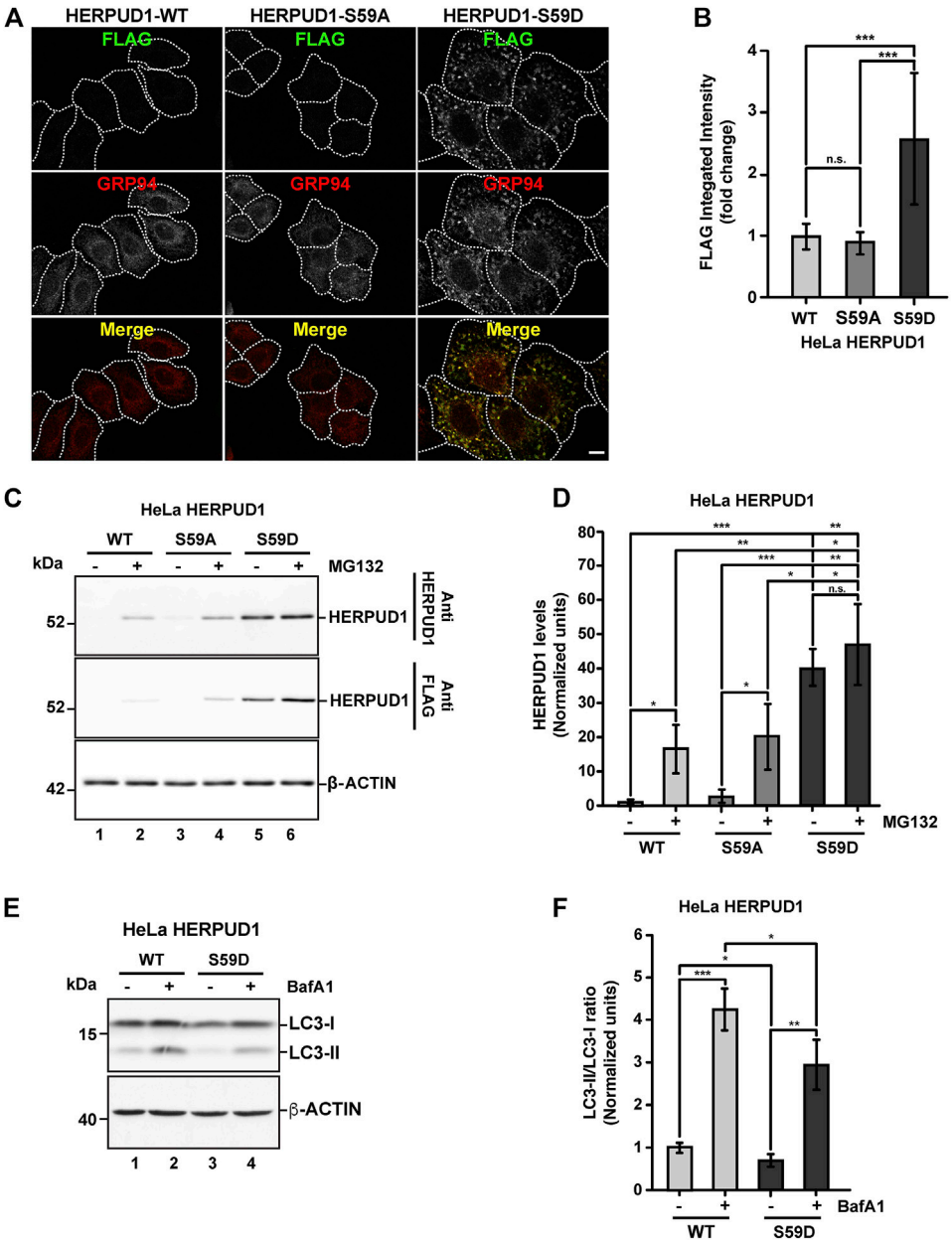

FIGURE 7 | Stabilization of HERPUD1 by S59D mutation alters the ER morphology and decreases autophagy. **(A)** HeLa cells stably expressing HERPUD1-WT-FLAG, HERPUD1-S59A-FLAG or HERPUD1-S59D-FLAG were grown in glass coverslips, fixed, permeabilized, and double-labeled with mouse monoclonal antibody against FLAG and with a rat monoclonal antibody against GRP94 followed by incubation with Alexa-488-conjugated donkey anti-rabbit IgG (green channel) and Alexa-594-conjugated donkey anti-rat IgG (red channel). Images were acquired using a TCS SP8 laser-scanning confocal microscope. The third image on each column is the merge of green and red channels; yellow indicates colocalization of red and green channels. Scale bar: 10 μm. **(B)** Quantification of fluorescence FLAG signal from indicated cells. **(C)** HeLa cells stably expressing HERPUD1-WT-FLAG, HERPUD1-S59A-FLAG or HERPUD1-S59D-FLAG were treated or not with 10 μM of MG132 for 4 h. Detergent-soluble protein extracts were analyzed by western blot with anti-HERPUD1 and anti-FLAG antibodies. β-ACTIN was used as a loading control. Position of molecular mass markers is indicated on the left. **(D)** Densitometry quantification of HERPUD1 western blot signal from images as those shown in **C**. Bars represent the mean ± standard deviation. **(E)** HeLa cells stably expressing HERPUD1-WT-FLAG or HERPUD1-S59D-FLAG untreated (lanes 1 and 3) or treated with 100 nM BafA1 for 4 h (lanes 2 and 4). Detergent-soluble protein extracts were analyzed by western blot with a rabbit polyclonal antibody to LC3B. Monoclonal antibody against β-ACTIN was used as a loading control. Position of molecular mass markers is indicated on the left. **(F)** Densitometry quantification of LC3-I and LC3-II protein levels from images as those shown in E. Relative levels are expressed as the ratio of LC3-II to LC3-I from images as those shown in **E**. Bars represent the mean ± standard deviation. Statistical analysis was performed using two-tailed unpaired Student's *t*-test ($n = 3$ n.s. not statistically significant, $^{*}p < 0.05$, $^{**}p < 0.01$, $^{***}p < 0.001$).

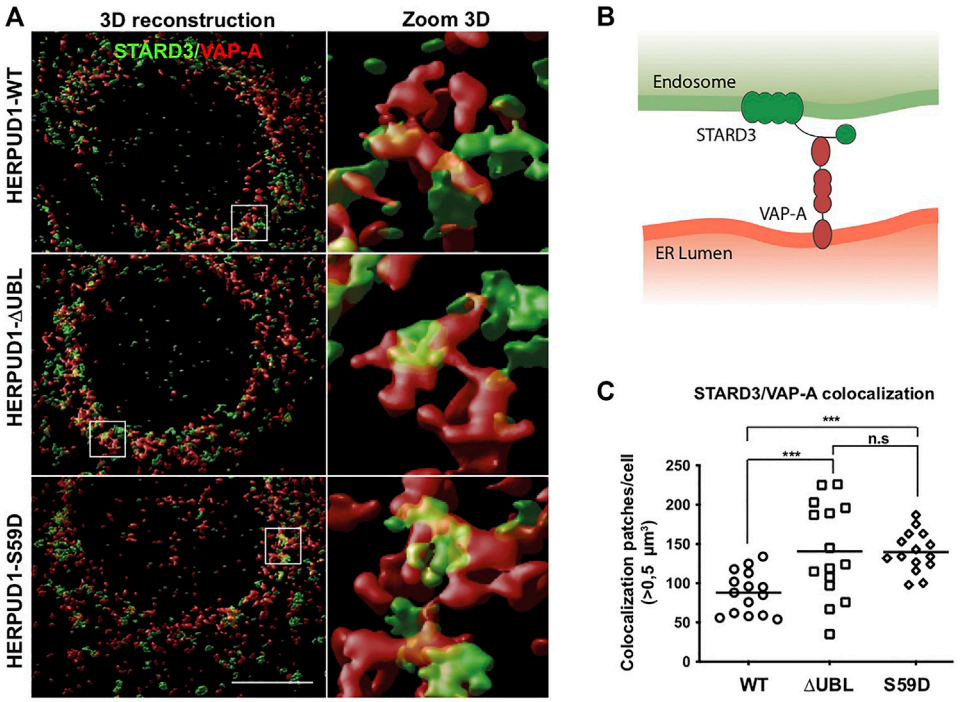

FIGURE 8 | Stabilization of HERPUD1 causes expansion of the ER-lysosomal network and an increase in size of ER-lysosomal contact sites. **(A)** HeLa cells stably expressing HERPUD1-WT-FLAG, HERPUD1-ΔUBL-FLAG or HERPUD1-S59D-FLAG were grown in glass coverslips and then fixed, permeabilized and double-labeled with a rabbit polyclonal antibody against STARD3 and a mouse monoclonal antibody against VAP-A followed by incubation with Alexa-488-conjugated donkey anti-rabbit IgG (green channel), Alexa-594-conjugated donkey anti-mouse IgG (red channel) and DAPI for nuclei staining. All images were acquired using a Leica TCS SP8 laser-scanning confocal microscope in z-series at nyquist rate oversampling parameters. Left panel shows 3D surface rendered images of STARD3 (green channel) and VAP-A (red channel) after deconvolution and chromatic aberration correction with Huygens software. Scale bar, 10 μm. Right panel shows a higher magnification of the 3D reconstructions. Box 5 × 5 μm. **(B)** Representative scheme of the interaction between the STARD3/VAP-A proteins. **(C)** Quantification of colocalization STARD3/VAP-A patches per cell. Open circle, square and rhombus represent the number of >0.5 μm^3 in HeLa HERPUD1-WT-FLAG (n = 15), HERPUD1-ΔUBL-FLAG (n = 15) and HERPUD1-S59D-FLAG (n = 15), respectively.

compared to lane 4 and **Figure 7D**). In contrast, we observed non-significant differences in the levels of HERPUD1-S59D in the absence (40.09 ± 5.31) or presence of MG132 (47.17 ± 11.74) (**Figure 7C**, lane 5 and 6 and **Figure 7D**). Further, and based on the negative impact of HERPUD1 stability on autophagy by the deletion of its UBL domain, we next investigated if the stability of HERPUD1-S59D could have a similar outcome. Biochemically, we found that HERPUD1-S59D cells have a significant reduction in the LC3-II/LC3-I ratio (0.66 ± 0.02), in comparison to HERPUD1-WT (1.00 ± 0.18) (**Figures 7E,F**). This result was corroborated by immunofluorescence analysis of LC3 in the absence or presence of BafA1 showing that HERPUD1-S59D cells present a lesser number of autophagosomes, compared to HERPUD1-WT (**Supplementary Figure S8**). Moreover, in agreement with previous reports indicating that a reduction in autophagy enhances ER expansion and cell size (Khaminets et al., 2015; Miettinen and Mikael, 2015), we noticed that HERPUD1-S59D cells were significantly larger in size (2.52 ± 0.98), compared to HERPUD1-WT (1.00 ± 0.4) and HERPUD1-S59A cells (0.88 ± 0.29) (**Figure 7A** and **Supplementary Figure S9A**). Importantly, cell size quantification showed HERPUD1-ΔUBL were also larger in size (1.36 ± 0.64) than HERPUD1-WT (1.00 ± 0.4), but smaller than HERPUD1-S59D (2.52 ± 0.98) (**Supplementary Figure S9A**). In addition, because nuclei size remains proportional to the cell size in a wide range of genetic backgrounds and growth conditions (Huber and Gerace, 2007), we studied the nuclei size in all cell lines. Surprisingly, nuclei size in HERPUD1-S59D cells were significantly larger (1.74 ± 0.72) in comparison to all tested cell lines; HERPUD1-WT (1.00 ± 0.49), HERPUD1-S59A (1.12 ± 0.47) and HERPUD1-ΔUBL (1.11 ± 0.52) (**Supplementary Figure S9B**). Altogether, our findings support the idea that HERPUD1 increased stability might play an important function in cellular plasticity by commanding a program that controls ER remodeling with impact in cell and nuclei size. The results with the phosphomimetic version of HERPUD1 opens the alternative of a program activated under the control of phosphorylation.

The Phosphomimetic HERPUD1-S59D Mutant Promotes ER-Lysosomal Network With Impact in Stress Cell Survival

Because of the increase in the number of functional lysosomes under the expression of HERPUD1-ΔUBL, we investigated if HERPUD1-S59D expressing cells could have a similar output. First, we performed immunofluorescence of LAMP1, observing a significant increase in the number of LAMP1 positive structures in HERPUD1-S59D cells (135.28 ± 21.32), in comparison to

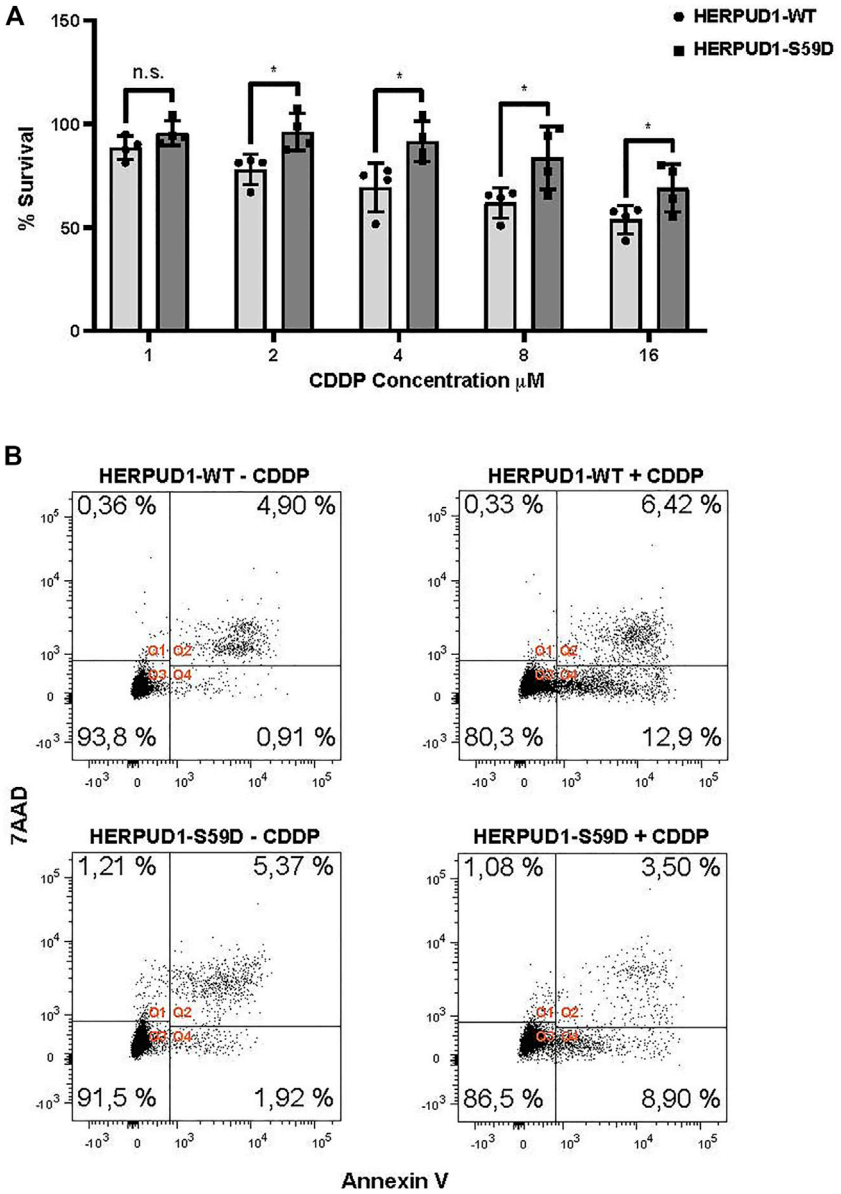

FIGURE 9 | Stabilization of HERPUD1 by S59D mutation decreases cell death mediated by CDDP. **(A)** HeLa cells stably expressing HERPUD1-WT-FLAG or HERPUD1-S59D-FLAG were treated with different concentrations of cisplatin (CDDP) and then a SRB assay was performed. The absorbance values of each point were normalized to control cells (without treatment) and transformed to a percentage. Experiments were performed at least three times, and the results are expressed as mean ± standard deviation. Statistical analysis was performed using two-tailed unpaired Student's *t*-test ($n = 4$ n.s. not statistically significant and $^*p < 0.05$) **(B)** HeLa cells stably expressing HERPUD1-WT-FLAG or HERPUD1-S59D-FLAG were treated or not with CDDP 10 μM for 24 h. Afterwards, cells were collected by trypsinization and stained with Annexin V-Pacific Blue and 7AAD. Scatter plots representing the different quadrants are labeled as Q1 (necrotic cells), Q2 (viable cells), Q3 (dead cells) and Q4 (apoptotic cells). The graph shows the percentage of cells present in each quadrant.

HERPUD1-WT (69.03 ± 13.79) and HERPUD1-S59A (58.42 ± 14.55) (**Supplementary Figures S10A,B**). Next, analysis with LysoTracker in HERPUD1-S59D cells (183.35 ± 60.05), in comparison to HERPUD1-WT (118.18 ± 51.00) and HERPUD1-S59A (86.13 ± 41.46) confirmed HERPUD1-S59D cells have a significant increase in the number of lysosomes per cell (**Supplementary Figures S10C,D**). Similar results were obtained with Magic Red where the quantification showed an increase of almost twice the integrated intensity of Magic Red in HERPUD1-S59D cells (2.25 ± 0.32) in comparison with HERPUD1-WT (1.00 ± 0.15) and HERPUD1-S59A (1.02 ± 0.24) (**Supplementary Figures S10E,F**). The integrated intensity analysis demonstrated the increase in lysosomal function is not a result of larger cell size suggesting the activation of an alternative mechanism that needs to be further investigated.

One important aspect of cellular plasticity is the establishment of a network between the ER and the lysosomes that helps in the

constant adaptation to particular cellular needs. In this regard, it is known that the ER forms membrane-contact sites (MCSs) with lysosomes (Valm and Alex, 2017), acting as a potent spatiotemporal organizer of endolysosomal biology (Neefjes et al., 2017). We hypothesized that ER-lysosomal network remodeling should be accompanied by the appearance of MCSs between these two organelles. Therefore, we studied in HERPUD1-WT, HERPUD1-ΔUBL and HERPUD1-S59D cells the spatial distribution of the STARD3 endo-lysosomal cholesterol-binding protein (Alpy et al., 2001) with VAP-A, an ER membrane protein (Skehel et al., 2000), known to form a novel molecular tether between endo-lysosomes and the ER referred as MCSs (Alpy et al., 2013), in a high-resolution scale. By three-dimensional (3D) reconstruction imaging we observed that expression of HERPUD1-ΔUBL and HERPUD1-S59D caused larger patches of colocalization between STARD3/VAP-A (**Figure 8A**, left panel white boxes). A higher zoom 3D magnification of these white boxes is indicated in **Figure 8A**, right panel. A representative scheme of the interaction between the STARD3/VAP-A proteins is indicated in **Figure 8B**. Quantification analysis confirmed a significant increase in the number of colocalization patches $>0.5\,\mu m^3$ per cell in HERPUD1-ΔUBL and HERPUD1-S59D expressing cells, compared to HERPUD1-WT (**Figure 8C**). Altogether, our findings strongly suggest that HERPUD1 stability at the ER compartment not only promotes the remodeling of the lysosomal network but also the size area of MCSs between these two organelles.

ER expansion has been known for decades as a trigger for crystalloid ER (Chin et al., 1982) and ER whorls (Feldman et al., 1981; Schuck et al., 2009), however only recent studies have proposed this phenomenon could be part of a program necessary to overcome ER stress with impact in stress cell survival (Schuck et al., 2009; Xu et al., 2021). Moreover, taking in consideration that HERPUD1 stability triggers ER expansion, ER-lysosomal network and MCSs between these two organelles, a protein known to be upregulated under ER stress, we studied the effect of HERPUD1 stability in the cell viability of HeLa cells in response to cisplatin (CDDP). CDDP is the most frequently used chemotherapeutic agent for the treatment of some types of cancers, including cervical cancer in accordance with the model of HeLa cells (Dasari and Bernard Tchounwou, 2014). In addition, it is known that alleviation of ER stress attenuates CDDP-induced apoptosis (Wu et al., 2018). Thus, we investigated the resistance to drug-induced cytotoxicity of HERPUD-WT and HERPUD1-S59D cells in response to varying doses of CDDP for 24 h with the Sulforhodamine B (SRB) assay. We found a significant increase in the resistance of HERPUD1-S59D cells in comparison with HERPUD1-WT at 2, 4, 8, and 16 μM of CDDP (**Figure 9A**). We corroborated this result measuring apoptosis of these cells in the absence or presence of 10 μM CDDP for 24 h by flow cytometry using Annexin-V staining method. In agreement with the SRB assay, we observed HERPUD1-S59D cells showed less apoptosis compared to HERPUD1-WT cells in response to CDDP treatment (**Figure 9B**). These results strongly indicate HERPUD1 stability helps to overcome cisplatin-induced cytotoxicity. In this regard, we propose that this differential response could be mediated by the expansion of the ER/lysosomal network, an aspect that should be investigated in other cancer cell models.

DISCUSSION

Post-translational events allow cells to respond swiftly to stress conditions with consequences in their proteome composition. Autophagy and the UPS are two closely related pathways that adjust their functions in response to cellular demands in order to maintain cellular homeostasis (Korolchuk et al., 2010). During starvation overall protein degradation rises by activation of both autophagy and the UPS (Mizushima et al., 2011; VerPlank et al., 2019). Indeed, before up-regulation of autophagy, efficient synthesis of new proteins is sustained by degradation of preexisting proteins by the proteasome, which shows that the proteasome also plays a crucial role in cell survival after nutritional stress (Vabulas and Ulrich Hartl, 2005). In agreement with this, it is known that the proteasome activity transits from a latent to an activated state (Asano et al., 2015; Collins and Goldberg, 2020). However, if UPS activation upon starvation mediates the degradation of specific proteins that could slow-down autophagy is unknown. Downregulation of HERPUD1 upon nutrient starvation in ATG5-depleted cells opens that alternative. In this regard, it has been previously proposed that HERPUD1 depletion up-regulates autophagy (Quiroga et al., 2013) and the degradation of cytosolic protein aggregates (Miura et al., 2010). These findings support the idea that basal levels of HERPUD1 could act as a break in the activation of basal autophagy.

Interestingly, another protein that was also robustly downregulated upon starvation in Atg5 KD cells was p62/SQSTM1. Been an autophagy receptor this protein could be also participating in endosomal microautophagy (Mejlvang et al., 2018), pathway that could be more activate with the lack of Atg5. $Atg5^{-/-}$ mice remain healthy until the perinatal period, therefore it is accepted that cells activate alternative mechanisms to compensate the lack of Atg5 (Yoshii et al., 2016). In agreement with this hypothesis, p62/SQSTM1 KO mice show an increase in the ER content in the liver (Yang et al., 2016), Further studies will help to clarify unconventional roles of p62/SQSTM1.

Under ER stress, HERPUD1 is upregulated even faster than ER chaperones (Kokame et al., 2000; Bergmann et al., 2018), where it participates in Endoplasmic Reticulum-Associated Degradation (ERAD) (Schulze et al., 2005). HERPUD1 facilitates the assembly of the HRD1 complex, also known as the retrotranslocon, key in the retrotranslocation of unfolded proteins from the ER to the cytosol for proteasomal degradation upon demand (Leitman et al., 2014; Schulz et al., 2017). However, the function of HERPUD1 in the absence of ER stress is less understood. Here, we propose HERPUD1 acts as a negative regulator of autophagy controlled by its proteasome dependent stability, a mechanism that could operate in the absence of ER stress under the control of phosphorylation of its UBL domain.

One interesting aspect of HERPUD1 is the UBL domain present in its N-terminus region. In general, UBL-containing proteins share the ability to interact with the 19S regulatory particle of the 26S proteasome promoting its activation (Hartmann-Petersen and Gordon, 2004b; Yu and Matouschek, 2017; Collins and Goldberg, 2020). The UBL domain itself can stimulate multiple proteasome activities in a similar fashion to ubiquitin chains (Kim et al., 2018; Collins and Goldberg, 2020). However, unlike ubiquitin and its homologous (e.g., SUMO and Nedd8), UBL-containing proteins cannot be conjugated to other proteins. The human genome encodes over 60 UBL-containing proteins, where 15 of them have been studied in their ability to bind and regulate proteasome activity (Collins and Goldberg, 2020). HERPUD1 is one member of this group, however its role as a positive modulator of the proteasomal activity remains uncharacterized. Moreover, because UBL-containing proteins can stimulate proteasome activity (Kim et al., 2018; Collins and Goldberg, 2020), it would be interesting to explore the effect of HERPUD1-ΔUBL and HERPUD1-S59D on the activity of the proteasome under normal and starvation conditions.

In addition, recent findings show UBL-containing proteins can also play a regulatory role in autophagy, such as USP14 (Kim et al., 2018), NUB1 (Guarascio et al., 2020), Elongin B (Antonioli et al., 2016), UHRF1 (Shi et al., 2020), OASL (Toledo Pinto et al., 2018), BAT3 (Sebti et al., 2014) and UBQLN (Rothenberg et al., 2010; Şentürk et al., 2019; Yang and Klionsky 2020). Our findings show that the stabilization of HERPUD1 by removing its UBL domain causes a reduction in LC3-II/LC3-I ratio, which positions HERPUD1 as a member of this growing list of UBL-containing proteins that function as regulators of autophagy. However, how HERPUD1 stability mediates the reduction in LC3-II/LC3-I ratio needs further studies. One aspect to be explored is the finding that HERPUD1 interacts with UBQLN (Kim et al., 2008). UBQLN is a cytosolic protein, that in addition to HERPUD1, interacts with LC3 and ubiquitinated cargos in autophagosomes (Rothenberg et al., 2010). Furthermore, it is known that silencing UBQLN leads to a reduction in the lipidation of LC3-I to LC3-II that correlates with a diminished number of autophagosomes (Rothenberg et al., 2010). Because UBQLN binds HERPUD1 independently of its UBL domain (Kim et al., 2008), it is possible that an increase in HERPUD1 stability at the ER could mediate the sequestration of UBQLN in this compartment affecting its function in other membranes such as autophagosomes (Rothenberg et al., 2010). In this regard, it has been previously proposed that recruitment of UBQLN to the ER by HERPUD1 could bring the proteasome and the ubiquitinated substrates to specific microdomains of the ER, which could hypothetically be the step that promotes the ERAD pathway (Kim et al., 2008). Because our results show that HERPUD1 stability maintain the ER-lysosomal network, additional work is needed to determine if HERPUD1:UBQLN interaction could play a role in the delivery of substrates to the ER-to-lysosomes-associated degradation (ERLAD) (Fregno et al., 2018; Fregno and Molinari 2019), considering the increase in the lysosomal degradation function. As HERPUD1-S59D mimics the effect on HERPUD1 stability we propose that recruitment of UBQLN at the ER is controlled by phosphorylation of HERPUD1.

Ubiquitin and UBL domains are targets of phosphorylation (Kondapalli et al., 2012; Koyano et al., 2014; Wauer et al., 2015). The best-known example is the phosphorylation of the UBL domain of the ubiquitin ligase PARKIN by the Ser/Thr kinase PINK1 on Ser65 (Kondapalli et al., 2012; Koyano et al., 2014). This post-translational modification orchestrates its enzymatic E3 ligase activity (Aguirre et al., 2017), participating in the ubiquitination of mitochondrial proteins during mitophagy. Here, we propose that phosphorylation of the UBL domain in HERPUD1 must affect its noncovalent binding to the proteasome explaining its stability increase, as occurs with HERPUD1-ΔUBL. Further studies are needed to define the physiological triggers of HERPUD1 phosphorylation, and the kinase involved.

This study is the first report indicating HERPUD1 stability mediates ER expansion but not as a consequence of ER stress. In this regard, it is well known that the ER expands to alleviate ER stress (Schuck et al., 2009). However, the ER expansion phenomenon is not always homeostatic. ER expansion requires an adequate supply of membrane lipids although the mechanisms that govern ER biogenesis are yet unclear. For example, the ER expands several folds when B lymphocytes differentiate into antibody-secreting plasma cells (Wiest et al., 1990), when hepatocytes increase its P450 detoxification system (Feldman et al., 1981), in response to Epidermal Growth Factor (EGF) (Caldieri et al., 2017) and statins (Chin et al., 1982). Interestingly, lipid synthesis activation causes expansion of the ER and resistance to ER stress even in cells lacking the UPR, highlighting the physiological importance of ER membrane biogenesis in homeostasis. Because ER adjust its size and shape according to need interacting with several other organelles (Schuck et al., 2009), it has been proposed ER size can impact other organelles allowing rapid transfer of ions and newly synthesized lipids, associated to the shape and distribution of the ER (Chan and Marshall, 2010). However, how cells control cell size is still an enigma. Nevertheless, because cell size controls flux across membranes, metabolism, biosynthetic capacity, and nutrient exchange, among others, (Chan and Marshall, 2010), our findings open the possibility that stabilized HERPUD1 could play an important role in cell physiology, a mechanism that could be related with mTOR pathway and its downstream targets (Fingar et al., 2022).

A future challenge will be to sort out the connection between HERPUD1 and lipid synthesis, a link recently suggested by genomics (Van Der Laan and Sander, 2018).

In this regard, an interesting observation to be considered is that HERPUD1 increased stability mimics the effect of statins in reference to the appearance of a crystalloid ER (Chin et al., 1982). Statins are cholesterol reducing agents acting as blockers of the cholesterol biosynthesis by the inhibition of 3-hydroxy-3-methylglutaryl coenzyme A (HMG-CoA) reductase. Interestingly, statins possess beneficial effects in a variety of human diseases. Importantly, a growing number of studies refer to statins as ER stress reducing agents (Mollazadeh et al., 2018; Zhang et al., 2018), modulators of autophagy (Ashrafizadeh et al., 2020) and inducers of lysosomal biogenesis (Zhang et al.,

2020). However, if statins promote those effects by a mechanism related with HERPUD1 stability is unknown.

ER expansion by HERPUD1 stability is correlated with a slow-down in autophagy. In agreement with this, it is known that the knockdown of the two major autophagy regulators, ATG5 and BECN1, likewise trigger ER expansion (Khaminets et al., 2015). Moreover, a similar ER expansion is also observed by ER-phagy inhibition, a selective form of autophagy responsible for the degradation of excess ER (Khaminets et al., 2015; Grumati et al., 2018). However, studies investigating if the UPR is activated or not in response to inhibition of autophagosomal biogenesis or ER-Phagy dysfunction are still lacking. While the opposite effect has been reported, observing that excessive ER-Phagy results in activation of the UPR response (Liao et al., 2019).

Our findings also indicate that ER expansion by HERPUD1 stability is accompanied by an increase in the number of functional lysosomes. Because several studies have indicated that UBL-containing proteins cause a positive modulation of the UPS system we can speculate that HERPUD1-ΔUBL and HERPUD1-S59D could have a negative impact in the proteasome activity. Disturbances in the UPS and autophagy function are known to be compensated by lysosome biogenesis (Jackson and Hewitt 2016). In addition, we have already discussed the possibility that HERPUD1 stability could trigger the recruitment of UBQLN to the ER. Interestingly, it has been recently discovered that UBQLN plays a crucial role in the maintenance of the acidic pH of lysosomes and in a closed interplay with the ER (Şentürk et al., 2019; Yang and Klionsky, 2020). Further work is needed to determine if HERPUD1:UBQLN interaction could play a role at this level. Furthermore, based on recent findings (Toulmay and Prinz, 2011; Henne, 2017), it is necessary to explore if MCSs between ER and lysosomes could play a role in the transfer of lipids to lysosomes to compensate for the massive expansion of the ER under HERPUD1 stability by degradation.

Together, our findings highlight novel insights into the possible role of HERPUD1 as a regulator of autophagy and its participation in the maintenance of the ER structure. Moreover, our results suggest that HERPUD1 stabilization promotes the lysosomal function which could promote ER-lysosome intercommunication even in conditions where the UPR is not activated. The mechanism behind this regulation remains to be elucidated, specially the UBL phosphorylation-dependent stabilization of HERPUD1 and its effect on the pathways discussed above. Furthermore, if this regulation has a role in cell pathological conditions it should be analyzed in future studies.

DATA AVAILABILITY STATEMENT

The datasets presented in this study can be found in online repositories. The names of the repository/repositories and accession number(s) can be found below: ProteomeXchange with identifier PXD024486.

AUTHOR CONTRIBUTIONS

Design of experiments: GV, OC, EA-M, SH, CC-T, LH, AEG, MHT, HAB, CR, JC, MV-G, RTH, AR-F, VAC, PVB. Development of experiments: GV, OC, EA-M, CC-T, LH, AEG, MHT, HAB, MV-G, AR-F, VAC. Writing: GV, OC, EA-M, SH, MHT, CR, MV-G, AR-F, VAC, PVB.

FUNDING

This research was funded by Fondo Nacional de Desarrollo Científico y Tecnológico of Chile (FONDECYT; http://www.conicyt.cl/fondecyt) 1190928 to MV-G, No. 1211261 to PVB and No. 11150532 to AR-F; Associative Investigation Program (PIA; https://www.conicyt.cl/pia) including No. No. ACT-172066 to PVB; Financiamiento Basal No. ANID/BASAL/ACE210009 to PVB; No. ANID/BASAL/FB210008 to PVB Academy Insertion Program (PAI; http://www.conicyt.cl/pai) No. 79150075 to AR-F; Fondo de Equipamiento Científico y Tecnológico of Chile (FONDEQUIP; http://www.conicyt.cl/fondequip) No. EQM150118 to PVB; Cooperation International Programme (CONICYT-RCUK; https://www.conicyt.cl/pci) No. DPI20140068 to PVB.

ACKNOWLEDGMENTS

We thank the generous donation of pCI-HERPUD1-Flag and pCI-HERPUD1-ΔUBL-Flag by Doctor Koichi Kokame from National Cerebral and Cardiovascular Center, Japan. We also thank Zanlungo for the generous donation of the anti-STARD3 commercial antibody. Additionally, we thank Lavandero and Quiroga for the critical discussion of the manuscript.

SUPPLEMENTARY MATERIAL

The Supplementary Material for this article can be found online at: https://www.frontiersin.org/articles/10.3389/fcell.2022.743287/full#supplementary-material

REFERENCES

Aguirre, J. D., Dunkerley, K. M., Mercier, P., and Shaw, G. S. (2017). Structure of Phosphorylated UBL Domain and Insights into PINK1-Orchestrated Parkin Activation. *Proc. Natl. Acad. Sci. USA* 114 (2), 298–303. doi:10.1073/pnas.1613040114

Alpy, F., Rousseau, A., Schwab, Y., Legueux, F., Stoll, I., Wendling, C., et al. (2013). STARD3 or STARD3NL and VAP Form a Novel Molecular Tether between Late Endosomes and the ER. *J. Cel Sci* 126 (Pt 23), 5500–5512. doi:10.1242/jcs.139295

Alpy, F., Stoeckel, M.-E., Dierich, A., Escola, J.-M., Wendling, C., Chenard, M.-P., et al. (2001). The Steroidogenic Acute Regulatory Protein Homolog MLN64, a Late Endosomal Cholesterol-Binding Protein. *J. Biol. Chem.* 276 (6), 4261–4269. doi:10.1074/jbc.m006279200

Anderson, R. G. W., Orci, L., and Brown, M. S. (1983). Ultrastructural Analysis of Crystalloid Endoplasmic Reticulum in UT-1 Cells and its Disappearance in Response to Cholesterol. *J. Cel Sci.* 63 (1), 1. doi:10.1242/jcs.63.1.1

Antonioli, M., Albiero, F., Piacentini, M., and Fimia, G. M. (2016). Temporal Regulation of Autophagy Response by the CULLIN 4-AMBRA1-CULLIN 5 Axis. *Mol. Cel Oncol* 3 (5), e1008304. doi:10.1080/23723556.2015.1008304

Asano, S., Fukuda, Y., Beck, F., Aufderheide, A., Förster, F., Danev, R., et al. (2015). A Molecular Census of 26 S Proteasomes in Intact Neurons. *Science* 347 (6220), 439–442. doi:10.1126/science.1261197

Ashrafizadeh, M., Ahmadi, Z., Farkhondeh, T., and Samarghandian, S. (2020). Modulatory Effects of Statins on the Autophagy: A Therapeutic Perspective. *J. Cel Physiol* 235 (4), 3157–3168. doi:10.1002/jcp.29227

Benes, P., Vetvicka, V., and Fusek, M. (2008). Cathepsin D-Many Functions of One Aspartic Protease. *Crit. Rev. Oncology/Hematology* 68 (1), 12–28. doi:10.1016/j.critrevonc.2008.02.008

Bergmann, T. J., Fregno, I., Fumagalli, F., Rinaldi, A., Bertoni, F., Boersema, P. J., et al. (2018). Chemical Stresses Fail to Mimic the Unfolded Protein Response Resulting from Luminal Load with Unfolded Polypeptides. *J. Biol. Chem.* 293 (15), 5600–5612. doi:10.1074/jbc.ra117.001484

Bertolotti, A., Zhang, Y., Hendershot, L. M., Harding, H. P., and Ron, D. (2000). Dynamic Interaction of BiP and ER Stress Transducers in the Unfolded-Protein Response. *Nat. Cel Biol* 2 (6), 326–332. doi:10.1038/35014014

Blois, J., Smith, A., and Josephson, L. (2011). The Slow Cell Death Response when Screening Chemotherapeutic Agents. *Cancer Chemother. Pharmacol.* 68 (3), 795–803. doi:10.1007/s00280-010-1549-9

Boonacker, E., Elferink, S., Bardai, A., Wormmeester, J., and Van Noorden, C. J. F. (2003). Rapid Assay to Detect Possible Natural Substrates of Proteases in Living Cells. *BioTechniques* 35 (4), 766–774. doi:10.2144/03354st07

Borgese, N., Francolini, M., and Snapp, E. (2006). Endoplasmic Reticulum Architecture: Structures in Flux. *Curr. Opin. Cel Biol.* 18 (4), 358–364. doi:10.1016/j.ceb.2006.06.008

Bustamante, H. A., González, A. E., Cerda-Troncoso, C., Shaughnessy, R., Otth, C., Soza, A., et al. (2018). Interplay between the Autophagy-Lysosomal Pathway and the Ubiquitin-Proteasome System: A Target for Therapeutic Development in Alzheimer's Disease. *Front Cel Neurosci* 12, 126. doi:10.3389/fncel.2018.00126

Bustamante, H. A., Cereceda, K., González, A. E., Valenzuela, G. E., Cheuquemilla, Y., Hernández, S., et al. (2020). The Proteasomal Deubiquitinating Enzyme PSMD14 Regulates Macroautophagy by Controlling Golgi-To-ER Retrograde Transport. *Cells* 9 (3), 777. doi:10.3390/cells9030777

Caldieri, G., Barbieri, E., Nappo, G., Raimondi, A., Bonora, M., Conte, A., et al. (2017). Reticulon 3-Dependent ER-PM Contact Sites Control EGFR Nonclathrin Endocytosis. *Science* 356 (6338), 617–624. doi:10.1126/science.aah6152

Camuzard, O., Santucci-Darmanin, S., Carle, G. F., and Pierrefite-Carle, V. (2020). Autophagy in the Crosstalk between Tumor and Microenvironment. *Cancer Lett.* 490, 143–153. doi:10.1016/j.canlet.2020.06.015

Cavieres, V. A., Cerda-Troncoso, C., Rivera-Dictter, A., Castro, R. I., Luchsinger, C., Santibañez, N., et al. (2020). Human Golgi Phosphoprotein 3 Is an Effector of RAB1A and RAB1B. *PLoS ONE* 15 (8 August), e0237514. doi:10.1371/journal.pone.0237514

Chan, Y.-H. M., and Marshall, W. F. (2010). Scaling Properties of Cell and Organelle Size. *Organogenesis* 6 (2), 88–96. doi:10.4161/org.6.2.11464

Chin, D. J., Luskey, K. L., Anderson, R. G., Faust, J. R., Goldstein, J. L., and Brown, M. S. (1982). Appearance of Crystalloid Endoplasmic Reticulum in Compactin-Resistant Chinese Hamster Cells with a 500-Fold Increase in 3-Hydroxy-3-Methylglutaryl-Coenzyme A Reductase. *Proc. Natl. Acad. Sci. U S A.* 79 (4 I), 1185–1189. doi:10.1073/pnas.79.4.1185

Chou, K.-M., Paul Krapcho, A., and Hacker, M. P. (2001). Impact of the Basic Amine on the Biological Activity and Intracellular Distribution of an Aza-Anthrapyrazole: BBR 342244Abbreviations: MDR, Multidrug Resistance; NHS-ASA, N-Hydroxysuccinimidyl-4-Azidosalicylic Acid; SRB, Sulforhodomine B; and P-Gp, P-Glycoprotein. *Biochem. Pharmacol.* 62 (10), 1337–1343. doi:10.1016/s0006-2952(01)00797-3

Collins, G. A., and Goldberg, A. L. (2020). Proteins Containing Ubiquitin-like (Ubl) Domains Not Only Bind to 26S Proteasomes but Also Induce Their Activation. *Proc. Natl. Acad. Sci. USA* 117 (9), 4664–4674. doi:10.1073/pnas.1915534117

Dasari, S., and Bernard Tchounwou, P. (2014). Cisplatin in Cancer Therapy: Molecular Mechanisms of Action. *Eur. J. Pharmacol.* 740, 364–378. doi:10.1016/j.ejphar.2014.07.025

De Duve, C., Poole, T. B., Trouet, A., Tulkens, P., and Van Hoof, F. (1974). Commentary. Lysosomotropic Agents. *Biochem. Pharmacol.* 23 (18), 2495–2531. doi:10.1016/0006-2952(74)90174-9

Demishtein, A., Fraiberg, M., Berko, D., Tirosh, B., Elazar, Z., and Navon, A. (2017). SQSTM1/P62-Mediated Autophagy Compensates for Loss of Proteasome Polyubiquitin Recruiting Capacity. *Autophagy* 13 (10), 1697–1708. doi:10.1080/15548627.2017.1356549

Feldman, D., Swarm, R. L., and Becker, J. (1981). *Ultrastructural Study of Rat Liver and Liver Neoplasms after Long-Term Treatment with Phenobarbital*. London, United Kingdom: Cancer Research 41 (6), 2151–2162.

Fingar, D. C., Salama, S., Tsou, C., Harlow, E., and Blenis, J. (2002). Mammalian Cell Size Is Controlled by mTOR and its Downstream Targets S6K1 and 4EBP1/eIF4E. *Genes Dev.* 16 (12), 1472–1487. doi:10.1101/gad.995802

Fregno, Ilaria., (2018). ER to Lysosome Associated Degradation of Proteasome Resistant ATZ Polymers Occurs via Receptor Mediated Vesicular Transport. *EMBO J.* 37 (17). doi:10.15252/embj.201899259

Fregno, I., and Molinari, M. (2019). Proteasomal and Lysosomal Clearance of Faulty Secretory Proteins: ER-Associated Degradation (ERAD) and ER-To-Lysosome-Associated Degradation (ERLAD) Pathways. *Crit. Rev. Biochem. Mol. Biol.* 54 (2), 153–163. doi:10.1080/10409238.2019.1610351

Friedman, J. R., DiBenedetto, J. R., West, M., Rowland, A. A., and Voeltz, G. K. (2013). Endoplasmic Reticulum-Endosome Contact Increases as Endosomes Traffic and Mature. *MBoC* 24 (7), 1030–1040. doi:10.1091/mbc.e12-10-0733

Golebiowski, F., Matic, I., Tatham, M. H., Cole, C., Yin, Y., Nakamura, A., et al. (2009). System-Wide Changes to Sumo Modifications in Response to Heat Shock. *Sci. Signal.* 2 (72), ra24. doi:10.1126/scisignal.2000282

González, A. E., Muñoz, V. C., Cavieres, V. A., Bustamante, H. A., Cornejo, V. H., Januário, Y. C., et al. (2017). Autophagosomes Cooperate in the Degradation of Intracellular C-Terminal Fragments of the Amyloid Precursor Protein via the MVB/Lysosomal Pathway. *FASEB J.* 31 (6), 2446–2459. doi:10.1096/fj.201600713R

Griffiths, G., Hoflack, B., Simons, K., Mellman, I., and Kornfeld, S. (1988). The Mannose 6-Phosphate Receptor and the Biogenesis of Lysosomes. *Cell* 52 (3), 329–341. doi:10.1016/s0092-8674(88)80026-6

Grumati, P., Dikic, I., and Stolz, A. (2018). ER-phagy at a Glance. *J. Cel Sci* 131 (17). doi:10.1242/jcs.217364

Guarascio, R., Salih, D., Yasvoina, M., Edwards, F. A., Cheetham, M. E., and van der Spuy, J. (2020). Negative Regulator of Ubiquitin-like Protein 1 Modulates the Autophagy-Lysosomal Pathway via P62 to Facilitate the Extracellular Release of Tau Following Proteasome Impairment. *Hum. Mol. Genet.* 29 (1), 80–96. doi:10.1093/hmg/ddz255

Harding, H. P., Novoa, I., Zhang, Y., Zeng, H., Wek, R., Schapira, M., et al. (2000). Regulated Translation Initiation Controls Stress-Induced Gene Expression in Mammalian Cells. *Mol. Cel* 6 (5), 1099–1108. doi:10.1016/s1097-2765(00)00108-8

Harding, H. P., Zhang, Y., Bertolotti, A., Zeng, H., and Ron, D. (2000). Perk Is Essential for Translational Regulation and Cell Survival during the Unfolded Protein Response. *Mol. Cel* 5 (5), 897–904. doi:10.1016/s1097-2765(00)80330-5

Hartmann-Petersen, R., and Gordon, C. (2004a). Integral UBL Domain Proteins: A Family of Proteasome Interacting Proteins. *Semin. Cel Dev. Biol.* 15 (2), 247–259. doi:10.1016/j.semcdb.2003.12.006

Hartmann-Petersen, R., and Gordon, C. (2004b). Ubiquitin-Proteasome System. *Cell Mol. Life Sci.* 61 (13). doi:10.1007/s00018-004-4132-x

Heifetz, A., Keenan, R. W., and Elbein, A. D. (1979). Mechanism of Action of Tunicamycin on the UDP-GlcNAc:dolichyl-Phosphate GlcNAc-1-Phosphate Transferase. *Biochemistry* 18 (11), 2186–2192. doi:10.1021/bi00578a008

Henne, W. M. (2017). Discovery and Roles of ER-Endolysosomal Contact Sites in Disease. *Adv. Exp. Med. Biol.* 997, 135–147. doi:10.1007/978-981-10-4567-7

Huber, M. D., and Gerace., L. (2007). The Size-Wise Nucleus: Nuclear Volume Control in Eukaryotes. *J. Cel Biol.* 179 (4), 583–584. doi:10.1083/jcb.200710156

Jackson, M. P., and Hewitt, E. W. (2016). Cellular Proteostasis: Degradation of Misfolded Proteins by Lysosomes. *Essays Biochem.* 60 (2), 173–180. doi:10.1042/ebc20160005

Jia, R., and Bonifacino, J. S. (2019). Negative Regulation of Autophagy by UBA6-BIRC6-Mediated Ubiquitination of LC3. *Elife* 8. doi:10.7554/eLife.50034

Jin, S. M., and Youle, R. J. (2012). PINK1- and Parkin-Mediated Mitophagy at a Glance. *J. Cel Sci.* 125 (4), 795–799. doi:10.1242/jcs.093849

Jung, H. S., Chung, K. W., Won Kim, J., Kim, J., Komatsu, M., Tanaka, K., et al. (2008). Loss of Autophagy Diminishes Pancreatic β Cell Mass and Function with Resultant Hyperglycemia. *Cel Metab.* 8 (4), 318–324. doi:10.1016/j.cmet.2008.08.013

Khaminets, A., Behl, C., and Dikic, I. (2016). Ubiquitin-Dependent and Independent Signals in Selective Autophagy. *Trends Cel Biol.* 26 (1), 6–16. doi:10.1016/j.tcb.2015.08.010

Khaminets, A., Heinrich, T., Mari, M., Grumati, P., Huebner, A. K., Akutsu, M., et al. (2015). Regulation of Endoplasmic Reticulum Turnover by Selective Autophagy. *Nature* 522 (7556), 354–358. doi:10.1038/nature14498

Kim, E., Park, S., Lee, J. H., Mun, J. Y., Choi, W. H., Yun, Y., et al. (2018). Dual Function of USP14 Deubiquitinase in Cellular Proteasomal Activity and Autophagic Flux. *Cel Rep.* 24 (3), 732–743. doi:10.1016/j.celrep.2018.06.058

Kim, H. T., and Goldberg, A. L. (2018). UBL Domain of Usp14 and Other Proteins Stimulates Proteasome Activities and Protein Degradation in Cells. *Proc. Natl. Acad. Sci. USA* 115 (50), E11642–E11650. doi:10.1073/pnas.1808731115

Kim, T.-Y., Kim, E., Yoon, S. K., and Yoon, J.-B., (2008). Herp Enhances ER-Associated Protein Degradation by Recruiting Ubiquilins. *Biochem. Biophysical Res. Commun.* 369 (2), 741–746. doi:10.1016/j.bbrc.2008.02.086

Kokame, K., Agarwala, K. L., Kato, H., and Miyata, T. (2000). Herp, a New Ubiquitin-like Membrane Protein Induced by Endoplasmic Reticulum Stress. *J. Biol. Chem.* 275 (42), 32846–32853. doi:10.1074/jbc.m002063200

Kokame, K., Kato, H., and Miyata, T. (2001). Identification of ERSE-II, a New Cis-Acting Element Responsible for the ATF6-dependent Mammalian Unfolded Protein Response. *J. Biol. Chem.* 276 (12), 9199–9205. doi:10.1074/jbc.m010486200

Kondapalli, C., Kazlauskaite, A., Zhang, N., Woodroof, H. I., Campbell, D. G., Gourlay, R., et al. (2012). PINK1 Is Activated by Mitochondrial Membrane Potential Depolarization and Stimulates Parkin E3 Ligase Activity by Phosphorylating Serine 65. *Open Biol.* 2 (MAY), 120080. doi:10.1098/rsob.120080

Korolchuk, V. I., Menzies, F. M., and Rubinsztein, D. C. (2010). Mechanisms of Cross-Talk between the Ubiquitin-Proteasome and Autophagy-Lysosome Systems. *FEBS Lett.* 584 (7), 1393–1398. doi:10.1016/j.febslet.2009.12.047

Koyano, F., Okatsu, K., Kosako, H., Tamura, Y., Go, E., Kimura, M., et al. (2014). Ubiquitin Is Phosphorylated by PINK1 to Activate Parkin. *Nature* 510 (7503), 162–166. doi:10.1038/nature13392

Lee, C. A., and Blackstone, C. (2020). ER Morphology and Endo-Lysosomal Crosstalk: Functions and Disease Implications. *Biochim. Biophys. Acta Mol. Cel Biol Lipids* 1865 (1), 158544. doi:10.1016/j.bbalip.2019.158544

Lee, D. H., and Goldberg, A. L. (1998). Proteasome Inhibitors: Valuable New Tools for Cell Biologists. *Trends Cel Biol.* 8 (10), 397–403. doi:10.1016/s0962-8924(98)01346-4

Leitman, J., Shenkman, M., Gofman, Y., Shtern, N. O., Ben-Tal, N., Hendershot, L. M., et al. (2014). Herp Coordinates Compartmentalization and Recruitment of HRD1 and Misfolded Proteins for ERAD. *MBoC* 25 (7), 1050–1060. doi:10.1091/mbc.e13-06-0350

Liao, Y., Duan, B., Zhang, Y., Zhang, X., and Xia, B. (2019). Excessive ER-Phagy Mediated by the Autophagy Receptor FAM134B Results in ER Stress, the Unfolded Protein Response, and Cell Death in HeLa Cells. *J. Biol. Chem.* 294 (52), 20009–20023. doi:10.1074/jbc.ra119.008709

Marzec, M., Eletto, D., and Argon, Y. (2012). GRP94: An HSP90-like Protein Specialized for Protein Folding and Quality Control in the Endoplasmic Reticulum. *Biochim. Biophys. Acta (Bba) - Mol. Cel Res.* 1823 (3), 774–787. doi:10.1016/j.bbamcr.2011.10.013

Mejlvang, J., Olsvik, H., Svenning, S., Bruun, J.-A., Abudu, Y. P., Larsen, K. B., et al. (2018). Starvation Induces Rapid Degradation of Selective Autophagy Receptors by Endosomal Microautophagy. *J. Cel Biol.* 217 (10), 3640–3655. doi:10.1083/jcb.201711002

Miettinen, T. P., and Björklund, M. (2015). Mevalonate Pathway Regulates Cell Size Homeostasis and Proteostasis through Autophagy. *Cel Rep.* 13 (11), 2610–2620. doi:10.1016/j.celrep.2015.11.045

Miura, H., Hashida, K., Sudo, H., Awa, Y., Takarada-Iemata, M., Kokame, K., et al. (2010). Deletion of Herp Facilitates Degradation of Cytosolic Proteins. *Genes Cells* 15 (8), 843–853. doi:10.1111/j.1365-2443.2010.01422.x

Mizushima, N., Levine, B., Cuervo, A. M., and Klionsky, D. J. (2008). Autophagy Fights Disease through Cellular Self-Digestion. *Nature* 451 (7182), 1069–1075. doi:10.1038/nature06639

Mizushima, N., Yoshimori, T., and Ohsumi, Y. (2011). The Role of Atg Proteins in Autophagosome Formation. *Annu. Rev. Cel Dev. Biol.* 27, 107–132. doi:10.1146/annurev-cellbio-092910-154005

Mollazadeh, H., Atkin, S. L., Butler, A. E., Ruscica, M., Sirtori, C. R., and Sahebkar, A. (2018). The Effect of Statin Therapy on Endoplasmic Reticulum Stress. *Pharmacol. Res.* 137, 150–158. doi:10.1016/j.phrs.2018.10.006

Moreau, K., Luo, S., and Rubinsztein, D. C. (2010). Cytoprotective Roles for Autophagy. *Curr. Opin. Cel Biol.* 22 (2), 206–211. doi:10.1016/j.ceb.2009.12.002

Murrow, L., and Debnath, J. (2013). Autophagy as a Stress-Response and Quality-Control Mechanism: Implications for Cell Injury and Human Disease. *Annu. Rev. Pathol. Mech. Dis.* 8, 105–137. doi:10.1146/annurev-pathol-020712-163918

Neefjes, J., Jongsma, M. M. L., and Berlin, I. (2017). Stop or Go? Endosome Positioning in the Establishment of Compartment Architecture, Dynamics, and Function. *Trends Cel Biol.* 27 (8), 580–594. doi:10.1016/j.tcb.2017.03.002

Ou, W.-J., Bergeron, J. J. M., Li, Y., Kang, C. Y., and Thomas, D. Y. (1995). Conformational Changes Induced in the Endoplasmic Reticulum Luminal Domain of Calnexin by Mg-ATP and Ca2+. *J. Biol. Chem.* 270 (30), 18051–18059. doi:10.1074/jbc.270.30.18051

Pathak, R. K., Luskey, K. L., and Anderson, R. G. (1986). Biogenesis of the Crystalloid Endoplasmic Reticulum in UT-1 Cells: Evidence that Newly Formed Endoplasmic Reticulum Emerges from the Nuclear Envelope. *J. Cel. Biol.* 102 (6), 2158–2168. doi:10.1083/jcb.102.6.2158

Quiroga, C., Gatica, D., Paredes, F., Bravo, R., Troncoso, R., Pedrozo, Z., et al. (2013). Herp Depletion Protects from Protein Aggregation by Up-Regulating Autophagy. *Biochim. Biophys. Acta (Bba) - Mol. Cel Res.* 1833 (12), 3295–3305. doi:10.1016/j.bbamcr.2013.09.006

Rothenberg, C., Srinivasan, D., Mah, L., Kaushik, S., Peterhoff, C. M., Ugolino, J., et al. (2010). Ubiquilin Functions in Autophagy and Is Degraded by Chaperone-Mediated Autophagy. *Hum. Mol. Genet.* 19 (16), 3219–3232. doi:10.1093/hmg/ddq231

Sai, X., Kokame, K., Shiraishi, H., Kawamura, Y., Miyata, T., Yanagisawa, K., et al. (2003). The Ubiquitin-like Domain of Herp Is Involved in Herp Degradation, but Not Necessary for its Enhancement of Amyloid Beta-Protein Generation. *FEBS Lett.* 553 (1–2), 151–156. doi:10.1016/s0014-5793(03)01009-3

Sauvé, V., Sung, G., Soya, N., Kozlov, G., Blaimschein, N., Miotto, L. S., et al. (2018). Mechanism of Parkin Activation by Phosphorylation. *Nat. Struct. Mol. Biol.* 25 (7), 623–630. doi:10.1038/s41594-018-0088-7

Schindelin, J., Arganda-Carreras, I., Frise, E., Kaynig, V., Longair, M., Pietzsch, T., et al. (2012). Fiji: An Open-Source Platform for Biological-Image Analysis. *Nat. Methods* 9 (7), 676–682. doi:10.1038/nmeth.2019

Schuck, S., Prinz, W. A., Thorn, K. S., Voss, C., and Walter, P. (2009). Membrane Expansion Alleviates Endoplasmic Reticulum Stress Independently of the Unfolded Protein Response. *J. Cel Biol.* 187 (4), 525–536. doi:10.1083/jcb.200907074

Schulz, J., Avci, D., Queisser, M. A., Gutschmidt, A., Dreher, L. S., Fenech, E. J., et al. (2017). Conserved Cytoplasmic Domains Promote Hrd1 Ubiquitin Ligase Complex Formation for ER-Associated Degradation (ERAD). *J. Cel Sci* 130 (19), 3322–3335. doi:10.1242/jcs.206847

Schulze, A., Standera, S., Buerger, E., Kikkert, M., van Voorden, S., Wiertz, E., et al. (2005). The Ubiquitin-Domain Protein HERP Forms a Complex with Components of the Endoplasmic Reticulum Associated Degradation Pathway. *J. Mol. Biol.* 354 (5), 1021–1027. doi:10.1016/j.jmb.2005.10.020

Sebti, S., Prebois, C., Perez-Gracia, E., Bauvy, C., Desmots, F., Pirot, N., et al. (2014). BAT3 Modulates P300-dependent Acetylation of P53 and Autophagy-Related Protein 7 (ATG7) during Autophagy. *Proc. Natl. Acad. Sci.* 111 (11), 4115–4120. doi:10.1073/pnas.1313618111

Sentürk, M., Lin, G., Zuo, Z., Mao, D., Watson, E., and Mikos, A. G., (2019). Ubiquilins Regulates Autophagic Flux through MTOR Signalling and Lysosomal Acidification. *Nat. Cel Biol.* 21 (3), 384–396. doi:10.1038/s41556-019-0281-x

Shi, X., Han, L., Sun, T., Zhang, F., Ji, S., Zhang, M., et al. (2020). Silencing UHRF1 Enhances Cell Autophagy to Prevent Articular Chondrocytes from Apoptosis in Osteoarthritis through PI3K/AKT/MTOR Signaling Pathway. *Biochem. Biophysical Res. Commun.* 529 (4), 1018–1024. doi:10.1016/j.bbrc.2020.06.032

Skehel, P. A., Fabian-Fine, R., and Kandel, E. R. (2000). Mouse VAP33 Is Associated with the Endoplasmic Reticulum and Microtubules. *Proc. Natl. Acad. Sci.* 97 (3), 1101–1106. doi:10.1073/pnas.97.3.1101

Swaney, D. L., Rodríguez Mias, R. A., and Villén, J. (2015). Phosphorylation of Ubiquitin at Ser65 Affects its Polymerization, Targets, and Proteome Wide Turnover. *EMBO Rep.* 16 (9), 1131–1144. doi:10.15252/embr.201540298

Tanida, I., Ueno, T., and Kominami, E. (2008). LC3 and Autophagy. *Methods Mol. Biol.* 445, 77–88. doi:10.1007/978-1-59745-157-4_4

Tapia, D., Jiménez, T., Zamora, C., Espinoza, J., Rizzo, R., González-Cárdenas, A., et al. (2019). KDEL Receptor Regulates Secretion by Lysosome Relocation- and Autophagy-dependent Modulation of Lipid-Droplet Turnover. *Nat. Commun.* 10 (1), 735. doi:10.1038/s41467-019-08501-w

Thastrup, O., Cullen, P. J., Drøbak, B. K., Hanley, M. R., and Dawson, A. P. (1990). Thapsigargin, a Tumor Promoter, Discharges Intracellular Ca2+ Stores by Specific Inhibition of the Endoplasmic Reticulum Ca2(+)-ATPase. *Proc. Natl. Acad. Sci. U S A.* 87 (7), 2466–2470. doi:10.1073/pnas.87.7.2466

Thayer, J. A., Awad, O., Hegdekar, N., Sarkar, C., Tesfay, H., Burt, C., et al. (2020). The PARK10 Gene USP24 Is a Negative Regulator of Autophagy and ULK1 Protein Stability. *Autophagy* 16 (1), 140–153. doi:10.1080/15548627.2019.1598754

Toledo Pinto, T. G., Batista-Silva, L. R., , Medeiros, R. C. A., Lara, F. A., and Moraes, M. O. (2018). Type I Interferons, Autophagy and Host Metabolism in Leprosy. *Front. Immunol.* 9, 806. doi:10.3389/fimmu.2018.00806

Toulmay, A., and Prinz, W. A. (2011). Lipid Transfer and Signaling at Organelle Contact Sites: The Tip of the Iceberg. *Curr. Opin. Cel Biol.* 23 (4), 458–463. doi:10.1016/j.ceb.2011.04.006

Tsubuki, S., Saito, Y., Tomioka, M., Ito, H., and Kawashima, S. (1996). Differential Inhibition of Calpain and Proteasome Activities by Peptidyl Aldehydes of Di-leucine and Tri-leucine. *J. Biochem.* 119 (3), 572–576. doi:10.1093/oxfordjournals.jbchem.a021280

Vabulas, R. M., and Hartl, F. U. (2005). Protein Synthesis upon Acute Nutrient Restriction Relies on Proteasome Function. *Science* 310 (5756), 1960–1963. doi:10.1126/science.1121925

Valm, A. M., Cohen, S., Legant, W. R., Melunis, J., Hershberg, U., Wait, E., et al. (2017). Applying Systems-Level Spectral Imaging and Analysis to Reveal the Organelle Interactome. *Nature* 546 (7656), 162–167. doi:10.1038/nature22369

Van Der Laan, S. W., Harshfield, E. L., Hemerich, D., Stacey, D., Wood, A. M., and Asselbergs, F. W. (2018). From Lipid Locus to Drug Target through Human Genomics. *Cardiovasc. Res.* 114 (9), 1258–1270. doi:10.1093/cvr/cvy120

VerPlank, J. J. S., Lokireddy, S., Zhao, J., and Goldberg, A. L. (2019). 26S Proteasomes Are Rapidly Activated by Diverse Hormones and Physiological States that Raise CAMP and Cause Rpn6 Phosphorylation. *Proc. Natl. Acad. Sci. USA* 116 (10), 4228–4237. doi:10.1073/pnas.1809254116

Walczak, M., and Martens., S. (2013). Dissecting the Role of the Atg12-Atg5-Atg16 Complex during Autophagosome Formation. *Autophagy* 9 (3), 424–425. doi:10.4161/auto.22931

Wauer, T., Swatek, K. N., Wagstaff, J. L., Gladkova, C., Pruneda, J. N., Michel, M. A., et al. (2015). Ubiquitin Ser65 Phosphorylation Affects Ubiquitin Structure, Chain Assembly and Hydrolysis. *Embo J.* 34 (3), 307–325. doi:10.15252/embj.201489847

Wiest, D. L., Burkhardt, J. K., Hester, S., Hortsch, M., Meyer, D. I., and Argon, Y. (1990). Membrane Biogenesis during B Cell Differentiation: Most Endoplasmic Reticulum Proteins Are Expressed Coordinately. *J. Cel Biol.* 110 (5), 1501–1511. doi:10.1083/jcb.110.5.1501

Wu, Y., Ma, C., Zhao, H., Zhou, Y., Chen, Z., and Wang, L. (2018). Alleviation of Endoplasmic Reticulum Stress Protects against Cisplatin-Induced Ovarian Damage. *Reprod. Biol. Endocrinol.* 16 (1), 85. doi:10.1186/s12958-018-0404-4

Xu, F., Du, W., Zou, Q., Wang, Y., Zhang, X., Xing, X., et al. (2021). COPII Mitigates ER Stress by Promoting Formation of ER Whorls. *Cell Res* 31 (2), 141–156. doi:10.38/s41422-020-00416-2

Xu, H., and Ren, D. (2015). Lysosomal Physiology. *Annu. Rev. Physiol.* 77, 57–80. doi:10.1146/annurev-physiol-021014-071649

Yan, L., Liu, W., Zhang, H., Liu, C., Shang, Y., Ye, Y., et al. (2014). Ube2g2-Gp78-Mediated HERP Polyubiquitylation Is Involved in ER Stress Recovery. *J. Cel Sci* 127 (7), 1417–1427. doi:10.1242/jcs.135293

Yang, H., Ni, H.-M., Guo, F., Ding, Y., Shi, Y.-H., Lahiri, P., et al. (2016). Sequestosome 1/P62 Protein Is Associated with Autophagic Removal of Excess Hepatic Endoplasmic Reticulum in Mice. *J. Biol. Chem.* 291 (36), 18663–18674. doi:10.1074/jbc.m116.739821

Yang, Y., and Klionsky, D. J. (2020). A Novel Role of UBQLNs (Ubiquilins) in Regulating Autophagy, MTOR Signaling and V-ATPase Function. *Autophagy* 16 (1), 1–2. doi:10.1080/15548627.2019.1665293

Yin, Y., Seifert, A., Chua, J. S., Maure, J.-F., Golebiowski, F., and Hay, R. T. (2012). SUMO-targeted Ubiquitin E3 Ligase RNF4 Is Required for the Response of Human Cells to DNA Damage. *Genes Dev.* 26 (11), 1196–1208. doi:10.1101/gad.189274.112

Yoshida, H., Matsui, T., Yamamoto, A., Okada, T., and Mori, K. (2001). XBP1 MRNA Is Induced by ATF6 and Spliced by IRE1 in Response to ER Stress to Produce a Highly Active Transcription Factor. *Cell* 107 (7), 881–891. doi:10.1016/s0092-8674(01)00611-0

Yoshii, S. R., Kuma, A., Akashi, T., Hara, T., Yamamoto, A., Kurikawa, Y., et al. (2016). Systemic Analysis of Atg5-Null Mice Rescued from Neonatal Lethality by Transgenic ATG5 Expression in Neurons. *Dev. Cel.* 39 (1), 116–130. doi:10.1016/j.devcel.2016.09.001

Yu, H., and Matouschek, A. (2017). Recognition of Client Proteins by the Proteasome. *Annu. Rev. Biophys.* 46, 149–173. doi:10.1146/annurev-biophys-070816-033719

Zhang, T., Lu, D., Yang, W., Shi, C., Zang, J., Shen, L., et al. (2018). HMG-CoA Reductase Inhibitors Relieve Endoplasmic Reticulum Stress by Autophagy Inhibition in Rats with Permanent Brain Ischemia. *Front. Neurosci.* 12 (JUN), 405. doi:10.3389/fnins.2018.00405

Zhang, Youzhi. (2020). Simvastatin Improves Lysosome Function via Enhancing Lysosome Biogenesis in Endothelial Cells. *Front. Biosci. - Landmark* 25 (2), 283–298. doi:10.2741/4807

Zhu, K., Dunner, K., and McConkey, D. J. (2010). Proteasome Inhibitors Activate Autophagy as a Cytoprotective Response in Human Prostate Cancer Cells. *Oncogene* 29 (3), 451–462. doi:10.1038/onc.2009.343

Conflict of Interest: The authors declare that the research was conducted in the absence of any commercial or financial relationships that could be construed as a potential conflict of interest.

Publisher's Note: All claims expressed in this article are solely those of the authors and do not necessarily represent those of their affiliated organizations or those of the publisher, the editors, and the reviewers. Any product that may be evaluated in this article, or claim that may be made by its manufacturer, is not guaranteed or endorsed by the publisher.

frontiers in Cell and Developmental Biology

ORIGINAL RESEARCH
published: 04 March 2022
doi: 10.3389/fcell.2022.837574

Efficient Cholesterol Transport in Dendritic Cells Defines Optimal Exogenous Antigen Presentation and Toxoplasma gondii Proliferation

*Cristina Croce[1], Facundo Garrido[1], Sofía Dinamarca[1], Julien Santi-Rocca[2], Sabrina Marion[3], Nicolas Blanchard[2], Luis S. Mayorga[1,4] and Ignacio Cebrian[1]**

[1]Instituto de Histología y Embriología de Mendoza (IHEM) - Universidad Nacional de Cuyo - CONICET, Mendoza, Argentina, [2]Institut Toulousain des Maladies Infectieuses et Inflammatoires (Infinity), Inserm/CNRS/Université Toulouse 3, Toulouse, France, [3]CNRS, Inserm, CHU Lille, U1019 - UMR 9017 - CIIL - Center for Infection and Immunity of Lille, Institut Pasteur de Lille, Université de Lille, Lille, France, [4]Facultad de Ciencias Exactas y Naturales, Universidad Nacional de Cuyo, Mendoza, Argentina

Dendritic cells are the most powerful antigen-presenting cells of the immune system. They present exogenous antigens associated with Major Histocompatibility Complex (MHC) Class II molecules through the classical pathway to stimulate CD4+ T cells, or with MHC-I to activate CD8+ T lymphocytes through the cross-presentation pathway. DCs represent one of the main cellular targets during infection by *Toxoplasma gondii*. This intracellular parasite incorporates essential nutrients, such as cholesterol, to grow and proliferate inside a highly specialized organelle, the parasitophorous vacuole (PV). While doing so, *T. gondii* modulates the host immune response through multiple interactions with proteins and lipids. Cholesterol is an important cellular component that regulates cellular physiology at the structural and functional levels. Although different studies describe the relevance of cholesterol transport for exogenous antigen presentation, the molecular mechanism underlying this process is not defined. Here, we focus our study on the inhibitor U18666A, a drug widely used to arrest multivesicular bodies biogenesis that interrupts cholesterol trafficking and changes the lipid composition of intracellular membranes. Upon bone marrow-derived DC (BMDC) treatment with U18666A, we evidenced a drastic disruption in the ability to present exogenous soluble and particulate antigens to CD4+ and CD8+ T cells. Strikingly, the presentation of *T. gondii*-associated antigens and parasite proliferation were hampered in treated cells. However, neither antigen uptake nor BMDC viability was significantly affected by the U18666A treatment. By contrast, this drug altered the transport of MHC-I and MHC-II molecules to the plasma membrane. Since U18666A impairs the formation of MVBs, we analyzed in *T. gondii* infected BMDCs the ESCRT machinery responsible for the generation of intraluminal vesicles. We observed that different MVBs markers, including ESCRT proteins, were recruited to the PV. Surprisingly, the main ESCRT-III component CHMP4b was massively recruited to the PV, and its expression level was upregulated upon BMDC infection by *T. gondii*. Finally, we demonstrated that BMDC treatment with U18666A interrupted cholesterol delivery and CHMP4b recruitment to the PV, which interfered with an efficient parasite replication.

OPEN ACCESS

Edited by:
Carlos Enrich,
University of Barcelona, Spain

Reviewed by:
Elodie Segura,
Institut Curie, France
Andrea Raimondi,
San Raffaele Hospital (IRCCS), Italy

***Correspondence:**
Ignacio Cebrian
icebrian@mendoza-conicet.gob.ar
orcid.org/0000-0001-6505-0875

Specialty section:
This article was submitted to Membrane Traffic, a section of the journal Frontiers in Cell and Developmental Biology

Received: *16 December 2021*
Accepted: *10 February 2022*
Published: *04 March 2022*

Citation:
Croce C, Garrido F, Dinamarca S, Santi-Rocca J, Marion S, Blanchard N, Mayorga LS and Cebrian I (2022) Efficient Cholesterol Transport in Dendritic Cells Defines Optimal Exogenous Antigen Presentation and Toxoplasma gondii Proliferation. Front. Cell Dev. Biol. 10:837574. doi: 10.3389/fcell.2022.837574

Altogether, our results highlight the importance of cholesterol trafficking and MVBs formation in DCs for optimal antigen presentation and *T. gondii* proliferation.

Keywords: dendritic cells, cholesterol, intraluminal vesicles, multivesicular bodies, CHMP4b, *Toxoplasma gondii*, antigen presentation, U18666A inhibitor

INTRODUCTION

Dendritic cells (DCs) are considered the most potent antigen presenting cells of the immune system. They present exogenous antigens on Major Histocompatibility Complex (MHC) class II molecules through the classical pathway to stimulate CD4+ T lymphocytes, or on MHC-I to activate CD8+ T cells through the cross-presentation pathway (Nutt and Chopin, 2020). On the one hand, newly synthesized MHC-II molecules associate with the invariant chain (Ii) in the ER, stabilizing the complex and preventing premature peptide binding. The cytoplasmic domain of Ii allows the translocation of the MHC-II/Ii complex from the Golgi to the endocytic network (Jurewicz and Stern, 2019). In this way, it reaches the MIIC compartment, where the requested proteins for efficient peptide loading are present (Rocha and Neefjes, 2008). MIIC compartments exhibit late endosomes characteristics (CD63+ and Lamp1+; Calafat et al., 1994), and there Ii is partially degraded, leaving a residual peptide attached to the peptide-binding site (CLIP) (Romagnoli and Germain, 1994). Moreover, MIIC compartments associate to other vesicles of the endocytic system, promoting the encounter with peptides derived from internalized antigens. The MIIC resident chaperone HLA-DM mediates the exchange of CLIP for the antigenic peptide (Jurewicz and Stern, 2019). Finally, MHC-II/peptide complexes reach the plasma membrane localizing at cholesterol-enriched domains (Bosch et al., 2013b).

On the other hand, during cross-presentation exogenous antigens uptaken by DCs are first partially degraded in the endocytic network, and then translocated to the cytosol, where they are further degraded by the proteasome (Kotsias et al., 2019). The generated peptides enter cross-presenting compartments to meet and be loaded onto MHC-I molecules. The intracellular source of MHC-I molecules for cross-presentation is still matter of debate, but different studies highlight the importance of the MHC-I pool present in the endocytic recycling compartment (ERC) (Nair-Gupta et al., 2014; Cebrian et al., 2016). There is also evidence about the interaction between MHC-I and Ii that impacts on cross-presentation, which is suggested to mediate the arrival of newly synthesized MHC-I to the endocytic network without affecting recycling (Basha et al., 2012). The specific location and intracellular compartment required for MHC-I/peptide complex formation is not fully defined (Blander, 2018), and this represents a key question in the field.

Cholesterol is an important component of biological membranes, being crucial both for maintaining their structure and for signaling events. Most of the cellular cholesterol is found in microdomains of the plasma membrane, called lipid rafts (Fessler, 2015). Lipid rafts serve as platforms where certain receptors and membrane proteins, such as MHC molecules, are grouped. An important role for lipid rafts grouping MHC-II/peptide complexes in order to activate immune responses was shown (Bosch et al., 2013b). Moreover, there is a cholesterol-binding site in the transmembrane domain of MHC-II, which allosterically modulates the loading of antigenic peptides, and contributes to the stabilization of MHC-II/peptide complexes at the plasma membrane (Roy et al., 2013). However, the role of cholesterol trafficking during MHC-II antigen presentation is not clearly defined yet. Regarding cross-presentation, it was reported that cationic lipids contribute to regulate antigen degradation by increasing the phagosomal pH (Gao et al., 2017). Furthermore, cholesterol depletion with lovastatin reduces macropinocytosis, and affects the cross-presentation ability of DCs (Albrecht et al., 2006). Increase in lipid bodies in IFNγ-activated DCs was found to correlate with improved cross-presentation efficacy (Bougnères et al., 2009; den Brok et al., 2016), although the underlying mechanism has not been identified.

Toxoplasma gondii is an obligate intracellular parasite that efficiently infects DCs, which are then instrumental in presenting parasite antigens to prime *T. gondii*-specific T cell responses (Mashayekhi et al., 2011; Dupont et al., 2014). After infection, the parasite remains confined inside a parasitophorous vacuole (PV), which is actively remodeled. From this niche, the parasite establishes several interactions with the host cell in order to optimally replicate (Coppens and Romano, 2018). In this sense, *T. gondii* is capable of incorporating cholesterol and fatty acids from endolysosomes and lipid droplets (LDs). Indeed, *T. gondii* replication is inhibited by disrupting cholesterol transport (Coppens et al., 2000). Other studies show that the cholesterol level in the host cell impacts on *T. gondii* replication (Bottova et al., 2009; Hu et al., 2017; Nolan et al., 2017; Sanfelice et al., 2017). Moreover, the complexity of parasite-host interactions and their impact on the modulation of antigen presentation (Poncet et al., 2019), make *T. gondii* an interesting model of study. For example, the relevance of Sec22b in driving retrotranslocation of *T. gondii*-derived antigens from the PV lumen to the host cytosol, mediating the ER-associated degradation machinery recruitment, has been demonstrated (Cebrian et al., 2011). However, membrane-associated antigen cross-presentation has been shown to be independent of Sec22b, suggesting that the biochemical nature of the antigens and their disposition in the PV determines their processing pathway (Buaillon et al., 2017). Furthermore, the interaction with recycling endosomes, mediated by Rab22a, has also been shown to be necessary for efficient cross-presentation (Cebrian et al., 2016). Regarding the presentation of antigens in MHC-II, this pathway seems important to keep parasite proliferation under control and develop the chronic phase of infection (Leroux et al., 2015), but the mechanism by which *T. gondii*-derived antigens reach degradative compartments to be presented by MHC-II, it has not been

completely defined (Poncet et al., 2019). The complexity of host-parasite interactions demands new approaches to understand how *T. gondii* modulates the functions of DCs.

In this work, we studied the impact of cholesterol trafficking on MHC-I and MHC-II antigen presentation. For this, we used the inhibitor U18666A, which interrupts the intracellular traffic of cholesterol by blocking the function of the NPC1 protein, leading to cholesterol accumulation in the endolysosomal compartments (Lu et al., 2015). We show that both MHC-II presentation and MHC-I cross-presentation were strongly disrupted in the presence of the inhibitor. Strikingly, the inhibitor not only blocks the presentation of *T. gondii*-associated antigens but also parasite proliferation. By EM analyzes, we observed intraluminal vesicles in the PVs. Since MVB biogenesis is inhibited by U18666A (Cenedella, 2009), we analyzed in *T. gondii* infected BMDCs the ESCRT machinery responsible for the generation of intraluminal vesicles. We observed that the main ESCRT-III component CHMP4b was massively recruited to the PV, and its expression level was upregulated upon *T. gondii* infection. U18666A treatment disrupted both the delivery of cholesterol and the recruitment of CHMP4b to the PV. Taken together, these results suggest an important role of cholesterol trafficking in antigen presentation, and on the proliferation of *T. gondii* within a functional PV.

MATERIALS AND METHODS

Cells

C57BL/6 mice from 6 to 10 weeks of age were used to obtain bone marrow stem cells from the femur and tibia. Animals were maintained in specific pathogen-free conditions (SPF), housed in temperature-controlled rooms (22–25°C), and received water and food *ad libitum*. All animal procedures were performed according to the bioethics rules of the "Comité Institucional para el Cuidado y Uso de Animales de Laboratorio (CICUAL), Facultad de Ciencias Médicas, Universidad Nacional de Cuyo". Cells were maintained in IMDM medium supplemented with 10% FBS and GM-CSF-containing supernatant to stimulate bone marrow-derived dendritic cell (BMDC) differentiation. After 9–14 days, immature BMDCs were used for experimental work. The GM-CSF-producing cell line J558 was kindly provided by Dr. Sebastian Amigorena (INSERM U932, Institute Curie, France). OT-IIZ, B3Z and BTg01Z (Grover et al., 2012) hybrid T cells were cultured with RPMI medium with 10% FBS. The different *T. gondii* strains were grown and maintained by infecting monolayers of HFF cells in DMEM complete medium. Intracellular parasites were recovered after HFF disruption by the use of a 23-G needle.

Reagents

The following reagents were used in this study: Ovalbumin (OVA), lyophilized powder (Worthington Biochemical Corporation); Bovine Serum Albumin (BSA), lyophilized powder (Santa Cruz); 3 µm latex beads and 3 µm blue latex beads (Polysciences Inc.); OVA conjugated to Alexa Fluor 488, Fluoromount-G with DAPI (Invitrogen); Dako Omnis without DAPI (Agilent); IMDM, DMEM and RPMI media (Gibco); poly-L-lysine, saponin, sucrose, protease inhibitor cocktail, filipin, and DMSO (Sigma-Aldrich); Tricine, Tris Base, TEMED, and U18666A (Calbiochem); glycine (Bio-Rad); acrylamide (Promega); Ponceau S solution (Abcam); Imidazole and NP-40 (ICN Biomedicals Inc.); Fetal Bovine Serum (FBS) was purchased in Natocor-Industria Biológica (Argentina); CPRG (Roche Diagnostic GmbH); ToPro3 (Molecular Probes). Synthetic peptides: $OVA_{(257–264)}$ SIINFEKL and $OVA_{(323–339)}$ ISQAVHAAHAEINEAGR (Polypeptide Group); and $CD4Ag28m_{(605–619)}$ AVEIHRPVPGTAPPS (Genecust).

Antibodies

The following antibodies were used in this study: purified rabbit polyclonal anti-OVA (Sigma-Aldrich), purified FITC mouse anti-H-$2K^b$ and PE mouse anti-IA^b (BD Pharmingen), rabbit polyclonal anti-Syntaxin 4 (Synaptic Systems), rabbit polyclonal anti-Rab11a (Aviva Systems Biology), rabbit polyclonal anti-CHMP4b and mouse monoclonal anti-TSG101 (Abcam), mouse monoclonal anti-SAG1 and rabbit polyclonal anti-CD63 (Santa Cruz). Purified rabbit anti-HPERVNVFDY (type I GRA6) and anti-GRA2 (Biotem). Anti-species conjugated to Alexa 488, 568, or 647 (Molecular Probes) or peroxidase (Jackson Laboratories) were used as secondary antibodies.

Antigen Presentation Assays

For all antigens tested, BMDCs were treated with 7.5 µg/ml of U18666A (or same volume of DMSO) for a total period of 8 h at 37°C. In the case of experiments involving *T. gondii*, BMDCs were incubated with the U18666A inhibitor during the whole infection period (8 h). The parasite strains TgRH *YFP SAG1-OVA* or TgRH *GRA6-OVA* were used at the indicated MOI. For soluble OVA (specific concentrations indicated in **Figures 1A, 2A**) or 3 µm latex beads coated with different ratios of OVA and BSA (10 mg/ml of OVA alone, 3 mg/ml of OVA and 7 mg/ml of BSA or 10 mg/ml of BSA alone), BMDCs were first pre-treated with U18666A for 3 h and then incubated 5 h more with the mentioned antigens. For the short control peptides ISQAVHAAHAEINEAGR (OVA 323–339 for OT-IIZ cells), AVEIHRPVPGTAPPS (AS15 for BTg01Z cells) or SIINFEKL (OVA 257-264 for B3Z cells), BMDCs were pre-treated for 6 h with U18666A plus 2 h with the corresponding peptide. After incubation, cells were washed three times with 0.5% BSA/PBS, fixed with 0.008% glutaraldehyde during 2 min at 4°C and quenched with 0.2M glycine. Finally, one final wash with PBS was performed, and the corresponding T cell hybridoma was added during 16 h at 37°C. T cell activation was colorimetrically determined detecting ß-galactosidase activity by optical density (absorbance at 595–655 nm) using CPRG as substrate for the reaction. When indicated, relative T cell response corresponds to the ratio between optical density of each experimental condition and the mean of optical densities of the highest antigen concentration of untreated cells, and it was expressed as arbitrary units (AU).

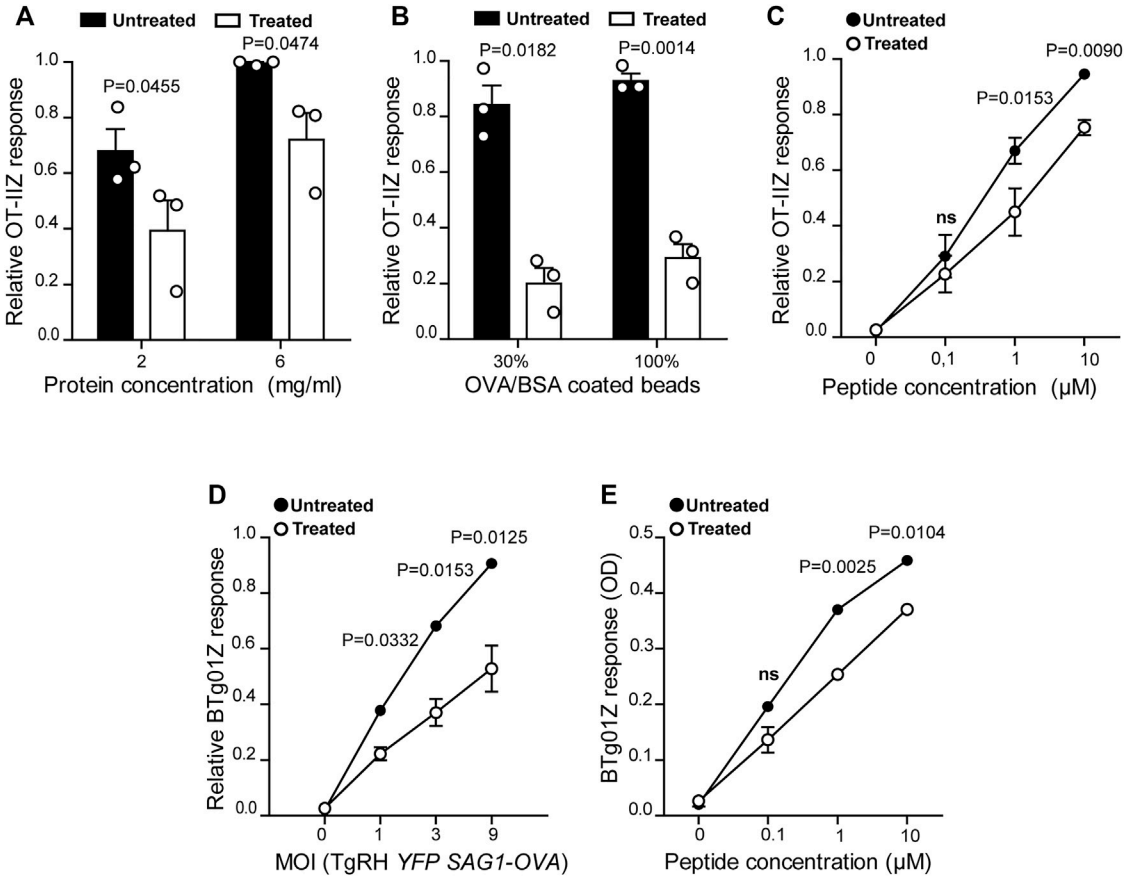

FIGURE 1 | MHC-II antigen presentation is hampered in U18666A-treated BMDCs. MHC-II antigen presentation ability of treated and untreated BMDCs was evaluated by OT-IIZ cell activation after the incubation with **(A)** soluble OVA, **(B)** OVA/BSA coated latex beads, and **(C)** the ISQAVHAAHAEINEAGR control peptide at the indicated concentrations. **(D)** The presentation of a natural antigen derived from the parasite TgRH *YFP SAG1-OVA* after 8 h of infection at the indicated MOI and **(E)** the AVEIHRPVPGTAPPS control peptide at the indicated concentrations, was evaluated by BTg01Z cell activation. In **(A–D)**, data represent mean ± SEM of triplicate values from three independent experiments. In panel **(E)**, data show mean ± SEM of triplicate values of a single experiment. The *P*-value for each experimental condition is indicted in figure. $p > 0.05$ (ns). The one-tailed Student's paired *t*-test was performed.

FACS Experiments

Cell Viability

To test cell viability after treatment, cells were incubated during 24 h in complete medium with 7.5 μg/ml of U18666A (or the same volume of DMSO) at 37°C. Then, cells were washed twice in PBS and stained with ToPro3 (1:3000) and immediately analyzed by flow cytometry. The population was selected and the doublets eliminated, using the gating strategy show in **Supplementary Figure S2A**, to determine the percentage of viable BMDCs (ToPro3 negative cells).

MHC-I and MHC-II Staining

BMDCs were incubated for 24 h in complete medium with 7.5 μg/ml of U18666A, or the same volume of DMSO. Then, cells were fixed with 2% PFA for 10 min at 4°C and quenched with 0.2M glycine. After this, cells were permeabilized with permeabilization buffer (0.05% saponin/0.2% BSA/PBS) for 20 min at RT, washed and incubated with FITC mouse anti-H-$2K^b$ (MHC-I) or PE mouse anti-IA^b (MHC-II) for 40 min at 4°C. To measure the cell surface expression of MHC molecules, intact cells were used (without fixing or permeabilizing). Finished staining, cells were washed three times with permeabilization buffer (or with PBS/0.5% BSA for intact cells), twice with PBS and mean fluorescent intensity (MFI) was obtained by flow cytometry analysis. MFI values were normalized to the mean of each control and expressed as AU.

Antigen Uptake and *T. gondii* Infection Assay

To determine the endocytic capacity of BMDCs in presence of the inhibitor, cells were pre-treated with 7.5 μg/ml of U18666A (or the same DMSO volume) during 7 h and incubated for 1 h more at 37°C with 0.1 or 0.3 mg/ml of OVA coupled to FITC in complete medium. To control unspecific binding of OVA-FITC, cells were incubated with the highest concentration of this fluorescent antigen at 4°C. Then, BMDCs were washed three times with 0.5% BSA/PBS and the MFI of FITC was determined by flow cytometry analysis.

To evaluate the phagocytic capacity of BMDCs, 3 μm blue latex beads were previously coated with 10 mg/ml of OVA. Cells were treated with 7.5 μg/ml of U18666A, or the same DMSO

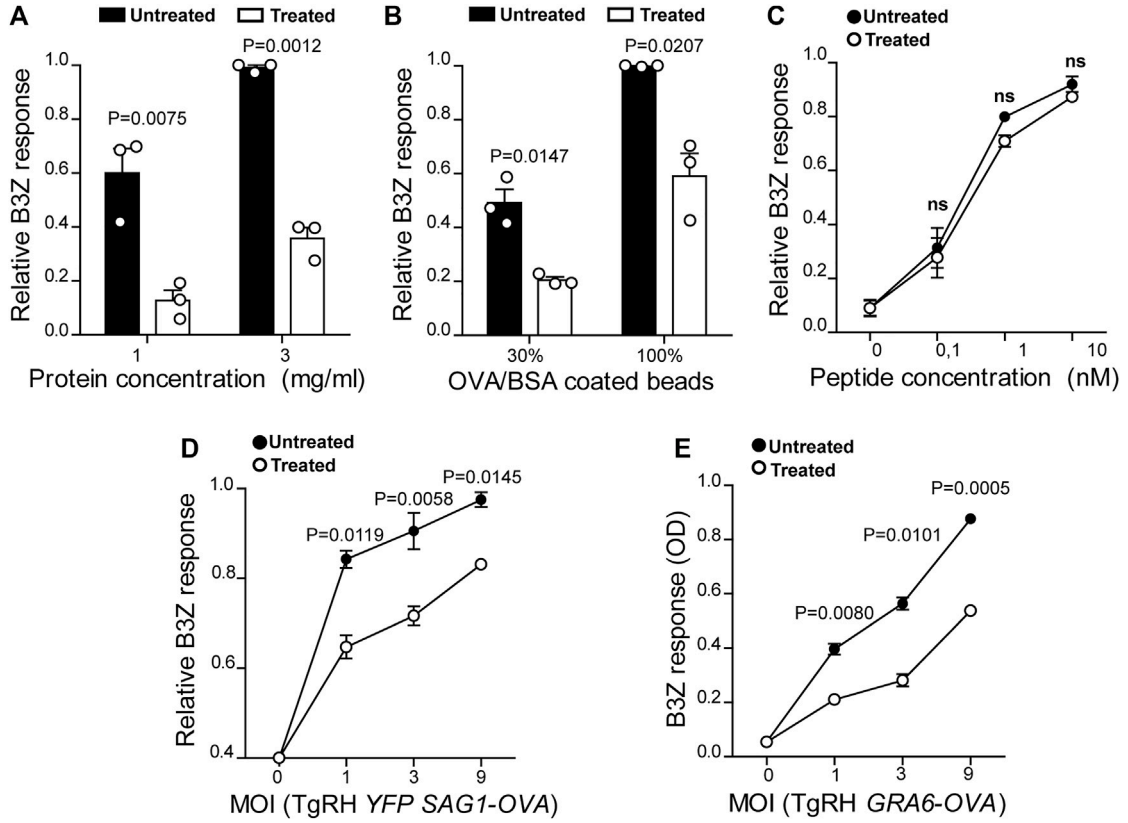

FIGURE 2 | U18666A treatment inhibits antigen cross-presentation by BMDCs. The cross-presentation of **(A)** soluble OVA, **(B)** OVA/BSA coated latex beads, and **(C)** the SIINFEKL control peptide at the indicated concentrations by treated and untreated BMDCs was evaluated with the B3Z hybridoma. **(D)** MHC-I presentation of OVA secreted by TgRH *YFP SAG1-OVA* and **(E)** the SIINFEKL peptide appended at the C-terminus of the GRA6 antigen expressed by TgRH *GRA6-OVA*, after 8 h of treated/untreated BMDCs infection at the indicated MOI was evaluated by B3Z activation. In **(A–D)**, data represent mean ± SEM of triplicate values from three independent experiments. In panel E, data show mean ± SEM of triplicate values of a single experiment. The *P*-value for each experimental condition is indicted in figure. $p > 0.05$ (ns). The one-tailed Student's paired *t*-test was performed.

volume, during 8 h and incubated for 1, 3 or 5 h at 37°C with the OVA-coated particles in complete medium. Control and treated BMDCs were also incubated for 5 h at 4°C with OVA-coated beads as negative control of phagocytosis. After each internalization period, cells were washed three times with 0.5% BSA/PBS, incubated 40 min at 4°C with a rabbit polyclonal anti-OVA antibody, then washed and labeled with a secondary anti-rabbit antibody coupled to Alexa 488 also 40 min at 4°C. After three final washes with 0.5% BSA/PBS, cells were analyzed by flow cytometry, as shown in **Figure 3C**. The percentage of internalized beads was normalized to the mean of 5 h phagocytosis of untreated cells and expressed as AU.

To test *T. gondii* infection upon U18666A treatment, BMDCs were incubated during 8 h at 37°C with the fluorescent strain TgRH *YFP SAG1-OVA* at MOI 1, 3 or 9 in complete medium with 7.5 µg/ml of inhibitor, or the equivalent DMSO volume. Then, cells were extensively washed with 0.5% BSA/PBS, fixed with 2% PFA during 10 min at 4°C, washed twice with 0.2M glycine, and one final wash with 0.5% BSA/PBS. The infection rate of BMDCs was determined by FACS analysis, as shown in **Figure 3E**. The percentage of infected cells was normalized to the mean of the condition "MOI 9" of untreated cells and expressed as AU.

Confocal Microscopy

BMDCs were cultured on poly-L-lysine-coated glass coverslips during 24 h in complete medium with 7.5 µg/ml of U18666A (or the same volume of DMSO). After extensive washing with PBS, BMDCs were first fixed with 2% PFA during 15 min at 37°C and then quenched with 0.2M glycine. After this, cells were permeabilized with 0.05% saponin/0.2% BSA/PBS for 20 min at RT, washed and incubated with mouse anti-H-2K^b (MHC-I) or mouse anti-I-A^b (MHC-II), combined with rabbit anti-Syn4, overnight at 4°C. The combinations of mouse anti-H-2K^b (MHC-I) plus rabbit anti-Rab11a, and mouse anti-I-A^b (MHC-II) plus filipin were also used. The next day, cells were washed with permeabilization buffer and incubated with a secondary antibody coupled to Alexa 488 or Alexa 555 for 60 min at 4°C. Cells were washed again three times with permeabilization buffer and twice with PBS. Finally, coverslips were mounted with Fluoromount-G (with DAPI).

To observe *T. gondii* infection, BMDCs were incubated at 37°C with TgRH *YFP SAG1-OVA* at MOI 1 on poly-L-lysine-coated

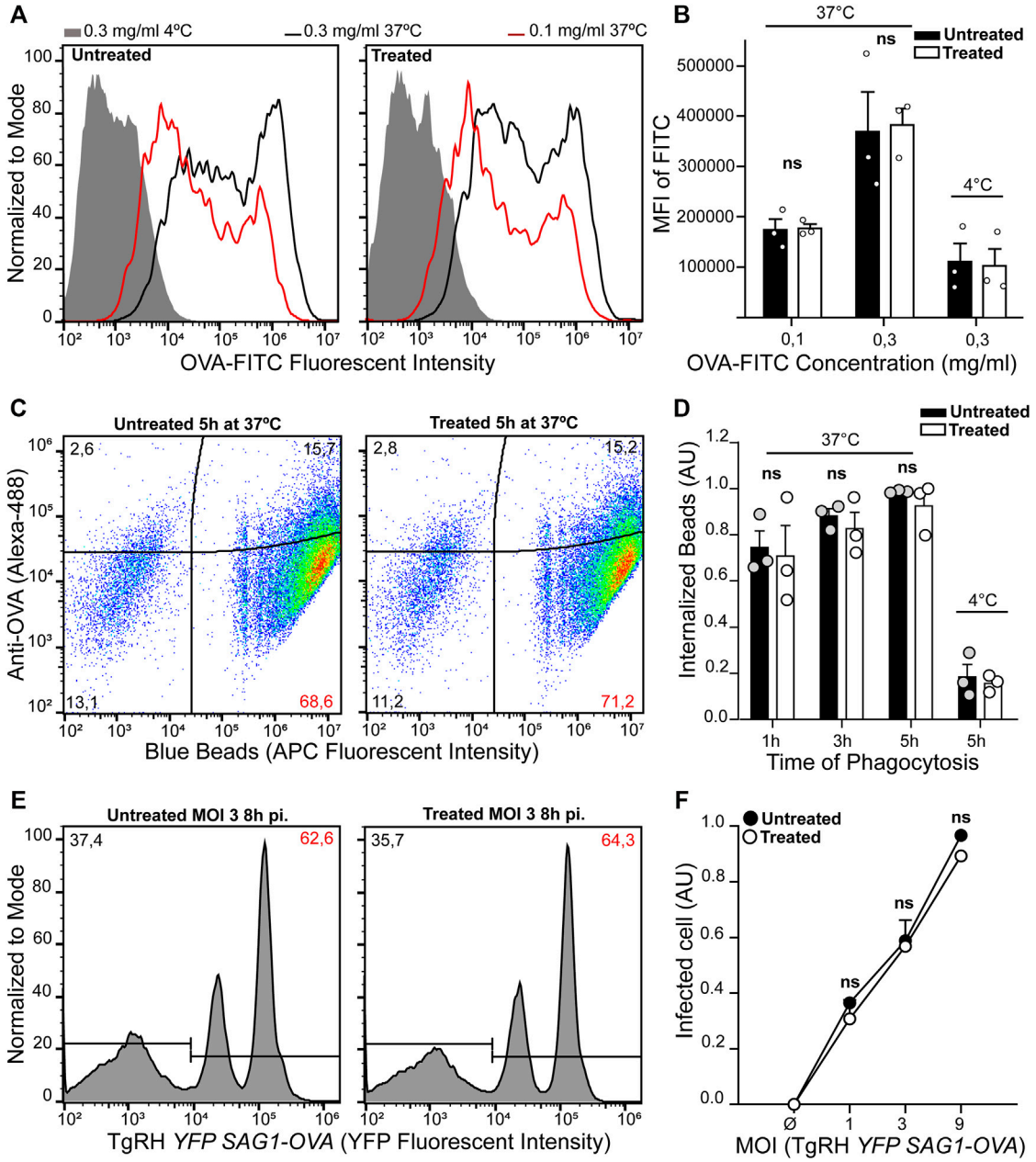

FIGURE 3 | BMDC treatment with U18666A does not affect their antigen internalization capacity. **(A–D)** Evaluation of endocytosis and phagocytosis in untreated and treated BMDCs. Fluid-phase endocytosis of fluorescent OVA after 1 h of internalization, and phagocytosis of 3 µm fluorescent latex beads at different times of internalization were assessed by FACS analysis. Antigen internalization was performed at 37°C for effective uptake, and at 4°C as negative control. **(A)** Representative FACS profiles of OVA-FITC fluorescent intensity corresponding to the endocytosis of 0.3 mg/ml (black lines), 0.1 mg/ml (red lines) or endocytosis of 0.3 mg/ml at 4°C (gray lines). **(B)** Histogram showing the mean fluorescence intensity of FITC in untreated and treated BMDCs. Data represent mean ± SEM of triplicate values from three independent experiments. **(C)** Representative FACS profiles of untreated and treated BMDCs after 5 h of phagocytosis with 3 µm fluorescent latex beads coated with OVA. Red numbers indicate the percentage of cells that have completely internalized particles (APC+/OVA–). **(D)** Histogram showing the normalized percentage (arbitrary units, AU) of efficient phagocytosis after 1, 3, and 5 h of latex beads internalization at 37°C, and 5 h at 4°C. Data represent mean ± SEM of triplicate values from three independent experiments. **(E,F)** The efficiency of untreated and treated BMDCs infection for 8 h with TgRH *YFP SAG1-OVA* was measured by FACS analysis at the indicated MOI. **(E)** Representative FACS profiles of infected BMDC at MOI 3. **(F)** Histograms showing the normalized percentage of infected cells as arbitrary units (AU). Data represent mean ± SEM of triplicate values from three independent experiments. The one-tailed Student's paired *t*-test was performed. $p > 0.05$ (ns).

glass coverslip for the indicated time in each section. Subsequently, cells were fixed and permeabilized the same way as for non-infected BMDCs. To detect endogenous MVBs component recruited to the PV, cells were incubated with rabbit anti-CD63, mouse anti-TSG101 or rabbit anti-CHMP4b, combined with mouse anti-SAG1, rabbit anti-GRA6 or mouse

anti-GRA2, respectively, overnight at 4°C. Next, cells were washed with permeabilization buffer and incubated with secondary antibodies coupled to Alexa 555 or Alexa 647 for 60 min at 4°C. Finally, cells were washed and mounted as described before for non-infected cells.

For cholesterol labeling, *T. gondii* infected (TgRH *YFP SAG1-OVA* at MOI 1) or non-infected BMDCs were incubated with 1 mg/ml of filipin for 1 h at RT, prior to fixing, and mounted with Dako Omnis mounting medium without DAPI.

Image acquisition was performed on an Olympus FV-1000 confocal microscope with a 63×/1.4 NA oil immersion objective. One z-stack plane is shown from the acquired images and they were processed with the ImageJ software (Wayne Rasband, National Institutes of Health). Image deconvolution was performed with the Parallel Spectral Deconvolution plugin (Piotr Wendykier) using a theoretical PSF generated by the Diffraction PSF 3D plugin (Robert Dougherty).

Immunoblotting

BMDCs were incubated with TgRH *YFP SAG1-OVA* at MOI 2 and 6 in complete medium, during 2, 8 or 24 h at 37°C. Then, 10^5 cells were washed three times with PBS and resuspended in 20 µl of sample buffer (50 mM Tris, 4% SDS, 9.5% glycerol and 2% β-mercaptoethanol). Total cell lysates were subjected to SDS-PAGE on 12% gel. After transferring, the membrane was stained with Ponceau S and washed with distilled water until all the dye was removed. Next, the membrane was blocked in 10% Milk/PBS during 1 h at RT and incubated with anti-CHMP4b, anti-SAG1 and then with peroxidase-conjugated antibodies. Bound antibodies were revealed using the kit Chemiluminescent Peroxidase Substrate-3 (Sigma-Aldrich), according to the manufacturers' instructions. The intensity of the bands was quantified by densitometry using Quantity One 4.6.6 software (Bio-Rad) and was expressed as arbitrary units.

Transmission Electron Microscopy

BMDCs were infected with TgRH *YFP SAG1-OVA* at MOI 1 during 24 h at 37°C. Then, cells were washed with ultrapure PBS three times, and fixed with 2.5% glutaraldehyde during 1 h at 4°C. Cells were washed again three times with ultrapure PBS (5 min at 4°C each), and incubated in 1% osmium tetroxide/PBS for 2 h at RT. Then they were dehydrated sequentially with increasing concentrations of ice-cold acetone and three times with 100% acetone for 15 min at RT. Cells were infiltrated in 1:1 acetone: EPON overnight at RT and finally embedded in fresh pure resin overnight at RT. Thin sections (60–80 nm) were cut with a diamond knife (Diatome, Washington, DC) on a Leica Ultracut R ultramicrotome and collected on 200-mesh copper grids. Grids were observed and photographed in a Zeiss 902 electron microscope at 50 kV.

Focused Ion Beam and Scanning Electron Microscopy (FIB-SEM)

HFF were brought to confluence on a plate with grid coverslip, infected for 24 h with TgRH *YFP SAG1-OVA* and fixed overnight at 4°C in 2.5% glutaraldehyde in 100 mM Hepes pH 7.4. Cells were incubated with 1% osmic acid, 1.5% potassium ferrocyanide in Hepes for 1 h at RT, then with 1% tannic acid in Hepes for 30 min at RT followed by 1% osmic acid in H_2O for 1 h at RT. Samples were dehydrated using ethanol gradient of 25, 50, 75, 95% for 10 min each, then 100% three times for 15 min. Cells were infiltrated in EPON overnight at RT and embedded in fresh pure resin for 2 h at RT, left to polymerize for 48 h at 60°C. Consecutive face-block imaging and milling was performed on a Zeiss Crossbeam 540. Voxel size of the xy-binned images is 10 × 10 × 5 nm (xyz).

Statistical Analysis

The one-tailed Student's paired *t*-test was performed at the indicated Figures by using the GraphPad Prism 5 software. The ImageJ software was used for imaging processing.

RESULTS

U18666A Treatment Impairs Exogenous Antigen Presentation by BMDCs

To confirm the critical importance of cholesterol transport for MHC-II antigen presentation by DCs (Anderson et al., 2000; Bosch et al., 2013b; Roy et al., 2013), we tested the impact of the inhibitor U18666A on this immune process. Therefore, we evaluated MHC-II antigen presentation by the use of OT-IIZ CD4+ T cells, which specifically recognizes the 17 amino acids sequence (ISQAVHAAHAEINEAGR) derived from ovalbumin (OVA), commonly known as 323–339 peptide, loaded onto I-A^b MHC-II molecules. We treated BMDCs with 7.5 µg/ml of U18666A, or the equivalent DMSO volume for the control condition, and incubated these cells with soluble OVA or OVA coupled to 3 µm latex beads for 5 h at 37°C. As shown in **Figures 1A,B**, U18666A treatment induced a strong reduction of CD4+ T cell activation in the context of endocytosis and phagocytosis, respectively. Also, the presentation of the short control 323–339 peptide, which does not require further processing to associate with MHC-II molecules, was significantly decreased in U18666A-treated BMDCs (**Figure 1C**). Consistent with previous reports, this result may reflect a reduced stability of MHC-II/peptide complexes at the cell surface due to cholesterol depletion (Bosch et al., 2013b). We next addressed the impact of U18666A treatment on the presentation of *T. gondii*-derived antigens. For this, we used a different CD4+ T hybridoma called BTg01Z, which recognizes a natural antigen of the parasite. BTg01Z cells are activated in response of recognizing the AS15 peptide (AVEIHRPVPGTAPPS) of the CD4Ag28m *T. gondii* protein loaded onto I-A^b MHC-II molecules at the plasma membrane of antigen-presenting cells (Grover et al., 2012). As shown in **Figure 1D**, BTg01Z CD4+ T cell activation was strikingly affected in the presence of U18666A after 8 h of *T. gondii* infection. Also in this experimental setup, the presentation of the corresponding short peptide was significantly inhibited after U18666A treatment (**Figure 1E**). These results indicate that correct cholesterol transport is necessary for adequate MHC-II antigen presentation.

DCs are highly adapted to process and present exogenous antigens in MHC-I molecules through the cross-presentation pathway. Although these cells require cholesterol in the plasma membrane to facilitate antigen internalization by macropinocytosis (Albrecht et al., 2006), the role of cholesterol trafficking in the context of cross-presentation remains unknown. To address this question, we treated BMDCs with U18666A and we used B3Z CD8+ T cells, which specifically recognizes the OVA-derived SIINFEKL peptide in association with H-2K^b MHC-I molecules. As shown in **Figures 2A,B**, U18666A-treated BMDCs fail to cross-present both soluble and particulate antigens, respectively. However, in this case no significant differences of CD8+ T activation were observed between control and treated cells after incubation with the short SIINFEKL peptide (**Figure 2C**). Similar to MHC-II presentation, the cross-presentation of *T. gondii*-derived antigens was impaired in U18666A-treated BMDCs after infection with TgRH *YFP SAG1-OVA* parasites, which secrete the model antigen OVA as a soluble protein into the vacuolar space (**Figure 2D**). Given that the distribution of *T. gondii* antigens inside the PV also determines the pathway followed by MHC-I molecules to activate CD8+ T lymphocytes (Buaillon et al., 2017; Poncet et al., 2019), we decided to analyze the presentation of a transmembrane antigen. Thus, we used the strain TgRH *GRA6-OVA*, which expresses a portion of OVA fused with the parasite membrane and immunodominant antigen GRA6 (Blanchard et al., 2008). Here again, MHC-I presentation of the GRA6-OVA antigen was significantly impaired in U18666A-treated BMDCs, as compared to control cells (**Figure 2E**). Altogether, these data show that cholesterol transport represents a key aspect of DC intracellular trafficking in order to carry out optimal MHC-II presentation and MHC-I cross-presentation of exogenous antigens.

U18666A Treatment Does Not Affect Cell Viability or Antigen Internalization by BMDCs

The drug U18666A inhibits cholesterol intracellular transport leading to an accumulation of this lipid within lysosomes (Cenedella, 2009; Lu et al., 2015). Since cholesterol is a key component of cell membranes, vital functions could be altered in treated DCs, thereby generating the defective phenotype of exogenous antigen presentation that we observe in our system. Therefore, we controlled the viability of U18666A-treated and untreated BMDCs. We used the fluorescent nuclear probe ToPro3 that binds to dead cell nucleus, but cannot access the DNA of viable cells. Cells were treated with the U18666A inhibitor (or the equivalent volume of DMSO) at 37°C for 24 h, a longer incubation period compared to the one used in the antigen presentation assays. In **Supplementary Figures S1A,B** is depicted the flow cytometry gating strategy for this experimental approach. Our results show that no significant differences of cell viability were found between control and U18666A-treated BMDCs (**Supplementary Figure S1C**).

Next, we decided to analyze the uptake capacity of exogenous antigens after U18666A treatment, since a defect at this level would determine the efficiency of CD4+/CD8+ T cell activation. After 7 h of U18666A treatment, BMDCs were incubated with different concentrations of OVA coupled to FITC for 1 h at 37°C, or the highest concentration of this antigen at 4°C, and the mean fluorescent intensity (MFI) of FITC was analyzed by flow cytometry. As shown in **Figures 3A,B**, no significant differences in fluid-phase endocytosis were found between control and U18666A-treated BMDCs.

Next, the phagocytic capacity of U18666A-treated BMDCs was evaluated by incubating these cells with 3 µm OVA-coated fluorescent latex beads for 1, 3, and 5 h. Again, the total period of U18666A treatment was 8 h. After each uptake time point, BMDCs were labeled with an anti-OVA antibody in order to discriminate between fluorescent particles attached to the cell surface (APC+/Alexa 488+) from those that were fully internalized (APC+/Alexa 488−), as shown in **Figure 3C**. As a control, we also incubated BMDCs with OVA-coated fluorescent beads for 5 h at 4°C to inhibit phagocytosis. We quantified the percentage of cells that fully internalized the particulate antigen in all experimental conditions, and did not find significant differences between control and U18666A-treated BMDCs (**Figure 3D**).

Finally, we investigated the infection rate by *T. gondii* in the presence or absence of the inhibitor. BMDCs were treated with U18666A or DMSO for 8 h and co-incubated with the fluorescent parasite strain TgRH *YFP SAG1-OVA* at different multiplicity of infection (MOI). **Figure 3E** shows representative flow cytometry profiles exhibiting uninfected cells (populations on the left), and BMDCs with one or two fluorescent parasites inside (populations on the right). As shown in **Figure 3F**, we quantified the percentage of infected cells by *T. gondii*, and no significant differences were observed between control and U18666A-treated BMDCs.

This set of experiments indicates that U18666A treatment does not affect fluid-phase endocytosis, phagocytosis, *T gondii* infection or cell viability, suggesting that another important intracellular trafficking step is perturbed upon BMDC incubation with this inhibitor and that it cripples exogenous antigen presentation.

U18666A Treatment Disrupts MHC-I and MHC-II Molecules Transport to the Plasma Membrane

We next decided to explore if U18666A treatment may be interfering with normal intracellular transport and distribution of MHC-I and MHC-II molecules in BMDCs, a key feature of antigen presentation. First, we analyzed cholesterol distribution in control and treated BMDCs by using filipin labeling and confocal microscopy. As shown in **Figure 4A**, control cells exhibited a uniform membrane distribution of cholesterol throughout the cytoplasm, whilst in U18666A-treated BMDCs, cholesterol was accumulated in a more marked patchy vesicular pattern, as described before in other cell types (Shoemaker et al., 2013; Elgner et al., 2016).

Since U18666A treatment interrupts cholesterol trafficking from lysosomes to the plasma membrane, we thought that the

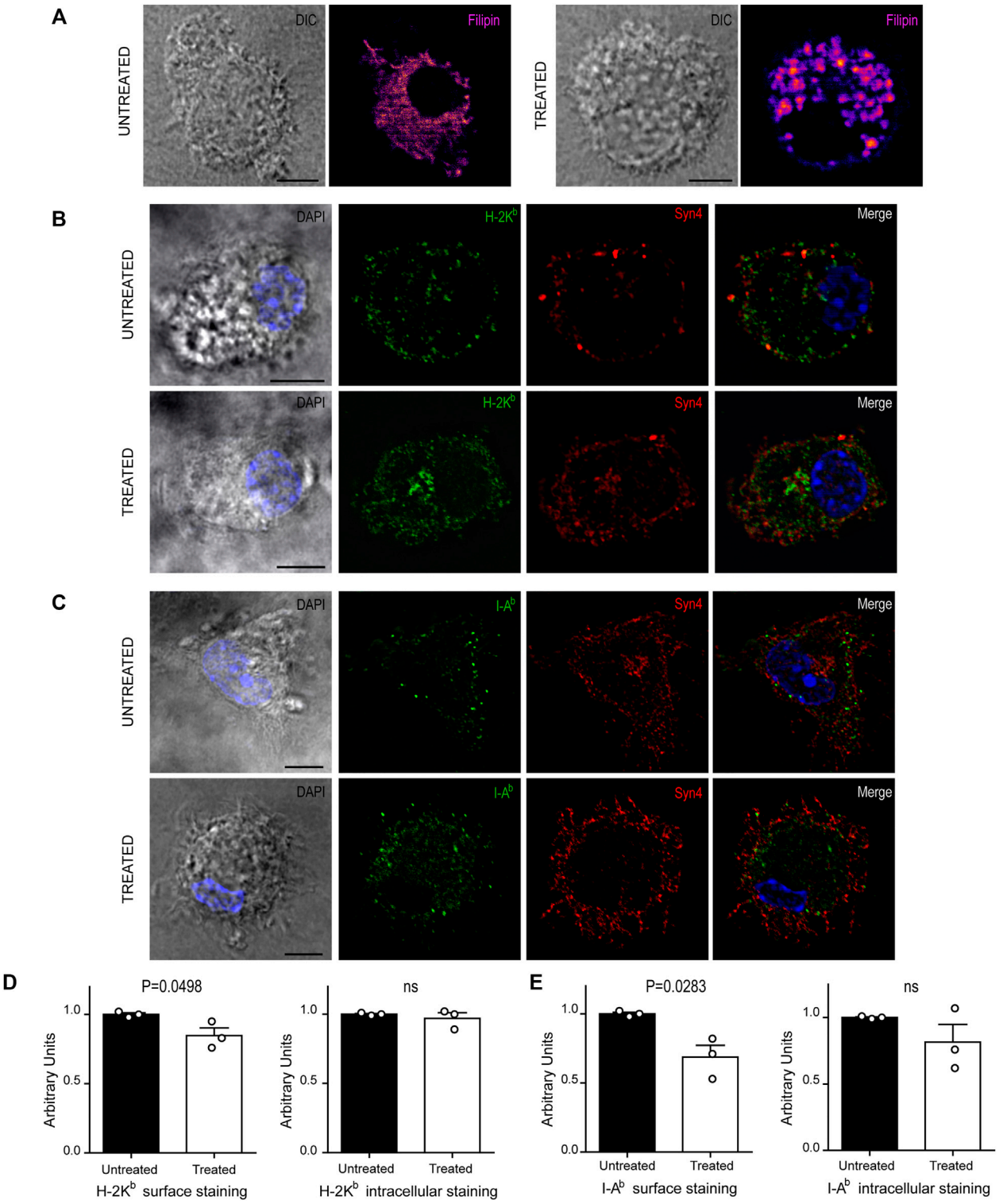

FIGURE 4 | U18666A treatment disrupt the arrival of MHC-I and MHC-II molecules to the cell surface. **(A–C)** Immunofluorescence labeling and confocal microscopy analysis showing the distribution of cholesterol, MHC molecules and a surface marker, in untreated and treated BMDCs for 24 h. **(A)** Cholesterol stained with filipin (fire). **(B)** H-2K^b MHC-I (green) and Syn4 (red). **(C)** I-A^b MHC-II (green) and Syn4 (red). Nuclei stained with DAPI. DIC images are shown on the left. Overlay of all fluorescent channels is shown in the right panels. Scale bars: 5 μm. Data are representative of 10 images analyzed for each experimental condition from three independent experiments. **(D,E)** FACS analysis of MHC-I and MHC-II molecules of untreated or treated BMDCs. Intact cells corresponding to surface expression (left) and permeabilized cells corresponding to total expression of MHC molecules (right). Histograms showing arbitrary units (AU) corresponding to values normalized to the mean of each control. Data represent mean ± SEM of triplicates values from three independent experiments. The *P*-value for each experimental condition is indicted in figure. $p > 0.05$ (ns). The one-tailed Student's paired *t*-test was performed.

regular transport of MHC molecules may be also altered. Therefore, we labeled BMDCs after 24 h of U18666A treatment with specific fluorescent tagged antibodies that detect endogenous H-2K^b MHC-I and I-A^b MHC-II molecules. We also included the detection of endogenous Syntaxin 4 (Syn4), a plasma membrane SNARE protein that can be present in DC endosomes and phagosomes (Cebrian et al., 2011). As shown in **Figures 4B,C**, MHC-I and MHC-II molecules seem to be more accumulated at the intracellular level and less in the periphery of U18666A-treated BMDCs, as compared to control BMDCs, suggesting a defect of transport to the plasma membrane. A perinuclear structure positive for Syn4 was more evident upon U18666A treatment than in control cells, suggesting an intracellular accumulation of MHC-I molecules in this region. Therefore, we performed a double staining to detect H-2K^b and Rab11a, a classical marker of recycling endosomes that highly co-localizes with the intracellular pool of MHC-I molecules (Nair-Gupta et al., 2014). As shown in **Supplementary Figure S2A**, U18666A-treated BMDCs exhibit higher accumulation of MHC-I molecules in Rab11a-positive endosomes and a weaker staining at the cell surface, as compared to untreated cells. Moreover, we decided to label I-A^b and filipin given that MHC-II molecules and cholesterol are present within acidic compartments of the endocytic network. Indeed, **Supplementary Figure S2B** shows that U18666A treatment induces stronger co-localization of MHC-II molecules with filipin than in control BMDCs, indicating higher intracellular accumulation of these molecules in endolysosomes. Conversely, the cell surface staining of I-A^b MHC-II molecules is weaker in treated than in untreated BMDCs.

To confirm this observation, we quantified intracellular and cell surface-associated MHC-I and MHC-II molecules in treated and untreated BMDCs by flow cytometry analysis. For the cell surface staining, we performed experiments with intact BMDCs, while the intracellular stainings were done with cells previously fixed and permeabilized with saponin. This experimental setup confirms that indeed, the cell surface expression levels of both MHC-I and MHC-II molecules, were significantly decreased in U18666A-treated BMDCs, as compared to control BMDCs (**Figures 4D,E**, respectively). By contrast, no major changes of intracellular staining were observed between control and treated cells. Although a tendency of lower amounts of intracellular MHC-II molecules was observed in U18666A-treated cells, this difference was not statistically significant (**Figure 4E**). Representative FACS histograms are shown in **Supplementary Figure S3**.

These results suggest that BMDC treatment with U18666A impacts on exogenous antigen presentation, at least partially, by arresting cholesterol intracellular trafficking and optimal transport of MHC-I and MHC-II molecules to the cell surface.

Intraluminal Vesicle Formation in the Vacuolar Space of *T. gondii* PV and CHMP4b Recruitment to the PV

Beyond its clear influence on MHC molecule trafficking and antigen presentation, intracellular transport of cholesterol is likely to also impact the host-parasite membrane interface, and in turn regulate *T. gondii* fitness within the host cell. The host-parasite membrane interface comprises not only the PV limiting membrane but also an intravacuolar network (IVN) of membrane tubules that is involved in sequestration of *T. gondii* membrane-bound antigens (Lopez et al., 2015), and in ingestion of host-derived proteins (Dou et al., 2014) and vesicles (Romano et al., 2017). Beside the tubules, by analyzing PVs at the ultrastructural level, we noticed the presence of numerous round-shaped vesicles in the lumen of *T. gondii* vacuoles. **Figure 5A** shows transmission electron microscopy (TEM) images depicting these intravacuolar vesicles. Although they exhibit some similarity with the intraluminal vesicles present in multivesicular bodies (MVBs), they are larger and more heterogeneous in size. Indeed, we frequently found big-size vesicles that are shown with higher magnification in the insets. To enhance the visualization of such intraluminal vesicles over the entire vacuolar space, we took advantage of an EM tomography approach called Focused Ion Beam-Scanning Electron Microscopy (FIB-SEM). Acting as a 'slicing nano-scalpel', the ion beam mills a bulk sample, progressively exposing the deeper regions of the material. The exposed block face is then imaged at high resolution with the electron beam, resulting in a stack of hundreds of serial images that encompass the entire PV (**Supplementary Figure S4 Movie**). As illustrated on planes extracted from the stack (**Figures 5B,C**), this approach confirmed the presence of tubules and vesicles in the lumen of the PV.

The molecular machinery responsible of generating intraluminal vesicles in MVBs is composed of the endosomal sorting complexes required for transport (ESCRT) proteins. This family of proteins, in association with other accessory molecules, form cytosolic complexes that sequentially interact to induce membrane deformation, invagination and inward endosomal budding (Henne et al., 2011). We hypothesized that the host cell ESCRT machinery required for MVB biogenesis could be involved also in the formation of such *T. gondii* intravacuolar vesicles. To test this idea, we first studied the recruitment of different MVBs markers to the PV, such as the tetraspanin CD63, the ESCRT-I member TSG101, and the ESCRT-III protein CHMP4b. We infected BMDCs with the fluorescent *T. gondii* strain TgRH *YFP-SAG1/OVA* for 8h, and we labeled the parasite proteins SAG1, GRA6 and GRA2 in combination with endogenous CD63, TSG101 and CHMP4b, respectively. As shown in **Figure 6A**, all three markers visibly localized to the PV membrane, indicating that *T. gondii* efficiently intercepts MVB components during DC infection. For CD63 and TSG101 labeling, the vesicular pattern displayed in BMDCs at steady state (**Supplementary Figures S5A,B**, respectively) was maintained after *T. gondii* infection (**Figure 6A**, top and middle panels). However, CHMP4b recruitment to the PV was striking and this protein re-localized almost completely to the parasite vacuole upon *T. gondii* infection (**Figure 6A**, lower panel). Moreover, the vesicular distribution of CHMP4b throughout the cytoplasm was lost upon *T. gondii* infection (**Supplementary Figures S5C,D**). A total redistribution of CHMP4b was accompanied

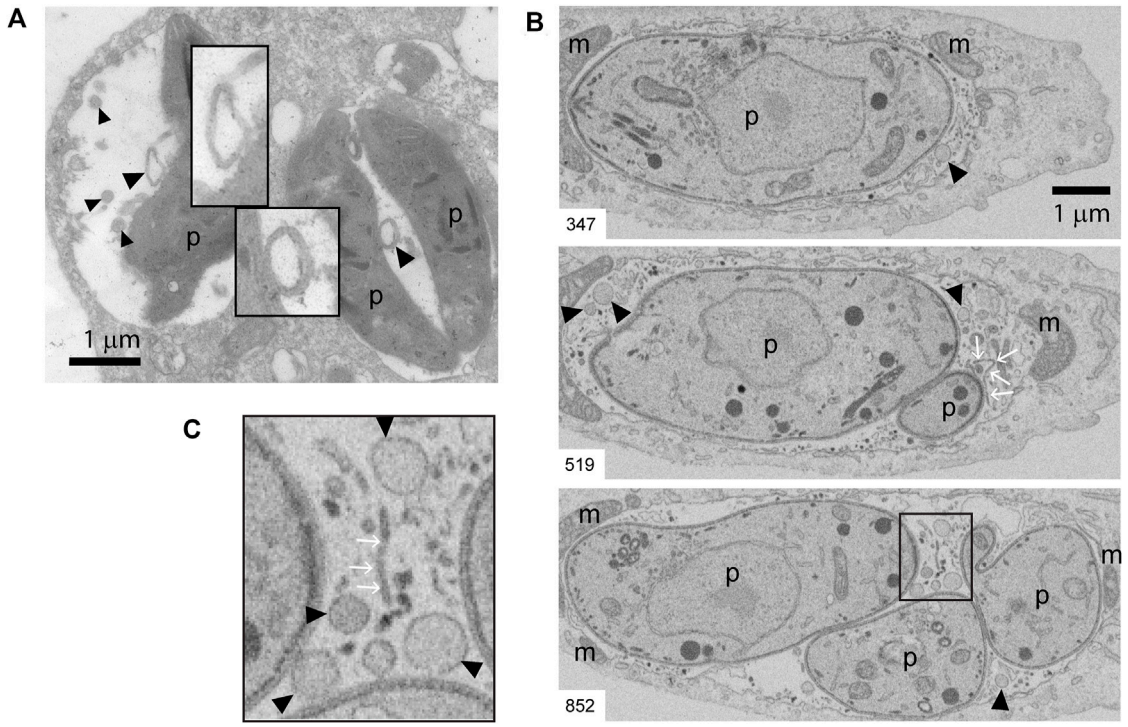

FIGURE 5 | TEM and FIB-SEM showing intravacuolar vesicles in infected BMDCs. **(A)** Transmission EM of *T. gondii*-infected BMDCs at MOI 1 for 24 h. Black arrowheads indicate intraluminal vesicles inside PVs. Magnification denote double-membrane surrounded vesicles. Data are representative of 30 images acquired and analyzed from three independent experiments. **(B,C)** Representative FIB-SEM images of a 24 h-infected human fibroblast, extracted from the stack that is shown as **Supplementary Figure S4 Movie**. The number at the bottom left indicates the position of the section in the stack. Black arrowheads point to intraluminal vesicles, white arrows point to tubules. **(C)** Inset of magnified area taken from slice #852. m: host mitochondria closely apposed to PV limiting membrane, p: parasite. A total of four movies (stacks) from different infected cells were analyzed. Intraluminal vesicles were observed in all the stacks.

by an increase of the fluorescence intensity, suggesting that *T. gondii* infection induces an upregulation of CHMP4b expression.

To directly test if *T. gondii* infection promotes the accumulation of CHMP4b, BMDCs incubated with two MOI were homogenized after different times of infection. The extracts were analyzed by SDS-PAGE and probed with anti-CHMP4b and anti-SAG1 antibodies. **Figures 6B,C** confirms that CHMP4b is strongly induced upon infection, correlating with the accumulation of the *T. gondii* SAG1 protein over time. Therefore, there is a clear positive correlation between the amount of parasites inside BMDCs and the expression level of CHMP4b along the active infection. Accordingly, CHMP4b expression was not augmented when BMDCs were incubated with heat-shock killed parasites, and importantly, the anti-CHMP4b antibody used does not cross-react with a potential *T. gondii* CHMP4b ortholog (**Supplementary Figure S5E**).

U18666A Treatment Inhibits CHMP4b Recruitment to the PV and *T. gondii* Replication

Previous work has shown a strong dependence of *T. gondii* replication on host-derived cholesterol supply (Coppens et al., 2000; Bottova et al., 2009; Sanfelice et al., 2017). However, these studies were not carried out in DCs, one of the preferred cellular targets of *T. gondii*. Given the singular interaction between *T. gondii* and DCs, we proposed to evaluate this scenario. For this, BMDCs were treated with 7.5 μg/ml U18666A (or with the equivalent volume of DMSO) during infection with TgRH *YFP SAG1-OVA* at MOI 1, and cholesterol was stained with filipin after 24 h. As shown in **Figure 7A**, a clear accumulation of cholesterol inside the PV of untreated cells was evidenced. Conversely, in the presence of the inhibitor, cholesterol was accumulated in large granules throughout the host cytosol, but not particularly at the PV.

In order to address if U18666A treatment of BMDCs impacts on *T. gondii* fitness, we followed parasite proliferation by flow cytometry analysis taking advantage of the fluorescence expressed by the TgRH *YFP SAG1-OVA* strain. The fluorescence profiles show that during the first 24 h pi *T. gondii* replicates similarly inside treated and untreated BMDCs. However, a significant delay of fluorescence incremental was observed in the treated condition from 48 h pi onwards, indicating an inhibition of parasite proliferation in these cells (**Figure 7C**, quantified in **Figure 7B**). Although a strong recruitment of CHMP4b to the replicating vacuoles was evident for both conditions at 48 h pi, the PVs observed were smaller, in size and number of parasites, in treated BMDCs than those present in untreated cells (**Figure 7D**). Moreover, CHMP4b was not recruited to small single parasite-

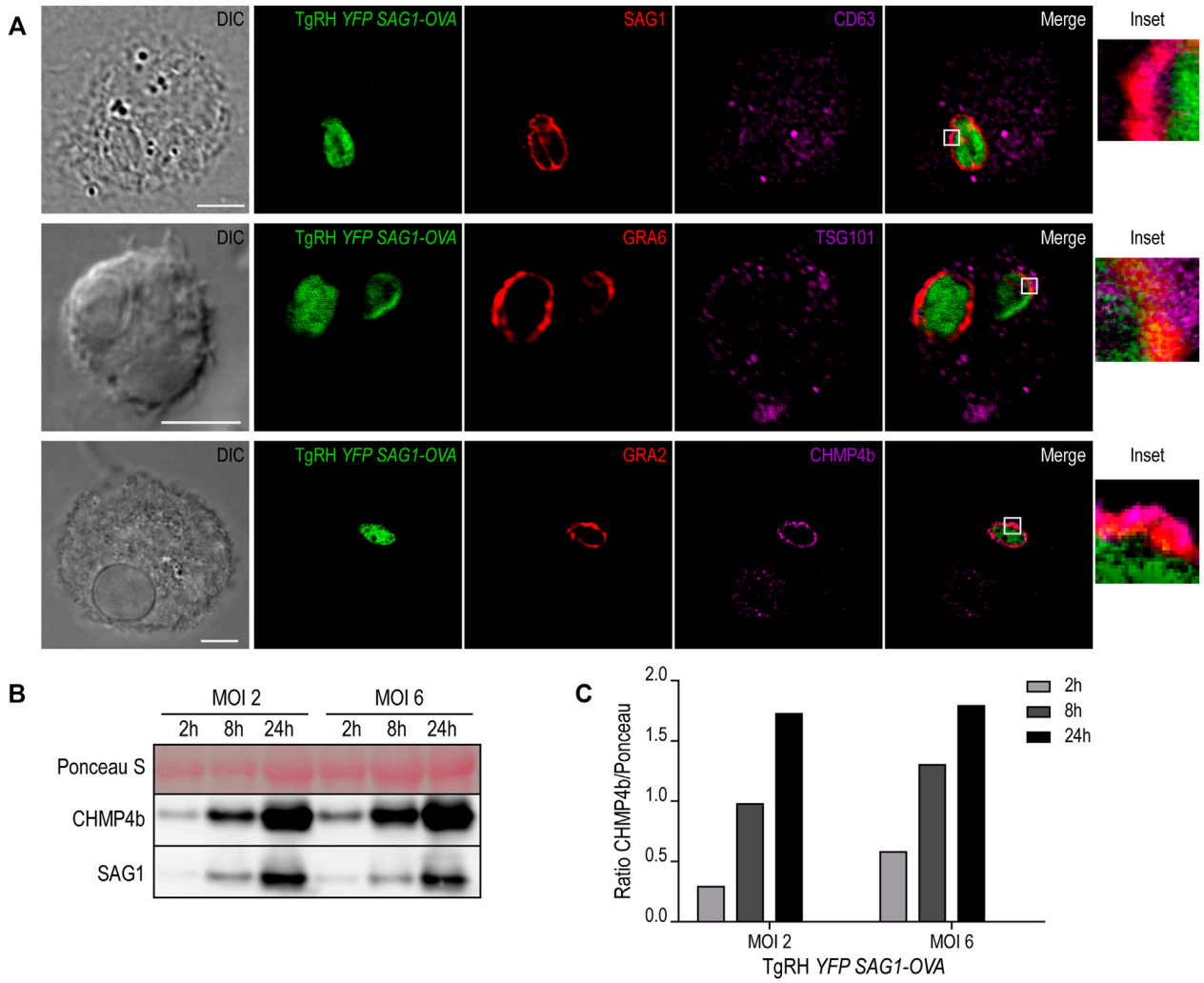

FIGURE 6 | MVBs components recruitment to the PV and CHMP4b over-expression in infected BMDCs. **(A)** Immunofluorescence labeling and confocal microscopy analysis showing the parasite proteins (SAG1, GRA6 or GRA2) in red and MVBs markers (CD63, TSG101 or CHMP4b) in magenta, in BMDCs infected with TgRH *YFP SAG1-OVA* (green) for 8 h. DIC images are shown on the left. Overlay of all fluorescent channels is shown in the right panels. Scale bars: 5 μm. Data are representative of 30 images analyzed for each experimental condition from three independent experiments. **(B)** Immunoblotting showing CHMP4b and SAG1 expression of BMDCs infected by TgRH *YFP SAG1-OVA* at MOI 2 and MOI 6, for 2, 8, and 24 h pi. **(C)** Densitometry quantification of Ponceau S and CHMP4b of BMDCs infected by TgRH *YFP SAG1-OVA*, at MOI 2 and MOI 6, at 2, 8, and 24 h pi. Data are representative of three independent experiments.

containing vacuoles in U18666A-treated BMDCs at 48 h pi, whilst in untreated cells, similar size PVs were strongly decorated with CHMP4b (**Figure 7E**). To further visualize these differences, the fluorescence intensity of CHMP4b, SAG1 and *TgRH YFP SAG1-OVA* was quantified in multiple and single parasite-containing vacuoles in control and treated cells (**Supplementary Figures S6A,B**, respectively). This result suggest that after the initial *T. gondii* infection and replication, CHMP4b cannot be efficiently recruited to the PV in successive replication rounds upon BMDC treatment with the drug.

Altogether, our data indicate an important participation of cholesterol in the *T. gondii* – DCs relationship, being necessary for both growth and proliferation, as well as for the optimal transport of MHC-I and MHC-II molecules to the cell surface required for efficient exogenous antigen presentation.

DISCUSSION

Cholesterol is a highly hydrophobic lipid that requires very tightly regulated molecular mechanisms to be transported along the cell. By and large, the efficacy of intracellular cholesterol transport depends on a proper subcellular distribution among organelles and the plasma membrane. This represents an essential feature of healthy cells that allows them to perform critical functions (Soccio and Breslow, 2004). In this study, we were interested to investigate the relevance of intracellular cholesterol transport during exogenous antigen presentation by DCs, which represent the most potent antigen presenting cells of the immune system. As general strategy, we altered cholesterol transport by the use of the drug U18666A, which has been widely characterized as a powerful inhibitor of NPC1 function and thereby retains

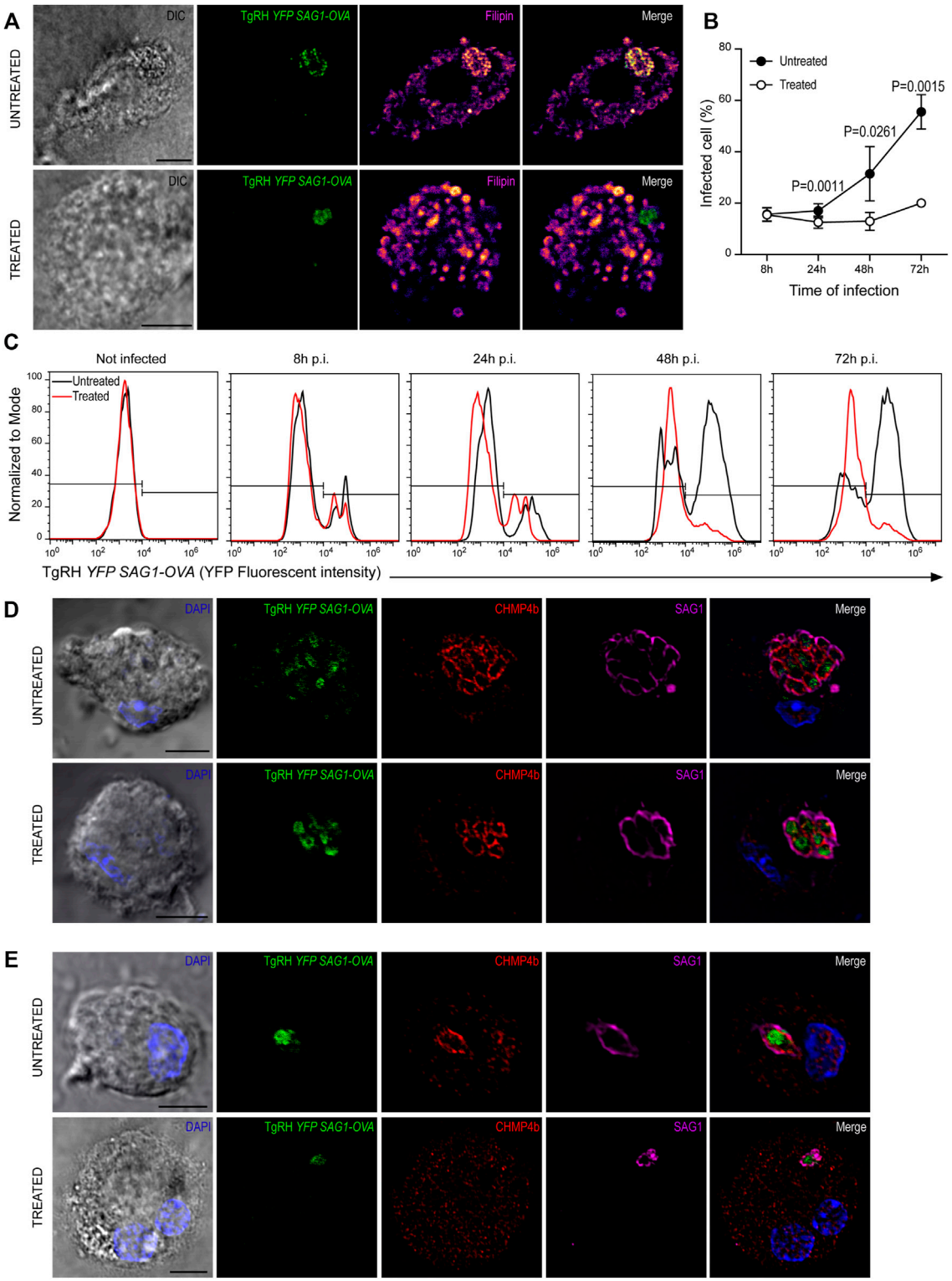

FIGURE 7 | U18666A treatment inhibits *T. gondii* replication. **(A)** Filipin labeling and confocal microscopy analysis showing the distribution of cholesterol in untreated (up) and treated (down) BMDCs infected with TgRH *YFP SAG1-OVA* (green) for 24 h. DIC images are shown on the left and overlay of all fluorescent channels is shown in the right panels. Scale bars: 5 μm. Data are representative of 15 images analyzed for each experimental condition from three independent experiments. **(B)** *T. gondii* proliferation curve in the presence of the inhibitor. Histograms showing the percentage of infected cells. Data represent mean ± SEM of triplicates values from three independent experiments. The *P*-value for each condition is indicted in figure. $p > 0.05$ (ns). The one-tailed Student's paired *t*-test was performed. **(C)**

(*Continued*)

FIGURE 7 | Representative FACS profile of *T. gondii* fluorescence in untreated (black lines) and treated (red lines) BMDCs. **(D,E)** Immunofluorescence labeling and confocal microscopy analysis showing CHMP4b and SAG1 in untreated and treated BMDCs infected with TgRH *YFP SAG1-OVA* for 48 h. **(D)** Shows big *T. gondii* PVs and **(E)** small *T. gondii* PVs (probably corresponding to a second round of replication). Nuclei stained with DAPI. DIC images are shown on the left, TgRH *YFP SAG1-OVA* (green), CHMP4b (red), SAG1 (magenta), and the overlay of all fluorescent channels is shown in the right panels. Scale bars: 5 μm. Data are representative of 15 images analyzed for each experimental condition from three independent experiments.

cholesterol inside endolysosomes (Lu et al., 2015). We decided to address this study by generating primary cultures of DCs differentiated from bone marrow of C57BL/6 mice. Hence, we set up a working concentration of U18666A that was not toxic for BMDCs, but clearly modified the intracellular distribution of cholesterol, as evidenced by filipin labeling and confocal microscopy. Although this experimental system was convenient to address our study, it also represents a limitation since we did not use other methods to change cholesterol levels or its transport. Besides, pharmacological intervention is not always a very specific approach because it may affect other important intracellular parameters.

A marked defect of MHC-I and MHC-II antigen presentation was evidenced in U18666A-treated BMDCs when we tested soluble, particulate and *T. gondii*-associated antigens. For the case of MHC-II antigen presentation, we also found a significant inhibition of CD4+ T lymphocyte activation by treated DCs when they were incubated with the corresponding short control peptides ($OVA_{(323–339)}$ for OT-IIZ and $CD4Ag28m_{(605–619)}$ for BTg01Z cells). However, the activation of B3Z CD8+ T cells upon BMDC incubation with the short control peptide $OVA_{(257–264)}$ was not diminished in treated cells. Accordingly, the deficiency of MHC-II molecule transport to the cell surface in treated BMDCs was stronger than for MHC-I, as analyzed by flow cytometry. A lack of flaw in the skill of U18666A-treated BMDCs to internalize exogenous antigens, make us consider that the inhibition of MHC-I and MHC-II transport to the cell surface is responsible, at least in part, of the defective antigen presentation phenotype that these cells exhibit. This conclusion is supported by the observation that the presentation defect observed in BMDCs from $NPC1^{-/-}$ mice is corrected when a subpopulation of cells with normal levels of MHC-II at the plasma membrane is selected (Bosch et al., 2013a).

In line with our results, previous studies have reported a loss of MHC-II expression at the cell surface when cholesterol transport is hampered (Kuipers et al., 2005; Vrljic et al., 2005) or a stability inhibition of MHC-II/peptide complexes accumulated at the plasma membrane in microclusters when cholesterol is depleted (Bosch et al., 2013b; Roy et al., 2013). An interesting experimental setup involving *Leishmania* infected macrophages demonstrate the relevance of cholesterol supply for efficient MHC-II antigen presentation (Roy et al., 2016). Regarding MHC-I expression, there is not much information available about the potential effect of cholesterol depletion, or cholesterol transport inhibition, during MHC-I trafficking to the cell surface. However, it was shown that cholesterol depletion with lovastatin impairs macropinocytosis and consequently, the MHC-I cross-presentation capacity of treated DCs was reduced (Albrecht et al., 2006). The use of U18666A in our experiments interrupts cholesterol transport without affecting fluid-phase endocytosis. Therefore, our study brings novel data about the relevance of cholesterol trafficking during MHC-I cross-presentation independently of the exogenous antigen uptake.

The striking defect observed for both MHC-I and MHC-II presentation of *T. gondii*-associated antigens, motivated us to investigate deeper into other aspects of the parasite fitness. The protozoan *T. gondii* is an obligate intracellular parasite that cannot synthesize sterols and must scavenge lipids from the host cell in order to grow and replicate inside the PV. This lipid acquisition includes cholesterol endocytosis by the parasite via the lysosomal low-density lipoprotein pathway (Coppens et al., 2000). Moreover, *T. gondii* also sequesters LDs, which represent a major intracellular source of cholesterol, and internalizes these organelles into the vacuole to achieve efficient proliferation (Hu et al., 2017; Nolan et al., 2017). In summary, different publications highlight the importance of host cholesterol supply for optimal *T. gondii* replication (Bottova et al., 2009; Sanfelice et al., 2017). In this sense, we provide further evidence to support this concept by showing that U18666A treatment of BMDCs inhibited cholesterol recruitment to the PV. As consequence, correct PV development and parasite growth were strongly blocked in our system. More importantly, our study is pioneer in addressing the relevance of cholesterol transport during *T. gondii* antigen presentation since this had not been tested before.

Probably one of the most remarkable findings of this study is the massive recruitment of CHMP4b to the PV and the subsequent over-expression of this ESCRT-III member in BMDCs infected by *T. gondii*. In accordance with our results, a very recent study shows that *T. gondii* drives the recruitment of the host ESCRT machinery through the parasite effector transmembrane dense granule protein TgGRA14. The interaction between TgGRA14 and host ESCRT components allows the efficient uptake of cytosolic proteins from the host cell important for parasite survival (Rivera-Cuevas et al., 2021). Another recent work from a different group that used a proximity-labeling strategy in combination with quantitative proteomics demonstrated that three components of the host ESCRT machinery are present at the host-parasite membrane interface in infected fibroblasts (Cygan et al., 2021). Interestingly, the vacuolar space of *T. gondii* PV comprises a sophisticated membranous IVN formed of tubules and vesicles. In this study, we also found round intraluminal vesicles in the vacuolar space of the parasite by performing both TEM and FIB-SEM experiments. The question of how these vesicles are generated inside the PV and if the host ESCRT machinery plays a relevant role in this process during the recruitment to the *T. gondii* vacuole remains open. Ongoing and future studies involving CHMP4b silencing in DCs will allow us to formally test this idea and define a more precise role for the ESCRT machinery during *T. gondii* infection.

DATA AVAILABILITY STATEMENT

The raw data supporting the conclusions of this article will be made available by the authors, without undue reservation.

ETHICS STATEMENT

The animal study was reviewed and approved by Comité Institucional para el Cuidado y Uso de Animales de Laboratorio (CICUAL) de la Facultad de Ciencias Médicas, Universidad Nacional de Cuyo.

AUTHOR CONTRIBUTIONS

CC, FG, SD, and JS-R performed experiments and prepared figures. NB, LM, and IC conceived, designed, and supervised the project. IC and CC wrote the manuscript. CC, FG, SM, NB, LM, and IC actively participated in the manuscript editing. All authors discussed results, data analysis, and commented on the manuscript preparation.

FUNDING

This work was supported by the "Agencia Nacional de Promoción Científica y Tecnológica" (PICT 2016-0013 to IC, PICT 2016-0894 and PICT 2018-4451 to LM), the "Centre National de la Recherche Scientifique" (CNRS) with the PICS (Projet International de Coopération Scientifique) collaborative program (TOXORAB 2017 to NB and IC), the PIA PARAFRAP Consortium (ANR-11-LABX0024 to NB and SM), 'Agence Nationale pour la Recherche' (ANR-18-CE15-0015 to NB).

ACKNOWLEDGMENTS

We thank S. Janssens, S. Lippens and the VIB Bioimaging core, University of Gent, Belgium, for FIB-SEM acquisitions; S. Allart and A. Canivet-Laffitte for technical assistance at Infinity-Inserm U1291 Imaging Facility (France). We also thank the Flow Cytometry Facility of the "Facultad de Ciencias Médicas, Universidad Nacional de Cuyo" (Argentina), and the Confocal and Electron Microscopy Facilities of IHEM - UNCuyo - CONICET (Argentina) for technical assistance.

SUPPLEMENTARY MATERIAL

The Supplementary Material for this article can be found online at: https://www.frontiersin.org/articles/10.3389/fcell.2022.837574/full#supplementary-material

Supplementary Figure 1 | U18666A treatment does not affect the viability of BMDCs. **(A)** Getting strategy used to determine the cell population to analyze. **(B)** Representative FACS profiles of ToPro3 fluorescent intensity corresponding to apoptotic cells. **(C)** Percentage of ToPro3 negative cells in control condition (black bar) and treated condition (white bar), after 24 h of treatment.

Supplementary Figure 2 | MHC-I and MHC-II molecules are accumulated in different intracellular endocytic compartments upon U18666A treatment. Immunofluorescence labeling and confocal microscopy analysis of U18666A-treated and untreated BMDCs showing **(A)** H-2K^b MHC-I (green) and Rab11a (red), and **(B)** filipin (green) and I-A^b MHC-II (red). Nuclei stained with DAPI. DIC images are shown on the left and the overlay of all fluorescent channels is shown in the right panels. Scale bars: 5 µm. Data are representative of 10 images analyzed for each labeling.

Supplementary Figure 3 | MHC-I and MHC-II molecules expression by FACS analysis. Representative FACS profiles of untreated and U18666A-treated BMDCs in intact (surface staining) and permeabilized (intracellular staining) cells showing the fluorescence intensity of H-2K^b-FITC (upper panels) and I-A^b-PE(lower panels) antibody labeling.

Supplementary Figure 4 | 3D imaging of an entire PV by FIB-SEM. HFF infected for 24 h with TgRH *YFP SAG1-OVA* were fixed and prepared for FIB-SEM imaging. This movie shows a stack of 1731 images binned in xy and cropped around the vacuolar space that contains four tachyzoites. Voxel size is 10 × 10 × 5 nm (xyz). Movie related to **Figure 5B** which shows an excerpt of three slices from the stack: #347, #519, and #852.

Supplementary Figure 5 | MVBs markers distribution in not infected BMDCs. Immunofluorescence labeling and confocal microscopy analysis of non-infected BMDCs showing **(A)** CD63, **(B)** TSG101 and **(C)** CHMP4b in red, and **(D)** BMDCs infected with TgRH *YFP SAG1-OVA* for 48 h showing the parasites in green, CHMP4b in red and SAG1 in magenta. Nuclei stained with DAPI. DIC images are shown on the left and the overlay of all fluorescent channels is shown in the right panels. Scale bars: 5 µm. Data are representative of 10 images analyzed for each labeling. **(E)** Immunoblotting of CHMP4b and SAG1 in BMDCs infected for 48 h with TgRH *YFP SAG1-OVA* at MOI 6 (1); in BMDCs that phagocytosed the heat killed and opsonized *T. gondii* strain TgRH *YFP SAG1-OVA* during 24 h (2) or 48 h (3), and in total lysates of the *T. gondii* strains TgRH *YFP SAG1-OVA* (4) or TgPru *Tomato SAG1-OVA* (5).

Supplementary Figure 6 | Fluorescence intensity profiles of CHMP4b in *T. gondii* PVs. Immunofluorescence labeling and confocal microscopy analysis related to **Figures 7D,E** showing the fluorescence intensity profiles of TgRH *YFP SAG1-OVA* (green), CHMP4b (red) and SAG1 (magenta) in **(A)** multiple and **(B)** single parasite-containing vacuoles of infected BMDCs. Straight lines were drawn delimiting the analyzed area.

REFERENCES

Albrecht, I., Gatfield, J., Mini, T., Jeno, P., and Pieters, J. (2006). Essential Role for Cholesterol in the Delivery of Exogenous Antigens to the MHC Class I-Presentation Pathway. *Int. Immunol.* 18, 755–765. doi:10.1093/intimm/dxl013

Anderson, H. A., Hiltbold, E. M., and Roche, P. A. (2000). Concentration of MHC Class II Molecules in Lipid Rafts Facilitates Antigen Presentation. *Nat. Immunol.* 1, 156–162. doi:10.1038/77842

Basha, G., Omilusik, K., Chavez-Steenbock, A., Reinicke, A. T., Lack, N., Choi, K. B., et al. (2012). A CD74-dependent MHC Class I Endolysosomal Cross-Presentation Pathway. *Nat. Immunol.* 13, 237–245. doi:10.1038/ni.2225

Blanchard, N., Gonzalez, F., Schaeffer, M., Joncker, N. T., Cheng, T., Shastri, A. J., et al. (2008). Immunodominant, Protective Response to the Parasite *Toxoplasma Gondii* Requires Antigen Processing in the Endoplasmic Reticulum. *Nat. Immunol.* 9, 937–944. doi:10.1038/ni.1629

Blander, J. M. (2018). Regulation of the Cell Biology of Antigen Cross-Presentation. *Annu. Rev. Immunol.* 36, 717–753. doi:10.1146/annurev-immunol-041015-055523

Bosch, B., Berger, A. C., Khandelwal, S., Heipertz, E. L., Scharf, B., Santambrogio, L., et al. (2013a). Disruption of Multivesicular Body Vesicles Does Not Affect Major Histocompatibility Complex (MHC) Class II-Peptide Complex Formation and Antigen Presentation by Dendritic Cells. *J. Biol. Chem.* 288, 24286–24292. doi:10.1074/jbc.M113.461996

Bosch, B., Heipertz, E. L., Drake, J. R., and Roche, P. A. (2013b). Major Histocompatibility Complex (MHC) Class II-Peptide Complexes Arrive at the Plasma Membrane in Cholesterol-Rich Microclusters. *J. Biol. Chem.* 288, 13236–13242. doi:10.1074/jbc.M112.442640

Bottova, I., Hehl, A. B., Štefanić, S., Fabriàs, G., Casas, J., Schraner, E., et al. (2009). Host Cell P-Glycoprotein Is Essential for Cholesterol Uptake and Replication of *Toxoplasma Gondii*. *J. Biol. Chem.* 284, 17438–17448. doi:10.1074/jbc.M809420200

Bougnères, L., Helft, J., Tiwari, S., Vargas, P., Chang, B. H.-J., Chan, L., et al. (2009). A Role for Lipid Bodies in the Cross-Presentation of Phagocytosed Antigens by MHC Class I in Dendritic Cells. *Immunity* 31, 232–244. doi:10.1016/j.immuni.2009.06.022

Buaillon, C., Guerrero, N. A., Cebrian, I., Blanié, S., Lopez, J., Bassot, E., et al. (2017). MHC I Presentation of *Toxoplasma Gondii* Immunodominant Antigen Does Not Require Sec22b and Is Regulated by Antigen Orientation at the Vacuole Membrane. *Eur. J. Immunol.* 47, 1160–1170. doi:10.1002/eji.201646859

Calafat, J., Nijenhuis, M., Janssen, H., Tulp, A., Dusseljee, S., Wubbolts, R., et al. (1994). Major Histocompatibility Complex Class II Molecules Induce the Formation of Endocytic MIIC-like Structures. *J. Cell Biol.* 126, 967–977. doi:10.1083/jcb.126.4.967

Cebrian, I., Croce, C., Guerrero, N. A., Blanchard, N., and Mayorga, L. S. (2016). Rab22a Controls MHC -I Intracellular Trafficking and Antigen Cross-presentation by Dendritic Cells. *EMBO Rep.* 17, 1753–1765. doi:10.15252/embr.201642358

Cebrian, I., Visentin, G., Blanchard, N., Jouve, M., Bobard, A., Moita, C., et al. (2011). Sec22b Regulates Phagosomal Maturation and Antigen Crosspresentation by Dendritic Cells. *Cell* 147, 1355–1368. doi:10.1016/j.cell.2011.11.021

Cenedella, R. J. (2009). Cholesterol Synthesis Inhibitor U18666A and the Role of Sterol Metabolism and Trafficking in Numerous Pathophysiological Processes. *Lipids* 44, 477–487. doi:10.1007/s11745-009-3305-7

Coppens, I., and Romano, J. D. (2018). Hostile Intruder: Toxoplasma Holds Host Organelles Captive. *Plos Pathog.* 14, e1006893. doi:10.1371/journal.ppat.1006893

Coppens, I., Sinai, A. P., and Joiner, K. A. (2000). Toxoplasma Gondii Exploits Host Low-Density Lipoprotein Receptor-Mediated Endocytosis for Cholesterol Acquisition. *J. Cell Biol.* 149, 167–180. doi:10.1083/jcb.149.1.167

Cygan, A. M., Jean Beltran, P. M., Mendoza, A. G., Branon, T. C., Ting, A. Y., Carr, S. A., et al. (2021). Proximity-labeling Reveals Novel Host and Parasite Proteins at the Toxoplasma Parasitophorous Vacuole Membrane. *mBio* 12, e0026021. doi:10.1128/mBio.00260-21

den Brok, M. H., Büll, C., Wassink, M., de Graaf, A. M., Wagenaars, J. A., Minderman, M., et al. (2016). Saponin-based Adjuvants Induce Cross-Presentation in Dendritic Cells by Intracellular Lipid Body Formation. *Nat. Commun.* 7, 13324. doi:10.1038/ncomms13324

Dou, Z., McGovern, O. L., Di Cristina, M., and Carruthers, V. B. (2014). *Toxoplasma Gondii* Ingests and Digests Host Cytosolic Proteins. *mBio* 5, e01188–14. doi:10.1128/mBio.01188-14

Dupont, C. D., Christian, D. A., Selleck, E. M., Pepper, M., Leney-Greene, M., Harms Pritchard, G., et al. (2014). Parasite Fate and Involvement of Infected Cells in the Induction of CD4+ and CD8+ T Cell Responses to Toxoplasma Gondii. *Plos Pathog.* 10, e1004047. doi:10.1371/journal.ppat.1004047

Elgner, F., Ren, H., Medvedev, R., Ploen, D., Himmelsbach, K., Boller, K., et al. (2016). The Intracellular Cholesterol Transport Inhibitor U18666A Inhibits the Exosome-dependent Release of Mature Hepatitis C Virus. *J. Virol.* 90, 11181–11196. doi:10.1128/jvi.01053-16

Fessler, R. D., Lebow, R. L., O'Toole, J. E., Fessler, R. G., and Eichholz, K. M. (2015). *Regulation of Adaptive Immunity in Health and Disease by Cholesterol Metabolism*, 1. London: Current Medicine Group LLC, 1–16. doi:10.1007/978-3-319-15206-6_109-1

Gao, J., Ochyl, L., Yang, E., and Moon, J. (2017). Cationic Liposomes Promote Antigen Cross-Presentation in Dendritic Cells by Alkalizing the Lysosomal pH and Limiting the Degradation of Antigens. *Ijn* 12, 1251–1264. doi:10.2147/IJN.S125866

Grover, H. S., Blanchard, N., Gonzalez, F., Chan, S., Robey, E. A., and Shastri, N. (2012). The *Toxoplasma Gondii* Peptide AS15 Elicits CD4 T Cells that Can Control Parasite burden. *Infect. Immun.* 80, 3279–3288. doi:10.1128/IAI.00425-12

Henne, W. M., Buchkovich, N. J., and Emr, S. D. (2011). The ESCRT Pathway. *Dev. Cell* 21, 77–91. doi:10.1016/j.devcel.2011.05.015

Hu, X., Binns, D., and Reese, M. L. (2017). The Coccidian Parasites Toxoplasma and Neospora Dysregulate Mammalian Lipid Droplet Biogenesis. *J. Biol. Chem.* 292, 11009–11020. doi:10.1074/jbc.m116.768176

Jurewicz, M. M., and Stern, L. J. (2019). Class II MHC Antigen Processing in Immune Tolerance and Inflammation. *Immunogenetics* 71, 171–187. doi:10.1007/s00251-018-1095-x

Kotsias, F., Cebrian, I., and Alloatti, A. (2019). *Antigen Processing and Presentation*. Amsterdam: Elsevier, 69–121. doi:10.1016/bs.ircmb.2019.07.005

Kuipers, H. F., Biesta, P. J., Groothuis, T. A., Neefjes, J. J., Mommaas, A. M., and van den Elsen, P. J. (2005). Statins Affect Cell-Surface Expression of Major Histocompatibility Complex Class II Molecules by Disrupting Cholesterol-Containing Microdomains. *Hum. Immunol.* 66, 653–665. doi:10.1016/j.humimm.2005.04.004

Leroux, L.-P., Nishi, M., El-Hage, S., Fox, B. A., Bzik, D. J., and Dzierszinski, F. S. (2015). Parasite Manipulation of the Invariant Chain and the Peptide Editor H2-DM Affects Major Histocompatibility Complex Class II Antigen Presentation during *Toxoplasma Gondii* Infection. *Infect. Immun.* 83, 3865–3880. doi:10.1128/IAI.00415-15

Lopez, J., Bittame, A., Massera, C., Vasseur, V., Effantin, G., Valat, A., et al. (2015). Intravacuolar Membranes Regulate CD8 T Cell Recognition of Membrane-Bound *Toxoplasma Gondii* Protective Antigen. *Cell Rep.* 13, 2273–2286. doi:10.1016/j.celrep.2015.11.001

Lu, F., Liang, Q., Abi-Mosleh, L., Das, A., De Brabander, J. K., Goldstein, J. L., et al. (2015). Identification of NPC1 as the Target of U18666A, an Inhibitor of Lysosomal Cholesterol export and Ebola Infection. *Elife* 4, e12177. doi:10.7554/eLife.12177

Mashayekhi, M., Sandau, M. M., Dunay, I. R., Frickel, E. M., Khan, A., Goldszmid, R. S., et al. (2011). CD8α+ Dendritic Cells Are the Critical Source of Interleukin-12 that Controls Acute Infection by Toxoplasma Gondii Tachyzoites α(+) Dendritic Cells Are the Critical Source of Interleukin-12 that Controls Acute Infection by *Toxoplasma Gondii* Tachyzoites. *Immunity* 35, 249–259. doi:10.1016/j.immuni.2011.08.008

Nair-Gupta, P., Baccarini, A., Tung, N., Seyffer, F., Florey, O., Huang, Y., et al. (2014). TLR Signals Induce Phagosomal MHC-I Delivery from the Endosomal Recycling Compartment to Allow Cross-Presentation. *Cell* 158, 506–521. doi:10.1016/j.cell.2014.04.054

Nolan, S. J., Romano, J. D., and Coppens, I. (2017). Host Lipid Droplets: An Important Source of Lipids Salvaged by the Intracellular Parasite *Toxoplasma Gondii*. *Plos Pathog.* 13, e1006362. doi:10.1371/journal.ppat.1006362

Nutt, S. L., and Chopin, M. (2020). Transcriptional Networks Driving Dendritic Cell Differentiation and Function. *Immunity* 52, 942–956. doi:10.1016/j.immuni.2020.05.005

Poncet, A. F., Blanchard, N., and Marion, S. (2019). Toxoplasma and Dendritic Cells: An Intimate Relationship that Deserves Further Scrutiny. *Trends Parasitol.* 35, 870–886. doi:10.1016/j.pt.2019.08.001

Rivera-Cuevas, Y., Mayoral, J., Di Cristina, M., Lawrence, A.-L. E., Olafsson, E. B., Patel, R. K., et al. (2021). *Toxoplasma Gondii* Exploits the Host ESCRT Machinery for Parasite Uptake of Host Cytosolic Proteins. *Plos Pathog.* 17, e1010138. doi:10.1371/journal.ppat.1010138

Rocha, N., and Neefjes, J. (2008). MHC Class II Molecules on the Move for Successful Antigen Presentation. *Embo J.* 27, 1–5. doi:10.1038/sj.emboj.7601945

Romagnoli, P., and Germain, R. N. (1994). The CLIP Region of Invariant Chain Plays a Critical Role in Regulating Major Histocompatibility Complex Class II Folding, Transport, and Peptide Occupancy. *J. Exp. Med.* 180, 1107–1113. doi:10.1084/jem.180.3.1107

Romano, J. D., Nolan, S. J., Porter, C., Ehrenman, K., Hartman, E. J., Hsia, R.-c., et al. (2017). The Parasite Toxoplasma Sequesters Diverse Rab Host Vesicles within an Intravacuolar Network. *J. Cell Biol.* 216, 4235–4254. doi:10.1083/jcb.201701108

Roy, K., Ghosh, M., Pal, T. K., Chakrabarti, S., and Roy, S. (2013). Cholesterol Lowering Drug May Influence Cellular Immune Response by Altering MHC II Function. *J. Lipid Res.* 54, 3106–3115. doi:10.1194/jlr.M041954

Roy, K., Mandloi, S., Chakrabarti, S., and Roy, S. (2016). Cholesterol Corrects Altered Conformation of Mhc-Ii Protein in *Leishmania Donovani* Infected

Macrophages: Implication in Therapy. *Plos Negl. Trop. Dis.* 10, e0004710. doi:10.1371/journal.pntd.0004710

Sanfelice, R. A., da Silva, S. S., Bosqui, L. R., Miranda-Sapla, M. M., Barbosa, B. F., Silva, R. J., et al. (2017). Pravastatin and Simvastatin Inhibit the Adhesion, Replication and Proliferation of *Toxoplasma Gondii* (RH Strain) in HeLa Cells. *Acta Tropica* 167, 208–215. doi:10.1016/j.actatropica.2016.12.006

Shoemaker, C. J., Schornberg, K. L., Delos, S. E., Scully, C., Pajouhesh, H., Olinger, G. G., et al. (2013). Multiple Cationic Amphiphiles Induce a Niemann-Pick C Phenotype and Inhibit Ebola Virus Entry and Infection. *PLoS ONE* 8, e56265. doi:10.1371/journal.pone.0056265

Soccio, R. E., and Breslow, J. L. (2004). Intracellular Cholesterol Transport. *Atvb* 24, 1150–1160. doi:10.1161/01.atv.0000131264.66417.d5

Vrljic, M., Nishimura, S. Y., Moerner, W. E., and McConnell, H. M. (2005). Cholesterol Depletion Suppresses the Translational Diffusion of Class II Major Histocompatibility Complex Proteins in the Plasma Membrane. *Biophysical J.* 88, 334–347. doi:10.1529/biophysj.104.045989

Conflict of Interest: The authors declare that the research was conducted in the absence of any commercial or financial relationships that could be construed as a potential conflict of interest.

frontiers in Cell and Developmental Biology

ORIGINAL RESEARCH
published: 18 March 2022
doi: 10.3389/fcell.2022.844297

c-Abl Activation Linked to Autophagy-Lysosomal Dysfunction Contributes to Neurological Impairment in Niemann-Pick Type A Disease

Tamara Marín[1], Andrés E. Dulcey[2], Fabián Campos[1], Catalina de la Fuente[3], Mariana Acuña[1,4], Juan Castro[1], Claudio Pinto[3], María José Yañez[5], Cristian Cortez[6], David W. McGrath[7], Pablo J. Sáez[7], Kirill Gorshkov[2], Wei Zheng[2], Noel Southall[2], Maria Carmo-Fonseca[8], Juan Marugán[2], Alejandra R. Alvarez[3]* and Silvana Zanlungo[1]**

[1]Department of Gastroenterology, Faculty of Medicine, Pontificia Universidad Católica de Chile, Santiago, Chile, [2]Early Translation Branch, National Center for Advancing Translational Sciences (NCATS), NIH, Rockville, MD, United States, [3]Laboratory of Cell Signaling, Center for Aging and Regeneration (CARE), Millennium Institute on Immunology and Immunotherapy (IMII), Department of Cellular and Molecular Biology, Biological Sciences Faculty, Pontificia Universidad Católica de Chile, Santiago, Chile, [4]Department of Medicine, Brigham and Women's Hospital, Harvard Medical School, Boston, MA, United States, [5]School of Medical Technology, Health Sciences Faculty, Universidad San Sebastián, Santiago, Chile, [6]Center for Genomics and Bioinformatics, Faculty of Science, Universidad Mayor, Santiago, Chile, [7]Cell Communication and Migration Laboratory, Institute of Biochemistry and Molecular Cell Biology, Center for Experimental Medicine, University Medical Center Hamburg-Eppendorf, Hamburg, Germany, [8]Instituto de Medicina Molecular João Lobo Antunes, Faculdade de Medicina, Universidade de Lisboa, Lisbon, Portugal*

Niemann-Pick type A (NPA) disease is a fatal lysosomal neurodegenerative disorder caused by the deficiency in acid sphingomyelinase (ASM) activity. NPA patients present severe and progressive neurodegeneration starting at an early age. Currently, there is no effective treatment for this disease and NPA patients die between 2 and 3 years of age. NPA is characterized by an accumulation of sphingomyelin in lysosomes and dysfunction in the autophagy-lysosomal pathway. Recent studies show that c-Abl tyrosine kinase activity downregulates autophagy and the lysosomal pathway. Interestingly, this kinase is also activated in other lysosomal neurodegenerative disorders. Here, we describe that c-Abl activation contributes to the mechanisms of neuronal damage and death in NPA disease. Our data demonstrate that: 1) c-Abl is activated *in-vitro* as well as *in-vivo* NPA models; 2) imatinib, a clinical c-Abl inhibitor, reduces autophagy-lysosomal pathway alterations, restores autophagy flux, and lowers sphingomyelin accumulation in NPA patient fibroblasts and NPA neuronal models and 3) chronic treatment with nilotinib and neurotinib, two c-Abl inhibitors with differences in blood-brain barrier penetrance and target binding mode, show further benefits. While nilotinib treatment reduces neuronal death in the cerebellum and improves locomotor functions, neurotinib decreases glial activation, neuronal disorganization, and loss in hippocampus and cortex, as well as the cognitive decline of NPA mice. Our results support the participation of c-Abl signaling in NPA neurodegeneration and autophagy-lysosomal alterations, supporting the potential use of c-Abl inhibitors for the clinical treatment of NPA patients.

Keywords: Niemann-Pick disease, neurodegeneration, c-Abl kinase, autophay-lysosomal pathway, lysosomal storage disorder (LSD)

OPEN ACCESS

Edited by:
Georg Haase,
INSERM U1106 Institut de Neurosciences des Systèmes, France

Reviewed by:
Marcello D'Amelio,
Campus Bio-Medico University, Italy
Carmen María García-Ruiz,
Spanish National Research Council (CSIC), Spain

****Correspondence:***
Juan Marugán
maruganj@mail.nih.gov
Alejandra R. Alvarez
aalvarez@bio.puc.cl
Silvana Zanlungo
szanlungo@uc.cl

Specialty section:
This article was submitted to Membrane Traffic, a section of the journal Frontiers in Cell and Developmental Biology

Received: *27 December 2021*
Accepted: *25 February 2022*
Published: *18 March 2022*

Citation:
Marín T, Dulcey AE, Campos F, de la Fuente C, Acuña M, Castro J, Pinto C, Yañez MJ, Cortez C, McGrath DW, Sáez PJ, Gorshkov K, Zheng W, Southall N, Carmo-Fonseca M, Marugán J, Alvarez AR and Zanlungo S (2022) c-Abl Activation Linked to Autophagy-Lysosomal Dysfunction Contributes to Neurological Impairment in Niemann-Pick Type A Disease. Front. Cell Dev. Biol. 10:844297. doi: 10.3389/fcell.2022.844297

INTRODUCTION

Mutations in the *SMPD1* gene that encodes for acid sphingomyelinase (ASM), a key lysosomal enzyme that hydrolyzes sphingomyelin to ceramide and phosphocholine, lead to Niemann Pick type A (NPA) disease (Schuchman, 2007). NPA disease is a fatal lysosomal neurodegenerative disorder characterized by sphingomyelin accumulation in lysosomes leading to lysosomal dysfunction and autophagy alterations (Yanez et al., 2020). NPA patients present with developmental delay, hepatosplenomegaly, and progressive neurodegeneration that initially affects Purkinje neurons in the cerebellum (Otterbach and Stoffel, 1995). Additionally, the brain shows astrogliosis, and the astrocytes in the NPA hippocampus and cortex present altered morphology (Perez-Canamas et al., 2017). Unfortunately, NPA patients typically die between 2 and 3 years of age (Schuchman and Desnick, 2017).

The mechanisms that lead to neuronal death in NPA disease are not fully understood. Previous work recognized the role of calcium imbalance (Perez-Canamas et al., 2017), neuronal endocannabinoid system alterations (Bartoll et al., 2020), and autophagy alterations (Gabande-Rodriguez et al., 2014; Li et al., 2014). Many neurodegenerative disorders are associated with autophagy alterations, reflecting the contribution of this process to neuronal physiology as it is involved in quality control of cytosolic components, such as damaged proteins and organelles, survival, and differentiation (Nixon, 2013; Lee et al., 2016; Menzies et al., 2017). Recent studies have shown autophagy-lysosomal pathway (ALP) alterations in NPA disease at different levels, including autophagosome-lysosome fusion (Li et al., 2014) and lysosomal membrane permeabilization (Gabande-Rodriguez et al., 2014). Therefore, pharmacological and genetic manipulations to promote better functioning of the ALP in clearing accumulated materials may be therapeutic in neurodegenerative disorders, including NPA disease.

c-Abl is a non-receptor tyrosine kinase that has different biological functions depending on the cell type and regulates several pathways including apoptosis and ALP, in response to different signals. c-Abl has been reported as a central signaling kinase in different neurodegenerative disorders including Alzheimer's (Alvarez et al., 2004; Cancino et al., 2008), Parkinson's (Ko et al., 2010), Amyotrophic lateral sclerosis (ALS) (Imamura et al., 2017) and Niemann Pick type C (NPC) disease (Klein et al., 2011; Contreras et al., 2020), among others (Yanez et al., 2020). Recently, c-Abl has been shown to be involved in autophagy. Chronic treatment with nilotinib, a clinically validated c-Abl inhibitor, improves autophagy, reduces Aβ levels, and prevents neurodegeneration in an Alzheimer's mouse model (La Barbera et al., 2021). In Parkinson's, nilotinib induces cellular clearance of α-synuclein, via autophagic degradation, and protects the dopaminergic neurons, improving locomotor function in mouse models of this disease (Hebron et al., 2013). In addition, c-Abl inhibition using a classic inhibitor, imatinib, induces autophagy through the overexpression of genes involved in this process (Can et al., 2011). Interestingly, c-Abl kinase regulates ALP through transcription factor EB (TFEB) modulation (Contreras et al., 2020), the master transcriptional factor that drives the expression of genes related to autophagy and lysosomal biogenesis, and exocytosis.

The relation between c-Abl kinase activation, neurodegeneration, and the ALP in NPA disease has not been explored yet. In this work, we show that c-Abl signaling participates in the pathogenic mechanisms leading to neurodegeneration in NPA disease. We found that c-Abl is activated in several NPA models and its inhibition promotes the improvement in the ALP inducing autophagy flux and reducing sphingomyelin accumulation *in vitro* NPA models. Moreover, c-Abl inhibition decreases neuronal death, astrogliosis, inflammation markers, neuronal disorganization, and improves locomotor and cognitive functions in NPA mice.

MATERIAL AND METHODS

NPA Models

NPA cellular models: i) Primary skin fibroblasts from an NPA patient (GM13205) carrying one mutation at the *SMPD1* gene were purchased from the Coriell Institute for Medical Research. These NPA fibroblasts have no detectable sphingomyelinase activity; donor subject (female Ashkenazi, 2 years old) had one allele with a deletion of a single cytosine in exon 2 at codon 330 of the *SMPD1* gene [990delC] resulting in a frameshift leading to the formation of a premature stop (TGA) at codon 382 [P330fsX382]. Fibroblasts from an unaffected individual (HC; healthy control) (GM05659) were used as control; ii) Primary cultures of neurons were prepared from the hippocampus of wild-type (WT) and NPA mouse embryos age E18 and kept in culture for 7 days as described by Kaech et al. (2006). iii) NPA Neural Stem cells (NPA NSC) derived from NPA fibroblasts (GM16195) which were previously described (Long et al., 2016) and iv) SH-SY5Y cells were treated with desipramine 5, 10, 20 μM by 24 h to mimic the NPA phenotype.

NPA mice (ASMKO; *Smpd1*$^{-/-}$): They were created by gene targeting, as described previously (Horinouchi et al., 1995) and were kindly donated by Dr. Fernández-Checa (University of Southern California Research Center for Alcoholic Liver and Pancreatic Diseases and Cirrhosis, Keck School of Medicine, University of Southern California, Los Angeles, CA, United States and Cell Death and Proliferation, Institute of Biomedical Research of Barcelona (IIBB), CSIC, Barcelona, España). *Smpd1*$^{-/-}$ mice were obtained using heterozygous C57BL/6 breeding pairs and the littermates were used as controls. Animals were maintained in the Animal Care Facility of Pontificia Universidad Católica de Chile. Genotypes were identified using a PCR-based screening as described previously (Horinouchi et al., 1995). All procedures were approved by the ad hoc committee of Chile (ANID) and the Institutional Animal Care and Bioethical and Biosafety Committee of the UC (Protocol #170912002).

Cellular and Animal Treatments

Human fibroblasts and NSC were maintained in Dulbecco's modified Eagle's medium (DMEM) supplied with 15% fetal bovine serum (FBS). Primary neurons were maintained in

Neurobasal supplemented with 2% B27, 2 mM glutamine, 100 U/ml penicillin, and 100 μg/ml streptomycin. The proliferation of non-neuronal cells was limited using cytosine arabinoside 1 μM. Cells were treated with imatinib for 24 h, the concentration used was dependent on each cellular type; fibroblasts were treated with 10 μM, primary neurons with 5 μM, and NSCs with 100 nM of imatinib.

Acute treatment with a c-Abl inhibitor: Male/female WT and NPA mice received daily intraperitoneal injections (i.p.) of imatinib mesylate (Novartis, Basel, Switzerland) 12.5 mg/kg in 0.9% NaCl from postnatal day 21 (P21) to P49. Control groups (WT and NPA) received daily intraperitoneal injections of 0.9% NaCl. Bodyweight was measured twice a week during the full period of treatment, as well as locomotors tests were realized once a week.

Chronic treatment with c-Abl inhibitors: Male/female WT and NPA mice received diets supplemented with the c-Abl inhibitor nilotinib or neurotinib *ad libitum* from P21 until 5, 7, and 11 months of age. Control groups received a control diet.The rodent chow diet was manufactured by Envigo/Teklad by incorporation of neurotinib 67 ppm (10 mg/kg) or nilotinib at 200 ppm (30 mg/kg) into the NIH-31 Open Formula Mouse/Rat Sterilizable Diet (7017), followed by irradiation handling of the final product. Animal bodyweight was measured twice a week during the full period of treatment. The distribution of male/females in the control and treatment groups was 60/40%. No gender-dependent differences were observed in any of the results.

Immunofluorescence Analysis of Cultured Cells

Fibroblasts and primary neurons were seeded on poly-lysine-coated coverslips (30,000 cells/cover). After treatment, cells were fixed in 4% paraformaldehyde/4% sucrose in PBS and permeabilized with 0.02% Triton X-100. Then, cells were blocked with 3% bovine serum albumin in PBS. Immunostaining was carried out using anti-tyrosine 412 phosphorylated of c-Abl (Y412) (anti-p-c-Abl) (C5240, Sigma Chemical co), anti-p62 (ab56416; Abcam), anti-LAMP1 (1D4B, sc-19992; Santa Cruz Biotechnology). Anti-rabbit IgG conjugated with Alexa Fluor-488 and anti-mouse IgG conjugated to Alexa Fluor-555 and Hoechst 33342 (H3570) were obtained from Invitrogen Detection Technologies. Fluorescent images were captured with an Olympus BX51 microscope (Olympus, Tokyo, Japan) and analyzed with the Image-Pro Express program (Media Cybernetics). We examined at least five images by cover and three covers by condition were stained by experiment in at least three independent experiments.

BODIPY-SM and Filipin Staining in Cells

Briefly, 20,000 cells/well were seeded on coverslips on 24-well plates after 4 h incubation at 37°C with 5% CO_2, 0.2 mg/ml BODIPY-FL C122 sphingomyelin (BODIPY-SM; catalog no. D7711, Thermo Fisher Scientific) was added to cells, and incubated overnight. Then, cells were fixed with 4% paraformaldehyde solution. Later, cells were incubated with 1 mg/ml Hoechst 33342 (H3570; Invitrogen) in PBS with incubation at room temperature for 10 min. After washing, covers were mounted with Fluoromount-G, and cells were imaged in the Olympus BX51 microscope (Olympus).

For Filipin staining, cells were fixed in 4% paraformaldehyde/4% sucrose in PBS for 30 min. After, cells were washed with PBS and treated with 1.5 mg/ml glycine for 20 min. Finally, cells were treated with 25 μg/mL Filipin (F-8765, Sigma Chemical Co.) for 30 min, washed with PBS and covered with Fluoromount-G. Images were captured with an Olympus BX51 microscope.

mRFP-GFP Tandem Fluorescent-Tagged LC3 Expression

Neural Stem Cells were transduced with 30 particles per cell of the mRFP-GFP tandem fluorescent-tagged LC3 (Premo™ Autophagy Tandem Sensor RFP-GFP-LC3B, P36239, Thermo Fisher Scientific), as described in the manufacturer's instructions. After 24 h, cells were rinsed in 1 × PBS, nuclei were stained with Hoechst 33342 (H3570; Invitrogen) and processed for analysis in an LSM510 META microscope (Carl Zeiss AG). Quantification of only RFP-positive dots or dots positive for GFP and RFP was performed with ImageJ software.

Western Blot Analysis

Proteins were prepared as described previously (Cancino et al., 2008). Tissue protein samples (30 μg) and cellular protein samples (50 μg) were resolved by SDS–PAGE. The immunoblot was carried out using anti-c-Abl (A5844, Sigma-Aldrich, USA), p-c-Abl (Tyr412) (07–788; Millipore), anti-LC3 (NB100-2220), anti-p62 (ab56416), and anti-GAPDH (0411; sc47724; Santa Cruz Biotechnology) antibodies. The secondary antibodies against rabbit or mouse IgGs conjugated with horseradish peroxidase were obtained from Upstate Biotechnology, Lake Placid, NY, United States.

Hanging and Memory Flexibility Test

During the treatments, locomotor coordination was evaluated through the Hanging test. The mouse was placed at the center of a horizontal bar (3 mm diameter; 35 mm long) hanging with its forepaws. The body position of the animal was observed for 30 s and scored as previously described (Voikar et al., 2002)

Spatial memory acquisition and learning of animals was assessed using the modified Morris water maze test called Memory flexibility test (Chen et al., 2000; Toledo and Inestrosa, 2010) which consisted of a dark blue plastic pool 100 cm in diameter and 40 cm in depth, located in a 2.5 × 2.5-m room with numerous extra-maze visual cues that remained constant throughout the experiment. The pool was filled with water (a depth of 28 cm) and a clear acrylic glass platform (10 cm in diameter and 26 cm high) was positioned in the pool and its location was changed every day during the test. Testing was performed for four consecutive days. Each day the animal completed 15 swim trials to find the platform, each trial for 40 s. The animal reaches the acceptable memory criteria when it reaches the platform in three consecutive trials in less than 20 s per attempt. A minimum of 5 min is expected between trials per animal. A mean of 15 trials to reach the platform for each mouse were used in the statistical analyses.

Tissue Immunohistochemical and Immunofluorescence Procedures

Mice were anesthetized with xylazine 0.12 mg/10 g and ketamine 0.8 mg/10 g and intracardially perfused with 0.9% NaCl. Then, the cerebellum and brain were removed and postfixed with 4% paraformaldehyde in PBS overnight, followed by 30% sucrose in PBS at 4°C overnight. Cerebella were cut in 30 μm sagittal sections, and brains were cut 20 μm coronal sections with a cryostat (Leica CM 1850) at −20°C. 2–3 slices by animal were stained by experiment. We examined at least three animals per condition for quantitative analysis. For immunohistochemistry, slices were treated with H_2O_2 0.3% for 30 min, washed four times with PBS, treated with $NaBH_4$ 10 mg/ml for 15 min, washed with PBS three times by 10 min, and blocked with BSA 0.5% triton x-100 0.2% for 1 h. Anti-calbindin D-28K antibody (AB1778, Chemicon International), anti-NeuN (ab177487, Abcam) were used with the avidin-biotin-horseradish peroxidase complex method (Vector Laboratories, Burlingame, CA, United States). Entellan was used as mounting medium.

For immunofluorescence, slices were treated with 0.4% triton x-100 for 30 min, glycine 0.15 M for 15 min, $NaBH_4$ 10 mg/ml for 15 min, washed with PBS three times by 10 min, and blocked with BSA 3% triton x-100 0.4% for 1 h. We used anti-GFAP (#3670, Cell signaling technology), anti-Iba-1 (NB100-1028, NovusBio), anti-CD68 (MCA1957GA; Bio-Rad), and Hoechst 33,342 (H3570, Invitrogen). Secondary antibodies anti-rabbit IgG conjugated with Alexa Fluor-488, anti-mouse IgG conjugated to Alexa Fluor-555, and anti-rat IgG conjugated with FITC were obtained from Invitrogen Detection Technologies. Fluoromount-G was used as mounting medium. Images were captured with an Olympus BX51 microscope (Olympus) and analyzed with the Image-Pro Express program (Media Cybernetics, Bethesda, MD, United States).

Analysis of astrocyte and microglia size and shape were performed in Fiji ImageJ from fluorescent images acquired in a DMi8 Leica microscope, with a PL FLUOTAR 40 × with a numerical aperture of 0.80. Then, images were analyzed by using a custom-made macro based on the principles previously described in other cellular systems (Saez et al., 2018). Briefly, after background subtraction, the maximal z-projection was obtained from the planes that contained the cells. Then, semi-automatic segmentation was performed by using Li's threshold method and manual post-correction of the region of interest. Shape descriptors, such as area and solidity [defined as: (Area/Convex area)], were calculated from segmented images.

Filipin Staining in Tissue

Slices were treated with $NaBH_4$ 10 mg/ml for 10 min. Then, slices were incubated with Filipin (F-8765, Sigma Chemical Co.) overnight. The next day, slices were washed with 1 × PBS and mounted with gelatin 0.1%. Fluoromount-G was used as mounting medium.

Statistical Analysis

Mean and standard error with the corresponding number of experiments are indicated in each figure legend. Probability values of the data for Student *t*-tests and ANOVA followed by Tukey *post-hoc* test were calculated using GraphPad Prism 8 (Graph Pad Software, Inc., San Diego, USA).

In the box-and-whisker plots, the center line denotes the median value, edges are upper and lower quartiles, whiskers show minimum and maximum values and points are individual experiments or number of animals or cells.

RESULTS

c-Abl Is Active and its Inhibition Decreases Autophagy and Lysosomal Alterations in NPA Patient Fibroblasts

c-Abl contributes to other neurodegenerative disorders linked to ALP alterations (Ren et al., 2018; Contreras et al., 2020). When this kinase is activated, it is phosphorylated at tyrosine 412 (p-c-Abl) and also partially changes its location from the cytosol to the nucleus. To evaluate if c-Abl is active in NPA disease, we analyzed the levels of p-c-Abl by Western blot in GM13205 NPA patient fibroblasts (NPA fibroblasts), which harbor one of the most common mutations in NPA disease (see material and methods section). Interestingly, we found that the p-c-Abl levels are increased in comparison to fibroblasts from a healthy subject (HC fibroblasts; GM05659) (**Figure 1A**). Moreover, we observed that p-c-Abl kinase is translocated to the nucleus in NPA fibroblasts (**Figure 1B**; **Supplementary Figure S1A**). These results show that c-Abl kinase is activated in fibroblasts from an NPA patient.

In order to test the involvement of c-Abl in NPA disease ALP alterations, we characterized NPA fibroblasts. In agreement with previous reports, NPA fibroblasts showed sphingomyelin accumulation (**Figure 1C**). We found that the autophagy and lysosomal markers, p62 and LC3II levels, were increased in NPA fibroblasts (**Figure 1D**), confirming autophagy alterations. Furthermore, immunofluorescence analysis showed an accumulation of p62 positive-autophagic vesicles around the nucleus (**Figure 1E**; **Supplementary Figure S1B**). Also, we found that Lamp1 levels were increased, confirming that NPA fibroblasts contain more acid vesicles and lysosomes than HC fibroblasts (**Figure 1F**; **Supplementary Figure S1C**).

Interestingly, when we treated NPA fibroblasts with imatinib, a classic c-Abl inhibitor, we found a significant decrease in the number of p62-positive vesicles. Moreover, imatinib treatment restored the p62-positive vesicles distribution (**Figure 1E**; **Supplementary Figure S1B**). A similar trend was observed for the Lamp1 signal, which decreased when NPA fibroblasts were treated with imatinib (**Figure 1F**; **Supplementary Figure S1C**). These results show that NPA fibroblasts present autophagy and lysosomal alterations and suggest that c-Abl activation is regulating them.

c-Abl Inhibition Improves Autophagy Flux and Decreases Sphingomyelin Accumulation in NPA Neuronal Models

Next, we explored the activation of c-Abl in a neuronal NPA model using NPA Neural Stem cells (NPA NSC) derived from

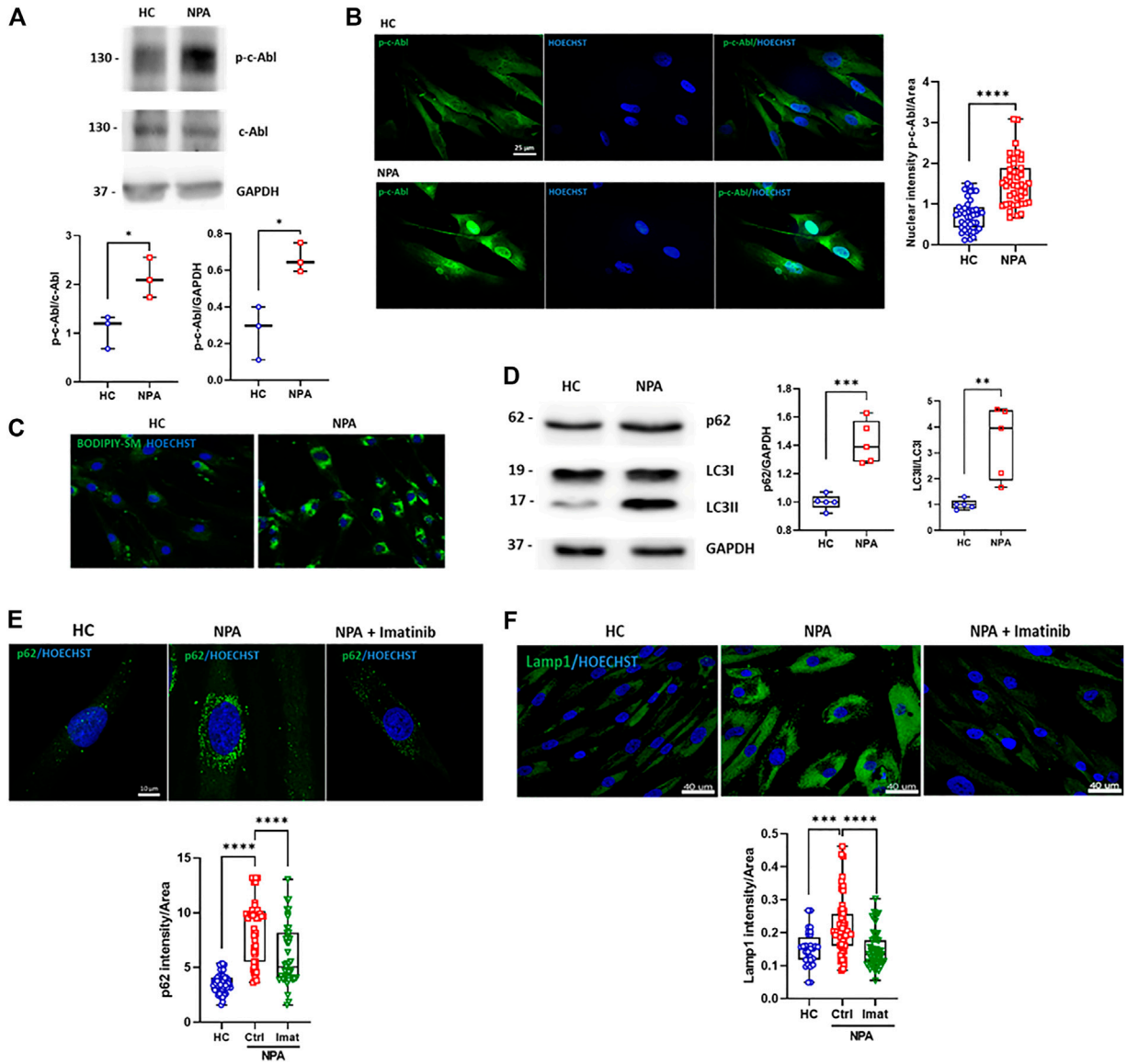

FIGURE 1 | c-Abl activation regulates autophagy and lysosomal alterations in NPA fibroblasts. **(A)** Human fibroblasts homogenates from NPA patient and healthy control (HC) subjects (50 µg protein/lane) were used to measure p-c-Abl levels. The graph shows quantifications of p-c-Abl levels normalized by GAPDH and c-Abl expression. The data shown are from three independent experiments. Student's *t*-test: $^{*}p < 0.05$. **(B)** HC and NPA fibroblasts were fixed and immunostained using an anti-p-c-Abl Tyr412 antibody (green) and Hoechst staining for nucleus (blue). For each condition, $n = 15$ cells were measured by experiment; three independent experiments were performed. Student's *t*-test: $^{****}p < 0.0001$. **(C)** HC and NPA fibroblasts were incubated with BODIPY-SM to confirm sphingomyelin accumulation. The images were taken with a × 40 objective lens. **(D)** Homogenates from fibroblasts from NPA patient and healthy control (HC) subject (50 µg protein/lane) were used to measure p62 and LC3II levels. The graph shows quantifications of protein levels normalized by GAPDH and LC3I expression, respectively. The image is representative of five independent experiments. Student's *t*-test: $^{**}p < 0.01$; $^{***}p < 0.001$; **(E)** HC and NPA fibroblasts were treated with imatinib (10 µM) for 24 h, fixed, and immunostained using an anti-p62 antibody (green) and **(F)** anti-Lamp1 (green). Hoechst staining for the nucleus (blue). For each condition, $n = 10–18$ cells were measured by experiment; three independent experiments were performed. ANOVA, Tukey *post-hoc*: $^{***}p < 0.001$; $^{****}p < 0.0001$. In the box-and-whisker plots, the center line denotes the median value, edges are upper and lower quartiles and whiskers show minimum and maximum values.

NPA fibroblasts (GM13205). The NPA NSCs exhibit a disease phenotype of lysosomal sphingomyelin accumulation and enlarged lysosomes and can be used as a cell-based disease model for studying the disease pathophysiology (Long et al., 2016). Interestingly, in this human neuronal NPA model, we also found that the levels of activated c-Abl are increased compared to NSCs derived from healthy individual fibroblasts (HC NSCs) (**Figure 2A**). We also confirmed c-Abl activation in another neuronal pharmacological NPA model, treating SH-SY5Y neuronal cells with the ASM inhibitor desipramine (Kornhuber et al., 2010). We confirmed the NPA phenotype through lipid accumulation using Filipin staining indicating the

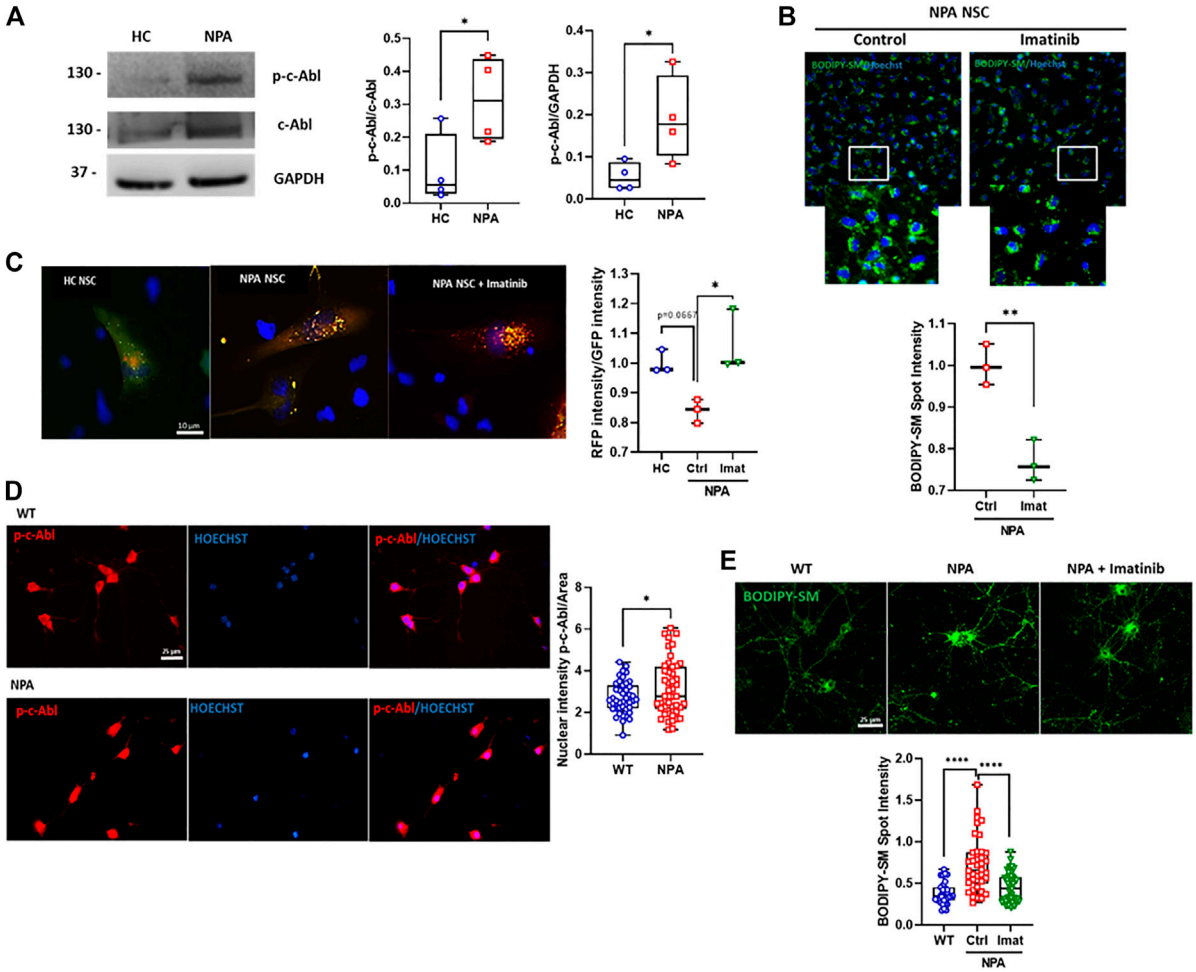

FIGURE 2 | c-Abl inhibition improves autophagy flux and decreases sphingomyelin accumulation in NPA neuronal models. **(A)** p-c-Abl levels were measured in Neural Stem Cells (NSCs) extracts by Western blot. Images representative from four independent experiments are shown. Student's *t*-test: $*p < 0.05$. **(B)** BODIPY-SM staining indicates sphingomyelin accumulation. Fluorescent microscopic images of NPA NSCs treated imatinib 0.001 μM by 24 h. For each condition, $n = 150$ cells were measured by experiment; three independent experiments were performed. Student's *t*-test: $**p < 0.01$. **(C)** NPA NSCs expressing mRFP-GFP-LC3 were treated with imatinib 0.001 μM by 24 h or vehicle. Graph shows the rate between RFP intensity and GFP intensity corresponding to autolysosomes. For each condition, $n = 50$ cells were measured by experiment; three different experiments were performed. Student's *t*-test: $*p < 0.05$. **(D)** Primary neurons were 7 days *in vitro*, fixed, and immunostained using anti-p-c-Abl Tyr412 antibody (red) and Hoechst staining for nucleus (blue). For each condition, $n = 10–20$ neurons were measured by experiment; three independent experiments were performed. Student's *t*-test: $*p < 0.05$. **(E)** Primary hippocampal neurons were treated with imatinib 5 μM by 24 h. Sphingomyelin accumulation was analyzed by BODIPY-SM. For each condition, $n = 10–20$ neurons were measured by experiment; three independent experiments were performed. ANOVA, Tukey *post-hoc*: $****p < 0.0001$. In the box-and-whisker plots, the center line denotes the median value, edges are upper and lower quartiles and whiskers show minimum and maximum values.

secondary accumulation of cholesterol (**Supplementary Figure S2A**) and a significant reduction in ASM activity in desipramine treated cells compared to control cells (**Supplementary Figure S2B**). Interestingly, we found an increase of p-c-Abl levels in SH-SY5Y cells treated with desipramine (**Supplementary Figure S3A**) and p-c-Abl nuclear localization in desipramine-treated cells (**Supplementary Figure S3B**).

To assess the contribution of c-Abl activity to the autophagy flux and cellular clearance dysfunction, we treated NPA NSCs with imatinib for 24 h and we evaluated sphingomyelin accumulation using BODIPY-SM. We found that imatinib treatment induces a decrease in sphingomyelin accumulation in NPA NSCs (**Figure 2B**).

We further analyzed the effect of c-Abl inhibition on autophagy flux using the Premo™ Autophagy Tandem Sensor RFP-GFP-LC3B in NPA NSCs. Cells incubated with this sensor express an LC3 fusion protein fused to an acid-sensitive GFP and an acid-insensitive RFP. The expression of this LC3 fusion protein allows visualizing the progression from autophagosome (neutral pH) to autolysosome (with an acidic pH) through the specific loss of the GFP fluorescence. Interestingly, HC NSCs mainly showed a diffuse green signal while NPA NSCs showed both punctuate GFP and RFP fluorescence (yellow colocalization), suggesting autophagosomes accumulation due to a decrease in

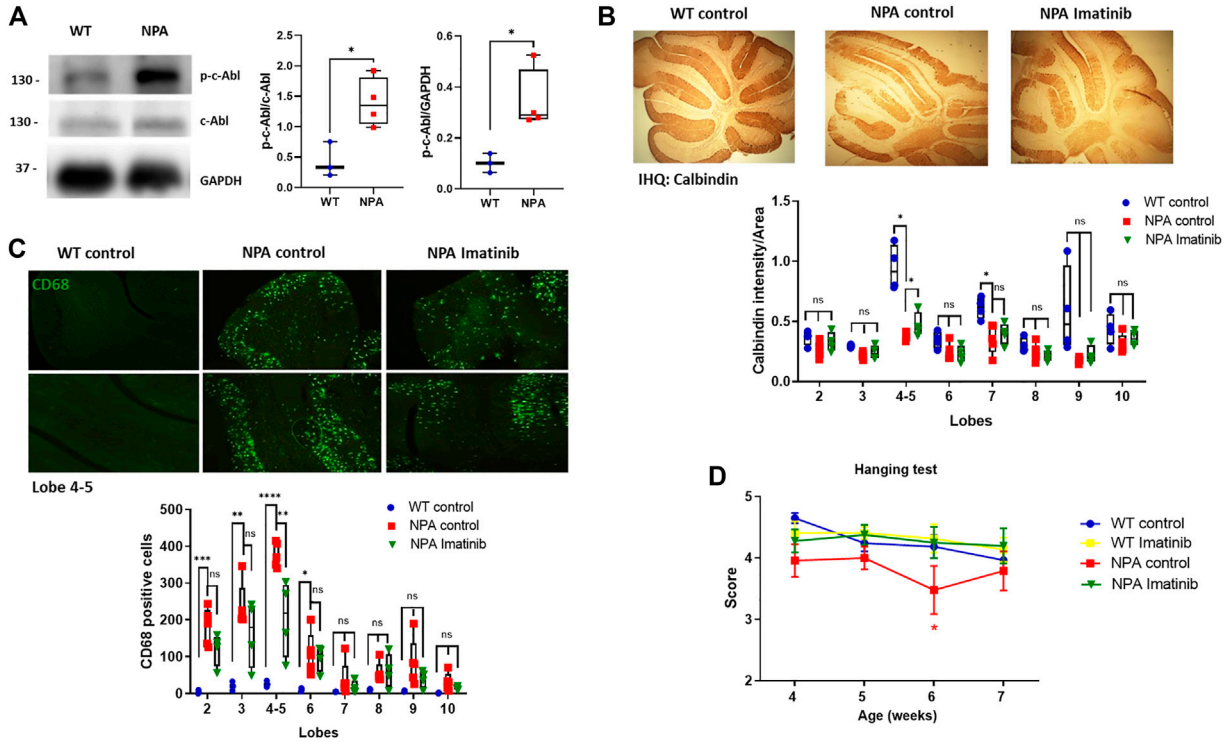

FIGURE 3 | Acute imatinib treatment decreases neuronal death in the cerebellum and improves locomotor function in NPA mice. **(A)** WT and NPA brain homogenates (50 μg protein/lane) from mice at 4 weeks old were analyzed by Western blot. The graph shows quantifications of p-c-Abl levels normalized by GAPDH and c-Abl levels. The number of animals was: WT = 3; NPA = 4; Student's *t*-test: $^{*}p < 0.05$. **(B)** WT and NPA mice were i.p. injected with imatinib (12.5 mg/kg) or vehicle from 3 weeks of age until 7 weeks of age. The Purkinje neuron marker calbindin was analyzed by immunohistochemistry. A quantification of calbindin-immunoreactive Purkinje cell bodies in cerebellar sections is shown. **(C)** CD68 marker was evaluated by immunofluorescence analysis in the cerebellum from WT and NPA mice. For **(B,C)**, the number of animals was WT control = 3; NPA control = 5; NPA imatinib = 4. Images were taken with × 4 objective. ANOVA, Tukey *post-hoc*: $^{*}p < 0.05$; $^{**}p < 0.01$; $^{***}p < 0.001$; $^{****}p < 0.0001$ **(D)** Mice were treated for 4 weeks and motor coordination was assessed weekly by the hanging test. Data are shown as mean ± SEM. ANOVA, Tukey *post-hoc*: $^{*}p < 0.05$, NPA control is statistically different from WT control and NPA with imatinib. The following number of animals was used: WT control = 11; WT imatinib = 10; NPA control = 8; NPA imatinib = 9. In the box-and-whisker plots, the center line denotes the median value, edges are upper and lower quartiles, whiskers show minimum and maximum values and points are individual experiments.

autophagosome-lysosome fusion in NPA (**Figure 2C**). Furthermore, the ratio between red intensity/green intensity was significantly increased with imatinib treatment in comparison to untreated NPA NSCs, suggesting that imatinib increases autolysosome formation (**Figure 2C**) thereby inducing autophagosome-lysosome fusion and increasing autophagy flux.

In addition, we analyzed c-Abl activation in primary cultures of hippocampal neurons obtained from the NPA mouse model, which was developed by the targeted deletion of the gene that codifies ASM (Horinouchi et al., 1995). The NPA mouse model (ASMKO; *Smpd1*$^{-/-}$) does not have residual ASM activity and exhibits progressive lipid storage in the reticuloendothelial (RES) organs, as well as in the brain (McGovern et al., 2017). First, we analyzed p-c-Abl levels by immunofluorescence from primary neurons from WT and NPA mouse embryos. We found that p-c-Abl levels and nuclear localization were increased in NPA primary neurons compared to WT neurons (**Figure 2D**; **Supplementary Figure S1D**). Moreover, we also found that imatinib treatment decreased sphingomyelin accumulation in NPA primary neurons (**Figure 2E**; **Supplementary Figure S1E**). These results show that c-Abl inhibition lowers sphingomyelin accumulation and suggests that c-Abl inhibition improves cellular clearance and autophagy flux in neuronal NPA models.

Acute c-Abl Inhibition Decreases the Neuronal Death in Cerebellum and Improves Locomotor Function in NPA Mice

To evaluate the relevance of c-Abl activity in neurodegeneration, we used the NPA mouse model described above, which exhibits progressive degeneration of Purkinje neurons in the cerebellum, gliosis, and demyelination (Otterbach and Stoffel, 1995). After we confirmed that c-Abl is active through Western blot in the central nervous system (CNS) in NPA mice (**Figure 3A**), we used an acute and short treatment scheme to evaluate the neuronal progression of NPA pathology. WT and NPA mice were injected intraperitoneally (i.p.) daily with imatinib (12.5 mg/kg) or vehicle from three until 7 weeks of age. The Purkinje cells loss was followed by immunohistochemistry analysis against calbindin. We found that the cerebellum of NPA mice showed less calbindin staining than WT mice at

anterior lobules, specifically 4–5, indicating Purkinje neurons loss (**Figure 3B**). This result is supported by previous studies that show that the loss of Purkinje neurons starts from the anterior lobes of the cerebellum and at older ages loss occurs in the posterior lobes (Macauley et al., 2008). Interestingly, the NPA mice treated with imatinib showed an increased calbindin staining, suggesting an improvement in the survival of the Purkinje neurons. A significant effect was found at lobules 4–5 (**Figure 3B**). Also, we evaluated the levels of the microglia marker CD68 by immunofluorescence. The cerebellum of NPA mice showed higher CD68 levels than the cerebellum of WT mice at anterior lobes and imatinib treatment significantly decreased CD68 positive cells specifically in lobules 4–5 compared to NPA mice cerebellum (**Figure 3C**).

Furthermore, we evaluated coordination and locomotor skills using the Hanging test (Voikar et al., 2002). We found that NPA mice showed impairment of the locomotor function compared to WT mice, whereas NPA mice treated with imatinib improved locomotor function in comparison to control NPA mice (**Figure 3D**). We did not find any difference in mice's gain of weight with the imatinib treatment (**Supplementary Figure S4**).

Chronic c-Abl Inhibition Treatment Delays Locomotor Impairment in NPA Mice

Our data above show that c-Abl inhibition decreases neuronal death in NPA mice at early ages. However, considering that NPA mice live for approximately 11 months, we decided to employ a longer, chronic, and less invasive treatment approach. We treated the animals with nilotinib and neurotinib-supplemented diets starting at 3 weeks of age. Both neurotinib and nilotinib are c-Abl inhibitors but these inhibitors have different mechanisms and brain penetration. Nilotinib binds to the ATP binding cleft between the N-terminal and C-terminal lobes, while neurotinib binds to an allosteric pocket for myristate at the C-terminal lobe of the kinase domain (Greuber et al., 2013; Wang, 2014). Nilotinib has been used in clinical trials for different neurodegenerative pathologies such as Parkinson's disease (Abushouk et al., 2018; Pagan et al., 2019) and Alzheimer's disease (Turner et al., 2020). Neurotinib is a new drug developed by our group in collaboration with the National Center for Advancing Translational Sciences at the National Institutes of Health (NCATS-NIH) which has favorable potency, selectivity, pharmacokinetics, and vastly improved central nervous system permeability that reaches higher concentration in the brain than nilotinib (**Supplementary Figure S5B**). The pharmacokinetic characterization of neurotinib is shown in **Supplementary Figure S5**. Animals were fed with a control diet or diets supplemented with neurotinib (67 ppm; 10 mg/kg) and nilotinib (200 ppm; 30 mg/kg) from 3 weeks of age to 11 months of age. We observed that p-c-Abl protein levels are increased in the cerebellum of control diet-treated NPA mice in comparison to WT mice with the same diet, indicating c-Abl activation at 5 months of age (**Figure 4A**). As we expected, diets supplemented with the c-Abl inhibitors nilotinib and neurotinib decreased p-c-Abl levels, suggesting that both treatments decreased c-Abl activation in the central nervous system (**Figure 4A**). To address if c-Abl inhibition is associated with an improvement in the locomotor function we evaluated the locomotor skills of mice through the Hanging test performed once a week from 4 weeks old until 11 months of age (**Figure 4B**). As expected, NPA mice fed with a control diet showed a significant and progressive impairment in locomotor function compared to WT mice (**Figure 4B**). Mice treated with neurotinib showed a modest delay in NPA-induced locomotor function impairment until 20 weeks of age. After that, the deterioration rate increased, similar to NPA mice treated with the control diet, until the end of treatment (**Figure 4B**). Surprisingly, we found that the NPA mice fed with the nilotinib supplemented diet maintained the locomotor function until the end of the treatment, showing very similar behaviour to WT mice.

The results were also analyzed by generating a deterioration curve with Hanging test data, which shows the percent of mice that score equal to or above three during treatment (a score less than three indicates locomotor impairment) (**Figure 4C**). As we expected, 100% of WT mice treated with the control diet had equal or above score 3 until the end of the treatment. Interestingly, 50% of NPA mice treated with the control diet had a score of three or higher at 10 weeks of treatment, while in the NPA mice treated with the neurotinib diet was at 21 weeks of treatment. Altogether, these results show a shift in the curve to the right for treatments with neurotinib and nilotinib, indeed the effect was bigger with the latter c-Abl inhibitor. At the end of treatment (46 weeks of treatment), 72% of NPA mice treated with the nilotinib diet and 30% of NPA mice treated with the neurotinib diet had a score 3 or higher. All of these analyses suggest that c-Abl inhibitors supplemented diets improved locomotor function and delayed deterioration, where nilotinib showed a significant and stable effect throughout the entire treatment (**Figure 4C**). NPA mice fed with control diet as well as NPA mice treated with diets supplemented with the c-Abl inhibitors showed similar loss of weight, starting around 5 months of age (150 days) (**Supplementary Figure S6**).

We next analyzed the histology of the cerebellum in mice at 5 months of age, after 4 months of treatment. We observed that the NPA cerebellum is smaller than the WT cerebellum at this age, indicating structural alterations in NPA mice. Furthermore, we found an impressive and significant loss of Purkinje neurons, followed by calbindin immunohistochemistry, at anterior and posterior lobules in the NPA mice cerebellum (**Figure 4D**). Interestingly, in accordance with our results using imatinib (acute treatment), we found that NPA mice treated with the nilotinib supplemented diet showed a significant increase in neuronal survival at posterior lobules 7 and 8, whereas mice treated with a neurotinib supplemented diet showed a trend for an increase in neuron survival that was not significant. Interestingly, this correlates with a better improvement in locomotor function with the nilotinib treatment compared with the neurotinib treatment (**Figure 4D**).

Chronic c-Abl Inhibition Treatment Improves Cognitive Decline and Decreases Brain Neuronal Disorganization and Gliosis in NPA Mouse Brains

Cerebellum damage in NPA disease has been well described, however, less is known about the pathological changes in other

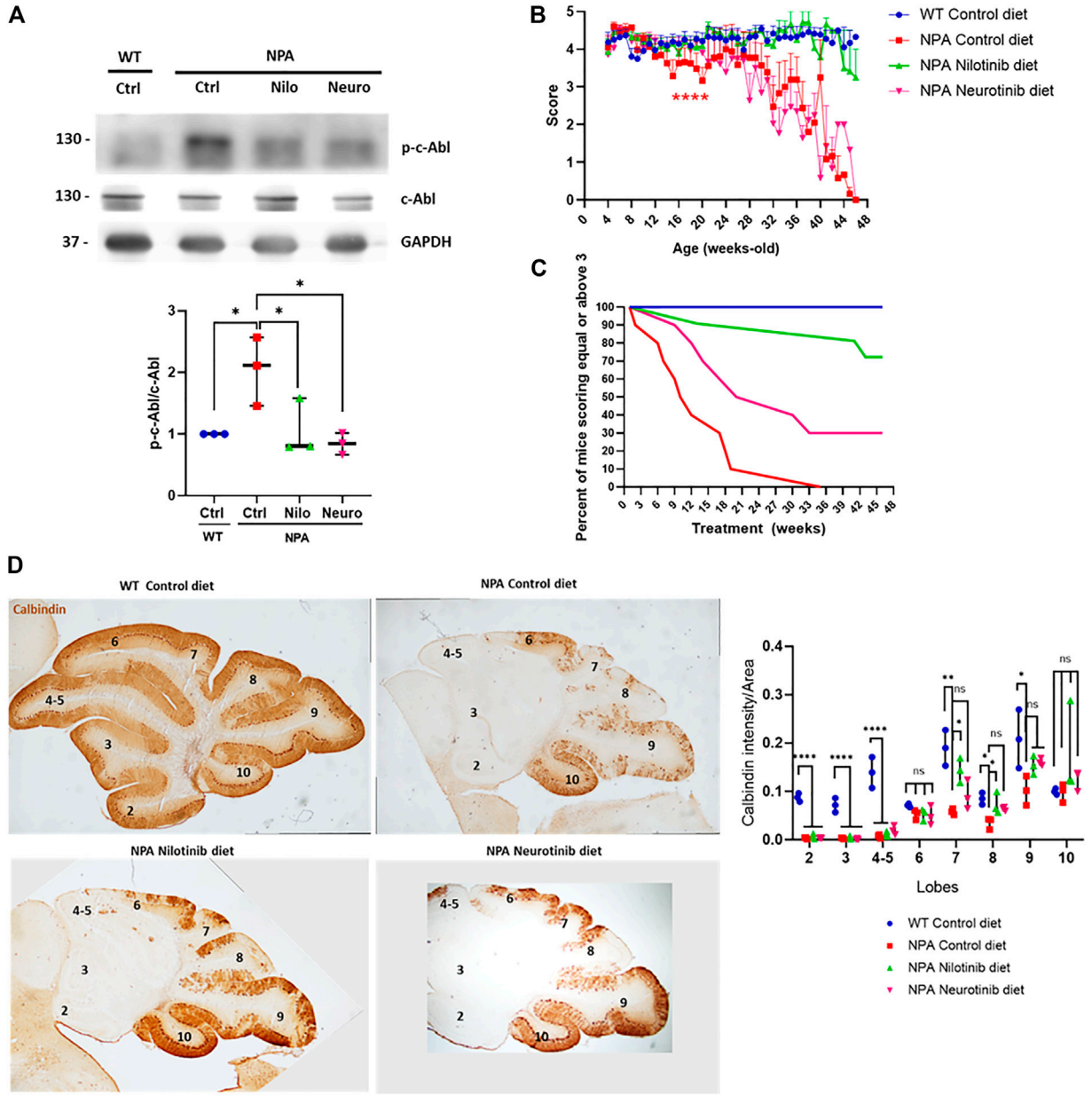

FIGURE 4 | Chronic c-Abl inhibition treatment delays locomotor impairment in NPA mice. WT and NPA mice received nilotinib (200 ppm; 30 mg/kg) and neurotinib (67 ppm; 10 mg/kg) supplemented diets or control diet starting at p21 until 11 months of age. **(A)** p-c-Abl protein levels were evaluated in cerebellum homogenates from WT and NPA mice of 5 months of age by Western blot. The number of animals was three by condition. ANOVA, Tukey *post-hoc*:*$p < 0.05$. **(B)** Motor coordination was assessed weekly by the Hanging test. Data are shown as mean ± SEM. ANOVA, Tukey *post-hoc*: ****$p < 0.0001$; NPA control is statistically different from WT control and nilotinib NPA. **(C)** Deterioration curve of mice was performed using percent of mice with a score equal to or above 3. For **(B,C)**, the following number of animals was used: WT control (Ctrl) = 10; NPA control (Ctrl) = 10; NPA nilotinib (Nilo) = 11; NPA neurotinib (Neuro) = 10. **(D)** Purkinje neuron marker Calbindin was analyzed by immunohistochemistry. Calbindin intensity was quantified. A representative image by condition is shown ($n = 3$ mice/group). Images were taken with × 2 objective. ANOVA, Tukey *post-hoc:* *$p < 0.05$; **$p < 0.01$; ***$p < 0.001$; ****$p < 0.0001$. In the box-and-whisker plots, the center line denotes the median value, edges are upper and lower quartiles, whiskers show minimum and maximum values and points are the number of animals used.

CNS regions. A previous report shows that cortex and hippocampus are affected in NPA pathology and associated with impairment in learning and memory (Arroyo et al., 2014). To asses the contribution of c-Abl in the cognitive impairment, we performed the Memory flexibility test, which is a modified Morris water maze test (Chen et al., 2000; Vorhees and Williams, 2006; Toledo and Inestrosa, 2010) in NPA mice at 7 months of age. The number of trials to reach the platform was used to evaluate cognitive function. As we expected, we found that NPA mice treated with control diet took significantly more

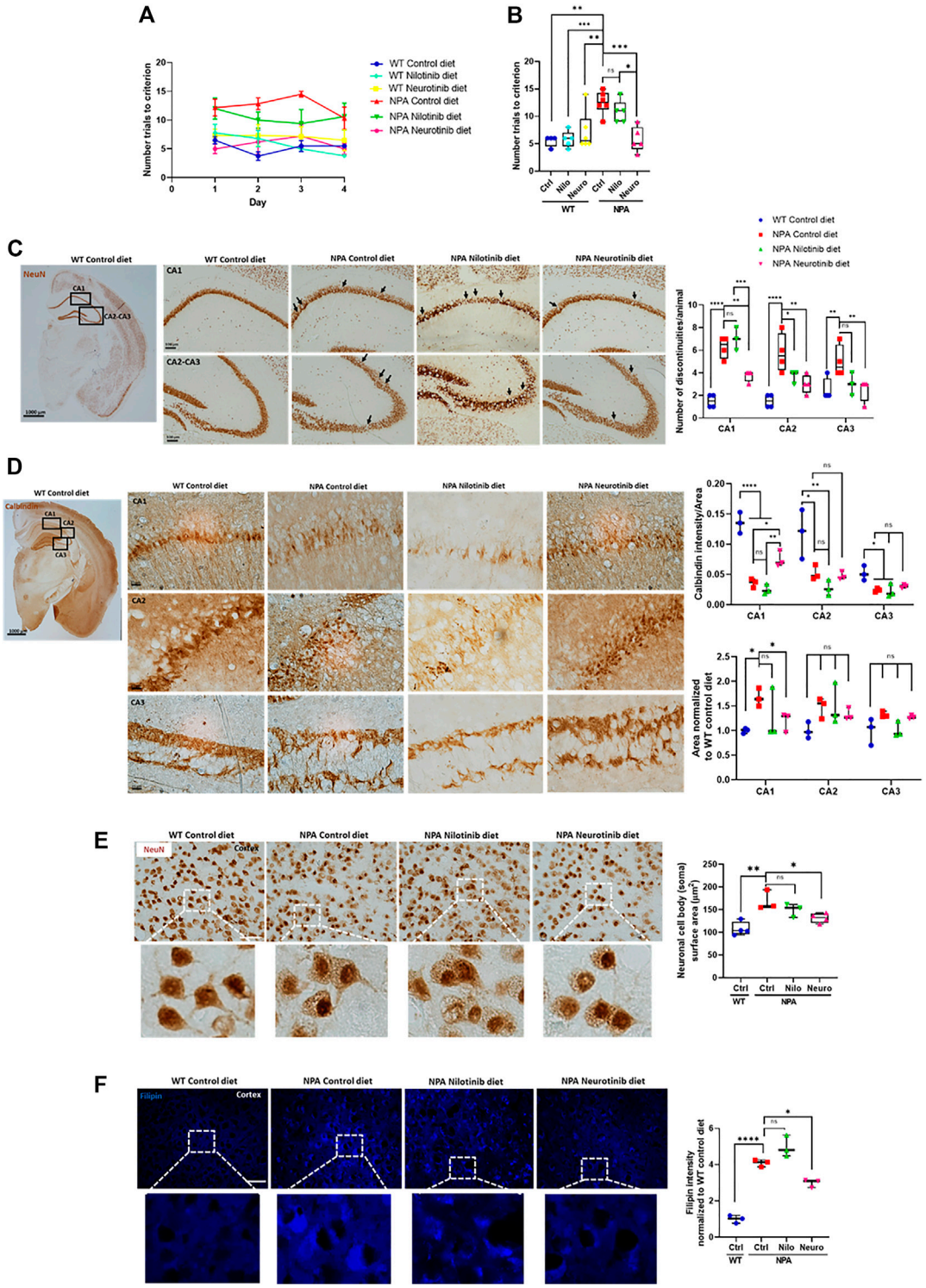

FIGURE 5 | Chronic c-Abl inhibition treatment improves cognitive decline and decreases brain neuronal disorganization in NPA mice. WT and NPA mice received nilotinib (200 ppm) and neurotinib (67 ppm) supplemented diets or control diet starting at p21 until 7 months of age. **(A)** Memory flexibility test was used to evaluate cognitive functions. Graphs show the number of trials every day during the test **(A)** and the average among 4 days of test **(B)**. The number of animals was: WT control (Ctrl) diet = 4; WT nilotinib (Nilo) diet = 5; WT neurotinib (Neuro) diet = 6; NPA control diet = 6; NPA nilotinib (Nilo) diet = 5; NPA neurotinib (Neuro) diet = 5. ANOVA, Tukey *post-hoc*: $*p < 0.05$; $**p < 0.01$; $***p < 0.001$ **(C)** Coronal sections of WT and NPA brain were stained with anti-NeuN antibody and 3,39-diaminobenzidine as chromogen. The rectangles in the first photo indicate where the magnification shown in the following photos comes from. Arrows point to actual discontinuities. Graph bars indicating discontinuity differences between WT and NPA mice with treatment in hippocampal subfields CA1, CA2, and CA3. Data are shown as the number of

(*Continued*)

FIGURE 5 | discontinuities/animal. The following number of animals was used: WT control = 4; NPA control = 4; NPA nilotinib = 3; NPA neurotinib = 4. ANOVA, Tukey *post-hoc*: *$p < 0.05$; **$p < 0.01$; ***$p < 0.001$; ****$p < 0.0001$. **(D)** Coronal sections were stained with calbindin which is a member of the large EF-hand family of calcium-binding proteins. These staining methods evidenced well-defined layers in the cortex and hippocampus structure. Neuronal disorganization with a decreased number of neurons is evident. The rectangles in the first photo indicate where the magnification shown in the following photos comes from. Image representative is shown. The following number of animals was used: WT control = 3; NPA control = 3; NPA nilotinib = 3; NPA neurotinib = 3. ANOVA, Tukey *post-hoc*: *$p < 0.05$; **$p < 0.01$; ****$p < 0.0001$. **(E)** Cortex neurons of the brains from WT and NPA mice were stained with NeuN antibody and 3,39-diaminobenzidine as chromogen. The area of the neuronal body was measured. 50 cells were measured by each mouse. The following number of animals was used: WT control (Ctrl) = 4; NPA control (Ctrl) = 3; NPA nilotinib = 3; NPA neurotinib = 4. ANOVA, Tukey *post-hoc*: *$p < 0.05$; **$p < 0.01$. **(F)** Slices were stained with Filipin staining to evaluate lipid accumulation. The following number of animals was used: WT control (Ctrl) = 3; NPA control (Ctrl) = 3; NPA nilotinib = 3; NPA neurotinib = 3. Image representative. ANOVA, Tukey *post-hoc*: *$p < 0.05$; ****$p < 0.0001$. Scale bar = 50 μm. In the box-and-whisker plots, the center line denotes the median value, edges are upper and lower quartiles, whiskers show minimum and maximum values and points are individual experiments.

trials to learn where the platform is, in comparison to WT mice during each day of testing (**Figure 5A**) or as an average of all days (**Figure 5B**), confirming a cognitive impairment in NPA mice at this age. Interestingly, NPA mice treated with a nilotinib supplemented diet showed a tendency toward improved cognitive function while the NPA mice treated with neurotinib supplemented diet showed a significant improvement in cognitive function in comparison to NPA mice treated with control diet, producing results similar to WT mice. Therefore, c-Abl inhibition improves cognitive functions of NPA mice and these results suggest that neurotinib is a better treatment than nilotinib for the cognitive alterations in NPA disease (**Figure 5B**).

After the memory flexibility test, mice were sacrificed and examined for neuronal damage and changes in the neuronal organization in the brain cortex and hippocampus. We stained tissues for neuronal-specific markers, the DNA-binding protein NeuN and the calcium-binding protein calbindin, which show well-defined layers in the cortex and hippocampus structure. NPA mice exhibited discontinuities in hippocampus zones CA1, CA2, and CA3 using NeuN immunostaining. Quantitation of the effect showed more discontinuities in the dorsal hippocampus of NPA mice (**Figure 5C**). Moreover, calbindin staining of the hippocampus from NPA mice also showed an increase of the zone area with a decrease in calbindin staining, suggesting structural disorganization and a decrease in number of calbindin positive neurons in the CA1 zone (**Figure 5D**). In addition, in the NPA mice cortex, the cell body of neurons was significantly bigger than the cell body of neurons from WT mice (**Figure 5E**). This correlated with a significant increase in Filipin staining levels in the cortex from NPA mice, confirming cholesterol accumulation in the NPA brain (**Figure 5F**). Interestingly, discontinuities and disorganization decreased in NPA mice treated with neurotinib and nilotinib supplemented diets, suggesting that c-Abl inhibition restores proper structuring and organization of the brain (**Figures 5C,D**). Additionally, c-Abl inhibition using only neurotinib diet treatment decreased neuronal cell body surface area and lipid accumulation, supporting the participation of c-Abl activation in ALP alterations (**Figures 5E,F**).

Previous studies have shown microglial activation in NPA disease (Gabande-Rodriguez et al., 2019). As expected, we found astrocyte and microglial activation in the cortex of NPA mice (**Figure 6A**). Interestingly, we found that the treatment with neurotinib reduced astrocyte activation, decreasing the size of astrocytes in the brains of NPA mice treated with neurotinib (**Figure 6B**; **Supplementary Figure S1F**). Moreover, we analyzed the cell shape of microglia as an index of activation, as resting-state microglia are ramified whereas activated microglia have an amoeboid form. Treatment with neurotinib restored the microglial shape in NPA brains, and the morphology of those cells is similar to that observed in WT brains (**Figure 6C**; **Supplementary Figure S1G**). These data show that c-Abl inhibition using neurotinib reduces both astrogliosis and microgliosis.

Altogether these results show that c-Abl inhibition decreases Purkinje cell death in the cerebellum correlating with an improvement in autophagy flux and locomotor function. Furthermore, our results show that there is glial activation and neuronal disorganization in NPA mice brains, which correlate with impairment of the cognitive function. Treatment with c-Abl inhibitors supplemented diets reduced these alterations improving memory and locomotor function in NPA mice. Our results strongly support the potential use of c-Abl inhibitors for clinical treatment of NPA patients.

DISCUSSION

Our work represents the first demonstration that c-Abl kinase plays an important role in neurodegeneration that is a hallmark of NPA pathology and that c-Abl inhibition can improve neurological decline of NPA mice. The major findings of this work are the following: 1) c-Abl kinase is activated in several NPA models; 2) *In vitro* NPA models show autophagy and lysosomal alterations; 3) c-Abl inhibition induces autophagy flux and lowers sphingomyelin accumulation in *in vitro* NPA models and 4) c-Abl inhibition associates with a decrease in neuronal death, brain neuronal disorganization, glial markers and with an improvement in locomotor and cognitive functions in NPA mice.

We found an increase of p-c-Abl protein levels and an increase in its nuclear localization in human NPA fibroblasts and NPA mouse primary neurons. Interestingly, c-Abl nuclear localization has been related to its pro-apoptotic functions, leading to cellular death (Wen et al., 1996). c-Abl is a non-receptor tyrosine kinase that has different biological functions depending on the cell type and can regulate several pathways in response to different signals (Wang, 2014). It has one nuclear export signal (NES) and three nuclear localization signal (NLS) motifs in its C-terminus consistent with its cytoplasmic and nuclear localization and its capacity to regulate gene expression through c-Abl substrates such as the transcription factors p73 (Klein

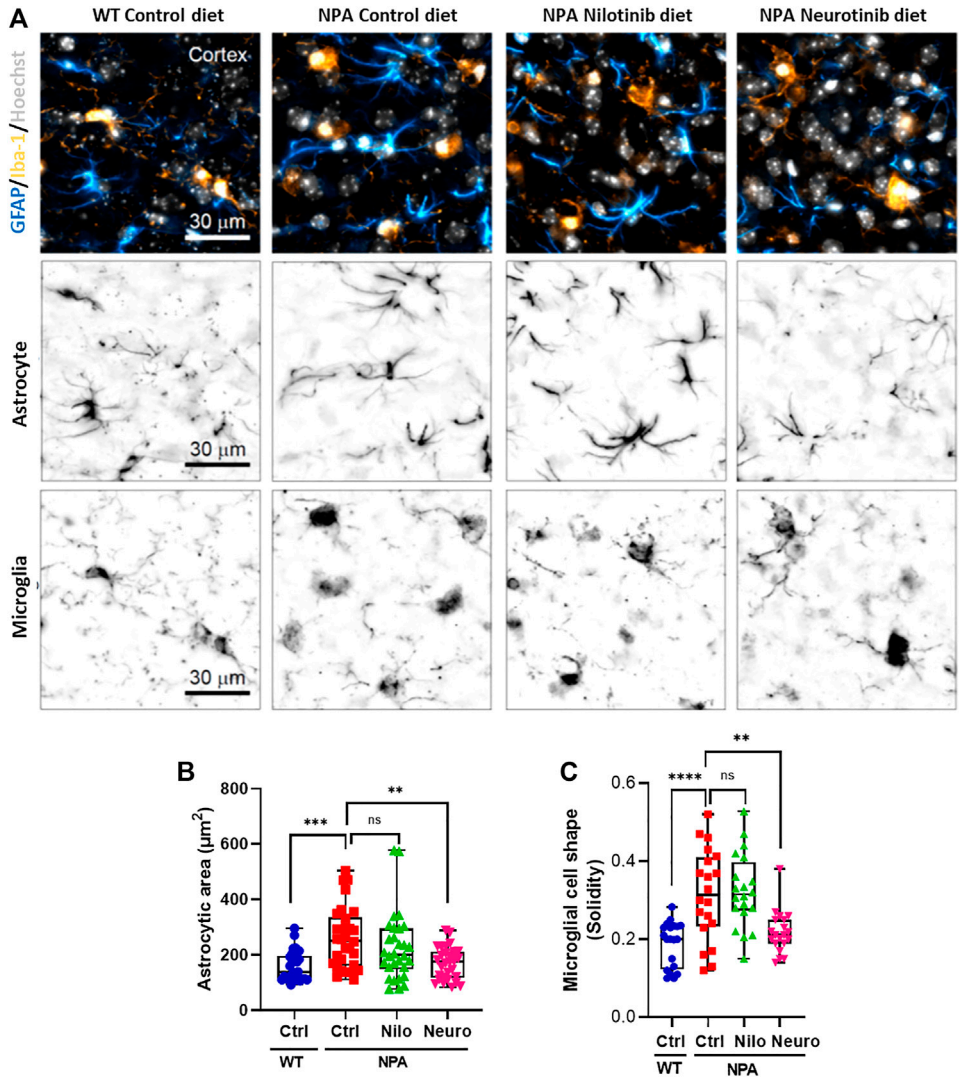

FIGURE 6 | Chronic c-Abl inhibition decreases glial activation in NPA mice. WT and NPA mice received nilotinib (200 ppm; 30 mg/kg) and neurotinib (67 ppm; 10 mg/kg) supplemented diets or control diet starting at p21 until 7 months of age. **(A)** Markers of astrocyte (GFAP) and microglia (Iba-1) were analyzed by immunofluorescence in slices of brain from WT and NPA mice. Confocal images were obtained of the cortex for each condition. A representative image of the cortex is shown in the first row; astrocytes (cyan hot), microglia (orange hot), and nucleus (grays). Representative images to visualize astrocyte and microglial shape are shown in the second and third row, respectively. **(B)** Astrocyte area was measured from GFAP positive cells. For each condition, $n = 10$ cells were measured by animal; three mice/group. ANOVA, Tukey *post-hoc*: $^{**}p < 0.01$, $^{***}p < 0.001$. **(C)** Microglia shape was determined from Iba-1 fluorescence. For each condition, $n = 5$–10 cells were measured by animal; three mice/group. ANOVA, Tukey *post-hoc*: $^{**}p < 0.01$, $^{****}p < 0.0001$. In the box-and-whisker plots, the center line denotes the median value, edges are upper and lower quartiles and whiskers show minimum and maximum values.

et al., 2011), TFEB (Contreras et al., 2020) and histone deacetylase HDAC2 (Gonzalez-Zuniga et al., 2014). Therefore, it is possible that in the NPA pathology the c-Abl kinase activation affects the expression of different genes. This possibility deserves further investigation.

c-Abl has been reported to be activated in other lysosomal and/or neurodegenerative diseases, including NPC disease, Gaucher disease (Yanez et al., 2021), Alzheimer's, and Parkinson's disease (Alvarez et al., 2004; Alvarez et al., 2008; Imam et al., 2011; La Barbera et al., 2021). Interestingly, NPC disease is a lysosomal storage and neurodegenerative disorder that shares several characteristics with NPA disease despite they are caused by mutations in different genes (Yanez et al., 2020). In NPC disease, the c-Abl signaling pathway impacts several of its downstream targets, including the p73 transcription factor (Alvarez et al., 2008), HDAC2 (Gonzalez-Zuniga et al., 2014; Contreras et al., 2016), APP (Yanez et al., 2016) and TFEB (Contreras et al., 2020). It would be interesting to study if these signaling pathways are also activated and participate in NPA pathological mechanisms. Thus, these diseases, which are different in their etiology, could share a common mechanism for neuronal death that involves activation of the c-Abl kinase.

It has been described that c-Abl kinase can be activated in response to distinct types of cellular stress (Sun et al., 2000; Shaul

and Ben-Yehoyada, 2005; Hopkins et al., 2012). However, the upstream stimulus and mechanism that activates c-Abl kinase in NPA disease remain unclear. The c-Abl kinase signaling activation in NPC neurons has been linked to increments in ROS levels (Klein et al., 2011). Interestingly, increased oxidative stress has also been described in NPA disease (Perez-Canamas et al., 2017). On the other hand, some studies suggest that c-Abl may be regulated in different cellular contexts by lipids (Van Etten, 2003). Therefore, there is a possibility that sphingomyelin or other lipids accumulation could activate c-Abl kinase in NPA pathology. Clearly, we have more to learn about the regulation of this kinase. This is an interesting topic that remains to be elucidated.

As previously mentioned, we utilized several NPA models including a pharmacological NPA model using desipramine which induces functional inhibition of ASM. The ASM enzyme is attached by electrostatic forces to the inner lysosomal membrane, thereby being protected against proteolysis. High concentrations of the protonated bases, such as desipramine, disturb the binding of ASM to the inner lysosomal membrane and result in detachment of ASM and subsequent inactivation possibly involving proteolysis (Kornhuber et al., 2010). However, considering desipramine is a promiscuous tricyclic antidepressant (TCA), we cannot rule out that part of the observed effect of c-Abl activation is produced through other targets of desipramine. Nevertheless, it is interesting that the ASM inhibition leads to c-Abl activation indicating that lipids homeostasis alterations are related to c-Abl regulation.

Autophagy is an important cellular process that eliminates damaged proteins, dysfunctional organelles, and protein aggregates, where lysosomes have a central role (Menzies et al., 2017). Neurons are particularly affected by disruptions of autophagy which are associated with many neurodegenerative disorders (Nixon, 2013; Lee et al., 2016; Menzies et al., 2017). It has been published that autophagy can be regulated by c-Abl kinase (Hebron et al., 2013; Contreras et al., 2020; Karim et al., 2020; La Barbera et al., 2021). Interestingly, we found that activated c-Abl levels and autophagy markers are increased in NPA cellular models. Furthermore, we found a high number of autophagy p62 positive vesicles around the nucleus. Our results are in accordance with what has been published before, fibroblasts from NPA patients accumulate elongated and unclosed autophagic membranes, as well as abnormally swollen autophagosomes (Corcelle-Termeau et al., 2016). Moreover, it has been described that autophagosome clearance is delayed leading to the accumulation of vesicles in other similar pathologies. For example, alterations in lysosomal function and autophagy are tightly associated with neurodegeneration in NPC disease (Liao et al., 2007) and other neurodegenerative disorders such as Parkinson's disease (Garcia-Sanz et al., 2018), Gaucher disease (Aflaki et al., 2016), and Alzheimer's disease (Cermak et al., 2016), among others (Lee et al., 2016; Menzies et al., 2017). In this sense, it has been described that lipid accumulation in NPA could contribute to autophagosomes accumulation because of autophagosome-lysosome fusion impairment (Li et al., 2014; Corcelle-Termeau et al., 2016). Moreover, lysosomal membrane permeabilization leading to the cytosolic release of lysosomal enzymes, such as Cathepsin B, has been described in NPA fibroblasts (Gabande-Rodriguez et al., 2014) and also in NPC models by our group (unpublished results).

We found that NPA cells exhibit alterations in lysosomal function and autophagy as well as c-Abl activation. Our results suggest that both mechanisms are connected. We observed that when c-Abl is inhibited, there is a decrease in sphingomyelin accumulation, autophagy markers, and cellular death. Also, we found that c-Abl inhibition increases autophagosome-lysosome fusion suggesting the induction of the autophagy flux. However, we can not rule out that c-Abl inhibition could be affecting different processes and characteristics related to lysosomes, such as membrane permeability and function, among others. The mechanism and how and what stage of autophagy flux could be regulated by c-Abl is not fully understood. One option is that c-Abl could be regulating gene expression through the transcription factor TFEB (Contreras et al., 2020). Thus, it could be regulating autophagy, lysosomal biogenesis, clearance, and exocytosis (Can et al., 2011; Ren et al., 2018). Accordingly, we propose that c-Abl inhibition is regulating different processes related to lysosomes at the same time. This could explain the decrease in sphingomyelin accumulation after 24 h of treatment with c-Abl inhibitors observed in this work. This effect is similar to the effect observed in NPC cells where c-Abl inhibition reduced cholesterol accumulation (Contreras et al., 2020). Another option is that c-Abl could phosphorylate some proteins related to the actin cytoskeleton (Mitsushima et al., 2006) and autophagy proteins such as beclin (Yu et al., 2020). This could directly affect the formation of autophagy vesicles and/or their movement. As mentioned, neurons are particularly affected by disruptions of autophagy (Nixon, 2013). Therefore, an improvement in autophagy could decrease neuronal death. This could positively affect Purkinje neurons in the cerebellum, hippocampal and cortical neurons in the brain, leading to a decrease in neuronal death and an improvement in locomotor and cognitive functions, respectively, in the NPA mouse. Actually, we found that mice treated with injections of imatinib show an increase in Purkinje neuron survival and a decrease in CD68 signal associated with cerebellar inflammation when c-Abl is inhibited. These results are similar to those published in NPC mice with an imatinib treatment (Alvarez et al., 2008). Here we also demonstrate a decrease in glial activation in NPA mice treated with c-Abl inhibitors. However, more studies are necessary to evaluate the effect of c-Abl inhibition on autophagy flux and its connection with neuronal death.

NPA mice live approximately 11 months, allowing us an opportunity to study the effects of a prolonged, chronic treatment using c-Abl inhibitors supplemented diets. This strategy is less invasive and is closer to an oral treatment such as that an NPA patient might receive. Also, a longer treatment allowed us the opportunity to explore different brain areas that could be involved in the impairment of other functions, such as learning and memory in the NPA pathology. It has been well described that the cortex and hippocampus in the brain are involved in learning and memory (Miller, 2000; Preston and

Eichenbaum, 2013; Opitz, 2014). Indeed, both areas before mentioned are affected in NPA pathology consistent with the impairment of the cognitive functions (Arroyo et al., 2014). Chronic treatment was performed using nilotinib and neurotinib supplemented diets. Imatinib was not considered for chronic treatment because it has a low Blood-Brain Barrier permeability (Wolff et al., 2003). Interestingly, we obtained differential results with the supplemented diets. On the one hand, our results show an outstanding improvement in the locomotor function in NPA mice treated with the nilotinib supplemented diet which correlates with an increase in Purkinje neuron survival in the cerebellum. And on the other side, we found a significant improvement in cognitive functions in NPA mice treated with neurotinib that correlated with a decrease in brain neuronal disorganization and gliosis in NPA mouse brain. Considering these results, it would be interesting to evaluate if a combined therapy has a synergistic effect.

The reasons that account for these differences between the treatments with these two c-Abl inhibitors neurotinib and nilotinib are not clear yet. Nilotinib is a classical c-Abl inhibitor that has been used in other neurodegenerative pathologies such as Parkinson's disease (Pagan et al., 2019) and Alzheimer's disease (Turner et al., 2020). Neurotinib is a new c-Abl inhibitor that was designed by our laboratory and the NCATS-NIH group. Nilotinib and neurotinib present different c-Abl inhibition mechanisms. Nilotinib binds to the ATP binding cleft between the N-terminal and C-terminal lobes, while neurotinib binds to an allosteric pocket for myristate at the C-terminal lobe of the kinase domain. In contrast to nilotinib which targets multiple kinases, the allosteric inhibitor neurotinib is highly selective for the c-Abl kinase. In addition, it is important to mention that the diets supplemented with the inhibitors were used with different concentrations: 67 ppm (10 mg/kg) for neurotinib, while 200 ppm (30 mg/kg) was used for nilotinib. Also, it is relevant that neurotinib has a better brain penetration and remains more time than nilotinib in the brain (**Supplementary Figure S5B**). Thus the concentrations of neurotinib and nilotinib for efficacy experiments were chosen to provide proper brain levels of the drug, where 200 ppm allows a reasonable concentration of nilotinib in the brain. A possible explanation for the differences in the observed results between these two compounds is that 200 ppm of nilotinib would provide better exposure toward the peripheral nervous system and muscle, which has been described showing functional defects in NPA mice (Michailowsky et al., 2019), while neurotinib distribute with better efficacy toward the CNS. More experiments are required to better understand pharmacokinetic to pharmacodynamic aspects of c-Abl inhibition. Although we obtained promising results, we did not observe an increase in the survival of NPA mice using a small number of animals, unlike a recent paper published where the authors found an increase in survival modulating the endocannabinoid signaling (Bartoll et al., 2020). It is possible that we need to increase the number of animals to obtain better results but also it could be that an increase in survival requires an integral effect including brain and peripheral organs.

Recent reports show that c-Abl inhibitors are being used in clinical trials for different neurodegenerative pathologies, including Parkinson's disease (Abushouk et al., 2018; Pagan et al., 2019) and other Dementias (Pagan et al., 2016), Huntington's disease (Clinical trial gov identifier NCT03764215) and Alzheimer's disease (NCT02947893) (Turner et al., 2020). Results in Parkinson's patients are promising because they show improvement in locomotor function and decreased synuclein accumulation, stimulating a new phase of this study (Pagan et al., 2019).

Considering these antecedents and our results, c-Abl is a promising therapeutic target for NPA. Moreover, c-Abl inhibitors are safe drugs that are well tolerated, with mild secondary effects already approved by the FDA for the treatment of chronic myeloid leukemia and another kind of cancers. Altogether, our work opens new perspectives for therapeutic interventions supporting the potential use of c-Abl inhibitors for the clinical treatment of NPA patients.

DATA AVAILABILITY STATEMENT

The original contributions presented in the study are included in the article/**Supplementary Material**, further inquiries can be directed to the corresponding authors.

ETHICS STATEMENT

The animal study was reviewed and approved by the Comité Ético Científico para el Cuidado de Animales y Ambiente PUC. Written informed consent was obtained from the owners for the participation of their animals in this study.

AUTHOR CONTRIBUTIONS

Conceptualization, TM, AA, and SZ; methodology, TM, FC, CD, MA, JC, MJY, CC, AD, DM, PS, and KG; drug design, AD and JM; formal analysis, TM, AA, and SZ; writing—original draft preparation, TM, AA, and SZ; PS wrote the scripts for analysis of cell shape, writing—review and editing, TM, MA, PS, KG, WZ, NS, CF, JM, AA, and SZ; funding acquisition, AA, CF, JM, and SZ. All authors have read and agreed to the published version of the manuscript.

FUNDING

This work was supported by the Comisión Nacional de Investigación Científica y Tecnológica-Chile: Fondecyt, 1201668 (AA), 1150186 and 1190334 (SZ), CARE-Chile-UC Center under grant number AFB170005 and FONDEF D10E1077, ID21I10347 (AA), PROGRAMA ICM-ANID, ICN 2021 045 (AA) and the intramural research program at the National Center for Advancing Translational Sciences, (NCATS), National Institutes of Health (JM), European Union's Horizon 2020–MSCA–RISE programme under grant agreement No 734825 (LysoMod) (CF and SZ), European Union's Horizon 2020 research and innovation programme under the Marie Sklodowska-Curie grant agreement No 953489 (PS), and CONICYT-PCHA/Doctorado-Nacional grant #2015-150038 (TM).

ACKNOWLEDGMENTS

PS and DM would like to acknowledge Dr. Antonio V. Failla and the UKE Microscopy Imaging Facility (UMIF) under the DFG Research Infrastructure Portal: RI_00489.

SUPPLEMENTARY MATERIAL

The Supplementary Material for this article can be found online at: https://www.frontiersin.org/articles/10.3389/fcell.2022.844297/full#supplementary-material

REFERENCES

Abushouk, A. I., Negida, A., Elshenawy, R. A., Zein, H., Hammad, A. M., Menshawy, A., et al. (2018). C-Abl Inhibition; A Novel Therapeutic Target for Parkinson's Disease. *Cnsnddt* 17 (1), 14–21. doi:10.2174/1871527316666170602101538

Aflaki, E., Moaven, N., Borger, D. K., Lopez, G., Westbroek, W., Chae, J. J., et al. (2016). Lysosomal Storage and Impaired Autophagy lead to Inflammasome Activation in G Aucher Macrophages. *Aging Cell* 15 (1), 77–88. doi:10.1111/acel.12409

Alvarez, A. R., Klein, A., Castro, J., Cancino, G. I., Amigo, J., Mosqueira, M., et al. (2008). Imatinib Therapy Blocks Cerebellar Apoptosis and Improves Neurological Symptoms in a Mouse Model of Niemann-Pick Type C Disease. *FASEB j.* 22 (10), 3617–3627. doi:10.1096/fj.07-102715

Alvarez, A. R., Sandoval, P. C., Leal, N. R., Castro, P. U., and Kosik, K. S. (2004). Activation of the Neuronal C-Abl Tyrosine Kinase by Amyloid-β-Peptide and Reactive Oxygen Species. *Neurobiol. Dis.* 17 (2), 326–336. doi:10.1016/j.nbd.2004.06.007

Arroyo, A. I., Camoletto, P. G., Morando, L., Sassoe-Pognetto, M., Giustetto, M., Van Veldhoven, P. P., et al. (2014). Pharmacological Reversion of Sphingomyelin-induced Dendritic Spine Anomalies in a Niemann Pick Disease Type A Mouse Model. *EMBO Mol. Med.* 6 (3), 398–413. doi:10.1002/emmm.201302649

Bartoll, A., Toledano-Zaragoza, A., Casas, J., Guzmán, M., Schuchman, E. H., and Ledesma, M. D. (2020). Inhibition of Fatty Acid Amide Hydrolase Prevents Pathology in Neurovisceral Acid Sphingomyelinase Deficiency by Rescuing Defective Endocannabinoid Signaling. *EMBO Mol. Med.* 12 (11), e11776. doi:10.15252/emmm.201911776

Can, G., Ekiz, H. A., and Baran, Y. (2011). Imatinib Induces Autophagy throughBECLIN-1andATG5genes in Chronic Myeloid Leukemia Cells. *Hematology* 16 (2), 95–99. doi:10.1179/102453311X12902908412039

Cancino, G. I., Toledo, E. M., Leal, N. R., Hernandez, D. E., Yévenes, L. F., Inestrosa, N. C., et al. (2008). STI571 Prevents Apoptosis, Tau Phosphorylation and Behavioural Impairments Induced by Alzheimer's β-amyloid Deposits. *Brain* 131 (Pt 9), 2425–2442. doi:10.1093/brain/awn125

Cermak, S., Kosicek, M., Mladenovic-Djordjevic, A., Smiljanic, K., Kanazir, S., and Hecimovic, S. (2016). Loss of Cathepsin B and L Leads to Lysosomal Dysfunction, NPC-like Cholesterol Sequestration and Accumulation of the Key Alzheimer's Proteins. *PLoS One* 11 (11), e0167428. doi:10.1371/journal.pone.0167428

Chen, G., Chen, K. S., Knox, J., Inglis, J., Bernard, A., Martin, S. J., et al. (2000). A Learning Deficit Related to Age and β-amyloid Plaques in a Mouse Model of Alzheimer's Disease. *Nature* 408 (6815), 975–979. doi:10.1038/35050103

Contreras, P. S., Gonzalez-Zuñiga, M., González-Hódar, L., Yáñez, M. J., Dulcey, A., Marugan, J., et al. (2016). Neuronal Gene Repression in Niemann-Pick Type C Models Is Mediated by the C-Abl/HDAC2 Signaling Pathway. *Biochim. Biophys. Acta (Bba) - Gene Regul. Mech.* 1859 (2), 269–279. doi:10.1016/j.bbagrm.2015.11.006

Contreras, P. S., Tapia, P. J., González-Hódar, L., Peluso, I., Soldati, C., Napolitano, G., et al. (2020). c-Abl Inhibition Activates TFEB and Promotes Cellular Clearance in a Lysosomal Disorder. *iScience* 23 (11), 101691. doi:10.1016/j.isci.2020.101691

Corcelle-Termeau, E., Vindeløv, S. D., Hämälistö, S., Mograbi, B., Keldsbo, A., Bräsen, J. H., et al. (2016). Excess Sphingomyelin Disturbs ATG9A Trafficking and Autophagosome Closure. *Autophagy* 12 (5), 833–849. doi:10.1080/15548627.2016.1159378

Gabandé-Rodríguez, E., Pérez-Cañamás, A., Soto-Huelin, B., Mitroi, D. N., Sánchez-Redondo, S., Martínez-Sáez, E., et al. (2019). Lipid-induced Lysosomal Damage after Demyelination Corrupts Microglia Protective Function in Lysosomal Storage Disorders. *EMBO J.* 38 (2). doi:10.15252/embj.201899553

Gabandé-Rodríguez, E., Boya, P., Labrador, V., Dotti, C. G., and Ledesma, M. D. (2014). High Sphingomyelin Levels Induce Lysosomal Damage and Autophagy Dysfunction in Niemann Pick Disease Type A. *Cell Death Differ* 21 (6), 864–875. doi:10.1038/cdd.2014.4

García-Sanz, P., Orgaz, L., Fuentes, J. M., Vicario, C., and Moratalla, R. (2018). Cholesterol and Multilamellar Bodies: Lysosomal Dysfunction in GBA-Parkinson Disease. *Autophagy* 14 (4), 717–718. doi:10.1080/15548627.2018.1427396

Gonzalez-Zuñiga, M., Contreras, P. S., Estrada, L. D., Chamorro, D., Villagra, A., Zanlungo, S., et al. (2014). c-Abl Stabilizes HDAC2 Levels by Tyrosine Phosphorylation Repressing Neuronal Gene Expression in Alzheimer's Disease. *Mol. Cel* 56 (1), 163–173. doi:10.1016/j.molcel.2014.08.013

Greuber, E. K., Smith-Pearson, P., Wang, J., and Pendergast, A. M. (2013). Role of ABL Family Kinases in Cancer: from Leukaemia to Solid Tumours. *Nat. Rev. Cancer* 13 (8), 559–571. doi:10.1038/nrc3563

Hebron, M. L., Lonskaya, I., and Moussa, C. E. H. (2013). Nilotinib Reverses Loss of Dopamine Neurons and Improves Motor Behavior via Autophagic Degradation of -synuclein in Parkinson's Disease Models. *Hum. Mol. Genet.* 22 (16), 3315–3328. doi:10.1093/hmg/ddt192

Hopkins, S., Linderoth, E., Hantschel, O., Suarez-Henriques, P., Pilia, G., Kendrick, H., et al. (2012). Mig6 Is a Sensor of EGF Receptor Inactivation that Directly Activates C-Abl to Induce Apoptosis during Epithelial Homeostasis. *Develop. Cel* 23 (3), 547–559. doi:10.1016/j.devcel.2012.08.001

Horinouchi, K., Erlich, S., Perl, D. P., Ferlinz, K., Bisgaier, C. L., Sandhoff, K., et al. (1995). Acid Sphingomyelinase Deficient Mice: a Model of Types A and B Niemann-Pick Disease. *Nat. Genet.* 10 (3), 288–293. doi:10.1038/ng0795-288

Imam, S. Z., Zhou, Q., Yamamoto, A., Valente, A. J., Ali, S. F., Bains, M., et al. (2011). Novel Regulation of Parkin Function through C-Abl-Mediated Tyrosine Phosphorylation: Implications for Parkinson's Disease. *J. Neurosci.* 31 (1), 157–163. doi:10.1523/JNEUROSCI.1833-10.2011

Imamura, K., Izumi, Y., Watanabe, A., Tsukita, K., Woltjen, K., Yamamoto, T., et al. (2017). The Src/c-Abl Pathway Is a Potential Therapeutic Target in Amyotrophic Lateral Sclerosis. *Sci. Transl. Med.* 9 (391). 3962. doi:10.1126/scitranslmed.aaf3962

Karim, M. R., Liao, E. E., Kim, J., Meints, J., Martinez, H. M., Pletnikova, O., et al. (2020). α-Synucleinopathy Associated C-Abl Activation Causes P53-dependent Autophagy Impairment. *Mol. Neurodegeneration* 15 (1), 27. doi:10.1186/s13024-020-00364-w

Klein, A., Maldonado, C., Vargas, L. M., Gonzalez, M., Robledo, F., Perez de Arce, K., et al. (2011). Oxidative Stress Activates the C-Abl/p73 Proapoptotic Pathway in Niemann-Pick Type C Neurons. *Neurobiol. Dis.* 41 (1), 209–218. doi:10.1016/j.nbd.2010.09.008

Ko, H. S., Lee, Y., Shin, J.-H., Karuppagounder, S. S., Gadad, B. S., Koleske, A. J., et al. (2010). Phosphorylation by the C-Abl Protein Tyrosine Kinase Inhibits Parkin's Ubiquitination and Protective Function. *Proc. Natl. Acad. Sci.* 107 (38), 16691–16696. doi:10.1073/pnas.1006083107

Kornhuber, J., Tripal, P., Reichel, M., Mühle, C., Rhein, C., Muehlbacher, M., et al. (2010). Functional Inhibitors of Acid Sphingomyelinase (FIASMAs): a Novel Pharmacological Group of Drugs with Broad Clinical Applications. *Cell Physiol Biochem* 26 (1), 9–20. doi:10.1159/000315101

La Barbera, L., Vedele, F., Nobili, A., Krashia, P., Spoleti, E., Latagliata, E. C., et al. (2021). Nilotinib Restores Memory Function by Preventing Dopaminergic Neuron Degeneration in a Mouse Model of Alzheimer's Disease. *Prog. Neurobiol.* 202, 102031. doi:10.1016/j.pneurobio.2021.102031

Lee, J.-A., Yue, Z., and Gao, F.-B. (2016). Autophagy in Neurodegenerative Diseases. *Brain Res.* 1649 (Pt B), 141–142. doi:10.1016/j.brainres.2016.09.030

Li, X., Xu, M., Pitzer, A. L., Xia, M., Boini, K. M., Li, P.-L., et al. (2014). Control of Autophagy Maturation by Acid Sphingomyelinase in Mouse Coronary Arterial

Smooth Muscle Cells: Protective Role in Atherosclerosis. *J. Mol. Med.* 92 (5), 473–485. doi:10.1007/s00109-014-1120-y

Liao, G., Yao, Y., Liu, J., Yu, Z., Cheung, S., Xie, A., et al. (2007). Cholesterol Accumulation Is Associated with Lysosomal Dysfunction and Autophagic Stress in Npc1−/− Mouse Brain. *Am. J. Pathol.* 171 (3), 962–975. doi:10.2353/ajpath.2007.070052

Long, Y., Xu, M., Li, R., Dai, S., Beers, J., Chen, G., et al. (2016). Induced Pluripotent Stem Cells for Disease Modeling and Evaluation of Therapeutics for Niemann-Pick Disease Type A. *Stem Cell Transl Med* 5 (12), 1644–1655. doi:10.5966/sctm.2015-0373

Macauley, S. L., Sidman, R. L., Schuchman, E. H., Taksir, T., and Stewart, G. R. (2008). Neuropathology of the Acid Sphingomyelinase Knockout Mouse Model of Niemann-Pick A Disease Including Structure-Function Studies Associated with Cerebellar Purkinje Cell Degeneration. *Exp. Neurol.* 214 (2), 181–192. doi:10.1016/j.expneurol.2008.07.026

McGovern, M. M., Dionisi-Vici, C., Giugliani, R., Hwu, P., Lidove, O., Lukacs, Z., et al. (2017). Consensus Recommendation for a Diagnostic Guideline for Acid Sphingomyelinase Deficiency. *Genet. Med.* 19 (9), 967–974. doi:10.1038/gim.2017.7

Menzies, F. M., Fleming, A., Caricasole, A., Bento, C. F., Andrews, S. P., Ashkenazi, A., et al. (2017). Autophagy and Neurodegeneration: Pathogenic Mechanisms and Therapeutic Opportunities. *Neuron* 93 (5), 1015–1034. doi:10.1016/j.neuron.2017.01.022

Michailowsky, V., Li, H., Mittra, B., Iyer, S. R., Mazála, D. A. G., Corrotte, M., et al. (2019). Defects in Sarcolemma Repair and Skeletal Muscle Function after Injury in a Mouse Model of Niemann-Pick Type A/B Disease. *Skeletal Muscle* 9 (1), 1. doi:10.1186/s13395-018-0187-5

Miller, E. K. (2000). The Prefontral Cortex and Cognitive Control. *Nat. Rev. Neurosci.* 1 (1), 59–65. doi:10.1038/35036228

Mitsushima, M., Takahashi, H., Shishido, T., Ueda, K., and Kioka, N. (2006). Abl Kinase Interacts with and Phosphorylates Vinexin. *FEBS Lett.* 580 (17), 4288–4295. doi:10.1016/j.febslet.2006.06.072

Nixon, R. A. (2013). The Role of Autophagy in Neurodegenerative Disease. *Nat. Med.* 19 (8), 983–997. doi:10.1038/nm.3232

Opitz, B. (2014). Memory Function and the hippocampus. *Front. Neurol. Neurosci.* 34, 51–59. doi:10.1159/000356422

Otterbach, B., and Stoffel, W. (1995). Acid Sphingomyelinase-Deficient Mice Mimic the Neurovisceral Form of Human Lysosomal Storage Disease (Niemann-Pick Disease). *Cell* 81 (7), 1053–1061. doi:10.1016/s0092-8674(05)80010-8

Pagan, F., Hebron, M., Valadez, E. H., Torres-Yaghi, Y., Huang, X., Mills, R. R., et al. (2016). Nilotinib Effects in Parkinson's Disease and Dementia with Lewy Bodies. *Jpd* 6 (3), 503–517. doi:10.3233/JPD-160867

Pagan, F. L., Hebron, M. L., Wilmarth, B., Torres-Yaghi, Y., Lawler, A., Mundel, E. E., et al. (2019). Pharmacokinetics and Pharmacodynamics of a Single Dose Nilotinib in Individuals with Parkinson's Disease. *Pharmacol. Res. Perspect.* 7 (2), e00470. doi:10.1002/prp2.470

Pérez-Cañamás, A., Benvegnù, S., Rueda, C. B., Rábano, A., Satrústegui, J., and Ledesma, M. D. (2017). Sphingomyelin-induced Inhibition of the Plasma Membrane Calcium ATPase Causes Neurodegeneration in Type A Niemann-Pick Disease. *Mol. Psychiatry* 22 (5), 711–723. doi:10.1038/mp.2016.148

Preston, A. R., and Eichenbaum, H. (2013). Interplay of hippocampus and Prefrontal Cortex in Memory. *Curr. Biol.* 23 (17), R764–R773. doi:10.1016/j.cub.2013.05.041

Ren, Y., Chen, J., Wu, X., Gui, C., Mao, K., Zou, F., et al. (2018). Role of C-Abl-Gsk3β Signaling in MPP+-Induced Autophagy-Lysosomal Dysfunction. *Toxicol. Sci.* 165 (1), 232–243. doi:10.1093/toxsci/kfy155

Sáez, P. J., Barbier, L., Attia, R., Thiam, H.-R., Piel, M., and Vargas, P. (2018). Leukocyte Migration and Deformation in Collagen Gels and Microfabricated Constrictions. *Methods Mol. Biol.* 1749, 361–373. doi:10.1007/978-1-4939-7701-7_26

Schuchman, E. H., and Desnick, R. J. (2017). Types A and B Niemann-Pick Disease. *Mol. Genet. Metab.* 120 (1-2), 27–33. doi:10.1016/j.ymgme.2016.12.008

Schuchman, E. H. (2007). The Pathogenesis and Treatment of Acid Sphingomyelinase-Deficient Niemann-Pick Disease. *J. Inherit. Metab. Dis.* 30 (5), 654–663. doi:10.1007/s10545-007-0632-9

Shaul, Y., and Ben-Yehoyada, M. (2005). Role of C-Abl in the DNA Damage Stress Response. *Cell Res* 15 (1), 33–35. doi:10.1038/sj.cr.7290261

Sun, X., Majumder, P., Shioya, H., Wu, F., Kumar, S., Weichselbaum, R., et al. (2000). Activation of the Cytoplasmic C-Abl Tyrosine Kinase by Reactive Oxygen Species. *J. Biol. Chem.* 275 (23), 17237–17240. doi:10.1074/jbc.C000099200

Toledo, E. M., and Inestrosa, N. C. (2010). Activation of Wnt Signaling by Lithium and Rosiglitazone Reduced Spatial Memory Impairment and Neurodegeneration in Brains of an APPswe/PSEN1ΔE9 Mouse Model of Alzheimer's Disease. *Mol. Psychiatry* 15 (3), 272228–272285. doi:10.1038/mp.2009.72

Turner, R. S., Hebron, M. L., Lawler, A., Mundel, E. E., Yusuf, N., Starr, J. N., et al. (2020). Nilotinib Effects on Safety, Tolerability, and Biomarkers in Alzheimer's Disease. *Ann. Neurol.* 88 (1), 183–194. doi:10.1002/ana.25775

Van Etten, R. A. (2003). c-Abl Regulation: a Tail of Two Lipids. *Curr. Biol.* 13 (15), R608–R610. doi:10.1016/s0960-9822(03)00528-1

Võikar, V., Rauvala, H., and Ikonen, E. (2002). Cognitive Deficit and Development of Motor Impairment in a Mouse Model of Niemann-Pick Type C Disease. *Behav. Brain Res.* 132 (1), 1–10. doi:10.1016/s0166-4328(01)00380-1

Vorhees, C. V., and Williams, M. T. (2006). Morris Water Maze: Procedures for Assessing Spatial and Related Forms of Learning and Memory. *Nat. Protoc.* 1 (2), 848–858. doi:10.1038/nprot.2006.116

Wang, J. Y. J. (2014). The Capable ABL: what Is its Biological Function? *Mol. Cel Biol* 34 (7), 1188–1197. doi:10.1128/MCB.01454-13

Wen, S. T., Jackson, P. K., and Van Etten, R. A. (1996). The Cytostatic Function of C-Abl Is Controlled by Multiple Nuclear Localization Signals and Requires the P53 and Rb Tumor Suppressor Gene Products. *EMBO J.* 15 (7), 1583–1595. doi:10.1002/j.1460-2075.1996.tb00503.x

Wolff, N. C., Richardson, J. A., Egorin, M., and Ilaria, R. L., Jr. (2003). The CNS Is a Sanctuary for Leukemic Cells in Mice Receiving Imatinib Mesylate for Bcr/Abl-Induced Leukemia. *Blood* 101 (12), 5010–5013. doi:10.1182/blood-2002-10-3059

Yáñez, M. J., Belbin, O., Estrada, L. D., Leal, N., Contreras, P. S., Lleó, A., et al. (2016). c-Abl Links APP-BACE1 Interaction Promoting APP Amyloidogenic Processing in Niemann-Pick Type C Disease. *Biochim. Biophys. Acta (Bba) - Mol. Basis Dis.* 1862 (11), 2158–2167. doi:10.1016/j.bbadis.2016.08.016

Yañez, M. J., Campos, F., Marín, T., Klein, A. D., Futerman, A. H., Alvarez, A. R., et al. (2021). c-Abl Activates RIPK3 Signaling in Gaucher Disease. *Biochim. Biophys. Acta (Bba) - Mol. Basis Dis.* 1867 (5), 166089. doi:10.1016/j.bbadis.2021.166089

Yañez, M. J., Marín, T., Balboa, E., Klein, A. D., Alvarez, A. R., and Zanlungo, S. (2020). Finding Pathogenic Commonalities between Niemann-Pick Type C and Other Lysosomal Storage Disorders: Opportunities for Shared Therapeutic Interventions. *Biochim. Biophys. Acta (Bba) - Mol. Basis Dis.* 1866 (10), 165875. doi:10.1016/j.bbadis.2020.165875

Yu, C., Gorantla, S. P., Müller-Rudorf, A., Müller, T. A., Kreutmair, S., Albers, C., et al. (2020). Phosphorylation of BECLIN-1 by BCR-ABL Suppresses Autophagy in Chronic Myeloid Leukemia. *Haematologica* 105 (5), 1285–1293. doi:10.3324/haematol.2018.212027

Conflict of Interest: The authors declare that the research was conducted in the absence of any commercial or financial relationships that could be construed as a potential conflict of interest.

Publisher's Note: All claims expressed in this article are solely those of the authors and do not necessarily represent those of their affiliated organizations, or those of the publisher, the editors and the reviewers. Any product that may be evaluated in this article, or claim that may be made by its manufacturer, is not guaranteed or endorsed by the publisher.

frontiers in Cell and Developmental Biology

ORIGINAL RESEARCH
published: 24 March 2022
doi: 10.3389/fcell.2022.820675

Erg25 Controls Host-Cholesterol Uptake Mediated by Aus1p-Associated Sterol-Rich Membrane Domains in *Candida glabrata*

*Michiyo Okamoto[1], Azusa Takahashi-Nakaguchi[1], Kengo Tejima[2], Kaname Sasamoto[1], Masashi Yamaguchi[1], Toshihiro Aoyama[3], Minoru Nagi[4], Kohichi Tanabe[5], Yoshitsugu Miyazaki[4], Hironobu Nakayama[6], Chihiro Sasakawa[1,7], Susumu Kajiwara[2], Alistair J. P. Brown[8], Miguel C. Teixeira[9] and Hiroji Chibana[1]**

[1]Medical Mycology Research Center, Chiba University, Chiba, Japan, [2]School of Life Science and Technology, Tokyo Institute of Technology, Yokohama, Japan, [3]Department of Electronic and Information Engineering, Suzuka National College of Technology, Suzuka, Japan, [4]National Institute of Infectious Diseases, Tokyo, Japan, [5]Department of Food Science and Human Nutrition, Faculty of Agriculture, Ryukoku University, Otsu, Japan, [6]Faculty of Pharmaceutical Sciences, Suzuka University of Medical Science, Suzuka, Japan, [7]Nippon Institute for Biological Science, Tokyo, Japan, [8]MRC Centre for Medical Mycology, University of Exeter, Exeter, United Kingdom, [9]Department of Bioengineering, Instituto Superior Técnico, Universidade de Lisboa, Lisbon, Portugal

OPEN ACCESS

Edited by:
Silvana Zanlungo,
Pontificia Universidad Católica de Chile, Chile

Reviewed by:
Thomas Günther-Pomorski,
Ruhr University Bochum, Germany
Allyson Faye O'Donnell,
University of Pittsburgh, United States

***Correspondence:**
Hiroji Chibana
chibana@faculty.chiba-u.jp

Specialty section:
This article was submitted to Membrane Traffic, a section of the journal Frontiers in Cell and Developmental Biology

Received: 23 November 2021
Accepted: 07 March 2022
Published: 24 March 2022

Citation:
Okamoto M, Takahashi-Nakaguchi A, Tejima K, Sasamoto K, Yamaguchi M, Aoyama T, Nagi M, Tanabe K, Miyazaki Y, Nakayama H, Sasakawa C, Kajiwara S, Brown AJP, Teixeira MC and Chibana H (2022) Erg25 Controls Host-Cholesterol Uptake Mediated by Aus1p-Associated Sterol-Rich Membrane Domains in Candida glabrata. Front. Cell Dev. Biol. 10:820675. doi: 10.3389/fcell.2022.820675

The uptake of cholesterol from the host is closely linked to the proliferation of pathogenic fungi and protozoa during infection. For some pathogenic fungi, cholesterol uptake is an important strategy for decreasing susceptibility to antifungals that inhibit ergosterol biosynthesis. In this study, we show that *Candida glabrata ERG25*, which encodes an enzyme that demethylates 4,4-dimethylzymosterol, is required for cholesterol uptake from host serum. Based on the screening of *C. glabrata* conditional knockdown mutants for each gene involved in ergosterol biosynthesis, *ERG25* knockdown was found to decrease lethality of infected mice. *ERG25* knockdown impairs the plasma membrane localization of the sterol importer Aus1p, suggesting that the accumulated 4,4-dimethylzymosterol destabilizes the lipid domain with which Aus1p functionally associates. *ERG25* knockdown further influences the structure of the membrane compartment of Can1p (MCC)/eisosomes (ergosterol-rich lipid domains), but not the localization of the membrane proteins Pma1p and Hxt1p, which localize to sterol-poor domains. In the sterol-rich lipid domain, Aus1p-contining domain was mostly independent of MCC/eisosomes, and the nature of these domains was also different: Ausp1-contining domain was a dynamic network-like domain, whereas the MCC/eisosomes was a static dot-like domain. However, deletion of MCC/eisosomes was observed to influence the localization of Aus1p after Aus1p was transported from the endoplasmic reticulum (ER) through the Golgi apparatus to the plasma membrane. These findings suggest that *ERG25* plays a key role in stabilizing sterol-rich lipid domains, constituting a promising candidate target for antifungal therapy.

Keywords: pathogenicity, plasma membrane, C4-sterol methyl oxidase (SMO), virulence factor, opportunistic pathogen, non-albicans, membrane compartment, micro domain

INTRODUCTION

Ergosterol is a significant component of the plasma membrane in fungi and protozoa, and its biosynthetic pathway has been successfully used as target in antifungal therapy. However, some pathogenic fungi and protozoa, such as *Candida glabrata*, *Aspergillus fumigatus*, and Trypanosoma brucei, have the ability to scavenge cholesterol from host-serum and utilize it as a surrogate for ergosterol (Coppens and Courtoy, 2000; Bard et al., 2005; Xiong et al., 2005; Nakayama et al., 2007; Nagi et al., 2013). Therefore, there is concern that the uptake of host cholesterol may decrease the susceptibility of these pathogens to antifungal drugs that target ergosterol biosynthesis. Elucidating the molecular mechanisms of cholesterol uptake will facilitate the development of more effective treatments for these fungal and protozoa infections.

Among pathogenic yeast, *C. glabrata* constitutes one of the organisms in which host-cholesterol uptake has been identified. *C. glabrata* also has been the focus of research as an opportunistic pathogen, since this fungus causes severe invasive infections associated to high mortality rates (Kullberg and Arendrup, 2015). *C. glabrata* is evolutionarily much closer to the non-pathogenic yeast *Saccharomyces cerevisiae* than is *Candida albicans*, the other well-characterized and common candida species. Almost 90% of *C. glabrata* genes demonstrate inferred orthology to *S. cerevisiae* genes (Lelandais et al., 2008), suggesting a strong conservation of physiology between these two species. *S. cerevisiae* can take up external cholesterol, but this process occurs only under anaerobic conditions or in cells with defects in heme biosynthesis, a situation that can mimic anaerobic conditions (Lorenz et al., 1986; Lorenz and Parks, 1991; Shianna et al., 2001; Vik and Rine, 2001). On the other hand, *C. glabrata* can take up cholesterol from serum even under aerobic conditions (Nagi et al., 2013). Therefore, *C. glabrata* appears to be an appropriate tool for investigating the molecular mechanism of host-cholesterol uptake.

C. glabrata displays intrinsically low susceptibility to azole drugs, like fluconazole, that target ergosterol biosynthesis, specifically inhibiting lanosterol 14-demethylase (Erg11p) activity. The expression of *ERG11,* of the transcription factor encoding gene *PDR1* and of its targets *CDR1*, *CDR2* and *SNQ2*, encoding multidrug transporters, is increased upon treatment with fluconazole (Henry et al., 2000; Sanglard et al., 2009; Vu et al., 2019), resulting in decreased susceptibility to azoles. In addition, the expression of some Drug:H^+ Antiporters of the Major Facilitator Superfamily, MFS, has also been associated with decreased azole susceptibility (Costa et al., 2014; Cannon and Holmes, 2015). In *C. glabrata,* the ATP-binding cassette transporter Aus1p has been shown to mediate cholesterol uptake, its expression being activated by Upc2A, a transcriptional activator of ergosterol biosynthesis genes (Nakayama et al., 2007). Interestingly, the expression of *PDR1* and *CDR1* is also dependent on Upc2A (Vu et al., 2019). The expression of *AUS1* is upregulated in the presence of fluconazole and *aus1*Δ cells are highly susceptible to fluconazole even in the presence of serum (Nagi et al., 2013). Furthermore, deletion of *AUS1* leads to reduced proliferation in mice (Nakayama et al., 2007; Nagi et al., 2013) and its expression is upregulated in response to serum or iron-poor environments, as would occur in the bloodstream of hosts (Nagi et al., 2013). Thus, Aus1p-mediated cholesterol uptake may play an important role in fungal infections, especially in bloodstream infections by *C. glabrata*. The detergent resistant membrane domains (DRMs) are resistant to extraction with low-temperature nonionic detergents, and sterol and sphingolipid-enriched. DRMs were used to explain protein-lipid interactions (Shogomori and Brown, 2003; Lichtenberg et al., 2005). Recently, DRMs have been used less as an experimental material to reflect the Lipid raft concept in cell membranes (Lingwood and Simons, 2010), however they can be easily tailored to examine the lateral association between the plasma membrane proteins and lipids. In *S. cerevisiae*, Aus1p has been reported to associate with DRMs (Gulati et al., 2015), but in *C. glabrata*, the association of CgAus1p with DRMs remains speculative.

Can1p (arginine permease) and Pma1p (H^+-ATPase) have been shown to be compartmentalized into distinct types of domains within the plasma membrane of *S. cerevisiae*: membrane compartment of Can1p (MCC) and membrane compartment of Pma1p (MCP), respectively. They appear microscopically to have a non-overlapping distribution with distinct patterns; the MCP domains have a network-like pattern, while the MCC domains have a punctate pattern (Malínská et al., 2003). Thus, the distribution of these proteins shows that the plasma membrane is not composed of a uniform arrangement of proteins and lipids, but rather a patchwork of domains with different compositions of proteins and lipids (Spira et al., 2012). The MCC has been suggested to be enriched in ergosterol (Grossmann and Malinsky, 2007), while the MCP has been suggested to be enriched in sphingolipids (van 't Klooster et al., 2020). The MCC corresponds to specific membrane invaginations that have been termed eisosomes (Strádalová et al., 2009). In pathogenic fungi, MCC/eisosomes appear to be functionally important, given that the deletion of eisosome-associated protein encoding genes leads to defects in cell wall synthesis, in the formation of invasive hyphal filaments, and in virulence in a murine model of *C. albicans* infection (Douglas et al., 2012, 2013; Li et al., 2015; Wang et al., 2016).

In this study, we screened a set of knockdown mutants in ergosterol biosynthetic genes (*ERG1*, *ERG7*, *ERG11*, *ERG25*, *ERG26*, and *ERG27*) to identify new players in cholesterol uptake *in vitro* and *in vivo*. Based on the observation that growth defects imposed by *ERG25* or *ERG26* knockdown are not rescued by the presence of serum, new insights into cholesterol uptake in *C. glabrata* were obtained. The role of the demethylation of 4,4-dimethylzymosterol by Erg25p in host-cholesterol uptake, mediated by Aus1p-associated membrane domains is scrutinized.

TABLE 1 | List of strains used in this study.

Strain	Parent: Modified genotype	References
ACG4	2001HT: *his3 trpl PScHOPZ-tetR-GAL4AD::TRP1*	(Nakayama et al., 1998)
HETS202	ACG4: FRT-*YKU80*	(Ueno et al., 2007)
KUE100	*his3 yku80::SAT1* flipper	(Ueno et al., 2007)
Tet-ERG1	HETS202: tet97p-*ERG1::CgHIS3*	This study
Tet-ERG7	ACG4: tet97p-*ERG7::CgHIS3*	This study
Tet-ERG11	ACG4: tet99p-*ERG11::CgHIS3*	This study
Tet-ERG25	HETS202: tet99p-*ERG25::CgHIS3*	This study
Tet-ERG26	HETS202: tet97p-*ERG26::CgHIS3*	This study
Tet-ERG27	ACG4: tet97p-*ERG27::CgHIS3*	This study
Δ*erg11*	KUE100: *ERG11::CgHIS3*	This study
Δerg25	CBS138: *ERG25::NAT^{R}*	This study
Tet-ERG25 Aus1G	Tet-ERG25: *AUS1-GFP ScURA3*	This study
WT_Aus1G	HETS202: *AUS1-GFP::ScURA3*	This study
WT_Aus1G/Pma1R	HETS202: *AUS1-GFP::ScURA3*, *PMA1-mCherry::natNT2*	This study
Tet-ERG25_ Aus1G/Hxt1R	Tet-ERG25: *AUS1-GFP::ScURA3*, *HXT1-mCherry:: natNT2*	This study
WT_Aus1G/Pil1R	HETS202: *AUS1-GFP::ScURA3*, *PIL1-mCherry::natNT2*	This study
Tet-ERG25_Aus1G/Pil1R	Tet-ERG25: *AUS1-GFP:ScURA3*, *PIL1-mCherry::natNT2*	This study
Tet-ERG25 *pil1*Δ_Aus1G	Tet-ERG25: Δ*C::NAT^{R} AUS1-GFP::ScURA3*	This study
Tet-ERG26_ Aus1G/Hxt1R	Tet-ERG26: *AUS1-GFP::ScURA3*, *HXT1-mCherry:: natNT2*	This study

MATERIALS AND METHODS

Strains and Media

Yeast strains used in this study are listed in **Table 1**. Yeast cells were grown in rich medium (YPD; 2% peptone, 1% yeast extract, 2% glucose) or minimal medium (SD; 0.17% yeast nitrogen base without amino acids and ammonium sulfate, 2% glucose, 5% ammonium sulfate, and appropriate amino acids) at 30 or 37°C. Bovine serum (Sigma-Aldrich, MO, United States) was added to the medium to a final concentration of 10%. Media supplementation with 20 μg/ml doxycycline (Dox) was used to repress gene expression in Tet-off strains.

Strain Construction

To construct Tet-off strains, *ERG11*, *ERG25* or *PIL1* deletion strain, each DNA cassette was amplified by polymerase chain reaction (PCR) using the primers listed in **Supplementary Table S1** and plasmid pTK916-97t (Ueno et al., 2010), pTK916-99t (Niimi et al., 2012), pCgHIS906 containing Cg*HIS3,* or pBM16.1 containing *NAT1* gene (Zordan et al., 2013) as a template. The resulting products were transformed into HETS202 cells, KUE100, or CBS138. Bovine serum was added to the selection medium for the construction of Δ*erg11* cells to maintain the growth of cells, and bovine serum and fluconazole were added for the construction of Δ*erg25* cells. Transformed cells were screened by colony PCR to verify that the tetracycline-dependent down-regulatable promoter had been inserted upstream of each target gene in the parent strain. Transformation and colony PCR methods were described in our previous report (Ueno et al., 2011). Strains expressing Aus1p-GFP, Hxt1p-mCherry, or Pil1p-mCherry were constructed using a PCR-based method with an integrative cassette. The cassette for tagging Aus1p with GFP was amplified using primers pAUS1F′ and pAUS1R' (**Supplementary Table S1**) and genomic DNA derived from the UTH*aus1*Δ/*AUS1-GFP* strain (Nagi et al., 2013) as template. *GFP-ScURA3* was inserted into the downstream end of *AUS1 via* homologous recombination. To tag Hxt1p with mCherry, Fragment 1 (encoding mCherry-natNT2) was amplified using primers pFA6aF and pFA6aR and plasmid pFA6a-mCherry-natNT2 (Okamoto et al., 2012) as template. Fragment 2, containing the downstream end of the *HXT1* open reading frame (ORF), was amplified using primers HXT1F1 and HXT1R and *C. glabrata* genomic DNA of HETS202 as template. Fragment 3, containing sequences downstream of the *HXT1* ORF, was amplified using primers HXT1F2 and HXT1R2 and *C. glabrata* genomic DNA as template. Fusion PCR was carried out using primers HXT1F1 and HXT1R2 and Fragments 1, 2, and 3 as templates, and then sequences encoding mCherry-natNT2 were inserted into the downstream end of the *HXT1* ORF by homologous recombination. The strains expressing Pil1p-mCherry or Pma1p-mCherry were constructed using the aforementioned cassette, derived from each of following primers (pFA6aF, pFA6aR, PIL1F1, PIL1R1, PIL1F2, and PIL1R2) or (pFA6aF, pFA6aR, PMA1F1, PMA1R1, PMA1F2, and PMA1R2), and using the same PCR method as employed for the mCherry-tagging of Hxt1p. Insertion of these cassettes into transformed cells was verified by colony PCR.

qRT-PCR

Cells were grown in minimal medium at 37°C overnight. This overnight pre-culture was used to inoculate a fresh culture at a density of 1×10^7 cells/ml in minimal medium in the presence or absence of 20 μg/ml Dox; the resulting culture was incubated at 37°C for 4 h with shaking. Cells then were collected by centrifugation and washed twice with sterile distilled water at 4°C. Total RNA was extracted using the RNeasy Mini extraction kit (Qiagen, Hilden, Germany). cDNA was synthesized from the total RNA using ReverTra Ace and random primers (Toyobo, Osaka, Japan). The amount of RNA for each gene was determined by quantitative real-time PCR (qRT-PCR) on a LightCycler® 96 System (Roche Diagnostics, Mannheim, Germany) with SYBR Green detection using the Thunderbird SYBR qPCR mix

(Toyobo). Transcript levels were normalized to that of *TEF1*, a housekeeping gene that encodes elongation factor 1. PCR conditions were as follows: pre-denaturation at 95°C for 1 min, followed by 40 cycles of denaturation at 95°C for 15 s and annealing/extension at 60°C for 1 min.

Assay of NBD-Cholesterol Uptake

Cells were grown to early exponential phase in minimal medium and then subcultured for 17 h in minimal medium containing 10% (v/v) bovine serum, 0.1% (w/v) Tween 80, and 5 μg/ml NBD-cholesterol (25-[N-[(7-nitro-2-1,3-benzoxadiazol-4-yl) methyl]amino]-27-norcholesterol; Avanti Polar Lipids, AL, United States) with or without Dox (20 μg/ml). Following culturing, the cells were washed twice with ice-cold phosphate-buffered saline (PBS) containing 0.5% (w/v) Nonidet P-40 and then once with PBS; the resulting pellet was resuspended in PBS. The cells were observed using a fluorescence microscope equipped with an NIBA filter (BX53; Olympus, Tokyo, Japan), and fluorescence intensity was quantified by flow cytometry (FACSVerse; Becton Dickinson, NJ, United States). Cells (1 ml volume of cells suspended in PBS) were pre-stained by the addition of propidium iodide (1 μl of a 1-mg/ml solution) to exclude dead cells from the analysis. Flow cytometry was performed as described previously (Marek et al., 2014). Cells cultured without NBD-cholesterol were analyzed as a control.

DRM Isolation and Immunoblotting

Cells were grown to logarithmic phase at 37°C in minimal medium containing 10% serum and 0.05% Tween 80 and incubated for 5.5 h after addition of 20 μg/ml Dox. Upon reaching an optical density at 600 nm (OD_{600}) of 20, the cells were treated with 10 mM NaN_3 and resuspended in TNE buffer (25 mM Tris-HCl [pH 7.5], 150 mM NaCl, and 5 mM EDTA) containing complete protease inhibitor cocktail (Sigma-Aldrich) and 1 mM PMSF. Cells were disrupted with glass beads using a Multi-beads Shocker (Yasui Kikai, Osaka, Japan). Debris and unbroken cells were removed by centrifugation for 5 min at 500× *g*. After incubation with 1% Triton X-100 (Sigma-Aldrich) for 30 min on ice, 840 μl of Optiprep solution (Alere Technologies AS, Oslo, Norway) was added to the lysate (420 μl) for a final Optiprep concentration of 40%, and the lysate was placed in a centrifuge tube. The sample was sequentially overlaid with 2.0 ml of 30% Optiprep (in TNE plus 0.1% Triton X-100) and 330 μl of TNE buffer containing 0.1% Triton X-100. The tube then was subjected to Optiprep density gradient flotation by centrifugation for 3.5 h at 35,000 rpm (168,000 g) in a P40ST rotor with a 4S13 adapter (Eppendorf Himac Technologies, Ibaraki, Japan) at 4°C. After centrifugation, 7 fractions of equal volume were collected starting from the top. Proteins in each fraction were precipitated with trichloroacetic acid (TCA) and resuspended in sample buffer. After incubation at 37°C for 10 min, the samples were resolved by 7.5% SDS-PAGE, transferred to a PVDF membrane (Immobilon-P, Merck Millipore, MA, United States), and subjected to western blotting. Western blotting was carried out using JL-8 anti-GFP monoclonal antibody (Clontech Laboratories, CA, United States) or anti-Pma1p polyclonal antibody (sc-33735, Santa Cruz Biotechnology, TX, United States).

Fluorescence Microscopy Analyses

The fluorescence microscopic images were observed with a BZ-9000 (Keyence, Osaka, Japan) equipped with a 100x oil-immersion objective lens or an Axio Observer Z.1 (Carl Zeiss, Jena, Germany) equipped with a 100x oil-immersion objective and a CMOS camera (Touptec photonics, Hangzhou, China). Basically, images were acquired with 1 s exposure. Confocal microscopy images were detected with a Stellaris 5 (Leica Microsystems, Wetzlar, Germany) equipped with a 100x objective lens and processed by lightning deconvolution on LAS X software. FM4-64 (FUJIFILM Wako Pure Chemical corporation, Osaka, Japan) was used to stain the vacuolar membrane. The cells expressing Aus1p-GFP were grown exponentially at 37°C in serum-containing SD medium and further incubated with or without Dox for 1 h. The FM4-64 stock solution (1.6 μM in DMSO) was added at a final concentration of 10 μM. After 30 min of incubation, cells were washed and further incubated with or without Dox for 1.5 h. To examine sterol localization, cells co-expressing Aus1p-GFP and Pma1p-mCherry were incubated with 5 μg/ml filipin (Polysciences, PA, United States) for 5 min at 30°C. After three rinses with PBS, the stained cells were observed by confocal fluorescence microscopy using excitation wavelengths of 405 nm for filipin, 488 nm for GFP, and 568 nm for mCherry. The brightness and contrast of images were adjusted with Fiji/ImageJ software (Schindelin et al., 2012). The EzColocalization plug-in was used for colocalization analysis and the assessment of Pearson's correlation coefficient.

Sterol Analysis

Cells were incubated under the conditions described above for the isolation of DRMs. After quantification of total protein using the Bradford method, DRMs were isolated by Optiprep density gradient flotation. Sterols were analyzed using GC. After cultivation, cells were harvested and freeze-dried to determine dry weight, and dried cells were resuspended in 4 ml of methanol. Following addition of an internal standard, 5-α-cholestane was added at 2 μg/g cell dry weight, and the cells were homogenized on ice for 10 min using a Hom-100 subsonic homogenizer (AGC Techno Glass, Shizuoka, Japan). The cell homogenate was transferred to a new tube, and 20% (w/w) solid KOH was added. The mixture then was vortexed until the KOH was completely dissolved. Lipids in DRMs were saponified at 85°C for 2 h. After the saponified mixture was cooled to room temperature, 4 ml of hexane and 1 ml of distilled water were added to extract alkali-stable lipids. After washing with 4 ml of distilled water, the extract was dried and then trimethylsilylated in pyridine at 70°C for 1 h using *N*,*O*-bis (trimethylsilyl) trifluoroacetamide (Tokyo Chemical Industry, Tokyo, Japan). After cooling to room temperature, the trimethylsilylated sterols were analyzed by GC (GC-18A, Shimadzu, Kyoto, Japan) using a 0.25 mm × 30 m Rtx-35MS column (Restek Corp., PA, United States) under the following conditions: the initial column temperature of 300°C was maintained for 1 min,

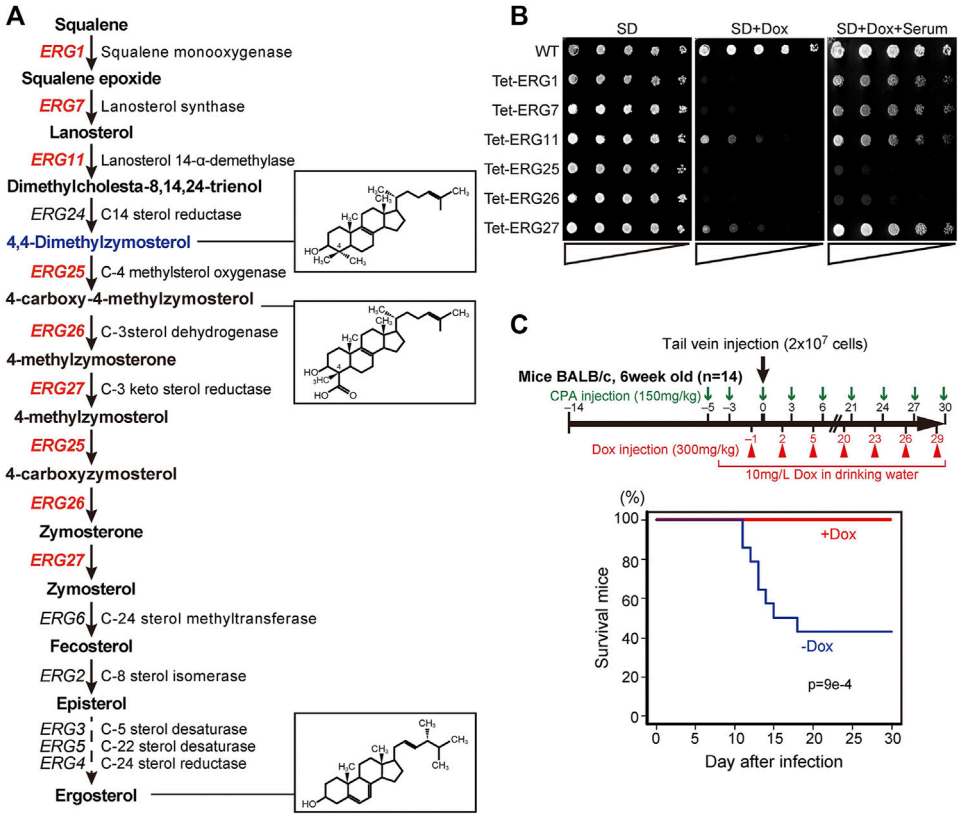

FIGURE 1 | ERG genes and the effects of knockdown. **(A)** Biosynthetic pathway from squalene to ergosterol, including genes, enzymes, and metabolic intermediates. Twelve genes encode enzymes of the ergosterol biosynthetic pathway in *S. cerevisiae*; the six genes in red are essential for growth in *S. cerevisiae*, in the absence of exogenous ergosterol. The chemical structures of ergosterol and 4, 4-dimethylzymosterol are indicated in the boxes to the right. **(B)** Effect of serum supplementation in cells subjected to gene repression. Wild-type (HETS202) and Tet-ERG cells in which the indicated *ERG* genes are knocked down by Dox diluted to OD_{600} (an optical density at 600 nm) of 0.5 in water. The diluted cells were spotted in 4-fold serial dilutions as indicated by triangles on agar plates of minimal medium (SD), SD containing 20 μg/ml Dox (SD + Dox), or SD containing 20 μg/ml Dox and 10% serum (SD + Dox + Serum), and incubated for 24 h at 37°C. The experiment was conducted three times. **(C)** Survival rate of mice after infection with Tet-ERG25 cells. As shown in the flowchart (upper panel), mice were dosed with 150 mg/kg body weight of cyclophosphamide (CPA) 3 and 5 days before the infection, and every 3 days after infection until the end of the experiment. The mice also were injected intraperitoneally with Dox in PBS (300 mg/kg body weight) every 3 days starting 1 day before the infection and also provided with drinking water containing Dox (10 mg/L) from starting from 4 days before infection. Log-phase Tet-ERG25 cells (2×10^7 yeast cells/animal) were administered to mice by tail vein injection. Red and blue lines indicate the survival rates of mice for the Dox-treated and Dox-untreated groups, respectively ($n = 14$ each). Vertical and horizontal axes indicate percentage of mice still alive and days after infection, respectively. *p* values were calculated using the log-rank (Mantel-Cox) test.

increased to 310°C at a rate of 10°C/min, and then maintained at 310°C for an additional 10 min. Trimethylsilylated sterols were detected by reference to pure substances; otherwise, sterols were identified by Shimadzu Corporation using GC-MS analysis.

Electron Microscopy

Tet-*ERG25* cells were pre-grown to exponential phase in minimal medium, and then inoculated to minimal medium containing serum with or without Dox. After 17 h, cells were collected by brief centrifugation and snap-frozen with melting propane in liquid nitrogen. Samples were freeze-substituted in OsO_4-acetone at −80°C for 4 days and embedded in epoxy resin. Ultrathin sections were cut to a thickness of 70 nm, stained with uranyl acetate and lead citrate, covered with Super support film (Nisshin EM, Tokyo, Japan), and observed using a JEM-1400 electron microscope (JEOL, Tokyo, Japan). The surface density of furrow-like invaginations was calculated from electron micrographs using the Fiji/ImageJ software.

Animal Infections

Male mice (6 weeks old, 19–24 g each, BALB/c; purchased from Oriental Yeast, Japan) were immunosuppressed by intraperitoneal injection of cyclophosphamide in saline (at 150 mg/kg body weight) 5 days before and 3 days before the infection, and every 3 days post-infection (dpi) until 27 dpi. Each group consisted of 14 mice. Mice were provided 5% (w/v) sucrose solution with or without Dox (10 mg/ml) as drinking water from 4 days prior to the injection until the end of the in-life interval. In the Dox-treated group, mice were injected intraperitoneally with Dox in PBS at a dose of 300 mg/kg body weight every 3 dpi. Mice were infected with 2×10^7 *C. glabrata* yeast cells in 200 μl of saline via tail vein injection. The mice experiments were performed strictly according to the guidelines of the Animal Care and Use Committee of Chiba University, Japan, which follows the NIH "Guide for the Care and Use of Laboratory Animals".

RESULTS

ERG25 is Required for *Candida glabrata* Serum-Dependent Growth *In Vitro* and for Lethality in Infected Mice

Among the ergosterol biosynthetic (*ERG*) genes, encoding enzymes for the conversion of squalene to ergosterol, six are essential for the growth in *Saccharomyces cerevisiae* in the absence of exogenous ergosterol (**Figure 1A**) (Giaever et al., 2002). The orthologous genes in *C. glabrata* include: *CgERG1* (CAGL0D05940g), *CgERG7* (CAGL0J10824g), *CgERG11* (CAGL0E04334g), *CgERG25* (CAGL0K04477g), *CgERG26* (CAGL0G00594g), and *CgERG27* (CAGL0G00594g). The deletion of each ERG gene results in the accumulation of individual sterol intermediates that are structurally distinct from ergosterol. To investigate whether these various intermediates may cause differences in the effects of cholesterol uptake on growth defects, we constructed conditional knockdown mutants (Tet-ERG) by replacing each promoter with a tetracycline-repressible (Tet-off) promoter (**Supplementary Figure S1A**). This Tet-off system is a useful tool for functional analysis of essential genes, since gene expression can be knocked down by the addition of tetracycline both *in vitro* and *in vivo* (Nakayama et al., 1998; Nakayama et al., 2000). We then checked the resulting Tet-ERG1, Tet-ERG7, Tet-ERG11, Tet-ERG25, Tet-ERG26, and Tet-ERG27 strains for their ability to grow in serum-supplemented medium. In each strain, the transcription of the corresponding gene was markedly knocked down in the presence of doxycycline (Dox) (**Supplementary Figure S1B**). Although Tet-ERG11 and Tet-ERG27 cells grew slightly in minimal (SD) medium containing Dox, these Tet-off strains exhibited a clear growth defect compared to the wild type cells (**Figure 1B**). Supplementation with serum permitted the Tet-ERG1, Tet-ERG7, Tet-ERG11, and Tet-ERG27 cells to grow in the presence of Dox. In contrast, Tet-ERG25 and Tet-ERG26 cells grown in the presence of Dox were not rescued by the addition of serum. Furthermore, to confirm whether the effect of knockdown by the Tet-off system on growth strictly reflects the effect of gene disruption, we performed the deletion of *ERG11* and *ERG25*. Similar to the knockdown of *ERG11*, Δ*erg11* cells displayed growth defect in minimal medium, and its growth defect was recovered by the addition of serum (**Supplementary Figure S2**). On the other hand, Δ*erg25* cells could grow in minimal medium containing serum when Erg11p, which is an upstream enzyme of Erg25p, was inhibited by fluconazole, but not in serum-free medium. *ERG25* encodes C-4 methyl sterol oxidase and *ERG26* encodes C-3 sterol dehydrogenase; together, the two enzymes catalyze a sequence of reactions that convert 4,4-dimethylzymosterol to zymosterone (**Figure 1A**). To clarify why cholesterol uptake did not rescue the growth defect caused by the inhibition of these demethylation steps, further analysis was performed using Tet-ERG25 cells. We investigated the requirement of Erg25p in blood-stream infection by examining the survival rate of mice administered Tet-ERG25 cells by tail vein injection. Because *Candida* causes an opportunistic infection, the infected host mice were immunosuppressed with cyclophosphamide prior to infection. The mice were infected with Tet-ERG25 cells and fed Dox to repress *ERG25* expression, as described in the Materials and Methods. In the group of mice not receiving Dox, survival decreased rapidly after the 11th day post-infection (dpi). In contrast, all mice receiving Dox survived until, at least, the 30th dpi (**Figure 1C**). The apparent difference in survival rates between the two groups was statistically significant ($p < 0.001$), revealing that *ERG25* knockdown reduces the lethality of mice infected with *C. glabrata*.

ERG25 Knockdown Leads to Decreased Cholesterol Uptake and Mis-Targeting of the Cholesterol Transporter Aus1p

To examine whether cholesterol uptake was functional in *ERG25* knockdown cells, we assessed the uptake of NBD-cholesterol, which is a fluorescently tagged analog of cholesterol, by fluorescence microscopy (**Figure 2A**). In wild-type and Tet-ERG11 cells grown in the absence of Dox, NBD-cholesterol is detected as clear intracellular punctate structures. Previously, these punctate structures have been described as lipid particles or droplets (Marek et al., 2014).The addition of Dox to wild-type cells did not affected the distribution of NBD-fluorescence. In Tet-ERG11 cells, although the NBD fluorescence was weaker, punctate signals were also observed under Dox conditions (i.e., conditions under which growth is maintained by the addition of serum.). On the other hand, in Tet-ERG25 and Tet-ERG26 cells, NBD-stained punctate structures no longer were observed in the presence of Dox and serum (**Figure 2A**; **Supplementary Figure S3A**). Additionally, we quantified NBD-cholesterol import in the cells using flow cytometry (**Figure 2B**). We pre-stained the cells with propidium iodide (PI), and excluded PI-staining cells from the analysis as dead cells. In wild-type cells, the fluorescence intensity of NBD was high regardless of the presence or absence of Dox. In Tet-ERG11 cells, the fluorescence intensity of NBD in the presence of Dox was lower than that in its absence, but higher than that of the non-stained cells. In Tet-ERG25 cells, the fluorescence intensity in the presence of Dox was clearly lower than that in its absence and was comparable to that of the non-stained cells. These results suggest that *ERG11* knockdown cells can partially take up NBD-cholesterol, while *ERG25* knockdown cells cannot take up NBD-cholesterol at all.

In *C. glabrata*, host-cholesterol uptake is mediated by the ATP-binding cassette transporter Aus1p, the expression of which is upregulated upon addition of serum (Nagi et al., 2013). To determine why *ERG25* knockdown cells are unable to take up cholesterol from serum, we focused on the expression of the *AUS1* gene and localization of Aus1p. We performed quantitative RT-PCR to examine the effect of *ERG25* knockdown on *AUS1* expression in the presence of serum (**Figure 2C**). The level of *AUS1* mRNA in Tet-ERG25 cells treated with Dox was comparable to those of Dox-treated wild-type and Tet-ERG11 cells. This result suggests that the transcription of *AUS1* is not affected by *ERG25* knockdown.

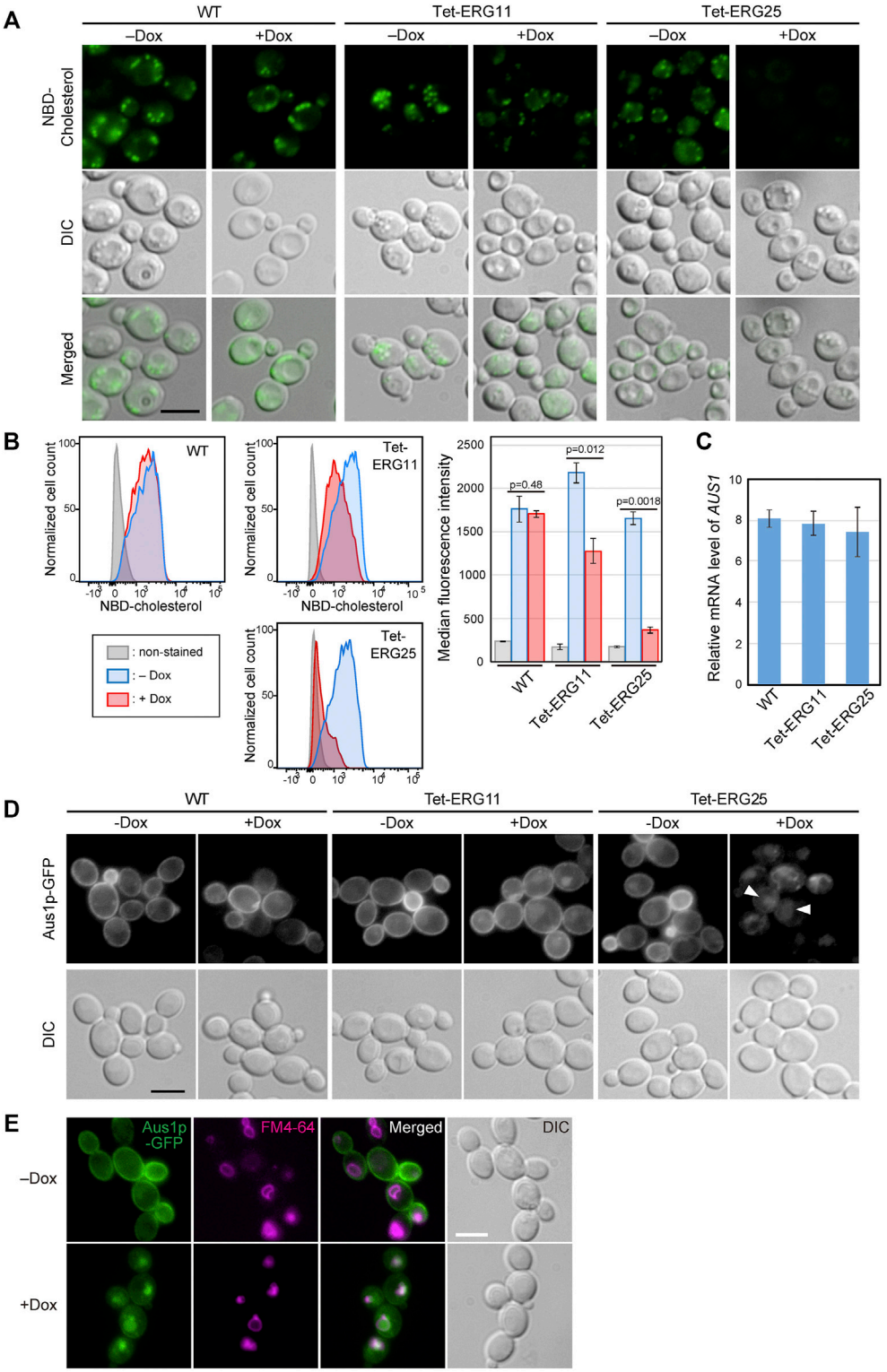

FIGURE 2 | *ERG25* knockdown causes defects in cholesterol uptake and the localization of Aus1p. **(A)** Uptake of fluorescent cholesterol analogues, NBD-cholesterol. Wild-type (HETS202), Tet-ERG11 and Tet-ERG25 cells were incubated with NBD-cholesterol in the presence (+Dox) or absence (–Dox) of Dox for 17 h in minimal medium containing 10% (v/v) serum. After washing, the fluorescence of NBD-cholesterol taken up into each cell was observed under a fluorescence microscope. **(B)** Wild-type, Tet-ERG11 and Tet-ERG25 cells were incubated as described in **(A)**, and then treated with propidium iodide (PI). Cells not stained with PI were defined as living cells, and the fluorescent intensity of NBD-cholesterol taken up into the cells was analyzed by flow cytometry. Cells incubated without NBD-cholesterol served as unstained controls. Cell

(*Continued*)

FIGURE 2 | count was normalized to the peak height at its mode of the distribution by FlowJo software. The maximum value of each peak was converted as 100%. Median fluorescence intensity was quantified from the result of each flow cytometry and represented as a graph. Values are presented as mean ± SD of three independent experiments. **(C)** *AUS1* transcript levels in wild-type (WT; KUE100), Tet-ERG11 and Tet-ERG25 cells. Cells were incubated at 37°C for 4 h in minimal medium with 20 μg/ml Dox in the presence of 10% bovine serum. *AUS1* mRNA was quantified by qRT-PCR, and the data were normalized against the corresponding levels of a housekeeping transcript (*TEF1*). Values are presented as mean ± standard deviation (SD) of three independent experiments. **(D)** Effect of *ERG25* knockdown on the localization of Aus1p. Wild-type, Tet-ERG11 or Tet-ERG25 cells that express Aus1p-GFP (WT_Aus1G, Tet-ERG11_Aus1G or Tet-ERG25_Aus1G) were incubated in minimal medium containing 10% (v/v) serum at 37°C with or without 20 μg/ml Dox. After 3.5 h, fluorescence associated with Aus1-GFP was observed using a microscope. DIC, Differential Interference Contrast. **(E)** *ERG25* knockdown causes the mislocalization of Aus1p to the vacuole. Tet-ERG25 cells that express Aus1p-GFP (Tet-ERG25_Aus1G) were incubated in minimal medium containing 10% (v/v) serum at 37°C with or without 20 μg/ml Dox for 3 h. Vacuole membrane was stained with FM4-64. All scale bars represent 5 μm.

Next, we investigated the effects of *ERG25* knockdown on Aus1p localization in a Tet-ERG25 strain using an Aus1p-Green Fluorescent Protein (GFP) fusion expressed from the endogenous *AUS1* locus. Since the Δ*aus1* strain is sensitive to fluconazole even in medium containing serum, the fact that the wild-type strain with GFP tagging on *AUS1* is not sensitive to fluconazole in medium containing serum suggests that Aus1p-GFP is functional. In the absence of Dox, the fluorescence of Aus1-GFP was detected on the cell surface in Tet-ERG11 and Tet-ERG25 cells (**Figure 2D**). In the presence of Dox, Aus1p-GFP localization to the plasma membrane was partially retained in Tet-ERG11 cells. In contrast, in Tet-ERG25 cells, the fluorescence of Aus1p-GFP disappeared from the cell surface; instead, atypical fluorescent clumps were observed (**Figure 2D**, white arrowhead). The fluorescence intensity profile also indicated that the fluorescence peak indicating localization to the cell membrane disappeared in the presence of Dox in Tet-ERG25 (**Figure 2D**, black arrowhead). The localization of Aus1p-GFP in Dox treated Tet-ERG25 cells appears to be vacuolar, its signal being surrounded by FM4-64, which stains vacuolar membranes (**Figure 2E**). These observations suggested that the inability of *ERG25* knockdown cells to uptake exogenous cholesterol is due to mislocalization of Aus1p, which may be unable to sort properly into the plasma membrane.

ERG25 Knockdown Leads to Loss of Aus1p-DRMs Association and Altered DRMs Sterol Composition

In *S. cerevisiae*, plasma membrane proteins have been suggested to associate with DRMs, which are enriched in ergosterol and sphingolipids. DRMs are proposed to be involved in the trafficking of proteins to the plasma membrane. Therefore, we evaluated whether the inability of Aus1p to localize to the plasma membrane in *ERG25* knockdown cells reflected the inability of Aus1p to associate with DRMs. Specifically, we isolated DRMs from Tet-ERG25 cells by the classical method, wherein a cell lysate is treated with Triton X-100 at 4°C and then fractionated by Optiprep density gradient centrifugation. Each fraction was analyzed by immunoblotting with antibodies against GFP to detect Aus1p-GFP or against Pma1p, a representative DRM-associated protein in *S. cerevisiae* (Gulati et al., 2015). When DRMs were isolated from cells grown in the absence of Dox, Pma1p was detected in Fraction 2, indicating that Fraction 2 was enriched in DRMs (**Figure 3A**). Aus1p-GFP also was detected in Fraction 2, similar to Pma1p. When DRMs were isolated from cells grown in the presence of Dox, Aus1p-GFP was no longer seen in Fraction 2. Instead, we observed an increase in low-molecular-weight proteins, presumably corresponding to free GFP, in the detergent-soluble fraction (Fractions 5-7) compared to cells grown in the absence of Dox. Because GFP tends to be resistant to vacuolar proteases (Conibear and Stevens, 2002), we speculated that the free GFP was derived from vacuolar degradation of Aus1p-GFP. This hypothesis is supported by the localization of the GFP fluorescence to the vacuole in *ERG25* knockdown cells (**Figure 2E**). In contrast, bands corresponding to Pma1p still were present in Fraction 2. Together, these results suggested that Aus1p associates with DRMs in *C. glabrata*, and that this association is disrupted in the *ERG25* knockdown cells.

To clarify why the association of Aus1p with DRMs is disrupted in the *ERG25* knockdown cells, we focused on 4,4-dimethylzymosterol, the precursor that is expected to accumulate in the *ERG25* knockdown cells. The formation of DRMs depends on specific interactions between sterols and sphingolipids (Klose et al., 2010) and a structural change of sterols affect the association of the plasma membrane with DRMs (Eisenkolb et al., 2002; Umebayashi and Nakano, 2003). We hypothesized that in cells knocked down for *ERG25* expression, the sterol in DRMs would change from ergosterol and cholesterol to 4,4-dimethylzymosterol, thereby affecting the association of Aus1p with DRMs. To test this hypothesis, we performed quantitative gas chromatography analysis (GC) of DRMs derived from Tet-ERG25 cells to investigate whether 4,4-dimethylzymosterol is contained primarily in the DRM fractions (**Figure 3B**). In the DRMs derived from Tet-ERG25 cells cultured with serum in the absence of Dox, the main sterol components were ergosterol and cholesterol, while 4,4-dimethylzymosterol was a minor sterol. In contrast, in DRMs derived from Tet-ERG25 cells cultured in the presence of Dox, the main sterol component was 4,4-dimethylzymosterol instead of ergosterol and cholesterol. Given that *ERG25* knockdown resulted in replacement of the ergosterol and cholesterol with 4,4-dimethylzymosterol as the DRM-forming sterol, it suggests that 4,4-dimethylzymosterol influences the association of Aus1p with DRMs.

ERG25 Knockdown Has Little Effect on the Plasma Membrane Localization of the DRM-Associated Proteins Pma1p and Hxt1p

Because the association of Pma1p with DRMs was not affected by *ERG25* knockdown (**Figure 3A**), we investigated whether *ERG25*

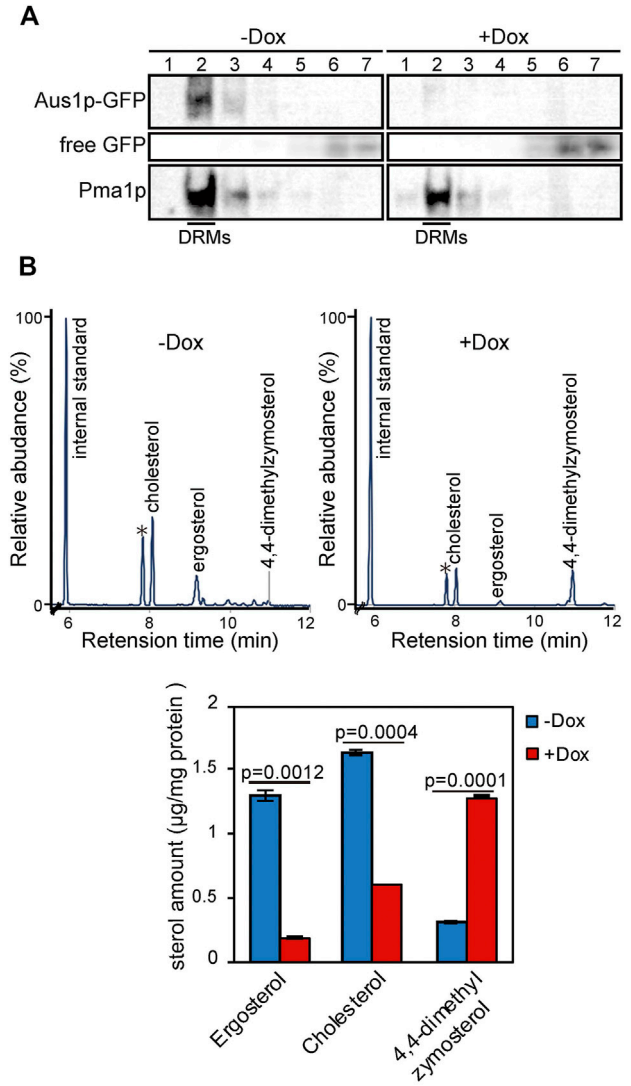

FIGURE 3 | *ERG25* knockdown causes the dissociation of Aus1p from detergent-resistant membranes (DRMs) and a component change of DRMs. **(A)** Biochemical analysis of the effect of *ERG25* knockdown on the association of Aus1p with DRMs. Tet-ERG25 cells that express Aus1p-GFP (Tet-ERG25_Aus1G) were grown to exponential phase at 37°C in minimal medium containing 10% (v/v) bovine serum and then incubated with or without 20 μg/ml Dox for 5.5 h. The cells were disrupted with glass beads, extracted with 1% Triton X-100, and subjected to Optiprep density gradient centrifugation. Seven fractions were collected and analyzed by western blotting with antibodies against GFP and Pma1p. Pma1p was used as a marker for DRM-associated proteins. Raw data was displayed in Supplementary Figure S4. **(B)** Sterol analysis of DRMs in Tet-*ERG25* cells. The DRM fraction was analyzed by gas chromatography. Before the centrifugation, the quantity of total protein was determined by protein assay. 5-α-Cholestane was used as an internal standard. Individual sterols are quantified and indicated in a lower panel. Individual sterols were identified by comparison to standards or GC-MS. Values are presented as mean ± SD of three independent experiments. ∗; Triton-100.

knockdown influenced the localization of Pma1p to the plasma membrane. We constructed a Tet-ERG25 strain that co-expressed Aus1p-GFP and Pma1p-mCherry by inserting sequences encoding the indicated fluorescent tag in-frame and downstream of the respective genes. The resulting strain encoded C-terminally tagged fusion proteins from the endogenous loci. We then observed cells of this strain using fluorescence microscopy to assess the intracellular localization of Pma1p. The fluorescence of Pma1p-mCherry was detected on the plasma membrane and in the vacuole in the absence of Dox. In the presence of Dox, the fluorescence of Aus1p-GFP on the cell surface disappeared, while that of Pma1p was maintained on the cell surface, although the fluorescence signal detected in the vacuole increased (**Figure 4A**). These results indicate that the localization of Pma1p to the plasma membrane was largely unaffected by *ERG25* knockdown.

Most plasma membrane proteins are compartmentalized in distinct domains on the plasma membrane, and their distribution is influenced by the lipid composition of the plasma membrane (Spira et al., 2012). Therefore, we speculated that Aus1p and Pma1p could be normally located in distinct domains of the plasma membrane, that have distinct lipid compositions, and that ergosterol is an important element in the distribution of Aus1p-associated domains. To confirm this hypothesis, we compared the distribution pattern of Aus1p and Pma1p on the plasma membrane by real-time observation of cells co-expressing *AUS1-GFP* and *PMA1-mCherry*, using high-resolution confocal microscopy. The fluorescence of Aus1p-GFP and Pma1p-mCherry were detected in the different region on the plasma membrane (**Figure 4B**). Further high-resolution observation clearly showed the difference in the distribution of Aus1p and Pma1p. In non-budding cells, the fluorescence of Aus1p-GFP exhibited a network-like localization pattern similar to that seen for Pma1p. Notably, however, most of the Aus1p-GFP fluorescence did not overlap with that of Pma1p-mCherry in the images that focused on the top and middle of the cell (**Figure 4C**). The fluorescence intensity profile and scatterplot of green (Aus1p-GFP) and magenta (Pma1p-mCherry) pixel intensities also clearly indicated a difference in the localization patterns of the two proteins. When daughter cells were smaller than mother cells, the fluorescence intensity of Aus1p-GFP was higher at the cell surface of daughter cells than in that of the mother cells, whereas that of Pma1p-mCherry was higher at the cell surface of mother cells (**Figure 4D**). These results indicated that Aus1p and Pma1p are compartmentalized to distinct domains on the plasma membrane under normal circumstances. Furthermore, to determine whether the differences in the localization patterns of Aus1p and Pma1p correlated with sterol distribution, we observed sterol by staining with filipin. In budding cells, filipin stained the cell surface of daughter cells more strongly than that of mother cells, and the filipin staining pattern was similar to the fluorescence pattern of Aus1p (**Figure 4D**, bottom panel). Furthermore, in the magnified image of budding cells, the fluorescence intensity profile indicated that the fluorescence of Pma1p-mCherry did not overlap with the distribution of sterol, while that of Aus1p-GFP showed partial overlap with the filipin-stained region (**Figure 4E**). To quantify the extent to which Aus1p and Pma1p are in close proximity to sterol-rich regions on the plasma membrane, we calculated Pearson's correlation

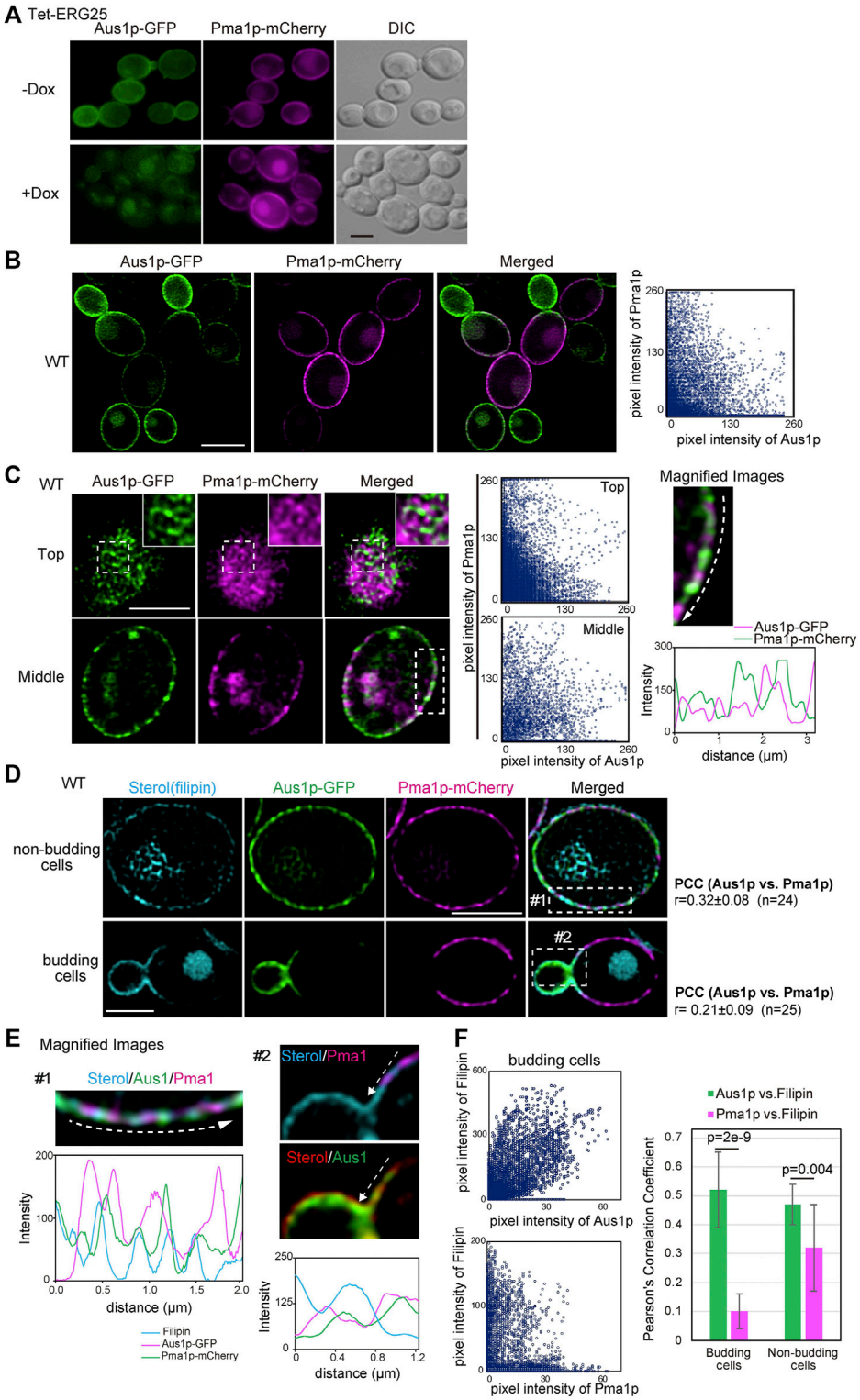

FIGURE 4 | *ERG25* knockdown has no effect on the localization of Pma1p. **(A)** Effect of *ERG25* knockdown on the localization of Pma1p. Tet-ERG25 cells that expresses Aus1p-GFP and Pma1p-mCherry (Tet-ERG25_Aus1G/Pma1R) were grown to exponential phase at 30°C in minimal medium containing 10% (v/v) bovine serum and observed using fluorescence microscopy after incubation with or without 20 μg/ml Dox for 3.5 h. **(B)** Distribution of Aus1p and Pma1p on the plasma membrane. Wild-type cells co-expressing Aus1p-GFP and Pma1p-mCherry (WT_Aus1G/Pma1R cells) were grown to exponential phase at 30°C in minimal medium containing 10% (v/v) bovine serum. Scatterplots of green and magenta pixel intensities of Aus1p-GFP and Pma1p-mCherry were performed using the Fiji/

(*Continued*)

FIGURE 4 | ImageJ software (right panel). **(C)** WT_Aus1G/Pma1R cells were observed at the cell surface (Top) and transverse region (Middle) using a high-resolution confocal fluorescence microscope in real time. Each area enclosed by the dashed lines also is provided as a magnified image. In the magnified image of the transverse region, intensity profiling of GFP (green) and mCherry (magenta) on the plasma membrane was carried out in the direction shown by the arrow. Scatterplots of green and magenta pixel intensities in each panel were indicated. **(D)** Comparison of distribution between Aus1p, Pma1p, and ergosterol in non-budding or budding cells. WT_Aus1G/Pma1R cells were stained with filipin and then observed by focusing on the middle of the cells using a confocal fluorescence microscope. In non-budding or budding cells, Person's correlation coefficient (PCC) between the fluorescent signals obtained with Aus1p-GFP and Pma1p-mCherry were indicated on the right side of the image. **(E)** Magnified image of each area enclosed by the dashed lines in **(D)**. Sterol was colored red or blue to facilitate comparison to the fluorescence of GFP (green) and mCherry (magenta). Intensity profiling of each fluorescence pattern was carried out along the dashed arrows and indicated in the corresponding light panel, respectively. **(F)** Scatterplots of green and cyan, or magenta and cyan pixel intensities in budding cells of **(D)**. PCC between Aus1p-GFP and Filipin, or Pma1p-mCherry and Filipin were graphically showed. All scale bars represent 2.5 μm.

coefficients (PCC) between fluorescene of Aus1p-GFP and Filipin, or that of Pma1p-mCherry and Filipin. The value of PCC between Aus1p-GFP and Filipin was higher than that of PCC between Pma1p-mCherry and Filipin (**Figure 4F**). These results suggested that the Aus1p-containing domains are enriched with sterol compared to the Pma1p-containing domains.

To further confirm that *ERG25* knockdown does not influence protein targeting in sterol-poor regions of the plasma membrane, we investigated the localization of the hexose transporter Hxt1p, which (like Pma1p) has been reported to be localized preferentially on mother cells in *S. cerevisiae* (Malínská et al., 2003). Using confocal microscopy, detailed observation of wild-type cells endogenously co-expressing Aus1p-GFP and Hxt1p-mCherry revealed that the fluorescence of Hxt1p-mCherry was detected primarily on the mother cells, unlike the filipin staining pattern in **Figure 4D** and the distribution of Hxt1p-mCherry was distinct from that of Aus1p (**Figure 5A**). High-resolution observation also clarified the difference in the distribution between Aus1p and Hxt1p (**Figure 5B**). When focusing on the middle of the cell, the fluorescence of Hxt1p-mCherry was observed primarily in the region from which Aus1p-GFP was excluded (**Figure 5C**). This distinction is apparent in the corresponding fluorescence intensity profile, which showed that the peaks of Aus1p-GFP and Hxt1p-mCherry fluorescence do not align. These results suggested that Aus1p and Hxt1p are compartmentalized to distinct domains on the plasma membrane. We then investigated the effect of *ERG25* knockdown on the localization of Hxt1p. While the fluorescence of Aus1p-GFP on the cell surface disappeared in Tet-ERG25 cells grown in the presence of Dox, the fluorescence of Hxt1p-mCherry still was detected on the cell surface regardless of the presence of Dox (**Figure 5D**). Taken together, our results suggested that the effect of *ERG25* knockdown was specific to Aus1p-containing domains, and not to Pma1p- or Hxt1p-containing domains.

MCC/Eisosome Structures Are Disrupted in *ERG25* Knockdown Cells

In *S. cerevisiae*, the MCC/eisosomes, which correspond to characteristic furrow-like invaginations in the plasma membrane (Strádalová et al., 2009), have been reported to be enriched in ergosterol (Grossmann and Malinsky, 2007). Therefore, to investigate whether *ERG25* knockdown affects the structure of the MCC/eisosomes, we observed the cell surface of Tet-ERG25 cells using transmission electron microscopy (TEM). In control cells untreated with Dox, furrow-like invaginations appeared as a bundle of lines with lengths of 130–200 nm, which are indicated by white arrowheads in tangential sections (**Figure 6A**); these invaginations exhibited depths of about 50 nm when viewed in transverse sections (**Figure 6B**). These structures were similar to the furrow-like invaginations corresponding to MCC/eisosomes of *S. cerevisiae* (Walther et al., 2006). By counting the number of invaginations in 13 *C. glabrata* cells, we quantified these structures at 3.2 ± 1.1/μm^2 (mean ± standard deviation) in the absence of Dox and 0.3 ± 0.5/μm^2 in the presence of Dox. In the presence of Dox, globular structures of 50–80 nm in diameter appeared on the cell surface, instead of furrow-like invaginations (black arrowheads in **Figures 6A,B**). The shape of these globular structures was similar to the shape of the remnants seen in *S. cerevisiae* with deletion of *PIL1*, which encodes a main organizer of MCC/eisosomes assembly (Moreira et al., 2012). These observations indicated that the influence of *ERG25* knockdown extended to the formation of furrow-like invaginations on the cell surface.

To further ascertain the effect of *ERG25* knockdown on MCC/eisosomes, we used fluorescence microscopy to observe the distribution of Pil1p in Tet-ERG25 cells. *PIL1* was endogenously tagged with sequences encoding mCherry so as to encode a C-terminally tagged protein. In wild-type cells, the fluorescence of Pil1-mCherry was detected in punctate compartments located on the cell surface in the presence or absence of Dox, suggesting that the localization of pil1p could not be affected by the addition of Dox (**Supplementary Figure S5**). On the other hand, in Tet-ERG25 cells, Pil1p-mCherry showed a punctate localization similar to wild-type cells (**Figure 6C**). In the absence of Dox, the fluorescence of Pil1p-mCherry was detected in punctate compartments located on the cell surface (**Figure 6C**). However, following *ERG25* knockdown with Dox, the punctate Pil1p fluorescence on the cell surface decreased, and fluorescence instead was observed in the cytoplasm. This result implied that *ERG25* knockdown causes diffusion of Pil1p from the plasma membrane to the cytoplasm.

Aus1p Associates With Dynamic Domains That Occasionally Overlap With MCC/Eisosomes

Because the structure of MCC/eisosomes diffused in the cells in which *ERG25* was knocked down, the relationship between the

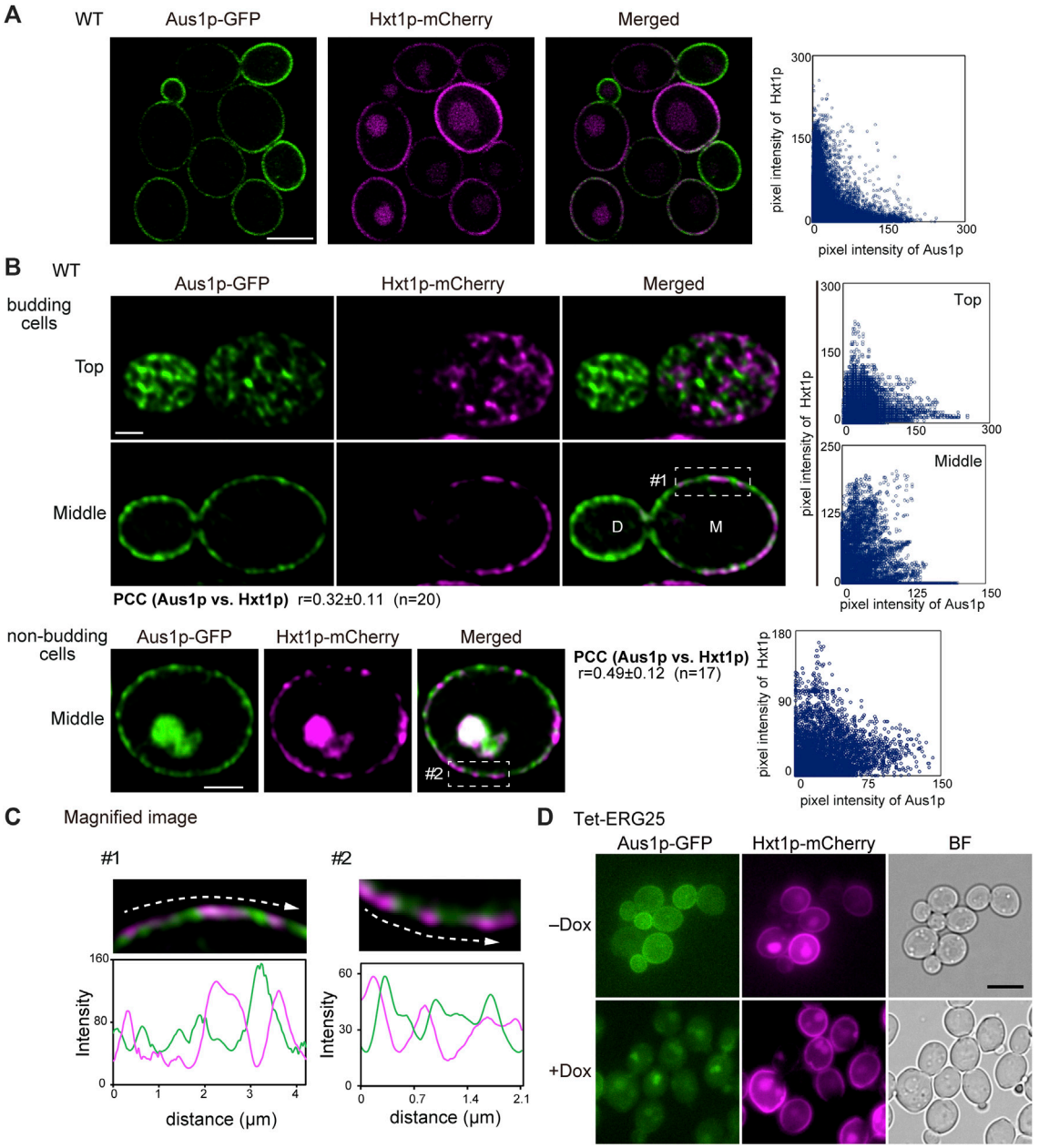

FIGURE 5 | The plasma membrane distributions of Aus1p and Hxt1p are different, and *ERG25* knockdown has no effect on the localization of Hxt1p. **(A)** Distribution of Aus1p and Hxt1p on the plasma membrane. Wild-type cells co-expressing Aus1p-GFP and Hxt1p-mCherry (WT_Aus1G/Hxt1R) cells were grown to exponential phase at 30°C in minimal medium containing bovine serum. Scatterplot of green and magenta pixel intensities of Aus1p-GFP and Hxt1p-mCherry was shown in the right panel. Scale bar represents 2.5 μm. **(B)** WT_Aus1G/Hxt1R cells were observed at high resolution by focusing on the top and middle of the cells using a confocal fluorescence microscope. Scatterplots in each cell were represented in the right panel. PCC between the fluorescent signals obtained with Aus1p-GFP and Hxt1p-mCherry in budding or non-budding cells were indicated. Scale bars represent 1 μm. D, daughter cell; M, mother cell. **(C)** Magnified image of the area enclosed by the dashed lines in **(B)**. Intensity profiling of GFP (green) and mCherry (magenta) on the plasma membrane was carried out along the dashed arrows. **(D)** Effect of *ERG25* knockdown on the localization of Hxt1p. Tet-ERG25 cells that expresses Aus1p-GFP and Hxt1p-mCherry (Tet-ERG25_Aus1G/Hxt1R) were grown to exponential phase at 30°C in minimal medium containing 10% (v/v) bovine serum and observed using fluorescence microscopy after incubation with or without 20 μg/ml Dox for 3.5 h. Scale bar represents 2.5 μm.

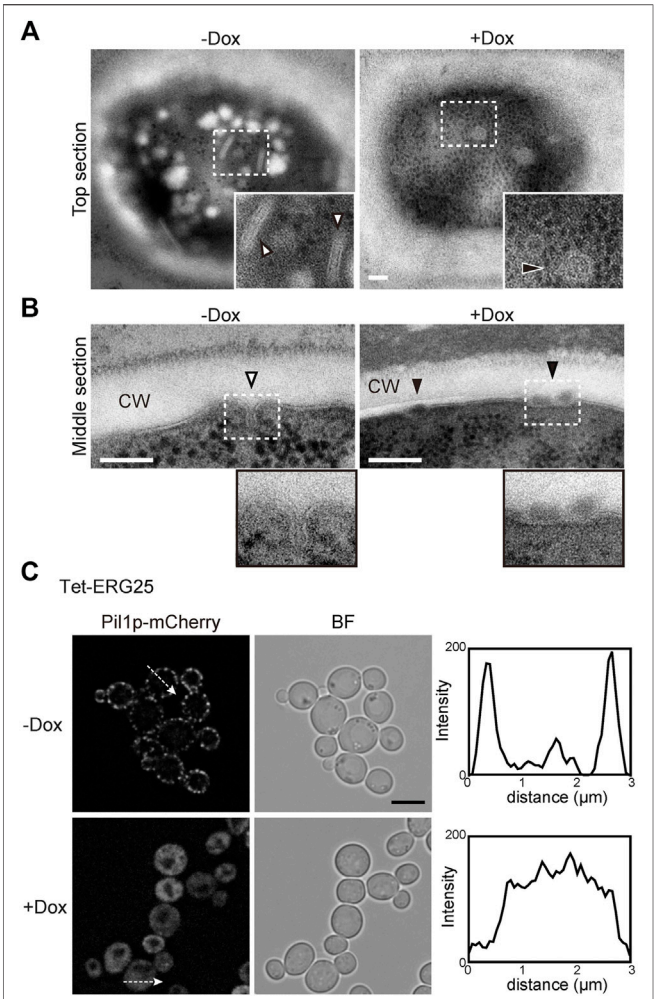

FIGURE 6 | *ERG25* knockdown has effect on the structure of MCC/eisosomes. **(A)** Observation of furrow-like invaginations in Tet-ERG25 cells using transmission electron microscopy (TEM). Cells were incubated at 37°C in minimal medium containing 10% (v/v) bovine serum with or without Dox for 17 h, and then fixed. Ultrathin sections (70-nm thicknesses) of the cell surface were observed. The furrow-like invaginations in Dox-untreated cells are indicated by white arrowheads, and abnormal invaginations in Dox-treated cells are indicated by black arrowheads. The dashed lines surround areas shown at higher magnifications in the lower right. Scale bars represent 100 nm. CW; cell wall. **(B)** TEM images of the cells sectioned through the middle of the cells. **(C)** Effect of *ERG25* knockdown on the localization of Pil1p-mCherry. Tet-ERG25 cells expressing Pil1p-mCherry (Tet-ERG25_Aus1G/Pil1R) were grown to exponential phase at 37°C in minimal medium containing bovine serum and further incubated for 17 h in the absence or presence of Dox. Intensity profiling of Pil1p-mCherry was carried out along the dashed arrows. Scale bar represents 5 μm.

diffusion and the mislocalization of Aus1p was investigated. We constructed Tet-ERG25Δ*pil1*, a double-mutant strain (with downregulation of *ERG25* and knockout of *PIL1*) that expresses Aus1p-GFP, and compared the localization of Aus1p when this strain was grown with and without Dox. In the absence of Dox, Aus1p was observed to be localized on the cell surface, but fluorescent aggregates were observed as indicated by the white arrowhead (**Figure 7A**). When Tet-ERG25Δ*pil1* was grown in the presence of Dox, Aus1p-GFP no longer localized to the plasma membrane, instead accumulating in the vacuole, as was seen previously in the case of *ERG25* knockdown. These observations show that the mislocalization of Aus1p by the knockdown of *ERG25* occurred independently of the aggregation of Aus1p on the plasma membrane, caused by the deletion of *PIL1*.

Given that the deletion of *PIL1* altered the inherent localization of Aus1p on the plasma membrane (as shown in **Figure 7A**), we investigated whether Aus1p associates with MCC/eisosomes on the plasma membrane. To compare the distributions of Aus1p and MCC/eisosomes, we performed dual-color imaging of Aus1p-GFP and Pil1-mCherry (a marker for MCC/eisosomes) in living cells. High-resolution imaging revealed that Aus1p fluorescence was detected primarily in the plasma membrane regions that did not contain Pil1p-mCherry (**Figures 7B,D**). Furthermore, we followed the behavior of Aus1p and Pil1p in detail by time-lapse observations. MCC/eisosomes (as indicated by Pil1p-mCherry) was static as reported in *S. cerevisiae* (Malínská et al., 2003), whereas Aus1p-GFP fluorescence migrated dynamically across the plasma membrane (**Figure 7C**) Supplemental Movie. Kymographs of the light panels also clearly highlight the dynamic differences between these domains, suggesting that Aus1p is dynamically localized to a domain that is distinct from MCC/eisosomes. However, the real-time imaging also showed some overlap between the fluorescence of Aus1p-GFP and that of Pil1-mCherry, as indicated by the white arrowheads in **Figure 7C**. Therefore, we performed time-lapse imaging of Aus1p-GFP, focusing on single MCC/eisosomes. We observed that some Aus1p-GFP was present in MCC/eisosomes for a short time, at intervals of about 1.5–4.5 s (frames surrounded by red lines in **Figure 7E**). These results suggested that Aus1p is mostly localized outside MCC/eisosomes, however, some Aus1p may access MCC/eisosomes occasionally.

DISCUSSION

Host-cholesterol uptake is one of the key survival strategies for successful infection, especially for *Candida glabrata*, which uses it to proliferate despite the presence of azole antifungal agents that inhibit ergosterol biosynthesis. In this study, among the screened ergosterol biosynthetic genes in *C. glabrata* (*ERG1, ERG7, ERG11, ERG25, ERG26*, and *ERG27*), we found that only the growth defects imposed by *ERG25* or *ERG26* knockdown were not rescued by the presence of serum (**Figure 1B**). Because the two genes are involved in a sequence of catalytic events, we concentrated our investigation on *ERG25*. In cells with little or no *ERG25* transcription, four observations were made: 4,4-dimethylzymosterol accumulates (**Figure 3B**); Aus1p-GFP delocalizes to the plasma membrane (**Figure 2D**); extracellular NBD-cholesterol is not uptaken (**Figures 2A,B**); the addition of serum cannot suppress their growth defects (**Figure 1B**). Based on these results, the effect of *ERG25* knockdown on Aus1p lipid domains was analyzed.

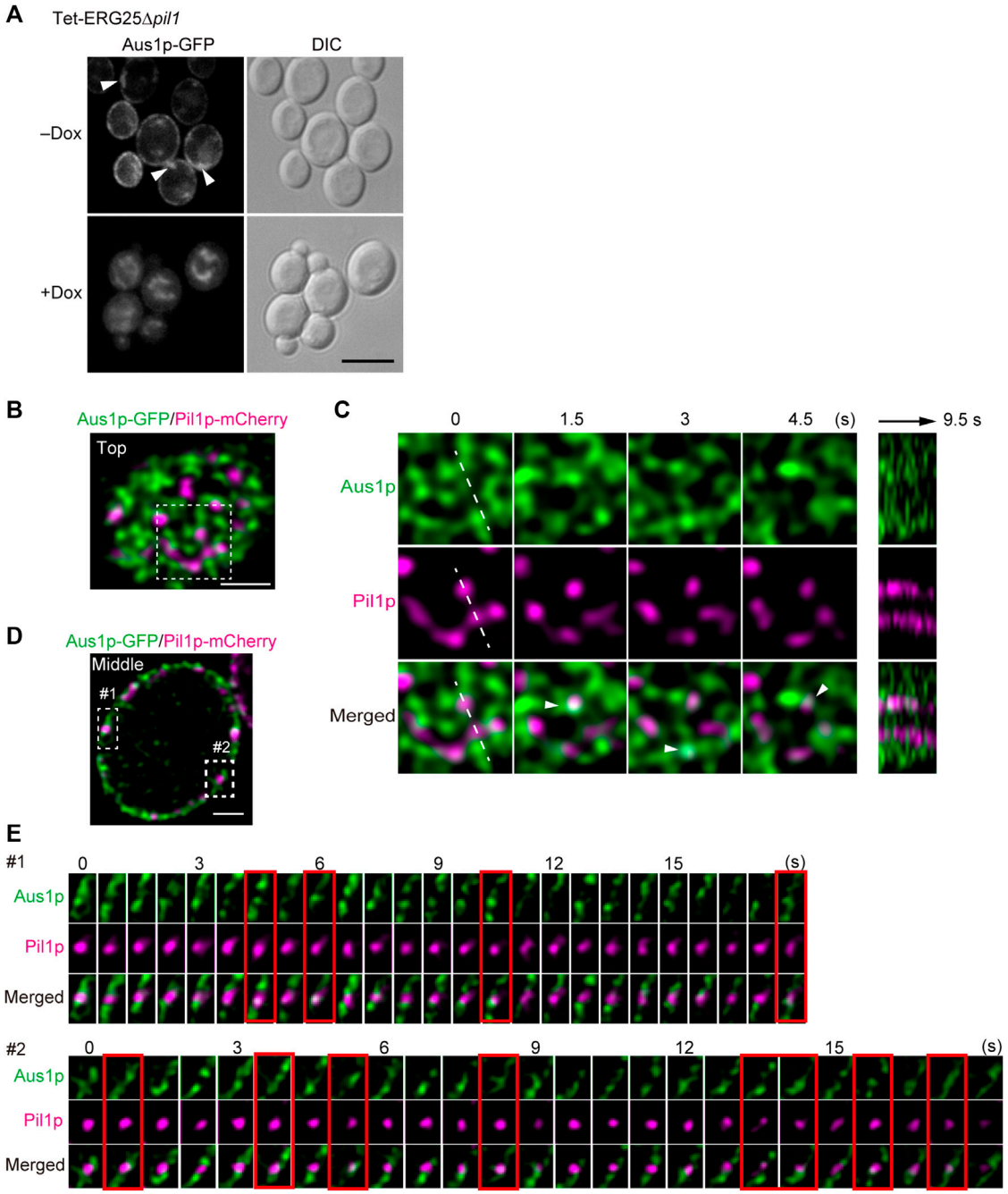

FIGURE 7 | Aus1p is compartmentalized into plasma membrane domains distinct from MCC/eisosomes. **(A)** Effect of *PIL1* deletion on the localization of Aus1p. Tet-ERG25 *pil1*Δ cells expressing Aus1p-GFP (Tet-ERG25 *pil1*Δ_Aus1G) were grown to exponential phase at 30°C in minimal medium containing bovine serum and observed using fluorescence microscopy after incubation with or without Dox for 3.5 h. Scale bar represents 5 μm. **(B)** Distribution of Aus1p and Pil1p on the plasma membrane. Wild-type cells co-expressing Aus1p-GFP and Pil1p-mCherry (WT_Aus1G/Pil1R) were incubated in the presence of serum and observed at the cell surface (Top) by high-resolution confocal microscopy. **(C)** Time-lapse imaging of the boxed region of **(A)**. Right panel shows the kymograph obtained by recording across the dashed line of the middle panels in a time-lapse image taken every 0.5 s. Co-localization of Aus1 and Pil1p appears in white, as indicated by arrowheads. **(D)** Distribution of Aus1p and Pil1p on the plasma membrane in the traverse region. **(E)** Time-lapse imaging of the boxed region of **(D)**. Images were taken at 0.75-s intervals. The images surrounded with red lines represent the co-localization of Aus1p-GFP and Pil1p-mCherry. All scale bars represent 2 μm.

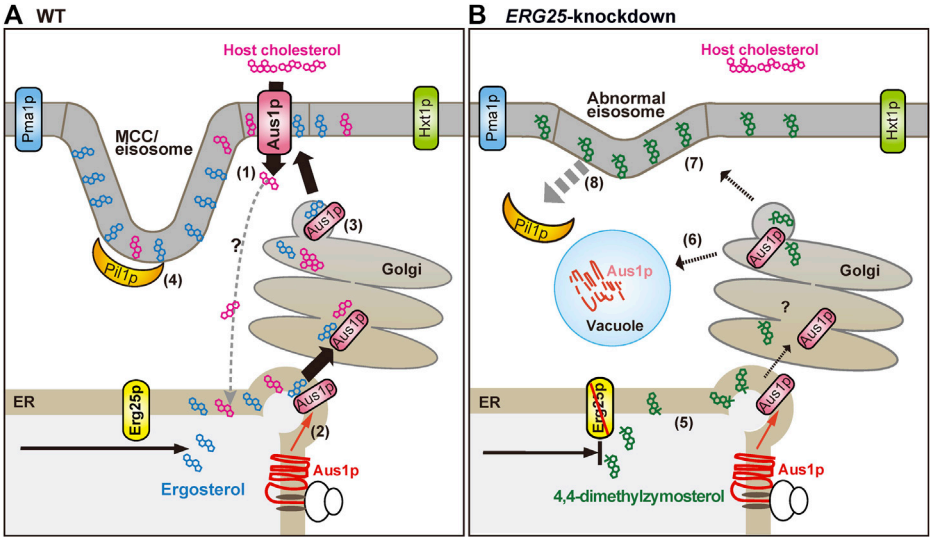

FIGURE 8 | Schematic diagram showing the proposed effects of *ERG25* knockdown on host-cholesterol uptake. **(A)** Ergosterol and cholesterol interact with sphingolipid to form lipid domains (liquid-ordered state domain). Host-cholesterol is incorporated from serum via Aus1p, which is normally localized on the plasma membrane (1) and then transported to the endoplasmic reticulum (ER), although the transport route is unknown. In *S. cerevisiae*, the association of proteins with lipid domain occurs during trafficking from the ER to the plasma membrane *via* the Golgi. Therefore, newly synthesized Aus1p is inferred to be transported from the ER to the Golgi while being incorporated into lipid domains containing endogenous ergosterol (2, 3). Pil1p localizes to the membrane compartment of Can1p (MCC)/eisosomes that are enriched in ergosterol, generating furrow-like plasma membrane invaginations (4). Aus1p-associated domains are distinct from membrane compartment of Pma1p (MCP), membrane domains containing Hxt1p, and MCC/eisosomes. **(B)** In *ERG25* knockdown cells, 4,4-dimethylzymosterol is contained in lipid domains in place of ergosterol (5), but the domains are not allowed to fit the Aus1p due to 4,4-dimethylzymosterol. Therefore, newly synthesized Aus1p is unable to associate with lipid domain, and is missorted to the vacuole, resulting in the degradation (6). 4,4-Dimethylzymosterol, which is transported to the plasma membrane (7) and the release of Pil1p from the MCC/eisosomes (8). However, there is no effect on the localization of membrane proteins Pma1 and Hxt1.

The selective interaction between ergosterol and sphingolipids has been reported to lead to phase separation into membrane domains with Liquid-ordered and Liquid-disordered like properties (Klose et al., 2010). The changes in sterol structure are known to destabilize or prevent the formation of liquid-ordered state domains (Xu et al., 2001; Megha et al., 2006). Since the liquid-ordered state conveys detergent resistance, we used DRMs to evaluate the liquid order state of membrane domains. In Tet-ERG25 cells under the Dox presence, Aus1p-GFP was scarcely detected in DRMs, whereas Pma1p had little or no effect on its distribution (**Figure 3A**). In addition, in Dox exposed Tet-ERG11 cells Aus1p-GFP was detected in the DRMs (**Supplementary Data S6A**). Furthermore, lipid analysis of DRMs showed that the abnormal sterol 4,4-dimethylzymosterol was detected as the major lipid component in Dox exposed Tet-ERG25 cells, whereas in Tet-ERG11 cells in the presence of Dox, the abnormal sterol, 4,14α-dimethylzymosterol was hardly or not detected in DRMs (**Supplementary Data S6B**). These results suggest that the loss of membrane localization of Aus1p-GFP was due to the presence of 4,4-dimethylzymosterol in the cell membrane, while in Tet-ERG11 cells in the presence of Dox, 4,14α-dimethylzymosterol hardly detected in the cell membrane, caused little effect in it and the localization of Aus1p-GFP was maintained.

The expression of Aus1p is regulated by Upc2A and Upc2B (Nagi et al., 2013), but the mechanism whereby Aus1p is transported to the plasma membrane remains unclear. The present study revealed that DRMs are required for the proper transport of Aus1p to the plasma membrane, as demonstrated by our analysis of cells knocked down for *ERG25* expression. We summarize our model for the transport of Aus1p in **Figure 8**. In *S. cerevisiae*, the association of membrane proteins with DRMs occurs in the ER or Golgi during intracellular transport (Bagnat et al., 2000; Okamoto et al., 2006), and some plasma membrane proteins are excluded from DRMs and are missorted to the vacuole from the late Golgi in the cells deleted for *ERG6*, which encodes an enzyme catalyzing a late step in ergosterol biosynthesis (Bagnat and Simons, 2002; Umebayashi and Nakano, 2003). Similar to Δ*erg6* cells, we showed, using *C. glabrata ERG25* knockdown cells, that Aus1p is mislocalized to the vacuole instead of the plasma membrane (**Figure 2E**). Therefore, in *ERG25*-knockdown cells, the association of Aus1p with DRMs in the ER and Golgi is prevented, and Aus1p appears to migrate from the late Golgi to the vacuole. Another experiment using *C. glabrata* supports this model. Specifically, while in the Tet-ERG25 cells absence of Dox, the deletion of *PIL1* affects the distribution of Aus1p in the plasma membrane after intracellular transport, the deletion of *PIL1* in combination with *ERG25* knockdown causes the mislocalization of Aus1p to the vacuole, similarly to the knockdown of *ERG25* alone (**Figure 7A**). These results suggest that Erg25p is a factor that transports newly synthesized Aus1p from the ER to the plasma membrane, and

that Pil1p is not associated with this process. However Pil1p may be involved in the localization of Aus1p after it reaches the plasma membrane.

In *S. cerevisiae*, ergosterol has been reported to be required for the proper localization of the MCC-associated proteins Can1p and Sur7p, as demonstrated using strains deleted for non-essential ergosterol biosynthesis genes such as *ERG6* and *ERG24* (Malínská et al., 2003; Grossmann et al., 2008). However, it is not yet clear whether ergosterol is required for the formation of eisosomes, because the deletion of these non-essential genes in *S. cerevisiae* did not result in an obvious defect in MCC/eisosomes formation or in the localization of Pil1p on the plasma membrane. *ERG25* knockdown in *C. glabrata* inhibited the normal formation of furrow-like invaginations (**Figures 6A,B**) and the retention of the MCC/eisosomes organizer Pil1p on the plasma membrane (**Figure 6C**), suggesting clearly the need for ergosterol in the formation and/or stability of eisosomes. The recruitment of Pil1p to the MCC/eisosomes is regulated by the phosphorylation of Pil1p via the Pkh1/2p kinases (Walther et al., 2007), which respond to the sphingolipid long-chain base (LCB) (Zhang et al., 2004). In *S. cerevisiae*, the *erg26* mutant cells, which are defective in the demethylation step of 4,4-dimethylzymosterol, exhibit a decrease in phytosphingosine-derived ceramide levels (Swain et al., 2002). Both ergosterol and cholesterol do not have a methyl group on the α-face, while 4,4-dimethyldysterol has a methyl group on the α-face (**Supplementary Figure S7**). Whether that clear structural difference interferes with the synthesis and association to sphingolipid is an important subject for further investigation.

Plasma membrane proteins are compartmentalized into distinct non-overlapping membrane domains. In addition to MCP and MCC/eisosomes, three non-overlapping plasma membrane domains have been identified in *S. cerevisiae*: membrane compartments containing the Target of Rapamycin kinase Complex 2 (TORC2; MCT) (Berchtold, 2009), the sterol transporters Ltc3/4 (MCL) (Murley et al., 2017), and the cell wall stress sensor Wsc1 (MCW) (Kock et al., 2016). These domains are characterized by their morphology and dynamics; the MCP shows a network-like distribution, while others show punctate distributions. Moreover, MCC/eisosomes, MCP, and MCL are static (Malínská et al., 2003; Murley et al., 2017), while the others are dynamic (Berchtold et al., 2012; Kock et al., 2016). Our observations indicate that the Aus1p-associated domain has a network-like distribution and is dynamic (**Figures 4C**, **7C**). Therefore, we propose that the Aus1p-associated domain constitutes a novel lipid domain.

It is not clear what mechanism is used to form and maintain the heterogeneous distribution of membrane proteins. Notably, *ERG25* knockdown in *C. glabrata* influences the localization of Aus1p, but not that of Pma1p or Hxt1p (**Figures 4A**, **5D**). These results support that ergosterol does not affect the localization of all membrane proteins. Additionally, *ERG26* knockdown also does not affect the localization of Hxt1p (**Supplementary Figure S3B**).

The Aus1p-related domain was shown to be preferentially concentrated in smaller daughter cells (**Figure 4D**). As reported about Pma1p in *S. cerevisiae*, the asymmetric localization of proteins in mother versus daughter cells is involved in promoting mother cell aging by affecting cellular homeostasis (Henderson et al., 2014; Yang et al., 2015), and sphingolipids contribute to maintain this asymmetric localization (Singh et al., 2017). On the other hand, ergosterol has been reported to be enriched in actively growing areas of the plasma membrane in various fungi, including *S. cerevisiae*, *C. albicans*, *Aspergillus nidulans*, and *Cryptococcus neoformans* (Bagnat and Simons, 2002; Martin and Konopka, 2004; Nichols et al., 2004; Pearson et al., 2004). Furthermore, many proteins identified to be enriched in daughter cells are needed for the emergence, construction, and division of the bud in *S. cerevisiae* (Yang et al., 2015). The Aus1p-associated domain is richer in ergosterol than the MCP in *C. glabrata* (**Figures 4E,F**). Therefore, the distribution of Aus1p in the cells appear to be correlated to the distribution of ergosterol. Although further studies are needed to clarify the mechanism by which Aus1p is distributed preferentially in daughter cells, we suggest that this Aus1p distribution bias to growing cells may allow cholesterol taken up from the host to be efficiently used for cell membrane synthesis in *C. glabrata*.

Recent studies also suggest that MCC/eisosomes act as reservoir domains for nutrient transporters, protecting them from endocytosis in response to nutrient starvation. The distribution of nutrient transporters to MCC/eisosomes has been suggested to be dependent on their conformational changes occurring upon substrate binding (Bianchi et al., 2018; Busto et al., 2018; Gournas et al., 2018; Moharir et al., 2018). For example, in *S. cerevisiae*, methionine permease Mup1p has been shown to be relocated from the MCC/eisosomes to a unique network-like domain at the plasma membrane in the presence of methionine (Busto et al., 2018). In recent years, MCC/eisosomes have been clarified to interact with MCT domains in the control of sphingolipid biosynthesis under conditions of membrane stress (Bartlett et al., 2015). Some MCT-associated proteins are spatially overlapped with MCC/eisosomes, and accumulate in a few large clusters reminiscent of eisosome remnants in Δ*pil1* cells (Bartlett et al., 2015). In our experiments with *C. glabrata*, some Aus1p was occasionally co-localized to MCC/eisosomes (**Figure 7E**) and accumulated in eisosome remnants-like structures in Δ*pil1* cells (arrowheads in **Figure 7A**). Therefore, Aus1p-associated domains may functionally be associated with MCC/eisosomes in *C. glabrata*. In *S. cerevisiae*, the transcription factors Upc2p and Sut1p, which regulate the expression of *AUS1* and of ergosterol biosynthesis genes in response to intracellular ergosterol abundance, regulate the expression of the genes encoding MCC/eisosome organizers, *NPC102* and *FHN2* (Wilcox et al., 2002; Foster et al., 2013), suggesting the involvement of the MCC/eisosomes in ergosterol homeostasis. We have observed that *C. glabrata* Aus1p localizes to novel network-like domains in the presence of serum. Although the specific role played by MCC/eisosomes to Aus1p localization requires further scrutiny, here, it is suggested that this role extends to sterol homeostasis mediated by the localization of Aus1p.

Clinical isolates of azole-resistant *C. glabrata* grow well in medium containing host serum even though they have lost the ability to synthesize endogenous ergosterol (Hanauer, 1992; Bard et al., 2005; Khan et al., 2014). Because such sterol-requiring strains

are not able to grow in the medium commonly used for diagnostic examination (Hanauer, 1992; Khan et al., 2014), consequently, the sterol-requiring strains are likely to be overlooked in the culture examinations of patients with candidemia. Therefore, the real incidence of *C. glabrata* infection must be higher than what can be deduced from the published detection rate. The key players underlying cholesterol uptake, once identified and characterized, are thus likely to constitute promising new drug targets, especially for the drug resistant strains against to ergosterol associates. Similarity analyses suggested that the amino acid sequence of Erg25p is more highly conserved than Erg11p and Erg26p (for example, in *Aspergillus fumigatus*, *Coccidioides immitis* and *Cryptococcus neoformans*) and is less similar to its human orthologue (CNBC4830) (**Supplementary Figure S8**; **Supplementary Table S2**). Additionally, *ERG25* is the most highly conserved of the *ERG* genes examined among the fungi, and the least closely related to its human orthologue. Based upon these results, Erg25p has potential as a target for the development of new allosteric antifungal agents.

DATA AVAILABILITY STATEMENT

The original contributions presented in the study are included in the article/**Supplementary Material**, further inquiries can be directed to the corresponding author.

ETHICS STATEMENT

The animal study was reviewed and approved by The Animal Care and Use Committee of Chiba University, Japan, which follows the NIH "Guide for the Care and Use of Laboratory Animals."

AUTHOR CONTRIBUTIONS

HC came up with a research idea, and HC and MO made experimental plans. KS, HC, AT-N and MO constructed mutants. TA performed qPCR. KT and SK performed sterol analysis. KS and AT-N carried out animal infections. MY performed electron microscopic analysis with MO. AT-N and TA performed a homology analysis. All other experiments were performed by MO. AT-N, MN, KT, YM, HN and SK provided informative discussions. MO and HC wrote the manuscript, and AT-N, CS, AB and MT supported to the editing.

FUNDING

This work was supported, in whole or in part, by MEXT/JSPS KAKENHI grant numbers 18H02653 to HC, 20K07475 and 18J40149 to MO. The work was also supported by AMED grant number JP18fk0108045 to YM.

ACKNOWLEDGMENTS

We thank Mari Ohiwa, Yuko Aida and Keiko Nakano from our laboratory for technical assistance.

SUPPLEMENTARY MATERIAL

The Supplementary Material for this article can be found online at: https://www.frontiersin.org/articles/10.3389/fcell.2022.820675/full#supplementary-material

REFERENCES

Bagnat, M., Keränen, S., Shevchenko, A., Shevchenko, A., and Simons, K. (2000). Lipid Rafts Function in Biosynthetic Delivery of Proteins to the Cell Surface in Yeast. *Proc. Natl. Acad. Sci.* 97, 3254–3259. doi:10.1073/pnas.97.7.3254

Bagnat, M., and Simons, K. (2002). Cell Surface Polarization during Yeast Mating. *Proc. Natl. Acad. Sci. U.S.A.* 99, 14183–14188. doi:10.1073/pnas.172517799

Bard, M., Sturm, A. M., Pierson, C. A., Brown, S., Rogers, K. M., Nabinger, S., et al. (2005). Sterol Uptake in Candida Glabrata: Rescue of Sterol Auxotrophic Strains. *Diagn. Microbiol. Infect. Dis.* 52, 285–293. doi:10.1016/j.diagmicrobio.2005.03.001

Bartlett, K., Gadila, S. K. G., Tenay, B., McDermott, H., Alcox, B., and Kim, K. (2015). TORC2 and Eisosomes Are Spatially Interdependent, Requiring Optimal Level of Phosphatidylinositol 4, 5-bisphosphate for Their Integrity. *J. Biosci.* 40, 299–311. doi:10.1007/s12038-015-9526-4

Berchtold, D., Piccolis, M., Chiaruttini, N., Riezman, I., Riezman, H., Roux, A., et al. (2012). Plasma Membrane Stress Induces Relocalization of Slm Proteins and Activation of TORC2 to Promote Sphingolipid Synthesis. *Nat. Cel Biol.* 14, 542–547. doi:10.1038/ncb2480

Berchtold, D., and Walther, T. C. (2009). TORC2 Plasma Membrane Localization Is Essential for Cell Viability and Restricted to a Distinct Domain. *MBoC* 20, 1565–1575. doi:10.1091/mbc.E0810.1091/mbc.e08-10-1001

Bianchi, F., Syga, L., Moiset, G., Spakman, D., Schavemaker, P. E., Punter, C. M., et al. (2018). Steric Exclusion and Protein Conformation Determine the Localization of Plasma Membrane Transporters. *Nat. Commun.* 9. doi:10.1038/s41467-018-02864-2

Busto, J. V., Elting, A., Haase, D., Spira, F., Kuhlman, J., Schäfer-Herte, M., et al. (2018). Lateral Plasma Membrane Compartmentalization Links Protein Function and Turnover. *EMBO J.* 37. doi:10.15252/embj.201899473

Cannon, R. D., and Holmes, A. R. (2015). Learning the ABC of Oral Fungal Drug Resistance. *Mol. Oral Microbiol.* 30, 425–437. doi:10.1111/omi.12109

Conibear, E., and Stevens, T. H. (2002). Studying Yeast Vacuoles. *Methods Enzymol.* 351. doi:10.1016/S0076-6879(02)51861-9

Coppens, I., and Courtoy, P. J. (2000). The Adaptative Mechanisms of Trypanosoma Brucei for Sterol Homeostasis in its Different Life-Cycle Environments. *Annu. Rev. Microbiol.* 54, 129–156. doi:10.1146/annurev.micro.54.1.129

Costa, C., Dias, P. J., Sã¡-Correia, I., and Teixeira, M. C. (2014). MFS Multidrug Transporters in Pathogenic Fungi: Do They Have Real Clinical Impact? *Front. Physiol.* 5. doi:10.3389/fphys.2014.00197

Douglas, L. M., Wang, H. X., Keppler-Ross, S., Dean, N., and Konopka, J. B. (2012). Sur7 Promotes Plasma Membrane Organization and Is Needed for Resistance to Stressful Conditions and to the Invasive Growth and Virulence of Candida Albicans. *MBio* 3, 1–12. doi:10.1128/mBio.00254-11

Douglas, L. M., Wang, H. X., and Konopka, J. B. (2013). The MARVEL Domain Protein Nce102 Regulates Actin Organization and Invasive Growth of Candida Albicans. *MBio* 4. doi:10.1128/mBio.00723-13

Eisenkolb, M., Zenzmaier, C., Leitner, E., and Schneiter, R. (2002). A Specific Structural Requirement for Ergosterol in Long-Chain Fatty Acid Synthesis Mutants Important for Maintaining Raft Domains in Yeast. *MBoC* 13, 4414–4428. doi:10.1091/mbc.E02-02-0116

Foster, H. A., Cui, M., Naveenathayalan, A., Unden, H., Schwanbeck, R., and Höfken, T. (2013). The Zinc Cluster Protein Sut1 Contributes to Filamentation in *Saccharomyces cerevisiae*. *Eukaryot. Cel* 12, 244–253. doi:10.1128/EC.00214-12

Giaever, G., Chu, A. M., Ni, L., Connelly, C., Riles, L., Véronneau, S., et al. (2002). Functional Profiling of the *Saccharomyces cerevisiae* Genome. *Nature* 418. doi:10.1038/nature00935

Gournas, C., Gkionis, S., Carquin, M., Twyffels, L., Tyteca, D., and André, B. (2018). Conformation-dependent Partitioning of Yeast Nutrient Transporters into Starvation-Protective Membrane Domains. *Proc. Natl. Acad. Sci. U.S.A.* 115. doi:10.1073/pnas.1719462115

Grossmann, G., Malinsky, J., Stahlschmidt, W., Loibl, M., Weig-Meckl, I., Frommer, W. B., et al. (2008). Plasma Membrane Microdomains Regulate Turnover of Transport Proteins in Yeast. *J. Cel Biol.* 183, 1075–1088. doi:10.1083/jcb.200806035

Grossmann, G., Opekarová, M., Malinsky, J., Weig-Meckl, I., and Tanner, W. (2007). Membrane Potential Governs Lateral Segregation of Plasma Membrane Proteins and Lipids in Yeast. *Embo J.* 26, 1–8. doi:10.1038/sj.emboj.7601466

Gulati, S., Balderes, D., Kim, C., Guo, Z. A., Wilcox, L., Area-Gomez, E., et al. (2015). ATP-binding Cassette Transporters and Sterol O -acyltransferases Interact at Membrane Microdomains to Modulate Sterol Uptake and Esterification. *FASEB j.* 29, 4682–4694. doi:10.1096/fj.14-264796

Hanauer, S. (1992). Primary Sclerosing Cholangitis and Ulcerative Colitis: Potential Cofactors in the Dysplasia Sequence. *Gastroenterology* 102, 2161–2162. doi:10.1016/0016-5085(92)90349-4

Henderson, K. A., Hughes, A. L., and Gottschling, D. E. (2014). Mother-daughter Asymmetry of pH Underlies Aging and Rejuvenation in Yeast. *Elife* 3. doi:10.7554/eLife.03504

Henry, K. W., Nickels, J. T., and Edlind, T. D. (2000). Upregulation of ERG Genes in Candida Species by Azoles and Other Sterol Biosynthesis Inhibitors. *Antimicrob. Agents Chemother.* 44, 2693–2700. doi:10.1128/AAC.44.10.2693-2700.2000

Khan, Z., Ahmad, S., Joseph, L., and Al-Obaid, K. (2014). Isolation of Cholesterol-dependent, Multidrug-Resistant Candida Glabrata Strains from Blood Cultures of a Candidemia Patient in Kuwait. *BMC Infect. Dis.* 14. doi:10.1186/1471-2334-14-188

Klose, C., Ejsing, C. S., García-Sáez, A. J., Kaiser, H.-J., Sampaio, J. L., Surma, M. A., et al. (2010). Yeast Lipids Can Phase-Separate into Micrometer-Scale Membrane Domains. *J. Biol. Chem.* 285, 30224–30232. doi:10.1074/jbc.M110.123554

Kock, C., Arlt, H., Ungermann, C., and Heinisch, J. J. (2016). Yeast Cell wall Integrity Sensors Form Specific Plasma Membrane Microdomains Important for Signalling. *Cell Microbiol.* 18, 1251–1267. doi:10.1111/cmi.12635

Kullberg, B. J., and Arendrup, M. C. (2015). Invasive Candidiasis. *N. Engl. J. Med.* 373, 1445–1456. doi:10.1056/NEJMra1315399

Lelandais, G., Tanty, V., Geneix, C., Etchebest, C., Jacq, C., and Devaux, F. (2008). Genome Adaptation to Chemical Stress: Clues from Comparative Transcriptomics in *Saccharomyces cerevisiae* and Candida Glabrata. *Genome Biol.* 9, R164. doi:10.1186/gb-2008-9-11-r164

Li, L., Naseem, S., Sharma, S., and Konopka, J. B. (2015). Flavodoxin-Like Proteins Protect Candida Albicans from Oxidative Stress and Promote Virulence. *Plos Pathog.* 11, e1005147–24. doi:10.1371/journal.ppat.1005147

Lichtenberg, D., Goñi, F. M., and Heerklotz, H. (2005). Detergent-Resistant Membranes Should not be Identified With Membrane Rafts. *Trends Biochem. Sci.* 30. doi:10.1016/j.tibs.2005.06.004

Lingwood, D., and Simons, K. (2010). Lipid Rafts as a Membrane-Organizing Principle. *Science* 80, 327. doi:10.1126/science.1174621

Lorenz, R. T., and Parks, L. W. (1991). Involvement of Heme Components in Sterol Metabolism of *Saccharomyces cerevisiae*. *Lipids* 26, 598–603. doi:10.1007/bf02536423

Lorenz, R. T., Rodriguez, R. J., Lewis, T. A., and Parks, L. W. (1986). Characteristics of Sterol Uptake in *Saccharomyces cerevisiae*. *J. Bacteriol.* 167, 981–985. doi:10.1128/jb.167.3.981-985.1986

Malínská, K., Malínský, J., Opekarová, M., and Tanner, W. (2003). Visualization of Protein Compartmentation within the Plasma Membrane of Living Yeast Cells. *MBoC* 14, 4427–4436. doi:10.1091/mbc.e03-04-0221

Marek, M., Silvestro, D., Fredslund, M. D., Andersen, T. G., and Pomorski, T. G. (2014). Serum Albumin Promotes ATP-Binding Cassette Transporter-dependent Sterol Uptake in Yeast. *FEMS Yeast Res.* 14, 1223–1233. doi:10.1111/1567-1364.12219

Martin, S. W., and Konopka, J. B. (2004). Lipid Raft Polarization Contributes to Hyphal Growth in Candida Albicans. *Eukaryot. Cel* 3, 675–684. doi:10.1128/EC.3.3.675-684.2004

MeghaBakht, O., and London, E. (2006). Cholesterol Precursors Stabilize Ordinary and Ceramide-Rich Ordered Lipid Domains (Lipid Rafts) to Different Degrees: Implications for the Bloch Hypothesis and Sterol Biosynthesis Disorders. *J. Biol. Chem.* doi:10.1074/jbc.M600395200

Moharir, A., Gay, L., Appadurai, D., Keener, J., and Babst, M. (2018). Eisosomes Are Metabolically Regulated Storage Compartments for APC-type Nutrient Transporters. *MBoC* 29, 2113–2127. doi:10.1091/mbc.E17-11-0691

Moreira, K. E., Schuck, S., Schrul, B., Fröhlich, F., Moseley, J. B., Walther, T. C., et al. (2012). Seg1 Controls Eisosome Assembly and Shape. *J. Cel Biol.* 198, 405–420. doi:10.1083/jcb.201202097

Murley, A., Yamada, J., Niles, B. J., Toulmay, A., Prinz, W. A., Powers, T., et al. (2017). Sterol Transporters at Membrane Contact Sites Regulate TORC1 and TORC2 Signaling. *J. Cel Biol.* 216, 2679–2689. doi:10.1083/jcb.201610032

Nagi, M., Tanabe, K., Ueno, K., Nakayama, H., Aoyama, T., Chibana, H., et al. (2013). The Candida Glabratasterol Scavenging Mechanism, Mediated by the ATP-Binding Cassette Transporter Aus1p, Is Regulated by Iron Limitation. *Mol. Microbiol.* 88, 371–381. doi:10.1111/mmi.12189

Nakayama, H., Izuta, M., Nagahashi, S., Sihta, E. Y., Sato, Y., Yamazaki, T., et al. (1998). A Controllable Gene-Expression System for the Pathogenic Fungus Candida Glabrata. *Microbiology* 144, 2407–2415. doi:10.1099/00221287-144-9-2407

Nakayama, H., Mio, T., Nagahashi, S., Kokado, M., Arisawa, M., and Aoki, Y. (2000). Tetracycline-Regulatable System to Tightly Control Gene Expression in the Pathogenic Fungus Candida Albicans. *Infect. Immun.* 68, 6712–6719. doi:10.1128/IAI.68.12.6712-6719.2000

Nakayama, H., Tanabe, K., Bard, M., Hodgson, W., Wu, S., Takemori, D., et al. (2007). The Candida Glabrata Putative Sterol Transporter Gene CgAUS1 Protects Cells against Azoles in the Presence of Serum. *J. Antimicrob. Chemother.* 60, 1264–1272. doi:10.1093/jac/dkm321

Nichols, C. B., Fraser, J. A., and Heitman, J. (2004). PAK Kinases Ste20 and Pak1 Govern Cell Polarity at Different Stages of Mating in Cryptococcus Neoformans. *MBoC* 15, 4476–4489. doi:10.1091/mbc.E04-05-0370

Niimi, K., Woods, M. A., Maki, K., Nakayama, H., Hatakenaka, K., Chibana, H., et al. (2012). Reconstitution of High-Level Micafungin Resistance Detected in a Clinical Isolate of Candida Glabrata Identifies Functional Homozygosity in Glucan Synthase Gene Expression. *J. Antimicrob. Chemother.* 67, 1666–1676. doi:10.1093/jac/dks112

Okamoto, M., Kurokawa, K., Matsuura-Tokita, K., Saito, C., Hirata, R., and Nakano, A. (2012). High-curvature Domains of the ER Are Important for the Organization of ER Exit Sites in *Saccharomyces cerevisiae*. *J. Cel Sci.* 125, 3412–3420. doi:10.1242/jcs.100065

Okamoto, M., Yoko-o, T., Umemura, M., Nakayama, K.-i., and Jigami, Y. (2006). Glycosylphosphatidylinositol-anchored Proteins Are Required for the Transport of Detergent-Resistant Microdomain-Associated Membrane Proteins Tat2p and Fur4p. *J. Biol. Chem.* 281, 4013–4023. doi:10.1074/jbc.M504684200

Pearson, C. L., Xu, K., Sharpless, K. E., and Harris, S. D. (2004). MesA, a Novel Fungal Protein Required for the Stabilization of Polarity Axes in Aspergillus Nidulans. *MBoC* 15, 3658–3672. doi:10.1091/mbc.E03-11-0803

Sanglard, D., Coste, A., and Ferrari, S. (2009). Antifungal Drug Resistance Mechanisms in Fungal Pathogens from the Perspective of Transcriptional Gene Regulation. *FEMS Yeast Res.* 9, 1029–1050. doi:10.1111/j.1567-1364.2009.00578.x

Schindelin, J., Arganda-Carreras, I., Frise, E., Kaynig, V., Longair, M., Pietzsch, T., et al. (2012). Fiji: An Open-Source Platform for Biological-Image Analysis. *Nat. Methods* 9, 676–682. doi:10.1038/nmeth.2019

Shianna, K. V., Dotson, W. D., Tove, S., and Parks, L. W. (2001). Identification of a UPC2 Homolog in *Saccharomyces cerevisiae* and its Involvement in Aerobic Sterol Uptake. *J. Bacteriol.* 183, 830–834. doi:10.1128/JB.183.3.830-834.2001

Shogomori, H., and Brown, D. A. (2003). Use of Detergents to Study Membrane Rafts: The Good, the Bad, and the Ugly. *Biol. Chem.* 384. doi:10.1515/BC.2003.139

Singh, P., Ramachandran, S. K., Zhu, J., Kim, B. C., Biswas, D., Ha, T., et al. (2017). Sphingolipids Facilitate Age Asymmetry of Membrane Proteins in Dividing Yeast Cells. *MBoC* 28, 2712–2722. doi:10.1091/mbc.E17-05-0335

Spira, F., Mueller, N. S., Beck, G., von Olshausen, P., Beig, J., Wedlich-Söldner, R., et al. (2012). Patchwork Organization of the Yeast Plasma Membrane into

Numerous Coexisting Domains. *Nat. Cel Biol.* 14, 640–648. doi:10.1038/ncb2487

Stra´dalova´, V., Stahlschmidt, W., Grossmann, G., Blazõi´kova´, M., Rachel, R., Tanner, W., et al. (2009). Furrow-like Invaginations of the Yeast Plasma Membrane Correspond to Membrane Compartment of Can1. *J. Cel Sci.* 122, 2887–2894. doi:10.1242/jcs.051227

Swain, E., Baudry, K., Stukey, J., McDonough, V., Germann, M., and Nickels, J. T. (2002). Sterol-Dependent Regulation of Sphingolipid Metabolism in *Saccharomyces cerevisiae*. *J. Biol. Chem.* 277. doi:10.1074/jbc.M204115200

Ueno, K., Matsumoto, Y., Uno, J., Sasamoto, K., Sekimizu, K., Kinjo, Y., et al. (2011). Intestinal Resident Yeast Candida Glabrata Requires Cyb2p-Mediated Lactate Assimilation to Adapt in Mouse Intestine. *PLoS One* 6, e24759. doi:10.1371/journal.pone.0024759

Ueno, K., Tamura, Y., and Chibana, H. (2010). Target Validation and Ligand Development for a Pathogenic Fungal Profilin, Using a Knock-Down Strain of Pathogenic Yeast Candida Glabrata and Structure-Based Ligand Design. *Yeast* 27, 369–378. doi:10.1002/yea.1759

Ueno, K., Uno, J., Nakayama, H., Sasamoto, K., Mikami, Y., and Chibana, H. (2007). Development of a Highly Efficient Gene Targeting System Induced by Transient Repression of YKU80 Expression in Candida Glabrata. *Eukaryot. Cel* 6, 1239–1247. doi:10.1128/EC.00414-06

Umebayashi, K., and Nakano, A. (2003). Ergosterol Is Required for Targeting of Tryptophan Permease to the Yeast Plasma Membrane. *J. Cel Biol.* 161, 1117–1131. doi:10.1083/jcb.200303088

van 't Klooster, J. S., Cheng, T.-Y., Sikkema, H. R., Jeucken, A., Moody, B., and Poolman, B. (2020). Periprotein Lipidomes of *Saccharomyces cerevisiae* Provide a Flexible Environment for Conformational Changes of Membrane Proteins. *Elife* 9. doi:10.7554/elife.57003

Vik, Å., and Rine, J. (2001). Upc2p and Ecm22p, Dual Regulators of Sterol Biosynthesis in *Saccharomyces cerevisiae*. *Mol. Cel. Biol.* 21, 6395–6405. doi:10.1128/mcb.21.19.6395-6405.2001

Vu, B. G., Thomas, G. H., and Moye-Rowley, W. S. (2019). Evidence that Ergosterol Biosynthesis Modulates Activity of the Pdr1 Transcription Factor in Candida Glabrata. *MBio* 10. doi:10.1128/mBio.00934-19

Walther, T. C., Aguilar, P. S., Fröhlich, F., Chu, F., Moreira, K., Burlingame, A. L., et al. (2007). Pkh-kinases Control Eisosome Assembly and Organization. *EMBO J.* 26, 4946–4955. doi:10.1038/sj.emboj.7601933

Walther, T. C., Brickner, J. H., Aguilar, P. S., Bernales, S., Pantoja, C., and Walter, P. (2006). Eisosomes Mark Static Sites of Endocytosis. *Nature* 439, 998–1003. doi:10.1038/Nature04472

Wang, H. X., Douglas, L. M., Veselá, P., Rachel, R., Malinsky, J., and Konopka, J. B. (2016). Eisosomes Promote the Ability of Sur7 to Regulate Plasma Membrane Organization inCandida Albicans. *MBoC* 27, 1663–1675. doi:10.1091/mbc.E16-01-0065

Wilcox, L. J., Balderes, D. A., Wharton, B., Tinkelenberg, A. H., Rao, G., and Sturley, S. L. (2002). Transcriptional Profiling Identifies Two Members of the ATP-Binding Cassette Transporter Superfamily Required for Sterol Uptake in Yeast. *J. Biol. Chem.* 277, 32466–32472. doi:10.1074/jbc.M204707200

Xiong, Q., Hassan, S. A., Wilson, W. K., Han, X. Y., May, G. S., Tarrand, J. J., et al. (2005). Cholesterol Import by Aspergillus fumigatus and its Influence on Antifungal Potency of Sterol Biosynthesis Inhibitors. *Antimicrob. Agents Chemother.* 49, 518–524. doi:10.1128/AAC.49.2.518-524.2005

Xu, X. L., Bittman, R., Duportail, G., Heissler, D., Vilcheze, C., and London, E. (2001). Effect of the Structure of Natural Sterols and Sphingolipids on the Formation of Ordered Sphingolipid/Sterol Domains (Rafts). *J. Biol. Chem.* 276, 33540–33546. doi:10.1074/jbc.M104776200

Yang, J., McCormick, M. A., Zheng, J., Xie, Z., Tsuchiya, M., Tsuchiyama, S., et al. (2015). Systematic Analysis of Asymmetric Partitioning of Yeast Proteome between Mother and Daughter Cells Reveals "Aging Factors" and Mechanism of Lifespan Asymmetry. *Proc. Natl. Acad. Sci. U.S.A.* 112, 11977–11982. doi:10.1073/pnas.1506054112

Zhang, X., Lester, R. L., and Dickson, R. C. (2004). Pil1p and Lsp1p Negatively Regulate the 3-phosphoinositide-dependent Protein Kinase-like Kinase Pkh1p and Downstream Signaling Pathways Pkc1p and Ypk1p. *J. Biol. Chem.* 279, 22030–22038. doi:10.1074/jbc.M400299200

Zordan, R. E., Ren, Y., Pan, S.-J., Rotondo, G., Peñas, A. D. L., Iluore, J., et al. (2013). Expression Plasmids for Use in Candida Glabrata. *G3 (Bethesda)* 3, 1675–1686. doi:10.1534/g3.113.006908

Conflict of Interest: The authors declare that the research was conducted in the absence of any commercial or financial relationships that could be construed as a potential conflict of interest.

Publisher's Note: All claims expressed in this article are solely those of the authors and do not necessarily represent those of their affiliated organizations, or those of the publisher, the editors and the reviewers. Any product that may be evaluated in this article, or claim that may be made by its manufacturer, is not guaranteed or endorsed by the publisher.

frontiers | Frontiers in Cell and Developmental Biology

TYPE Original Research
PUBLISHED 20 October 2022
DOI 10.3389/fcell.2022.911664

OPEN ACCESS

EDITED BY
Maria Isabel Colombo,
Universidad Nacional de Cuyo,
Argentina

REVIEWED BY
Ruben Claudio Aguilar,
Purdue University, United States
Yang Sun,
Stanford University, United States

*CORRESPONDENCE
María-Paz Marzolo,
mmarzolo@bio.puc.cl

†PRESENT ADDRESS
Centre for Cancer Cell Reprogramming and Institute for Cancer Research, Department of Molecular Cell Biology, Oslo University Hospital, Oslo, Norway

SPECIALTY SECTION
This article was submitted to Membrane Traffic, a section of the journal Frontiers in Cell and Developmental Biology

RECEIVED 03 April 2022
ACCEPTED 10 October 2022
PUBLISHED 20 October 2022

CITATION
Sandoval L, Fuentealba LM and Marzolo M-P (2022), Participation of OCRL1, and APPL1, in the expression, proteolysis, phosphorylation and endosomal trafficking of megalin: Implications for Lowe Syndrome. *Front. Cell Dev. Biol.* 10:911664. doi: 10.3389/fcell.2022.911664

Participation of OCRL1, and APPL1, in the expression, proteolysis, phosphorylation and endosomal trafficking of megalin: Implications for Lowe Syndrome

Lisette Sandoval[1,2†], Luz M. Fuentealba[1] and María-Paz Marzolo[1*]

[1]Laboratorio de Tráfico Intracelular y Señalización, Departamento de Biología Celular y Molecular, Facultad de Ciencias Biológicas, Pontificia Universidad Católica de Chile, Santiago, Chile, [2]Instituto de Ciencias Biomédicas, Facultad de Ciencias de la Salud, Universidad Autónoma de Chile, Santiago, Chile

Megalin/LRP2 is the primary multiligand receptor for the re-absorption of low molecular weight proteins in the proximal renal tubule. Its function is significantly dependent on its endosomal trafficking. Megalin recycling from endosomal compartments is altered in an X-linked disease called Lowe Syndrome (LS), caused by mutations in the gene encoding for the phosphatidylinositol 5-phosphatase OCRL1. LS patients show increased low-molecular-weight proteins with reduced levels of megalin ectodomain in the urine and accumulation of the receptor in endosomal compartments of the proximal tubule cells. To gain insight into the deregulation of megalin in the LS condition, we silenced OCRL1 in different cell lines to evaluate megalin expression finding that it is post-transcriptionally regulated. As an indication of megalin proteolysis, we detect the ectodomain of the receptor in the culture media. Remarkably, in OCRL1 silenced cells, megalin ectodomain secretion appeared significantly reduced, according to the observation in the urine of LS patients. Besides, the silencing of APPL1, a Rab5 effector associated with OCRL1 in endocytic vesicles, also reduced the presence of megalin's ectodomain in the culture media. In both silencing conditions, megalin cell surface levels were significantly decreased. Considering that GSK3ß-mediated megalin phosphorylation reduces receptor recycling, we determined that the endosomal distribution of megalin depends on its phosphorylation status and OCRL1 function. As a physiologic regulator of GSK3ß, we focused on insulin signaling that reduces kinase activity. Accordingly, megalin phosphorylation was significantly reduced by insulin in wild-type cells. Moreover, even though in cells with low activity of OCRL1 the insulin response was reduced, the phosphorylation of megalin was significantly decreased and the receptor at the cell surface increased, suggesting a protective role of insulin in a LS cellular model.

KEYWORDS
megalin, lowe syndrome, ocrl1, APPL1, renal disease, proteolysis, GSK3, insulin

Introduction

Megalin is an endocytic receptor belonging to the low-density lipoprotein receptors family (Saito et al., 1994; Marzolo and Farfán, 2011). This receptor is found in the apical surface of several epithelia and is highly expressed in the kidney, specifically in the proximal tubular epithelium (PT) (Saito et al., 1994; Farquhar et al., 1995). The function of megalin in epithelial kidney cells is related to the recapture of low molecular weight proteins (LMW) from the glomerular filtrate (Leheste et al., 1999). Megalin ligands, including calcium, albumin, insulin, leptin, parathyroid hormone (PTH), angiotensin II, retinol-binding protein (RBP), and vitamin D binding protein (DBP), are involved in pathological kidney conditions (Marzolo and Farfán, 2011). Renal defects of megalin knockout (KO) mice (Leheste et al., 2003, 1999) include phosphaturia, hypercalciuria, and proteinuria, due to loss of megalin ligands such as RBP, DBP and albumin (Bockenhauer et al., 2008; Bothwell et al., 2011). These defects are explained in terms of inefficient endocytosis of megalin ligands and, importantly, to additional megalin trafficking functions related to the regulation of inorganic sodium phosphate cotransporter (NaPi-IIa) (Bachmann et al., 2004) and sodium-proton exchanger 3 (NHE3) (Alexander and Grinstein, 2009). Also, the lack of megalin is associated to significant ultrastructural changes in the endosomal compartments of PT epithelial cells, including the absence of dense apical tubules, which correspond to the apical recycling endosomes, and other endocytic structures, such as clathrin-coated pits and vesicles (Leheste et al., 1999). On the other hand, under physiological conditions, it is possible to find megalin fragments in the urine (Pisitkun et al., 2004; Thrailkill et al., 2009; Suruda et al., 2017). The predominant species is megalin ectodomain (A-megalin), probably released by shedding, a process that would take place at the cell surface through a mechanism involving the activity of protein kinase C (PKC) and matrix metalloproteases (Zou et al., 2004). Besides, it is also possible to detect, but at low levels, the full-length receptor (C-megalin) present in exosomes (Suruda et al., 2017). C-megalin levels are increased in diabetes patients (Kurita et al., 2022) and negatively correlated with serum 1,25(OH)2D and 24,25(OH)2D (Toi et al., 2019). However, there are still open questions regarding the mechanisms explaining the presence and the change in the levels of megalin in the urine, especially in different pathologies affecting the kidney.

The cytoplasmic domain of megalin has an essential role in determining its apical distribution and recycling (Marzolo et al., 2003; Yuseff et al., 2007; Farfán et al., 2013; Perez Bay et al., 2016). In polarized epithelial cells, internalized megalin follows an endosomal itinerary including the apical sorting endosome (ASE), the common recycling endosome (CRE) (where it meets with basolateral internalized cargoes such as TfR), and the Rab11 positive apical recycling endosome (ARE), from which it recycles to the cell surface (Mattila et al., 2014; Perez Bay et al., 2016; Eshbach and Weisz, 2017). Also, the already mentioned ectodomain shedding can modify megalin surface levels. Besides, it is known that glycogen synthase kinase-3 ß (GSK3ß) binds directly to the megalin cytoplasmic domain (Marzolo and Farfán, 2011) and phosphorylates the PPPSP motif within the intracellular domain of the receptor, decreasing the efficiency of megalin recycling and therefore reducing its cell surface expression (Yuseff et al., 2007).

Lowe Syndrome (LS) is a human pathological and lethal condition caused by mutations in the *OCRL* gene, encoding a phosphatidylinositol 5-phosphatase OCRL1, affecting the brain, eye, and kidney (Lowe et al., 1952; Attree et al., 1992). The disease is characterized by congenital cataracts, central hypotonia, and renal proximal tubular dysfunction (Preston et al., 2020). There are different mutations in *OCRL* causing LS, which decrease the function or expression of the enzyme (Lichter-Konecki et al., 2006; De Matteis et al., 2017). LS patients also exhibit high concentrations of proteins in their urine, including megalin ligands. Besides, the secretion of megalin itself, as A-megalin, seems to be specifically decreased, contrasting with the normal secretion of cubilin, a megalin co-receptor (Norden et al., 2002; Suruda et al., 2017). The mechanism that explains the A-megalin decrease is not known.

OCRL1 modulates the endocytic trafficking of several cargo receptors (Choudhury et al., 2005; Erdmann et al., 2007; Noakes et al., 2011; Vicinanza et al., 2011). We have described significant alterations in endocytic trafficking of various receptors, including megalin, in OCRL1 silenced cells (Vicinanza et al., 2011). This last study showed defects in early endosomal compartments characterized by the abnormal presence of phosphatidylinositol 4,5-P2, a preferential substrate of OCRL1 (Zhang et al., 1998), and by the ectopic accumulation of actin filaments (Dambournet et al., 2011; Vicinanza et al., 2011; Kühbacher et al., 2012) that impede efficient recycling of cargoes. As a consequence of these defects, cells deficient in OCRL1 exhibit a reduction in the cell surface expression of megalin. Besides, data obtained from humanized Lowe Syndrome animals (Festa et al., 2019) and zebrafish (Oltrabella et al., 2015) indicate that cell surface and total megalin are decreased in proximal tubule cells. On the other hand, APPL1 is an endocytic protein that associates with OCRL1 (Erdmann et al., 2007). In some LS OCRL1 mutants, the interaction with APPL1 is disrupted (McCrea et al., 2008; Noakes et al., 2011). The presence of megalin in APPL1 endosomes is also reduced in OCRL1 knock-down cells (Vicinanza et al., 2011).

Here we explored the expression of megalin in a "cellular Lowe condition", finding a post-transcriptional regulation of megalin levels in OCRL1 silenced cells. We also evaluated megalin proteolysis and ectodomain secretion. When OCRL1 levels were low, the secretion of the receptor ectodomain was decreased. These results indicate that OCRL1 knock-down (KD) cells show a phenotype that mimics the situation found in the urine of LS patients (Norden et al., 2002; Suruda et al., 2017). In addition, we found that silencing of APPL1 also reduced cell surface expression and secretion of the megalin ectodomain to cell culture.

The reported reduction and surface expression of megalin in LS could be partly explained by defects in endosomal recycling due to ectopic actin polymerization in the endosomes as described (Vicinanza et al., 2011) but also can be the result of changes in intracellular signaling processes that increases GSK3ß activity. Our results showed that the basal megalin phosphorylation was rather decreased in LS conditions and that the endosomal distribution of the receptor depended on its phosphorylation status as well as on the activity of OCRL1. Interestingly, we uncovered a role of insulin in megalin phosphorylation and cell surface expression, finding that the stimulation of cells with the hormone reduces megalin phosphorylation, consistent with a decreased activity of GSK3ß, and increases its surface expression. Finally, although insulin signaling was decreased in cells with reduced function of OCRL1, megalin was still less phosphorylated and more present at the plasma membrane, indicating that although less efficient, insulin could promote megalin recycling in LS conditions.

Materials and methods

Antibodies and reagents

The monoclonal anti-HA and the polyclonal anti-human cytoplasmic domain of megalin antibodies have been described before (Marzolo et al., 2003; Yuseff et al., 2007). Polyclonal antibody against human OCRL was described before (Vicinanza et al., 2011). Two rabbit anti-APPL1 human antibodies were used, one kindly provided by Dr. David Kaplan (Lin et al., 2006), and the other was from Cell signaling (D83H4; XP® Rabbit mAb #3858). Anti-tubulin monoclonal antibody (MAB3408)was purchased from Chemicon (Temecula, CA, USA). Antibodies against E-cadherin and GSK3ß (610202) were from BD Bioscience-Pharmingen (San Jose, CA, USA). The antibodies for phospho-GSK3ß (Ser-9) (D85E12), phospho-AKT S473 (D9E) 4060, AKT 9272, EEA1 (C45B10), Rab7 (D95F2) were purchased from Cell signaling. Alexa Fluor-594 goat anti-rabbit IgG, Alexa Fluor-488 goat anti-mouse IgG, and anti-HA-Alexa-488 were purchased from Molecular Probes (Europe BV, Leiden, the Netherlands). LiCl and Coomassie blue were obtained from Winkler (Santiago, Chile). Protein A-agarose and G-agarose were from Pierce (Rockford, IL, USA) [^{35}S] methionine/cysteine was obtained from ICN (Costa Mesa, CA, USA) [^{32}P] orthophosphate was purchased from the Chilean Commission of Nuclear Energy (CCHEN, Chile). All tissue culture media, serum and plastics, were from Life Technologies, Inc. (Rockville, MI, USA). Matrix metalloproteinase inhibitor (GM6001) was from Calbiochem (San Diego, CA, USA). YU142670 was obtained from Merck & Co., Inc. (Kenilworth, NJ, USA). Sulfo-NHS-LC-biotin and Immunopure Streptavidin-agarose were from Pierce (Rockford, IL, USA).

Plasmids and primers sequences

Megalin mini receptor (mMeg) was generated from a human kidney cDNA library (Marzolo et al., 2003; Farfán et al., 2013). Plasmids for phosphomimetic mMeg (mMeg S170D), non-phosphorylatable mMeg (mMeg S170A) and mMeg lacking the ectodomain (Meg0) were described previously (Yuseff et al., 2007; Marzolo and Farfán, 2011). mCherry-Rab11 was kindly provided by Dr. Alexis Gautreau (Derivery et al., 2009). Human OCRL1-EGFP was described before (Vicinanza et al., 2011). Plasmids for short hairpin RNAs were MISSION® pLKO.1-puro Non-Target shRNA Control Plasmid DNA (Sigma-Aldrich), pLKO vectors purchased from Open Biosystems (shOCRL1 5′- GCCAAGTATAAGAAA GTTCAA -3′ and shAPPL1 5′- GCATTGTTAGAACCTCTACTT-3′). The primers used in quantitative PCR reactions were as follows: megalin forward, 5′- CTGCTCTTGTAGACCTGGGTTC -' 3; megalin reverse, 5′- TCGGCACAGCTACACTCATAAC -3; glyceraldehyde-3-phosphate dehydrogenase forward, 5′- TCA AGGCTGAGAATGGGAAG -`3; glyceraldehyde-3-phosphate dehydrogenase reverse, 5′- AGCAGAAGGGGCAGAGATG -`3.

Cell lines and culture conditions

LLC-PK1 epithelial cells, derived from porcine kidney were cultured in alpha-MEM supplemented with 7.5% FBS containing 100 U/ml penicillin and 100 mg/ml streptomycin) and 2 mM glutamine (Invitrogen). These cells have been previously used in studies on proximal tubule function and megalin expression (Marzolo et al., 2003; Yuseff et al., 2007; Cabezas et al., 2019, 2011). MDCK epithelial cells are derived from dog kidneys and correspond to the distal tubule. These cells have been used previously to study megalin and LRP1 trafficking (Marzolo et al., 2003; Yuseff et al., 2007; Farfán et al., 2013) and were obtained from ATCC. HEK 293T cells were used to produce lentivirus as described (Sotelo et al., 2014). HeLa cells were maintained in DMEM with 10% FBS, 2 mM glutamine, and antibiotics. All the cells were grown at 37°C in humidified air containing 5% CO2.

Lentivirus production and cell transfection

Plasmids encoding shRNA, pCMVR8.91, and VSVg were transfected in HEK293 cells using calcium method phosphate (Chen and Okayama, 1987). The supernatant with lentivirus was collected after 48 h and used to infect cells in the presence of 8 μg/ml of polybrene. Stably silenced clones were selected with 2 μg/ml puromycin in growing media for 3 days after infection. Cells were transfected with Lipofectamine 2,000 (Invitrogen), according to the manufacturer's instructions. For the generation of stably-expressing minireceptors, mMeg or Meg0 (Marzolo et al., 2003), cells lines were transfected and selected using 0.8 mg/ml of G418 for 2 weeks and then maintained with 0.4 mg/ml of G418.

Western blot

Cells were lysed with lysis buffer (PBS containing 1% Triton X-100, 1 mM glycerophosphate, 1 mM sodium orthovanadate, 5 mM sodium fluoride, and the protease inhibitors 2 mM PMSF, 1 mM pepstatin, 2 μM antipain, 1 μM leupeptin, and 0.3 μM aprotinin). Extracts were centrifuged at 12.000 rpm for 10 min, and the pellet was discarded. Protein from lysates and the immune complexes (for immunoprecipitation samples) were boiled in Laemmli sample buffer (62.5 mM Tris-HCl, pH 6.8; 2% w/v SDS, 10% v/v glycerol, and 5% ß-mercaptoethanol) and then analyzed by SDS-PAGE or tris-tricine under reducing conditions. Gels were transferred to an Immobilon-P membrane (Millipore, Billerica, MA). The membranes were blocked in TBS containing 1% Triton X-100 and 3% BSA and subjected to incubation overnight with primary antibodies and for 2 h with secondary antibodies. Blots were developed with the ECL system from Amersham Life Science (Arlington Heights, IL, USA) and analyzed with ImageJ.

Quantitative PCR

Total RNA was isolated using RNA-Solv (Omega Bio-Tek, Norcross, GA, USA) following the manufacturer's instructions and treated with DNAse I. Then, the reverse transcription was performed with random primers and RevertAidTM MMuLV Reverse Transcriptase in the presence of RNAseOUT (Fermentas Glen Burnie, MD, USA). PCR reactions were performed using a 7,500 Real-Time PCR System (Applied Biosystems, Carlsbad, CA, USA) and Brilliant SybrGreen I (Stratagene). Results were analyzed with the 7,500 System Software.

Metabolic labeling

To measure megalin biosynthesis, the cells were incubated with 200 uCi/ml of [35S]-methionine/cysteine at 37°C for 4 h, followed by a wash with ice-cold PBS and lysing procedure. Radiolabeled mMeg was immunoprecipitated with rabbit polyclonal anti-megalin antibody (Marzolo et al., 2003) and protein A–agarose beads (Pierce). Samples were separated by SDS-PAGE and visualized by autoradiography.

Megalin half-life and intracellular proteolytic products accumulation

For mMeg half-life measurement, 5×10^6 cells/cm2 (shControl and shOCRL LLC-PK1) were plated on 6-well plates and treated with cycloheximide (100 μM) for indicated times in culture media (DMEM) without serum, up to 12 h. At the end of the incubation, cells were lysed using lysis buffer (PBS containing 1% Triton X-100, 1 mM glycerophosphate, 1 mM sodium orthovanadate, 5 mM sodium fluoride, and the protease inhibitors 2 mM PMSF, 1 mM pepstatin, 2 μM antipain, 1 μM leupeptin, and 0.3 μM aprotinin). The samples were separated by SDS-PAGE and analyzed by western blot.

Immunofluorescence staining and colocalization analysis

LLC-PK1 cells were grown in glass coverslips for 24 h, then, co-transfected with plasmids encoding the chaperone RAP and mMeg using Lipofectamin 2000. For the colocalization experiments wild-type mMeg, mMeg S/D or mMeg S/A were used. To visualize Rab11 the receptor was co-transfected with mCherry -Rab11. After 24 h of expression, cells were treated with 50 μM YU142670 or vehicle for 4 h. Cells were fixed with 4% paraformaldehyde in PBS and then permeabilized with 0.2% Triton X-100 in PBS. Next, the cells were blocked with 5% BSA in PBS and incubated successively with the primary antibodies (anti-HA and anti-EEA1 or anti-Rab7) and the corresponding secondary antibodies. Images were captured by Inverted Nikon Ti2-E and deconvolved with DeconvolutionLab (Sage et al., 2017) Manders coefficient was calculated with JaCoP (Bolte and Cordelières, 2006), a plugin for ImageJ (NIH). Briefly, images of cells with the two stains were selected and separated. Cells were analyzed with the JaCoP function of Manders' Coefficient and data was stored for analysis.

Determination of megalin ectodomain secretion

Silenced or control cells were seeded at a density of 8×10^5 and grown in DMEM plus 10% SBF for 48 h to accumulate the proteolytic fragment of mMeg in the culture media. For matrix

metalloproteinases inhibition (MMPi) treatment, cells were treated with or without 10 μM GM6001 for 48 h, replenishing every 12 h. The medium was collected, and the cells were lysed. The media were clarified by centrifugation at 10,000 *g* for 10 min and then concentrated with Centricon® 100. Proteins from the concentrated medium were immunoprecipitated with anti-HA antibody coupled with protein G–agarose beads (Pierce). Samples were separated by SDS-PAGE and analyzed by Western blot.

Flow cytometry

For measurements of total mMeg, cells expressing the mini receptor were grown on 100-mm dishes until 80% confluency. Cells were detached with PBS containing 5 mM EDTA and permeabilized with 0.75% saponin in PBS before incubation with Alexa488-conjugated anti-HA antibody. The results were displayed as mean fluorescence per cell. For measurements of surface mMeg, non-permeabilized cells were detached with PBS containing 5 mM EDTA and incubated with monoclonal Alexa488-conjugated anti-HA antibody. Cells from another set were permeabilized with 0.75% saponin in PBS and incubated with anti-HA-488 to measure the total amount of receptors. Results were plotted as surface (non-permeabilized cells) mean fluorescence *versus* total (permeabilized cells) mean fluorescence. Background fluorescence intensity was assessed without the primary antibody and subtracted from mean fluorescence. Mean fluorescence values were obtained in triplicate with a FACScalibur (BD Biosciences-Pharmingen, Sweden), and the data were analyzed with the Weasel software.

Phosphorylation assay and insulin treatment

The strategy to measure phosphorylation was described before (Li et al., 2000; Yuseff et al., 2007). Briefly, seeded cells were washed and incubated twice with phosphate-free minimal essential medium (Gibco) for 20 min, followed by the addition of 200 uCi/ml of [^{32}P]-orthophosphate at 37°C for 2 h. Then, cells were washed and lysed in a PBS buffer containing 1% Triton X-100, 1 mM glycerophosphate, 1 mM sodium orthovanadate, 5 mM sodium fluoride, and protease inhibitors. For insulin treatment, the protein was included at a final concentration of 100 nM in all steps of the phosphorylation assay. Following immunoprecipitation with anti-megalin antibody, samples were examined *via* SDS–PAGE and autoradiography. The percentage of megalin phosphorylation was calculated by densitometry using ImageJ and normalized to the levels of mMeg detected by western blot from an aliquot of cell lysate.

Cell-surface biotinylation

To determine cell surface mMeg localization, the cells were biotinylated as described (Marzolo et al., 2003). Briefly, control or OCRL1 silenced cells were serum-starved for 2 h and incubated with 100 nM insulin for 2 or 4 h. The cells were washed in ice-cold PBS and biotinylated at 4°C with 0.5 mg/ml sulfo-NHS-LC-biotin for 1 h. Then, the cells were washed with PBS and the biotin was quenched with 50 mM NH_4Cl for 10 min. Cells were lysed and biotinylated cell-surface proteins were adsorbed to streptavidin agarose beads for 2 h at 4°C in rotation. Beads were washed, boiled in Laemmli sample buffer and the proteins of interest were separated by SDS-PAGE and analyzed by western blot.

Insulin signaling

Cells were serum-starved for 4 h with or without 50 μM YU142670 (Pirruccello et al., 2014). Next, cells were incubated with 100 nM insulin (with or without 50 μM YU142670), to promote AKT and GSK3β phosphorylation due to insulin signaling. Cells were washed twice with PBS, lysed, and analyzed by western blot.

Statistical analysis

The blots were quantified with the ImageJ software, and qPCR analyses were performed using a relative quantification mathematical model, as previously described (Pfaffl, 2001). Data were expressed as the mean ± SEM (standard error of the mean) from at least three independent experiments. Comparisons of two conditions were performed using Student's t-test or Mann-Whitney. For multiple comparisons data was analyzed using ANOVA with Bonferroni and Dunnett´s correction. The statistical analyses and graphs were performed using GraphPad Prism 5.

Results

Megalin is post-transcriptionally regulated in a cellular model of Lowe Syndrome

It has been proposed that the defect in re-absorption function and secretion of megalin in LS result from receptor trafficking deregulation (Norden et al., 2002; Vicinanza et al., 2011). As was reported, the lack of OCRL1 does not affect megalin apical distribution or its internalization, but the recycling of the receptor is significantly reduced in both proximal and distal epithelial tubular cells (Vicinanza et al., 2011). To study megalin expression and trafficking, we silenced OCRL1 in the porcine

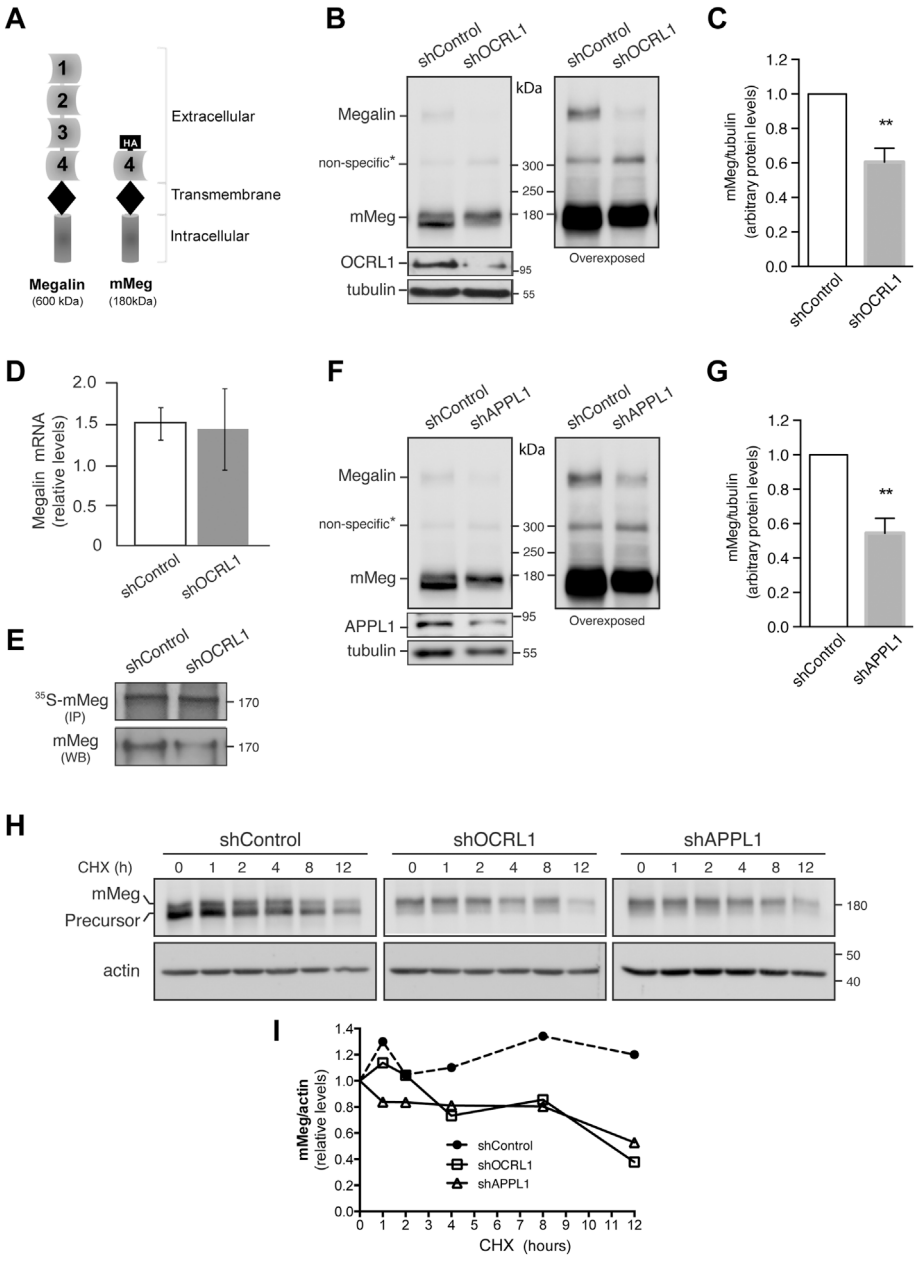

FIGURE 1
Megalin is down-regulated in OCRL1 and APPL1 KD proximal tubule cells. **(A)** Schematic representation of the full-length megalin with its four ligand-binding domains and the mini receptor with the fourth ligand-binding domain tagged with HA-epitope (mMeg). **(B–H)** LLC-PK1 cells stably expressing mMeg (mMeg-LLC-PK1) were infected with non-target shRNA (shControl), shRNA directed against OCRL1 (shOCRL1) or APPL1 (shAPPL1) lentiviruses. **(B)** Endogenous megalin and mMeg were analyzed in whole-cell lysates of control and OCRL1 silenced cells by western blot. **(C)** Quantification of mMeg protein levels corrected with tubulin levels in control and OCRL1 KD cells. Data are expressed as the means ± SEM of N = 5 independent experiments (*t*-test, $^{**}p < 0.01$). **(D)** Quantitative PCR was used to analyze mRNA levels of megalin. Three independent assays were performed, and the average ±SD was plotted on the graph. **(E)** Metabolic labeling of control or OCRL1 silenced cells with [^{35}S]-methionine/cysteine for 4 h mMeg was immunoprecipitated (IP) and analyzed by autoradiography. Additionally, an aliquot of the whole-cell lysate was used to total mMeg by western blot (WB). **(F)** Endogenous megalin and mMeg were analyzed in whole-cell lysates of control and APPL1 silenced cells by western blot. **(G)** Quantification of mMeg protein levels corrected with tubulin levels in control and APPL1 KD cells. Data are expressed as the means ± SEM of five independent experiments (*t*-test, $^{**}p < 0.01$). **(H)** Control or silenced cells were treated with CHX (100 μM), and the expression of mMeg, Precursor-mMeg, and actin were determined by western blot at indicated times. **(I)** Graph corresponds to mMeg protein levels corrected with actin levels in control and silenced cells.

kidney proximal tubule cells LLC-PK1. In this model, we evaluated the protein levels of the receptor, both endogenous megalin and the megalin mini receptor, mMeg, an accepted model to study trafficking and phosphorylation of the full-length receptor (Yuseff et al., 2007; Farfán et al., 2013) (Figure 1A). Interestingly we observed a significant decrease in megalin expression, at the protein level, in OCRL1 silenced cells (Figures 1B,C). On the other hand, and in line with findings in zebrafish (Oltrabella et al., 2015), the reduction of megalin protein levels in OCRL KD cells was not a result of a transcriptional regulation because megalin mRNA expression, evaluated by quantitative PCR, did not change (Figure 1D). Besides, the amount of mMeg found after a pulse of ^{35}S-methionine was similar in control and OCRL1 KD cells (Figure 1E), confirming that the decreased total levels of the receptor were not due to a reduction in its biosynthesis. These results suggest that OCRL1 regulates megalin at a post-transcriptional level in the proximal kidney cell line.

OCRL1 and the endosomal protein APPL1 are present in endocytic vesicles (Erdmann et al., 2007). The recruitment of OCRL1 to the phagosomes and endosomes is regulated by Rab proteins, including Rab5, Rab22a, and Rab35 (Hyvola et al., 2006; Fukuda et al., 2008; Noakes et al., 2011). Besides, the association of OCRL1 to endosomes is indirectly regulated by APPL1 by its interaction with Rab5 (McCrea et al., 2008; Bohdanowicz et al., 2012) and APPL1 interacts with megalin (Erdmann et al., 2007). Previous results showed that in OCRL KD cells, the presence of megalin in APPL1-positive endosomes is reduced, whereas its presence in EEA1-positive endosomes is increased (Vicinanza et al., 2011; Festa et al., 2019). However, the role of APPL1 in megalin expression has not been evaluated. Therefore, we determined whether silencing APPL1 modifies megalin levels. Our findings indicate that this was the case; as is shown in Figures 1F,G, megalin protein levels were significantly reduced in APPL1 KD cells. To explore if the reduction of OCRL1 and APPL1 decreases megalin by promoting its degradation, the receptor half-life was evaluated by measuring its disappearance over time in control and OCRL1 or APPL1 KD cells. Cells were treated with cycloheximide (CHX) for up to 12 h. The disappearance of megalin in OCRL1 and APPL1 silenced cells was faster than in control cells (Figures 1H,I). These results underscored the roles of OCRL1 and APPL1 in megalin protein stability.

In control cells treated with CHX, the inhibition of proteasome by epoxomycin partially recovered megalin levels but the inhibition of lysosome, with NH4Cl, had no effect (Supplementary Figure S1A,B). In OCRL1 silenced cells the recovery of megalin levels was significant upon proteasome inhibition. Compared with the control cells, the inhibition of lysosome in shOCRL1 cells had a slight but not significant effect. These results suggest that the lack of OCRL1 induces megalin degradation by the proteasome and possibly in less extension by the lysosome. APPL1 silenced cells also show a more predominant role of proteasome than lysosome in megalin degradation.

Megalin proteolytic processing, ectodomain secretion and surface levels are decreased in OCRL1 and APPL1 knock-down cells

LS patients have reduced megalin levels in the urine (Norden et al., 2002; Suruda et al., 2017). Besides the reduction in total megalin levels, explained by increased receptor degradation, a possible mechanism involved in the decrease of megalin in the urine of LS patients is related to alterations in the proteolysis of the receptor ectodomain. Endogenous megalin is first proteolyzed by matrix metalloproteinases (MMPs), stimulated by PKC; this process is followed by a γ-secretase mediated intramembrane processing of the resulting megalin C-terminal fragment; this sequential proteolytic processing has been documented in opossum renal cell line (OK) (Zou et al., 2004) as well in LLC-PK1 cells (Cabezas et al., 2019) among others. To evaluate the proteolytic processing in our system, we first characterized and compared the processing of mMeg, expressed in LLC-PK1 and MDCK renal epithelial cells. We determined the distribution of the extracellular and intracellular fragments of mMeg since a differential localization of these domains originated from endogenous megalin in rat proximal tubule epithelium was previously reported (Bachinsky et al., 1993; Zou et al., 2004). In MDCK cells mMeg extracellular and cytoplasmic domains were not always colocalizing within the cell (Supplementary Figure S2A,B), consistent with constitutive processing of the receptor as occurs with other members of the family (Larios and Marzolo, 2012). Moreover, it was also possible to observe that, in addition to the detection of N- and C-terminal megalin in the same structure, amino and carboxy-terminal fragments were also found separated (Supplementary Figure S2B), corroborating the observations in renal tissues analyzed by electron microscopy (Bachinsky et al., 1993; Zou et al., 2004).

Furthermore, by immunofluorescence, we found an interesting distribution pattern of the receptor in LLC-PK1 cells overexpressing mMeg (in which minimegalin levels are several times higher than endogenous megalin, see Figure 1B); some cells exhibited the label corresponding to both domains while in others, only the label corresponding to the ectodomain (N-terminal, containing HA epitope) was detected (Figure 2A). Besides, this dual pattern was not observed in cells expressing mMeg0, a mini receptor lacking the extracellular domain but including an amino-terminal HA-epitope (Figure 2B). This result suggests that the cells exclusively positive for the ectodomain staining (Figure 2A) could capture the N-terminal part of the receptor from the media. Accordingly, western blot evaluation of the cellular proteins showed a band recognized by the anti-

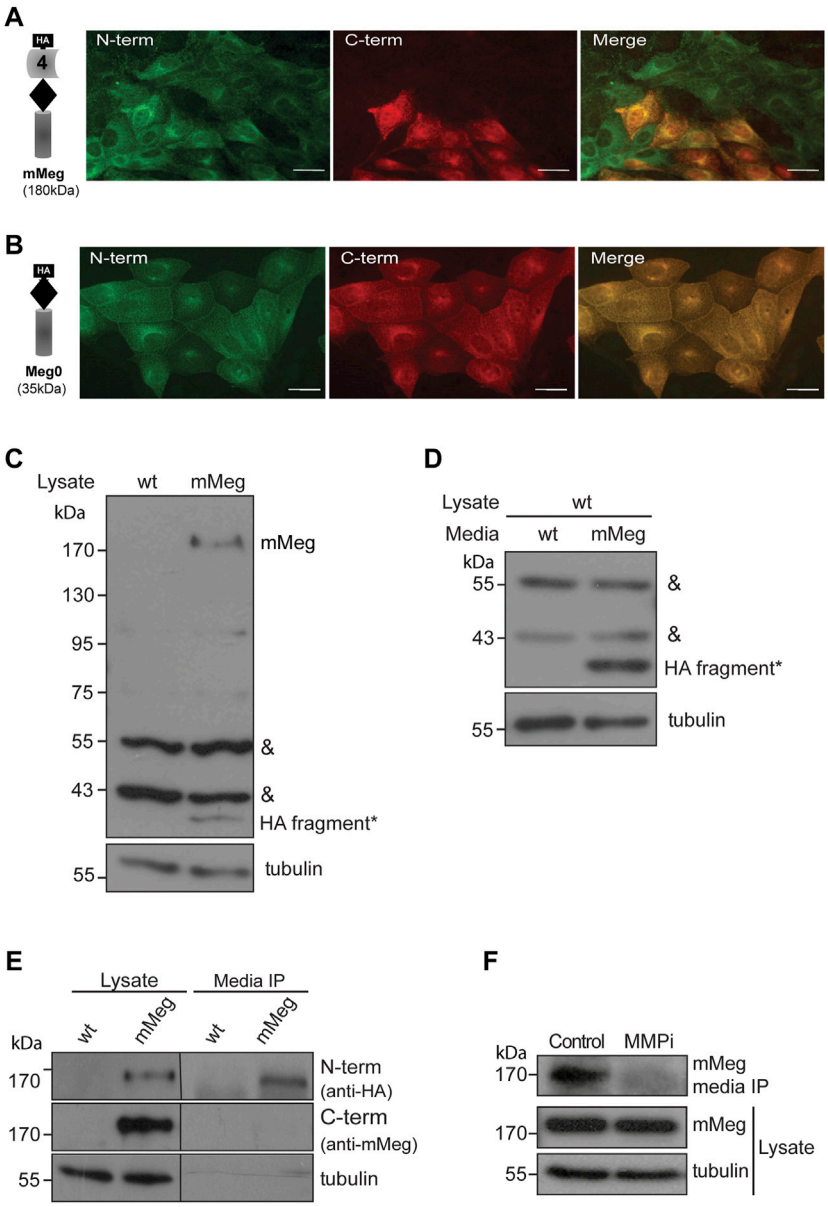

FIGURE 2
Characterization of megalin intracellular and secreted fragments. Immunofluorescence of LLC-PK1 cells stably expressing **(A)** mMeg or **(B)** Meg0 to detect amino-terminal (N-term) or carboxy-terminal (C-term) domains of the receptor with anti-HA (green) and anti-Megalin (red) antibodies, respectively. The images were acquired by epifluorescence microscopy. Scale bar, 10 μm. **(C)** Whole-cell lysates of wt LLC-PK1 and mMeg-LLC-PK1 cells were analyzed by western blot using anti-HA to detect mMeg or its N-term fragments. Symbols correspond to a non-specific band (&) and the low molecular weight band exclusive to the mMeg expressing cell lysate (*). **(D)** Whole-cell lysates of wt LLC-PK1 cells were incubated with conditioned media of either wt or mMeg -LLC-PK1 cells, analyzed by western blot using an anti-HA antibody, which recognizes the N-terminal portion of mMeg. Symbols correspond to the non-specific band (&) and low molecular weight band found in the cell lysate of wt LLC-PK1 cells incubated with conditioned media from mMeg-expressing LLC-PK1 cells (*). **(E)** mMeg-LLC-PK1 cells were grown to confluence for 48 h. The conditioned medium was concentrated and then immunoprecipitated with an anti-HA antibody. Protein samples, immunoprecipitated media, and cell lysates were analyzed with an anti-HA antibody to detect megalin ectodomain (N-term) and with an anti-megalin cytoplasmic domain polyclonal antibody to detect megalin carboxy-terminal fragment (C-term). Tubulin was used as a loading control. **(F)** mMeg expressing cells were incubated with vehicle (Control) or 10 μM MMPi (GM6001, general matrix metalloprotease inhibitor) for 48 h and replenished every 12 h. The immunoprecipitated media and cell lysates were analyzed by western blot to detect mMeg and tubulin as load control.

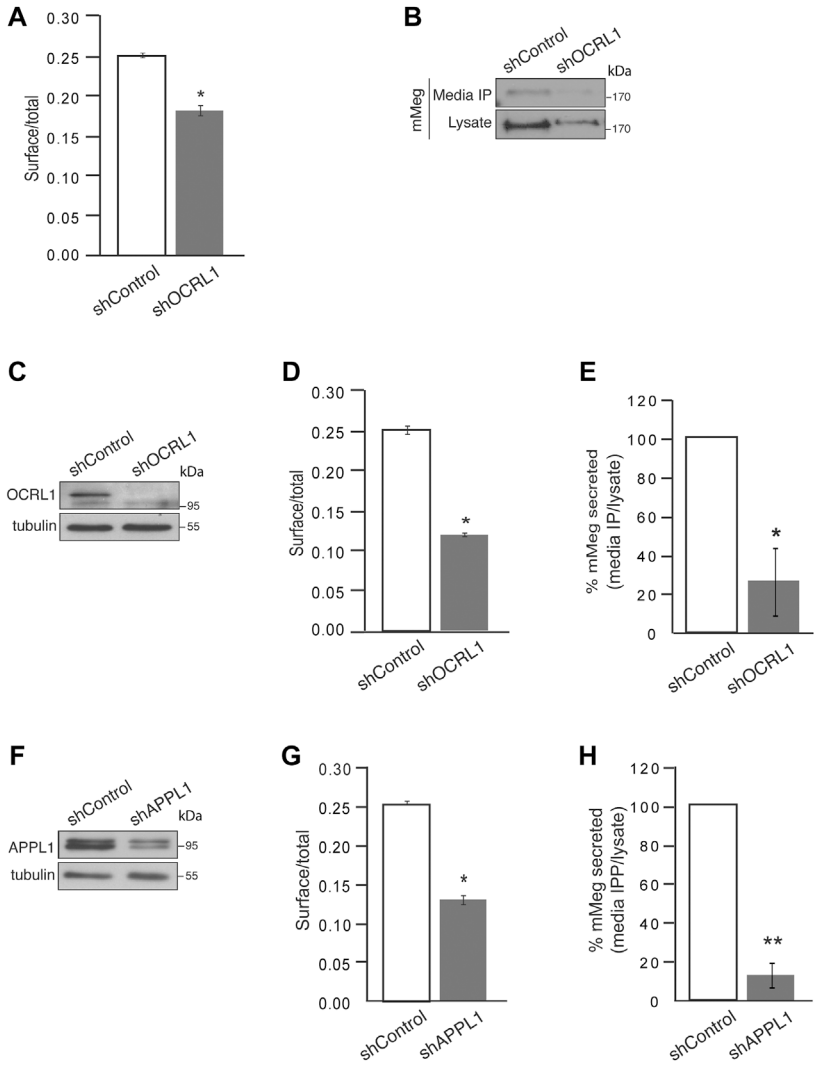

FIGURE 3
Cell surface megalin distribution and extracellular domain release decrease under OCRL1 and APPL1 silencing. **(A)** mMeg-LLC-PK1 cells, non-permeabilized or permeabilized, control, or OCRL1-silenced were incubated with an anti-HA-488-conjugated antibody and analyzed by flow cytometry. The results are plotted as the ratio of expression levels observed in non-permeabilized (surface) *versus* permeabilized cells (total). Data are expressed as the means ± SEM of N = 3 independent experiments (*t*-test, **p* < 0.05). **(B)** Conditioned media of control or OCRL1 silenced mMeg-LLC-PK1 cells were processed by anti-HA immunoprecipitation (Media IP). Samples of IP and cell lysates were analyzed by western blot with an anti-HA antibody to detect the megalin ectodomain (N-term). **(C–H)** MDCK cells stably expressing mMeg (mMeg-MDCK) were infected with non-target shRNA (shControl), shRNA directed against OCRL1 (shOCRL1) or APPL1 (shAPPL1) lentiviruses. **(C)** Protein levels of OCRL1 were analyzed in whole-cell lysates of control and OCRL1 silenced cells by western blot. **(D)** Flow cytometry analyzes mMeg surface localization in control and OCRL1 silenced cells. The plot shows the surface vs. total ratio of expression levels. Data are expressed as the means ± SEM of N = 3 independent experiments (*t*-test, **p* < 0.05). **(E)** Analysis of immunoprecipitated conditioned medium and cell lysates of control or OCRL1 silenced cells by western blot with an anti-HA antibody. The plot shows the levels of mMeg in the immunoprecipitated media corrected by total. Data are expressed as the means ± SEM N = 3 independent experiments (*t*-test, **p* < 0.05). **(F)** Protein levels of APPL1 were analyzed in whole-cell lysates of control and APPL1 silenced cells by western blot. **(G)** Flow cytometry analyzes mMeg surface localization in control and APPL1 silenced cells. The plot shows the surface vs. total ratio of expression levels. Data are expressed as the means ± SEM of N = 3 independent experiments (*t*-test, **p* < 0.05). **(H)** Analysis of immunoprecipitated conditioned medium and cell lysates of control or APPL1 silenced cells by western blot with an anti-HA antibody. The plot shows the levels of mMeg in media IP corrected by total. Data are expressed as the means ± SEM N = 3 independent experiments (*t*-test, ***p* < 0.01).

ectodomain antibody (anti-HA), of around 40 kDa, only present in lysates from mMeg transfected cells (Figure 2C). To test if this band corresponds to an endocytosed minimegalin N-terminal fragment, we incubated non-transfected cells with the conditioned media obtained either from wild-type or mMeg expressing cells. The result shows a band, 40 kDa, only detected in lysates of the cells exposed to the conditioned media of mMeg expressing cells (Figure 2D). Overall, these

observations suggest that megalin ectodomain secretion would be followed by the internalization of this domain, or a fragment of it, in our cellular model.

Then, we evaluated the conditioned media of LLC-PK1 mMeg cells. We detected a fragment of mMeg recognized only by anti-HA but not by an anti-C terminal antibody, indicating that this soluble N-terminal fragment of the protein probably results from a shedding process. This band is slightly smaller than the one present in cell lysates, corresponding to the full-length mMeg (Figure 2E). Similar results were found in mMeg expressing MDCK cells (Supplementary Figure S3), indicating that megalin is secreted to the culture media as a proteolytic product. Similar to the endogenous receptor, matrix metalloproteinases (MMPs) and a disintegrin and metalloproteinase domain-containing (ADAM) proteins would be involved in the shedding of mMeg because the inhibition of these enzymes with the general inhibitor GM6001 reduced the secretion of the receptor ectodomain (Figure 2F).

To determine if megalin processing is altered in LS cellular models, we evaluated the cell surface expression and secretion of mMeg, to the culture media, in OCRL1 and APPL1 KD cells. As previously found in HK2 cells (Vicinanza et al., 2011), the reduction of OCRL1 in LLC-PK1 cells induced a significant decrease in mMeg levels at the cell surface (Figure 3A). The ectodomain of megalin in the media was also evidently reduced in this proximal tubule cell (Figure 3B). Similar results were observed in OCRL1 KD MDCK cells (Figures 3C–E). These results highlight a role for OCRL1 in regulating megalin surface expression, proteolysis, and ectodomain secretion.

Additionally, we evaluated whether the previous relationship between OCRL and APPL1 exists in our model, specifically if the effects on mMeg trafficking observed in OCRL1 silenced cells replicate under APPL1 silencing conditions (Figure 3F). Our results show a significant reduction in megalin cell surface expression in APPL1 silenced cells (Figure 3G). Interestingly, APPL1 silencing also significantly reduced mMeg secretion to the culture media (Figure 3H). The similarity of the effects of APPL1 KD with OCRL1 KD again suggests a link between these two endosomal proteins in regulating mMeg trafficking and processing.

OCRL1 regulates the phosphorylation and the endosomal distribution of megalin

Megalin trafficking is particularly affected at the early endosomes in OCRL1 silenced cells due to inefficient recycling back to the plasma membrane, partly due to an accumulation of actin filaments around the endosomes (Vicinanza et al., 2011). On the other hand, we have described that megalin's recycling and cell surface levels are inhibited by GSK3-mediated phosphorylation of its cytoplasmic domain (Yuseff et al., 2007). Thus, we wondered whether GSK3β-mediated megalin phosphorylation could be increased in OCRL1 KD cells as an additional explanation for its reduction at the cell surface. To address this possibility, we evaluated megalin phosphorylation in mMeg-MDCK silenced for OCRL1 (Vicinanza et al., 2011). In OCRL1 KD cells, protein levels and the basal activation of GSK3ß, analyzed by phosphorylation of its inhibitory residue Ser9, were not changed (Figure 4A). Then, we evaluated the phosphorylation of mMeg by metabolic labeling with ^{32}P-orthophosphate, as described (Yuseff et al., 2007). Contrarily to our initial idea, in OCRL1 KD cells megalin phosphorylation was reduced to 59% of the control cells (Figures 4B,C), something unexpected considering that the basal inhibition GSK3ß (phosphorylated in Ser 9) was similar in both wild-type and OCRL1 KD cells. Part of the remaining phosphorylated megalin was GSK3-dependent as LiCl, a GSK3 inhibitor (Serretti et al., 2009), diminished even more the phosphorylation of the receptor (Figures 4B,C). Overall, these results indicate that in our LS cellular model, the reduced surface expression of megalin is not explained by an increase in its GSK3ß-mediated phosphorylation. In contrast with the effect due to the lack of OCRL1, silencing APPL1 did not significantly affect the basal levels of megalin phosphorylation, although there was a reduction trend (Figures 4D,E).

One possibility to explain a lower megalin phosphorylation in LS cells is that GSK3ß has less access to its substrate. To test this possibility, we determined the colocalization of endogenous megalin and transfected GSK3-HA in LLC-PK1 cells. Cells were treated with YU142670, an inhibitor of OCRL1 (Pirruccello et al., 2014), or vehicle, and the colocalization of megalin with GSK3ß was analyzed after the immunodetection of both proteins. The blocking effect of the inhibitor was assessed by determining the size of the EEA1 positive endosomes (Supplementary Figure S4A,B). The results show megalin and GSK3ß colocalize similarly in control and inhibitor-treated cells (Supplementary Figure S4C,D), a result that does not support the option of decreased substrate-kinase encounter in LS conditions.

Then, we asked if megalin is differentially distributed in the endosomal compartments dependent on phosphorylation status and how this localization could be changed if OCRL1 activity is decreased. To have insights into the endosomal distribution of megalin in its phosphorylated and non-phosphorylated forms, the wild-type having the cytoplasmic PPPSP motif recognized by GSK3ß, the phosphomimetic PPPDP (S/D) and the non-phosphorylated PPPAP (S/A) forms of mMegs (Yuseff et al., 2007; Marzolo and Farfán, 2011) were expressed in LLC-PK1 treated or not with YU142670. The steady-state distribution of mMeg was determined by colocalization with EEA1, Rab11 and Rab7 under control conditions (Figures 5A–F). Due to the lack of specific staining of the Rab11 antibody in LLC-PK1 cells, the distribution of the megalin in the recycling compartment was assessed upon transfection of mCherry-Rab11. In YU142670 treated cells, the wild-type and S/D mutant mMegs were significantly increased in EEA1 positive early endosomes (Figures 5A,B) and in Rab11 recycling endosomes (Figures 5 C, D). In

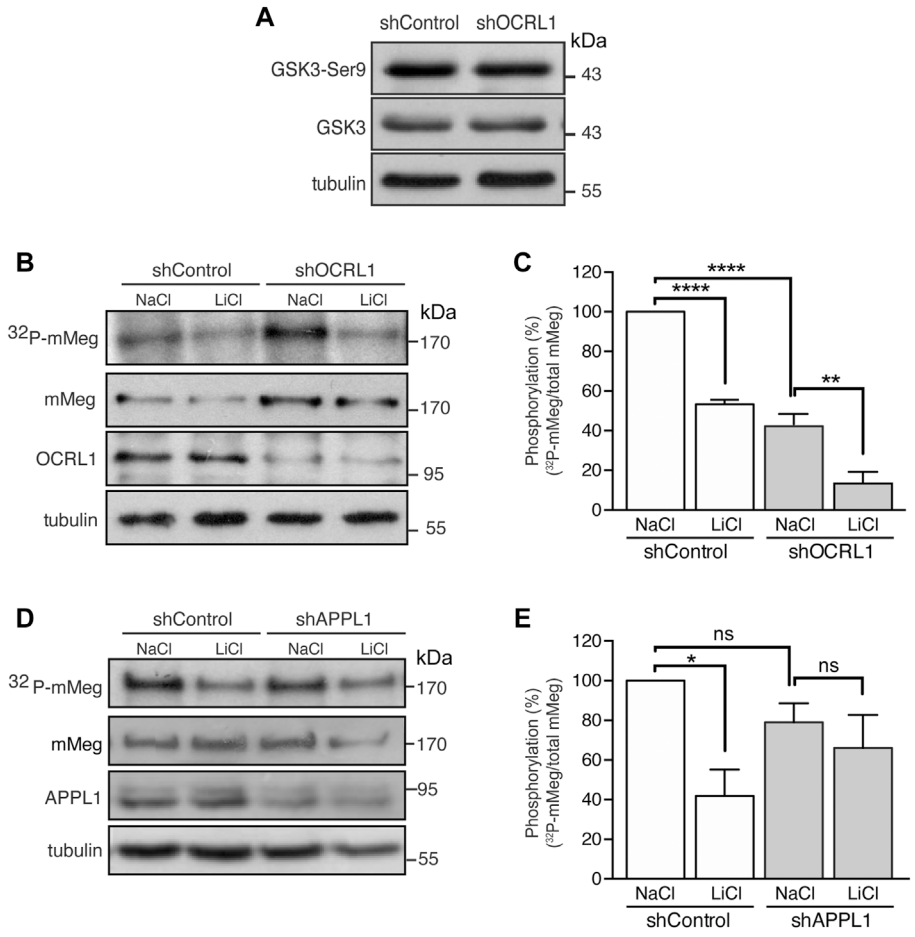

FIGURE 4
Reduced mMeg phosphorylation in mMeg-MDCK OCRL1 silenced cells. **(A)** Control or OCRL1 silenced cells were lysed and analyzed by western blot with antibodies against phosphorylated GSK3ß (Ser9) and total GSK3ß. **(B)** Control or silenced for OCRL were treated with LiCl (50 mM) or NaCl (50 mM) as control. For phosphorylation assays, the cells were incubated with [^{32}P]-orthophosphate for 2 h at 37°C, followed by immunoprecipitation of megalin from cell lysates using an anti-megalin cytoplasmic domain. The immune complexes were analyzed by SDS-PAGE and visualized by autoradiography. Aliquots of whole-cell lysates were used to detect mMeg by western blot. **(C)** Graph shows the percentage of phosphorylated mMeg related to the total. Data are expressed as the means ± SEM of N = 3 independent experiments (ANOVA, ****$p < 0.0001$, **$p < 0.01$). **(D)** Control or silenced for APPL1 were treated with LiCl (50 mM) or NaCl (50 mM) as control. For phosphorylation assays, the cells were incubated with [^{32}P]-orthophosphate for 2 h at 37°C, followed by immunoprecipitation of megalin from cell lysates using an anti-megalin cytoplasmic domain. The immune complexes were analyzed by SDS-PAGE and visualized by autoradiography. Aliquots of whole-cell lysates were used to detect mMeg by western blot **(E)** Graph corresponds to the percentage of phosphorylated mMeg related to the total of control or APPL1 silenced cells. Data are expressed as the means ± SEM of N = 3 independent experiments (ANOVA, *$p < 0.05$).

contrast, upon the inhibition of OCRL1 only the mMeg S/D mutant was increased in Rab7 positive endosomes, even though the wild-type mMeg was more present in this compartment under control conditions (10.8% wt vs. 3.1% S/D) (Figures 5 E, F). Interestingly, the mMegS/A that is not a substrate of GSK3ß was rather refractory to the reduction of OCRL1 activity. This mutant has a fast-cycling behavior (Yuseff et al., 2007), something evident when its presence in the different endosomal compartments is analyzed under control conditions; compared with the wild-type mMeg, the mMeg S/A mutant was more present in early/recycling endosomes (18.5% wt; 41.05% S/A) and less in late Rab7 positive endosomes (10.4 wt% vs. 3.1% S/A). Overall, these pieces of evidence suggest that the endosomal trafficking of megalin is differentially affected by the reduction in the activity of OCRL1 and the phosphorylation status of the receptor.

It is important to consider that the increased presence of megalin in the Rab11-endosomal compartments in YU142670 treated cells probably reflects that the inhibition of megalin recycling also takes place from a more mature recycling compartment and not only from an EEA1-sorting endosome. Moreover, our data also show that the inhibition of OCRL activity affects the identity of the endosomal compartments; cells treated with YU142670 showed a significant increase in the colocalization of EEA1 with Rab11 (Supplementary Figure S4E,F).

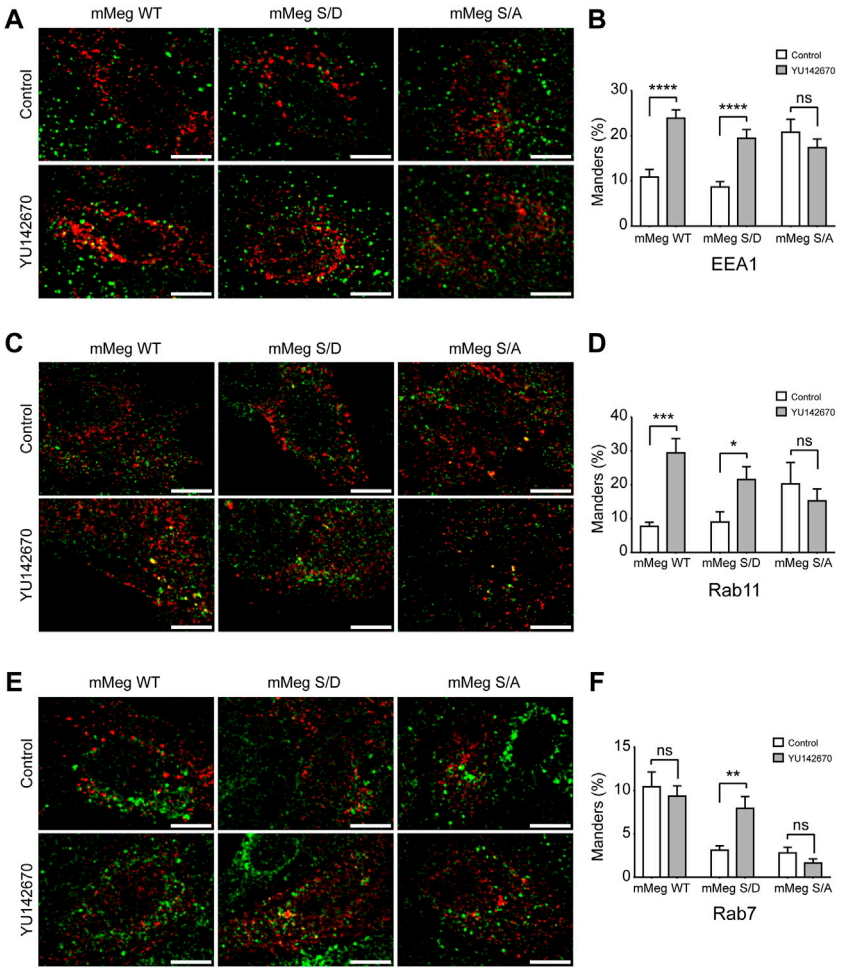

FIGURE 5
Endosomal distribution of megalin and its phosphorylated and non-phosphorylated forms in control and OCRL inhibition conditions. LLC-PK1 were transfected with HA-tagged minimegalins (mMeg) wt, phosphomimetic (mMeg S/D) or non-phosphorylatable mMeg S/A. Then, cells were treated with 50 μM YU142670 or vehicle for 4 h, fixed and processed for fluorescence microscopy. Preparations were imaged with Confocal Nikon Timelapse. Scale Bars 10 μM. **(A)** Cells were stained with anti-EEA1 (green) and anti-HA (red). **(B)** At least 34 separated cells were analyzed with ImageJ to measure the Manders percentage between EEA1 endosomes and HA-tagged mMeg structures. ANOVA, $^{****}p < 0.0001$. **(C)** LLC-PK1 cells were co-transfected with mCherry-Rab11 and HA-tagged mMeg. Then, cells were treated with 50 μM YU142670 for 4 h, fixed and processed to detect mMeg (HA, red) and Rab11 (green). The color was changed for consistency with the other panels. **(D)** At least 12 separated cells were analyzed with ImageJ to measure the Manders percentage between Rab11-positive endosomes and mMeg structures. ANOVA, $^{***}p < 0.001$, $^{*}p < 0.05$. **(E)** LLC-PK1 transfected with HA-tagged mMeg. Then, cells were treated with 50 μM YU142670 for 4 h, fixed and processed to detect mMeg (HA, red) and Rab7 (green). **(F)** At least 18 separated cells were analyzed with ImageJ to measure the Manders percentage between Rab7-positive endosomes and mMeg structures. ANOVA, $^{**}p < 0.01$.

Insulin treatment decreases megalin phosphorylation and increases megalin at the cell surface despite a reduction in the signaling pathway in OCRL1-and APPL1-silenced cells

Insulin increases megalin levels in cell culture under conditions resembling hypertension and type-2 diabetes, both associated with chronic kidney disease (Hosojima et al., 2009; Bryniarski et al., 2018). Besides, insulin inhibits GSK3 (Cross et al., 1995). As mentioned before, megalin's recycling from endosomes to the cell surface is reduced by GSK3-mediated phosphorylation of its cytoplasmic domain, decreasing the amount of megalin available for ligand binding (Yuseff et al., 2007). Therefore, insulin could mediate a physiological way to inhibit megalin phosphorylation and, eventually, increase the receptor surface levels. First, we tested the effect of 100 nM insulin on megalin phosphorylation in LLC-PK1 cells (Figure 6). Interestingly, 4 h of insulin treatment significantly reduced megalin phosphorylation up to 60% of the control

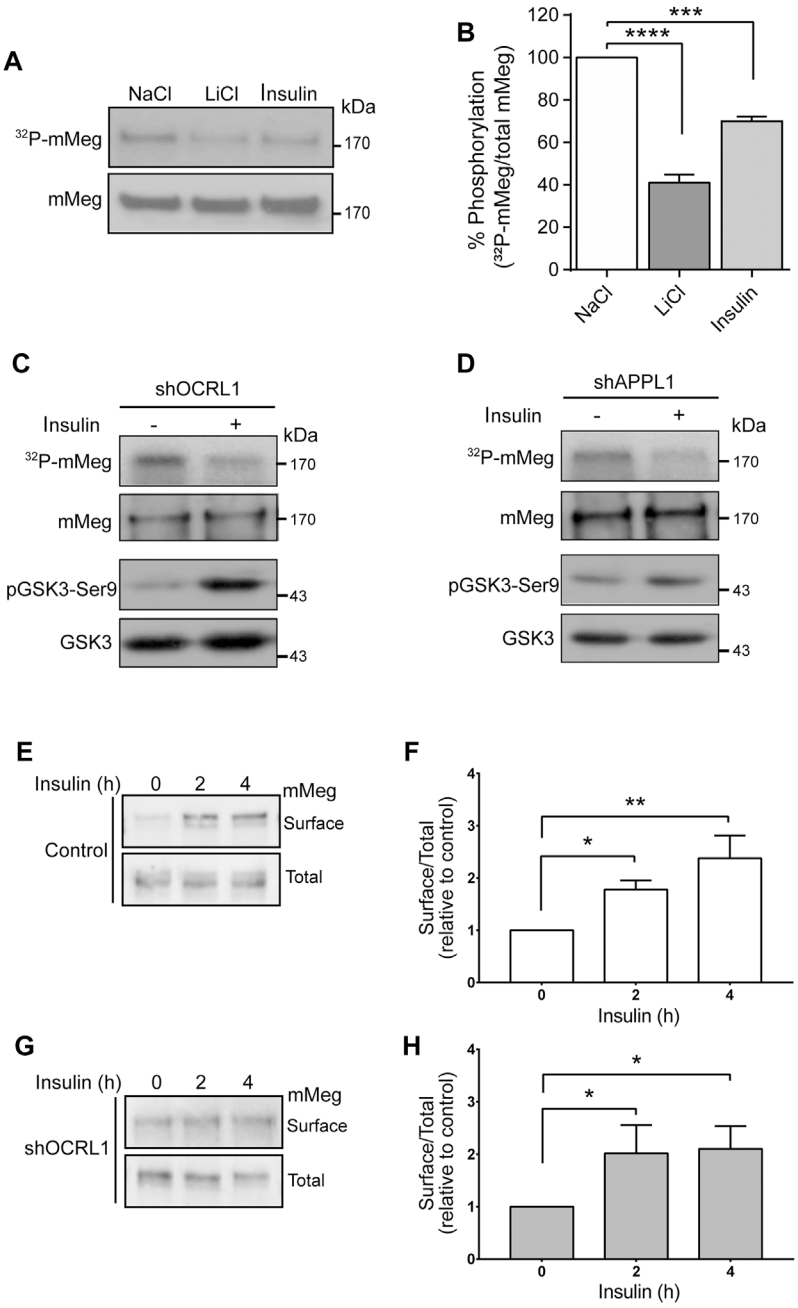

FIGURE 6
Insulin decreases megalin phosphorylation and increases megalin surface expression in control and LS cellular models. **(A)** mMeg-LLC-PK1 cells treated with NaCl (50 mM), LiCl (50 mM) or insulin (100 nM) were labeled [^{32}P]-orthophosphate for 2 h at 37°C, followed by immunoprecipitation of megalin with an anti-megalin cytoplasmic domain. The immune complexes were analyzed by SDS-PAGE and visualized by autoradiography. Aliquots of whole-cell lysates were used to detect mMeg by western blot. **(B)** Graph corresponds to the percentage of phosphorylated mMeg related to the total of NaCl, LiCl or insulin-treated cells. Data are expressed as the means ± SEM of N = 3 independent experiments (ANOVA, ****$p < 0.0001$, ***$p < 0.001$). Phosphorylation assays were performed in OCRL1 **(C)** or APPL1 **(D)** silenced cells in the presence or the absence of 100 nM insulin. Immunoprecipitated radiolabeled mMeg was evaluated by autoradiography. Total mMeg and GSK3ß (total and phosphorylated forms) were detected by western blot. **(E,F)** Control or **(G,H)** OCRL1 silenced cells were serum-starved for 2 h before the incubation with 100 nM insulin by the indicated period of time. Cells were biotinylated to determine the surface levels of mMeg. The whole lysates were used for total receptor levels. Samples were analyzed by western blot. The graphs shows surface vs. total ratio of mMeg expression levels relative to control time 0. N = 4; ANOVA, *$p < 0.05$, **$p < 0.01$.

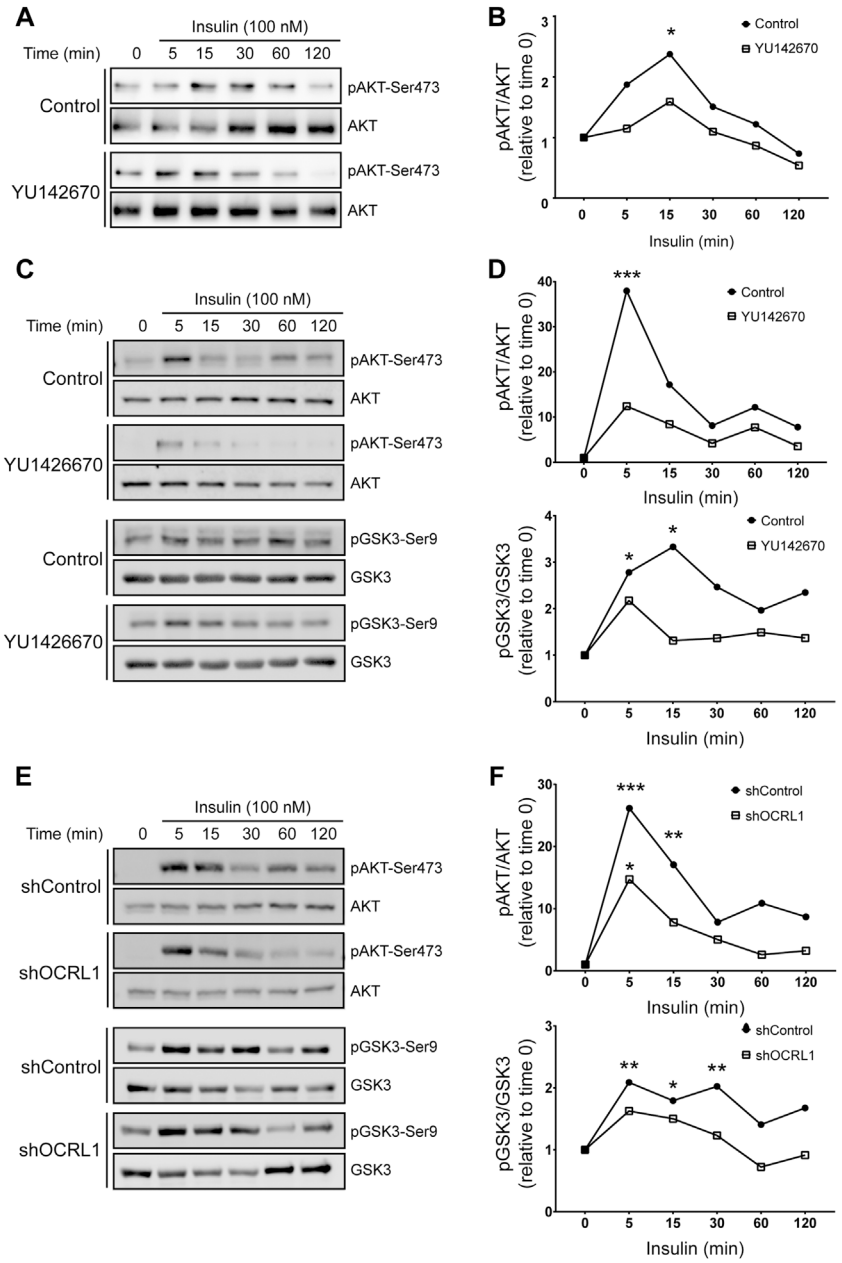

FIGURE 7
Insulin signaling is decreased in LS cellular models. mMeg-LLC-PK1 **(A–B)** or HeLa **(C–D)** cells were serum starved for 4 h ± 50 μM YU1426670 and then incubated with 100 nM insulin ± 50 μM YU1426670 for indicated periods of time. **(A,C)** Cell lysates were analyzed by western blot to detect total and phosphorylated forms of AKT. **(B)**. Graph corresponds to the protein levels of phosphorylated AKT corrected by total levels of AKT relative to time 0. N = 3; ANOVA, *$p < 0.05$.**(D)** Graph corresponds to the protein levels of phosphorylated protein corrected by total levels relative to control, time 0, AKT (upper) or GSK3β (lower). N = 3, ANOVA, ***$p < 0.001$, **$p < 0.01$, *$p < 0.05$. **(E–F)** HeLa control or OCRL1 silenced cells were serum starved for 4 h and then incubated with 100 nM insulin ± 50 μM YU1426670 for indicated periods of time. **(E)** Cell lysates were analyzed by western blot to detect total and phosphorylated forms of AKT and GSK3β. **(F)** Graph corresponds to the protein levels of phosphorylated protein corrected by total levels relative to control, time 0, AKT (upper) or GSK3β (lower). N = 3 ANOVA, ***$p < 0.001$, **$p < 0.01$, *$p < 0.05$.

(Figures 6A,B). Moreover, in OCRL1 and APPL1 KD cells, insulin was still able to reduce megalin phosphorylation as well as GSK3ß activity, measured by the PKB/AKT-mediated phosphorylation in Ser9 (Figures 6C,D).

Accordingly, insulin treatment of both wild-type and LS cells (OCRL KD) significantly increased megalin surface expression after 4 h of treatment (Figures 6E–H). These results suggest that insulin, *via* inhibition of GSK3ß -mediated megalin

phosphorylation, could promote more efficient recycling of the receptor in normal and in OCRL1 dysfunction conditions.

Considering this insulin effect on megalin phosphorylation and cell surface expression, we were interested to know if LS cellular models respond differently to insulin (Figure 7). We measured insulin signaling up to 2 h in LLC-PK1 cells treated with 50uM of YU142670 to inhibit OCRL1. Cells showed a decreased insulin response, evaluated by a lower activation of AKT at 15 min of activation (Figures 7A,B). In order to test if the absence of OCRL1 affects insulin signaling in a different cell type, we tested Hela cells, a human cell line that does not express megalin. Hela cells were treated with YU142670 or vehicle (Figures 7C,D) or silenced for OCRL1 (Figures 7E,F). There was an evident difference in the time of response to insulin in Hela cells compared to LLC-PK1. In Hela cells, the phosphorylation peak of AKT was at 5 min of insulin stimulation. In both models (cells treated with YU142670 and OCRL KD), the response to the hormone was significantly decreased compared to the control cells, specifically by reducing AKT phosphorylation. Similar results were observed regarding pGSK3ß. Therefore, cells with decreased function of OCRL1 are less responsive to insulin. Similarly, we tested insulin response in APPL1 KD Hela cells, finding that both AKT and its downstream substrate GSK3 show a reduction in phosphorylation (Supplementary Figure S5).

Overall, these results indicate that insulin signaling operates under cellular LS conditions, although with significantly reduced efficiency. Potentially, insulin could be considered a tool to reduce the constitutive GSK3ß-mediated megalin phosphorylation, which decreases the receptor cell surface levels (Yuseff et al., 2007).

Discussion

The elucidation of the molecular mechanisms underlying the regulation of megalin function and trafficking is a central issue in understanding the receptor's role in human pathologies. In the present paper, we focused on the regulation of megalin by the phosphatidylinositol 5-phosphatase OCRL1 in a cellular model that simulates the LS condition specifically at the level of the proximal tubule of the kidney. First, we show evidence of megalin down-regulation protein and a reduction of the receptor shedding under the OCRL1 silencing condition reinforcing the proposed trafficking defects of megalin in LS renal phenotype (Pisitkun et al., 2004; Erdmann et al., 2007; Alexander and Grinstein, 2009; Suruda et al., 2017). Megalin proteolysis could be of physiological importance in regulating its own expression due to the transcriptional role proposed for its intracellular domain in the nucleus (Li et al., 2008; Marzolo and Farfán, 2011). The mechanisms underlying the shedding process include ligand binding, different metalloproteinases, and PKC-dependent regulation (Zou et al., 2004; Marzolo and Farfán, 2011; Mazzocchi et al., 2017). In the present study, we complement these observations by showing the importance of OCRL1 and its interacting endosomal protein APPL1 in regulating total and cell surface levels of megalin and the secretion of the receptor ectodomain. Besides, we described how OCRL1 regulates the megalin phosphorylation and the endosomal distribution of the receptor depending on its phosphorylation status. Finally, and physiologically relevant, we showed that megalin phosphorylation and cell surface expression is regulated by insulin.

In our proximal tubule cells model for the Lowe condition, endogenous megalin was reduced without changes in the receptor's mRNA, similar to what was found in the humanized Lowe Syndrome mouse model (Festa et al., 2019). The reduction in megalin protein, observed in OCRL1 silenced LLC-PK1 cells, is similar to what was reported in a mouse model of Dent1 disease, another pathology with a related renal phenotype as LS (Christensen et al., 2003). Dent1 disease occurs due to gene mutations of the chloride channel CLC-5 (Fisher et al., 1995), a protein that interacts with megalin and regulates its trafficking in renal proximal tubule cells (Christensen et al., 2003). Moreover, the evaluation of megalin, secreted in the urine of Dent patients, also shows a reduction in the presence of the receptor (Norden et al., 2002). Thus, our results corroborate the evidence indicating a correlation between renal defects that affect megalin function in LS and Dent1 disease (Norden et al., 2002; Shrimpton et al., 2009; Vicinanza et al., 2011).

In revealing megalin degradation in cells with reduced OCRL1 protein, we found that protein stability, but not its synthesis, was decreased upon OCRL1 silencing. In the absence of OCRL1, cargoes accumulate in EEA1-positive early/sorting endosomes and cannot recycle from tubular structures to the plasma membrane (Vicinanza et al., 2011). Therefore, we initially speculated that in LLC-PK1 cells deficient in OCRL1 the receptor could be favored to get into the degradative lysosomal pathway, explaining the significant reduction in megalin protein. Our results in cells with inhibition of lysosomal activity (Supplementary Figure S1) added to the similar presence of megalin in Rab7-late endosomes in control and inhibited OCRL1 cells (Figure 5), did not support this possibility. In contrast, our data favor the role of the proteasomal degradation pathway in megalin half-life. Another possibility to explain the decrease of megalin in OCRL1 silenced LLC-PK1 cells relates to the role of the enzyme dipeptidyl-peptidase 4 (DPP4) (Aroor et al., 2016). This enzyme plays a relevant role in the proximal tubule (Lee et al., 2015). DPP4 is activated by EGFR stimulation and is associated with a reduction of megalin in mice (Aroor et al., 2016). In this regard, it is worth mentioning that in OCRL1 KD cells, the activation level of EGFR is significantly increased due to its accumulation in endosomes, where it persists in its signaling mode, activating ERK (Vicinanza et al., 2011). The total protein

levels and the half-life of megalin were reduced in APPL1 silenced cells, similar to what was found in OCRL1 KD cells.

To study the role of OCRL1 and APPL1 in megalin ectodomain secretion, we first validated mMeg as a proper model to study the proteolysis (shedding) and trafficking of megalin. It has been reported that the overexpression of the expected product of γ-secretase activity over the MCTF, to the so-called megalin intracellular carboxy-terminal domain (MICD), down-regulates megalin and also a Na+/H+ exchanger 3 at a transcriptional level in a proximal tubule cell lines (Li et al., 2008). However, we were unable to detect this proteolytic product in our system. The expected MICD has been challenging to identify at the moment in tissue and cell cultures. Using inhibitors of proteasomal degradation, we have tried unsuccessfully to detect MICD (data not shown). Despite these results, our cellular models allow us to establish a role of OCRL1 as well as APPL1 in megalin regulation; the silencing of these proteins reduced both cell surface levels and megalin secretion to the extracellular media (corrected by the total levels of the receptor), compared to the control cells in kidney epithelial cells, LLC-PK1 and MDCK. The reduction of megalin cell surface levels in OCRL1 knock-down is also explained by an impairment of the receptor recycling from the sorting endosome, as was already described (Vicinanza et al., 2011).

Among the possible mechanisms underlying the reduction in megalin shedding observed in OCRL1 and APPL1 knock-down cells is the reduced presence of megalin at the cell surface. In general, the events triggered by MMPs and ADAM proteins metalloproteinases occur at the plasma membrane (Edwards et al., 2008; Larios and Marzolo, 2012; Zakiyanov et al., 2019). In lung epithelial cells, the metalloproteinases directly associated with megalin proteolytic processing are MMP-2 and MMP-14 (Mazzocchi et al., 2017) (also known as MT1-MMP). MMP-2 is secreted as a pro-enzyme, activated by other metalloproteinases, including MMP-14, and binds to the megalin ectodomain (Mazzocchi et al., 2017). MMP-14 directly interacts with and processes megalin (Mazzocchi et al., 2017) and is also present in the proximal tubule (Zakiyanov et al., 2019). Like megalin, MMP-14 localizes at the apical surface and is found in apical vesicles in epithelial cells from the prostate and uterus (Thathiah and Carson, 2004; Sroka et al., 2008). Besides, MMP-14 can be released in exosomes in an active form (Hakulinen et al., 2008) and potentially could process exosomal megalin present in the urine (Marzolo and Farfán, 2011; De et al., 2017). Besides the reduction of surface megalin, it is also conceivable that the trafficking of these metalloproteinases could be affected in the LS condition, either its presence at the cell surface or its intracellular activity. MMP-14 traffics through the endosomal pathway and in this could be affected by an OCRL1 deficiency; MMP14 is endocytosed and localized first to early endosomes and later gets recycled through either early endosomes and the trans-Golgi network (TGN) (Wang et al., 2004) or late endosomes (Hakulinen et al., 2008; Williams and Coppolino, 2011; Macpherson et al., 2014). Megalin could also be a substrate of the ADAMs family (Zou et al., 2004; Larios and Marzolo, 2012). These membrane proteins locate in perinuclear regions, but they are also found in lesser amounts at the cell surface (Edwards et al., 2008), where they process many of their substrates, such as adhesion proteins and surface receptors (Reiss et al., 2006; Murphy, 2009). However, active forms of ADAMs are also found in intracellular compartments (Shirakabe et al., 2001); for example, ADAM10 and 17/TACE induce the shedding of APP in the TGN (Skovronsky et al., 2000). In the same direction, ADAM10 efficiently processes CD23 and possibly other substrates at the endosome (Mathews et al., 2010), and therefore, its activity could be directly affected in an LS condition.

The similar results obtained upon APPL1 silencing are probably due to the role that this adaptor protein has in the recruitment of OCRL1 to early endosomes (McCrea et al., 2008; Noakes et al., 2011; Bohdanowicz et al., 2012), besides the functions of the small endosomal GTPases Rab5 and Rab35 have in the recruitment of the phosphatase (Hyvola et al., 2006; Kanno et al., 2008; Dambournet et al., 2011). On the other hand, the internalization pathway of megalin includes its trafficking through APPL1 positive early endosomes; however, in cells lacking OCRL1, the presence of internalized megalin in APPL1 endosomes is reduced, contrasting with its increase in early endosomes positive for EEA1 (Vicinanza et al., 2011; Festa et al., 2019). These observations imply that even when megalin interacts with APPL1 (Erdmann et al., 2007), its presence in endosomes positive for this adaptor protein requires the presence of OCRL1.

Considering the negative role that the GSK3ß-mediated phosphorylation of the cytoplasmic domain of megalin has in receptor surface expression (Yuseff et al., 2007), we evaluated this modification in our cellular models. Our first hypothesis was that a defect in the phosphorylation of megalin, reflected by higher levels of this modification, could explain the lower surface levels of megalin in OCRL1 silenced cells. Cells with decreased levels of OCRL1 showed no change in basal GSK3ß activity, but, in contrast to our prediction, they exhibited lower levels of megalin phosphorylation. There is no information concerning where GSK3ß phosphorylates megalin and how this phosphorylation is controlled by the action of phosphatases or other kinases. However, it is known that AKT controls GSK3ß activity when both proteins are in PI (3,4) P2-enriched endosomal membranes and recruited by APPL1 (Schenck et al., 2008) suggesting that megalin phosphorylation would occur in the endosomal pathway. Then, we hypothesized that inhibition of OCRL1 could decrease the colocalization of GSK3ß with megalin. However, our results did not support this option, at least using our experimental strategy. On the other hand, megalin is also phosphorylated by PKC, PKA and CKII, although to a much smaller extent than by GSK3ß (Yuseff et al., 2007), but the

physiological significance of these modifications is still unknown. We could speculate that under LS conditions, the non-GSK3ß dependent phosphorylation of megalin and mediated by any of the kinases mentioned, could be inhibited explaining part of the reduction in megalin phosphorylation observed in OCRL KD cells. If any of these phosphorylation sites would have a positive role in the expression of megalin at the plasma membrane, their inhibition could result in a reduction of cell surface megalin. This effect would add to the recycling impairment caused by the accumulation of actin cytoskeleton at the endosomal membrane (Vicinanza et al., 2011). Future experiments would be required to address this possibility.

Of note, there was residual but still significant phosphorylation of megalin in our LS cellular model susceptible to inhibition of GSK3ß with LiCl. Considering this finding, we tested a physiological stimulus that activates PI3K and AKT as insulin, to reduce GSK3ß activity and megalin phosphorylation. For the first time, our results showed that insulin significantly reduced megalin phosphorylation and increases its expression at the plasma membrane under normal conditions. Moreover, in LLC-PK1 cells with reduced levels of OCRL1 and APPL1, the treatment with insulin significantly decreased GSK3ß activity and megalin phosphorylation, suggesting that this signaling pathway is still functional under these conditions. Accordingly, insulin treatment also increased megalin cell surface expression in cells with reduced OCRL1 activity. Potentially, the insulin pathway could be considered a tool to reduce the constitutive GSK3ß-mediated megalin phosphorylation and increase the receptor cell surface levels (Yuseff et al., 2007).

LS patients exhibit a urinary waste of several growth factors, including insulin (Norden et al., 2001; Bökenkamp and Ludwig, 2016). From this point of view, it is expected that insulin signaling could be affected in LS as we found in our study. Moreover, the reduction in insulin signaling evidenced in our experiments at the cellular level, specifically in conditions of reduction of OCRL1 function, not only would reduce megalin recycling but also would potentially decrease megalin endocytosis as pAKT is required for the efficient megalin-mediated endocytosis of albumin, a physiologically relevant ligand of the receptor present in the proximal tubule (Silva-Aguiar et al., 2022). Regarding AKT activity, it has been recently found that the mTORC1 complex is inactivated in OCRL1 deficient cells (Madhivanan et al., 2020), a defect that triggers a lack of nutrient-sensing (Wang et al., 2021) due to mTORC1 is required for proper insulin signaling (Saltiel and Kahn, 2001). Insulin signaling is also highly dependent on the cell type, something we observed in our experiments, and is associated with insulin receptor trafficking (Iraburu et al., 2021). For instance, the activation of PI3K and pAKT takes place at the plasma membrane as well as in endosomes, with higher activation at the endosome (Ceresa et al., 1998; Iraburu et al., 2021), being possible that under LS conditions at least the endosomal signaling, would be affected. Therefore, it is expected that the response to insulin and megalin phosphorylation mediated by GSK3ß are affected in LS cellular models and, in general, cells with decreased function of OCRL1 would be less responsive to insulin. Moreover, in LS patients' insulin signaling could be partially inhibited, affecting other processes including the stimulation of megalin expression under chronic kidney disease (Hosojima et al., 2009; Bryniarski et al., 2018) and the insulin-mediated surface expression of GLUT4, a trafficking response that is inhibited by GSK3ß (Duan X et al., 2021).

Endosomal compartments are part of the trafficking route of cargo proteins. They also have roles in membrane turnover and intracellular communication being a platform characterized by endosomal adaptor proteins, where components of signaling pathways are recruited (Vicinanza et al., 2011). Regarding insulin, APPL1 has been identified as an AKT-interacting endosomal adaptor (Mitsuuchi et al., 1999; Schenck et al., 2008) required for insulin signaling (Sato et al., 2007; Ryu et al., 2014). Here, we present insulin signaling kinetics showing a similar disruption of AKT and GSK3ß phosphorylation upon APPL1 KD and OCRL1 KD cells.

As mentioned before, in LS and Dent disease there are significant decreases in A-megalin in the urine (Suruda et al., 2017). Furthermore, other pathologies leading to chronic kidney diseases, such as diabetes (Ogasawara et al., 2012; De et al., 2017) and IgA nephropathy (Seki et al., 2014), exhibit an increase in the presence of C-megalin, probably secreted into the urine as exosomes. With the evidence described in this work, we highlight the importance of establishing cellular models for studying proteolysis, trafficking and phosphorylation of megalin in pathologies in which this receptor is affected to find potential therapeutic tools for these diseases.

Data availability statement

The original contributions presented in the study are included in the article/Supplementary Material, further inquiries can be directed to the corresponding author.

Author contributions

LS carried out experiments, analyzed the data, and made the first draft of the figures and manuscript. LMF performed experiments, analyzed the data and edited some manuscript sections. MPM is the corresponding author, supervised the research design, the laboratory activities, analyzed the data, including the structure of the article and figures, the list of

references, and wrote and edited the final version of the manuscript and figures.

Funding

This work was supported by Fondo Nacional de Ciencia y Tecnología, FONDECYT of Chile, project 1200393 to MPM, CONICYT doctoral thesis support scholarship AT24100200 to LS and Doctorado Nacional/2017-21171004 to LMF.

Acknowledgments

We thank Antonella de Matteis (TIGEM, Italy) for her conceptual and technical and for providing OCRL1 antibodies. We thank David Kaplan (Program in Neurosciences and Mental Health, Hospital for Sick Children and Department of Molecular Genetics, University of Toronto, Toronto, Ontario, Canada) for providing the APPL1 antibody used in this study. We also thank Alexis Gautreau (Ecole Polytechnique, IP Paris, Palaiseau, France) for giving as the plasmid mCherry-Rab11.

Conflict of interest

The authors declare that the research was conducted in the absence of any commercial or financial relationships that could be construed as a potential conflict of interest.

Publisher's note

All claims expressed in this article are solely those of the authors and do not necessarily represent those of their affiliated organizations, or those of the publisher, the editors and the reviewers. Any product that may be evaluated in this article, or claim that may be made by its manufacturer, is not guaranteed or endorsed by the publisher.

Supplementary material

The Supplementary Material for this article can be found online at: https://www.frontiersin.org/articles/10.3389/fcell.2022.911664/full#supplementary-material

References

Alexander, R. T., and Grinstein, S. (2009). Tethering, recycling and activation of the epithelial sodium-proton exchanger, NHE3. *J. Exp. Biol.* 212, 1630–1637. doi:10.1242/JEB.027375

Aroor, A., Zuberek, M., Duta, C., Meuth, A., Sowers, J. R., Whaley-Connell, A., et al. (2016). Angiotensin II stimulation of DPP4 activity regulates megalin in the proximal tubules. *Int. J. Mol. Sci.* 17, E780. doi:10.3390/IJMS17050780

Attree, O., Olivos, I. M., Okabe, I., Bailey, L. C., Nelson, D. L., Lewis, R. A., et al. (1992). The Lowe's oculocerebrorenal syndrome gene encodes a protein highly homologous to inositol polyphosphate-5-phosphatase. *Nature* 358, 239–242. doi:10.1038/358239A0

Bachinsky, D. R., Zheng, G., Niles, J. L., McLaughlin, M., Abbate, M., Andres, G., et al. (1993). Detection of two forms of GP330. Their role in Heymann nephritis. *Am. J. Pathol.* 143, 598–611.

Bachmann, S., Schlichting, U., Geist, B., Mutig, K., Petsch, T., Bacic, D., et al. (2004). Kidney-specific inactivation of the megalin gene impairs trafficking of renal inorganic sodium phosphate cotransporter (NaPi-IIa). *J. Am. Soc. Nephrol.* 15, 892–900. doi:10.1097/01.ASN.0000120389.09938.21

Bockenhauer, D., Bokenkamp, A., van't Hoff, W., Levtchenko, E., Kist-van Holthe, J. E., Tasic, V., et al. (2008). Renal phenotype in Lowe syndrome: A selective proximal tubular dysfunction. *Clin. J. Am. Soc. Nephrol.* 3, 1430–1436. doi:10.2215/CJN.00520108

Bohdanowicz, M., Balkin, D. M., De Camilli, P., and Grinstein, S. (2012). Recruitment of OCRL and Inpp5B to phagosomes by Rab5 and APPL1 depletes phosphoinositides and attenuates Akt signaling. *Mol. Biol. Cell* 23, 176–187. doi:10.1091/mbc.E11-06-0489

Bökenkamp, A., and Ludwig, M. (2016). The oculocerebrorenal syndrome of Lowe: an update. *Pediatr. Nephrol.* 31, 2201–2212. doi:10.1007/s00467-016-3343-3

Bolte, S., and Cordelières, F. P. (2006). A guided tour into subcellular colocalization analysis in light microscopy. *J. Microsc.* 224 (3), 213–232. doi:10.1111/j.1365-2818.2006.01706.x

Bothwell, S. P., Chan, E., Bernardini, I. M., Kuo, Y. M., Gahl, W. A., and Nussbaum, R. L. (2011). Mouse model for Lowe syndrome/Dent Disease 2 renal tubulopathy. *J. Am. Soc. Nephrol.* 22, 443–448. doi:10.1681/ASN.2010050565

Bryniarski, M. A., Yee, B. M., Jaffri, I., Chaves, L. D., Yu, J. A., Guan, X., et al. (2018). Increased megalin expression in early type 2 diabetes: Role of insulin-signaling pathways. *Am. J. Physiol. Ren. Physiol.* 315, F1191–F1207. doi:10.1152/ajprenal.00210.2018

Cabezas, F., Lagos, J., Céspedes, C., Vio, C. P., Bronfman, M., and Marzolo, M. P. (2011). Megalin/LRP2 expression is induced by peroxisome proliferator-activated receptor -alpha and -gamma: implications for PPARs' roles in renal function. *PloS One* 6, e16794. doi:10.1371/JOURNAL.PONE.0016794

Cabezas, F., Farfán, P., and Marzolo, M. P. (2019). Participation of the SMAD2/3 signalling pathway in the down regulation of megalin/LRP2 by transforming growth factor beta (TGF-ß1). *PloS One* 14, e0213127. doi:10.1371/JOURNAL.PONE.0213127

Ceresa, B. P., Kao, A. W., Santeler, S. R., and Pessin, J. E. (1998). Inhibition of clathrin-mediated endocytosis selectively attenuates specific insulin receptor signal transduction pathways. *Mol. Cell. Biol.* 18, 3862–3870. doi:10.1128/MCB.18.7.3862

Chen, C., and Okayama, H. (1987). High-efficiency transformation of mammalian cells by plasmid DNA. *Mol. Cell. Biol.* 7, 2745–2752. doi:10.1128/mcb.7.8.2745

Choudhury, R., Diao, A., Zhang, F., Eisenberg, E., Saint-Pol, A., Williams, C., et al. (2005). Lowe syndrome protein OCRL1 interacts with clathrin and regulates protein trafficking between endosomes and the trans -golgi network. *Mol. Biol. Cell* 16, 3467–3479. doi:10.1091/mbc.e05-02-0120

Christensen, E. I., Devuyst, O., Dom, G., Nielsen, R., Van der Smissen, P., Verroust, P., et al. (2003). Loss of chloride channel ClC-5 impairs endocytosis by defective trafficking of megalin and cubilin in kidney proximal tubules. *Proc. Natl. Acad. Sci. U. S. A.* 100, 8472–8477. doi:10.1073/pnas.1432873100

Cross, D. A. E., Alessi, D. R., Cohen, P., Andjelkovich, M., and Hemmings, B. A. (1995). Inhibition of glycogen synthase kinase-3 by insulin mediated by protein kinase B. *Nature* 378, 785–789. doi:10.1038/378785A0

Dambournet, D., MacHicoane, M., Chesneau, L., Sachse, M., Rocancourt, M., El Marjou, A., et al. (2011). Rab35 GTPase and OCRL phosphatase remodel lipids and F-actin for successful cytokinesis. *Nat. Cell Biol.* 13, 981–988. doi:10.1038/ncb2279

De, S., Kuwahara, S., Hosojima, M., Ishikawa, T., Kaseda, R., Sarkar, P., et al. (2017). Exocytosis-mediated urinary full-length megalin excretion is linked with the pathogenesis of diabetic nephropathy. *Diabetes* 66, 1391–1404. doi:10.2337/DB16-1031

De Matteis, M. A., Staiano, L., Emma, F., and Devuyst, O. (2017). The 5-phosphatase OCRL in Lowe syndrome and Dent disease 2. *Nat. Rev. Nephrol.* 13, 455–470. doi:10.1038/nrneph.2017.83

Derivery, E., Sousa, C., Gautier, J. J., Lombard, B., Loew, D., and Gautreau, A. (2009). The Arp2/3 activator WASH controls the fission of endosomes through a large multiprotein complex. *Dev. Cell* 17 (5), 712–723. doi:10.1016/j.devcel.2009.09.010

Duan, X., Norris, D. M., Humphrey, S. J., Yang, P., Cooke, K. C., Bultitude, W. P., et al. (2021). Trafficking regulator of GLUT4-1 (TRARG1) is a GSK3 substrate. *Biochem. J.* 479 (11), 1237–1256. doi:10.1042/BCJ20220153

Edwards, D. R., Handsley, M. M., and Pennington, C. J. (2008). The ADAM metalloproteinases. *Mol. Asp. Med.* 29, 258–289. doi:10.1016/J.MAM.2008.08.001

Erdmann, K. S., Mao, Y., McCrea, H. J., Zoncu, R., Lee, S., Paradise, S., et al. (2007). A role of the Lowe syndrome protein OCRL in early steps of the endocytic pathway. *Dev. Cell* 13, 377–390. doi:10.1016/j.devcel.2007.08.004

Eshbach, M. L., and Weisz, O. A. (2017). Receptor-mediated endocytosis in the proximal tubule. *Annu. Rev. Physiol.* 79, 425–448. doi:10.1146/ANNUREV-PHYSIOL-022516-034234

Farfán, P., Lee, J., Larios, J., Sotelo, P., Bu, G., and Marzolo, M.-P. (2013). A sorting nexin 17-binding domain within the LRP1 cytoplasmic tail mediates receptor recycling through the basolateral sorting endosome. *Traffic* 14, 823–838. doi:10.1111/tra.12076

Farquhar, M. G., Saito, A., Kerjaschki, D., and Orlando, R. A. (1995). The heymann nephritis antigenic complex: megalin (gp330) and RAP. *J. Am. Soc. Nephrol.* 6, 35–47. doi:10.1681/ASN.V6135

Festa, B. P., Berquez, M., Gassama, A., Amrein, I., Ismail, H. M., Samardzija, M., et al. (2019). OCRL deficiency impairs endolysosomal function in a humanized mouse model for Lowe syndrome and Dent disease. *Hum. Mol. Genet.* 28, 1931–1946. doi:10.1093/hmg/ddy449

Fisher, S. E., Van Bakel, I., Lloyd, S. E., Pearce, S. H. S., Thakker, R. V., and Craig, I. W. (1995). Cloning and characterization of CLCN5, the human kidney chloride channel gene implicated in Dent disease (an X-linked hereditary nephrolithiasis). *Genomics* 29, 598–606. doi:10.1006/GENO.1995.9960

Fukuda, M., Kanno, E., Ishibashi, K., and Itoh, T. (2008). Large scale screening for novel rab effectors reveals unexpected broad Rab binding specificity. *Mol. Cell. Proteomics* 7, 1031–1042. doi:10.1074/MCP.M700569-MCP200

Hakulinen, J., Sankkila, L., Sugiyama, N., Lehti, K., and Keski-Oja, J. (2008). Secretion of active membrane type 1 matrix metalloproteinase (MMP-14) into extracellular space in microvesicular exosomes. *J. Cell. Biochem.* 105, 1211–1218. doi:10.1002/JCB.21923

Hosojima, M., Sato, H., Yamamoto, K., Kaseda, R., Soma, T., Kobayashi, A., et al. (2009). Regulation of megalin expression in cultured proximal tubule cells by angiotensin II type 1A receptor- and insulin-mediated signaling cross talk. *Endocrinology* 150, 871–878. doi:10.1210/EN.2008-0886

Hyvola, N., Diao, A., McKenzie, E., Skippen, A., Cockcroft, S., and Lowe, M. (2006). Membrane targeting and activation of the Lowe syndrome protein OCRL1 by rab GTPases. *Embo J.* 25, 3750–3761. doi:10.1038/sj.emboj.7601274

Iraburu, M. J., Garner, T., and Montiel-Duarte, C. (2021). Revising endosomal trafficking under insulin receptor activation. *Int. J. Mol. Sci.* 22, 6978. doi:10.3390/ijms22136978

Kanno, E., Ishibashi, K., , et al.Fukuda, M., Kanno, E., Ishibashi, K., Itoh, T. (2008). Large scale screening for novel rab effectors reveals unexpected broad rab binding specificity. *Mol. Cell. Proteomics* 7, 1031–1042. doi:10.1074/mcp.M700569-MCP200

Kühbacher, A., Dambournet, D., Echard, A., Cossart, P., and Pizarro-Cerdá, J. (2012). Phosphatidylinositol 5-phosphatase oculocerebrorenal syndrome of Lowe protein (OCRL) controls actin dynamics during early steps of Listeria monocytogenes infection. *J. Biol. Chem.* 287, 13128–13136. doi:10.1074/JBC.M111.315788

Kurita, N., Kinoshita, M., Fujimura, M., Kurosawa, K., Sakuramachi, Y., Takano, K., et al. (2022). Association of urinary C-megalin with albuminuria and renal function in diabetes: a cross-sectional study (diabetes distress and care registry at tenri [DDCRT 21]). *J. Nephrol.* 35, 201–210. doi:10.1007/s40620-021-00995-2

Larios, J., and Marzolo, M. P. (2012). Novel aspects of the apolipoprotein-E receptor family: regulation and functional role of their proteolytic processing. *Front. Biol.* 7, 113–143. doi:10.1007/s11515-011-1186-7

Lee, J. W., Chou, C. L., and Knepper, M. A. (2015). Deep sequencing in microdissected renal tubules identifies nephron segment-specific transcriptomes. *J. Am. Soc. Nephrol.* 26, 2669–2677. doi:10.1681/ASN.2014111067

Leheste, J. R., Rolinski, B., Vorum, H., Hilpert, J., Nykjaer, A., Jacobsen, C., et al. (1999). Megalin knockout mice as an animal model of low molecular weight proteinuria. *Am. J. Pathol.* 155, 1361–1370. doi:10.1016/S0002-9440(10)65238-8

Leheste, J. R., Melsen, F., Wellner, M., Jansen, P., Schlichting, U., Renner-Müller, I., et al. (2003). Hypocalcemia and osteopathy in mice with kidney-specific megalin gene defect. *FASEB J. Off. Publ. Fed. Am. Soc. Exp. Biol.* 17, 247–249. doi:10.1096/FJ.02-0578FJE

Li, Y., Marzolo, M.-P., Kerkhof, P. V., Strous, G. J., and Bu, G. (2000). The YXXL motif , but not the two NPXY motifs , serves as the dominant endocytosis signal for low density lipoprotein. *Recept. Relat. Protein* * 275, 17187–17194. doi:10.1074/jbc.M000490200

Li, Y., Cong, R., and Biemesderfer, D. (2008). The COOH terminus of megalin regulates gene expression in opossum kidney proximal tubule cells. *Am. J. Physiol. Cell Physiol.* 295, C529–C537. doi:10.1152/AJPCELL.00037.2008

Lichter-Konecki, U., Farber, L. W., Cronin, J. S., Suchy, S. F., and Nussbaum, R. L. (2006). The effect of missense mutations in the RhoGAP-homology domain on ocrl1 function. *Mol. Genet. Metab.* 89, 121–128. doi:10.1016/J.YMGME.2006.04.005

Lin, D. C., Quevedo, C., Brewer, N. E., Bell, A., Testa, J. R., Grimes, M. L., et al. (2006). APPL1 associates with TrkA and GIPC1 and is required for nerve growth factor-mediated signal transduction. *Mol. Cell. Biol.* 26, 8928–8941. doi:10.1128/MCB.00228-06

Lowe, C., Terrey, M., and MaClachlan, E. A. (1952). Organic-aciduria, decreased renal ammonia production, hydrophthalmos, and mental retardation; a clinical entity. *AMA. Am. J. Dis. Child.* 83, 164–184. doi:10.1001/ARCHPEDI.1952.02040060030004

Macpherson, I. R., Rainero, E., Mitchell, L. E., van den Berghe, P. V. E., Speirs, C., Dozynkiewicz, M. A., et al. (2014). CLIC3 controls recycling of late endosomal MT1-MMP and dictates invasion and metastasis in breast cancer. *J. Cell Sci.* 127, 3893–3901. doi:10.1242/JCS.135947

Madhivanan, K., Ramadesikan, S., Hsieh, W-C., Aguilar, M. C., Hanna, C. B., Bacallao, R. L., et al. (2020). Lowe syndrome patient cells display mTOR- and RhoGTPase-dependent phenotypes alleviated by rapamycin and statins. *Hum. Mol. Genet.* 29 (10), 1700–1715. doi:10.1093/hmg/ddaa086

Marzolo, M. P., and Farfán, P. (2011). New insights into the roles of megalin/LRP2 and the regulation of its functional expression. *Biol. Res.* 44, 89–105. doi:10.4067/S0716-97602011000100012

Marzolo, M. P., Yuseff, M. I., Retamal, C., Donoso, M., Ezquer, F., Farfán, P., et al. (2003). Differential distribution of low-density lipoprotein-receptor-related protein (LRP) and megalin in polarized epithelial cells is determined by their cytoplasmic domains. *Traffic* 4, 273–288. doi:10.1034/J.1600-0854.2003.00081.X

Mathews, J. A., Gibb, D. R., Chen, B. H., Scherle, P., and Conrad, D. H. (2010). CD23 Sheddase A disintegrin and metalloproteinase 10 (ADAM10) is also required for CD23 sorting into B cell-derived exosomes. *J. Biol. Chem.* 285, 37531–37541. doi:10.1074/JBC.M110.141556

Mattila, P. E., Raghavan, V., Rbaibi, Y., Baty, C. J., and Weisz, O. A. (2014). Rab11a-positive compartments in proximal tubule cells sort fluid-phase and membrane cargo. *Am. J. Physiol. Cell Physiol.* 306, 441–449. doi:10.1152/ajpcell.00236.2013

Mazzocchi, L. C., Vohwinkel, C. U., Mayer, K., Herold, S., Morty, R. E., Seeger, W., et al. (2017). TGF-β inhibits alveolar protein transport by promoting shedding, regulated intramembrane proteolysis, and transcriptional downregulation of megalin. *Am. J. Physiol. Lung Cell. Mol. Physiol.* 313, L807–L824. doi:10.1152/AJPLUNG.00569.2016

McCrea, H. J., Paradise, S., Tomasini, L., Addis, M., Melis, M. A., De Matteis, M. A., et al. (2008). All known patient mutations in the ASH-RhoGAP domains of OCRL affect targeting and APPL1 binding. *Biochem. Biophys. Res. Commun.* 369, 493–499. doi:10.1016/j.bbrc.2008.02.067

Mitsuuchi, Y., Johnson, S. W., Sonoda, G., Tanno, S., Golemis, E. A., and Testa, J. R. (1999). Identification of a chromosome 3p14.3-21.1 gene, APPL, encoding an adaptor molecule that interacts with the oncoprotein-serine/threonine kinase AKT2. *Oncogene* 18, 4891–4898. doi:10.1038/sj.onc.1203080

Murphy, G. (2009). Regulation of the proteolytic disintegrin metalloproteinases, the "Sheddases. *Semin. Cell Dev. Biol.* 20, 138–145. doi:10.1016/J.SEMCDB.2008.09.004

Noakes, C. J., Lee, G., and Lowe, M. (2011). The PH domain proteins IPIP27A and B link OCRL1 to receptor recycling in the endocytic pathway. *Mol. Biol. Cell* 22, 606–623. doi:10.1091/mbc.E10-08-0730

Norden, A. G. W., Lapsley, M., Lee, P. J., Pusey, C. D., Scheinman, S. J., Tam, F. W. K., et al. (2001). Glomerular protein sieving and implications for renal failure in Fanconi syndrome. *Kidney Int.* 60, 1885–1892. doi:10.1046/j.1523-1755.2001.00016.x

Norden, A. G. W., Lapsley, M., Igarashi, T., Kelleher, C. L., Lee, P. J., Matsuyama, T., et al. (2002). Urinary megalin deficiency implicates abnormal tubular endocytic function in Fanconi syndrome. *J. Am. Soc. Nephrol.* 13, 125–133. doi:10.1681/ASN.V131125

Ogasawara, S., Hosojima, M., Kaseda, R., Kabasawa, H., Yamamoto-Kabasawa, K., Kurosawa, H., et al. (2012). Significance of urinary full-length and ectodomain forms of megalin in patients with type 2 diabetes. *Diabetes Care* 35, 1112–1118. doi:10.2337/DC11-1684

Oltrabella, F., Pietka, G., Ramirez, I. B. R., Mironov, A., Starborg, T., Drummond, I. A., et al. (2015). The Lowe syndrome protein OCRL1 is required for endocytosis in the zebrafish pronephric tubule. *PLoS Genet.* 11, e1005058. doi:10.1371/journal.pgen.1005058

Perez Bay, A. E., Schreiner, R., Benedicto, I., Paz Marzolo, M., Banfelder, J., Weinstein, A. M., et al. (2016). The fast-recycling receptor Megalin defines the apical recycling pathway of epithelial cells. *Nat. Commun.* 7, 11550–11615. doi:10.1038/ncomms11550

Pfaffl, M. W. (2001). A new mathematical model for relative quantification in real-time RT-PCR. *Nucleic Acids Res.* 29, E45. doi:10.1093/NAR/29.9.E45

Pirruccello, M., Nandez, R., Idevall-Hagren, O., Alcazar-Roman, A., Abriola, L., Berwick, S. A., et al. (2014). Identification of inhibitors of inositol 5-phosphatases through multiple screening strategies. *ACS Chem. Biol.* 9, 1359–1368. doi:10.1021/cb500161z

Pisitkun, T., Shen, R. F., and Knepper, M. A. (2004). Identification and proteomic profiling of exosomes in human urine. *Proc. Natl. Acad. Sci. U. S. A.* 101, 13368–13373. doi:10.1073/PNAS.0403453101

Preston, R., Naylor, R. W., Stewart, G., Bierzynska, A., Saleem, M. A., Lowe, M., et al. (2020). A role for OCRL in glomerular function and disease. *Pediatr. Nephrol.* 35, 641–648. doi:10.1007/s00467-019-04317-4

Reiss, K., Ludwig, A., and Saftig, P. (2006). Breaking up the tie: disintegrin-like metalloproteinases as regulators of cell migration in inflammation and invasion. *Pharmacol. Ther.* 111, 985–1006. doi:10.1016/J.PHARMTHERA.2006.02.009

Ryu, J., Galan, A. K., Xin, X., Dong, F., Abdul-Ghani, M. A., Zhou, L., et al. (2014). APPL1 potentiates insulin sensitivity by facilitating the binding of IRS1/2 to the insulin receptor. *Cell Rep.* 7, 1227–1238. doi:10.1016/J.CELREP.2014.04.006

Sage, D., Donati, L., Soulez, F., Fortun, D., Schmit, G., Seitz, A., et al. (2017). DeconvolutionLab2: An open-source software for deconvolution microscopy. *Methods* 115, 28–41. doi:10.1016/j.ymeth.2016.12.015

Saito, A., Pietromonaco, S., Loo, A. K. C., and Farquhar, M. G. (1994). Complete cloning and sequencing of rat gp330/" megalin, " a distinctive member of the low density lipoprotein receptor gene family. *Proc. Natl. Acad. Sci. U. S. A.* 91, 9725–9729. doi:10.1073/PNAS.91.21.9725

Saltiel, A. R., and Kahn, C. R. (2001). Insulin signalling and the regulation of glucose and lipid metabolism. *Nature* 414, 799–806. doi:10.1038/414799a

Sato, Y., Taoka, M., Sugiyama, N., Kubo, K. I., Fuchigami, T., Asada, A., et al. (2007). Regulation of the interaction of Disabled-1 with CIN85 by phosphorylation with Cyclin-dependent kinase 5. *Genes cells.* 12, 1315–1327. doi:10.1111/j.1365-2443.2007.01139.x

Schenck, A., Goto-Silva, L., Collinet, C., Rhinn, M., Giner, A., Habermann, B., et al. (2008). The endosomal protein Appl1 mediates akt substrate specificity and cell survival in vertebrate development. *Cell* 133, 486–497. doi:10.1016/j.cell.2008.02.044

Seki, T., Asanuma, K., Asao, R., Nonaka, K., Sasaki, Y., Trejo, J. A. O., et al. (2014). Significance of urinary full-length megalin in patients with IgA nephropathy. *PloS One* 9, e114400. doi:10.1371/JOURNAL.PONE.0114400

Serretti, A., Drago, A., and De Ronchi, D. (2009). Lithium pharmacodynamics and pharmacogenetics: focus on inositol mono phosphatase (IMPase), inositol poliphosphatase (IPPase) and glycogen sinthase kinase 3 beta (GSK-3 beta). *Curr. Med. Chem.* 16 (15), 1917–1948. doi:10.2174/092986709788186101

Shirakabe, K., Wakatsuki, S., Kurisaki, T., and Fujisawa-Sehara, A. (2001). Roles of Meltrin beta/ADAM19 in the processing of neuregulin. *J. Biol. Chem.* 276, 9352–9358. doi:10.1074/JBC.M007913200

Shrimpton, A. E., Hoopes, R. R., Knohl, S. J., Hueber, P., Reed, A. A. C., Christie, P. T., et al. (2009). OCRL1 mutations in dent 2 patients suggest a mechanism for phenotypic variability. *Nephron. Physiol.* 112, 27–36. doi:10.1159/000213506

Silva-Aguiar, R. P., Peruchetti, D. B., Florentino, L. S., Takiya, C. M., Marzolo, M.-P., Dias, W. B., et al. (2022). Albumin expands albumin reabsorption capacity in proximal tubule epithelial cells through a positive feedback loop between AKT and megalin. *Int. J. Mol. Sci.* 23, 848. doi:10.3390/ijms23020848

Skovronsky, D. M., Moore, D. B., Milla, M. E., Doms, R. W., and Lee, V. M. Y. (2000). Protein kinase C-dependent alpha-secretase competes with beta-secretase for cleavage of amyloid-beta precursor protein in the trans-golgi network. *J. Biol. Chem.* 275, 2568–2575. doi:10.1074/JBC.275.4.2568

Sotelo, P., Farfán, P., Milla, M. E., Benitez, M. L., Bu, G., and Marzolo, M-P. (2014). Sorting nexin 17 regulates ApoER2 recycling and reelin signaling. *PLoS One* 9 (4), e93672. doi:10.1371/journal.pone.0093672

Sroka, I. C., McDaniel, K., Nagle, R. B., and Bowden, G. T. (2008). Differential localization of MT1-MMP in human prostate cancer tissue: role of IGF-1R in MT1-MMP expression. *Prostate* 68, 463–476. doi:10.1002/PROS.20718

Suruda, C., Tsuji, S., Yamanouchi, S., Kimata, T., Huan, N. T., Kurosawa, H., et al. (2017). Decreased urinary excretion of the ectodomain form of megalin (A-megalin) in children with OCRL gene mutations. *Pediatr. Nephrol.* 32, 621–625. doi:10.1007/S00467-016-3535-X

Thathiah, A., and Carson, D. D. (2004). MT1-MMP mediates MUC1 shedding independent of TACE/ADAM17. *Biochem. J.* 382, 363–373. doi:10.1042/BJ20040513

Thraillkill, K. M., Nimmo, T., Bunn, R. C., Cockrell, G. E., Moreau, C. S., Mackintosh, S., et al. (2009). Microalbuminuria in type 1 diabetes is associated with enhanced excretion of the endocytic multiligand receptors megalin and cubilin. *Diabetes Care* 32, 1266–1268. doi:10.2337/DC09-0112

Toi, N., Inaba, M., Ishimura, E., Tsugawa, N., Imanishi, Y., Emoto, M., et al. (2019). Significance of urinary C-megalin excretion in vitamin D metabolism in pre-dialysis CKD patients. *Sci. Rep.* 9, 2207. doi:10.1038/s41598-019-38613-8

Vicinanza, M., Di Campli, A., Polishchuk, E., Santoro, M., Di Tullio, G., Godi, A., et al. (2011). OCRL controls trafficking through early endosomes via PtdIns4, $5P_2$-dependent regulation of endosomal actin. *EMBO J.* 30, 4970–4985. doi:10.1038/emboj.2011.354

Wang, X., Ma, D., Keski-Oja, J., and Pei, D. (2004). Co-recycling of MT1-MMP and MT3-MMP through the trans-Golgi network. Identification of DKV582 as a recycling signal. *J. Biol. Chem.* 279, 9331–9336. doi:10.1074/JBC.M312369200

Wang, B., He, W., Prosseda, P. P., Li, L., Kowal, T. J., Alvarado, J. A., et al. (2021). OCRL regulates lysosome positioning and mTORC1 activity through SSX2IP-mediated microtubule anchoring. *EMBO Rep.* 22, e52173. doi:10.15252/embr.202052173

Williams, K. C., and Coppolino, M. G. (2011). Phosphorylation of membrane type 1-matrix metalloproteinase (MT1-MMP) and its vesicle-associated membrane protein 7 (VAMP7)-dependent trafficking facilitate cell invasion and migration. *J. Biol. Chem.* 286, 43405–43416. doi:10.1074/JBC.M111.297069

Yuseff, M. I., Farfan, P., Bu, G., and Marzolo, M.-P. (2007). A cytoplasmic PPPSP motif determines megalin's phosphorylation and regulates receptor's recycling and surface expression. *Traffic* 8, 1215–1230. doi:10.1111/j.1600-0854.2007.00601.x

Zakiyanov, O., Kalousová, M., Zima, T., and Tesař, V. (2019). Matrix metalloproteinases in renal diseases: A critical appraisal. *Kidney Blood Press. Res.* 44, 298–330. doi:10.1159/000499876

Zhang, X., Hartz, P. A., Philip, E., Racusen, L. C., and Majerus, P. W. (1998). Cell lines from kidney proximal tubules of a patient with Lowe syndrome lack OCRL inositol polyphosphate 5-phosphatase and accumulate phosphatidylinositol 4, 5-bisphosphate. *J. Biol. Chem.* 273, 1574–1582. doi:10.1074/jbc.273.3.1574

Zou, Z., Chung, B., Nguyen, T., Mentone, S., Thomson, B., and Biemesderfer, D. (2004). Linking receptor-mediated endocytosis and cell signaling: Evidence for regulated intramembrane proteolysis of megalin in proximal tubule. *J. Biol. Chem.* 279, 34302–34310. doi:10.1074/jbc.M405608200

Frontiers in
Cell and Developmental Biology

Explores the fundamental biological processes of life, covering intracellular and extracellular dynamics.

The world's most cited developmental biology journal, advancing our understanding of the fundamental processes of life. It explores a wide spectrum of cell and developmental biology, covering intracellular and extracellular dynamics.

Discover the latest Research Topics

See more →

Frontiers

Avenue du Tribunal-Fédéral 34
1005 Lausanne, Switzerland
frontiersin.org

Contact us

+41 (0)21 510 17 00
frontiersin.org/about/contact